



## Supplementary Materials for

### **All topological bands of all nonmagnetic stoichiometric materials**

Maia G. Vergniory *et al.*

Corresponding authors: Maia G. Vergniory, maiagvergniory@dipc.org; Benjamin J. Wieder, bwieder@mit.edu; Nicolas Regnault, regnault@princeton.edu

*Science* **376**, eabg9094 (2022)  
DOI: 10.1126/science.abg9094

#### **The PDF file includes:**

Supplementary Text  
Figs. S1 to S103  
Tables S1 to S33  
References

## CONTENTS

<b>. List of Tables</b>	<b>4</b>
<b>S1. Introduction to the Supplementary Material</b>	<b>5</b>
<b>S2. Topological Quantum Chemistry Review</b>	<b>6</b>
A. Elementary Band Representations . . . . .	6
B. The Compatibility Relations . . . . .	8
<b>S3. Overview of the Previous Functionality of the VASP2Trace Program and New Features of the Check Topological Mat Program</b>	<b>9</b>
A. Overview of the Previous Functionality of the VASP2Trace and Check Topological Mat Programs . . . . .	10
B. New Features of the Check Topological Mat Program Introduced in this Work . . . . .	12
<b>S4. VASP Calculation Details and Data Set Preparation</b>	<b>13</b>
<b>S5. Computation Time and Resources</b>	<b>16</b>
A. Supercomputers and General Computational Resource Usage Statistics . . . . .	16
B. Computational Resources Expended per SG and per Number of Atoms in the Primitive Cell . . . . .	17
C. Disk Storage Requirements and Statistics . . . . .	29
<b>S6. Topological Material Classes in the Absence of Spin-Orbit Coupling</b>	<b>34</b>
A. Relative Numbers of Materials in Each Topological Class with and without SOC . . . . .	35
B. Physical Interpretation of the NLC and SEBR Materials Classes in the Absence of SOC . . . . .	37
<b>S7. Major Updates to the Topological Materials Database</b>	<b>41</b>
<b>S8. Statistics for all of the Topological Bands and Band Connectivity in the ICSD</b>	<b>44</b>
A. Topological Classification at the Fermi Level for all of the Stoichiometric Unique Materials in the ICSD with and w/o SOC . . . . .	44
B. Topological Classification and Connectivity of all of the Bands in all of the Stoichiometric Unique Materials in the ICSD with and w/o SOC . . . . .	55
<b>S9. Repeat-Topology and Supertopology</b>	<b>75</b>
A. Definition of Repeat-Topology . . . . .	75
B. Definition of Supertopology . . . . .	76
C. Statistics for Supertopological Materials in the ICSD . . . . .	77
<b>S10. SOC-Driven Topological Phase Transitions</b>	<b>89</b>
<b>S11. Lists of Representative Topological Materials</b>	<b>103</b>
A. Symmetry-Indicated TIs, TCIs, and HOTIs . . . . .	105
1. 3D Strong TIs . . . . .	105
2. $S_4$ -Rotoinversion-Indicated Strong TIs and Weyl Semimetals . . . . .	116
3. Inversion-Symmetry-Protected HOTIs . . . . .	118

4. Inversion-Symmetry-Indicated Weak TIs and TCIs . . . . .	127
5. Rotation-Anomaly TCIs and High-Fold-Rotation Mirror TCIs . . . . .	144
6. Other TCIs with Trivial $Z_4$ Indices . . . . .	150
7. TCIs with Threefold Rotation Symmetry . . . . .	156
B. Repeat-Topological Materials . . . . .	157
C. Enforced Topological Semimetals . . . . .	166
1. ESFD-Classified Semimetals . . . . .	166
2. ES-Classified Semimetals . . . . .	189
D. Semimetal-Insulator Transitions Driven by Spin-Orbit Coupling . . . . .	196
E. Materials with Fragile Topological Bands at or Close to $E_F$ . . . . .	203
. References	<b>209</b>

## LIST OF TABLES

S1. Topology of all of the bands in the RTopo and STopo compound Bi <sub>2</sub> Mg <sub>3</sub> . . . . .	13
S2. Number of analyzed compounds . . . . .	15
S3. Percentage of unique materials with at least one magnetic ICSD entry and with valence <i>f</i> electrons as determined by VASP (see <a href="https://www.smcm.iqfr.csic.es/docs/vasp/node248.html">https://www.smcm.iqfr.csic.es/docs/vasp/node248.html</a> for further details) . . . . .	15
S4. Total CPU hours expended in each of the four VASP calculation steps, subdivided by calculations performed with and without incorporating the effects of SOC (with SOC and w/o SOC, respectively) . . . . .	17
S5. Total CPU hours expended for ab-initio calculations with SOC per SG . . . . .	18
S6. Total CPU hours expended for ab-initio calculations w/o SOC per SG . . . . .	22
S7. Total CPU hours expended for ab-initio calculations with SOC per number of atoms in the primitive cell . . . . .	26
S8. Total CPU hours expended for ab-initio calculations w/o SOC per number of atoms in the primitive cell . . . . .	27
S9. Total disk storage space for ab-initio calculations per SG . . . . .	29
S10. Total disk storage space for ab-initio calculations per number of atoms in the primitive cell . . . . .	33
S11. Number of unique materials in each topological class where both SOC and w/o SOC calculations have converged . . . . .	35
S12. List of all nonmagnetic NLC-SM unique materials without <i>f</i> electrons . . . . .	39
S13. List of all nonmagnetic SEBR-SM unique materials without <i>f</i> electrons . . . . .	40
S14. Number of unique materials in each topological class per SG with SOC . . . . .	44
S15. Number of materials in each topological class per SG w/o SOC . . . . .	50
S16. Topology of all of the bands in the ES compound Ni <sub>2</sub> SnZr . . . . .	56
S17. Number of topological bands per SG among the unique materials with SOC . . . . .	57
S18. Number of unique materials per SG with topological bands at any filling with SOC . . . . .	61
S19. Number of topological bands per SG w/o SOC among the unique materials . . . . .	65
S20. Number of unique materials per SG with topological bands w/o SOC at any filling . . . . .	69
S21. High-connectivity nonmagnetic unique materials without <i>f</i> electrons . . . . .	74
S22. Topology of all of the bands in the RTopo and STopo compound Bi . . . . .	77
S23. Statistics for supertopological materials with SOC . . . . .	78
S24. Supertopological nonmagnetic unique materials without <i>f</i> electrons that are NLC at $E_F$ . . . . .	79
S25. Supertopological nonmagnetic unique materials without <i>f</i> electrons that are SEBR at $E_F$ . . . . .	79
S26. Supertopological nonmagnetic unique materials without <i>f</i> electrons that are ES at $E_F$ . . . . .	81
S27. Supertopological nonmagnetic unique materials without <i>f</i> electrons that are ESFD at $E_F$ . . . . .	83
S28. Supertopological nonmagnetic unique materials without <i>f</i> electrons that are LCEBR at $E_F$ . . . . .	87
S29. SOC-driven topological phase transition statistics for ES materials w/o SOC . . . . .	90
S30. SOC-driven topological phase transition statistics for ESFD materials w/o SOC . . . . .	93
S31. SOC-driven topological phase transition statistics for LCEBR materials w/o SOC . . . . .	99
S32. SOC-driven topological phase transition statistics for NLC-SM materials w/o SOC . . . . .	103
S33. SOC-driven topological phase transition statistics for SEBR-SM materials w/o SOC . . . . .	103

## S1. INTRODUCTION TO THE SUPPLEMENTARY MATERIAL

In this work, we have introduced a complete catalogue of the symmetry-indicated stable and fragile topology of all of the bands in all of the stoichiometric materials in the Inorganic Crystal Structure Database (ICSD) [41]. Below, we provide Supplementary Material (SM) containing a description of our methodology, as well as detailed statistics for the materials studied in this work. First, in S2, we will review the methods employed in this work, which derive from the recently introduced theory of *Topological Quantum Chemistry* (TQC) [28]. Next, in S3 and S4, we will document the computational machinery that we developed to apply TQC to the ICSD database. Specifically, in S3 and S4, we will respectively review the `VASP2Trace` program previously implemented for Ref. [38], and will detail updates to the `Check Topological Mat` program implemented for this work – for both programs, we will additionally detail their interface with the density functional theory (DFT) Vienna Ab-initio Simulation Package (VASP) [78, 79]. In S5, we will next discuss how we prepared the data used to generate this work, and will detail the CPU time invested per number of atoms in the unit cell of each material, and per each crystallographic space group (SG) [56]. In the following section – S6, we will then review the theory of TQC in the absence of spin-orbit coupling (SOC), and will specifically discuss the physical interpretation of symmetry-based indicators of band topology [16, 17, 29, 33, 36, 37, 87] in material calculations performed in the absence of SOC (w/o SOC). In the following section – S7 – we will then provide detailed descriptions of the significant **Topological Materials Database** (<https://www.topologicalquantumchemistry.com/>) updates implemented for this work.

In the remaining sections of the Supplementary Material, we will present detailed statistics, tables, and lists supporting the results shown in the main text. First, in S8, we will provide extensive statistics for all of the topological bands and band connectivity in the materials studied in this work. Next, in S9, we will rigorously define the *repeat-topological* (RTopo) and *supertopological* (STopo) material classes introduced in this work, and will provide a list of all of the symmetry-indicated STopo materials in the ICSD. Then, in S10, we will analyze the role of SOC in driving phase transitions between topological (semi)metals w/o SOC and topological (crystalline) insulators with SOC. In S10, we will additionally provide detailed statistics for all of the topological phase transitions observed in this work between materials with and w/o SOC. Finally, in S11, we will present an extensive list of all of the highest-quality topological (crystalline) insulators and semimetals among all of the stoichiometric materials in the ICSD. Though some of the materials in S11 are well known – such as the archetypal 3D topological insulator (TI)  $\text{Bi}_2\text{Se}_3$  [18] [ICSD 617079, SG 166 ( $R\bar{3}m$ )] – others are relatively unstudied, and should inspire new experimental investigations as well as provide new context for previously unexplained experimental data.

## S2. TOPOLOGICAL QUANTUM CHEMISTRY REVIEW

### A. Elementary Band Representations

Topological Quantum Chemistry (TQC) [28] is a position-space theory of band topology in crystalline solids. The building blocks of TQC are trivial atomic limits, which transform in elementary band representations (EBRs) [88–90]. Most generally, a band representation (band rep), elementary or otherwise, is a collection of momentum-space states (bands) induced from (exponentially) localized orbitals placed throughout each unit cell of a crystal [89, 91]. If the band rep is induced from a *maximal* Wyckoff position  $\omega$  and a set of atomic orbitals that transform in an irreducible corepresentation (corep) of the site-symmetry group  $G_\omega$  [defined in detail in Refs. [28, 58, 92, 93]], then the band rep can be further classified as *elementary* (*i.e.*, as an EBR), provided that the band rep is not an *exceptional case* (see Refs. [28, 29, 93]). Conversely, if the band rep is not elementary, then it can be expressed as a sum of EBRs [93]. In this work and in TQC, we restrict analysis to nonmagnetic (paramagnetic) crystals [*i.e.* Type-II Shubnikov space groups (SGs) [29, 56]], which respect time-reversal ( $\mathcal{T}$ ) symmetry. The EBRs of the nonmagnetic SGs can be accessed through the **BANDREP** tool [28, 58] on the **Bilbao Crystallographic Server (BCS)** [94, 95]. During the preparation of this work, the EBRs of the magnetic SGs were also computed in Ref. [29] (see **MBANDREP** on the **BCS**), and were used to perform the first high-throughput search for magnetic topological materials [37].

For the purposes of this work, we are primarily concerned with the small coreps at high-symmetry (maximal)  $\mathbf{k}$  points. Specifically, given a set of bands in a first-principles or tight-binding calculation, one can extract the coreps of the occupied bands at the maximal  $\mathbf{k}$  points to construct a *symmetry data vector* [38]. Given a symmetry data vector, the first step is to determine if the symmetry data vector is compatible with an insulating gap along all high-symmetry lines and planes – this can be accomplished using the compatibility relations, which are explained in detail in S2B. If the symmetry data is incompatible with an insulating gap, then the bulk bands are necessarily (semi)metallic. Semimetals that fail to satisfy the compatibility relations can then be further classified by whether a multiplet of Bloch states (transforming in an irreducible small corep of the little group) at a maximal  $\mathbf{k}$  point is partially occupied [enforced semimetal with Fermi degeneracy (ESFD)], or whether the compatibility relations fail along a high-symmetry line or plane [enforced semimetal (ES)]. If the symmetry data vector is compatible with an insulating gap (along high-symmetry lines and planes), we then determine if the symmetry data can be re-expressed as a linear combination of EBRs (LCEBR) with integer coefficients. As we will shortly see, in order for a set of bands to be topologically trivial, it is a necessary (but not sufficient) condition that the bands are classified as LCEBR.

The EBRs also provide a means of characterizing the topology of a set of bands obtained from a DFT or tight-binding calculation. Specifically, given an energetically isolated set of bands, the small coreps (symmetry eigenvalues) can imply one of two broad topological classes. First, there are stable topological bands, which characterize strong and weak topological (crystalline) insulators (TIs and TCIs) [5, 16, 17, 30, 33] that cannot be rendered topologically trivial through the addition of bands that are not themselves stable topological. A subset of topological bands, known as *symmetry-indicated* topological bands [5, 16, 17, 30, 33, 87], can be recognized as topologically stable because their symmetry data cannot be expressed as a linear combination of EBRs with integer coefficients. In this work, we follow the nomenclature established in Ref. [38] in which a symmetry-indicated topological band is classified as originating from a split EBR (SEBR) if its symmetry data can be expressed as a linear combination of connected pieces of EBRs that are themselves disconnected (while continuing to not match any linear combination of full EBRs). Continuing to employ the nomenclature of Ref. [38], we classify symmetry-indicated topological bands as NLC if their symmetry data cannot be expressed as an integer-valued linear combination of pieces of EBRs. Additionally, it was recently discovered that there also exist *fragile* topological bands [43–48, 96–101], which, unlike stable topological bands, can characterize a trivial insulator (or an “obstructed” atomic limit [34, 59, 102]) if they are combined with trivial or other fragile bands. TIs and TCIs characterized by stable topological bands can be classified using methods including K-theory [103], surface-state anomalies [14, 16, 17, 29, 104, 105], and layer constructions [16, 29, 106], whereas fragile topological bands can be characterized by corner filling anomalies [34, 46, 59, 96, 99, 102] and quantized twisted-boundary [47, 100] and defect [107] responses. For both stable and fragile TCIs, a complete diagnosis of nontrivial band topology can

be obtained by performing (nested) Wilson loop calculations [13, 14, 34, 102, 108–112].

For each SG, symmetry-indicated topological bands labeled NLC or SEBR can be further characterized using symmetry-based indicators (SIs). Specifically, following a prescription detailed in Ref. [32], the authors of Refs. [16, 17, 33] compared the EBRs, small coreps, and compatibility relations in each SG to determine the linearly independent sets of NLC and SEBR symmetry data [we provide specific details of this calculation in the text below]. In each SG, the calculation prescribed in Ref. [32] returned a set of positive-definite integers – known as the *SI group* (*e.g.* {4, 2, 2, 2} in SG 2) – that aligned with the symmetry-indicated classification of strong and weak stable topological (crystalline) insulators in that SG (*e.g.*  $\mathbb{Z}_4 \otimes \mathbb{Z}_2^3$ ). In Refs. [16, 17], the authors then matched the SI groups (*e.g.*  $\mathbb{Z}_4 \otimes \mathbb{Z}_2^3$ ) to anomalous boundary states and occupied bands with specific combinations of crystal symmetry eigenvalues – known as *SI formulas* (*i.e.* generalized Fu-Kane formulas [30]) – to construct a complete enumeration of all possible symmetry-indicated stable TIs and TCIs in the nonmagnetic SGs. This method was then expanded in Ref. [36] to the nonmagnetic SGs without SOC to compute the stable SIs for special classes of topological semimetals, which in this work we designate as SEBR-SM and NLC-SM (see S6 for further details). Finally, building upon the first demonstration of symmetry-indicated fragile topology in TQC [43], the authors of Refs. [45, 46] discovered the existence of fragile SIs, specifically showing that if a set of bands is classified as LCEBR, then it can be further classified as fragile if some of the integer coefficients in the linear combination of EBRs are negative.

In summary, TQC provides a unique, deterministic method for diagnosing the topology of any set of energetically isolated bands. Using TQC, we can analyze the full energy spectrum of any material up to any number of bands using the following procedure. First, using VASP2Trace [38, 84, 113] – a program that was implemented by Zhijun Wang to be used in conjunction with VASP [78, 79, 81] – we calculate the characters  $\chi(g)$  of all of the unitary symmetries  $g$  of the occupied Bloch wavefunctions at all high-symmetry (maximal)  $\mathbf{k}$  points, where  $\chi(g)$  is equal to the trace of the matrix representative of the symmetry element  $g$  in the reducible small corep corresponding to the set of all of the occupied Bloch states at  $\mathbf{k}$ . Next, using  $\chi(g)$ , we compute the multiplicity  $m_\alpha$  of the  $\alpha$ -th *irreducible* small corep of each little group  $G_{\mathbf{k}}$  by systematically applying the so-called *magic formula*:

$$m_\alpha = \frac{1}{\|G_{\mathbf{k}}\|} \sum_{g \in G_{\mathbf{k}}} \chi_\alpha^*(g) \chi(g), \quad (\text{S1})$$

where  $\chi_\alpha(g)$  is the character of  $g$  in the  $\alpha$ -th irreducible small corep of  $G_{\mathbf{k}}$ , and where  $\|G_{\mathbf{k}}\|$  is the order of the little group (*i.e.*, the number of symmetry operations in the little group not including operations related by integer lattice translations). The characters of the irreducible small coreps of the little groups of all  $\mathbf{k}$  points in all 230 nonmagnetic SGs can be accessed using the **REPRESENTATIONS DSG** tool on the **BCS** implemented for TQC [28, 43, 58, 92, 93, 97]. Next, using an upgraded implementation of the **Check Topological Mat** [113] tool on the **BCS** (see S3 for a detailed description of new features), we analyze each set of isolated bands. Specifically, we first obtain a symmetry data vector  $B$ , defined as:

$$B = (m(\rho_{G_{K_1}}^1), m(\rho_{G_{K_1}}^1), \dots, m(\rho_{G_{K_1}}^2), m(\rho_{G_{K_1}}^2) \dots)^T, \quad (\text{S2})$$

where  $m(\rho_{G_{K_i}}^j)$  is the multiplicity of the  $j$ -th small corep of the little group  $G_{K_i}$  at the maximal momentum  $K_i$ . Next, we denote the symmetry data vector of the  $i$ -th EBR as  $EBR_i$ . Then, for any isolated subset of bands characterized by a symmetry vector that satisfies the compatibility relations, we solve a linear system of equations given by:

$$B = EBR \cdot X, \quad (\text{S3})$$

in which the solution  $X = (X_1, X_2, \dots, X_N)$  indicates the coefficients of the linear combination of EBRs corresponding to  $B$ . The presence of non-integer coefficients in  $\{X_1, X_2, \dots, X_N\}$  in Eq. (S3) implies that some or all of the stable SIs are nontrivial for the bands characterized by  $B$ . For each SG, the possible existence of non-integer solutions to Eq. (S3), and hence the existence of nontrivial stable SIs, may be predicted through the Smith decomposition of the EBR matrix [32]. Specifically, because an EBR is a non-square matrix with integer coefficients,

then its Smith decomposition can be expressed as a product of three matrices with integer coefficients:

$$EBR = L \cdot D \cdot R, \quad (\text{S4})$$

where  $L$  and  $R$  are unimodular matrices and  $D$  is a diagonal matrix. The number of nonzero diagonal elements in  $D$  is the rank of the stable SI group, and the matrices  $L$  and  $R$  can be chosen such that the (diagonal) entries in  $D$  are positive integers [29, 114]. If some of diagonal entries  $\{n_1, n_2, \dots\}$  are greater than one, then the stable SI group is nontrivial, and is given by  $\mathbb{Z}_{n_1} \otimes \mathbb{Z}_{n_2} \otimes \dots$  [e.g., the nonzero elements in  $D$  in SG 2 ( $P\bar{1}$ ) are  $\{4, 2, 2, 2\}$ , corresponding to a stable SI group  $\mathbb{Z}_4 \otimes \mathbb{Z}_2^3$ ]. By then systematically applying [VASP2Trace](#) and [Check Topological Mat](#) to each isolated set of bands in the electronic structure of each material in the ICSD [41], we obtain the symmetry-indicated stable and fragile band topology of every known stoichiometric, nonmagnetic material.

## B. The Compatibility Relations

To determine the connectivity of electronic bands characterized by a given symmetry data vector [Eq. (S3)], one must use the compatibility relations between  $\mathbf{k}$  points throughout the BZ. Specifically, in a given SG, the compatibility relations are defined as the dependencies between the multiplicity of the small coreps of the little groups of a  $\mathbf{k}$  point in the BZ and the multiplicities of the small coreps of the little groups along a line or plane in which the point sits [92]. The compatibility relations exist because the little group of a line (or a plane) is necessarily a subgroup of the little group of a high-symmetry point along the line (or plane) [56].

A set of bands can be *partially* identified by its decomposition into integer-valued linear combinations of the irreducible small coreps of the little group of each  $\mathbf{k}$  point in the BZ. However, in general, it is not necessary to consider the multiplicities of the coreps in the whole BZ to analyze the connectivity of a given symmetry data vector, due to the compatibility relations between the coreps of two connected subsets of  $\mathbf{k}$ -vectors. This renders the problem of decomposing bands into the coreps of the little group of the continuous variable  $\mathbf{k}$  feasible, because the corep decomposition in the whole BZ is fully fixed by the corep decomposition at only a finite (and in practice very small) number of  $\mathbf{k}$  points known as the *maximal*  $\mathbf{k}$  vectors [28, 58, 92, 93]. For example, consider a  $\mathbf{k}$  point that belongs to a line ( $l$ )  $\mathbf{k}_l$  for which the little group  $\mathcal{G}^{\mathbf{k}}$  of  $\mathbf{k}$  is a supergroup of the little group of  $\mathbf{k}_l$ ,  $\mathcal{G}^{\mathbf{k}_l} \leq \mathcal{G}^{\mathbf{k}}$ . The matrix representatives of a small corep  $\rho_{\mathcal{G}^{\mathbf{k}}}^i$  of the little group  $\mathcal{G}^{\mathbf{k}}$  associated with the symmetry operations that belong to  $\mathcal{G}^{\mathbf{k}_l}$  transform in a small representation, not necessarily irreducible, of  $\mathcal{G}^{\mathbf{k}_l}$ . This representation, in general, is equivalent to a direct sum of the irreducible small coreps  $\rho_{\mathcal{G}^{\mathbf{k}_l}}^j$  of  $\mathcal{G}^{\mathbf{k}_l}$ :

$$\rho_{\mathcal{G}^{\mathbf{k}}}^i \downarrow \mathcal{G}^{\mathbf{k}_l} = \bigoplus_{i=1}^s m_{ij}^{\mathbf{k}, \mathbf{k}_l} \rho_{\mathcal{G}^{\mathbf{k}_l}}^j \quad (\text{S5})$$

where  $s$  is the number of irreducible small coreps of  $\mathcal{G}^{\mathbf{k}_l}$  and  $m_{ij}^{\mathbf{k}, \mathbf{k}_l}$  is the (integer) multiplicity of  $\rho_{\mathcal{G}^{\mathbf{k}_l}}^j$  in the decomposition of  $\rho_{\mathcal{G}^{\mathbf{k}}}^i$ . The same arguments can also be employed to calculate the compatibility relations between the multiplicities of the coreps in the symmetry data at a high-symmetry point and the corep multiplicities in a plane containing the high-symmetry point, or between the corep multiplicities along a line and the corep multiplicities in a plane containing the line. For TQC, we previously implemented the program [DCOMPREL](#) [28, 43, 58, 92, 93, 97] for obtaining the compatibility relations between each pair of connected  $\mathbf{k}$ -vectors in the BZ of each nonmagnetic double (spinful) SG.

The compatibility relations provide a means of analyzing a given symmetry data vector obtained from first-principles or tight-binding calculations. Specifically, as shown in Refs. [37, 38], there are three cases for the connectivity of a set of Bloch eigenstates characterized by a symmetry data vector, given a specified number of filled Bloch eigenstates (electrons):

1. We observe that a set of small coreps at a maximal point  $\mathbf{k}$  corresponds to a set of Bloch states in which a band degeneracy is partially occupied. Numerically using [Check Topological Mat](#), this occurs when the number of bands (small coreps corresponding to the occupied Bloch states) is not the same at every maximal

$\mathbf{k}$ -vector (*i.e.*, the sum of the dimensions of the coreps is different from the number of occupied bands in at least at one maximal  $\mathbf{k}$ -vector, which can occur because [Check Topological Mat](#) does not output fractional numbers of coreps). In this case, the bands below the Fermi level characterized by the symmetry data vector are necessarily connected to states above the Fermi energy, and therefore fail to satisfy the compatibility relations at a maximal  $\mathbf{k}$  point. Following the nomenclature established in Ref. [38], we label a material with a partially filled multiplet of Bloch eigenstates at a maximal  $\mathbf{k}$  point as an “enforced semimetal with Fermi degeneracy” (ESFD). A well-known example of an ESFD-classified material is HgTe in SG 216 ( $F\bar{4}3m$ ) [4] ([ICSD 31845](#), see [S11 C 1](#)).

2. The symmetry data vector corresponds to fully occupied Bloch-state multiplets at all maximal  $\mathbf{k}$  points, but the small corep multiplicities in the symmetry data vector do not satisfy the compatibility relations along a line or a plane connecting at least one pair of maximal  $\mathbf{k}$  points. Specifically, using [Check Topological Mat](#), this numerically occurs when the number of bands (small coreps corresponding to the occupied Bloch states) at a maximal vector  $\mathbf{k}$  is *different than* the corep multiplicities at  $\mathbf{k}$  implied through the compatibility relations by the Bloch states that transform in the symmetry data at a different maximal vector  $\mathbf{k}'$ . This implies that the bands described by the symmetry data vector necessarily connect along a high-symmetry line or plane to bands above the Fermi energy not included in the symmetry data. In this case, because the symmetry data necessarily characterizes a topological semimetal, then we label the partially occupied connected set of electronic bands characterized by the symmetry data as an “enforced semimetal” (ES). A well-studied example of an ES material is the archetypal Dirac semimetal  $Cd_3As_2$  in SG 137 ( $P4_2/nmc$ ) [6, 19, 115, 116] ([ICSD 107918](#), see [S11 C 2](#)), which was recently confirmed in theory [59] and experiment [60] to be a *higher-order* topological semimetal.
3. The symmetry data vector corresponds to fully occupied Bloch-state multiplets at all maximal  $\mathbf{k}$  points, and the small corep multiplicities in the symmetry data vector *satisfy* the compatibility relations along all lines and planes connecting the maximal  $\mathbf{k}$  points. Specifically, using [Check Topological Mat](#), this numerically occurs when the number of bands (small coreps corresponding to the occupied Bloch states) at all maximal  $\mathbf{k}$  vectors is *the same* as the corep multiplicities at  $\mathbf{k}$  implied through the compatibility relations by the Bloch states that transform in the symmetry data at all other maximal vectors  $\mathbf{k}'$ .

The bands described by the symmetry data are therefore compatible with an insulating gap along all high-symmetry lines and planes, and the symmetry data vector is labeled either LCEBR, NLC, or SEBR (see [S2 A](#) for further details). It is important to emphasize that LCEBR, NLC, and SEBR bands may still be connected to bands at other energies not described by the symmetry data by topological Weyl points or nodal lines in the BZ interior (*i.e.* away from all high-symmetry lines and planes) [29, 31, 36, 112]; NLC- and SEBR-classified topological semimetal phases are discussed in further detail in [S6](#) for further details). In particular, as established in Refs. [31, 36] and discussed in [S6](#), *all* NLC and SEBR bands in nonmagnetic crystals w/o SOC characterize topological semimetal phases with nodal degeneracies in the BZ interior (respectively termed NLC-SM and SEBR-SM phases in this work).

Finally, we note that in [Check Topological Mat](#), it is occasionally possible for a set of characters in the symmetry data to appear to violate time-reversal ( $\mathcal{T}$ ) symmetry. We attribute this situation to numerical error, and in all cases, we have confirmed that the characters match the small irreps of the little groups of the Type-I magnetic (unitary) SG [29, 56] that is a subgroup of the nonmagnetic SG for the symmetry data. In the calculations performed for this work on nonmagnetic materials, we have merged all Bloch states that exhibit  $\mathcal{T}$ -breaking splitting on an energy scale of less than 1 meV to ensure that the symmetry data and band structures displayed on <https://www.topologicalquantumchemistry.com/> are  $\mathcal{T}$ -symmetric.

### S3. OVERVIEW OF THE PREVIOUS FUNCTIONALITY OF THE VASP2TRACE PROGRAM AND NEW FEATURES OF THE CHECK TOPOLOGICAL MAT PROGRAM

In a recent previous work [38], the authors introduced the [VASP2Trace](#) [84] and [Check Topological Mat](#) programs on the [BCS](#) to diagnose the topology of materials whose electronic structure has been calculated using

VASP [78, 79]. The input files for **Check Topological Mat** are the output files of **VASP2Trace**, which calculates the traces (eigenvalues) of the unitary symmetries of the electronic Bloch wavefunctions obtained from VASP [78, 79]. For this work, we have for the first time used **VASP2Trace** to compute band topology away from  $E_F$ , and have introduced new features for **Check Topological Mat**. In this section, we will first provide in S3 A an overview of the previous functionality of the **VASP2Trace** and **Check Topological Mat** programs implemented for Ref. [38]. We will then in S3 B subsequently detail the new features in **Check Topological Mat** implemented for this work.

### A. Overview of the Previous Functionality of the **VASP2Trace** and **Check Topological Mat** Programs

In this section, we will briefly summarize the algorithm and output of **VASP2Trace** and the previous functionality of **Check Topological Mat**. To begin, in the SG of a crystalline solid, each unitary symmetry operation is defined as  $\mathcal{O} = \{R|t\}$ , where  $R$  is a point group symmetry operation (rotation or rotoinversion) and  $t$  is a translation vector (which may have a fractional value in the units of the lattice constants) [56]. For each maximal  $\mathbf{k}$  point (defined in Refs. [28, 58]), we first obtain the single-particle Bloch wavefunctions  $\psi_{n\mathbf{k}}(\vec{r}) \equiv \langle \vec{r} | \psi_{n\mathbf{k}} \rangle$  using the DFT package VASP [78, 79] and identify a set of orthonormal wavefunctions  $\{\psi_{n\mathbf{k}}^1(\vec{r}), \psi_{n\mathbf{k}}^2(\vec{r}), \dots, \psi_{n\mathbf{k}}^m(\vec{r})\}$  with a degeneracy  $m$  that each have the same energy eigenvalue  $E_n(\mathbf{k})$ . If the symmetry operation  $\mathcal{O}$  belongs to the little group  $G_{\mathbf{k}}$  of  $\mathbf{k}$ , then acting on any of the wavefunctions  $\psi_{n\mathbf{k}}^i(\vec{r})$  with  $\mathcal{O}$  results in a linear combination of all of the  $m$  degenerate Bloch states at  $E_n$  and  $\mathbf{k}$ :

$$\mathcal{O} |\psi_{n\mathbf{k}}^i\rangle = \sum_{j=1}^m O_{ij}^{\mathbf{k}} |\psi_{n\mathbf{k}}^j\rangle, \quad (\text{S6})$$

where  $O^{\mathbf{k}}$  is the matrix representative of symmetry operation  $\mathcal{O}$ . The  $ij$ -th element of  $O^{\mathbf{k}}$  is in turn given by:

$$O_{ij}^{\mathbf{k}} = \langle \psi_{n\mathbf{k}}^j | \mathcal{O} | \psi_{n\mathbf{k}}^i \rangle. \quad (\text{S7})$$

The matrix representatives  $O^{\mathbf{k}}$  form a (generically reducible) small corep of  $G_{\mathbf{k}}$ .

It is important to emphasize that in the output of a DFT calculation, numerical precision and symmetry-breaking effects (*e.g.* weak magnetism) may lead to several nondegenerate states appearing as degenerate, or may lead to degenerate states appearing weakly split. Hence, it is necessary to implement a numerical tolerance factor for the energies of states at the same  $\mathbf{k}$  point, such that states within the energy range of the tolerance factor are taken to be degenerate. To avoid accidental degeneracies, it is desirable to have as small a tolerance factor as possible up to the energy scale at which numerical precision issues lead to symmetry-breaking splitting. For this work, we have chosen a tolerance factor of 0.002 eV.

As discussed in S2, the multiplicities of the irreducible small coreps in the (generically reducible) representation corresponding to the degenerate states  $\{\psi_{n\mathbf{k}}^1(\vec{r}), \psi_{n\mathbf{k}}^2(\vec{r}), \dots, \psi_{n\mathbf{k}}^m(\vec{r})\}$  can be obtained by computing the symmetry characters (traces) of the matrix representatives  $O^{\mathbf{k}}$  in Eq. (S7). Hence, it is sufficient to calculate:

$$\chi_{n\mathbf{k}}^{\mathcal{O}} = \sum_{i=1}^m \langle \psi_{n\mathbf{k}}^i | \mathcal{O} | \psi_{n\mathbf{k}}^i \rangle, \quad (\text{S8})$$

for the matrix representative  $\mathcal{O}$  of each unitary symmetry operation  $g \in G_{\mathbf{k}}$ . The traces (characters)  $\chi_{n\mathbf{k}}^{\mathcal{O}}$  in Eq. (S8) may straightforwardly be obtained from the WAVECAR output file of VASP, in which the Bloch wavefunctions at each  $\mathbf{k}$  point are each expressed as a linear combination of plane waves:

$$\psi_{n\mathbf{k}}^i(\mathbf{r}) = \sum_j C_{j,n\mathbf{k}}^i e^{i(\mathbf{k} + \mathbf{G}_j) \cdot \mathbf{r}}. \quad (\text{S9})$$

In Eq. (S9), each  $\mathbf{G}_j$  is a reciprocal lattice vector, and states in different BZs related by reciprocal lattice vectors

are orthonormal such that  $\langle \mathbf{k} + \mathbf{G}_i | \mathbf{k} + \mathbf{G}_j \rangle = \delta_{ij}$ . Although the reciprocal lattice contains an infinite number of BZs related by the vectors  $\mathbf{G}_j$ , in practice, VASP only considers the truncated finite set of  $\mathbf{k}$  points for which  $\frac{\hbar^2}{2m_e}(\mathbf{k} + \mathbf{G}_j)^2 < E_{\text{cutoff}}$ , where the energy cutoff  $E_{\text{cutoff}}$  is an input parameter.

Given  $\psi_{n\mathbf{k}}^i(\mathbf{r})$  in the plane-wave basis in Eq. (S9), the action of the symmetry operation  $O$  is given by:

$$\begin{aligned}\mathcal{O}\psi_{n\mathbf{k}}^i(\mathbf{r}) &= \{R|\mathbf{t}\}\psi_{n\mathbf{k}}^i(\mathbf{r}) = \psi_{n\mathbf{k}}^i(\{R|\mathbf{t}\}^{-1}\mathbf{r}) = \sum_j C_{j,n\mathbf{k}}^i e^{i(\mathbf{k}+\mathbf{G}_j)\cdot R^{-1}(\mathbf{r}-\mathbf{t})} = \\ &= \sum_j C_{j,n\mathbf{k}}^i e^{iR(\mathbf{k}+\mathbf{G}_j)\cdot(\mathbf{r}-\mathbf{t})} = e^{-i\mathbf{k}\cdot\mathbf{t}} \sum_j C_{j,n\mathbf{k}}^i e^{i(\mathbf{k}+\mathbf{G}_{j'})\cdot\mathbf{r}} e^{-i\mathbf{G}_{j'}\cdot\mathbf{t}},\end{aligned}\quad (\text{S10})$$

where  $\mathbf{G}_{j'}$  is the reciprocal lattice vector for which:

$$\mathbf{k} + \mathbf{G}_{j'} = R\mathbf{k} + \mathbf{G}_j. \quad (\text{S11})$$

Hence, the  $i$ -th element of the diagonal of the matrix representative  $O^k$  is given by:

$$\langle \psi_{n\mathbf{k}}^i | \mathcal{O} | \psi_{n\mathbf{k}}^i \rangle = e^{-i\mathbf{k}\cdot\mathbf{t}} \sum_j (C_{j',n\mathbf{k}}^i)^* C_{j,n\mathbf{k}}^i e^{-i\mathbf{G}_{j'}\cdot\mathbf{t}}, \quad (\text{S12})$$

where in each term in the sum over  $j$ , the index  $j'$  is individually determined through Eq. (S11). The trace of the matrix representative  $O^k$  defined in Eq. (S8) is thus given by:

$$\chi_{n,\mathbf{k}}^O = e^{-i\mathbf{k}\cdot\mathbf{t}} \sum_{i=i}^m \sum_j (C_{j',n\mathbf{k}}^i)^* C_{j,n\mathbf{k}}^i e^{-i\mathbf{G}_{j'}\cdot\mathbf{t}}, \quad (\text{S13})$$

such that the trace of the identity operation  $\mathcal{O} = \{E|0\}$  is equal to the band degeneracy  $m$  at  $E_n(\mathbf{k})$ .

In summary, **VASP2Trace** obtains the plane-wave coefficients  $C_{j,n\mathbf{k}}^i$  from the WAVECAR output file generated by VASP for the  $m$  degenerate states at an energy  $E_n$  and a point  $\mathbf{k}$ . **VASP2Trace** then produces the following output data:

1. The symmetry operations of the SG (one symmetry operation for each element of the point group of the SG), given in a primitive basis that in general does not correspond to the standard setting of the SG listed in the International Tables for Crystallography [117] or the **BCS**.
2. The coordinates of the maximal  $\mathbf{k}$  vectors of the SG expressed in a reciprocal basis consistent with the (generically non-standard) setting of the outputted symmetry operations.
3. For each maximal  $\mathbf{k}$  vector and band  $n$ , **VASP2Trace** outputs the traces of the symmetry operations of the little group  $G_{\mathbf{k}}$  (one trace for each element of the point group of  $G_{\mathbf{k}}$ ).

In Ref. [38], together with the **VASP2Trace** program written by Zhijun Wang [84], the authors also introduced the **Check Topological Mat** program to diagnose the topology of a material using the output of **VASP2Trace**. To diagnose the bulk topology, **Check Topological Mat** first compares the symmetry operation traces computed *ab initio* to the little group character tables on the **BCS**, allowing the determination of the little group small coreps in the symmetry data at a set of (typically, but not necessarily) maximal  $\mathbf{k}$  points.

To identify the multiplicities of the irreducible small coreps in the symmetry data at each maximal  $\mathbf{k}$  point, the previous implementation of **Check Topological Mat** first converts the data given by **VASP2Trace** into the standard setting of the SG used by the programs on the **BCS**. The conversion between the SG setting in the output of **VASP2Trace** and the standard setting of the **BCS** is performed using the **IDENTIFY GROUP** program on the **BCS** [118] to calculate a transformation matrix between the output of **VASP2Trace** and the standard setting. The transformation matrix additionally allows the identification of the maximal  $\mathbf{k}$  vector labels used by VASP given the output of **VASP2Trace**. Next, given the characters of the SG symmetry elements in the standard setting

[Eq. (S13) after using the **IDENTIFY GROUP** program] and the  $\mathbf{k}$  vector labels, the small corep multiplicities are obtained through the Schur orthogonality relation (magic formula), as detailed in the text surrounding Eq. (S1) in S2. Lastly, the irreducible small corep multiplicities corresponding to the symmetry data are then analyzed using the machinery of TQC to obtain the topological classification of the occupied bands, as detailed in Ref. [38] and S2.

However, it is important to emphasize that due to numerical precision issues with bands far above  $E_F$ , or symmetry-breaking effects such as magnetism, the Bloch wavefunctions at  $\mathbf{k}$  in Eq. (S9) may exhibit unitary symmetry eigenvalues (characters) that are not possible given the symmetry elements in the little group  $G_{\mathbf{k}}$ . Specifically, for  $m$  degenerate Bloch states at a point  $\mathbf{k}$  and an energy  $E_n$  in the output of a VASP calculation, Eq. (S13) may return impossible combinations of characters for the set of symmetry-operation matrix representatives  $\{O^{\mathbf{k}}\}$  if symmetries have become broken, or if the DFT calculations did not converge at  $E_n$  and  $\mathbf{k}$ . We refer to this situation, in which a group of degenerate states exhibits a set of characters that are together incompatible with the little group  $G_{\mathbf{k}}$ , as a *bad trace*. At each of the maximal  $\mathbf{k}$  vectors, **Check Topological Mat** searches in increasing integer electronic fillings for a filling  $\nu$  at which there is a bad trace at  $\mathbf{k}$ . If **Check Topological Mat** at any  $\mathbf{k}$  vector encounters a bad trace with  $\nu \leq N_e$ , where  $N_e$  is the number of valence electrons, then the topological classification at  $E_F$  cannot be determined. In this work, we have discarded the 655 ICSD entries for which VASP calculations converged to a (meta)stable state with bad traces at or below  $E_F$ .

## B. New Features of the **Check Topological Mat** Program Introduced in this Work

In addition to the previous functionality of the **VASP2Trace** and **Check Topological Mat** programs, we have introduced several new features in this work:

1. The most recent version of **VASP2Trace** [84] now allows users to input a number of bands that differs from the number of electrons (*i.e.* a number of bands that differs from the intrinsic electronic filling). In this work, we have used this new feature to perform the first high-throughput analysis of band topology *away from*  $E_F$  in nonmagnetic materials, specifically varying the number of electrons used in the input for **VASP2Trace** to analyze the topology all of the energetically isolated bands in the electronic structure of each ICSD entry.
2. **Check Topological Mat** can now identify small corep multiplicities both with and w/o SOC – the previous iteration of **Check Topological Mat** implemented for Ref. [38] could only identify small corep multiplicities in the presence of SOC.
3. **Check Topological Mat** now generates a file containing topological data for all energetically isolated sets of bands. For each set of energetically isolated bands (*i.e.* bands that are separated from all other bands at all high-symmetry  $\mathbf{k}$  points and along all high-symmetry BZ lines and planes), **Check Topological Mat** now indicates if the set of bands is trivial, fragile topological, or stable topological (further differentiating between SEBR or NLC). In the case in which the bands are stable topological, **Check Topological Mat** additionally provides the values of the stable SIs using the convention established in Refs. [16, 36]. As an example, we have reproduced in Table S1 the output of **Check Topological Mat** for the repeat-topological (RTopo) and supertopological (STopo) compound  $\text{Bi}_2\text{Mg}_3$  [ICSD 659569, SG 164 ( $P\bar{3}m1$ )] discussed in the main text (see S9 for precise definitions of RTopo and STopo compounds).
4. When **Check Topological Mat** diagnoses a partially filled set of bands in a material to be an ES or ESFD semimetal, **Check Topological Mat** now provides the compatibility relations along the high-symmetry BZ lines and planes, thus identifying the location(s) of the protected crossing point(s).

For the present work, we have also made the updated version of **Check Topological Mat** detailed in this section publicly available on the **BCS** at [www.cryst.ehu.es/cryst/checktopologicalmat](http://www.cryst.ehu.es/cryst/checktopologicalmat).

A	$\Gamma$	H	K	L	M	dim	top. type	ind/band	filling $\nu$	top. type/all	type/all	ind/all
-A8(2)	-GM8(2)	-H4-H5(2)	-K4-K5(2)	-L3-L4(2)	-M5-M6(2)	2	SEBR	0 0 0 3	2	SEBR	0 0 0 3	
-A9(2)	-GM9(2)	-H6(2)	-K6(2)	-L5-L6(2)	-M3-M4(2)	2	SEBR	0 0 0 1	4	LCEBR	0 0 0 0	
-A9(2)	-GM8(2)	-H4-H5(2)	-K6(2)	-L3-L4(2)	-M3-M4(2)	4	SEBR	0 0 0 3	8	SEBR	0 0 0 3	
-A8(2)	-GM8(2)	-H6(2)	-K4-K5(2)	-L5-L6(2)	-M5-M6(2)							
-A9(2)	-GM9(2)	-H6(2)	-K6(2)	-L3-L4(2)	-M5-M6(2)	2	SEBR	0 0 1 1	10	SEBR	0 0 1 0	
-A8(2)	-GM4-GM5(2)	-H6(2)	-K6(2)	-L5-L6(2)	-M3-M4(2)	4	SEBR	0 0 0 3	14	SEBR	0 0 1 3	
-A6-A7(2)	-GM8(2)	-H4-H5(2)	-K4-K5(2)	-L3-L4(2)	-M5-M6(2)							
-A4-A5(2)	-GM6-GM7(2)	-H6(2)	-K6(2)	-L5-L6(2)	-M3-M4(2)	2	SEBR	0 0 1 0	16	SEBR	0 0 0 3	
-A8(2)	-GM9(2)	-H4-H5(2)	-K6(2)	-L3-L4(2)	-M3-M4(2)	6	SEBR	0 0 0 2	22	SEBR	0 0 0 1	
-A9(2)	-GM9(2)	-H6(2)	-K6(2)	-L5-L6(2)	-M5-M6(2)							
-A6-A7(2)	-GM6-GM7(2)	-H6(2)	-K4-K5(2)	-L5-L6(2)	-M3-M4(2)							
-A9(2)	-GM9(2)	-H6(2)	-K6(2)	-L3-L4(2)	-M5-M6(2)	2	SEBR	0 0 1 1	24	SEBR	0 0 1 2	
-A8(2)	-GM8(2)	-H6(2)	-K4-K5(2)	-L3-L4(2)	-M3-M4(2)	8	SEBR	0 0 1 1	32	SEBR	0 0 0 3	
-A4-A5(2)	-GM8(2)	-H4-H5(2)	-K6(2)	-L5-L6(2)	-M5-M6(2)							
-A8(2)	-GM4-GM5(2)	-H6(2)	-K4-K5(2)	-L5-L6(2)	-M5-M6(2)							
-A9(2)	-GM8(2)	-H4-H5(2)	-K6(2)	-L3-L4(2)	-M3-M4(2)							

Table S1. A typical table generated by [Check Topological Mat](#). Here, we have used as an example the repeat-topological (RTopo) and supertopological (STopo) compound  $\text{Bi}_2\text{Mg}_3$  [ICSD [659569](#), SG 164 ( $P\bar{3}m1$ )] discussed in the main text (see [S9](#) for precise definitions of RTopo and STopo compounds). In this table, the horizontal lines indicate the electronic fillings  $\nu$  at which the occupied bands satisfy the compatibility relations. Columns  $A$ ,  $\Gamma$ ,  $H$ ,  $K$ ,  $L$ , and  $M$  contain the coreps at each maximal  $\mathbf{k}$  point for each energetically isolated set of bands that satisfy the compatibility relations. Column “dim” shows the dimension of each set of bands, Column “top. type” indicates the topology of the isolated bands [which can either be LCEBR, FRAGILE, NLC, or SEBR], and Column “ind/band” contains the stable symmetry-based indicators (SIs) ( $Z_{2,1} Z_{2,2} Z_{2,3} Z_4$ ) that result from subducing onto SG 2 ( $P\bar{1}$ ). The remaining three columns contain the cumulative information of several combined sets of energetically isolated bands that are filled up to a total number of valence electrons specified by the column “filling  $\nu$ .” Column “top. type/all” provides the cumulative topology (LCEBR, FRAGILE, NLC, or SEBR) at the gap specified by the electronic filling in the “filling  $\nu$ ” column, and Column “ind/all” provides the cumulative stable SIs of all of the filled bands up to the same gap. Hence, the values of “ind/all” at each filling  $\nu$  listed in this table can be obtained by summing the values in the “ind/band” column up to the same filling  $\nu$ . In  $\text{Bi}_2\text{Mg}_3$ , the Fermi level lies at a valence filling  $\nu = 16$ , indicating that the gap at  $E_F$  exhibits symmetry-indicated stable (SEBR) topology characterized by the subduced stable SIs (0003).

#### S4. VASP CALCULATION DETAILS AND DATA SET PREPARATION

In this work, we performed ab-initio calculations using Density Functional Theory (DFT) [[119](#), [120](#)] as implemented in the Vienna Ab-initio Simulation Package (VASP) [[78](#), [80](#)]. For each material calculation, we used as input the structural parameters reported on the ICSD [[41](#)]. We treated the interaction between the ion cores and the valence electrons using the projector augmented-wave method [[81](#)]. For the exchange-correlation potential, we used the generalized gradient approximation (GGA) with the Perdew-Burke-Ernzerhof parameterization for solids [[82](#)]. For calculations incorporating the effects of spin-orbit coupling (SOC), we accounted for the effects of SOC using the second variation method [[83](#)]. For the plane-wave expansion, we employed a  $\Gamma$ -centered  $\mathbf{k}$ -point grid of size  $(11 \times 11 \times 11)$  for reciprocal space integration and a 550 eV energy cutoff. Because small changes in the structural parameters of a material with a similarly small gap size can drive a topological phase transition, then for this work, we have analyzed *all* of the entries in the ICSD, including duplicate entries for the same compound that feature only minor variation in the reported parameters. For example in PbTe, there are 42 total entries in the ICSD, of which only 5 have a negative (inverted) gap corresponding to a higher-order topological crystalline insulating (TCI) phase (see Ref. [[121](#)] and [S11 A 5](#)). Therefore, rather than simply report PbTe as a TCI, we provide on <https://www.topologicalquantumchemistry.com/> a complete analysis of all 42 ICSD entries for PbTe, allowing users to choose between entries with and without nontrivial symmetry-indicated topology.

For each material, we prepared input files for VASP using the CIF structure files provided on the ICSD. Specifically, we first used the Atomic Simulation Environment (ASE) [[122](#)] to transform the CIF file from the ICSD

into a VASP POSCAR structure input file. This step must be performed with caution, because some CIF files on the ICSD are missing atoms that are listed in the chemical formula (typically, but not always, hydrogen atoms), and some unit-cell coordinates are reported in a non-standard basis. To account for the latter issue of differing unit-cell bases, we have employed the PHONOPY [123] package to convert the coordinates of the atoms in the CIF files into positions in a primitive cell chosen in a consistent (standard) basis for each SG. In Table S2, we provide statistics regarding the number of ICSD entries considered in our analysis. In this work, we began by considering the complete list of 193,426 entries in the ICSD. Of the 193,426 ICSD entries, 181,218 contain experimentally-obtained atomic positions, and the remaining 12,208 entries contain theoretically-obtained atomic positions. Separately, of the 193,426 ICSD entries, 96,196 (49.73%) have stoichiometric chemical formulas and processable (non-corrupt) CIF structure files, whereas the remaining 97,230 (50.27%) entries are either not stoichiometric or exhibit corrupted CIF structure files. In general, non-stoichiometric materials cannot be analyzed using TQC without constructing exceedingly large unit cells representing the average structure, and corrupted CIF files can only be processed if repaired using a case-by-case methodology.

Next, having established the primitive cell, we construct the pseudopotential file for each compound and execute VASP. This process is performed in an automated, high-throughput fashion through a script that uses each ICSD CIF file as an input, and then outputs the topological analysis, electronic band structure, and density of states. As shown in Fig. 1 of the main text, our topological analysis is performed by computing the characters of the unitary symmetry operations of the little groups at the maximal  $\mathbf{k}$  vectors (see S3). For each SG, the list of maximal  $\mathbf{k}$  vectors may be obtained by choosing an EBR of the SG using the **BANDREP** tool on the **BCS** ([www.cryst.ehu.es/cryst/bandrep](http://www.cryst.ehu.es/cryst/bandrep)). The first column in the output of **BANDREP** contains the maximal  $\mathbf{k}$  vectors of the SG.

Beyond the Bloch states at the maximal  $\mathbf{k}$  vectors, we also compute for each material the electronic structure (bands) along an SG-dependent  $\mathbf{k}$  path to generate band structure plots, and the density of states. For each band structure calculation, we specifically calculate the energies of the Bloch eigenstates at 20  $\mathbf{k}$  points along each  $\mathbf{k}$  path segment. At each  $\mathbf{k}$  point along each path segment, we calculate the energies of at least  $2N_e$  Bloch states, where  $N_e$  is the number of valence electrons in the primitive cell; we do not include bands originating from core-shell atomic orbitals. We note that because VASP can be parallelized over bands, the number of bands included in some material calculations is larger than  $2N_e$ . For completeness and consistency with other previous works [39, 124], we have included in our electronic structure calculations both the minimal paths connecting all  $\mathbf{k}$  vectors, as well as additional paths that are not required by band connectivity [28, 92], but are nevertheless commonly employed in earlier works. For each of the 14 Bravais classes and crystallographic point groups, we have constructed  $\mathbf{k}$  paths in reduced coordinates (independent of the lattice parameters) using a combination of symmetry considerations and band-structure compatibility relations [114]. We emphasize that this approach differs from other programs, such as the *Seek-path* package [125], which use different criteria to generate  $\mathbf{k}$  paths in non-reduced units of the lattice vectors, causing the  $\mathbf{k}$  paths to become structure-dependent and vary for materials within the same SG. For example, the high-throughput first-principles calculations performed in Ref. [39] were performed without rescaled  $\mathbf{k}$  vectors. Hence, in the **Catalogue of Topological Materials** introduced in Ref. [39], there exist materials with the same SG and different displayed  $\mathbf{k}$  paths, whereas the electronic structures of all of the ICSD entries on <https://www.topologicalquantumchemistry.com/> with the same SG are plotted along the same (reduced-coordinate)  $\mathbf{k}$  paths. We additionally emphasize that in order to locate all of the band crossings in topological semimetal phases, we found that it was necessary to search for crossing points not just along the minimal set of high-symmetry lines between pairs of maximal  $\mathbf{k}$  vectors, but also along lines connecting the first and second BZs. In some SGs, we also include additional  $\mathbf{k}$  paths beyond the first BZ in order to avoid plotting discontinuous band structures. For each ICSD entry on <https://www.topologicalquantumchemistry.com/>, we have made the  $\mathbf{k}$  paths and POSCAR files available for users to download directly from the page for each ICSD entry on <https://www.topologicalquantumchemistry.com/>.

As stated in the main text, we define a unique material as the set of ICSD entries that share the same stoichiometric formula, topological subclassification with SOC, SG, and, in the case of a topological semimetal, type of crossing at the Fermi level in the presence of SOC. We emphasize that our definition of a unique material does not account for the topological subclassification of a material w/o SOC, or account for variation in the topology of energetically isolated bands away from  $E_F$ . Specifically, for simplicity, two ICSD entries with the same stoichiometric formula, SG, and topological classification (and crossing points if semimetallic) at  $E_F$  in

the presence of SOC are grouped together as a single unique material, whether or not the topology of the two ICSD entries is different at  $E_F$  w/o SOC, or away from  $E_F$  with or w/o SOC. Hence as discussed in S9, there may exist variation in the topology away from  $E_F$  across ICSD entries associated to the same unique material. Additionally, we note that for a fraction of the analyzed ICSD entries, calculations only converged with SOC, and for the same material did not converge w/o SOC. Specifically, calculations performed w/o SOC failed to converge for 3,504 ICSD entries, representing 4.78% of the 73,234 total materials for which calculations converged with SOC. We have further classified our data by tagging materials that are either listed as magnetic on the Materials Project (<https://materialsproject.org/>) [126], or display nonzero magnetic moments in the output of our VASP calculations. Finally, we have also identified the compounds that contain valence  $f$  electrons as determined by VASP (*i.e.* the compounds containing atoms with partially filled  $f$  orbitals, see <https://www.smcm.iqfr.csic.es/docs/vasp/node248.html> for further details); these materials may exhibit non-negligible electron-electron correlation effects. Throughout this work, we follow the VASP pseudopotential documentation on <https://www.smcm.iqfr.csic.es/docs/vasp/node248.html> in determining whether a material does not carry valence  $f$  electrons, which we denote in this work using the shorthand expression “without  $f$  electrons.” In Table S3, we list the percentage of unique materials in which any of the associated ICSD entries are magnetic (either as listed on the Materials Project or in our first-principles calculations), and the percentage of unique materials with  $f$  electrons at  $E_F$  as determined by VASP.

Table S2. Number of analyzed compounds.

	Total	Experimentally-Obtained Atomic Positions	Theoretically-Obtained Atomic Positions
Entries	193,426	181,218	12,208
Stoichiometric and Valid CIF File	96,196	85,701	10,495
Non-Stoichiometric or Corrupted CIF File	97,230	95,517	1,713

Table S3. Percentage of unique materials with at least one magnetic ICSD entry and with valence  $f$  electrons as determined by VASP (see <https://www.smcm.iqfr.csic.es/docs/vasp/node248.html> for further details).

Unique Materials with Magnetism	35.82%
Unique Materials with Valence $f$ Electrons	28.69%

Lastly, it is important to emphasize additional issues that arise regarding magnetic ground states in VASP. In this work, all of the calculations were performed with a zero initial magnetic moment on each atom. However for a given compound, there may exist a magnetic ground state that is lower in energy than a metastable non-(para-)magnetic state. Hence in this case, the nonmagnetic solution is a local minimum in the total energy landscape of the system, but may still correspond to the final state in the VASP calculation. Depending on the details of the calculation, then VASP will either remain close to the initialized paramagnetic state, or may find a magnetic state that is lower in energy, but not necessarily the correct magnetic ground state (*i.e.*, there may exist a different magnetic state, or a structurally distorted nonmagnetic state, that is lower in energy). In VASP, the magnetism of a (meta)stable final state is most dependent on the following parameters:

- The total number of bands (NBANDS) in the calculation. Because VASP is parallelized, then the number of bands must be divisible by the number of cores (NPAR) for an accurate and convergent calculation. Hence, VASP adjusts NBANDS to be a multiple of the number of cores. Because NPAR depends on the details of the VASP configuration and hardware used to perform the calculation, then NPAR may vary for the same VASP calculation performed across two different (super)computers.
- The block size in the blocked Davidson algorithm (NSIM).

In most VASP calculations, NBANDs only affects the rate of convergence, and not the quantitative features (*e.g.* magnetic configuration) of the final state. However, in the presence of multiple nearby local minima in the total energy landscape, NBANDs, NPAR, and NSIM may (uncontrollably) bias the final local minimum of the VASP calculation. In general, when using VASP to perform topological material calculations and to reproduce the calculations performed for this work, we recommend performing several tests with varying NBANDS, NPAR, NSIM, and other parameters, in particular confirming that all calculations converge to the same (ideally global) minimum.

In the high-throughput calculations performed for this work, we found it to be prohibitively difficult to systematically evaluate each ICSD entry for the appearance of metastable (potentially magnetic) final states. However, by manually comparing intermediate self-consistent and band-structure output files in our VASP calculations, we were able to detect only  $\sim 100$  compounds with magnetic and nonmagnetic local minima that were close in energy. Specifically, we compared the magnetization in the self-consistent and band structure output files of each VASP calculation, finding only  $\sim 100$  ICSD entries with large magnetization discrepancies (though we detected slight variations when our tests were performed on different supercomputers, due to varying NPAR, as discussed earlier in this section). This makes us confident that the large majority of our material calculations exhibit reliable (*i.e.* physically realistic) nonmagnetic final states.

## S5. COMPUTATION TIME AND RESOURCES

In this section, we detail the computational resources used in this work. First, in S5A, we list the supercomputers used to perform the ab-initio calculations in this work, and the number CPU hours expended. Then, in S5B, we provide a more detailed breakdown of our computational resource usage, focusing specifically on the number of CPU hours expended per SG and per number of atoms in the primitive cell. Lastly, in S5C, we detail the disk storage usage requested for the calculations performed in this work, focusing specifically on the disk storage requested per SG and per number of atoms in the primitive cell.

### A. Supercomputers and General Computational Resource Usage Statistics

Our calculations were primarily executed on the Draco and Cobra supercomputers of the Max Planck Society (MPG) and on the Cori and Edison supercomputers of the United States Department of Energy (DOE). Below, we provide information about the node architecture, communication network, and peak performance of each supercomputer:

- Draco: HPC system with Intel 'Haswell' Xeon E5-2698 processors (880 nodes with 32 cores @ 2.3 GHz each). 106 of the nodes are equipped with accelerator cards (each with two PNY GTX980 GPUs). Draco also contains 64 Intel 'Broadwell' processors that each have 40 cores and a main memory of 256 GB. In total Draco has 30,688 cores and a total main memory of 128 TB, and provides a peak performance of 1.12 petaflop/s. Beyond the compute nodes used for calculations, Draco has 4 login nodes and 8 I/O nodes, each with 1.5 petabytes of disk storage.
- Cobra: HPC system with 3424 compute nodes, 136,960 CPU cores, 128 Tesla V100-32 GPUs, 240 Quadro RTX 5000 GPUs, 529 TB RAM DDR4, 7.9 TB HBM2, 11.4 petaflop/s peak DP, and 2.64 petaflop/s peak SP.
- Cori: Cray XC40 system with 622,336 Intel processor cores and a theoretical peak performance of 30 petaflop/s (30 quadrillion operations per second).
- Edison: Cray XC30 with 133,824 compute cores for running scientific applications, 357 TB of memory, and 7.56 petabytes of online disk storage with a peak I/O bandwidth of 168 GB/s.

We performed first-principles calculations on a total of 73,234 ICSD entries. As shown in Fig. 1 of the main text and discussed in S4, the calculations that we performed can be divided into four steps, which we respectively label as VASP1, VASP2, VASP3, and VASP4:

- VASP1: Self-consistent DFT calculations. The calculations performed in VASP1 generate charge density (CHGCAR) files, which served as input for the remaining three calculation steps.
- VASP2: Generating the Bloch wavefunctions at the maximal  $\mathbf{k}$  vectors, using the input from VASP1. VASP2 generates the output files used to calculate the characters of the unitary symmetry operations of the little groups at the maximal  $\mathbf{k}$  points, which we then used to diagnose the material topology, as detailed in [S3](#).
- VASP3: Calculating the band structure along high-symmetry lines and planes, using the input from VASP1. Each segment of the  $\mathbf{k}$  path contains 20  $\mathbf{k}$  points. At each  $\mathbf{k}$  point along each path segment, we calculated the energies of at least  $2N_e$  Bloch states, where  $N_e$  is the number of valence electrons in the primitive cell; we did not include bands originating from core-shell atomic orbitals. As discussed in [S4](#), because VASP is parallelized, then the number of bands must be divisible by the number of cores (NPAR) for an accurate and convergent calculation. Hence, VASP adjusts the number of bands to be a multiple of the number of cores. Because NPAR depends on the details of the VASP configuration and hardware used to perform the calculation, then NPAR may vary for the same VASP calculation performed across two different (super)computers.
- VASP4: Self-consistent calculations of the density of states, using the input from VASP1. To calculate the density of states in VASP4, we employed an  $(11 \times 11 \times 11)$   $\mathbf{k}$ -point grid.

In Table [S4](#), we show the number of CPU hours expended in the calculations performed in this work divided into each of the four calculation steps.

Job	CPU h. with SOC	CPU h. w/o SOC
VASP1	9,500,801.70	2,298,583.30
VASP2	170,633.80	56,520.70
VASP3	2,560,882.60	56,520.70
VASP4	5,804,948.80	1,397,550.30
Total Time	18,037,266.90	4,525,673.80

Table S4. Total CPU hours expended in each of the four VASP calculation steps, subdivided by calculations performed with and without incorporating the effects of SOC (with SOC and w/o SOC, respectively).

## B. Computational Resources Expended per SG and per Number of Atoms in the Primitive Cell

In this section, we provide tables containing a detailed statistical breakdown of the computational resources expended for this work. First, in Table [S5](#) (Table [S6](#)), we list the CPU hours expended to perform ab-initio calculations with SOC (w/o SOC), subdivided by SG. Next, in Table [S7](#) (Table [S8](#)), we list the CPU hours expended to perform ab-initio calculations with SOC (w/o SOC), subdivided by the number of atoms in the primitive cell of each material. Most interestingly, we observe that there are vanishingly few stoichiometric materials in the ICSD with greater than 60 atoms in the primitive cell. Specifically, we find that there are 10,835 ICSD entries with greater than 60 in the primitive cell, representing 11.26% of the 96,196 total stoichiometric entries in the ICSD.

Table S5: Total CPU time expended for all of the ab-initio calculations performed in this work incorporating the effects of SOC (with SOC), subdivided by space group (SG). In order, the columns in this table list the SG, the number of ICSDs successfully analyzed in the SG, the CPU hours expended per each of the four calculation steps (VASP1 through VASP4) detailed in [S5 A](#), and the total CPU hours expended for materials in the SG.

SG	# ICSDs	VASP1 (CPU hours)	VASP2 (CPU hours)	VASP3 (CPU hours)	VASP4 (CPU hours)	Total (CPU hours)
1	225	67534.5	718.9	4560.6	38488.5	111302.5
2	1885	572989.9	7439.1	81830.9	322951.5	985211.3
3	19	6489.8	26.9	400.9	2675.3	9592.9
4	305	97974.7	576	9153.7	61414.5	169118.9
5	195	73484.8	305.5	4328.2	56460.5	134579
6	39	7746	32.5	429.6	3391.4	11599.5
7	143	52621.6	267.8	4131.8	29000.3	86021.5
8	173	58561.7	188.4	2737.3	36156.2	97643.7
9	278	194291.8	662.5	9442.9	123863.5	328260.7
10	44	7407.7	59.6	938.5	3597	12002.9
11	790	172295.1	1916.7	30243.2	126423.2	330878.2
12	1844	473531.1	3539	46170.5	360788.5	884029.2
13	314	76186.3	801.5	12216.9	39632.1	128836.8
14	3787	1799616	16665.5	259458.6	1067200.4	3142940.5
15	2526	1372458.9	8181.1	124624.6	830990.6	2336255.2
16	2	73	24.3	49.2	70.7	217.1
17	8	909.6	27.1	510.5	618.8	2066
18	42	10938.8	300.9	5175.5	7024	23439.2
19	364	84374.7	2351.3	41287.4	55194.6	183208
20	85	15247.2	134.8	2707	8951.7	27040.7
21	21	1548.9	13.9	244.3	863.6	2670.6
22	17	1404.3	9.9	181.6	775.1	2370.9
23	16	2789.7	17.4	259.2	1087.5	4153.9
24	3	168.2	2.4	28.7	101.3	300.6
25	59	2666.1	58	957.1	1603.2	5284.4
26	85	21846.5	391.8	6848.2	11396.8	40483.4
27	1	89.2	2.2	40.4	67.5	199.3
28	18	1498.6	37.6	635.1	1114.7	3286
29	89	19338.2	522.8	9292.9	14563.9	43717.7
30	6	2866.8	58.1	925.4	1629.4	5479.7
31	247	37185.5	889.3	15277.5	23724.4	77076.7
32	12	3779.4	108.2	1962.8	2783.8	8634.2
33	406	102540.7	2171.8	38634.4	60282.2	203629.2
34	30	8458.9	208.5	3488.3	5763.3	17919.1
35	8	1291	11	213.4	824.7	2340.2
36	412	101801.2	649.6	12947.5	58890.4	174288.7
37	7	1654.4	15.9	338	1094.4	3102.7
38	173	15730.8	118	2542.3	11316.3	29707.4
39	15	3302.6	68.5	887.3	2430	6688.3
40	67	11630.1	122.5	3051.6	10744.8	25549
41	44	14186.7	102	2590	7891	24769.7
42	4	500.1	7.2	96.2	374.8	978.3
43	126	27111.4	224.5	4999.9	21284	53619.8
44	100	10278.7	85.1	1294.8	7763.2	19421.7
45	11	7084.3	52.7	1032.5	3797.5	11967
46	91	23841.1	177.4	3333.6	14095.6	41447.6
47	95	4588.5	161	3059.2	2737.8	10546.5
48	3	153.7	7.4	121.3	110.8	393.2

49	1	98.5	4	65.5	59.1	227.2
50	11	2279.1	79.4	1386.9	1409.5	5154.9
51	147	10885.8	449.7	8318.7	7566.8	27220.9
52	51	9752	378.4	6759.2	6091.3	22981
53	27	1699.2	77.7	1410.5	1275.7	4463.1
54	25	5666.9	261.5	4925.9	4427.9	15282.2
55	548	118860.4	3849.4	67835.6	61494.5	252039.9
56	31	5994.3	212.2	3642.1	3354.3	13202.9
57	208	49081.8	1486.3	27007.4	25043.3	102618.7
58	493	37096.3	1289.4	22742.3	20676.6	81804.6
59	338	37551.5	1166.3	20022.8	18167.1	76907.7
60	252	36258.7	1677.5	31542.6	28260.9	97739.8
61	233	54377.6	2172.4	36147.1	32512.4	125209.5
62	5664	905383.9	28981.3	523829.7	469273.2	1927468.1
63	2188	279088.8	2394.2	43507.4	169019	494009.4
64	435	131710.8	1377.2	26477.8	91983.7	251549.5
65	372	31828	893.7	8655.2	31429.7	72806.6
66	51	7580.5	124.5	2536.3	6356.4	16597.8
67	63	1465.3	25.8	331.3	873.2	2695.6
68	21	5123.5	70.1	1519.6	3280.9	9994
69	75	6718.6	81.2	1652.5	4493.9	12946.1
70	208	30036.8	431.6	10250.5	21787.5	62506.4
71	666	68696.9	797.7	13262.9	44634.7	127392.2
72	240	26125.3	312	5526.8	18592.2	50556.3
73	29	18882.4	222.6	4164.3	8777.1	32046.4
74	370	28410	362.5	6227.7	18657.3	53657.5
75	5	732.2	12.3	234.5	451.8	1430.8
76	12	3354.8	81.1	1256.1	2268.4	6960.4
77	2	42.3	1.4	14.9	28.8	87.4
78	2	942.2	19.3	259.8	523.5	1744.8
79	14	2200.4	19.3	285	1418.3	3923
80	3	1735.2	15	270.9	1017.7	3038.9
81	19	1657.2	48	656.3	1147.8	3509.3
82	275	23777.8	230.4	2910.7	17937	44855.9
83	11	2863.5	59.8	1052.8	1052.8	5029
84	35	2992.7	123	2087.3	2218.5	7421.5
85	54	11358	381.4	6312.3	6706.7	24758.4
86	71	8051.1	262.8	4838.5	5006.1	18158.5
87	298	20912.8	278.2	4524.8	16391.6	42107.3
88	332	30525.1	529.7	8039.4	24842.2	63936.4
90	5	2335.3	65	1021.4	994	4415.7
91	9	534.8	20.6	367.3	368.7	1291.5
92	135	12743	495.2	7427.4	7669.5	28335.1
94	1	22.3	2.3	12.6	14.1	51.4
95	3	196.6	6.2	105.9	106.8	415.6
96	37	1705	94.1	1286.5	1349.4	4435.1
97	2	215.7	3.6	58.2	175.9	453.3
98	7	685.8	10	158.4	547.3	1401.6
99	195	1644.6	74.9	729.8	960.1	3409.3
100	38	6227.6	180.1	2927.2	3610.2	12945.1
102	15	3196.3	73.5	1364.5	1754.2	6388.5
103	9	258.2	15.3	298.5	405.9	977.9
104	4	458.6	17	397.8	521.2	1394.7
105	4	393	16	228	310.3	947.3
106	1	139.3	6.9	54	70.3	270.4
107	159	4325.5	51.9	653.4	3190	8220.7

108	15	2502.9	32.7	551.2	2098.6	5185.4
109	54	2504.3	29.3	408	2427.1	5368.7
110	36	11290.9	117.1	2034.2	6727.7	20169.9
111	27	541.8	22.5	389.6	444.1	1398
112	4	102.9	7	125.2	142.5	377.5
113	167	13435.6	527.2	7351.6	8437.9	29752.3
114	42	5869.9	160.9	2567.3	2881.2	11479.3
115	24	1012.6	39.6	520.7	588.4	2161.3
116	25	1923.3	73.6	1298	1485	4779.8
117	12	2826.3	87.2	1414.2	1608	5935.8
118	12	1583.2	59.4	990.9	1129	3762.4
119	50	2606.9	40.3	595.8	2441.6	5684.5
120	25	3680.8	58.2	953	2724.3	7416.4
121	216	9964.4	182.4	2435.8	9008.1	21590.7
122	515	18306.3	359.9	4071.3	14727.5	37464.9
123	727	9138.4	527	7910.2	6013.3	23589
124	34	3013.3	187.5	3373.3	2539.7	9113.9
125	73	4167.4	193.3	4022.9	2916.9	11300.5
126	12	910.5	58.8	1009	726.2	2704.5
127	574	37869.2	1968.8	32145.3	22982.4	94965.6
128	94	17718.4	723.2	12642.4	9418.7	40502.7
129	1549	19001.8	1879.5	18025.9	13538.8	52446
130	59	8942.4	418.6	7886.6	5681.1	22928.6
131	58	651.5	274.5	676.8	536.3	2139
132	10	341.5	74.1	423	312.5	1151.1
133	5	238.3	14.1	269.8	195.2	717.4
134	9	304.6	24.9	354.4	262.4	946.3
135	91	6534.5	310.8	4810.7	3525.2	15181.1
136	790	29152.5	3660.6	25817.1	18624.4	77254.6
137	160	7048.9	632.4	6872.3	5063.7	19617.3
138	26	5684.8	210.1	3361.3	2476	11732.2
139	3533	107816.6	1729.5	24559.3	86811.5	220916.8
140	959	56603.1	982.3	16694.7	41044.6	115324.6
141	733	44661.2	895.1	14205.8	29961.4	89723.4
142	104	38012.6	655.3	11937.5	21227.4	71832.8
143	19	6765.7	103.9	1502.8	3837.2	12209.5
144	32	9948.2	190.1	2751.8	6470.5	19360.6
145	5	1075.4	20.9	308.2	760.5	2165.1
146	113	25918.6	127.2	1764.4	16159.4	43969.5
147	84	13832.8	382.6	5773.4	7442.1	27430.9
148	822	91747.5	841	12476.9	67723.6	172789
149	15	809.2	76.8	403.9	546.5	1836.4
150	91	10043.7	534.5	3985.8	5418.4	19982.4
151	5	881	29.6	494.5	691.1	2096.1
152	273	6662.8	1740.9	3458.7	4898.2	16760.6
153	2	276.7	12.4	125.3	170.4	584.8
154	140	1804.1	140.6	1111.2	1481	4537
155	70	8848.2	73.4	926.8	5156.8	15005.1
156	255	128759	3557	39738.8	63758.3	235813.1
157	29	1159.6	34.8	509	864.6	2568
158	3	688.1	14.8	306.5	395	1404.3
159	59	6786	438.6	2846	4625.1	14695.6
160	306	44692.4	444.9	6463	35660.1	87260.5
161	252	29282.3	237.9	3457.2	20565.9	53543.3
162	73	1615.2	596.8	1122.7	994.2	4329
163	88	17151.5	1898.2	10981.6	9491.5	39522.8

164	1025	20013.8	5203.1	13803.1	11970.2	50990.2
165	68	6490.7	1406.1	3987	3404.9	15288.7
166	1795	159909.7	1392.2	18670.5	88486.6	268459
167	959	63955.4	925.7	13857.5	43213.4	121952
169	1	90.5	3.5	65.1	86.5	245.7
173	196	37263	1038.7	15754.4	20274.7	74330.8
174	72	12286.9	390.6	4588.3	6398.7	23664.5
175	2	66.1	6.3	62.9	44.6	179.9
176	369	28937.9	1519.5	27429.4	20322.5	78209.3
177	3	242.9	13.7	250.1	171.2	677.9
180	95	740.6	72.6	1000.4	709.4	2522.9
181	15	241	20.9	275.1	186.8	723.9
182	51	1957.6	146.9	2619.7	1891.9	6616.2
183	3	3.7	0.3	1.6	1.6	7.1
185	97	16176.6	429.3	7369.6	7161.5	31137
186	877	45454.6	1691.8	32979.6	32104.5	112230.4
187	251	2258.5	146.1	1794.5	1664.5	5863.6
188	28	2412.5	84	1407.6	1314.6	5218.7
189	871	25895.7	1193.9	21404.6	19445.2	67939.5
190	73	7812.5	442.4	5770.9	5294.1	19319.9
191	1401	21880.5	992.8	15193.9	8156.1	46223.3
192	15	1522.4	134.8	2550.4	1385.5	5593.1
193	498	36772.9	1806.1	39473.2	21158.7	99210.9
194	3433	127489.3	5781.7	101337.4	57052.7	291661.1
195	1	90.5	3.7	62	63.7	219.9
196	1	78.3	0.9	12.1	21.7	112.9
197	36	3709.5	75.2	1465.2	2454.8	7704.8
198	327	17350.1	889.9	13603.1	13919	45762.1
199	41	4559.4	86.5	1664.4	2976.9	9287.2
200	27	1317.3	117.4	1819.9	1197.2	4451.8
201	8	1462.7	82.1	1427.1	970.6	3942.5
202	26	823.7	22.5	397.6	451	1694.9
203	8	828.5	28	591.4	737.5	2185.4
204	331	9737.2	206.2	4302.3	5233.5	19479.2
205	368	8392.1	884.3	12607	8132	30015.4
206	213	72674.7	1026.3	22110.1	30663	126474.2
208	2	11.4	1.5	7	4.2	24
210	1	32.1	1.2	19.1	26.7	79.1
211	1	39.3	2.9	49.7	28.6	120.5
212	29	1946.3	134.8	2104	1203.1	5388.2
213	41	1574.5	167.6	1492	875.9	4110
214	19	2204.1	73.9	1867.9	1419.5	5565.6
215	98	4124.9	248.1	4278.8	3403	12054.8
216	1826	18159.4	415.4	5503	9330	33407.9
217	185	16382.1	354.9	6838.9	7300	30875.9
218	98	8681.2	489.5	8172.1	6399.2	23742.1
219	14	1595.8	34.1	716.4	1094	3440.3
220	299	22985.3	501.7	9567.4	22312.4	55366.7
221	3559	13622.7	2031	13444.2	7459	36556.8
223	578	36140.1	2172.2	38604.6	18647.8	95564.8
224	48	587.7	59.8	618.7	381	1647.1
225	5740	51102.3	1755	26600	27342.9	106800.2
226	110	3272.1	145.4	2975.3	2116.1	8508.9
227	3108	53642.1	1892.3	32005.3	37696.5	125236.2
229	589	7518.1	257.6	5123.9	4291.5	17191.2
230	6	609.8	26.5	704.3	499.2	1839.8

Total	73234	9500790.9	170632.8	2560878.8	5804953.8	18037256.3
-------	-------	-----------	----------	-----------	-----------	------------

Table S6: Total CPU time expended for all of the ab-initio calculations performed in this work without incorporating the effects of SOC (w/o SOC), subdivided by SG. In order, the columns in this table list the SG, the number of ICSDs successfully analyzed in the SG, the CPU hours expended per each of the four calculation steps (VASP1 through VASP4) detailed in [S5 A](#), and the total CPU hours expended for materials in the SG.

SG	# ICSDs	VASP1 (CPU hours)	VASP2 (CPU hours)	VASP3 (CPU hours)	VASP4 (CPU hours)	Total (CPU hours)
1	222	16640.5	263.4	2250.8	10564.9	29719.6
2	1755	235667.3	3350.5	33564.7	152953.3	425535.9
3	16	930.1	7	81.8	538.9	1557.8
4	291	17447.8	156	2082.8	11934.1	31620.7
5	186	6913.4	57.2	653.8	4689	12313.4
6	39	1515.9	10.7	124	809.5	2460.1
7	143	8217.1	130.3	1050.1	5396.9	14794.4
8	168	5057.3	41.9	424.9	3167.5	8691.6
9	276	14522.1	112	1485	10613.8	26732.8
10	39	1873.5	14.9	185.8	1110.9	3185.1
11	749	53377.6	554.4	6215.3	33315.3	93462.6
12	1722	87000.4	614.7	7800	50440	145855.1
13	274	19194	170.8	2384.8	12399.9	34149.5
14	3602	391541.5	3358.7	48706.8	272488.3	716095.2
15	2419	177227	1461.2	18799.9	123027.7	320515.8
16	2	16.1	2	14.2	12.1	44.5
17	8	258.1	14.1	213.5	187.3	673
18	42	2809.3	127.5	2381.5	2167.5	7485.8
19	352	21449.7	940.1	17090.4	15336.1	54816.2
20	77	2538.6	36.2	556.2	1810.3	4941.3
21	20	306.5	5	65.1	165.5	542
22	14	312.4	2.9	39.7	134.5	489.6
23	15	510.5	5	58.8	204	778.3
24	3	41.8	0.8	8.6	26.7	77.9
25	58	872.9	42.9	476.7	406	1798.5
26	84	4907.6	169.8	3080.8	2775.5	10933.7
27	1	20.4	1	16.4	14.7	52.5
28	18	403.1	20.4	281.8	255.4	960.7
29	87	4800.4	237.4	4132.5	3720.1	12890.4
30	6	693.3	24.8	465.5	421.4	1605.1
31	245	8475	393.3	6672.2	5951	21491.5
32	12	1042.7	58.7	844	763.6	2709
33	399	22961	912.6	16815.8	15095.1	55784.5
34	30	2285.8	93.4	1827.2	1636.7	5843
35	8	253	16.4	67.5	166.3	503.1
36	392	14360.2	181.5	2621.9	8920	26083.6
37	7	328.9	14.2	99.8	250.9	693.7
38	162	2810.1	193.8	876.2	1508.4	5388.5
39	14	497.3	7.2	134.7	386.3	1025.5
40	64	2449.7	32.1	682.7	2050.8	5215.3
41	44	2926.4	30.2	600.1	1822.1	5378.8
42	4	183.7	2.4	31.6	161.4	379.1
43	125	4866	57.3	1071	3696.1	9690.4
44	93	1896.8	21.7	270.3	878.4	3067.2
45	11	1428.1	12.9	230.8	880.2	2552

46	83	4135.5	40.4	620.8	2283	7079.7
47	86	2117.4	71.1	869.9	787.8	3846.2
48	3	86.4	5.6	64.6	55.3	211.9
50	11	1020	38.6	773.3	700.8	2532.8
51	138	4387.5	181.6	3072.2	2766.1	10407.3
52	48	3899.3	186.1	2798.5	2550.8	9434.7
53	27	798.4	37.4	594.6	557.5	1988
54	23	1833.7	84.6	1722.7	1536.3	5177.3
55	466	37375	1328.4	24747.9	22131.1	85582.4
56	31	1967	89.6	1661.6	1522.9	5241
57	185	21454.5	582.5	11391.2	10321	43749.3
58	481	12890.5	576.2	9232.8	8317.6	31017.1
59	317	14493.3	466	7550.1	6710.8	29220.3
60	247	13852.8	686.1	11583.1	10368.2	36490.2
61	227	17496.1	856.6	15266	13530	47148.7
62	5327	302331.6	10405.5	187244.1	167174.9	667156.1
63	2021	51822.1	601.2	7947.2	23375.5	83745.9
64	421	19419.8	240.5	4187.2	13338.9	37186.4
65	331	11135.8	102.4	1487.7	3952.3	16678.2
66	49	2818.5	33.8	573.4	1907.5	5333.3
67	48	900.2	9.6	108.1	372.4	1390.3
68	21	1599.4	20.6	333.9	1121.1	3075
69	73	2870.6	26.3	413.9	1294.6	4605.5
70	197	7537.8	99.4	1998.5	5604.2	15239.8
71	574	17088	168.7	2306.6	7159	26722.3
72	227	7369.5	83.8	1192.4	3970.2	12615.9
73	21	3113.5	36.8	535.6	2081.5	5767.5
74	342	7896	104.2	1446.9	4571.6	14018.8
75	5	192.3	7.1	112.5	119.3	431.2
76	12	661.9	26.4	487.1	508.3	1683.7
77	2	17.2	1.1	9.9	11	39.2
78	2	289.9	8	148.1	155.6	601.5
79	14	376.5	5.5	69.7	239	690.7
80	3	362.8	3.8	58.2	234	658.8
81	18	373.5	20.3	259.4	289.8	942.9
82	265	3631.4	86.6	708.4	2588	7014.5
83	10	716.2	20.7	345.2	370.8	1452.9
84	35	1121.1	48.9	776.1	802.4	2748.6
85	51	3973.6	130.9	2511	2619.6	9235.2
86	68	2795.4	104.2	1759.5	1788.1	6447.3
87	291	8338	89.3	1091.6	4117.1	13636
88	314	9571.3	128.6	1716.2	6876.7	18292.9
90	5	614.1	23	491.8	363.5	1492.5
91	9	136.1	8.9	130.2	95.1	370.3
92	133	3393.2	182.5	2995.1	2221.3	8792.1
94	1	4.3	0.3	3.7	3	11.2
95	3	44.4	3.2	43.1	31.6	122.3
96	37	350.3	28.3	364.8	291.4	1034.8
97	2	16.6	1.1	12.5	21.8	51.9
98	7	144.1	2.9	37.6	111.9	296.5
99	195	625.5	100.6	527.8	425.9	1679.8
100	38	1376	74	1256.1	897.9	3604
102	15	717.3	34	662.3	473.2	1886.8
103	9	39.2	5.3	43.6	32.8	120.9
104	4	100.9	8.4	127.8	96	333.1
105	4	73.7	4.6	75.3	52.6	206.2

106	1	24	1.7	25.6	18.5	69.8
107	145	789.3	22.7	179.5	450.5	1442
108	14	488.2	8.9	125.7	369.3	992.2
109	50	436.9	12.2	103.3	241.3	793.8
110	36	2058.5	29.2	446.8	1440.3	3974.8
111	26	203.8	18.3	179.9	132.7	534.8
112	4	22.6	2.5	20.4	15.6	61
113	150	2409.9	164.4	2336.3	1741.1	6651.8
114	42	1054.6	67.5	1108.7	791.4	3022.2
115	24	298	19.7	289.5	198.4	805.7
116	25	616.6	40.7	650.1	473.7	1781
117	12	917.1	35.6	684.9	552.7	2190.2
118	12	449.8	28.7	480.6	402.5	1361.6
119	50	631.4	15.4	154.9	413.9	1215.5
120	25	884.6	16.5	220.3	561.1	1682.5
121	205	2258.1	62.4	631.7	1603	4555.2
122	510	3995.8	123.2	1103.7	2803.2	8026
123	699	4342.5	352	2844.7	2142	9681.2
124	33	1119.5	62.1	1194.5	922	3298.1
125	67	1841.9	79.5	1149.6	841.2	3912.1
126	11	372.2	23.8	451.5	321.3	1168.7
127	523	15351.3	591.5	9138.4	6490.3	31571.5
128	89	8301.5	285.2	5630.7	4071.6	18289
129	1506	10738.6	814.4	5929.9	4520.7	22003.5
130	58	4060.1	179.9	3491.2	2537.5	10268.7
131	57	240.7	27.9	179.6	138.2	586.4
132	10	94.2	7.4	87.6	65.6	254.8
133	5	100.6	5.9	104.2	74.5	285.2
134	9	67.8	5.7	62.8	46.3	182.7
135	84	1695.1	107	1590.2	1141.8	4534.1
136	766	9562.1	608.4	8214.9	5921.6	24307
137	158	3107.1	200.6	2993.2	2197.4	8498.4
138	20	1175.6	44.3	776.5	560.3	2556.7
139	3345	30000.9	577	5821.5	14249.1	50648.5
140	916	16784.1	307.6	3577.2	8459.7	29128.5
141	658	12790	221	2852.3	6060.4	21923.7
142	98	8273.9	136.8	2139.7	5064	15614.4
143	18	1468.6	54.8	792.1	1086	3401.5
144	31	3401.4	88.3	1256.7	1685.7	6432
145	5	254.5	10.9	143.7	192.5	601.7
146	108	2882.8	29	293.2	1969.9	5174.9
147	80	3872.6	108.9	1913.7	2397.8	8293
148	794	26005.2	236.8	2812.5	16800	45854.5
149	15	142.5	10.1	100.6	89	342.3
150	88	2728.6	122.8	1604.5	1334.5	5790.4
151	4	199.4	10.1	186.2	154.2	549.9
152	269	1454.2	172	1229.5	1091	3946.7
153	1	35.4	1.9	33.2	28.1	98.5
154	138	617.1	83.1	535.7	460.5	1696.4
155	66	1133	23.4	200.9	729.4	2086.7
156	224	24561.7	714.8	13269.3	11261.8	49807.6
157	27	320.9	27.2	263.3	226.9	838.4
158	3	158.5	7.2	128.9	105.8	400.5
159	57	1159.9	82	985.1	841	3068.1
160	298	5234.3	116.7	1256.6	3419	10026.6
161	251	5052.8	71.6	814.7	3616.4	9555.5

162	70	461.9	43.7	358.9	317.6	1182.1
163	80	4697	193.1	3418.7	2948.8	11257.6
164	996	6051.4	596.2	4239	3709	14595.6
165	66	2066.5	114.8	1803	1511.3	5495.5
166	1679	43048.6	429.4	3973.1	15148.7	62599.9
167	913	34970.4	517.1	4992.7	25149.1	65629.3
169	1	26	2.7	34.2	24.8	87.7
173	176	6442.7	300.5	5379.9	3825.6	15948.7
174	62	1834.8	110.3	1473.5	1136.8	4555.4
175	2	18.4	1.6	19.2	13.7	52.9
176	339	10426.4	599	10057.4	7233.8	28316.6
177	3	83.6	6.6	98.5	54.2	242.9
180	95	302.6	63.2	380.9	220.5	967.3
181	15	65.6	7.7	85.6	48	206.9
182	49	578.1	61.7	816.5	442.3	1898.7
183	3	3.2	1.5	3.8	2.4	10.9
185	84	2742.7	174.9	3049.8	1572.5	7539.9
186	842	8956.8	849.5	10271.5	5688.3	25766.1
187	246	812.3	170.3	771.2	489.3	2243.1
188	27	367	34.1	458.9	250.3	1110.3
189	768	7479.3	674.7	6256.1	3510.8	17920.8
190	67	1486.7	148.8	1859.8	1013.6	4508.9
191	1269	10049.9	680.1	4765	2736.8	18231.8
192	14	627.6	49.3	890.2	482.5	2049.6
193	439	10935.5	515.5	7762.6	4193.8	23407.3
194	3269	42642.6	2690.8	30749.5	16916.5	92999.5
195	1	26.5	1.6	26	16.7	70.7
196	1	12.7	0.4	3.3	4.5	21
197	36	521.6	24.7	355	351.2	1252.6
198	323	4050	333.9	4925.2	3259.5	12568.7
199	40	823.9	22.4	341.6	496.3	1684.2
200	27	526.7	47.7	693.7	452.5	1720.5
201	7	496.5	26.8	473.5	306.3	1303.2
202	26	236.9	7.3	100.6	151	495.8
203	8	285.6	7	133.6	243.8	670.1
204	323	2843.6	73.5	1114.7	1249.5	5281.4
205	364	3012.8	299.7	3650	2415.6	9378.1
206	208	14306.2	184.2	3907.3	6257.4	24655
208	2	2.9	0.9	2.8	1.7	8.4
210	1	10	0.5	4.6	8.1	23.1
211	1	15.9	1.4	22.2	10.5	50.1
212	29	609.5	47.2	738.8	363.7	1759.3
213	41	328.5	36.8	497	244.6	1106.9
214	18	367.9	16.8	373	268.2	1025.9
215	95	1020.6	118	1625.3	810.9	3574.8
216	1798	4916.7	210.6	1411.7	3321.6	9860.6
217	178	2790.9	88	1441.5	1304	5624.4
218	98	1925.3	194.4	3060.3	1496	6676.1
219	13	261.8	8.1	146.6	213.9	630.4
220	295	5456.1	151	2266.3	2167.5	10040.9
221	3493	10189.3	3401	9912.1	6474.7	29977.1
223	568	17296.6	978.4	14360.2	7033.1	39668.4
224	45	271.5	45.9	265.3	142.2	724.8
225	5619	21321.7	842.1	6760.4	12191.7	41116
226	102	984.3	41.3	635.8	757.3	2418.7
227	3012	17366.8	594.4	7540.4	8656.2	34157.8

229	583	3066.4	107	1221.7	1359.9	5755
230	6	219.5	8	159.2	199.3	586
Total	69730	2298583.3	56520.7	773019.5	1397550.3	4525673.8

Table S7: Total CPU time expended for all of the ab-initio calculations performed in this work incorporating the effects of SOC (with SOC), subdivided by the number of atoms in the primitive cell in each material. In order, the columns in this table list the number of atoms, the number of ICSDs successfully analyzed with the same number of atoms, the CPU hours expended per each of the four calculation steps (VASP1 through VASP4) detailed in [S5 A](#), and the total CPU hours expended for materials with the listed number of atoms in the primitive cell.

# atoms	# ICSDs	VASP1 (CPU hours)	VASP2 (CPU hours)	VASP3 (CPU hours)	VASP4 (CPU hours)	Total (CPU hours)
1	1178	1692.2	133	455.7	1315.1	3596
2	5838	8707.1	1229	4630.6	5155.7	19722.4
3	2429	8457.2	586.1	2543.2	5180.9	16767.4
4	4851	24909	1465	8512.3	17989.5	52875.8
5	3912	38653.7	1437.9	9362.6	26276.9	75731.1
6	6280	62655.4	3812.2	25308	46531.7	138307.2
7	1169	20558.6	378.2	3953.5	21107.7	45997.9
8	4239	69498.4	1969.7	26406.4	66879.8	164754.4
9	1745	38455.6	1040.8	16788.1	36746.4	93030.9
10	3498	101882.1	3068.6	38573.3	108096.9	251620.9
11	488	37159.7	846.8	8064.9	39050.5	85121.8
12	5023	271212.6	8527.4	131051	280299.7	691090.8
13	748	59115.8	1356.4	12500.1	43733.6	116705.8
14	2462	178253.4	4446.4	48149	209175.9	440024.7
15	429	44783.7	1372.9	9509.1	57785.1	113450.9
16	2980	291702.3	6978.2	101610.2	187394.1	587684.7
17	336	32322.2	607.5	8352.8	25039.6	66322.1
18	1607	187947	5758	57464.4	127823.4	378992.8
19	271	59358.6	475.7	5950.7	24315.9	90100.9
20	3618	480741.1	10167.6	149467.9	299831.8	940208.3
21	199	30273.9	1085.7	6403.3	15711.2	53474.2
22	1613	254127.1	3484	47223.3	131763.9	436598.3
23	148	20209.7	636	4955.5	12606.8	38408
24	2635	452531.4	11618.9	135134.3	232471.7	831756.3
25	65	31170.7	200.7	2461.6	13554.2	47387.2
26	686	151359.6	1566	26140.2	79825.2	258891
27	154	26557.3	325.8	5019.3	15649.1	47551.5
28	2663	520778.7	9095	168200.4	279719.3	977793.3
29	441	64277.5	969.1	18818.8	28707.4	112772.8
30	855	222765	3328.8	51435.4	120702.2	398231.4
31	37	11691.3	96.4	1306.8	7565.8	20660.3
32	1446	529701.1	5729.5	104171.6	335148.4	974750.5
33	76	24907.1	274.1	5145.1	12343.3	42669.6
34	341	171411.2	1259	20640.5	102531.1	295841.7
35	44	34184	188.7	3082.9	21339.5	58795.1
36	1644	674688.5	12436.8	220457.8	371435.6	1279018.7
37	34	23767.8	224	2484.9	8439.8	34916.5
38	494	227118.6	3134.9	53355.6	105738.9	389348.1
39	67	41008.1	654.9	11049.4	16198.3	68910.7
40	1533	590881.7	11528.7	209582.4	338425.5	1150418.3
41	46	32255.1	242.9	4046	17630.1	54174.1

42	495	217781.5	2799.9	47968.9	131825.1	400375.5
43	16	6440.2	87.5	1193.6	3602.1	11323.3
44	791	535425.1	6427.7	111650.2	327926	981429
45	45	23017.7	390.7	6707.1	14180.8	44296.5
46	390	211540.2	2535	43916.8	112491.1	370483
47	10	15904.4	84.5	1334.3	5832.3	23155.4
48	846	523845.7	8847.3	151462.9	312179.8	996335.7
49	33	29334.5	229.2	3864.4	10371.8	43799.9
50	183	121677.3	1375.6	22310.1	68542.9	213905.9
51	12	9202.6	147.6	2251.9	5709.7	17311.7
52	641	574723.4	6738.7	111780.4	280305	973547.6
53	10	10657	54.7	688.1	2446.9	13846.7
54	257	146755.9	2628.7	44400.6	90529.7	284314.9
55	13	10828.9	128.6	2068.7	4207	17233.2
56	552	398960.4	6814.9	116851.8	239838.5	762465.7
57	11	8036.9	158.9	2340.2	3750.3	14286.3
58	161	120980.8	2010.7	29671	57301	209963.4
59	4	6722.4	45.1	706.8	4153.5	11627.8
60	417	351268.4	5045.2	84244.6	208210.1	648768.3
62	2	894.3	21.5	355.4	1717.5	2988.7
64	2	2286.1	35.9	573.9	1571.7	4467.6
68	2	1585.7	22.4	382.6	969	2959.6
70	3	2061.2	28.3	477.9	1953.5	4520.9
72	7	10535.4	119.5	2050	10071.1	22776
74	2	1022.6	21.8	354.5	1834.5	3233.4
76	6	4563.8	81.7	1275.2	4981.3	10902
78	1	1007.7	14.1	227.9	1214.2	2463.9
Total	73234	9500790.9	170632.8	2560878.8	5804953.8	18037256.3

Table S8: Total CPU time expended for all of the ab-initio calculations performed in this work without incorporating the effects of SOC (w/o SOC), subdivided by the number of atoms in the primitive cell in each material. In order, the columns in this table list the number of atoms, the number of ICSDs successfully analyzed with the same number of atoms, the CPU hours expended per each of the four calculation steps (VASP1 through VASP4) detailed in [S5 A](#), and the total CPU hours expended for materials with the listed number of atoms in the primitive cell.

# atoms	# ICSDs	VASP1 (CPU hours)	VASP2 (CPU hours)	VASP3 (CPU hours)	VASP4 (CPU hours)	Total (CPU hours)
1	1174	1428.4	150.8	237.9	1464.8	3281.8
2	5757	8494.6	1997.5	4335.5	6970.2	21797.9
3	2375	4654.8	538.7	1930.2	3119.6	10243.2
4	4724	13122.2	1848.2	6104.9	7951.1	29026.4
5	3768	17086.8	1570.1	5693.8	8010.7	32361.4
6	6005	27415.5	1914.6	11614.4	13057.6	54002.1
7	1121	5835.6	302.4	1686	3342.6	11166.6
8	4087	26286.6	1597.5	11208	14378.5	53470.6
9	1634	11539.6	781.9	5615	5671	23607.5
10	3366	29405.9	1002.8	8577.2	16863.4	55849.3
11	442	9348.1	148.4	1500.1	4025.6	15022.2
12	4721	74161.1	2387	25867.7	37434.5	139850.3
13	687	13310.1	255.6	2598	5464.7	21628.4
14	2346	36977.7	811.9	8930.2	19695.8	66415.6
15	404	10900.2	161.3	1705.1	5488.7	18255.3
16	2800	66554.1	1869.7	23967.2	35630.9	128021.8

17	325	8368.3	160.3	1947.3	4687.1	15163
18	1527	43958.1	1050.3	12785.7	21962.3	79756.5
19	235	13056.8	108.7	1274.3	4504.2	18943.9
20	3436	105041.5	2622.5	37317.1	60273.3	205254.4
21	180	6459.4	161.4	2000.5	3555	12176.3
22	1507	54674.8	925	11862.2	31129.2	98591.2
23	143	4653.5	105	1261.1	2887.3	8906.8
24	2445	107421.5	2878.4	44166.6	65128.8	219595.2
25	56	6339.8	50.3	595.5	2730.8	9716.4
26	636	27235.2	577.1	8100.2	15875.6	51788.1
27	144	8156.7	144	1874.2	4699.9	14874.7
28	2484	130370.6	3425.9	56219.6	75007.8	265023.9
29	421	18100.3	276.5	4305.2	7713	30395
30	771	44759.9	1138.5	17363.1	28079.2	91340.7
31	36	2787.1	41.6	430.6	1939.6	5198.9
32	1336	101776.4	2053.3	34289.6	63445.4	201564.7
33	71	7223.7	112.9	1889.5	3001.4	12227.6
34	315	28517.9	359	5176.1	18254	52307
35	42	6647.6	57.5	746.3	3465	10916.3
36	1535	180424.4	4037.4	73477.6	108486.3	366425.8
37	33	5944.5	66.1	823.5	3392.1	10226.2
38	438	58361.8	976.5	16280.2	30233.3	105851.8
39	63	10970.5	200.3	3261.2	5283.2	19715.2
40	1484	164516.7	3821.1	67853.9	103775.8	339967.5
41	39	4761	59.6	888.3	3289	8997.9
42	441	50165.2	858.1	13486.9	33587.9	98098.2
43	14	2472.3	34.2	393.1	1583	4482.6
44	708	115514.9	1865.9	32835.9	80554.8	230771.5
45	38	7729.9	160.7	2177.1	4031.6	14099.4
46	382	48077.9	773.4	12418.4	30508.1	91777.8
47	10	2162	26.9	385.5	1425.3	3999.6
48	815	132027.4	2797.2	51535.4	92872.3	279232.3
49	33	7950.4	65.4	919.6	4103.8	13039.2
50	176	29245.7	426.7	5948.3	19606.6	55227.2
51	10	1858.8	24.8	458	1336.6	3678.3
52	596	112774.2	1755.4	31895.2	73103.5	219528.3
53	10	2535.4	20	249.8	1016.3	3821.5
54	252	42895.2	844.6	14972.5	28809.5	87521.8
55	12	3719.9	39.5	617.8	1600.3	5977.6
56	529	103002.2	2019.1	38861.8	73748.8	217631.9
57	10	1918.4	48.2	717.9	1319.2	4003.8
58	151	28945.3	493.5	9623.3	18075	57137
59	4	1545.6	13.2	182.4	1055.2	2796.4
60	401	86389.7	1441.7	26559.6	61958.9	176349.8
62	2	562.1	3.8	60.9	360.9	987.8
64	2	1124.3	7.9	128.6	701.5	1962.3
68	2	433.1	3.5	49.8	287.9	774.2
70	3	928.2	5.9	95.4	583.8	1613.3
72	7	4042.6	23.3	370.4	2161.8	6598.1
74	2	471.9	3.6	57.1	333.6	866.2
76	6	2508	14.5	222.7	1237.4	3982.6
78	1	533.6	2.2	35.9	218.1	789.7
Total	73234	2298583.3	56520.7	773019.5	1397550.3	4525673.8

### C. Disk Storage Requirements and Statistics

In this section, we provide tables detailing the amount of disk storage requested for this work. Overall, we have used 2,037.80Gb of storage for this work, which can be subdivided into 1,694.50Gb (83.15%) for the SOC DFT calculations and 343.30Gb (16.85%) for the DFT calculations performed w/o SOC. To conserve disk space, we have only stored the OUTCAR files outputted by VASP, the CHGCAR files generated during the self-consistent DFT calculations, and the PROCAR files generated during the density of states (DOS) evaluation. All of these files are stored in a compressed BZIP2 format. The majority of the storage is dedicated to the SOC computation output – specifically, the CHGCAR files use 559.30Gb (27.45%), and the PROCAR files use 1,013.80Gb (49.75%). For a more detailed overview, we list in Table S9 the disk storage expended to perform ab-initio calculations subdivided by SG, and in Table S10 we list the disk storage expended to perform ab-initio calculations subdivided by the number of atoms in the primitive cell of each material.

Table S9: Total disk storage space (in Gb) expended for all of the ab-initio calculations performed in this work, subdivided by SG. In order, the columns in this table list the SG, the number of ICSDs successfully analyzed in the SG, the total storage space (in Gb) for the calculations performed with and w/o SOC, the storage for the compressed CHGCAR files generated during the SOC self-consistent DFT calculations, the storage for the compressed PROCAR files generated during the SOC DFT DOS calculations, and the total storage space for the calculations performed w/o SOC.

SG	# ICSDs	Total Storage SOC+w/o SOC (Gb)	CHGCAR SCC Storage (Gb)	PROCAR DOS Storage (Gb)	Total w/o SOC Storage (Gb)
1	225	14	1.54	8.25	2.05
2	1885	119.7	19.8	67.9	27.05
3	19	1.32	0.15	0.95	0.15
4	305	18.92	3.13	11.85	2.9
5	195	9.83	1.83	6.2	1.3
6	39	1.8	0.17	1.32	0.21
7	143	8.53	1.46	5.29	1.36
8	173	5.86	1.15	3.61	0.79
9	278	17.1	3.37	10.42	2.62
10	44	1.76	0.22	1.12	0.25
11	790	39.49	6.18	23.58	6.17
12	1844	70.2	17.18	37	11.06
13	314	16.93	3.31	9.41	2.84
14	3787	244.55	55.26	119.39	51.72
15	2526	135.25	33.73	63.14	25.98
16	2	0.03	0.01	0.02	—
17	8	0.43	0.06	0.29	0.05
18	42	2.15	0.43	1.21	0.39
19	364	20.31	4.55	10.45	3.36
20	85	3.75	0.96	1.96	0.53
21	21	0.51	0.11	0.29	0.07
22	17	0.6	0.14	0.35	0.06
23	16	0.73	0.22	0.38	0.09
24	3	0.11	0.04	0.05	0.02
25	59	1.04	0.12	0.7	0.12
26	85	3.5	0.71	1.99	0.57
27	1	0.05	0.01	0.03	0.01
28	18	0.65	0.07	0.49	0.06
29	89	4.38	0.96	2.44	0.78
30	6	0.36	0.08	0.17	0.09
31	247	11.18	1.73	7.45	1.46
32	12	0.44	0.12	0.14	0.14

33	406	19.5	3.84	11.47	3.27	
34	30	1.22	0.27	0.56	0.3	
35	8	0.26	0.06	0.12	0.05	
36	412	18.25	4.43	10.31	2.32	
37	7	0.3	0.09	0.11	0.07	
38	173	3.47	0.8	1.86	0.45	
39	15	0.81	0.22	0.41	0.11	
40	67	2.7	0.67	1.42	0.41	
41	44	2.21	0.76	0.81	0.49	
42	4	0.2	0.07	0.09	0.03	
43	126	6.35	2.4	2.53	1.11	
44	100	3.18	0.96	1.64	0.38	
45	11	1.01	0.4	0.35	0.21	
46	91	5.7	1.71	2.96	0.74	
47	95	2.03	0.28	1.21	0.27	
48	3	0.09	0.02	0.05	0.01	
49	1	0.05	0.01	0.03	—	
50	11	0.54	0.07	0.31	0.12	
51	147	3.95	0.53	2.51	0.57	
52	51	2.92	0.59	1.73	0.46	
53	27	0.76	0.2	0.37	0.14	
54	25	1.29	0.34	0.63	0.23	
55	548	31.89	3.65	20.84	4	
56	31	1.58	0.35	0.86	0.3	
57	208	11.18	2.23	6.58	1.75	
58	493	11.97	2.43	6.69	1.98	
59	338	8.63	1.53	4.93	1.39	
60	252	11.75	2.22	6.91	2.03	
61	233	12.52	2.74	6.99	2.21	
62	5664	223.07	40	133.95	34.07	
63	2188	53.41	15.98	24.99	7.7	
64	435	17.57	4.28	9.16	2.88	
65	372	10.18	2.81	5	1.39	
66	51	1.81	0.61	0.64	0.39	
67	63	0.7	0.16	0.35	0.11	
68	21	1.06	0.34	0.42	0.22	
69	75	2.77	0.87	1.27	0.43	
70	208	9.04	3.09	3.96	1.4	
71	666	21.53	8.92	7.59	2.96	
72	240	9.68	3.05	4.63	1.4	
73	29	2.25	1.31	0.21	0.43	
74	370	10.91	3.5	4.92	1.72	
75	5	0.33	0.05	0.24	0.03	
76	12	0.56	0.18	0.25	0.11	
77	2	0.03	0.01	0.01	—	
78	2	0.07	0.04	—	0.03	
79	14	0.64	0.2	0.32	0.09	
80	3	0.43	0.22	0.13	0.07	
81	19	0.81	0.14	0.53	0.09	
82	275	8.88	2.63	4.57	1.14	
83	11	0.46	0.08	0.27	0.06	
84	35	1.31	0.24	0.8	0.21	
85	54	2.13	0.54	1.03	0.39	
86	71	3.63	0.59	2.34	0.48	
87	298	7.36	2.69	2.87	1.3	
88	332	10.59	4.68	3.15	2.07	

90	5	0.19	0.08	0.03	0.06	
91	9	0.48	0.09	0.32	0.06	
92	135	3.52	0.98	1.79	0.58	
94	1	0.02	—	0.01	—	
95	3	0.12	0.03	0.07	0.02	
96	37	0.93	0.24	0.51	0.13	
97	2	0.23	0.04	0.05	0.14	
98	7	0.24	0.1	0.09	0.04	
99	195	1.23	0.26	0.62	0.18	
100	38	1.62	0.29	1.07	0.2	
102	15	0.77	0.1	0.56	0.09	
103	9	0.13	0.03	0.08	0.02	
104	4	0.22	0.04	0.15	0.02	
105	4	0.15	0.02	0.1	0.02	
106	1	0.06	0.01	0.04	0.01	
107	159	2.22	0.79	0.96	0.28	
108	15	0.63	0.24	0.26	0.1	
109	54	1.37	0.62	0.48	0.2	
110	36	2.5	0.71	1.24	0.42	
111	27	0.38	0.09	0.21	0.05	
112	4	0.07	0.02	0.03	0.01	
113	167	5.09	1.1	3.07	0.56	
114	42	1.6	0.4	0.89	0.23	
115	24	0.34	0.07	0.17	0.05	
116	25	1.25	0.14	0.92	0.14	
117	12	0.67	0.12	0.41	0.1	
118	12	0.57	0.11	0.36	0.07	
119	50	1.14	0.52	0.34	0.2	
120	25	1.18	0.46	0.47	0.19	
121	216	4.82	1.86	1.84	0.7	
122	515	10.77	4.49	3.87	1.74	
123	727	5.85	1.34	2.59	0.92	
124	34	0.62	0.2	0.24	0.13	
125	73	1.92	0.48	1.05	0.26	
126	12	0.54	0.13	0.31	0.08	
127	574	14.47	2.42	8.93	1.73	
128	94	4.95	1.05	2.91	0.69	
129	1549	13.71	3.68	6.05	2.23	
130	59	3	0.58	1.86	0.43	
131	58	0.4	0.11	0.17	0.07	
132	10	0.22	0.07	0.1	0.03	
133	5	0.19	0.01	0.14	0.03	
134	9	0.19	0.04	0.11	0.03	
135	91	3.28	0.7	1.92	0.47	
136	790	11.58	2.43	6.49	1.67	
137	160	3.88	0.69	2.36	0.57	
138	26	1.41	0.25	0.89	0.13	
139	3533	54.9	30.93	10.47	9.08	
140	959	21.54	8.14	8.68	3.12	
141	733	19.92	8.65	6.91	3.04	
142	104	8.49	3.69	3.04	1.33	
143	19	1.42	0.28	0.86	0.21	
144	32	1.61	0.54	0.63	0.36	
145	5	0.38	0.08	0.24	0.05	
146	113	5.79	1.28	3.63	0.64	
147	84	3.49	0.98	1.62	0.63	

148	822	33.51	9.81	16.67	5.36	
149	15	0.45	0.14	0.22	0.06	
150	91	3.99	0.82	2.48	0.5	
151	5	0.27	0.07	0.15	0.04	
152	273	4.95	1.38	2.57	0.7	
153	2	0.09	0.02	0.05	0.01	
154	140	1.81	0.58	0.81	0.28	
155	70	2.51	0.86	1.16	0.35	
156	255	11.97	3.71	5.41	1.69	
157	29	1	0.19	0.66	0.1	
158	3	0.14	0.04	0.07	0.02	
159	59	2.89	0.55	1.91	0.33	
160	306	20.34	14.24	2.56	3.24	
161	252	7.86	2.48	3.82	1.21	
162	73	1.14	0.35	0.5	0.17	
163	88	3.39	1.23	1.34	0.57	
164	1025	10.28	3.4	4.07	1.59	
165	68	2.87	0.69	1.63	0.43	
166	1795	51.92	25.8	14.99	8.24	
167	959	25.83	10.4	10.02	4.1	
169	1	0.04	0.01	0.02	—	
173	196	11.41	2.42	6.14	1.12	
174	72	3.58	0.7	2.29	0.39	
175	2	0.05	0.01	0.03	0.01	
176	369	13.22	3.03	7.23	2.19	
177	3	0.12	0.05	0.05	0.02	
180	95	0.91	0.3	0.36	0.16	
181	15	0.23	0.08	0.09	0.04	
182	51	1.25	0.38	0.62	0.18	
183	3	0.01	—	—	—	
185	97	5.59	1.11	3.69	0.52	
186	877	19	5.02	10.71	2.14	
187	251	1.52	0.54	0.54	0.24	
188	28	1.15	0.35	0.58	0.15	
189	871	16.66	4.33	8.77	1.9	
190	73	3.06	0.73	1.76	0.38	
191	1401	11.26	3.08	4.84	1.72	
192	15	0.85	0.26	0.42	0.13	
193	498	11.96	4.03	5.47	1.53	
194	3433	50.85	15.29	23.62	7.07	
195	1	0.04	0.02	0.02	0.01	
196	1	0.03	0.01	0.01	—	
197	36	1.97	0.65	0.94	0.27	
198	327	7.67	2.36	3.84	1.1	
199	41	1.64	0.54	0.75	0.23	
200	27	0.81	0.21	0.43	0.12	
201	8	0.52	0.12	0.3	0.07	
202	26	0.69	0.33	0.19	0.12	
203	8	0.5	0.23	0.16	0.08	
204	331	6.73	2.69	2.3	1.12	
205	368	5.8	1.95	2.58	0.93	
206	213	13.02	4.11	6.17	1.94	
208	2	0.01	0.01	—	—	
210	1	0.03	0.01	0.01	0.01	
211	1	0.03	0.02	0.01	0.01	
212	29	1.02	0.32	0.5	0.16	

213	41	1	0.3	0.49	0.15	
214	19	0.92	0.41	0.31	0.14	
215	98	2.18	0.45	1.35	0.24	
216	1826	9.11	3.7	2.52	1.41	
217	185	6.53	2.14	3.04	0.82	
218	98	4.17	1.4	2.06	0.57	
219	14	0.8	0.26	0.39	0.1	
220	299	10.02	3.84	4.06	1.43	
221	3559	11.29	3.52	3.15	2.19	
223	578	11.28	3.19	5.65	1.65	
224	48	0.39	0.13	0.15	0.06	
225	5740	33.64	14.19	8.95	5.6	
226	110	3.17	1.21	1.23	0.46	
227	3108	41.14	18.06	12.18	6.54	
229	589	4.79	1.79	1.59	0.8	
230	6	0.37	0.12	0.17	0.06	
Total	73234	2072.48	559.38	1013.81	342.62	

Table S10: Total disk storage space (in Gb) expended for all of the ab-initio calculations performed in this work, subdivided by the number of atoms in the primitive cell in each material. In order, the columns in this table list the number of atoms, the number of ICSDs successfully analyzed with the same number of atoms, the total storage space (in Gb) for the calculations performed with and w/o SOC, the storage space used for the compressed CHGCAR files generated during the SOC self-consistent DFT calculations, the storage used for the compressed PROCAR files generated during the SOC DOS DFT calculations, and the total storage space used for the calculations performed w/o SOC.

# atoms	# ICSDs	Total Storage SOC+w/o SOC (Gb)	CHGCAR SCC Storage (Gb)	PROCAR DOS Storage (Gb)	Total w/o SOC Storage (Gb)
1	1178	1.34	0.4	0.08	0.38
2	5838	11.9	4.61	1.48	2.63
3	2429	8.76	3.86	1.6	1.7
4	4851	23.6	9.84	5.7	4.36
5	3912	29.83	13.5	7.48	5.1
6	6280	50.21	19.69	15.6	8.55
7	1169	15.36	7.41	4.05	2.58
8	4239	50.43	17.46	19.92	8.05
9	1745	28.19	10.26	11.35	3.98
10	3498	52.59	17.43	22.76	8.06
11	488	15.25	5.89	6.03	2.21
12	5023	111.11	30.79	56.24	15.91
13	748	20.16	6.82	9.18	2.76
14	2462	62.23	20.79	28.02	8.88
15	429	16.07	4.83	8.12	2.22
16	2980	99.57	24.13	55.9	13.01
17	336	13.85	5.66	5.38	2.06
18	1607	64.96	16.25	34.47	8.18
19	271	13.42	3.58	7.3	1.73
20	3618	152.47	29.56	91.29	20.03
21	199	10.08	1.92	6.4	1.21
22	1613	78.63	19.28	44.71	10.33
23	148	8.11	2.55	4.1	1.05
24	2635	141	26.83	88.31	17.75
25	65	4.93	1.03	3.02	0.62
26	686	45.4	10.52	27.66	5.33

27	154	10.82	2.03	7.03	1.34	
28	2663	159.49	33.06	97.87	20.74	
29	441	18.63	5.6	8.85	2.69	
30	855	60.95	11.88	38.63	7.48	
31	37	3.07	0.52	1.89	0.56	
32	1446	92.83	19.94	51.6	14.87	
33	76	4.35	1.42	1.9	0.74	
34	341	21.8	5.94	9.98	4.51	
35	44	3.32	1.2	1.13	0.8	
36	1644	113.2	25.87	61.42	19.17	
37	34	2.13	0.86	0.48	0.66	
38	494	34.24	8.51	17.76	5.72	
39	67	5.23	1.9	2.04	0.98	
40	1533	110.22	25.88	59.04	19.35	
41	46	2.93	0.76	1.37	0.6	
42	495	37.54	6.64	19.17	6.45	
43	16	0.95	0.15	0.45	0.28	
44	791	50.33	11.77	21.13	12.38	
45	45	2.49	0.84	0.76	0.65	
46	390	22.18	8.24	6.98	5.49	
47	10	0.45	0.21	—	0.2	
48	846	50.64	17.71	14.2	14.46	
49	33	2.86	0.84	1.27	0.61	
50	183	10.95	3.95	2.87	3.22	
51	12	0.51	0.21	0.05	0.17	
52	641	37.57	14.32	6.9	11.54	
53	10	0.44	0.16	0.08	0.17	
54	257	15.03	6.1	3.5	4.36	
55	13	0.86	0.25	0.35	0.19	
56	552	31.41	13	4.45	10.8	
57	11	0.66	0.35	0.04	0.2	
58	161	9.55	3.8	2.12	2.73	
59	4	0.25	0.1	—	0.12	
60	417	23.81	9.86	2.24	9.17	
62	2	0.1	0.04	—	0.05	
64	2	0.12	0.05	—	0.05	
68	2	0.1	0.04	—	0.04	
70	3	0.14	0.07	—	0.06	
72	7	0.45	0.19	0.06	0.14	
74	2	0.1	0.04	—	0.05	
76	6	0.29	0.12	—	0.13	
78	1	0.06	0.02	—	0.03	
Total	73234	2072.48	559.38	1013.81	342.62	

## S6. TOPOLOGICAL MATERIAL CLASSES IN THE ABSENCE OF SPIN-ORBIT COUPLING

In real materials, spin-orbit interaction (SOC) is always present [2, 127]; however, depending on the orbitals at the Fermi energy, the dispersion, and the specific atoms in the material, the effects of SOC can be approximated to be negligible. For each of the materials on <https://www.topologicalquantumchemistry.com/>, we have performed DFT calculations (the details of which are specified in S4) both incorporating and neglecting the effects of SOC (though as noted in S4, there exist materials on <https://www.topologicalquantumchemistry.com/> for which only calculations incorporating SOC were convergent). As shown in Fig. S1, users on <https://www.topologicalquantumchemistry.com/> can toggle be-

tween the results of first-principles calculations performed with and w/o SOC for the same material using the switch on the top-right corner of each material page [light blue box in Fig. S1(A,B)].

In the absence of SOC, the possible stable topological (TQC) classes [28, 38, 43, 58, 92, 93, 97] for each material – NLC, SEBR, ES, ESFD, and LCEBR – are the same as the possible classes in the presence of SOC. However, as we will detail in the text below, the relative number of materials within each topological class, and the physical meaning of the NLC and SEBR classes, strongly differ with and w/o SOC. First, in S6 A, we will discuss the relative preponderance of ES-classified materials compared to the relative dearth of NLC- and SEBR-classified compounds in the absence of SOC. Then, in S6 B, we will review the physical meaning and expected topological boundary states of each topological class in the absence of SOC. In particular, in S6 B, we will focus on the cases of NLC- and SEBR-classified nonmagnetic materials, which were shown in Ref. [36] to be topological semimetals – as opposed to topological (crystalline) insulators – when the effects of SOC are neglected. Throughout this work, we specifically term ICSD entries that are classified as NLC (SEBR) at  $E_F$  w/o SOC as NLC-SM (SEBR-SM) topological semimetals. In the language of Refs. [29, 37], NLC-SM and SEBR-SM phases w/o SOC are *Smith-index semimetals*, as they are characterized by nontrivial values of the SIs of the nonmagnetic (Type-II Shubnikov) single (spinless) SGs [36].

### A. Relative Numbers of Materials in Each Topological Class with and without SOC

Number of Unique Materials in Each Stable Topological Class Among the Materials with Convergent Calculations in the Absence of SOC (36,163 Unique Materials)		
Topological Class	Without SOC	With SOC
NLC (-SM)	251 (0.69%)	2,568 (7.10%)
SEBR (-SM)	44 (0.12%)	2,814 (7.78%)
ES	6,006 (16.61%)	3,785 (10.47%)
ESFD	13,997 (38.71%)	9,485 (26.23%)
LCEBR	15,865 (43.87%)	17,511 (48.42%)

Table S11. On <https://www.topologicalquantumchemistry.com/>, there are 36,163 unique materials (as defined in Ref. [38] and in the main text) for which DFT calculations were successfully performed both with and without incorporating the effects of SOC. For each of the stable topological classes, we list the number of materials in the class with and without SOC. As will be discussed in S6 B, we have added a parenthetical (-SM) following the NLC and SEBR classes, because NLC- and SEBR-classified nonmagnetic materials are necessarily topological semimetals in the absence of SOC [16, 17, 36]. As discussed in this section, the number of LCEBR compounds is relatively similar whether SOC is incorporated or neglected, whereas there are vanishingly few NLC-SM- and SEBR-SM-classified materials in the absence of SOC. Most specifically, the combined numbers of SEBR- and ESFD-classified materials with SOC ( $2,814 + 9,485 = 12,299$ ) is close to the number of ESFD-classified materials without SOC (13,997), the number of NLC- and ES-classified materials with SOC ( $2,568 + 3,785 = 6,353$ ) is close to the number of NLC-SM- and ES-classified materials without SOC ( $251 + 6,006 = 6,257$ ), and the number of SEBR-SM-classified materials without SOC (44) is small compared to the overall number of calculated materials (0.12% of 36,163). As explained in the text below, the relative absence of NLC-SM and SEBR-SM materials can be understood by recognizing that most NLC- and SEBR-classified materials with SOC become ES-classified when SOC is neglected, because there are significantly many more ways for materials to fail to satisfy the compatibility relations [28, 92, 93] in the absence of SOC [58].

In Table S11, we show the number (and percentage) of materials in each stable topological class at  $E_F$  in the calculations performed with and w/o SOC for the unique materials (defined in Ref. [38] and in the main text) for which DFT calculations (performed as detailed in S4) converged both with and without incorporating the effects of SOC. We note that while the number of LCEBR-classified materials are similar with and w/o SOC, there are large differences across the other four stable topological classes. Most notably, in Table S11, the number of NLC-

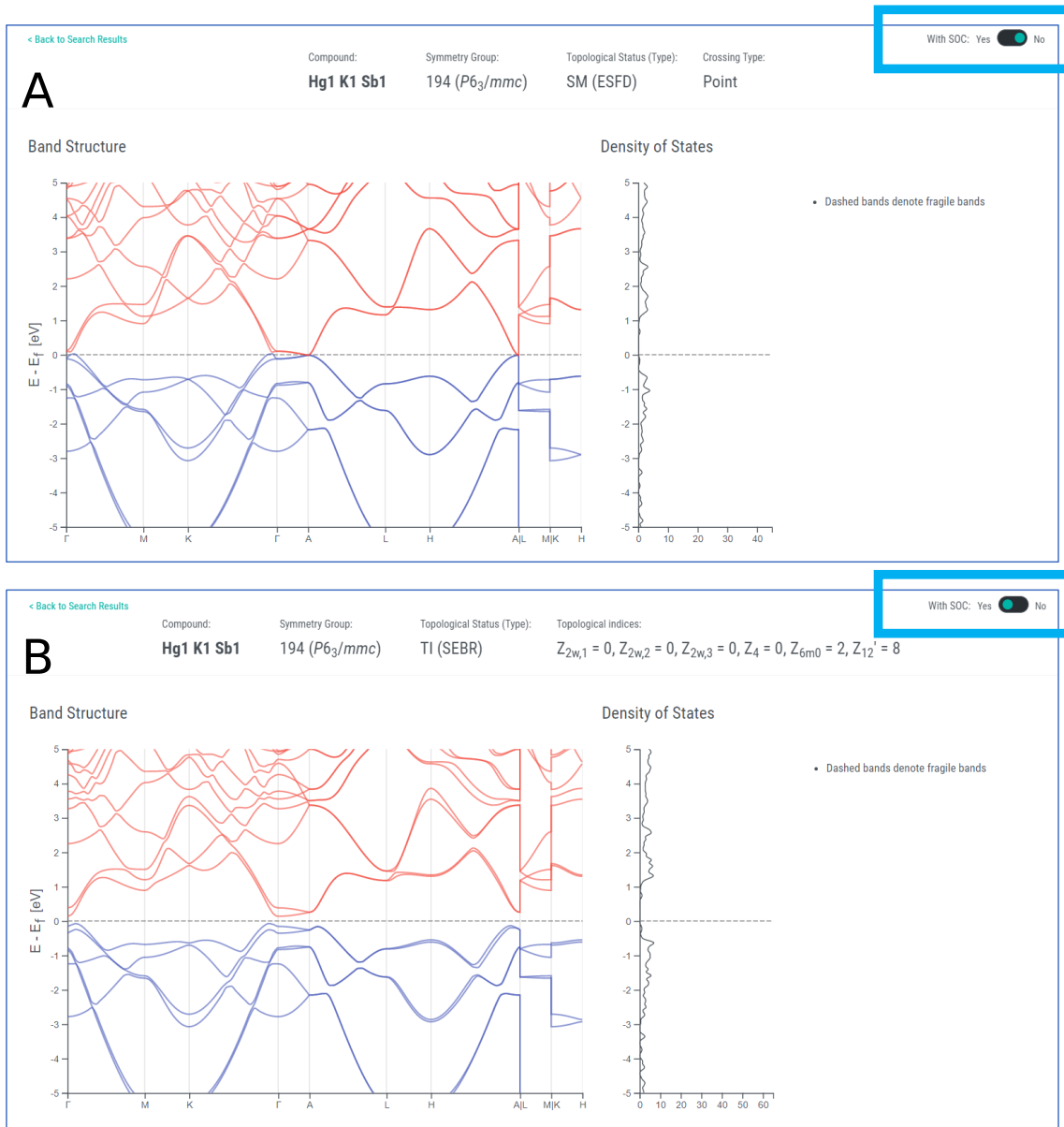


Figure S1. The electronic structure of the candidate hourglass TCI KHgSb (ICSD 56201, see Refs. [13, 14, 110, 128, 129] and S11A6) without (A) and with (B) the effects of SOC incorporated. Users can toggle between the first-principles analysis and topological data for each material on <https://www.topologicalquantumchemistry.com/> with and without SOC by clicking the switch highlighted in the blue box in the top-right corners of panels A and B.

and ES-classified materials with SOC ( $2,568 + 3,785 = 6,353$ ) is close to the number of NLC-SM- and ES-classified materials w/o SOC ( $251 + 6,006 = 6,257$ ), and the number of SEBR-SM-classified materials w/o SOC (44) is small compared to the overall number of calculated materials (0.12% of 36,163). In particular, the number of NLC-SM- and SEBR-SM-classified materials w/o SOC in Table S11 ( $251 + 44 = 295$ ) is smaller by roughly a factor of 20 than the number of NLC- and SEBR-classified materials with SOC ( $2,568 + 2,814 = 5,382$ ).

This difference can be understood by recognizing that the matrix representatives of twofold symmetries, such as mirror reflection and twofold rotation, anticommute in the presence of SOC, but *commute* in the absence of SOC, and that twofold crystal symmetries without translations have real-valued (imaginary-valued) eigenvalues in the absence (presence) of SOC [56, 130]. This implies that many more symmetry operations have simultaneously well-defined eigenvalues at each  $\mathbf{k}$  point in the absence of SOC than in the presence of SOC in nonmagnetic materials. Consequently, along high-symmetry lines and planes with the same symmetry, there are typically many more small irreducible corepresentation (corep) labels in the absence of SOC than in its presence. For this reason, when bands are inverted in a material w/o SOC, the material is much more likely to become ES-classified (and thus fail to satisfy the compatibility relations) than it is to become NLC-SM-classified, whereas in the presence of SOC, the material has a significantly greater chance of becoming NLC-classified after a bulk band inversion.

As an example, consider a TRIM point  $\mathbf{k}$  in a material where the little group  $G_{\mathbf{k}}$  contains twofold rotation  $\{C_{2z}|000\}$ , inversion  $\{\mathcal{I}|000\}$ , and time-reversal  $\{\mathcal{T}|000\}$  symmetries. The combination of inversion and twofold rotation also implies the presence of a mirror symmetry  $\{M_z|000\} = \{\mathcal{I}|000\}\{C_{2z}|000\}$ . Without SOC, the matrix representatives of inversion, twofold rotation, and mirror symmetries commute, and hence all three symmetries have simultaneously well-defined (real-valued) eigenvalues. There are therefore four one-dimensional (per spin), single-valued coreps at  $\mathbf{k}$ , which may be labeled by their  $\{C_{2z}|000\}$  and  $\{\mathcal{I}|000\}$  eigenvalues. When bands with distinct parity (inversion) eigenvalues are inverted at  $\mathbf{k}$  in the absence of SOC, protected crossing points appear along the twofold rotation axis if the bands carry distinct  $\{C_{2z}|000\}$  eigenvalues and the same  $\{M_z|000\}$  eigenvalues, or appear in the mirror plane if the inverted bands instead carry distinct  $\{M_z|000\}$  eigenvalues and the same  $\{C_{2z}|000\}$  eigenvalues. Conversely with SOC, the eigenvalues of  $\{C_{2z}|000\}$  are imaginary numbers  $\pm i$ , and states with distinct  $\{C_{2z}|000\}$  eigenvalues are paired by  $\{\mathcal{T}|000\}$  symmetry at  $\mathbf{k}$ , and by  $\{\mathcal{I} \times \mathcal{T}|000\}$  symmetry away from  $\mathbf{k}$ . Therefore in the presence of SOC,  $G_{\mathbf{k}}$  has only two, two-dimensional, double-valued small coreps that may be labeled by their Kramers pairs of distinct parity (inversion) eigenvalues. Hence, when bands with distinct parity eigenvalues are inverted at  $\mathbf{k}$  with SOC, protected crossing points do not appear, absent additional symmetries.

Lastly, we note that the general trend of increased band connectivity w/o SOC also extends away from  $E_F$  across the stoichiometric materials in the ICSD. We specifically find that 1,047 ICSD entries with SOC (corresponding to 508 unique materials) contain a connected grouping of bands with at least  $N_e$  states at each  $\mathbf{k}$  point, where  $N_e$  is the number of valence electrons. Conversely, 20,899 ICSD entries w/o SOC (corresponding to 10,313 unique materials) contain a connected grouping of bands with at least  $N_e$  states at each  $\mathbf{k}$  point (taking bands w/o SOC to be spin-degenerate). In S8 we will also discuss the extreme case of *supermetallic* (SMetal) materials, in which *all* of the bands included in our VASP calculations are connected (see S4 for calculation details). Further supporting the trend of increased band connectivity in the absence of SOC, <https://www.topologicalquantumchemistry.com/> contains 17 unique SMetal materials with SOC, whereas there are 1,138 unique SMetal materials w/o SOC, representing a hundred-fold increase compared to calculations performed with SOC in the number of materials with fully-connected valence bands up to the energy (filling) cutoff of  $\sim 2N_e$  imposed in our VASP calculations (see S4). Further statistics for materials with highly connected bands on <https://www.topologicalquantumchemistry.com/>, as well as material examples, are provided in S8.

## B. Physical Interpretation of the NLC and SEBR Materials Classes in the Absence of SOC

To determine the topological class of a material in the absence of SOC, we use the same methods previously employed in Ref. [38]. First, we determine if the coreps of the occupied bands at all high-symmetry points satisfy the compatibility relations [28, 92, 93] for an insulating gap to exist at  $E_F$ . If the insulating compatibility relations are not satisfied, then the material is classified as either an ESFD semimetal (in which a band degeneracy at a high-symmetry point is partially occupied) or an ES semimetal (in which the compatibility relations fail along a line or plane in the BZ).

Without SOC, ES and ESFD semimetals exhibit topological boundary states analogous to those of topological semimetals with strong SOC. For ESFD materials, it has been extensively shown [131–133] that if the little group of the  $\mathbf{k}$  point of the nodal degeneracy is isomorphic to a chiral SG (defined in this work as an SG without rotoin-

version symmetries, more formally referenced as a *Sohncke* SG, see Ref. [134]), then the nodal point will carry a topological chiral charge, and will exhibit associated topological surface Fermi arcs. As demonstrated in several recent theoretical and experimental studies [9, 23–25, 131, 135, 136], the surface Fermi arcs are qualitatively the same in dispersion and length in strong- and weak-SOC ESFD semimetals whose nodal degeneracies lie at high-symmetry points with chiral little groups. Specifically, large topological Fermi arcs are typically present in ESFD semimetals in chiral SGs both with and without SOC – in the weak-SOC case, the Fermi arcs are spin-degenerate, whereas in the strong-SOC case, the Fermi arcs are highly-spin-polarized [25, 131], but are typically only weakly split by SOC [23, 24, 135, 136]. In weak-SOC ES semimetals, the nodal degeneracies are typically nodal lines, which are protected by a combination of coreps with different symmetry eigenvalues and weak-SOC topological invariants (*e.g.*, local  $\mathcal{I} \times \mathcal{T}$ -symmetry protection, as introduced in Ref. [31]). When SOC is negligible, all bulk nodal lines carry associated flat-band-like topological “drumhead” surface states [31, 137], which represent the weak-SOC (nondispersing) limit of the twofold surface Dirac cones of 3D TIs and TCIs. Additionally, it has recently been shown that more exotic, “monopole-charged” variants [138–141] of weak-SOC nodal lines also exhibit flat-band-like hinge states that are representative of a *higher-order* bulk-boundary correspondence, and correspond to the weak-SOC (nondispersing) limit of the helical hinge states of higher-order TIs [34].

In the cases where a material w/o SOC is classified as NLC or SEBR, the differences with the strong-SOC case are more pronounced. First, it was shown in Refs. [16, 17, 36] that 3D, time-reversal- ( $\mathcal{T}$ -) symmetric (*i.e.* nonmagnetic), symmetry-indicated, topological insulating phases are only stable in the presence of non-negligible SOC. However, it was also shown in Refs. [29, 36, 37, 39, 142] that the valence bands of real materials, when SOC is neglected, are still capable of simultaneously satisfying the insulating compatibility relations while not being equivalent to a linear combination of trivial bands. This presents an apparent contradiction: namely, a set of valence bands in a 3D material without SOC cannot be topologically nontrivial if stable (strong) topological bands do not exist in 3D,  $\mathcal{T}$ -symmetric systems without SOC. The resolution – discovered in Ref. [36] – is that in fact *all* NLC- and SEBR-classified materials in the absence of SOC are special cases of topological semimetals that satisfy the compatibility relations for insulators. Specifically, the compatibility relations are only capable of determining if the symmetry eigenvalues (small coreps) of the occupied bands can be smoothly connected to each other along all  $k$  paths with crystal symmetry eigenvalues. However, bulk nodal degeneracies such as Weyl points [143] and nodal lines w/o SOC [138, 139] can also be stabilized by topological invariants evaluated on closed manifolds in momentum space (*e.g.* the Chern number evaluated on a sphere surrounding a Weyl point), *even if the crossing bands have the same corep labels*. In the relatively few materials on <https://www.topologicalquantumchemistry.com/> that are classified as NLC-SM or SEBR-SM in the calculations performed w/o SOC (Tables S12 and S13, respectively), a bulk gap is permitted along all high-symmetry lines and planes, but there is no gap in the BZ interior in the calculations performed w/o SOC.

To classify the NLC-SM and SEBR-SM phases of the materials on <https://www.topologicalquantumchemistry.com/> in the calculations performed w/o SOC, we have employed the SI formulas (topological indices and notation) of Ref. [36]. We note that in the notation of Ref. [36], the  $\mathbb{Z}_2$ -valued strong nodal-line-semimetal parity index introduced in Ref. [31] (which is the vanishing-SOC analog of the Fu-Kane parity index [5, 30]), does not appear on <https://www.topologicalquantumchemistry.com/>. Instead, the  $\mathbb{Z}_2$  nodal-line index from Ref. [31] has been subsumed by the  $\mathbb{Z}_4$ -valued parity index  $z_4$  that captures both monopole-charged and uncharged nodal lines, and is the vanishing-SOC (spinless) analog of the  $\mathbb{Z}_4$ -valued index  $Z_4$  for spinful HOTIs discussed in Refs. [16, 17, 29, 33, 34, 139] and in S11A3. Specifically, in nonmagnetic materials with inversion symmetry,  $z_4 = 1, 2, 3$  phases are all nodal-line semimetals. If the values of all other spinless SIs (*e.g.* weak indices) are trivial, then the nodal lines in a  $z_4 = 1, 3$  ( $z_4 = 2$ ) NLC-SM or SEBR-SM carry trivial (nontrivial) monopole charges [34, 139].

To compare the ES nodal-line semimetals that are prevalent throughout <https://www.topologicalquantumchemistry.com/> (S6A) to the nodal-line topological indices previously introduced in Refs. [31, 36], we have produced subduction tables at the bottom of each material page on <https://www.topologicalquantumchemistry.com/>. Specifically, following the procedure employed in Refs [38, 114, 144], the most familiar [31, 34, 36] strong  $\mathbb{Z}_4$  and weak  $\mathbb{Z}_2$  parity indices for ES-classified, centrosymmetric, nodal line semimetals w/o SOC ( $z_4$  and  $z_{2,i}$  respectively) can be obtained by consulting the subduction table entry for SG 2 ( $P\bar{1}$ ) in calculations performed w/o SOC [noting

that, if  $z_4$  and  $z_{2,i}$  are trivial for all  $i = 1, 2, 3$ , then the subduction table will not display an entry for SG 2 ( $P\bar{1}$ ). During the preparation of this work, an alternative method for diagnosing the topology of ES-classified nodal-line semimetals in the absence of SOC was also introduced in Refs. [145, 146], providing additional context for the subduction tables on <https://www.topologicalquantumchemistry.com/> generated for the present work.

Table S12: List of all nonmagnetic unique materials without  $f$  electrons that are classified as NLC-SM in calculations performed w/o SOC. In this table, a chemical formula with a \* indicates that some (but not all) of the ICSDs associated to the same unique material (defined using its topological class with SOC) are classified as NLC-SM in calculations for the same ICSD entries performed w/o SOC. In this table, the topological indices (spinless SIs) at  $E_F$  of the calculations performed w/o SOC are listed in the notation of Ref. [36]. Further details and the physical interpretation of each spinless SI in this table are provided in Ref. [36].

Chem. formula	SG #	SG symbol	ICSD	Line/Weyl	no-SOC topological indices
CaAs <sub>3</sub>	2	$P\bar{1}$	<a href="#">193</a>	Line	$z_{2,1} = 1 \ z_{2,2} = 0 \ z_{2,3} = 0 \ z_4 = 1$
CaP <sub>3</sub>	2	$P\bar{1}$	<a href="#">74479</a>	Line	$z_{2,1} = 0 \ z_{2,2} = 1 \ z_{2,3} = 0 \ z_4 = 1$
Ba(Mo <sub>6</sub> S <sub>8</sub> )	2	$P\bar{1}$	<a href="#">85490</a>	Line	$z_{2,1} = 0 \ z_{2,2} = 0 \ z_{2,3} = 0 \ z_4 = 3$
Bi	2	$P\bar{1}$	<a href="#">426929</a>	Line	$z_{2,1} = 0 \ z_{2,2} = 0 \ z_{2,3} = 1 \ z_4 = 3$
YAsS	14	$P2_1/c$	<a href="#">611344</a>	Line	$z'_2 = 1 \ z_4 = 2$
FeH <sub>4</sub>	11	$P2_1/m$	<a href="#">187148</a>	Line	$z'_2 = 1 \ z_4 = 2$
Al <sub>2</sub> Fe <sub>3</sub> Si <sub>3</sub>	2	$P\bar{1}$	<a href="#">422342</a>	Line	$z_{2,1} = 0 \ z_{2,2} = 1 \ z_{2,3} = 0 \ z_4 = 3$
Sr <sub>2</sub> Co(SeO <sub>3</sub> ) <sub>3</sub>	2	$P\bar{1}$	<a href="#">79204</a>	Line	$z_{2,1} = 0 \ z_{2,2} = 1 \ z_{2,3} = 1 \ z_4 = 1$
KH <sub>2</sub> PO <sub>3</sub>	14	$P2_1/c$	<a href="#">37072</a>	Line	$z'_2 = 1 \ z_4 = 2$
YAsSe	14	$P2_1/c$	<a href="#">611398</a>	Line	$z'_2 = 1 \ z_4 = 2$
Ag(SO <sub>4</sub> )	2	$P\bar{1}$	<a href="#">421341</a>	Line	$z_{2,1} = 1 \ z_{2,2} = 1 \ z_{2,3} = 1 \ z_4 = 1$
ScH <sub>3</sub>	12	$C2/m$	<a href="#">670220</a>	Line	$z'_2 = 1 \ z_{2,2} = 1 \ z_{2,1} = 1 \ z_4 = 2$
Cu <sub>4</sub> Mo <sub>6</sub> Se <sub>8</sub>	2	$P\bar{1}$	<a href="#">171431</a>	Line	$z_{2,1} = 1 \ z_{2,2} = 1 \ z_{2,3} = 1 \ z_4 = 1$
K(OS <sub>2</sub> O <sub>6</sub> )	2	$P\bar{1}$	<a href="#">419880</a>	Line	$z_{2,1} = 1 \ z_{2,2} = 1 \ z_{2,3} = 0 \ z_4 = 3$
Cu(N(CN) <sub>2</sub> ) <sub>2</sub> (NH <sub>3</sub> ) <sub>2</sub>	2	$P\bar{1}$	<a href="#">425593</a>	Line	$z_{2,1} = 0 \ z_{2,2} = 1 \ z_{2,3} = 0 \ z_4 = 1$
Rh <sub>3</sub> Ga <sub>5</sub>	2	$P\bar{1}$	<a href="#">240179</a>	Line	$z_{2,1} = 1 \ z_{2,2} = 0 \ z_{2,3} = 0 \ z_4 = 0$
(PCl <sub>4</sub> ) <sub>2</sub> (Mo <sub>2</sub> Cl <sub>10</sub> )	2	$P\bar{1}$	<a href="#">50441</a>	Line	$z_{2,1} = 1 \ z_{2,2} = 0 \ z_{2,3} = 0 \ z_4 = 3$
PbPt <sub>2</sub> O <sub>4</sub>	2	$P\bar{1}$	<a href="#">59657</a>	Line	$z_{2,1} = 0 \ z_{2,2} = 1 \ z_{2,3} = 1 \ z_4 = 0$
SrMo <sub>6</sub> S <sub>8</sub>	2	$P\bar{1}$	<a href="#">65941</a>	Line	$z_{2,1} = 0 \ z_{2,2} = 0 \ z_{2,3} = 0 \ z_4 = 3$
Li <sub>5</sub> (W <sub>2</sub> O <sub>7</sub> )	2	$P\bar{1}$	<a href="#">194127</a>	Line	$z_{2,1} = 1 \ z_{2,2} = 1 \ z_{2,3} = 1 \ z_4 = 2$
Ta <sub>6</sub> S	2	$P\bar{1}$	<a href="#">202564</a>	Line	$z_{2,1} = 0 \ z_{2,2} = 0 \ z_{2,3} = 1 \ z_4 = 2$
CaMo <sub>6</sub> S <sub>8</sub>	2	$P\bar{1}$	<a href="#">619422</a>	Line	$z_{2,1} = 0 \ z_{2,2} = 0 \ z_{2,3} = 0 \ z_4 = 3$
CaCu(SiO <sub>4</sub> )(H <sub>2</sub> O)	14	$P2_1/c$	<a href="#">30926</a>	Line	$z'_2 = 1 \ z_4 = 2$
LiCuC <sub>3</sub> H <sub>4</sub> PO <sub>5</sub>	15	$C2/c$	<a href="#">243640</a>	Line	$z'_2 = 1 \ z_{2,2} = 1 \ z_{2,1} = 1 \ z_4 = 2$
Tc <sub>2</sub> P <sub>3</sub>	2	$P\bar{1}$	<a href="#">41017</a>	Line	$z_{2,1} = 0 \ z_{2,2} = 0 \ z_{2,3} = 0 \ z_4 = 1$
HgK	2	$P\bar{1}$	<a href="#">104302</a>	Line	$z_{2,1} = 0 \ z_{2,2} = 1 \ z_{2,3} = 0 \ z_4 = 2$
AgHgO <sub>2</sub>	2	$P\bar{1}$	<a href="#">670059</a>	Line	$z_{2,1} = 0 \ z_{2,2} = 1 \ z_{2,3} = 1 \ z_4 = 2$
CuAuO <sub>2</sub>	12	$C2/m$	<a href="#">670103</a>	Line	$z'_2 = 1 \ z_{2,2} = 1 \ z_{2,1} = 1 \ z_4 = 2$
Cu(WO <sub>4</sub> ) <sup>*</sup>	2	$P\bar{1}$	<a href="#">69759</a>	Line	$z_{2,1} = 0 \ z_{2,2} = 1 \ z_{2,3} = 1 \ z_4 = 3$
Cu(WO <sub>4</sub> )	2	$P\bar{1}$	<a href="#">84558</a>	Line	$z_{2,1} = 0 \ z_{2,2} = 1 \ z_{2,3} = 1 \ z_4 = 1$
FeSe	2	$P\bar{1}$	<a href="#">196300</a>	Line	$z_{2,1} = 0 \ z_{2,2} = 0 \ z_{2,3} = 1 \ z_4 = 1$
FeO <sub>3</sub>	2	$P\bar{1}$	<a href="#">671721</a>	Line	$z_{2,1} = 0 \ z_{2,2} = 1 \ z_{2,3} = 1 \ z_4 = 2$
Li <sub>4</sub> N <sub>1</sub>	2	$P\bar{1}$	<a href="#">675136</a>	Line	$z_{2,1} = 0 \ z_{2,2} = 0 \ z_{2,3} = 0 \ z_4 = 3$
CLi <sub>2</sub>	12	$C2/m$	<a href="#">670915</a>	Line	$z'_2 = 1 \ z_{2,2} = 1 \ z_{2,1} = 1 \ z_4 = 2$
Ti <sub>11</sub> Ni <sub>9</sub> Pt <sub>4</sub>	15	$C2/c$	<a href="#">168948</a>	Line	$z'_2 = 1 \ z_{2,2} = 0 \ z_{2,1} = 0 \ z_4 = 2$
VO <sub>2</sub> <sup>*</sup>	2	$P\bar{1}$	<a href="#">1502</a>	Line	$z_{2,1} = 0 \ z_{2,2} = 0 \ z_{2,3} = 1 \ z_4 = 1$
Cu(MoO <sub>4</sub> )	2	$P\bar{1}$	<a href="#">39439</a>	Line	$z_{2,1} = 1 \ z_{2,2} = 1 \ z_{2,3} = 0 \ z_4 = 0$
Tc <sub>2</sub> As <sub>3</sub>	2	$P\bar{1}$	<a href="#">66662</a>	Line	$z_{2,1} = 0 \ z_{2,2} = 0 \ z_{2,3} = 0 \ z_4 = 1$
Mo <sub>3</sub> S <sub>4</sub>	2	$P\bar{1}$	<a href="#">237587</a>	Line	$z_{2,1} = 0 \ z_{2,2} = 0 \ z_{2,3} = 1 \ z_4 = 3$
(CuCl <sub>3</sub> )(Cu <sub>2</sub> TeO <sub>3</sub> )	2	$P\bar{1}$	<a href="#">431558</a>	Line	$z_{2,1} = 0 \ z_{2,2} = 0 \ z_{2,3} = 0 \ z_4 = 3$
V <sub>6</sub> O <sub>13</sub> <sup>*</sup>	12	$C2/m$	<a href="#">50409</a>	Line	$z'_2 = 1 \ z_{2,2} = 1 \ z_{2,1} = 1 \ z_4 = 2$

Sc <sub>5</sub> Cl <sub>8</sub> N	12	<i>C</i> 2/ <i>m</i>	60856	Line	$z'_2 = 1 \ z_{2,2} = 1 \ z_{2,1} = 1 \ z_4 = 2$
Li <sub>4</sub> N <sub>1</sub>	2	<i>P</i> 1̄	675127	Line	$z_{2,1} = 0 \ z_{2,2} = 0 \ z_{2,3} = 1 \ z_4 = 0$
CsHg	2	<i>P</i> 1̄	62000	Line	$z_{2,1} = 0 \ z_{2,2} = 0 \ z_{2,3} = 1 \ z_4 = 2$
CsHg	2	<i>P</i> 1̄	150974	Line	$z_{2,1} = 0 \ z_{2,2} = 0 \ z_{2,3} = 1 \ z_4 = 0$
NiOOH	2	<i>P</i> 1̄	674656	Line	$z_{2,1} = 1 \ z_{2,2} = 0 \ z_{2,3} = 0 \ z_4 = 1$
Ti <sub>5</sub> O <sub>5</sub>	12	<i>C</i> 2/ <i>m</i>	56694	Line	$z'_2 = 1 \ z_{2,2} = 1 \ z_{2,1} = 1 \ z_4 = 2$
BaBiO <sub>3</sub>	12	<i>C</i> 2/ <i>m</i>	61499	Line	$z'_2 = 1 \ z_{2,2} = 1 \ z_{2,1} = 1 \ z_4 = 2$
Ag(V <sub>2</sub> P <sub>2</sub> O <sub>10</sub> )	14	<i>P</i> 2 <sub>1</sub> / <i>c</i>	73824	Line	$z'_2 = 1 \ z_4 = 2$
Hf <sub>8</sub> Ni <sub>21</sub>	2	<i>P</i> 1̄	2416	Line	$z_{2,1} = 0 \ z_{2,2} = 0 \ z_{2,3} = 0 \ z_4 = 1$
Ni <sub>21</sub> Zr <sub>8</sub>	2	<i>P</i> 1̄	402864	Line	$z_{2,1} = 0 \ z_{2,2} = 1 \ z_{2,3} = 0 \ z_4 = 2$
V <sub>B</sub> 3	12	<i>C</i> 2/ <i>m</i>	672902	Line	$z'_2 = 0 \ z_{2,2} = 1 \ z_{2,1} = 1 \ z_4 = 0$
Ni <sub>21</sub> Zr <sub>8</sub>	2	<i>P</i> 1̄	647148	Line	$z_{2,1} = 0 \ z_{2,2} = 1 \ z_{2,3} = 0 \ z_4 = 0$
Ag(SO <sub>4</sub> )	2	<i>P</i> 1̄	290374	Line	$z_{2,1} = 0 \ z_{2,2} = 0 \ z_{2,3} = 0 \ z_4 = 2$
BaPd <sub>2</sub> Bi <sub>2</sub>	11	<i>P</i> 2 <sub>1</sub> / <i>m</i>	416299	Line	$z'_2 = 1 \ z_4 = 2$
Ni <sub>11</sub> As <sub>8</sub>	15	<i>C</i> 2/ <i>c</i>	164878	Line	$z'_2 = 1 \ z_{2,2} = 1 \ z_{2,1} = 1 \ z_4 = 2$
BC <sub>5</sub>	2	<i>P</i> 1̄	166556	Line	$z_{2,1} = 0 \ z_{2,2} = 1 \ z_{2,3} = 1 \ z_4 = 3$
Li <sub>6</sub> P	2	<i>P</i> 1̄	673928	Line	$z_{2,1} = 0 \ z_{2,2} = 1 \ z_{2,3} = 0 \ z_4 = 3$
NiOOH	58	<i>P</i> n <i>nm</i>	674650	Line	$z'_2 = 1 \ z_4 = 2 \ z_2^- = 1 \ z_2^+ = 1$
Pb <sub>2</sub> Sr <sub>2</sub> YC <sub>3</sub> O <sub>8</sub>	2	<i>P</i> 1̄	74154	Line	$z_{2,1} = 1 \ z_{2,2} = 1 \ z_{2,3} = 0 \ z_4 = 1$
Cu(WO <sub>4</sub> )	2	<i>P</i> 1̄	169004	Line	$z_{2,1} = 1 \ z_{2,2} = 0 \ z_{2,3} = 0 \ z_4 = 3$
Sc <sub>3</sub> NiSi <sub>3</sub>	12	<i>C</i> 2/ <i>m</i>	48004	Line	$z'_2 = 1 \ z_{2,2} = 0 \ z_{2,1} = 0 \ z_4 = 2$
CLi <sub>8</sub>	2	<i>P</i> 1̄	670922	Line	$z_{2,1} = 0 \ z_{2,2} = 0 \ z_{2,3} = 1 \ z_4 = 0$
SrPd <sub>2</sub> Bi <sub>2</sub>	11	<i>P</i> 2 <sub>1</sub> / <i>m</i>	416300	Line	$z'_2 = 1 \ z_4 = 2$
Na <sub>6</sub> Ti <sub>6</sub> O <sub>13</sub>	12	<i>C</i> 2/ <i>m</i>	238302	Line	$z'_2 = 1 \ z_{2,2} = 1 \ z_{2,1} = 1 \ z_4 = 2$
Ag(SO <sub>4</sub> )	15	<i>C</i> 2/ <i>c</i>	290375	Line	$z'_2 = 1 \ z_{2,2} = 0 \ z_{2,1} = 0 \ z_4 = 2$
Au <sub>2</sub> Ca <sub>5</sub>	15	<i>C</i> 2/ <i>c</i>	58403	Line	$z'_2 = 0 \ z_{2,2} = 1 \ z_{2,1} = 1 \ z_4 = 0$
Pt <sub>5</sub> P <sub>2</sub>	15	<i>C</i> 2/ <i>c</i>	24327	Line	$z'_2 = 0 \ z_{2,2} = 1 \ z_{2,1} = 1 \ z_4 = 0$
Sb <sub>2</sub> Te <sub>3</sub>	15	<i>C</i> 2/ <i>c</i>	187497	Line	$z'_2 = 1 \ z_{2,2} = 0 \ z_{2,1} = 0 \ z_4 = 2$
NiS <sub>2</sub>	60	<i>P</i> bcn	169571	Line	$z'_2 = 1 \ z_4 = 2$
Ni <sub>10</sub> Sn <sub>5</sub> P <sub>3</sub>	2	<i>P</i> 1̄	59641	Line	$z_{2,1} = 0 \ z_{2,2} = 1 \ z_{2,3} = 1 \ z_4 = 0$
TiNi	2	<i>P</i> 1̄	150629	Line	$z_{2,1} = 1 \ z_{2,2} = 0 \ z_{2,3} = 1 \ z_4 = 3$
Cu <sub>7</sub> In <sub>3</sub>	2	<i>P</i> 1̄	429530	Line	$z_{2,1} = 0 \ z_{2,2} = 0 \ z_{2,3} = 0 \ z_4 = 2$
WNi <sub>4</sub> Pb <sub>16</sub>	15	<i>C</i> 2/ <i>c</i>	67920	Line	$z'_2 = 1 \ z_{2,2} = 1 \ z_{2,1} = 1 \ z_4 = 2$
Pd <sub>13</sub> Pb <sub>9</sub>	15	<i>C</i> 2/ <i>c</i>	648362	Line	$z'_2 = 1 \ z_{2,2} = 0 \ z_{2,1} = 0 \ z_4 = 2$
Pb <sub>9</sub> Pd <sub>13</sub>	15	<i>C</i> 2/ <i>c</i>	105593	Line	$z'_2 = 1 \ z_{2,2} = 0 \ z_{2,1} = 0 \ z_4 = 2$

Table S13: List of all nonmagnetic unique materials without *f* electrons that are classified as SEBR-SM in calculations performed w/o SOC. In this table, a chemical formula with a \* indicates that some (but not all) of the ICSDs associated to the same unique material (defined using its topological class with SOC) are classified as SEBR-SM in calculations for the same ICSD entries performed w/o SOC. In this table, the topological indices (spinless SIs) at  $E_F$  of the calculations performed w/o SOC are listed in the notation of Ref. [36]. Further details and the physical interpretation of each spinless SI in this table are provided in Ref. [36].

Chem. formula	SG #	SG symbol	ICSD	Line/Weyl	no-SOC topological indices
Tl <sub>6</sub> TeO <sub>12</sub>	148	<i>R</i> 3	37134	Line	$z_{2,3} = 0 \ z_4 = 3 \ z_{2,1} = 0 \ z_{2,2} = 0$
Mo <sub>6</sub> Te <sub>8</sub>	148	<i>R</i> 3̄	59375	Line	$z_{2,3} = 1 \ z_4 = 3 \ z_{2,1} = 1 \ z_{2,2} = 1$
Sc <sub>7</sub> Cl <sub>12</sub> N	148	<i>R</i> 3̄	201976	Line	$z_{2,3} = 1 \ z_4 = 3 \ z_{2,1} = 1 \ z_{2,2} = 1$
Mo <sub>3</sub> Te <sub>4</sub>	148	<i>R</i> 3̄	644477	Line	$z_{2,3} = 1 \ z_4 = 1 \ z_{2,1} = 1 \ z_{2,2} = 1$
Mo <sub>3</sub> S <sub>4</sub>	148	<i>R</i> 3̄	600385	Line	$z_{2,3} = 1 \ z_4 = 2 \ z_{2,1} = 1 \ z_{2,2} = 1$
NiTi <sub>3</sub> S <sub>6</sub>	148	<i>R</i> 3̄	26312	Line	$z_{2,3} = 1 \ z_4 = 3 \ z_{2,1} = 1 \ z_{2,2} = 1$
Mo <sub>3</sub> Se <sub>4</sub>	148	<i>R</i> 3̄	600386	Line	$z_{2,3} = 1 \ z_4 = 1 \ z_{2,1} = 1 \ z_{2,2} = 1$
Mo <sub>8</sub> Ga <sub>40</sub> C	148	<i>R</i> 3̄	617918	Line	$z_{2,3} = 1 \ z_4 = 3 \ z_{2,1} = 1 \ z_{2,2} = 1$
Ni <sub>3</sub> AsIn	148	<i>R</i> 3̄	671511	Line	$z_{2,3} = 1 \ z_4 = 3 \ z_{2,1} = 1 \ z_{2,2} = 1$

MoN <sub>2</sub>	166	<i>R</i> $\bar{3}m$	<a href="#">674587</a>	Line	$z'_2 = 1 \ z_4 = 2$
Mo <sub>6</sub> S <sub>8</sub>	148	<i>R</i> $\bar{3}$	<a href="#">252376</a>	Line	$z_{2,3} = 1 \ z_4 = 2 \ z_{2,1} = 1 \ z_{2,2} = 1$
SiO <sub>2</sub>	162	<i>P</i> $\bar{3}1m$	<a href="#">170552</a>	Line	$z'_2 = 1 \ z_4 = 2$
Ca <sub>3</sub> Au <sub>4</sub>	148	<i>R</i> $\bar{3}$	<a href="#">54547</a>	Line	$z_{2,3} = 1 \ z_4 = 0 \ z_{2,1} = 1 \ z_{2,2} = 1$
Na <sub>4</sub> Cl <sub>3</sub>	148	<i>R</i> $\bar{3}$	<a href="#">672989</a>	Line	$z_{2,3} = 1 \ z_4 = 2 \ z_{2,1} = 1 \ z_{2,2} = 1$
Bi <sub>2</sub> Pt	147	<i>P</i> $\bar{3}$	<a href="#">58847</a>	Line	$z_{2,3} = 1 \ z_4 = 2$
Ni <sub>4</sub> Ti <sub>3</sub>	148	<i>R</i> $\bar{3}$	<a href="#">105422</a>	Line	$z_{2,3} = 1 \ z_4 = 2 \ z_{2,1} = 1 \ z_{2,2} = 1$
Ge <sub>9</sub> Pd <sub>25</sub>	147	<i>P</i> $\bar{3}$	<a href="#">637543</a>	Line	$z_{2,3} = 1 \ z_4 = 3$

## S7. MAJOR UPDATES TO THE TOPOLOGICAL MATERIALS DATABASE

In this section, we will briefly overview the most significant changes implemented on the [Topological Materials Database](https://www.topologicalquantumchemistry.com/) (<https://www.topologicalquantumchemistry.com/>) for this work, following its initial introduction in Ref. [38]. To begin, in one of the most significant changes implemented on <https://www.topologicalquantumchemistry.com/> for this work, we have processed the complete set of stoichiometric materials in the ICSD, leading to a current total set of 73,234 ICSD entries on <https://www.topologicalquantumchemistry.com/> with electronic structures and topological data in the presence of SOC (see S4 for first-principles calculation details). This represents an increase of roughly  $\sim 50,000$  ICSD entries from the previous content of <https://www.topologicalquantumchemistry.com/> generated for Ref. [38]. Beyond the large increase in the number of listed ICSD entries, we have also for this work implemented the following major changes on <https://www.topologicalquantumchemistry.com/>:

- For the large majority of the ICSD entries accessible on <https://www.topologicalquantumchemistry.com/> (69,730 of 73,234 ICSD entries), the electronic structures and topological data are now available with and without the effects of SOC incorporated (see S6).
- The electronic band structure and density of states for each entry on <https://www.topologicalquantumchemistry.com/> are displayed with dynamical zoom options. Additionally, by hovering the pointer over a Bloch state in the electronic structure plot or over an energy in the density of states, contextual information can now be accessed, including the energy and the magnitude of the direct gaps above and below a given Bloch state.
- We have for the first time computed the complete set of symmetry-indicated fragile bands above the core shell [43–46] for each stoichiometric ICSD entry. In each band structure plot, the largest sets of bands with cumulative symmetry-indicated fragile topology are labeled with dashed lines. On each entry on <https://www.topologicalquantumchemistry.com/> with fragile topological bands, we have also provided a table summarizing the details of the fragile bands.
- We have introduced a “Topological Data” table for each entry on <https://www.topologicalquantumchemistry.com/> that lists the symmetry-indicated stable and fragile topology of each connected grouping of bands, as well as the cumulative stable and fragile topology of the total set of bands occupied up to each insulating electronic filling as determined by band connectivity (see S2 and S8).
- For each electronic structure calculation on <https://www.topologicalquantumchemistry.com/>, we have made the VASP input POSCAR files and the k-path files available for download through links provided below the crystallographic lattice data.

In addition to the basic search options based on chemical composition and ICSD accession codes previously implemented for Ref. [38], we have for this work implemented advanced materials search criteria (see Fig. S2), which include:

- The SG of the ICSD entry.
- The number of atoms in the unit cell (denoted as “No. of elements”).
- The number of valence electrons.
- The direct and indirect band gaps at  $E_F$ .
- The dimensionality (point, line, or plane) of the high-symmetry manifold(s) containing the crossing point(s) at  $E_F$  if the bulk at  $E_F$  is an enforced topological semimetal (ES- or ESFD-classified).
- The number of times that the bands at  $E_F$  cross the Fermi level along the plotted  $\mathbf{k}$ -path, subdivided by valence and conduction bands.
- The values of the stable SIs [5, 16, 17, 22, 29, 30, 32–34, 87] if the bulk is an NLC- or SEBR-classified topological (crystalline) insulator at  $E_F$  when the effects of SOC are incorporated (see S2).

Importantly, users may simultaneously specify several advanced search criteria. For example, users may search for weak TIs that contain the element Bi and have  $z$ -directed weak-index vectors [5, 16, 30, 147, 148] by entering Bi into the “Compound Contains” bar while specifying the stable SIs  $Z_{2w,1} = 0$ ,  $Z_{2w,2} = 0$ , and  $Z_{2w,3} = 1$  and either  $Z_4 = 0$  or  $Z_4 = 2$  in the “Topological Insulator Filters” in the “Advanced Search” drop-down menu (see Fig. S2). Further discussions regarding the differences between  $Z_4 = 0$  and  $Z_4 = 2$  weak TIs are provided in S11 A 6.

After performing a basic or advanced search, users are provided a list of matching ICSD entries sorted by the symmetry-indicated stable topological class at  $E_F$  in the presence of SOC [“TI” (NLC or SEBR), “SM” (ES or ESFD), or “Trivial” (LCEBR), see Fig. S2]. After choosing an ICSD entry from the search results, users are redirected to the specific page on <https://www.topologicalquantumchemistry.com/> for the ICSD entry; in Fig. S3 we show as an example the material page on <https://www.topologicalquantumchemistry.com/> for the (obstructed) weak TI  $\text{Bi}_3\text{S}\text{Te}_2$  [ICSD 107587, SG 164 ( $P\bar{3}m1$ )] (see S11 A 6 and Refs. [5, 16, 26, 30, 147–150]). On the page for each ICSD entry on <https://www.topologicalquantumchemistry.com/>, we provide data including:

- The stoichiometric chemical formula, the SG, the crystal lattice parameters, the topological classification at  $E_F$ , a dropdown menu of the other ICSD entries associated to the same unique material (see S4), the values of the stable SIs [5, 16, 17, 22, 29, 30, 32–34, 87] if the ICSD entry is NLC- or SEBR-classified at  $E_F$ , and, if the bulk at  $E_F$  is an enforced topological semimetal (ES- or ESFD-classified), whether the crossing point lies at a high-symmetry point or along a high-symmetry line or plane.
- Interactive 3D plots of the real-space crystal structure and the first BZ.
- Interactive plots of the electronic band structure and the density of states.
- The direct gaps at  $E_F$  at the high-symmetry  $\mathbf{k}$  points, defined both by occupation as determined by VASP and by band index.
- The “Topological Data” table discussed earlier in this section, which contains the individual and cumulative symmetry-indicated topology of each connected of bands as determined by the compatibility relations (*i.e.* by band connectivity, see S2).
- Information for the largest sets of bands with cumulative symmetry-indicated fragile topology in the electronic structure [43–46].
- If the topological classification at  $E_F$  is ES, then we provide a table listing the high-symmetry manifolds along which enforced crossing points are required to appear.

- The stable SIs [5, 16, 17, 22, 29, 30, 32–34, 87] of the lowest-symmetry nonmagnetic NLC and SEBR phases that can be realized by breaking crystal symmetries, computed by subduction onto lower-symmetry SGs as detailed in Refs. [29, 114]. There are two cases in which the “Transitions upon symmetry lowering” table is not displayed. First, the “Transitions upon symmetry lowering,” table is not displayed if the bulk cannot be driven by infinitesimal symmetry-breaking into a nonmagnetic NLC or SEBR phase (*i.e.* if the symmetry-indicated stable topology is trivial for all possible group-subgroup subductions). Second, the “Transitions upon symmetry lowering” table is also absent for ESFD materials that are filling-enforced (semi)metals [see Refs. [130, 151, 152]] with accidental degeneracies at  $E_F$  [defined in S3 A], which prevent the unambiguous identification of subduced small coreps.

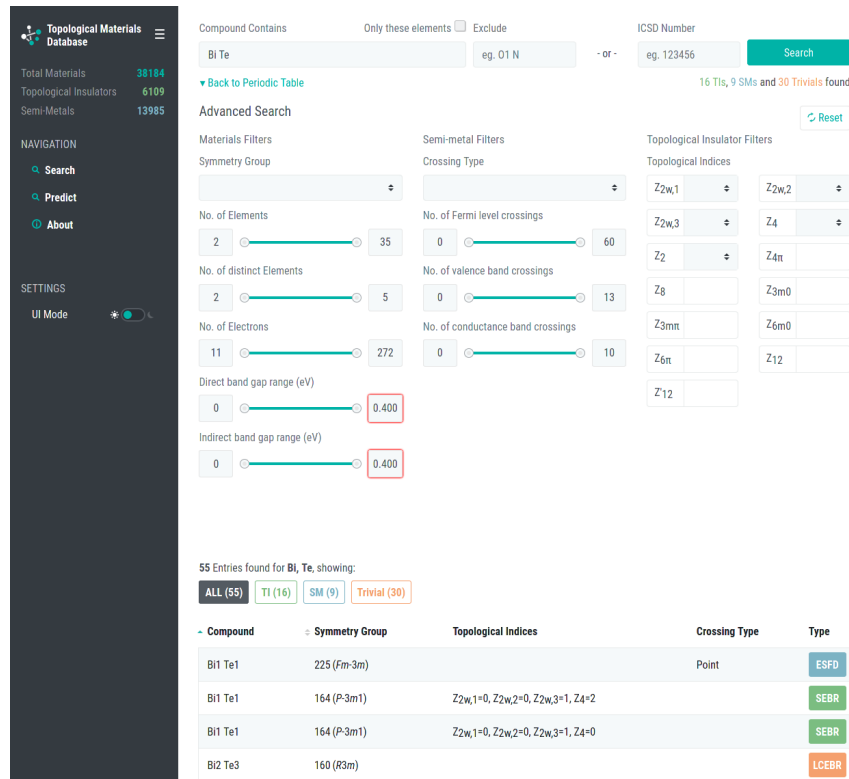


Figure S2. A screenshot of the search interface of the updated Topological Materials Database (<https://www.topologicalquantumchemistry.com/>). The top three search bars allow basic search options based on chemical composition and ICSD accession codes. For this work, we have additionally implemented the “Advanced Search” features displayed below the “Back to Periodic Table” button, which are further detailed in this section.

Finally, many of the ICSD entries listed on <https://www.topologicalquantumchemistry.com/> are also analyzed on the Materials Project (MP) [126]. While the Topological Materials Database introduced in Ref. [38] and expanded in this work focuses on the electronic band topology of a given material, the MP provides a general analysis focused on magnetic, structural, and chemical material properties. For materials that are listed both on <https://www.topologicalquantumchemistry.com/> and on the MP, we provide on each ICSD entry page on <https://www.topologicalquantumchemistry.com/> a link to the corresponding MP page. Additionally, for materials that are listed both on <https://www.topologicalquantumchemistry.com/> and on the MP, the MP entry page extracts and reproduces the topological classification at  $E_F$  with SOC from the corresponding ICSD entry page on <https://www.topologicalquantumchemistry.com/>.

## S8. STATISTICS FOR ALL OF THE TOPOLOGICAL BANDS AND BAND CONNECTIVITY IN THE ICSD

The ICSD contains 193,426 entries [41]. In this work, we have analyzed the complete set of 96,196 ICSD entries with stoichiometric chemical formulas and processable (non-corrupt) CIF structure files, achieving convergent electronic-structure calculations for 73,234 ICSD entries with SOC and 69,730 ICSD entries w/o SOC, corresponding to 38,298 unique materials (see S4 for calculation details and for the definition of unique materials employed in this work). In this section, we will provide a detailed statistical breakdown of the symmetry-indicated topological classification of all isolated sets of bands in all of the ICSD entries analyzed in this work as determined by band connectivity through TQC (see S2). This includes diagnoses of both symmetry-indicated stable [5, 16, 17, 22, 29, 30, 32–34, 87] and fragile [43, 45, 46] topology across all of the bands included in our first-principles calculations, as well as statistics for and examples of materials with large band connectivities. First, in S8 A, we will provide detailed statistics for the stable topological classification at  $E_F$  with and w/o SOC of all of the stoichiometric materials in the ICSD. Then, in S8 B, we will provide detailed statistics for the stable and fragile topological classification of all of the isolated bands (as defined by band connectivity, see S2) in the ICSD. We will also in S8 B provide statistics for and examples of materials with extremely large band connectivities.

### A. Topological Classification at the Fermi Level for all of the Stoichiometric Unique Materials in the ICSD with and w/o SOC

In this section, we will provide statistics for the topological classification at the Fermi level for the unique materials studied in this work (defined in the main text and in S4). Specifically, in Table S14 (Table S15), we list the number of materials whose valence bands are in total classified by one of the four stable topological classes introduced in Ref. [38]: NLC (-SM), SEBR (-SM), ES, and ESFD. We note that, using the symmetry-based indicators for fragile topology introduced in Refs. [43, 45, 46], we did not identify any ICSD entries in which the total set of occupied (valence) bands was fragile topological with or w/o SOC (though we did identify energetically-isolated fragile bands near the Fermi energy in many materials, see S8 B and S11 E).

Table S14: The number of unique materials in each of the topological classes (as defined in the main text and in Ref. [38]) in calculations performed with SOC. In this table, the topology of a material is taken to be the total (cumulative) topology of all of the bands occupied up to  $E_F$ . In order, the columns in this table list the SG, the number of unique materials in the SG, the number of TIs and TCIs (defined as either NLC or SEBR) in the SG, the number of semimetals (SMs) in the SG (defined as either ES or ESFD), the number of unique materials with trivial symmetry-indicated topology (LCEBR) in the SG, the number of NLC-classified TIs and TCIs in the SG, the number of SEBR-classified TIs and TCIs in the SG, the number of ES-classified SMs in the SG, and the number of ESFD-classified SMs in the SG. For all of the topological classification categories in the table, each number of materials is accompanied by the percentage of materials in the SG in the topological class. When there are no materials in the topological class, the table entry is marked with a dashed horizontal line.

SG	# Mat.	TIs	SMs	Trivial	NLC	SEBR	ES	ESFD
1	151	—	9 (6.0%)	142 (94.0%)	—	—	—	9 (6.0%)
2	1574	182 (11.6%)	116 (7.4%)	1276 (81.1%)	182 (11.6%)	—	—	116 (7.4%)
3	13	—	—	13 (100%)	—	—	—	—
4	228	—	8 (3.5%)	220 (96.5%)	—	—	8 (3.5%)	—
5	156	—	15 (9.6%)	141 (90.4%)	—	—	—	15 (9.6%)
6	28	—	1 (3.6%)	27 (96.4%)	—	—	—	1 (3.6%)
7	85	—	3 (3.5%)	82 (96.5%)	—	—	3 (3.5%)	—
8	144	—	13 (9.0%)	131 (91.0%)	—	—	—	13 (9.0%)
9	199	—	11 (5.5%)	188 (94.5%)	—	—	11 (5.5%)	—
10	38	20 (52.6%)	5 (13.2%)	13 (34.2%)	20 (52.6%)	—	—	5 (13.2%)
11	587	95 (16.2%)	105 (17.9%)	387 (65.9%)	95 (16.2%)	—	—	105 (17.9%)

12	1345	432 (32.1%)	204 (15.2%)	709 (52.7%)	219 (16.3%)	213 (15.8%)	—	204 (15.2%)
13	195	20 (10.3%)	36 (18.5%)	139 (71.3%)	20 (10.3%)	—	—	36 (18.5%)
14	2665	298 (11.2%)	224 (8.4%)	2143 (80.4%)	298 (11.2%)	—	74 (2.8%)	150 (5.6%)
15	1485	122 (8.2%)	200 (13.5%)	1163 (78.3%)	122 (8.2%)	—	—	200 (13.5%)
16	2	—	—	2 (100%)	—	—	—	—
17	8	—	—	8 (100%)	—	—	—	—
18	30	—	2 (6.7%)	28 (93.3%)	—	—	—	2 (6.7%)
19	270	—	20 (7.4%)	250 (92.6%)	—	—	20 (7.4%)	—
20	66	—	2 (3.0%)	64 (97.0%)	—	—	2 (3.0%)	—
21	16	—	6 (37.5%)	10 (62.5%)	—	—	—	6 (37.5%)
22	17	—	—	17 (100%)	—	—	—	—
23	16	—	2 (12.5%)	14 (87.5%)	—	—	—	2 (12.5%)
24	2	—	—	2 (100%)	—	—	—	—
25	45	—	2 (4.4%)	43 (95.6%)	—	—	—	2 (4.4%)
26	60	—	4 (6.7%)	56 (93.3%)	—	—	—	4 (6.7%)
27	1	—	—	1 (100%)	—	—	—	—
28	11	—	2 (18.2%)	9 (81.8%)	—	—	2 (18.2%)	—
29	61	—	1 (1.6%)	60 (98.4%)	—	—	1 (1.6%)	—
30	5	—	1 (20.0%)	4 (80.0%)	—	—	—	1 (20.0%)
31	159	—	14 (8.8%)	145 (91.2%)	—	—	—	14 (8.8%)
32	10	—	—	10 (100%)	—	—	—	—
33	257	—	24 (9.3%)	233 (90.7%)	—	—	24 (9.3%)	—
34	21	—	3 (14.3%)	18 (85.7%)	—	—	—	3 (14.3%)
35	8	—	2 (25.0%)	6 (75.0%)	—	—	—	2 (25.0%)
36	261	—	40 (15.3%)	221 (84.7%)	—	—	—	40 (15.3%)
37	5	—	—	5 (100%)	—	—	—	—
38	104	—	33 (31.7%)	71 (68.3%)	—	—	—	33 (31.7%)
39	13	—	—	13 (100%)	—	—	—	—
40	57	—	5 (8.8%)	52 (91.2%)	—	—	5 (8.8%)	—
41	31	—	1 (3.2%)	30 (96.8%)	—	—	1 (3.2%)	—
42	4	—	—	4 (100%)	—	—	—	—
43	84	—	13 (15.5%)	71 (84.5%)	—	—	—	13 (15.5%)
44	69	—	11 (15.9%)	58 (84.1%)	—	—	—	11 (15.9%)
45	8	—	—	8 (100%)	—	—	—	—
46	57	—	7 (12.3%)	50 (87.7%)	—	—	7 (12.3%)	—
47	51	31 (60.8%)	13 (25.5%)	7 (13.7%)	31 (60.8%)	—	—	13 (25.5%)
48	3	—	—	3 (100%)	—	—	—	—
49	1	—	—	1 (100%)	—	—	—	—
50	7	4 (57.1%)	—	3 (42.9%)	3 (42.9%)	1 (14.3%)	—	—
51	107	47 (43.9%)	36 (33.6%)	24 (22.4%)	47 (43.9%)	—	—	36 (33.6%)
52	39	1 (2.6%)	4 (10.3%)	34 (87.2%)	1 (2.6%)	—	4 (10.3%)	—
53	18	2 (11.1%)	3 (16.7%)	13 (72.2%)	—	2 (11.1%)	—	3 (16.7%)
54	19	4 (21.1%)	2 (10.5%)	13 (68.4%)	4 (21.1%)	—	2 (10.5%)	—
55	394	217 (55.1%)	45 (11.4%)	132 (33.5%)	217 (55.1%)	—	—	45 (11.4%)
56	19	—	4 (21.1%)	15 (79.0%)	—	—	4 (21.1%)	—
57	142	34 (23.9%)	18 (12.7%)	90 (63.4%)	34 (23.9%)	—	18 (12.7%)	—
58	208	41 (19.7%)	47 (22.6%)	120 (57.7%)	41 (19.7%)	—	12 (5.8%)	35 (16.8%)
59	227	70 (30.8%)	72 (31.7%)	85 (37.4%)	32 (14.1%)	38 (16.7%)	—	72 (31.7%)
60	142	14 (9.9%)	11 (7.8%)	117 (82.4%)	14 (9.9%)	—	11 (7.8%)	—
61	122	10 (8.2%)	6 (4.9%)	106 (86.9%)	10 (8.2%)	—	6 (4.9%)	—
62	3006	693 (23.1%)	692 (23.0%)	1621 (53.9%)	693 (23.1%)	—	692 (23.0%)	—
63	1396	466 (33.4%)	490 (35.1%)	440 (31.5%)	271 (19.4%)	195 (14.0%)	—	490 (35.1%)
64	257	59 (23.0%)	46 (17.9%)	152 (59.1%)	—	59 (23.0%)	6 (2.3%)	40 (15.6%)
65	241	135 (56.0%)	73 (30.3%)	33 (13.7%)	77 (31.9%)	58 (24.1%)	—	73 (30.3%)
66	36	6 (16.7%)	9 (25.0%)	21 (58.3%)	6 (16.7%)	—	—	9 (25.0%)
67	30	10 (33.3%)	6 (20.0%)	14 (46.7%)	10 (33.3%)	—	—	6 (20.0%)

68	19	—	4 (21.1%)	15 (79.0%)	—	—	—	4 (21.1%)
69	66	23 (34.9%)	18 (27.3%)	25 (37.9%)	—	23 (34.9%)	—	18 (27.3%)
70	139	32 (23.0%)	11 (7.9%)	96 (69.1%)	—	32 (23.0%)	—	11 (7.9%)
71	452	188 (41.6%)	162 (35.8%)	102 (22.6%)	—	188 (41.6%)	—	162 (35.8%)
72	192	45 (23.4%)	58 (30.2%)	89 (46.4%)	30 (15.6%)	15 (7.8%)	—	58 (30.2%)
73	24	2 (8.3%)	3 (12.5%)	19 (79.2%)	2 (8.3%)	—	3 (12.5%)	—
74	218	64 (29.4%)	80 (36.7%)	74 (33.9%)	64 (29.4%)	—	—	80 (36.7%)
75	5	—	2 (40.0%)	3 (60.0%)	—	—	—	2 (40.0%)
76	12	—	2 (16.7%)	10 (83.3%)	—	—	2 (16.7%)	—
77	2	—	—	2 (100%)	—	—	—	—
78	2	—	—	2 (100%)	—	—	—	—
79	11	—	1 (9.1%)	10 (90.9%)	—	—	1 (9.1%)	—
80	3	—	—	3 (100%)	—	—	—	—
81	14	—	—	14 (100%)	—	—	—	—
82	136	18 (13.2%)	11 (8.1%)	107 (78.7%)	18 (13.2%)	—	1 (0.7%)	10 (7.3%)
83	10	5 (50.0%)	4 (40.0%)	1 (10.0%)	2 (20.0%)	3 (30.0%)	4 (40.0%)	—
84	28	2 (7.1%)	5 (17.9%)	21 (75.0%)	2 (7.1%)	—	3 (10.7%)	2 (7.1%)
85	39	4 (10.3%)	10 (25.6%)	25 (64.1%)	—	4 (10.3%)	2 (5.1%)	8 (20.5%)
86	51	10 (19.6%)	28 (54.9%)	13 (25.5%)	—	10 (19.6%)	17 (33.3%)	11 (21.6%)
87	181	22 (12.2%)	86 (47.5%)	73 (40.3%)	—	22 (12.2%)	23 (12.7%)	63 (34.8%)
88	139	7 (5.0%)	21 (15.1%)	111 (79.9%)	—	7 (5.0%)	4 (2.9%)	17 (12.2%)
90	5	—	2 (40.0%)	3 (60.0%)	—	—	—	2 (40.0%)
91	7	—	1 (14.3%)	6 (85.7%)	—	—	1 (14.3%)	—
92	47	—	16 (34.0%)	31 (66.0%)	—	—	11 (23.4%)	5 (10.6%)
94	1	—	—	1 (100%)	—	—	—	—
95	3	—	1 (33.3%)	2 (66.7%)	—	—	1 (33.3%)	—
96	16	—	1 (6.2%)	15 (93.8%)	—	—	1 (6.2%)	—
97	2	—	1 (50.0%)	1 (50.0%)	—	—	1 (50.0%)	—
98	4	—	—	4 (100%)	—	—	—	—
99	98	—	22 (22.4%)	76 (77.5%)	—	—	7 (7.1%)	15 (15.3%)
100	20	—	12 (60.0%)	8 (40.0%)	—	—	1 (5.0%)	11 (55.0%)
102	12	—	3 (25.0%)	9 (75.0%)	—	—	2 (16.7%)	1 (8.3%)
103	3	—	3 (100%)	—	—	—	—	3 (100%)
104	3	—	1 (33.3%)	2 (66.7%)	—	—	—	1 (33.3%)
105	4	—	—	4 (100%)	—	—	—	—
106	1	—	1 (100%)	—	—	—	1 (100%)	—
107	121	—	68 (56.2%)	53 (43.8%)	—	—	16 (13.2%)	52 (43.0%)
108	15	—	5 (33.3%)	10 (66.7%)	—	—	2 (13.3%)	3 (20.0%)
109	40	—	16 (40.0%)	24 (60.0%)	—	—	1 (2.5%)	15 (37.5%)
110	8	—	2 (25.0%)	6 (75.0%)	—	—	2 (25.0%)	—
111	21	1 (4.8%)	4 (19.1%)	16 (76.2%)	—	1 (4.8%)	—	4 (19.1%)
112	4	—	—	4 (100%)	—	—	—	—
113	84	6 (7.1%)	20 (23.8%)	58 (69.0%)	6 (7.1%)	—	—	20 (23.8%)
114	31	2 (6.5%)	1 (3.2%)	28 (90.3%)	—	2 (6.5%)	1 (3.2%)	—
115	21	4 (19.1%)	6 (28.6%)	11 (52.4%)	—	4 (19.1%)	—	6 (28.6%)
116	17	1 (5.9%)	—	16 (94.1%)	—	1 (5.9%)	—	—
117	11	1 (9.1%)	1 (9.1%)	9 (81.8%)	1 (9.1%)	—	—	1 (9.1%)
118	11	1 (9.1%)	1 (9.1%)	9 (81.8%)	1 (9.1%)	—	—	1 (9.1%)
119	35	2 (5.7%)	6 (17.1%)	27 (77.1%)	2 (5.7%)	—	—	6 (17.1%)
120	15	2 (13.3%)	2 (13.3%)	11 (73.3%)	2 (13.3%)	—	2 (13.3%)	—
121	126	19 (15.1%)	20 (15.9%)	87 (69.0%)	—	19 (15.1%)	—	20 (15.9%)
122	124	16 (12.9%)	10 (8.1%)	98 (79.0%)	—	16 (12.9%)	2 (1.6%)	8 (6.5%)
123	473	90 (19.0%)	313 (66.2%)	70 (14.8%)	52 (11.0%)	38 (8.0%)	98 (20.7%)	215 (45.5%)
124	23	1 (4.3%)	19 (82.6%)	3 (13.0%)	1 (4.3%)	—	7 (30.4%)	12 (52.2%)
125	52	11 (21.1%)	24 (46.1%)	17 (32.7%)	5 (9.6%)	6 (11.5%)	10 (19.2%)	14 (26.9%)
126	12	—	5 (41.7%)	7 (58.3%)	—	—	3 (25.0%)	2 (16.7%)

127	403	71 (17.6%)	282 (70.0%)	50 (12.4%)	71 (17.6%)	—	109 (27.1%)	173 (42.9%)
128	76	15 (19.7%)	34 (44.7%)	27 (35.5%)	—	15 (19.7%)	24 (31.6%)	10 (13.2%)
129	884	230 (26.0%)	435 (49.2%)	219 (24.8%)	108 (12.2%)	122 (13.8%)	102 (11.5%)	333 (37.7%)
130	38	4 (10.5%)	13 (34.2%)	21 (55.3%)	3 (7.9%)	1 (2.6%)	3 (7.9%)	10 (26.3%)
131	44	7 (15.9%)	27 (61.4%)	10 (22.7%)	7 (15.9%)	—	10 (22.7%)	17 (38.6%)
132	10	—	1 (10.0%)	9 (90.0%)	—	—	1 (10.0%)	—
133	3	1 (33.3%)	1 (33.3%)	1 (33.3%)	1 (33.3%)	—	1 (33.3%)	—
134	4	—	3 (75.0%)	1 (25.0%)	—	—	—	3 (75.0%)
135	30	5 (16.7%)	11 (36.7%)	14 (46.7%)	5 (16.7%)	—	8 (26.7%)	3 (10.0%)
136	266	38 (14.3%)	135 (50.8%)	93 (35.0%)	—	38 (14.3%)	76 (28.6%)	59 (22.2%)
137	70	10 (14.3%)	27 (38.6%)	33 (47.1%)	—	10 (14.3%)	10 (14.3%)	17 (24.3%)
138	22	4 (18.2%)	3 (13.6%)	15 (68.2%)	4 (18.2%)	—	3 (13.6%)	—
139	1622	493 (30.4%)	900 (55.5%)	229 (14.1%)	—	493 (30.4%)	307 (18.9%)	593 (36.6%)
140	457	86 (18.8%)	243 (53.2%)	128 (28.0%)	56 (12.2%)	30 (6.6%)	68 (14.9%)	175 (38.3%)
141	267	57 (21.4%)	108 (40.5%)	102 (38.2%)	—	57 (21.4%)	27 (10.1%)	81 (30.3%)
142	77	10 (13.0%)	25 (32.5%)	42 (54.5%)	—	10 (13.0%)	15 (19.5%)	10 (13.0%)
143	18	—	5 (27.8%)	13 (72.2%)	—	—	2 (11.1%)	3 (16.7%)
144	13	—	1 (7.7%)	12 (92.3%)	—	—	—	1 (7.7%)
145	5	—	—	5 (100%)	—	—	—	—
146	87	—	15 (17.2%)	72 (82.8%)	—	—	5 (5.8%)	10 (11.5%)
147	75	8 (10.7%)	9 (12.0%)	58 (77.3%)	—	8 (10.7%)	6 (8.0%)	3 (4.0%)
148	496	70 (14.1%)	142 (28.6%)	284 (57.3%)	—	70 (14.1%)	34 (6.8%)	108 (21.8%)
149	10	—	3 (30.0%)	7 (70.0%)	—	—	1 (10.0%)	2 (20.0%)
150	66	—	11 (16.7%)	55 (83.3%)	—	—	3 (4.5%)	8 (12.1%)
151	5	—	—	5 (100%)	—	—	—	—
152	42	—	12 (28.6%)	30 (71.4%)	—	—	3 (7.1%)	9 (21.4%)
153	2	—	—	2 (100%)	—	—	—	—
154	19	—	2 (10.5%)	17 (89.5%)	—	—	1 (5.3%)	1 (5.3%)
155	54	—	12 (22.2%)	42 (77.8%)	—	—	3 (5.6%)	9 (16.7%)
156	57	—	13 (22.8%)	44 (77.2%)	—	—	7 (12.5%)	6 (10.5%)
157	16	—	3 (18.8%)	13 (81.2%)	—	—	1 (6.2%)	2 (12.5%)
158	3	—	2 (66.7%)	1 (33.3%)	—	—	1 (33.3%)	1 (33.3%)
159	26	—	6 (23.1%)	20 (76.9%)	—	—	4 (15.4%)	2 (7.7%)
160	160	—	42 (26.2%)	118 (73.8%)	—	—	7 (4.4%)	35 (21.9%)
161	87	—	15 (17.2%)	72 (82.8%)	—	—	8 (9.2%)	7 (8.1%)
162	54	7 (13.0%)	20 (37.0%)	27 (50.0%)	—	7 (13.0%)	8 (14.8%)	12 (22.2%)
163	63	5 (7.9%)	21 (33.3%)	37 (58.7%)	—	5 (7.9%)	8 (12.7%)	13 (20.6%)
164	598	113 (18.9%)	207 (34.6%)	278 (46.5%)	—	113 (18.9%)	48 (8.0%)	159 (26.6%)
165	34	4 (11.8%)	16 (47.1%)	14 (41.2%)	—	4 (11.8%)	7 (20.6%)	9 (26.5%)
166	1029	216 (21.0%)	415 (40.3%)	398 (38.7%)	—	216 (21.0%)	112 (10.9%)	303 (29.4%)
167	325	16 (4.9%)	108 (33.2%)	201 (61.9%)	—	16 (4.9%)	32 (9.8%)	76 (23.4%)
169	1	—	—	1 (100%)	—	—	—	—
173	124	—	42 (33.9%)	82 (66.1%)	—	—	39 (31.4%)	3 (2.4%)
174	59	—	42 (71.2%)	17 (28.8%)	—	—	3 (5.1%)	39 (66.1%)
175	2	—	2 (100%)	—	—	—	—	2 (100%)
176	206	6 (2.9%)	82 (39.8%)	118 (57.3%)	—	6 (2.9%)	24 (11.7%)	58 (28.2%)
177	1	—	—	1 (100%)	—	—	—	—
180	28	—	16 (57.1%)	12 (42.9%)	—	—	6 (21.4%)	10 (35.7%)
181	8	—	4 (50.0%)	4 (50.0%)	—	—	1 (12.5%)	3 (37.5%)
182	34	—	22 (64.7%)	12 (35.3%)	—	—	20 (58.8%)	2 (5.9%)
183	1	—	—	1 (100%)	—	—	—	—
185	51	—	29 (56.9%)	22 (43.1%)	—	—	13 (25.5%)	16 (31.4%)
186	392	—	206 (52.5%)	186 (47.5%)	—	—	76 (19.4%)	130 (33.2%)
187	158	13 (8.2%)	111 (70.2%)	34 (21.5%)	13 (8.2%)	—	51 (32.3%)	60 (38.0%)
188	21	—	5 (23.8%)	16 (76.2%)	—	—	2 (9.5%)	3 (14.3%)
189	592	118 (19.9%)	418 (70.6%)	56 (9.5%)	—	118 (19.9%)	138 (23.3%)	280 (47.3%)

190	45	4 (8.9%)	23 (51.1%)	18 (40.0%)	4 (8.9%)	—	5 (11.1%)	18 (40.0%)
191	506	81 (16.0%)	420 (83.0%)	5 (1.0%)	—	81 (16.0%)	194 (38.3%)	226 (44.7%)
192	2	—	—	2 (100%)	—	—	—	—
193	302	15 (5.0%)	268 (88.7%)	19 (6.3%)	—	15 (5.0%)	114 (37.8%)	154 (51.0%)
194	1619	220 (13.6%)	1120 (69.2%)	279 (17.2%)	—	220 (13.6%)	594 (36.7%)	526 (32.5%)
195	1	—	—	1 (100%)	—	—	—	—
196	1	—	1 (100%)	—	—	—	—	1 (100%)
197	20	—	9 (45.0%)	11 (55.0%)	—	—	—	9 (45.0%)
198	173	—	78 (45.1%)	95 (54.9%)	—	—	2 (1.2%)	76 (43.9%)
199	33	—	8 (24.2%)	25 (75.8%)	—	—	1 (3.0%)	7 (21.2%)
200	22	3 (13.6%)	14 (63.6%)	5 (22.7%)	—	3 (13.6%)	—	14 (63.6%)
201	7	1 (14.3%)	3 (42.9%)	3 (42.9%)	—	1 (14.3%)	—	3 (42.9%)
202	18	—	10 (55.6%)	8 (44.4%)	—	—	—	10 (55.6%)
203	6	—	1 (16.7%)	5 (83.3%)	—	—	1 (16.7%)	—
204	151	12 (8.0%)	109 (72.2%)	30 (19.9%)	—	12 (8.0%)	—	109 (72.2%)
205	130	9 (6.9%)	38 (29.2%)	83 (63.9%)	9 (6.9%)	—	4 (3.1%)	34 (26.1%)
206	61	11 (18.0%)	17 (27.9%)	33 (54.1%)	—	11 (18.0%)	2 (3.3%)	15 (24.6%)
208	2	—	—	2 (100%)	—	—	—	—
210	1	—	1 (100%)	—	—	—	—	1 (100%)
211	1	—	1 (100%)	—	—	—	—	1 (100%)
212	14	—	8 (57.1%)	6 (42.9%)	—	—	3 (21.4%)	5 (35.7%)
213	22	—	17 (77.3%)	5 (22.7%)	—	—	3 (13.6%)	14 (63.6%)
214	14	—	8 (57.1%)	6 (42.9%)	—	—	1 (7.1%)	7 (50.0%)
215	54	3 (5.6%)	13 (24.1%)	38 (70.4%)	—	3 (5.6%)	—	13 (24.1%)
216	777	69 (8.9%)	458 (58.9%)	250 (32.2%)	69 (8.9%)	—	24 (3.1%)	434 (55.9%)
217	111	6 (5.4%)	55 (49.5%)	50 (45.0%)	—	6 (5.4%)	1 (0.9%)	54 (48.6%)
218	42	1 (2.4%)	11 (26.2%)	30 (71.4%)	—	1 (2.4%)	6 (14.3%)	5 (11.9%)
219	9	—	3 (33.3%)	6 (66.7%)	—	—	2 (22.2%)	1 (11.1%)
220	143	11 (7.7%)	102 (71.3%)	30 (21.0%)	11 (7.7%)	—	2 (1.4%)	100 (69.9%)
221	1352	133 (9.8%)	1059 (78.5%)	160 (11.8%)	4 (0.3%)	129 (9.5%)	163 (12.1%)	896 (66.3%)
223	222	9 (4.0%)	210 (94.6%)	3 (1.4%)	—	9 (4.0%)	47 (21.2%)	163 (73.4%)
224	17	—	11 (64.7%)	6 (35.3%)	—	—	2 (11.8%)	9 (52.9%)
225	1693	183 (10.8%)	1112 (65.7%)	398 (23.5%)	—	183 (10.8%)	175 (10.3%)	937 (55.4%)
226	46	2 (4.3%)	43 (93.5%)	1 (2.2%)	—	2 (4.3%)	7 (15.2%)	36 (78.3%)
227	841	148 (17.6%)	498 (59.2%)	195 (23.2%)	—	148 (17.6%)	149 (17.7%)	349 (41.5%)
229	210	7 (3.3%)	182 (86.7%)	21 (10.0%)	—	7 (3.3%)	18 (8.6%)	164 (78.1%)
230	6	1 (16.7%)	4 (66.7%)	1 (16.7%)	—	1 (16.7%)	1 (16.7%)	3 (50.0%)
Total	38298	6128 (16.0%)	14037 (36.6%)	18133 (47.4%)	3000 (7.8%)	3128 (8.2%)	4102 (10.7%)	9935 (25.9%)

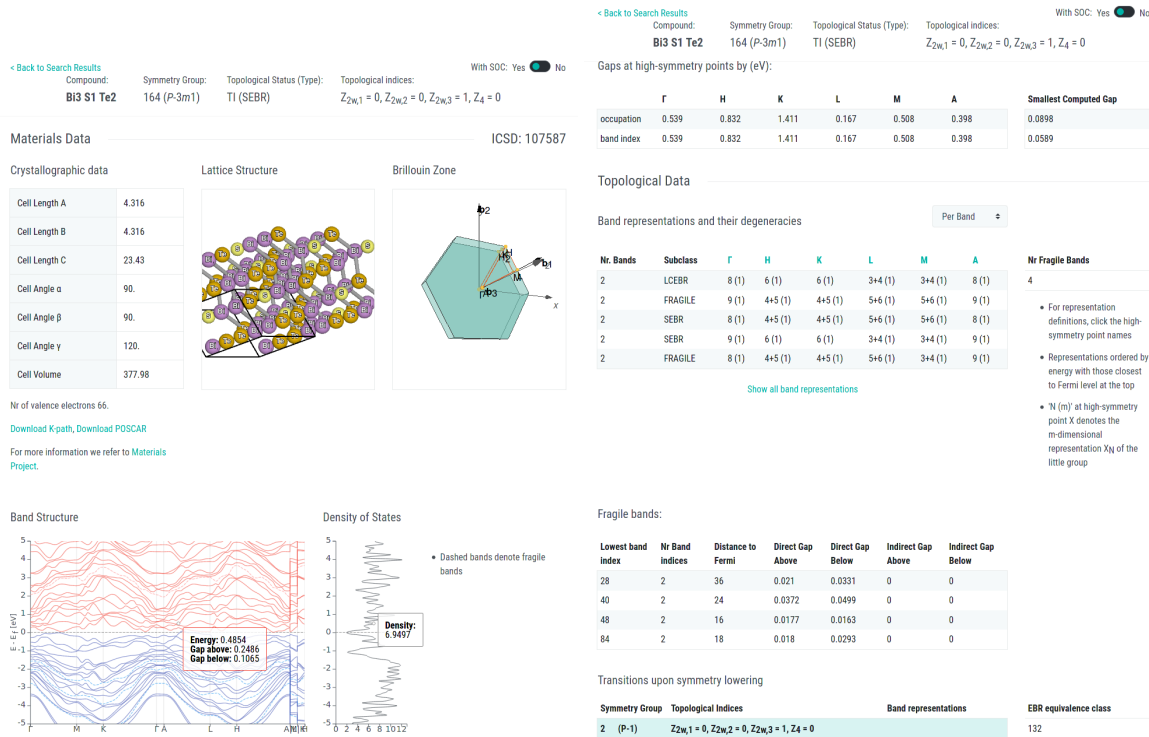


Figure S3. An ICSD entry page on <https://www.topologicalquantumchemistry.com/>. We have chosen as an example the (obstructed) weak TI  $\text{Bi}_3\text{S}\text{Te}_2$  [ICSD 107587, SG 164 ( $P\bar{3}m1$ )] (see S11A6 and Refs. [5, 16, 26, 30, 147–150]). *Left panel* We first list the chemical formula, SG, topological classification at  $E_F$ , the stable SIs if the topological classification at  $E_F$  is NLC (-SM) or SEBR (-SM) [see S2 and S6], and, if the bulk at  $E_F$  is an enforced topological semimetal (ES- or ESFD-classified), whether the crossing point lies at a high-symmetry point or along a high-symmetry line or plane. On the top-left corner, there is a switch that allows users to toggle between the electronic structures and topological data for the same ICSD entry computed with and without incorporating the effects of SOC. We then display the “Materials Data” for the ICSD entry, which consists of the ICSD accession code, a dropdown list of all other ICSD entries associated to the same unique material (see S4), the crystallographic lattice data, interactive plots of the real-space unit cell and the first BZ, and the number of valence electrons. For ICSD entries that are also listed on the Materials Project (MP) [126], we additionally provide a link to the corresponding page on the MP. Lastly, below the Materials Data, we provide interactive band structure and density-of-states plots. *Right panel* A continuation of the example page on <https://www.topologicalquantumchemistry.com/> shown in the left panel. We first list the direct gaps at  $E_F$  at the high-symmetry  $\mathbf{k}$  points, defined both by occupation as determined by VASP and by band index. We then list the “Topological Data” table discussed in this section. Next, we list information for the largest sets of bands with cumulative symmetry-indicated fragile topology in the electronic structure [43–46]. Next, if the topological classification at  $E_F$  is ES, then we provide a table listing the high-symmetry manifolds along which enforced crossing points are required to appear. Lastly, using subduction onto lower-symmetry SGs as detailed in Refs. [29, 114], we compute the stable SIs [5, 16, 17, 22, 29, 30, 32–34, 87] of the lowest-symmetry nonmagnetic NLC and SEBR phases that can be realized by breaking crystal symmetries. If the “Transitions upon symmetry lowering” table is not displayed, then the bulk cannot be driven by infinitesimal symmetry-breaking into a nonmagnetic NLC or SEBR phase, or is a filling-enforced, ESFD-classified (semi)metal [see Refs. [130, 151, 152]] with at least one accidental degeneracy at  $E_F$  [defined in S3A].

Table S15: The number of unique materials in each of the topological classes (as defined in the main text and in S6) in calculations performed w/o SOC. In this table, the topology of a material is taken to be the total (cumulative) topology of all of the bands occupied up to  $E_F$ . In order, the columns in this table list the SG, the number of unique materials in the SG (which we emphasize to be defined using the topological classification with SOC, see S4), the number of semimetals (SMs) in the SG (defined as either NLC-SM, SEBR-SM, ES, or ESFD), the number of unique materials with trivial symmetry-indictated topology (LCEBR) in the SG, the number of NLC-SM-classified SMs in the SG, the number of SEBR-SM-classified SMs in the SG, the number of ES-classified SMs in the SG, and the number of ESFD-classified SMs in the SG. For all of the topological classification categories in the table, each number of materials is accompanied by the percentage of materials in the SG in the topological class. When there are no materials in the topological class, the table entry is marked with a dashed horizontal line.

SG	# Mat.	SMs	Trivial	NLC-SM	SEBR-SM	ES	ESFD
1	151	9 (6.0%)	142 (94.0%)	—	—	—	9 (6.0%)
2	1466	277 (18.9%)	1189 (81.1%)	165 (11.3%)	—	—	112 (7.6%)
3	10	7 (70.0%)	3 (30.0%)	—	—	7 (70.0%)	—
4	219	20 (9.1%)	199 (90.9%)	—	—	14 (6.4%)	6 (2.7%)
5	148	31 (20.9%)	117 (79.0%)	—	—	19 (12.8%)	12 (8.1%)
6	28	5 (17.9%)	23 (82.1%)	—	—	4 (14.3%)	1 (3.6%)
7	85	9 (10.6%)	76 (89.4%)	—	—	6 (7.1%)	3 (3.5%)
8	141	26 (18.4%)	115 (81.6%)	—	—	14 (9.9%)	12 (8.5%)
9	197	15 (7.6%)	182 (92.4%)	—	—	4 (2.0%)	11 (5.6%)
10	33	21 (63.6%)	12 (36.4%)	—	—	16 (48.5%)	5 (15.2%)
11	547	197 (36.0%)	350 (64.0%)	4 (0.7%)	—	97 (17.7%)	96 (17.6%)
12	1250	621 (49.7%)	629 (50.3%)	24 (1.9%)	—	406 (32.5%)	191 (15.3%)
13	164	42 (25.6%)	122 (74.4%)	1 (0.6%)	—	21 (12.8%)	20 (12.2%)
14	2520	491 (19.5%)	2029 (80.5%)	24 (0.9%)	—	330 (13.1%)	137 (5.4%)
15	1402	332 (23.7%)	1070 (76.3%)	22 (1.6%)	—	137 (9.8%)	173 (12.3%)
16	2	1 (50.0%)	1 (50.0%)	—	—	1 (50.0%)	—
17	8	3 (37.5%)	5 (62.5%)	—	—	3 (37.5%)	—
18	30	6 (20.0%)	24 (80.0%)	—	—	4 (13.3%)	2 (6.7%)
19	261	28 (10.7%)	233 (89.3%)	—	—	9 (3.5%)	19 (7.3%)
20	58	5 (8.6%)	53 (91.4%)	—	—	3 (5.2%)	2 (3.5%)
21	15	9 (60.0%)	6 (40.0%)	—	—	3 (20.0%)	6 (40.0%)
22	14	11 (78.6%)	3 (21.4%)	—	—	11 (78.6%)	—
23	15	5 (33.3%)	10 (66.7%)	—	—	3 (20.0%)	2 (13.3%)
24	2	—	2 (100%)	—	—	—	—
25	45	14 (31.1%)	31 (68.9%)	—	—	12 (26.7%)	2 (4.4%)
26	59	12 (20.3%)	47 (79.7%)	—	—	8 (13.6%)	4 (6.8%)
27	1	—	1 (100%)	—	—	—	—
28	11	7 (63.6%)	4 (36.4%)	—	—	5 (45.5%)	2 (18.2%)
29	59	2 (3.4%)	57 (96.6%)	—	—	1 (1.7%)	1 (1.7%)
30	5	2 (40.0%)	3 (60.0%)	—	—	1 (20.0%)	1 (20.0%)
31	158	33 (20.9%)	125 (79.1%)	—	—	19 (12.0%)	14 (8.9%)
32	10	—	10 (100%)	—	—	—	—
33	251	43 (17.1%)	208 (82.9%)	—	—	20 (8.0%)	23 (9.2%)
34	21	5 (23.8%)	16 (76.2%)	—	—	2 (9.5%)	3 (14.3%)
35	8	4 (50.0%)	4 (50.0%)	—	—	2 (25.0%)	2 (25.0%)
36	241	53 (22.0%)	188 (78.0%)	—	—	21 (8.7%)	32 (13.3%)
37	5	—	5 (100%)	—	—	—	—
38	95	69 (72.6%)	26 (27.4%)	—	—	38 (40.0%)	31 (32.6%)
39	12	3 (25.0%)	9 (75.0%)	—	—	3 (25.0%)	—
40	54	7 (13.0%)	47 (87.0%)	—	—	3 (5.6%)	4 (7.4%)

41	31	10 (32.3%)	21 (67.7%)	—	—	9 (29.0%)	1 (3.2%)
42	4	—	4 (100%)	—	—	—	—
43	83	21 (25.3%)	62 (74.7%)	—	—	8 (9.6%)	13 (15.7%)
44	62	35 (56.5%)	27 (43.5%)	—	—	24 (38.7%)	11 (17.7%)
45	8	2 (25.0%)	6 (75.0%)	—	—	2 (25.0%)	—
46	55	30 (54.5%)	25 (45.5%)	—	—	23 (41.8%)	7 (12.7%)
47	45	42 (93.3%)	3 (6.7%)	—	—	29 (64.4%)	13 (28.9%)
48	3	1 (33.3%)	2 (66.7%)	—	—	1 (33.3%)	—
50	7	5 (71.4%)	2 (28.6%)	—	—	5 (71.4%)	—
51	100	77 (77.0%)	23 (23.0%)	—	—	42 (42.0%)	35 (35.0%)
52	36	4 (11.1%)	32 (88.9%)	—	—	—	4 (11.1%)
53	18	6 (33.3%)	12 (66.7%)	—	—	3 (16.7%)	3 (16.7%)
54	18	6 (33.3%)	12 (66.7%)	—	—	4 (22.2%)	2 (11.1%)
55	336	252 (75.0%)	84 (25.0%)	—	—	211 (62.8%)	41 (12.2%)
56	19	5 (26.3%)	14 (73.7%)	—	—	1 (5.3%)	4 (21.1%)
57	128	48 (37.5%)	80 (62.5%)	—	—	31 (24.2%)	17 (13.3%)
58	202	98 (48.5%)	104 (51.5%)	1 (0.5%)	—	62 (30.7%)	35 (17.3%)
59	208	143 (68.8%)	65 (31.2%)	—	—	78 (37.5%)	65 (31.2%)
60	139	30 (21.6%)	109 (78.4%)	1 (0.7%)	—	20 (14.4%)	9 (6.5%)
61	119	18 (15.1%)	101 (84.9%)	—	—	16 (13.4%)	2 (1.7%)
62	2800	1451 (51.8%)	1349 (48.2%)	—	—	777 (27.8%)	674 (24.1%)
63	1277	924 (72.4%)	353 (27.6%)	—	—	454 (35.5%)	470 (36.8%)
64	244	111 (45.5%)	133 (54.5%)	—	—	72 (29.5%)	39 (16.0%)
65	213	193 (90.6%)	20 (9.4%)	—	—	123 (57.8%)	70 (32.9%)
66	34	16 (47.1%)	18 (52.9%)	—	—	7 (20.6%)	9 (26.5%)
67	29	17 (58.6%)	12 (41.4%)	—	—	11 (37.9%)	6 (20.7%)
68	19	6 (31.6%)	13 (68.4%)	—	—	2 (10.5%)	4 (21.1%)
69	65	43 (66.2%)	22 (33.9%)	—	—	25 (38.5%)	18 (27.7%)
70	130	47 (36.1%)	83 (63.9%)	—	—	36 (27.7%)	11 (8.5%)
71	385	315 (81.8%)	70 (18.2%)	—	—	162 (42.1%)	153 (39.7%)
72	182	109 (59.9%)	73 (40.1%)	—	—	51 (28.0%)	58 (31.9%)
73	16	1 (6.2%)	15 (93.8%)	—	—	—	1 (6.2%)
74	202	152 (75.2%)	50 (24.8%)	—	—	75 (37.1%)	77 (38.1%)
75	5	2 (40.0%)	3 (60.0%)	—	—	—	2 (40.0%)
76	12	2 (16.7%)	10 (83.3%)	—	—	1 (8.3%)	1 (8.3%)
77	2	—	2 (100%)	—	—	—	—
78	2	—	2 (100%)	—	—	—	—
79	11	1 (9.1%)	10 (90.9%)	—	—	—	1 (9.1%)
80	3	—	3 (100%)	—	—	—	—
81	13	4 (30.8%)	9 (69.2%)	1 (7.7%)	—	—	3 (23.1%)
82	130	37 (28.5%)	93 (71.5%)	2 (1.5%)	—	10 (7.7%)	25 (19.2%)
83	9	8 (88.9%)	1 (11.1%)	—	—	2 (22.2%)	6 (66.7%)
84	28	7 (25.0%)	21 (75.0%)	—	—	4 (14.3%)	3 (10.7%)
85	36	14 (38.9%)	22 (61.1%)	2 (5.6%)	—	3 (8.3%)	9 (25.0%)
86	49	38 (77.5%)	11 (22.4%)	—	—	9 (18.4%)	29 (59.2%)
87	175	106 (60.6%)	69 (39.4%)	2 (1.1%)	—	15 (8.6%)	89 (50.9%)
88	129	27 (20.9%)	102 (79.1%)	—	—	12 (9.3%)	15 (11.6%)
90	5	4 (80.0%)	1 (20.0%)	—	—	2 (40.0%)	2 (40.0%)
91	7	3 (42.9%)	4 (57.1%)	—	—	1 (14.3%)	2 (28.6%)
92	47	18 (38.3%)	29 (61.7%)	—	—	6 (12.8%)	12 (25.5%)
94	1	1 (100%)	—	—	—	1 (100%)	—
95	3	1 (33.3%)	2 (66.7%)	—	—	1 (33.3%)	—
96	16	1 (6.2%)	15 (93.8%)	—	—	—	1 (6.2%)
97	2	1 (50.0%)	1 (50.0%)	—	—	—	1 (50.0%)
98	4	1 (25.0%)	3 (75.0%)	—	—	—	1 (25.0%)
99	98	27 (27.6%)	71 (72.5%)	—	—	1 (1.0%)	26 (26.5%)

100	20	14 (70.0%)	6 (30.0%)	—	—	1 (5.0%)	13 (65.0%)
102	12	6 (50.0%)	6 (50.0%)	—	—	3 (25.0%)	3 (25.0%)
103	3	3 (100%)	—	—	—	—	3 (100%)
104	3	1 (33.3%)	2 (66.7%)	—	—	—	1 (33.3%)
105	4	1 (25.0%)	3 (75.0%)	—	—	1 (25.0%)	—
106	1	1 (100%)	—	—	—	—	1 (100%)
107	112	101 (90.2%)	11 (9.8%)	—	—	13 (11.6%)	88 (78.6%)
108	14	7 (50.0%)	7 (50.0%)	—	—	2 (14.3%)	5 (35.7%)
109	37	23 (62.2%)	14 (37.8%)	—	—	7 (18.9%)	16 (43.2%)
110	8	3 (37.5%)	5 (62.5%)	—	—	2 (25.0%)	1 (12.5%)
111	20	7 (35.0%)	13 (65.0%)	—	—	1 (5.0%)	6 (30.0%)
112	4	—	4 (100%)	—	—	—	—
113	71	26 (36.6%)	45 (63.4%)	—	—	5 (7.0%)	21 (29.6%)
114	31	6 (19.4%)	25 (80.7%)	—	—	3 (9.7%)	3 (9.7%)
115	21	15 (71.4%)	6 (28.6%)	—	—	1 (4.8%)	14 (66.7%)
116	17	3 (17.6%)	14 (82.3%)	—	—	3 (17.6%)	—
117	11	6 (54.5%)	5 (45.5%)	—	—	3 (27.3%)	3 (27.3%)
118	11	3 (27.3%)	8 (72.7%)	—	—	2 (18.2%)	1 (9.1%)
119	35	17 (48.6%)	18 (51.4%)	—	—	8 (22.9%)	9 (25.7%)
120	15	6 (40.0%)	9 (60.0%)	—	—	3 (20.0%)	3 (20.0%)
121	123	56 (45.5%)	67 (54.5%)	—	—	17 (13.8%)	39 (31.7%)
122	124	23 (18.6%)	101 (81.5%)	—	—	11 (8.9%)	12 (9.7%)
123	450	391 (86.9%)	59 (13.1%)	—	—	66 (14.7%)	325 (72.2%)
124	22	19 (86.4%)	3 (13.6%)	—	—	4 (18.2%)	15 (68.2%)
125	49	32 (65.3%)	17 (34.7%)	—	—	7 (14.3%)	25 (51.0%)
126	11	4 (36.4%)	7 (63.6%)	—	—	2 (18.2%)	2 (18.2%)
127	368	326 (88.6%)	42 (11.4%)	—	—	78 (21.2%)	248 (67.4%)
128	71	45 (63.4%)	26 (36.6%)	—	—	12 (16.9%)	33 (46.5%)
129	861	691 (80.3%)	170 (19.7%)	—	—	213 (24.7%)	478 (55.5%)
130	37	23 (62.2%)	14 (37.8%)	—	—	10 (27.0%)	13 (35.1%)
131	43	36 (83.7%)	7 (16.3%)	—	—	11 (25.6%)	25 (58.1%)
132	10	1 (10.0%)	9 (90.0%)	—	—	1 (10.0%)	—
133	3	2 (66.7%)	1 (33.3%)	—	—	—	2 (66.7%)
134	4	3 (75.0%)	1 (25.0%)	—	—	—	3 (75.0%)
135	26	15 (57.7%)	11 (42.3%)	—	—	9 (34.6%)	6 (23.1%)
136	251	188 (74.9%)	63 (25.1%)	—	—	95 (37.9%)	93 (37.0%)
137	68	37 (54.4%)	31 (45.6%)	—	—	10 (14.7%)	27 (39.7%)
138	16	7 (43.8%)	9 (56.2%)	—	—	4 (25.0%)	3 (18.8%)
139	1543	1384 (89.7%)	159 (10.3%)	—	—	332 (21.5%)	1052 (68.2%)
140	431	319 (74.0%)	112 (26.0%)	—	—	100 (23.2%)	219 (50.8%)
141	246	169 (68.7%)	77 (31.3%)	—	—	77 (31.3%)	92 (37.4%)
142	73	35 (48.0%)	38 (52.0%)	—	—	11 (15.1%)	24 (32.9%)
143	17	5 (29.4%)	12 (70.6%)	—	—	—	5 (29.4%)
144	13	2 (15.4%)	11 (84.6%)	—	—	—	2 (15.4%)
145	5	—	5 (100%)	—	—	—	—
146	83	20 (24.1%)	63 (75.9%)	—	—	—	20 (24.1%)
147	71	19 (26.8%)	52 (73.2%)	—	3 (4.2%)	1 (1.4%)	15 (21.1%)
148	479	224 (46.8%)	255 (53.2%)	—	35 (7.3%)	5 (1.0%)	184 (38.4%)
149	10	5 (50.0%)	5 (50.0%)	—	—	—	5 (50.0%)
150	64	15 (23.4%)	49 (76.6%)	—	—	4 (6.2%)	11 (17.2%)
151	4	—	4 (100%)	—	—	—	—
152	40	9 (22.5%)	31 (77.5%)	—	—	2 (5.0%)	7 (17.5%)
153	1	1 (100%)	—	—	—	1 (100%)	—
154	17	2 (11.8%)	15 (88.2%)	—	—	1 (5.9%)	1 (5.9%)
155	50	19 (38.0%)	31 (62.0%)	—	—	2 (4.0%)	17 (34.0%)
156	57	16 (28.1%)	41 (71.9%)	—	—	7 (12.3%)	9 (15.8%)

157	14	5 (35.7%)	9 (64.3%)	—	—	2 (14.3%)	3 (21.4%)
158	3	3 (100%)	—	—	—	1 (33.3%)	2 (66.7%)
159	24	6 (25.0%)	18 (75.0%)	—	—	—	6 (25.0%)
160	158	58 (36.7%)	100 (63.3%)	—	—	6 (3.8%)	52 (32.9%)
161	87	18 (20.7%)	69 (79.3%)	—	—	3 (3.5%)	15 (17.2%)
162	52	27 (51.9%)	25 (48.1%)	—	1 (1.9%)	5 (9.6%)	21 (40.4%)
163	57	25 (43.9%)	32 (56.1%)	—	—	3 (5.3%)	22 (38.6%)
164	574	320 (55.8%)	254 (44.2%)	—	2 (0.3%)	47 (8.2%)	271 (47.2%)
165	33	24 (72.7%)	9 (27.3%)	—	—	6 (18.2%)	18 (54.5%)
166	957	620 (64.8%)	337 (35.2%)	2 (0.2%)	2 (0.2%)	153 (16.0%)	463 (48.4%)
167	301	122 (40.5%)	179 (59.5%)	—	1 (0.3%)	21 (7.0%)	100 (33.2%)
169	1	—	1 (100%)	—	—	—	—
173	113	39 (34.5%)	74 (65.5%)	—	—	11 (9.7%)	28 (24.8%)
174	50	33 (66.0%)	17 (34.0%)	—	—	—	33 (66.0%)
175	2	2 (100%)	—	—	—	—	2 (100%)
176	189	82 (43.4%)	107 (56.6%)	—	—	5 (2.6%)	77 (40.7%)
177	1	—	1 (100%)	—	—	—	—
180	28	18 (64.3%)	10 (35.7%)	—	—	2 (7.1%)	16 (57.1%)
181	8	5 (62.5%)	3 (37.5%)	—	—	1 (12.5%)	4 (50.0%)
182	33	24 (72.7%)	9 (27.3%)	—	—	5 (15.2%)	19 (57.6%)
183	1	—	1 (100%)	—	—	—	—
185	49	29 (59.2%)	20 (40.8%)	—	—	10 (20.4%)	19 (38.8%)
186	370	203 (54.9%)	167 (45.1%)	—	—	40 (10.8%)	163 (44.0%)
187	154	123 (79.9%)	31 (20.1%)	—	—	31 (20.1%)	92 (59.7%)
188	20	4 (20.0%)	16 (80.0%)	—	—	—	4 (20.0%)
189	537	483 (89.9%)	54 (10.1%)	—	—	94 (17.5%)	389 (72.4%)
190	41	25 (61.0%)	16 (39.0%)	—	—	3 (7.3%)	22 (53.7%)
191	452	447 (98.9%)	5 (1.1%)	—	—	63 (13.9%)	384 (85.0%)
192	2	—	2 (100%)	—	—	—	—
193	270	257 (95.2%)	13 (4.8%)	—	—	24 (8.9%)	233 (86.3%)
194	1530	1278 (83.5%)	252 (16.5%)	—	—	235 (15.4%)	1043 (68.2%)
195	1	—	1 (100%)	—	—	—	—
196	1	1 (100%)	—	—	—	—	1 (100%)
197	20	10 (50.0%)	10 (50.0%)	—	—	—	10 (50.0%)
198	170	77 (45.3%)	93 (54.7%)	—	—	1 (0.6%)	76 (44.7%)
199	32	9 (28.1%)	23 (71.9%)	—	—	1 (3.1%)	8 (25.0%)
200	22	17 (77.3%)	5 (22.7%)	—	—	2 (9.1%)	15 (68.2%)
201	6	4 (66.7%)	2 (33.3%)	—	—	—	4 (66.7%)
202	18	10 (55.6%)	8 (44.4%)	—	—	—	10 (55.6%)
203	6	1 (16.7%)	5 (83.3%)	—	—	—	1 (16.7%)
204	145	123 (84.8%)	22 (15.2%)	—	—	4 (2.8%)	119 (82.1%)
205	130	49 (37.7%)	81 (62.3%)	—	—	9 (6.9%)	40 (30.8%)
206	60	30 (50.0%)	30 (50.0%)	—	—	1 (1.7%)	29 (48.3%)
208	2	2 (100%)	—	—	—	2 (100%)	—
210	1	1 (100%)	—	—	—	—	1 (100%)
211	1	1 (100%)	—	—	—	—	1 (100%)
212	14	8 (57.1%)	6 (42.9%)	—	—	2 (14.3%)	6 (42.9%)
213	22	17 (77.3%)	5 (22.7%)	—	—	1 (4.5%)	16 (72.7%)
214	13	7 (53.9%)	6 (46.1%)	—	—	1 (7.7%)	6 (46.1%)
215	53	23 (43.4%)	30 (56.6%)	—	—	—	23 (43.4%)
216	751	517 (68.8%)	234 (31.2%)	—	—	21 (2.8%)	496 (66.0%)
217	108	66 (61.1%)	42 (38.9%)	—	—	6 (5.6%)	60 (55.6%)
218	42	12 (28.6%)	30 (71.4%)	—	—	—	12 (28.6%)
219	8	5 (62.5%)	3 (37.5%)	—	—	2 (25.0%)	3 (37.5%)
220	142	115 (81.0%)	27 (19.0%)	—	—	15 (10.6%)	100 (70.4%)
221	1334	1170 (87.7%)	164 (12.3%)	—	—	107 (8.0%)	1063 (79.7%)

223	217	214 (98.6%)	3 (1.4%)	—	—	13 (6.0%)	201 (92.6%)
224	16	9 (56.2%)	7 (43.8%)	—	—	—	9 (56.2%)
225	1651	1277 (77.3%)	374 (22.6%)	—	—	74 (4.5%)	1203 (72.9%)
226	43	42 (97.7%)	1 (2.3%)	—	—	3 (7.0%)	39 (90.7%)
227	816	673 (82.5%)	143 (17.5%)	—	—	131 (16.1%)	542 (66.4%)
229	205	185 (90.2%)	20 (9.8%)	—	—	8 (3.9%)	177 (86.3%)
230	6	5 (83.3%)	1 (16.7%)	—	—	1 (16.7%)	4 (66.7%)
Total	36163	20298 (56.1%)	15865 (43.9%)	251 (0.7%)	44 (0.1%)	6006 (16.6%)	13997 (38.7%)

## B. Topological Classification and Connectivity of all of the Bands in all of the Stoichiometric Unique Materials in the ICSD with and w/o SOC

In this section, we will provide statistics on the symmetry-indicated stable [5, 16, 17, 22, 30, 32–34, 87] and fragile [43, 45, 46] topology of *all* of the isolated bands in all of the stoichiometric unique materials in the ICSD, where in the calculations performed for this work, we have taken the conduction manifold to contain at least as many states as the valence manifold (*i.e.* there are  $\geq 2N_e$  total bands, see S4 for further calculation details). We have also compiled statistics for materials with large or complete band connectivities [defined as *supermetallic* (SMetal) materials in the text below]. For the statistics compiled in this section for symmetry-indicated insulating topology at varying electronic fillings, we emphasize that the isolated bands (as determined by band connectivity through the compatibility relations in TQC, see S2) can never be classified as ESFD- or ES-classified semimetals, which by definition require a connected group of bands to be partially occupied at a high-symmetry point or along a high-symmetry line or plane [38]. Consequently, all of the isolated topological bands analyzed in this section are labeled as either NLC, SEBR, LCEBR, or FRAGILE. We emphasize that in the absence of SOC, all symmetry-indicated topological (NLC-SM- and SEBR-SM-classified) bands in nonmagnetic materials correspond to topological semimetal phases, and are thus connected to other bands at higher or lower energies by nodal points in the BZ interior. However, NLC-SM and SEBR-SM bands are still considered to be isolated by band connectivity, as they satisfy the insulating compatibility relations, which are only defined along high-symmetry BZ lines and planes (see S6 and Ref. [36]).

To begin, in this work, we are uniquely able to analyze the symmetry-indicated topology of bands away from the Fermi level by using new features of the [Check Topological Mat](#) program, which we have detailed in S3. In Table S16, we show the output of [Check Topological Mat](#) for the candidate ES compound Ni<sub>2</sub>SnZr [ICSD 105383, SG 225 ( $Fm\bar{3}m$ )]. Though Ni<sub>2</sub>SnZr is an ES-classified SM at  $E_F$  with SOC, none of the entries in Table S16 are labeled as “ES,” because the symmetry-indicated topology of energetically isolated groups of bands can only be meaningfully defined by taking the connected bands to be fully occupied (whereas partial occupancy is required to realize an ES-classified semimetal).

Next, in Table S17, we list the number of isolated sets of bands in each topological class per SG with SOC as determined by band connectivity. Remarkably, we find that nearly 2/3 of all of the bands in all of the stoichiometric unique materials in the ICSD exhibit symmetry-indicated stable (NLC or SEBR) topology when incorporating the effects of SOC. Then, in Table S18, we list the number of unique materials in each SG with at least one symmetry-indicated stable or fragile topological set of bands with SOC. We further find that an overwhelming 87.99% of the stoichiometric unique materials in the ICSD have at least one stable or fragile topological band when the effects of SOC are incorporated. For completeness, we next respectively provide in Tables S19 and S20 the number of isolated sets of bands in each topological class per SG w/o SOC as determined by band connectivity, and the number of unique materials in each SG with at least one symmetry-indicated stable or fragile topological set of bands w/o SOC.

Lastly, in this work we have discovered the existence of SMetal materials, which realize an extreme limit of band connectivity in which *all* of the bands included our VASP calculations are connected (*i.e.* materials in which there does not exist an LCEBR-, NLC-, or SEBR-classified gap at any integer electronic filling, including filling the complete set of  $\sim 2N_e$  bands in the VASP calculation, see S4 for calculation details). As previously discussed in S6, <https://www.topologicalquantumchemistry.com/> contains 17 unique SMetal materials with SOC (Table S18), whereas there are 1,138 unique SMetal materials w/o SOC (Table S20), representing a hundred-fold increase w/o SOC in the number of materials with fully-connected valence bands up to the energy (filling) cutoff of  $\sim 2N_e$  imposed in our VASP calculations (see S4). We have in this work also discovered the existence of materials in which a very large number of bands ( $\geq 130$ ) are connected, even in the presence of SOC. In Table S21, we list the nonmagnetic unique materials without *f* electrons that exhibit connected groupings of bands with total dimension greater than or equal to 130 in the calculations performed with SOC.

$\Gamma$	X	L	W	dim	top. type	ind/band	filling $\nu$	top. type/all	ind/all
-GM6(2)	-X6(2)	-L8(2)	-W7(2)	2	TRIVIAL	0 0 0	2	TRIVIAL	0 0 0
-GM8(2)	-X8(2)	-L9(2)	-W6(2)	2	TRIVIAL	0 0 0	4	TRIVIAL	0 0 0
-GM11(4)	-X7(2)	-L9(2)	-W7(2)	4	SEBR	2 0 6	8	SEBR	2 0 6
	-X6(2)	-L6-L7(2)	-W6(2)						
-GM10(4)	-X8(2)	-L9(2)	-W6(2)	4	SEBR	2 0 2	12	TRIVIAL	0 0 0
	-X9(2)	-L6-L7(2)	-W7(2)						
-GM10(4)	-X9(2)	-L9(2)	-W6(2)	6	SEBR	3 1 7	18	SEBR	3 1 7
-GM7(2)	-X7(2)	-L4-L5(2)	-W7(2)						
	-X6(2)	-L8(2)	-W6(2)						
-GM11(4)	-X9(2)	-L8(2)	-W7(2)	4	TRIVIAL	0 0 0	22	SEBR	3 1 7
	-X8(2)	-L4-L5(2)	-W6(2)						
-GM10(4)	-X9(2)	-L8(2)	-W7(2)	4	SEBR	3 1 3	26	SEBR	2 0 2
	-X6(2)	-L6-L7(2)	-W7(2)						
-GM7(2)	-X8(2)	-L9(2)	-W6(2)	14	SEBR	2 0 6	40	TRIVIAL	0 0 0
-GM10(4)	-X7(2)	-L9(2)	-W6(2)						
-GM8(2)	-X7(2)	-L8(2)	-W7(2)						
-GM11(4)	-X6(2)	-L9(2)	-W6(2)						
-GM6(2)	-X7(2)	-L6-L7(2)	-W7(2)						
	-X6(2)	-L8(2)	-W7(2)						
	-X6(2)	-L4-L5(2)	-W7(2)						
-GM9(2)	-X7(2)	-L9(2)	-W6(2)	2	SEBR	1 1 1	42	SEBR	1 1 1
-GM8(2)	-X8(2)	-L6-L7(2)	-W7(2)	6	SEBR	0 0 4	48	SEBR	1 1 5
-GM11(4)	-X9(2)	-L9(2)	-W6(2)						
	-X8(2)	-L8(2)	-W6(2)						
-GM10(4)	-X6(2)	-L4-L5(2)	-W7(2)	4	TRIVIAL	0 0 0	52	SEBR	1 1 5
	-X7(2)	-L8(2)	-W6(2)						

Table S16. A typical table generated by [Check Topological Mat](#) (see S3). Here, we have used as an example the ES-classified compound Ni<sub>2</sub>SnZr [[ICSD 105383](#), SG 225 ( $Fm\bar{3}m$ )]. In this table, the horizontal lines indicate the electronic fillings  $\nu$  at which the occupied bands satisfy the compatibility relations. Columns  $\Gamma$ , X, L, and W contain the coreps at each maximal  $\mathbf{k}$  point for each energetically isolated set of bands that satisfy the compatibility relations. Column “dim” shows the dimension of each set of bands, Column “top. type” indicates the topology of the isolated bands [which can either be LCEBR, FRAGILE, NLC, or SEBR], and Column “ind/band” contains the minimal ( $Z_8$ ) and non-minimal ( $Z_4 = Z_8 \text{ mod } 4$ ,  $Z_2 = Z_8 \text{ mod } 2$ ) stable SIs [16, 29] of SG 225 ( $Fm\bar{3}m$ ), given in the order ( $Z_4$ ,  $Z_2$ ,  $Z_8$ ). The remaining three columns contain the cumulative information of several combined sets of energetically isolated bands that are filled up to a total number of valence electrons specified by the column “filling  $\nu$ .” Column “top. type/all” provides the cumulative topology (LCEBR, FRAGILE, NLC, or SEBR) at the gap specified by the electronic filling in the “filling  $\nu$ ” column, and Column “ind/all” provides the cumulative stable SIs of all of the filled bands up to the same gap. Hence, the values of “ind/all” at each filling  $\nu$  listed in this table can be obtained by summing the values in the “ind/band” column up to the same filling  $\nu$ . We emphasize that even though Ni<sub>2</sub>SnZr is ES-classified at the Fermi level (there are 28 valence electrons in Ni<sub>2</sub>SnZr), none of the entries in this table are labeled as “ES,” because the symmetry-indicated topology of energetically isolated groups of bands can only be meaningfully defined by taking the connected bands to be fully occupied (whereas partial occupancy is required to realize an ES-classified semimetal).

Table S17: In this table, we list the number of isolated sets of bands with SOC as determined by band connectivity (see S2) in unique materials in each SG in each topological class. In order, the columns in this table list the SG, the number of unique materials in the SG, the number of NLC-classified sets of bands, the number of SEBR-classified sets of bands, the number of LCEBR-classified sets of bands, the number of sets of connected fragile bands, and the total number of sets of isolated (connected) bands. For all of the topological classification categories in the table, each number of bands is accompanied by the percentage of bands in the SG in the topological class. When there are no bands in the topological class, the table entry is marked with a dashed horizontal line.

SG	# Mat.	# NLC bands	# SEBR bands	# LCEBR bands	# Fragile bands	Total # isolated bands
1	151	—	—	13263 (100%)	—	13263
2	1574	191942 (81.2%)	—	44364 (18.8%)	—	236306
3	13	—	—	1708 (100%)	—	1708
4	228	—	—	15934 (100%)	—	15934
5	156	—	—	16121 (100%)	—	16121
6	28	—	—	2232 (100%)	—	2232
7	85	—	—	6211 (100%)	—	6211
8	144	—	—	10382 (100%)	—	10382
9	199	—	—	12836 (100%)	—	12836
10	38	3426 (86.0%)	—	556 (14.0%)	—	3982
11	587	25889 (64.1%)	—	14479 (35.9%)	—	40368
12	1345	74986 (54.5%)	33987 (24.7%)	28550 (20.8%)	—	137523
13	195	10984 (68.5%)	—	5058 (31.5%)	—	16042
14	2665	194380 (81.2%)	—	45057 (18.8%)	—	239437
15	1485	75378 (62.2%)	—	45743 (37.8%)	—	121121
16	2	—	—	125 (100%)	—	125
17	8	—	—	563 (100%)	—	563
18	30	—	—	2825 (100%)	—	2825
19	270	—	—	12867 (100%)	—	12867
20	66	—	—	5007 (100%)	—	5007
21	16	—	—	1102 (100%)	—	1102
22	17	—	—	1371 (100%)	—	1371
23	16	—	—	1486 (100%)	—	1486
24	2	—	—	88 (100%)	—	88
25	45	—	—	2184 (100%)	—	2184
26	60	—	—	4400 (100%)	—	4400
27	1	—	—	54 (100%)	—	54
28	11	—	—	500 (100%)	—	500
29	61	—	—	2651 (100%)	—	2651
30	5	—	—	558 (100%)	—	558
31	159	—	—	10121 (100%)	—	10121
32	10	—	—	1129 (100%)	—	1129
33	257	—	—	11039 (100%)	—	11039
34	21	—	—	1695 (100%)	—	1695
35	8	—	—	878 (100%)	—	878
36	261	—	—	16116 (100%)	—	16116
37	5	—	—	415 (100%)	—	415
38	104	—	—	6817 (100%)	—	6817
39	13	—	—	859 (100%)	—	859
40	57	—	—	3548 (100%)	—	3548
41	31	—	—	2464 (100%)	—	2464
42	4	—	—	321 (100%)	—	321
43	84	—	—	5305 (100%)	—	5305
44	69	—	—	4843 (100%)	—	4843
45	8	—	—	917 (100%)	—	917

46	57	—	—	3774 (100%)	—	3774
47	51	3820 (80.8%)	—	907 (19.2%)	—	4727
48	3	65 (40.4%)	47 (29.2%)	49 (30.4%)	—	161
49	1	56 (69.1%)	—	25 (30.9%)	—	81
50	7	258 (40.8%)	128 (20.2%)	246 (38.9%)	—	632
51	107	4669 (75.5%)	—	1513 (24.5%)	—	6182
52	39	870 (48.7%)	—	918 (51.3%)	—	1788
53	18	—	821 (79.3%)	214 (20.7%)	—	1035
54	19	521 (56.8%)	—	397 (43.2%)	—	918
55	394	30767 (86.8%)	—	4699 (13.2%)	—	35466
56	19	592 (59.3%)	—	407 (40.7%)	—	999
57	142	4217 (61.1%)	—	2681 (38.9%)	—	6898
58	208	7453 (67.6%)	—	3577 (32.4%)	—	11030
59	227	5527 (40.3%)	2537 (18.5%)	5664 (41.3%)	—	13728
60	142	3238 (51.1%)	—	3100 (48.9%)	—	6338
61	122	4948 (83.9%)	—	949 (16.1%)	—	5897
62	3006	62367 (52.4%)	—	56672 (47.6%)	—	119039
63	1396	34318 (55.8%)	5070 (8.2%)	22069 (35.9%)	—	61457
64	257	—	15714 (81.5%)	3559 (18.5%)	—	19273
65	241	9201 (55.2%)	4432 (26.6%)	3046 (18.3%)	—	16679
66	36	1430 (68.3%)	—	663 (31.7%)	—	2093
67	30	680 (68.8%)	—	308 (31.2%)	—	988
68	19	—	1039 (61.7%)	644 (38.3%)	—	1683
69	66	—	5218 (78.8%)	1406 (21.2%)	—	6624
70	139	898 (10.6%)	3632 (42.8%)	3965 (46.7%)	—	8495
71	452	8741 (22.2%)	18476 (47.0%)	12128 (30.8%)	—	39345
72	192	6264 (57.1%)	1068 (9.7%)	3628 (33.1%)	—	10960
73	24	993 (60.0%)	—	663 (40.0%)	—	1656
74	218	7724 (72.5%)	—	2928 (27.5%)	—	10652
75	5	—	—	396 (100%)	—	396
76	12	—	—	380 (100%)	—	380
77	2	—	—	20 (100%)	—	20
78	2	—	—	108 (100%)	—	108
79	11	—	—	841 (100%)	—	841
80	3	—	—	214 (100%)	—	214
81	14	—	816 (48.0%)	885 (52.0%)	—	1701
82	136	5741 (46.7%)	—	6550 (53.3%)	1 (0.0%)	12292
83	10	206 (47.9%)	151 (35.1%)	73 (17.0%)	—	430
84	28	821 (65.1%)	—	440 (34.9%)	—	1261
85	39	730 (33.1%)	718 (32.6%)	755 (34.3%)	—	2203
86	51	—	1266 (70.7%)	525 (29.3%)	—	1791
87	181	1369 (12.7%)	6836 (63.4%)	2563 (23.8%)	11 (0.1%)	10779
88	139	253 (4.1%)	3586 (58.7%)	2263 (37.1%)	3 (0.1%)	6105
90	5	—	—	569 (100%)	—	569
91	7	—	—	173 (100%)	—	173
92	47	—	—	1156 (100%)	—	1156
94	1	—	—	37 (100%)	—	37
95	3	—	—	66 (100%)	—	66
96	16	—	—	386 (100%)	—	386
97	2	—	—	138 (100%)	—	138
98	4	—	—	103 (100%)	—	103
99	98	—	—	2228 (100%)	—	2228
100	20	—	—	1175 (100%)	—	1175
102	12	—	—	461 (100%)	—	461
103	3	—	—	29 (100%)	—	29
104	3	—	—	118 (100%)	—	118

105	4	—	—	139 (100%)	—	139	
106	1	—	—	29 (100%)	—	29	
107	121	—	—	3497 (100%)	—	3497	
108	15	—	—	653 (100%)	—	653	
109	40	—	—	1117 (100%)	—	1117	
110	8	—	—	350 (100%)	—	350	
111	21	—	678 (49.8%)	683 (50.2%)	—	1361	
112	4	57 (39.0%)	—	89 (61.0%)	—	146	
113	84	2055 (35.3%)	—	3767 (64.7%)	—	5822	
114	31	—	1524 (64.9%)	823 (35.1%)	—	2347	
115	21	—	669 (45.4%)	806 (54.6%)	—	1475	
116	17	—	504 (40.4%)	743 (59.6%)	—	1247	
117	11	517 (40.8%)	—	749 (59.2%)	—	1266	
118	11	364 (43.0%)	—	482 (57.0%)	—	846	
119	35	1067 (46.7%)	—	1218 (53.3%)	—	2285	
120	15	565 (39.1%)	—	880 (60.9%)	—	1445	
121	126	—	4553 (45.6%)	5441 (54.4%)	—	9994	
122	124	—	3323 (66.4%)	1684 (33.6%)	—	5007	
123	473	8145 (58.1%)	3494 (24.9%)	2385 (17.0%)	2 (0.0%)	14026	
124	23	72 (23.8%)	80 (26.4%)	151 (49.8%)	—	303	
125	52	659 (32.7%)	696 (34.5%)	662 (32.8%)	1 (0.1%)	2018	
126	12	—	210 (46.5%)	242 (53.5%)	—	452	
127	403	10069 (80.6%)	—	2412 (19.3%)	7 (0.1%)	12488	
128	76	113 (3.4%)	2320 (70.6%)	836 (25.4%)	16 (0.5%)	3285	
129	884	6683 (32.6%)	5794 (28.2%)	8029 (39.1%)	6 (0.0%)	20512	
130	38	330 (30.6%)	134 (12.4%)	613 (56.9%)	—	1077	
131	44	429 (63.5%)	—	247 (36.5%)	—	676	
132	10	—	249 (62.9%)	147 (37.1%)	—	396	
133	3	29 (43.3%)	11 (16.4%)	27 (40.3%)	—	67	
134	4	—	51 (78.5%)	14 (21.5%)	—	65	
135	30	560 (59.3%)	—	384 (40.7%)	—	944	
136	266	—	5570 (57.4%)	4098 (42.3%)	29 (0.3%)	9697	
137	70	—	1827 (59.4%)	1249 (40.6%)	—	3076	
138	22	517 (60.0%)	—	344 (40.0%)	—	861	
139	1622	7320 (13.0%)	37938 (67.4%)	10985 (19.5%)	68 (0.1%)	56311	
140	457	7845 (57.6%)	2501 (18.4%)	3264 (24.0%)	4 (0.0%)	13614	
141	267	611 (6.5%)	5800 (62.1%)	2907 (31.1%)	26 (0.3%)	9344	
142	77	—	1352 (48.7%)	1425 (51.3%)	—	2777	
143	18	2 (0.1%)	—	1393 (89.1%)	168 (10.8%)	1563	
144	13	—	—	502 (100%)	—	502	
145	5	—	—	203 (100%)	—	203	
146	87	—	—	7694 (100%)	—	7694	
147	75	—	4625 (73.0%)	1481 (23.4%)	232 (3.7%)	6338	
148	496	—	29625 (68.3%)	13720 (31.6%)	57 (0.1%)	43402	
149	10	—	—	435 (86.1%)	70 (13.9%)	505	
150	66	—	—	3456 (89.2%)	419 (10.8%)	3875	
151	5	—	—	165 (100%)	—	165	
152	42	—	—	892 (100%)	—	892	
153	2	—	—	44 (100%)	—	44	
154	19	—	—	423 (100%)	—	423	
155	54	—	—	4560 (100%)	—	4560	
156	57	—	—	1146 (89.5%)	134 (10.5%)	1280	
157	16	—	—	696 (86.9%)	105 (13.1%)	801	
158	3	—	—	82 (97.6%)	2 (2.4%)	84	
159	26	—	—	904 (98.7%)	12 (1.3%)	916	
160	160	—	—	6273 (100%)	—	6273	

161	87	—	—	3311 (100%)	—	3311
162	54	—	1617 (72.4%)	482 (21.6%)	135 (6.0%)	2234
163	63	309 (11.0%)	897 (32.0%)	1466 (52.4%)	127 (4.5%)	2799
164	598	—	14976 (68.5%)	5093 (23.3%)	1810 (8.3%)	21879
165	34	1 (0.1%)	432 (48.9%)	419 (47.4%)	32 (3.6%)	884
166	1029	—	39673 (68.7%)	17908 (31.0%)	144 (0.2%)	57725
167	325	1717 (14.2%)	3830 (31.8%)	6501 (54.0%)	1 (0.0%)	12049
169	1	—	—	6 (100%)	—	6
173	124	—	—	2898 (98.4%)	47 (1.6%)	2945
174	59	1403 (64.2%)	—	783 (35.8%)	—	2186
175	2	—	39 (60.9%)	25 (39.1%)	—	64
176	206	671 (12.5%)	2483 (46.2%)	2199 (40.9%)	22 (0.4%)	5375
177	1	—	—	33 (100%)	—	33
180	28	—	—	276 (100%)	—	276
181	8	—	—	62 (100%)	—	62
182	34	—	—	668 (96.2%)	26 (3.8%)	694
183	1	—	—	9 (75.0%)	3 (25.0%)	12
185	51	—	—	975 (94.2%)	60 (5.8%)	1035
186	392	—	—	6973 (97.8%)	160 (2.2%)	7133
187	158	1193 (58.9%)	—	828 (40.9%)	4 (0.2%)	2025
188	21	147 (32.7%)	—	297 (66.0%)	6 (1.3%)	450
189	592	2850 (12.6%)	14666 (64.7%)	5125 (22.6%)	25 (0.1%)	22666
190	45	741 (49.2%)	—	749 (49.7%)	17 (1.1%)	1507
191	506	—	6987 (78.2%)	1929 (21.6%)	17 (0.2%)	8933
192	2	—	17 (68.0%)	8 (32.0%)	—	25
193	302	13 (0.4%)	1705 (54.9%)	1368 (44.0%)	21 (0.7%)	3107
194	1619	5224 (18.7%)	14644 (52.3%)	7725 (27.6%)	393 (1.4%)	27986
195	1	—	—	91 (100%)	—	91
196	1	—	—	83 (100%)	—	83
197	20	—	—	966 (100%)	—	966
198	173	—	—	3771 (100%)	—	3771
199	33	—	—	679 (85.2%)	118 (14.8%)	797
200	22	113 (8.3%)	951 (69.6%)	290 (21.2%)	12 (0.9%)	1366
201	7	117 (23.0%)	299 (58.9%)	92 (18.1%)	—	508
202	18	—	598 (47.5%)	648 (51.4%)	14 (1.1%)	1260
203	6	7 (1.7%)	314 (76.8%)	82 (20.1%)	6 (1.5%)	409
204	151	—	4138 (74.2%)	1353 (24.3%)	83 (1.5%)	5574
205	130	1196 (52.9%)	—	1066 (47.1%)	—	2262
206	61	—	1045 (72.7%)	350 (24.3%)	43 (3.0%)	1438
208	2	—	—	10 (83.3%)	2 (16.7%)	12
210	1	—	—	16 (64.0%)	9 (36.0%)	25
211	1	—	—	22 (100%)	—	22
212	14	—	—	282 (100%)	—	282
213	22	—	—	243 (100%)	—	243
214	14	—	—	233 (90.0%)	26 (10.0%)	259
215	54	178 (7.2%)	909 (36.8%)	1239 (50.1%)	146 (5.9%)	2472
216	777	6971 (44.8%)	—	7464 (48.0%)	1110 (7.1%)	15545
217	111	—	1584 (34.5%)	2843 (61.9%)	163 (3.5%)	4590
218	42	—	547 (41.8%)	755 (57.7%)	6 (0.5%)	1308
219	9	6 (1.6%)	173 (44.6%)	206 (53.1%)	3 (0.8%)	388
220	143	795 (37.8%)	—	1187 (56.4%)	124 (5.9%)	2106
221	1352	1836 (15.8%)	5688 (49.0%)	4070 (35.1%)	7 (0.1%)	11601
223	222	—	1343 (57.4%)	903 (38.6%)	93 (4.0%)	2339
224	17	—	206 (81.1%)	48 (18.9%)	—	254
225	1693	—	23368 (64.0%)	12701 (34.8%)	421 (1.1%)	36490
226	46	38 (6.0%)	342 (54.3%)	243 (38.6%)	7 (1.1%)	630

227	841	285 (1.5%)	14032 (75.5%)	3786 (20.4%)	473 (2.5%)	18576
229	210	42 (1.2%)	2740 (76.1%)	813 (22.6%)	7 (0.2%)	3602
230	6	22 (43.1%)	8 (15.7%)	20 (39.2%)	1 (2.0%)	51
Total	38298	859606 (43.0%)	379321 (19.0%)	750504 (37.6%)	7297 (0.4%)	1996728

Table S18: In this table, we list the number of unique materials that contain at least some topological features with SOC in each SG. In order, the columns in this table list the SG, the number of unique materials in the SG, the number of unique materials with either at least one stable or fragile band in the spectrum or symmetry-enforced crossing points at  $E_F$  (*i.e.* materials that are either ES- or ESFD-classified semimetals or exhibit stable or fragile topological bands at any filling). From left to right, in the following columns we list, per SG, the number of unique materials with at least one stable or fragile topological connected set of bands at any filling, at least one fragile topological set of bands at any filling, at least one NLC-classified stable topological band at any filling, at least one SEBR-classified stable topological band at any filling, and at least one stable topological set of bands at any filling. In the remaining three columns, we list the number of materials that do not contain *any* symmetry-indicated stable or fragile topological bands (STriv), the number of supermetallic (SMetal) materials in which *all* of the bands in at least one of the ICSDs associated to the unique material are *fully* connected, and the number of unique materials in which all bands are stable topological [*i.e.* supertopological (STopo) materials, see S9]. For all of the topological classification categories in the table, each number of materials is accompanied by the percentage of materials in the SG in the topological class. When there are no materials in the topological class, the table entry is marked with a dashed horizontal line.

SG	# Mat.	Topology	$\geq 1$ topo. band	$\geq 1$ frag. band	$\geq 1$ NLC band	$\geq 1$ SEBR band	$\geq 1$ NLC or SEBR band	STriv	SMetal	STopo
1	151	9 (6.0%)	—	—	—	—	151 (100%)	—	—	—
2	1574	1574 (100%)	1574 (100%)	—	1574 (100%)	—	1574 (100%)	—	—	7 (0.4%)
3	13	—	—	—	—	—	—	13 (100%)	—	—
4	228	8 (3.5%)	—	—	—	—	—	228 (100%)	—	—
5	156	15 (9.6%)	—	—	—	—	—	156 (100%)	—	—
6	28	1 (3.6%)	—	—	—	—	—	28 (100%)	—	—
7	85	3 (3.5%)	—	—	—	—	—	85 (100%)	—	—
8	144	13 (9.0%)	—	—	—	—	—	144 (100%)	—	—
9	199	11 (5.5%)	—	—	—	—	—	199 (100%)	—	—
10	38	38 (100%)	38 (100%)	—	38 (100%)	—	38 (100%)	—	—	1 (2.6%)
11	587	587 (100%)	587 (100%)	—	587 (100%)	—	587 (100%)	—	—	1 (0.2%)
12	1345	1345 (100%)	1345 (100%)	—	1345 (100%)	1341 (99.7%)	1345 (100%)	—	—	9 (0.7%)
13	195	195 (100%)	195 (100%)	—	195 (100%)	—	195 (100%)	—	—	1 (0.5%)
14	2665	2665 (100%)	2665 (100%)	—	2665 (100%)	—	2665 (100%)	—	—	24 (0.9%)
15	1485	1485 (100%)	1485 (100%)	—	1485 (100%)	—	1485 (100%)	—	—	—
16	2	—	—	—	—	—	—	2 (100%)	—	—
17	8	—	—	—	—	—	—	8 (100%)	—	—
18	30	2 (6.7%)	—	—	—	—	—	30 (100%)	—	—
19	270	20 (7.4%)	—	—	—	—	—	270 (100%)	—	—
20	66	2 (3.0%)	—	—	—	—	—	66 (100%)	—	—
21	16	6 (37.5%)	—	—	—	—	—	16 (100%)	—	—
22	17	—	—	—	—	—	—	17 (100%)	—	—
23	16	2 (12.5%)	—	—	—	—	—	16 (100%)	—	—
24	2	—	—	—	—	—	—	2 (100%)	—	—
25	45	2 (4.4%)	—	—	—	—	—	45 (100%)	—	—
26	60	4 (6.7%)	—	—	—	—	—	60 (100%)	—	—

27	1	—	—	—	—	—	—	—	1 (100%)	—	—
28	11	2 (18.2%)	—	—	—	—	—	—	11 (100%)	—	—
29	61	1 (1.6%)	—	—	—	—	—	—	61 (100%)	—	—
30	5	1 (20.0%)	—	—	—	—	—	—	5 (100%)	—	—
31	159	14 (8.8%)	—	—	—	—	—	—	159 (100%)	—	—
32	10	—	—	—	—	—	—	—	10 (100%)	—	—
33	257	24 (9.3%)	—	—	—	—	—	—	257 (100%)	—	—
34	21	3 (14.3%)	—	—	—	—	—	—	21 (100%)	—	—
35	8	2 (25.0%)	—	—	—	—	—	—	8 (100%)	—	—
36	261	40 (15.3%)	—	—	—	—	—	—	261 (100%)	—	—
37	5	—	—	—	—	—	—	—	5 (100%)	—	—
38	104	33 (31.7%)	—	—	—	—	—	—	104 (100%)	—	—
39	13	—	—	—	—	—	—	—	13 (100%)	—	—
40	57	5 (8.8%)	—	—	—	—	—	—	57 (100%)	—	—
41	31	1 (3.2%)	—	—	—	—	—	—	31 (100%)	—	—
42	4	—	—	—	—	—	—	—	4 (100%)	—	—
43	84	13 (15.5%)	—	—	—	—	—	—	84 (100%)	—	—
44	69	11 (15.9%)	—	—	—	—	—	—	69 (100%)	—	—
45	8	—	—	—	—	—	—	—	8 (100%)	—	—
46	57	7 (12.3%)	—	—	—	—	—	—	57 (100%)	—	—
47	51	51 (100%)	51 (100%)	—	51 (100%)	—	—	51 (100%)	—	—	—
48	3	3 (100%)	3 (100%)	—	3 (100%)	3 (100%)	—	3 (100%)	—	—	—
49	1	1 (100%)	1 (100%)	—	1 (100%)	—	—	1 (100%)	—	—	—
50	7	7 (100%)	7 (100%)	—	7 (100%)	7 (100%)	—	7 (100%)	—	—	—
51	107	107 (100%)	107 (100%)	—	107 (100%)	—	—	107 (100%)	—	—	2 (1.9%)
52	39	39 (100%)	39 (100%)	—	39 (100%)	—	—	39 (100%)	—	—	—
53	18	18 (100%)	18 (100%)	—	—	18 (100%)	—	18 (100%)	—	—	—
54	19	19 (100%)	19 (100%)	—	19 (100%)	—	—	19 (100%)	—	—	—
55	394	394 (100%)	394 (100%)	—	394 (100%)	—	—	394 (100%)	—	—	5 (1.3%)
56	19	19 (100%)	19 (100%)	—	19 (100%)	—	—	19 (100%)	—	—	—
57	142	142 (100%)	142 (100%)	—	142 (100%)	—	—	142 (100%)	—	—	—
58	208	208 (100%)	208 (100%)	—	208 (100%)	—	—	208 (100%)	—	—	1 (0.5%)
59	227	227 (100%)	227 (100%)	—	226 (99.6%)	225 (99.1%)	—	227 (100%)	—	—	—
60	142	142 (100%)	142 (100%)	—	142 (100%)	—	—	142 (100%)	—	—	—
61	122	122 (100%)	122 (100%)	—	122 (100%)	—	—	122 (100%)	—	—	9 (7.4%)
62	3006	3002 (99.9%)	3002 (99.9%)	—	3002 (99.9%)	—	—	3002 (99.9%)	5 (0.2%)	—	3 (0.1%)
63	1396	1396 (100%)	1396 (100%)	—	1396 (100%)	1187 (85.0%)	—	1396 (100%)	—	—	6 (0.4%)
64	257	257 (100%)	257 (100%)	—	—	257 (100%)	257 (100%)	—	—	—	5 (1.9%)
65	241	241 (100%)	241 (100%)	—	241 (100%)	238 (98.8%)	—	241 (100%)	—	—	2 (0.8%)
66	36	36 (100%)	36 (100%)	—	36 (100%)	—	—	36 (100%)	—	—	—
67	30	30 (100%)	30 (100%)	—	30 (100%)	—	—	30 (100%)	—	—	—
68	19	19 (100%)	19 (100%)	—	—	19 (100%)	19 (100%)	—	—	—	—
69	66	66 (100%)	66 (100%)	—	—	66 (100%)	66 (100%)	—	—	—	—
70	139	139 (100%)	139 (100%)	—	133 (95.7%)	139 (100%)	139 (100%)	—	—	—	—
71	452	452 (100%)	451 (99.8%)	—	449 (99.3%)	450 (99.6%)	451 (99.8%)	1 (0.2%)	—	—	—
72	192	192 (100%)	192 (100%)	—	192 (100%)	173 (90.1%)	192 (100%)	—	—	—	—
73	24	24 (100%)	24 (100%)	—	24 (100%)	—	—	24 (100%)	—	—	—
74	218	218 (100%)	218 (100%)	—	218 (100%)	—	—	218 (100%)	—	—	2 (0.9%)
75	5	2 (40.0%)	—	—	—	—	—	—	5 (100%)	—	—
76	12	2 (16.7%)	—	—	—	—	—	—	12 (100%)	—	—
77	2	—	—	—	—	—	—	—	2 (100%)	—	—
78	2	—	—	—	—	—	—	—	2 (100%)	—	—
79	11	1 (9.1%)	—	—	—	—	—	—	11 (100%)	—	—
80	3	—	—	—	—	—	—	—	3 (100%)	—	—
81	14	14 (100%)	14 (100%)	—	—	14 (100%)	14 (100%)	—	—	—	—
82	136	136 (100%)	136 (100%)	1 (0.7%)	136 (100%)	—	136 (100%)	—	—	—	—

83	10	10 (100%)	10 (100%)	—	10 (100%)	10 (100%)	10 (100%)	—	—	—	1 (10.0%)
84	28	28 (100%)	28 (100%)	—	28 (100%)	—	28 (100%)	—	—	—	—
85	39	39 (100%)	39 (100%)	—	39 (100%)	39 (100%)	39 (100%)	—	—	—	—
86	51	51 (100%)	51 (100%)	—	—	51 (100%)	51 (100%)	—	—	—	—
87	181	181 (100%)	181 (100%)	11 (6.1%)	177 (97.8%)	181 (100%)	181 (100%)	—	—	—	1 (0.6%)
88	139	139 (100%)	139 (100%)	3 (2.2%)	93 (66.9%)	139 (100%)	139 (100%)	—	—	—	1 (0.7%)
90	5	2 (40.0%)	—	—	—	—	—	5 (100%)	—	—	—
91	7	1 (14.3%)	—	—	—	—	—	7 (100%)	—	—	—
92	47	16 (34.0%)	—	—	—	—	—	47 (100%)	—	—	—
94	1	—	—	—	—	—	—	1 (100%)	—	—	—
95	3	1 (33.3%)	—	—	—	—	—	3 (100%)	—	—	—
96	16	1 (6.2%)	—	—	—	—	—	16 (100%)	—	—	—
97	2	1 (50.0%)	—	—	—	—	—	2 (100%)	—	—	—
98	4	—	—	—	—	—	—	4 (100%)	—	—	—
99	98	22 (22.4%)	—	—	—	—	—	98 (100%)	—	—	—
100	20	12 (60.0%)	—	—	—	—	—	20 (100%)	—	—	—
102	12	3 (25.0%)	—	—	—	—	—	12 (100%)	—	—	—
103	3	3 (100%)	—	—	—	—	—	3 (100%)	—	—	—
104	3	1 (33.3%)	—	—	—	—	—	3 (100%)	—	—	—
105	4	—	—	—	—	—	—	4 (100%)	—	—	—
106	1	1 (100%)	—	—	—	—	—	1 (100%)	—	—	—
107	121	68 (56.2%)	—	—	—	—	—	121 (100%)	—	—	—
108	15	5 (33.3%)	—	—	—	—	—	15 (100%)	—	—	—
109	40	16 (40.0%)	—	—	—	—	—	40 (100%)	—	—	—
110	8	2 (25.0%)	—	—	—	—	—	8 (100%)	—	—	—
111	21	21 (100%)	21 (100%)	—	—	21 (100%)	21 (100%)	—	—	—	—
112	4	4 (100%)	4 (100%)	—	4 (100%)	—	4 (100%)	—	—	—	—
113	84	84 (100%)	84 (100%)	—	84 (100%)	—	84 (100%)	—	—	—	—
114	31	31 (100%)	31 (100%)	—	—	31 (100%)	31 (100%)	—	—	—	—
115	21	21 (100%)	21 (100%)	—	—	21 (100%)	21 (100%)	—	—	—	—
116	17	17 (100%)	17 (100%)	—	—	17 (100%)	17 (100%)	—	—	—	—
117	11	11 (100%)	11 (100%)	—	11 (100%)	—	11 (100%)	—	—	—	—
118	11	11 (100%)	11 (100%)	—	11 (100%)	—	11 (100%)	—	—	—	—
119	35	35 (100%)	35 (100%)	—	35 (100%)	—	35 (100%)	—	—	—	—
120	15	15 (100%)	15 (100%)	—	15 (100%)	—	15 (100%)	—	—	—	—
121	126	126 (100%)	126 (100%)	—	—	126 (100%)	126 (100%)	—	—	—	—
122	124	124 (100%)	124 (100%)	—	—	124 (100%)	124 (100%)	—	—	—	4 (3.2%)
123	473	473 (100%)	472 (99.8%)	3 (0.6%)	469 (99.2%)	429 (90.7%)	472 (99.8%)	—	—	—	41 (8.7%)
124	23	23 (100%)	23 (100%)	—	18 (78.3%)	22 (95.7%)	23 (100%)	—	—	—	—
125	52	52 (100%)	52 (100%)	1 (1.9%)	52 (100%)	52 (100%)	52 (100%)	—	—	—	—
126	12	12 (100%)	12 (100%)	—	—	12 (100%)	12 (100%)	—	—	—	—
127	403	403 (100%)	403 (100%)	7 (1.7%)	403 (100%)	—	403 (100%)	—	—	—	6 (1.5%)
128	76	76 (100%)	76 (100%)	14 (18.4%)	56 (73.7%)	76 (100%)	76 (100%)	—	—	—	—
129	884	884 (100%)	884 (100%)	6 (0.7%)	852 (96.4%)	874 (98.9%)	884 (100%)	—	—	—	1 (0.1%)
130	38	38 (100%)	38 (100%)	—	38 (100%)	35 (92.1%)	38 (100%)	—	—	—	—
131	44	44 (100%)	44 (100%)	—	44 (100%)	—	44 (100%)	—	—	—	—
132	10	10 (100%)	10 (100%)	—	—	10 (100%)	10 (100%)	—	—	—	—
133	3	3 (100%)	3 (100%)	—	3 (100%)	3 (100%)	3 (100%)	—	—	—	—
134	4	4 (100%)	4 (100%)	—	—	4 (100%)	4 (100%)	—	—	—	—
135	30	30 (100%)	30 (100%)	—	30 (100%)	—	30 (100%)	—	—	—	—
136	266	264 (99.2%)	264 (99.2%)	28 (10.5%)	—	264 (99.2%)	264 (99.2%)	2 (0.8%)	—	—	—
137	70	70 (100%)	70 (100%)	—	—	70 (100%)	70 (100%)	—	—	—	—
138	22	22 (100%)	22 (100%)	—	22 (100%)	—	22 (100%)	—	—	—	—
139	1622	1622 (100%)	1622 (100%)	69 (4.2%)	1508 (93.0%)	1618 (99.8%)	1622 (100%)	—	—	—	43 (2.6%)
140	457	457 (100%)	457 (100%)	4 (0.9%)	457 (100%)	432 (94.5%)	457 (100%)	—	—	—	45 (9.8%)
141	267	267 (100%)	267 (100%)	23 (8.6%)	203 (76.0%)	267 (100%)	267 (100%)	—	—	—	2 (0.8%)

142	77	77 (100%)	77 (100%)	—	—	77 (100%)	77 (100%)	—	—	—
143	18	16 (88.9%)	15 (83.3%)	15 (83.3%)	1 (5.6%)	—	1 (5.6%)	—	—	—
144	13	1 (7.7%)	—	—	—	—	—	13 (100%)	—	—
145	5	—	—	—	—	—	—	5 (100%)	—	—
146	87	15 (17.2%)	—	—	—	—	—	87 (100%)	—	—
147	75	75 (100%)	75 (100%)	46 (61.3%)	—	75 (100%)	75 (100%)	—	—	—
148	496	496 (100%)	496 (100%)	52 (10.5%)	—	496 (100%)	496 (100%)	—	—	—
149	10	8 (80.0%)	8 (80.0%)	8 (80.0%)	—	—	—	—	—	—
150	66	48 (72.7%)	46 (69.7%)	46 (69.7%)	—	—	—	1 (1.5%)	—	—
151	5	—	—	—	—	—	—	5 (100%)	—	—
152	42	12 (28.6%)	—	—	—	—	—	42 (100%)	—	—
153	2	—	—	—	—	—	—	2 (100%)	—	—
154	19	2 (10.5%)	—	—	—	—	—	19 (100%)	—	—
155	54	12 (22.2%)	—	—	—	—	—	54 (100%)	—	—
156	57	42 (73.7%)	37 (64.9%)	37 (64.9%)	—	—	—	11 (19.3%)	—	—
157	16	14 (87.5%)	13 (81.2%)	13 (81.2%)	—	—	—	—	—	—
158	3	3 (100%)	2 (66.7%)	2 (66.7%)	—	—	—	1 (33.3%)	—	—
159	26	12 (46.1%)	7 (26.9%)	7 (26.9%)	—	—	—	20 (76.9%)	—	—
160	160	42 (26.2%)	—	—	—	—	—	160 (100%)	—	—
161	87	15 (17.2%)	—	—	—	—	—	87 (100%)	—	—
162	54	54 (100%)	54 (100%)	40 (74.1%)	—	54 (100%)	54 (100%)	—	—	—
163	63	63 (100%)	63 (100%)	46 (73.0%)	62 (98.4%)	63 (100%)	63 (100%)	—	—	—
164	598	598 (100%)	598 (100%)	459 (76.8%)	—	598 (100%)	598 (100%)	—	—	13 (2.2%)
165	34	34 (100%)	33 (97.1%)	13 (38.2%)	1 (2.9%)	33 (97.1%)	33 (97.1%)	1 (2.9%)	—	—
166	1029	1029 (100%)	1029 (100%)	129 (12.5%)	—	1029 (100%)	1029 (100%)	—	—	6 (0.6%)
167	325	324 (99.7%)	324 (99.7%)	1 (0.3%)	303 (93.2%)	323 (99.4%)	324 (99.7%)	3 (0.9%)	—	—
169	1	—	—	—	—	—	—	1 (100%)	—	—
173	124	63 (50.8%)	28 (22.6%)	28 (22.6%)	—	—	—	92 (74.2%)	—	—
174	59	59 (100%)	59 (100%)	—	59 (100%)	—	59 (100%)	—	—	—
175	2	2 (100%)	2 (100%)	—	—	2 (100%)	2 (100%)	—	—	—
176	206	206 (100%)	205 (99.5%)	12 (5.8%)	162 (78.6%)	203 (98.5%)	205 (99.5%)	—	—	5 (2.4%)
177	1	—	—	—	—	—	—	—	—	—
180	28	16 (57.1%)	—	—	—	—	—	28 (100%)	—	—
181	8	4 (50.0%)	—	—	—	—	—	8 (100%)	—	—
182	34	28 (82.3%)	15 (44.1%)	15 (44.1%)	—	—	—	19 (55.9%)	—	—
183	1	1 (100%)	1 (100%)	1 (100%)	—	—	—	—	—	—
185	51	38 (74.5%)	21 (41.2%)	21 (41.2%)	—	—	—	24 (47.1%)	—	—
186	392	255 (65.0%)	80 (20.4%)	80 (20.4%)	—	—	—	288 (73.5%)	—	—
187	158	155 (98.1%)	155 (98.1%)	2 (1.3%)	155 (98.1%)	—	155 (98.1%)	3 (1.9%)	—	1 (0.6%)
188	21	20 (95.2%)	18 (85.7%)	5 (23.8%)	18 (85.7%)	—	18 (85.7%)	3 (14.3%)	—	—
189	592	592 (100%)	592 (100%)	23 (3.9%)	577 (97.5%)	592 (100%)	592 (100%)	—	—	10 (1.7%)
190	45	45 (100%)	45 (100%)	10 (22.2%)	45 (100%)	—	45 (100%)	—	—	—
191	506	506 (100%)	501 (99.0%)	20 (4.0%)	—	501 (99.0%)	501 (99.0%)	—	4 (0.8%)	63 (12.4%)
192	2	2 (100%)	2 (100%)	—	—	2 (100%)	2 (100%)	—	—	—
193	302	302 (100%)	300 (99.3%)	13 (4.3%)	11 (3.6%)	299 (99.0%)	300 (99.3%)	3 (1.0%)	—	3 (1.0%)
194	1619	1607 (99.3%)	1571 (97.0%)	240 (14.8%)	1246 (77.0%)	1542 (95.2%)	1571 (97.0%)	27 (1.7%)	5 (0.3%)	130 (8.0%)
195	1	—	—	—	—	—	—	1 (100%)	—	—
196	1	1 (100%)	—	—	—	—	—	1 (100%)	—	—
197	20	9 (45.0%)	—	—	—	—	—	20 (100%)	—	—
198	173	78 (45.1%)	—	—	—	—	—	173 (100%)	—	—
199	33	29 (87.9%)	28 (84.8%)	28 (84.8%)	—	—	—	2 (6.1%)	—	—
200	22	22 (100%)	22 (100%)	8 (36.4%)	22 (100%)	22 (100%)	22 (100%)	—	—	—
201	7	7 (100%)	7 (100%)	—	7 (100%)	7 (100%)	7 (100%)	—	—	—
202	18	18 (100%)	18 (100%)	7 (38.9%)	—	18 (100%)	18 (100%)	—	—	—
203	6	6 (100%)	6 (100%)	3 (50.0%)	5 (83.3%)	6 (100%)	6 (100%)	—	—	—
204	151	151 (100%)	151 (100%)	57 (37.8%)	—	151 (100%)	151 (100%)	—	1 (0.7%)	—

205	130	129 (99.2%)	129 (99.2%)	—	129 (99.2%)	—	129 (99.2%)	1 (0.8%)	—	2 (1.5%)	
206	61	61 (100%)	59 (96.7%)	25 (41.0%)	—	59 (96.7%)	59 (96.7%)	—	—	4 (6.6%)	
208	2	2 (100%)	2 (100%)	2 (100%)	—	—	—	—	—	—	
210	1	1 (100%)	1 (100%)	1 (100%)	—	—	—	—	—	—	
211	1	1 (100%)	—	—	—	—	—	—	—	—	
212	14	8 (57.1%)	—	—	—	—	—	14 (100%)	—	—	
213	22	17 (77.3%)	—	—	—	—	—	22 (100%)	—	—	
214	14	13 (92.9%)	10 (71.4%)	10 (71.4%)	—	—	—	1 (7.1%)	—	—	
215	54	54 (100%)	54 (100%)	36 (66.7%)	47 (87.0%)	53 (98.2%)	54 (100%)	—	—	—	
216	777	774 (99.6%)	772 (99.4%)	502 (64.6%)	768 (98.8%)	—	768 (98.8%)	5 (0.6%)	—	1 (0.1%)	
217	111	111 (100%)	111 (100%)	72 (64.9%)	—	111 (100%)	111 (100%)	—	—	—	
218	42	42 (100%)	42 (100%)	5 (11.9%)	—	42 (100%)	42 (100%)	—	—	—	
219	9	9 (100%)	9 (100%)	2 (22.2%)	4 (44.4%)	9 (100%)	9 (100%)	—	—	—	
220	143	143 (100%)	142 (99.3%)	95 (66.4%)	142 (99.3%)	—	142 (99.3%)	2 (1.4%)	—	—	
221	1352	1338 (99.0%)	1299 (96.1%)	7 (0.5%)	899 (66.5%)	1273 (94.2%)	1299 (96.1%)	30 (2.2%)	2 (0.1%)	196 (14.5%)	
223	222	222 (100%)	218 (98.2%)	74 (33.3%)	—	218 (98.2%)	218 (98.2%)	2 (0.9%)	—	9 (4.0%)	
224	17	17 (100%)	17 (100%)	—	—	17 (100%)	17 (100%)	—	—	1 (5.9%)	
225	1693	1679 (99.2%)	1671 (98.7%)	337 (19.9%)	—	1664 (98.3%)	1664 (98.3%)	25 (1.5%)	—	37 (2.2%)	
226	46	46 (100%)	44 (95.7%)	7 (15.2%)	22 (47.8%)	44 (95.7%)	44 (95.7%)	1 (2.2%)	—	—	
227	841	841 (100%)	840 (99.9%)	322 (38.3%)	231 (27.5%)	840 (99.9%)	840 (99.9%)	1 (0.1%)	1 (0.1%)	33 (3.9%)	
229	210	209 (99.5%)	196 (93.3%)	7 (3.3%)	31 (14.8%)	196 (93.3%)	196 (93.3%)	6 (2.9%)	5 (2.4%)	31 (14.8%)	
230	6	6 (100%)	6 (100%)	1 (16.7%)	6 (100%)	4 (66.7%)	6 (100%)	—	—	—	
Total	38298	34664 (90.5%)	33636 (87.8%)	3162 (8.3%)	24841 (64.9%)	19688 (51.4%)	33312 (87.0%)	4529 (11.8%)	17 (0.0%)	769 (2.0%)	

Table S19: In this table, we list the number of isolated sets of bands w/o SOC as determined by band connectivity (see S2) in unique materials in each SG in each topological class. In order, the columns in this table list the SG, the number of unique materials in the SG, the number of NLC-classified sets of bands, the number of SEBR-classified sets of bands, the number of LCEBR-classified sets of bands, the number of sets of connected fragile bands, and the total number of sets of isolated (connected) bands. For all of the topological classification categories in the table, each number of bands is accompanied by the percentage of bands in the SG in the topological class. When there are no bands in the topological class, the table entry is marked with a dashed horizontal line.

SG	# Mat.	# NLC bands	# SEBR bands	# LCEBR bands	# Fragile bands	Total # isolated bands
1	151	—	—	13271 (100%)	—	13271
2	1466	181126 (81.7%)	—	40496 (18.3%)	—	221622
3	10	89 (29.0%)	—	218 (71.0%)	—	307
4	219	—	—	9057 (100%)	—	9057
5	148	—	—	7054 (100%)	—	7054
6	28	—	—	692 (100%)	—	692
7	85	—	—	3498 (100%)	—	3498
8	141	—	—	4171 (100%)	—	4171
9	197	—	—	8834 (100%)	—	8834
10	33	40 (14.0%)	—	245 (85.7%)	1 (0.3%)	286
11	547	411 (3.9%)	—	10218 (96.1%)	—	10629
12	1250	7793 (26.8%)	—	21273 (73.0%)	56 (0.2%)	29122
13	164	721 (21.4%)	—	2648 (78.6%)	—	3369
14	2520	14220 (18.0%)	—	64657 (82.0%)	2 (0.0%)	78879
15	1402	14168 (34.3%)	—	27162 (65.7%)	—	41330
16	2	—	—	9 (100%)	—	9
17	8	—	—	61 (100%)	—	61
18	30	—	—	820 (100%)	—	820
19	261	—	—	7018 (100%)	—	7018
20	58	—	—	1463 (100%)	—	1463

21	15	—	—	147 (100%)	—	147	
22	14	—	—	184 (100%)	—	184	
23	15	—	—	427 (100%)	—	427	
24	2	—	—	23 (100%)	—	23	
25	45	—	—	280 (100%)	—	280	
26	59	—	—	838 (100%)	—	838	
27	1	—	—	4 (100%)	—	4	
28	11	—	—	91 (100%)	—	91	
29	59	—	—	1124 (100%)	—	1124	
30	5	—	—	107 (100%)	—	107	
31	158	—	—	3384 (100%)	—	3384	
32	10	—	—	268 (100%)	—	268	
33	251	—	—	5382 (100%)	—	5382	
34	21	—	—	504 (100%)	—	504	
35	8	—	—	131 (100%)	—	131	
36	241	—	—	4848 (100%)	—	4848	
37	5	9 (15.2%)	—	50 (84.8%)	—	59	
38	95	—	—	1057 (100%)	—	1057	
39	12	—	—	120 (100%)	—	120	
40	54	—	—	998 (100%)	—	998	
41	31	—	—	591 (100%)	—	591	
42	4	—	—	96 (100%)	—	96	
43	83	—	—	2409 (100%)	—	2409	
44	62	—	—	933 (100%)	—	933	
45	8	—	—	121 (100%)	—	121	
46	55	—	—	667 (100%)	—	667	
47	45	—	—	299 (100%)	—	299	
48	3	—	—	21 (100%)	—	21	
50	7	7 (11.5%)	—	54 (88.5%)	—	61	
51	100	—	—	638 (100%)	—	638	
52	36	27 (8.1%)	—	307 (91.9%)	—	334	
53	18	23 (12.4%)	—	162 (87.6%)	—	185	
54	18	1 (0.5%)	—	201 (99.5%)	—	202	
55	336	—	—	2814 (100%)	—	2814	
56	19	28 (11.3%)	—	220 (88.7%)	—	248	
57	128	—	—	1161 (100%)	—	1161	
58	202	351 (14.8%)	—	2012 (85.1%)	1 (0.0%)	2364	
59	208	—	—	1754 (100%)	—	1754	
60	139	151 (10.2%)	—	1330 (89.8%)	—	1481	
61	119	—	—	1359 (100%)	—	1359	
62	2800	—	—	28024 (100%)	—	28024	
63	1277	—	—	8619 (100%)	1 (0.0%)	8620	
64	244	—	—	2488 (99.9%)	2 (0.1%)	2490	
65	213	—	—	1209 (99.8%)	2 (0.2%)	1211	
66	34	17 (6.7%)	—	237 (92.9%)	1 (0.4%)	255	
67	29	—	—	170 (100%)	—	170	
68	19	8 (4.3%)	—	178 (95.7%)	—	186	
69	65	—	—	841 (99.5%)	4 (0.5%)	845	
70	130	222 (15.4%)	—	1218 (84.6%)	—	1440	
71	385	—	—	2847 (99.9%)	3 (0.1%)	2850	
72	182	—	—	1031 (100%)	—	1031	
73	16	—	—	186 (100%)	—	186	
74	202	—	—	1121 (99.9%)	1 (0.1%)	1122	
75	5	24 (16.0%)	—	126 (84.0%)	—	150	
76	12	—	—	337 (100%)	—	337	
77	2	1 (7.7%)	—	12 (92.3%)	—	13	

78	2	—	—	89 (100%)	—	89	
79	11	—	—	294 (99.7%)	1 (0.3%)	295	
80	3	—	—	137 (100%)	—	137	
81	13	196 (46.9%)	—	221 (52.9%)	1 (0.2%)	418	
82	130	1936 (40.6%)	—	2762 (58.0%)	65 (1.4%)	4763	
83	9	4 (5.6%)	—	67 (94.4%)	—	71	
84	28	36 (9.6%)	—	341 (90.5%)	—	377	
85	36	111 (20.4%)	—	433 (79.6%)	—	544	
86	49	28 (7.3%)	—	353 (92.7%)	—	381	
87	175	567 (22.8%)	—	1917 (77.1%)	2 (0.1%)	2486	
88	129	350 (17.3%)	—	1655 (82.0%)	13 (0.6%)	2018	
90	5	—	—	122 (97.6%)	3 (2.4%)	125	
91	7	—	—	59 (100%)	—	59	
92	47	—	—	611 (100%)	—	611	
94	1	—	—	10 (100%)	—	10	
95	3	—	—	21 (100%)	—	21	
96	16	—	—	207 (100%)	—	207	
97	2	—	—	25 (96.2%)	1 (3.9%)	26	
98	4	—	—	32 (100%)	—	32	
99	98	—	—	544 (99.5%)	3 (0.6%)	547	
100	20	—	—	419 (98.1%)	8 (1.9%)	427	
102	12	—	—	132 (100%)	—	132	
103	3	—	—	9 (100%)	—	9	
104	3	—	—	32 (100%)	—	32	
105	4	—	—	39 (100%)	—	39	
106	1	—	—	7 (100%)	—	7	
107	112	—	—	735 (100%)	—	735	
108	14	—	—	174 (100%)	—	174	
109	37	—	—	486 (100%)	—	486	
110	8	—	—	138 (100%)	—	138	
111	20	—	—	119 (100%)	—	119	
112	4	—	—	33 (100%)	—	33	
113	71	—	—	1092 (99.5%)	6 (0.6%)	1098	
114	31	—	—	420 (100%)	—	420	
115	21	—	—	166 (100%)	—	166	
116	17	—	—	91 (98.9%)	1 (1.1%)	92	
117	11	—	—	155 (100%)	—	155	
118	11	—	—	117 (100%)	—	117	
119	35	—	—	379 (98.4%)	6 (1.6%)	385	
120	15	—	—	194 (99.5%)	1 (0.5%)	195	
121	123	—	—	1509 (99.5%)	7 (0.5%)	1516	
122	124	—	—	1373 (96.5%)	49 (3.5%)	1422	
123	450	—	—	1646 (99.6%)	7 (0.4%)	1653	
124	22	—	—	98 (100%)	—	98	
125	49	—	—	370 (100%)	—	370	
126	11	—	—	86 (100%)	—	86	
127	368	—	—	2074 (100%)	—	2074	
128	71	64 (9.2%)	—	623 (90.0%)	5 (0.7%)	692	
129	861	—	—	3736 (99.8%)	8 (0.2%)	3744	
130	37	5 (1.6%)	21 (6.8%)	281 (91.5%)	—	307	
131	43	—	—	132 (100%)	—	132	
132	10	—	—	100 (100%)	—	100	
133	3	—	—	8 (100%)	—	8	
134	4	—	—	6 (100%)	—	6	
135	26	—	—	160 (100%)	—	160	
136	251	—	—	1707 (99.9%)	1 (0.1%)	1708	

137	68	—	—	541 (99.5%)	3 (0.6%)	544
138	16	—	—	117 (100%)	—	117
139	1543	—	—	6983 (99.8%)	16 (0.2%)	6999
140	431	—	—	2133 (100%)	1 (0.1%)	2134
141	246	—	—	1659 (99.3%)	11 (0.7%)	1670
142	73	—	—	468 (100%)	—	468
143	17	—	—	954 (97.3%)	26 (2.6%)	980
144	13	—	—	439 (100%)	—	439
145	5	—	—	182 (100%)	—	182
146	83	—	—	4154 (100%)	—	4154
147	71	47 (1.9%)	1351 (55.5%)	1015 (41.7%)	22 (0.9%)	2435
148	479	1857 (7.2%)	16880 (65.0%)	7035 (27.1%)	199 (0.8%)	25971
149	10	—	—	237 (97.5%)	6 (2.5%)	243
150	64	—	—	1298 (98.3%)	22 (1.7%)	1320
151	4	—	—	78 (100%)	—	78
152	40	—	—	333 (100%)	—	333
153	1	—	—	6 (100%)	—	6
154	17	—	—	171 (100%)	—	171
155	50	—	—	1351 (100%)	—	1351
156	57	—	—	750 (99.5%)	4 (0.5%)	754
157	14	—	—	238 (97.9%)	5 (2.1%)	243
158	3	—	—	61 (100%)	—	61
159	24	—	—	439 (100%)	—	439
160	158	—	—	2593 (100%)	—	2593
161	87	—	—	1691 (100%)	—	1691
162	52	—	22 (6.0%)	337 (92.3%)	6 (1.6%)	365
163	57	5 (0.5%)	100 (10.3%)	841 (87.0%)	21 (2.2%)	967
164	574	2 (0.1%)	218 (4.9%)	4060 (92.0%)	132 (3.0%)	4412
165	33	—	16 (6.5%)	230 (93.5%)	—	246
166	957	828 (7.9%)	52 (0.5%)	9314 (88.8%)	290 (2.8%)	10484
167	301	37 (1.0%)	448 (12.1%)	3202 (86.8%)	3 (0.1%)	3690
169	1	—	—	5 (100%)	—	5
173	113	—	—	2121 (100%)	1 (0.1%)	2122
174	50	—	—	655 (99.8%)	1 (0.1%)	656
175	2	—	—	16 (100%)	—	16
176	189	14 (0.6%)	62 (2.8%)	2156 (96.5%)	1 (0.0%)	2233
177	1	—	—	9 (100%)	—	9
180	28	—	—	87 (100%)	—	87
181	8	—	—	24 (100%)	—	24
182	33	—	—	263 (98.9%)	3 (1.1%)	266
183	1	—	—	3 (100%)	—	3
185	49	—	—	465 (99.4%)	3 (0.6%)	468
186	370	—	—	3674 (100%)	—	3674
187	154	—	—	737 (99.9%)	1 (0.1%)	738
188	20	—	—	247 (100%)	—	247
189	537	—	—	2614 (99.8%)	4 (0.1%)	2618
190	41	—	—	439 (99.3%)	3 (0.7%)	442
191	452	—	—	1214 (99.6%)	5 (0.4%)	1219
192	2	—	—	8 (100%)	—	8
193	270	—	—	916 (99.8%)	2 (0.2%)	918
194	1530	—	—	6630 (99.3%)	44 (0.7%)	6674
195	1	—	—	28 (100%)	—	28
196	1	—	—	36 (100%)	—	36
197	20	—	—	324 (100%)	—	324
198	170	—	—	2866 (100%)	—	2866
199	32	—	—	426 (100%)	—	426

200	22	—	—	161 (99.4%)	1 (0.6%)	162	
201	6	14 (14.6%)	—	82 (85.4%)	—	96	
202	18	—	—	324 (97.6%)	8 (2.4%)	332	
203	6	23 (18.1%)	—	101 (79.5%)	3 (2.4%)	127	
204	145	—	—	833 (100%)	—	833	
205	130	—	—	1134 (97.2%)	33 (2.8%)	1167	
206	60	—	—	415 (100%)	—	415	
208	2	—	—	6 (100%)	—	6	
210	1	—	—	9 (60.0%)	6 (40.0%)	15	
211	1	—	—	5 (100%)	—	5	
212	14	—	—	165 (100%)	—	165	
213	22	—	—	154 (100%)	—	154	
214	13	—	—	105 (100%)	—	105	
215	53	—	—	412 (99.0%)	4 (1.0%)	416	
216	751	—	—	4815 (92.3%)	404 (7.7%)	5219	
217	108	—	—	924 (99.9%)	1 (0.1%)	925	
218	42	—	—	418 (99.8%)	1 (0.2%)	419	
219	8	—	—	104 (100%)	—	104	
220	142	—	—	819 (99.4%)	5 (0.6%)	824	
221	1334	—	—	3387 (99.8%)	8 (0.2%)	3395	
223	217	—	—	690 (100%)	—	690	
224	16	—	—	59 (100%)	—	59	
225	1651	—	—	8290 (97.3%)	232 (2.7%)	8522	
226	43	—	—	131 (100%)	—	131	
227	816	—	—	3640 (98.0%)	76 (2.0%)	3716	
229	205	—	—	755 (99.6%)	3 (0.4%)	758	
230	6	—	—	9 (100%)	—	9	
Total	36163	225561 (32.6%)	19170 (2.8%)	444191 (64.3%)	1882 (0.3%)	690804	

Table S20: In this table, we list the number of unique materials that contain at least some topological features w/o SOC in each SG. In order, the columns in this table list the SG, the number of unique materials in the SG, the number of unique materials with either at least one stable or fragile band in the spectrum or symmetry-enforced crossing points at  $E_F$  (*i.e.* materials that are either ES-, ESFD-, NLC-SM- or SEBR-SM- classified semimetals at  $E_F$  or exhibit NLC, SEBR, or fragile topological bands at any filling at which the compatibility relations are satisfied). From left to right, in the following columns we list, per SG, the number of unique materials with at least one stable or fragile topological connected set of bands at any filling, at least one fragile topological set of bands at any filling, at least one NLC-classified stable topological band at any filling, at least one SEBR-classified stable topological band at any filling, and at least one stable topological set of bands at any filling. In the remaining three columns, we list the number of materials that do not contain *any* symmetry-indicated stable or fragile topological bands (STriv), the number of supermetallic (SMetal) materials in which *all* of the bands in at least one of the ICSDs associated to the unique material are *fully* connected, and the number of unique materials in which all bands are stable topological [*i.e.* supertopological (STopo) materials, see S9]. For all of the topological classification categories in the table, each number of materials is accompanied by the percentage of materials in the SG in the topological class. When there are no materials in the topological class, the table entry is marked with a dashed horizontal line.

SG	# Mat.	Topology	$\geq 1$ topo. band	$\geq 1$ frag. band	$\geq 1$ NLC band	$\geq 1$ SEBR band	$\geq 1$ NLC or SEBR band	STriv	SMetal	STopo
1	151	9 (6.0%)	—	—	—	—	—	151 (100%)	—	—

2	1466	1466 (100%)	1466 (100%)	—	1466 (100%)	—	1466 (100%)	—	—	6 (0.4%)
3	10	10 (100%)	9 (90.0%)	—	9 (90.0%)	—	9 (90.0%)	1 (10.0%)	—	—
4	219	20 (9.1%)	—	—	—	—	—	218 (99.5%)	—	—
5	148	31 (20.9%)	—	—	—	—	—	148 (100%)	—	—
6	28	5 (17.9%)	—	—	—	—	—	28 (100%)	—	—
7	85	9 (10.6%)	—	—	—	—	—	85 (100%)	—	—
8	141	26 (18.4%)	—	—	—	—	—	138 (97.9%)	—	—
9	197	15 (7.6%)	—	—	—	—	—	197 (100%)	—	—
10	33	27 (81.8%)	22 (66.7%)	1 (3.0%)	22 (66.7%)	—	22 (66.7%)	10 (30.3%)	—	—
11	547	308 (56.3%)	182 (33.3%)	—	182 (33.3%)	—	182 (33.3%)	349 (63.8%)	3 (0.6%)	—
12	1250	1203 (96.2%)	1151 (92.1%)	46 (3.7%)	1144 (91.5%)	—	1144 (91.5%)	90 (7.2%)	1 (0.1%)	3 (0.2%)
13	164	144 (87.8%)	141 (86.0%)	—	141 (86.0%)	—	141 (86.0%)	26 (15.8%)	—	—
14	2520	2353 (93.4%)	2325 (92.3%)	2 (0.1%)	2325 (92.3%)	—	2325 (92.3%)	216 (8.6%)	—	—
15	1402	1376 (98.2%)	1366 (97.4%)	—	1366 (97.4%)	—	1366 (97.4%)	46 (3.3%)	1 (0.1%)	—
16	2	1 (50.0%)	—	—	—	—	—	1 (50.0%)	—	—
17	8	3 (37.5%)	—	—	—	—	—	7 (87.5%)	—	—
18	30	6 (20.0%)	—	—	—	—	—	30 (100%)	—	—
19	261	28 (10.7%)	—	—	—	—	—	261 (100%)	—	—
20	58	5 (8.6%)	—	—	—	—	—	58 (100%)	—	—
21	15	9 (60.0%)	—	—	—	—	—	12 (80.0%)	—	—
22	14	11 (78.6%)	—	—	—	—	—	14 (100%)	—	—
23	15	5 (33.3%)	—	—	—	—	—	15 (100%)	—	—
24	2	—	—	—	—	—	—	2 (100%)	—	—
25	45	14 (31.1%)	—	—	—	—	—	39 (86.7%)	—	—
26	59	12 (20.3%)	—	—	—	—	—	57 (96.6%)	—	—
27	1	—	—	—	—	—	—	1 (100%)	—	—
28	11	7 (63.6%)	—	—	—	—	—	8 (72.7%)	1 (9.1%)	—
29	59	2 (3.4%)	—	—	—	—	—	59 (100%)	—	—
30	5	2 (40.0%)	—	—	—	—	—	5 (100%)	—	—
31	158	33 (20.9%)	—	—	—	—	—	158 (100%)	—	—
32	10	—	—	—	—	—	—	10 (100%)	—	—
33	251	43 (17.1%)	—	—	—	—	—	251 (100%)	—	—
34	21	5 (23.8%)	—	—	—	—	—	20 (95.2%)	—	—
35	8	4 (50.0%)	—	—	—	—	—	7 (87.5%)	—	—
36	241	53 (22.0%)	—	—	—	—	—	238 (98.8%)	—	—
37	5	5 (100%)	5 (100%)	—	5 (100%)	—	5 (100%)	—	—	—
38	95	69 (72.6%)	—	—	—	—	—	78 (82.1%)	3 (3.2%)	—
39	12	3 (25.0%)	—	—	—	—	—	11 (91.7%)	—	—
40	54	7 (13.0%)	—	—	—	—	—	53 (98.2%)	—	—
41	31	10 (32.3%)	—	—	—	—	—	28 (90.3%)	—	—
42	4	—	—	—	—	—	—	4 (100%)	—	—
43	83	21 (25.3%)	—	—	—	—	—	83 (100%)	—	—
44	62	35 (56.5%)	—	—	—	—	—	58 (93.5%)	—	—
45	8	2 (25.0%)	—	—	—	—	—	8 (100%)	—	—
46	55	30 (54.5%)	—	—	—	—	—	51 (92.7%)	—	—
47	45	42 (93.3%)	—	—	—	—	—	32 (71.1%)	2 (4.4%)	—
48	3	1 (33.3%)	—	—	—	—	—	3 (100%)	—	—
50	7	6 (85.7%)	2 (28.6%)	—	2 (28.6%)	—	2 (28.6%)	4 (57.1%)	1 (14.3%)	—
51	100	77 (77.0%)	—	—	—	—	—	36 (36.0%)	20 (20.0%)	—
52	36	17 (47.2%)	14 (38.9%)	—	14 (38.9%)	—	14 (38.9%)	22 (61.1%)	—	—
53	18	12 (66.7%)	8 (44.4%)	—	8 (44.4%)	—	8 (44.4%)	12 (66.7%)	—	—
54	18	7 (38.9%)	1 (5.6%)	—	1 (5.6%)	—	1 (5.6%)	16 (88.9%)	—	—
55	336	252 (75.0%)	—	—	—	—	—	172 (51.2%)	8 (2.4%)	—
56	19	12 (63.2%)	11 (57.9%)	—	11 (57.9%)	—	11 (57.9%)	10 (52.6%)	—	—
57	128	48 (37.5%)	—	—	—	—	—	98 (76.6%)	—	—
58	202	163 (80.7%)	129 (63.9%)	1 (0.5%)	129 (63.9%)	—	129 (63.9%)	69 (34.2%)	—	—

59	208	143 (68.8%)	—	—	—	—	—	136 (65.4%)	8 (3.9%)	—
60	139	76 (54.7%)	54 (38.9%)	—	54 (38.9%)	—	54 (38.9%)	84 (60.4%)	1 (0.7%)	—
61	119	18 (15.1%)	—	—	—	—	—	116 (97.5%)	—	—
62	2800	1451 (51.8%)	—	—	—	—	—	2257 (80.6%)	10 (0.4%)	—
63	1277	924 (72.4%)	—	—	—	—	—	735 (57.6%)	25 (2.0%)	—
64	244	113 (46.3%)	2 (0.8%)	2 (0.8%)	—	—	—	182 (74.6%)	13 (5.3%)	—
65	213	193 (90.6%)	2 (0.9%)	2 (0.9%)	—	—	—	57 (26.8%)	13 (6.1%)	—
66	34	22 (64.7%)	10 (29.4%)	1 (2.9%)	9 (26.5%)	—	9 (26.5%)	17 (50.0%)	—	—
67	29	17 (58.6%)	—	—	—	—	—	25 (86.2%)	1 (3.5%)	—
68	19	8 (42.1%)	4 (21.1%)	—	4 (21.1%)	—	4 (21.1%)	12 (63.2%)	1 (5.3%)	—
69	65	46 (70.8%)	3 (4.6%)	3 (4.6%)	—	—	—	44 (67.7%)	3 (4.6%)	—
70	130	105 (80.8%)	88 (67.7%)	—	88 (67.7%)	—	88 (67.7%)	40 (30.8%)	—	—
71	385	316 (82.1%)	2 (0.5%)	2 (0.5%)	—	—	—	144 (37.4%)	19 (4.9%)	—
72	182	109 (59.9%)	—	—	—	—	—	112 (61.5%)	7 (3.9%)	—
73	16	1 (6.2%)	—	—	—	—	—	16 (100%)	—	—
74	202	153 (75.7%)	1 (0.5%)	1 (0.5%)	—	—	—	105 (52.0%)	8 (4.0%)	—
75	5	5 (100%)	5 (100%)	—	5 (100%)	—	5 (100%)	—	—	—
76	12	2 (16.7%)	—	—	—	—	—	12 (100%)	—	—
77	2	1 (50.0%)	1 (50.0%)	—	1 (50.0%)	—	1 (50.0%)	1 (50.0%)	—	—
78	2	—	—	—	—	—	—	2 (100%)	—	—
79	11	2 (18.2%)	1 (9.1%)	1 (9.1%)	—	—	—	11 (100%)	—	—
80	3	—	—	—	—	—	—	3 (100%)	—	—
81	13	13 (100%)	13 (100%)	1 (7.7%)	13 (100%)	—	13 (100%)	—	—	—
82	130	130 (100%)	130 (100%)	40 (30.8%)	130 (100%)	—	130 (100%)	—	—	—
83	9	8 (88.9%)	2 (22.2%)	—	2 (22.2%)	—	2 (22.2%)	1 (11.1%)	1 (11.1%)	—
84	28	18 (64.3%)	15 (53.6%)	—	15 (53.6%)	—	15 (53.6%)	13 (46.4%)	—	—
85	36	32 (88.9%)	30 (83.3%)	—	30 (83.3%)	—	30 (83.3%)	7 (19.4%)	—	—
86	49	43 (87.8%)	21 (42.9%)	—	21 (42.9%)	—	21 (42.9%)	19 (38.8%)	—	—
87	175	166 (94.9%)	146 (83.4%)	2 (1.1%)	146 (83.4%)	—	146 (83.4%)	20 (11.4%)	3 (1.7%)	7 (4.0%)
88	129	91 (70.5%)	85 (65.9%)	9 (7.0%)	84 (65.1%)	—	84 (65.1%)	49 (38.0%)	—	—
90	5	5 (100%)	2 (40.0%)	2 (40.0%)	—	—	—	3 (60.0%)	—	—
91	7	3 (42.9%)	—	—	—	—	—	6 (85.7%)	—	—
92	47	18 (38.3%)	—	—	—	—	—	46 (97.9%)	1 (2.1%)	—
94	1	1 (100%)	—	—	—	—	—	1 (100%)	—	—
95	3	1 (33.3%)	—	—	—	—	—	3 (100%)	—	—
96	16	1 (6.2%)	—	—	—	—	—	16 (100%)	—	—
97	2	1 (50.0%)	1 (50.0%)	1 (50.0%)	—	—	—	1 (50.0%)	—	—
98	4	1 (25.0%)	—	—	—	—	—	4 (100%)	—	—
99	98	28 (28.6%)	3 (3.1%)	3 (3.1%)	—	—	—	87 (88.8%)	1 (1.0%)	—
100	20	15 (75.0%)	8 (40.0%)	8 (40.0%)	—	—	—	15 (75.0%)	—	—
102	12	6 (50.0%)	—	—	—	—	—	10 (83.3%)	—	—
103	3	3 (100%)	—	—	—	—	—	1 (33.3%)	—	—
104	3	1 (33.3%)	—	—	—	—	—	2 (66.7%)	—	—
105	4	1 (25.0%)	—	—	—	—	—	4 (100%)	—	—
106	1	1 (100%)	—	—	—	—	—	1 (100%)	—	—
107	112	101 (90.2%)	—	—	—	—	—	97 (86.6%)	—	—
108	14	7 (50.0%)	—	—	—	—	—	11 (78.6%)	—	—
109	37	23 (62.2%)	—	—	—	—	—	37 (100%)	—	—
110	8	3 (37.5%)	—	—	—	—	—	8 (100%)	—	—
111	20	7 (35.0%)	—	—	—	—	—	19 (95.0%)	—	—
112	4	—	—	—	—	—	—	4 (100%)	—	—
113	71	29 (40.9%)	5 (7.0%)	5 (7.0%)	—	—	—	62 (87.3%)	—	—
114	31	6 (19.4%)	—	—	—	—	—	30 (96.8%)	—	—
115	21	15 (71.4%)	—	—	—	—	—	16 (76.2%)	1 (4.8%)	—
116	17	4 (23.5%)	1 (5.9%)	1 (5.9%)	—	—	—	15 (88.2%)	—	—
117	11	6 (54.5%)	—	—	—	—	—	10 (90.9%)	—	—

118	11	3 (27.3%)	—	—	—	—	—	10 (90.9%)	—	—
119	35	20 (57.1%)	5 (14.3%)	5 (14.3%)	—	—	—	30 (85.7%)	—	—
120	15	7 (46.7%)	1 (6.7%)	1 (6.7%)	—	—	—	10 (66.7%)	—	—
121	123	60 (48.8%)	5 (4.1%)	5 (4.1%)	—	—	—	112 (91.1%)	1 (0.8%)	—
122	124	45 (36.3%)	30 (24.2%)	30 (24.2%)	—	—	—	92 (74.2%)	—	—
123	450	395 (87.8%)	5 (1.1%)	5 (1.1%)	—	—	—	122 (27.1%)	76 (16.9%)	—
124	22	19 (86.4%)	—	—	—	—	—	6 (27.3%)	—	—
125	49	32 (65.3%)	—	—	—	—	—	30 (61.2%)	—	—
126	11	4 (36.4%)	—	—	—	—	—	10 (90.9%)	—	—
127	368	326 (88.6%)	—	—	—	—	—	74 (20.1%)	18 (4.9%)	—
128	71	55 (77.5%)	30 (42.2%)	5 (7.0%)	29 (40.9%)	—	29 (40.9%)	27 (38.0%)	1 (1.4%)	—
129	861	697 (81.0%)	8 (0.9%)	8 (0.9%)	—	—	—	422 (49.0%)	18 (2.1%)	—
130	37	28 (75.7%)	9 (24.3%)	—	2 (5.4%)	8 (21.6%)	9 (24.3%)	13 (35.1%)	—	—
131	43	36 (83.7%)	—	—	—	—	—	10 (23.3%)	—	—
132	10	1 (10.0%)	—	—	—	—	—	10 (100%)	—	—
133	3	2 (66.7%)	—	—	—	—	—	1 (33.3%)	—	—
134	4	3 (75.0%)	—	—	—	—	—	2 (50.0%)	1 (25.0%)	—
135	26	15 (57.7%)	—	—	—	—	—	18 (69.2%)	—	—
136	251	188 (74.9%)	1 (0.4%)	1 (0.4%)	—	—	—	131 (52.2%)	26 (10.4%)	—
137	68	38 (55.9%)	3 (4.4%)	3 (4.4%)	—	—	—	47 (69.1%)	—	—
138	16	7 (43.8%)	—	—	—	—	—	14 (87.5%)	—	—
139	1543	1388 (90.0%)	15 (1.0%)	15 (1.0%)	—	—	—	437 (28.3%)	122 (7.9%)	—
140	431	319 (74.0%)	1 (0.2%)	1 (0.2%)	—	—	—	163 (37.8%)	58 (13.5%)	—
141	246	175 (71.1%)	10 (4.1%)	10 (4.1%)	—	—	—	160 (65.0%)	3 (1.2%)	—
142	73	35 (48.0%)	—	—	—	—	—	55 (75.3%)	2 (2.7%)	—
143	17	10 (58.8%)	7 (41.2%)	7 (41.2%)	—	—	—	10 (58.8%)	—	—
144	13	2 (15.4%)	—	—	—	—	—	13 (100%)	—	—
145	5	—	—	—	—	—	—	5 (100%)	—	—
146	83	20 (24.1%)	—	—	—	—	—	83 (100%)	—	—
147	71	71 (100%)	71 (100%)	17 (23.9%)	34 (47.9%)	71 (100%)	71 (100%)	—	—	—
148	479	479 (100%)	479 (100%)	116 (24.2%)	429 (89.6%)	479 (100%)	479 (100%)	—	—	3 (0.6%)
149	10	8 (80.0%)	3 (30.0%)	3 (30.0%)	—	—	—	6 (60.0%)	—	—
150	64	24 (37.5%)	12 (18.8%)	12 (18.8%)	—	—	—	49 (76.6%)	—	—
151	4	—	—	—	—	—	—	4 (100%)	—	—
152	40	9 (22.5%)	—	—	—	—	—	39 (97.5%)	—	—
153	1	1 (100%)	—	—	—	—	—	1 (100%)	—	—
154	17	2 (11.8%)	—	—	—	—	—	17 (100%)	—	—
155	50	19 (38.0%)	—	—	—	—	—	50 (100%)	—	—
156	57	18 (31.6%)	3 (5.3%)	3 (5.3%)	—	—	—	54 (94.7%)	—	—
157	14	8 (57.1%)	3 (21.4%)	3 (21.4%)	—	—	—	9 (64.3%)	—	—
158	3	3 (100%)	—	—	—	—	—	3 (100%)	—	—
159	24	6 (25.0%)	—	—	—	—	—	24 (100%)	—	—
160	158	58 (36.7%)	—	—	—	—	—	156 (98.7%)	—	—
161	87	18 (20.7%)	—	—	—	—	—	87 (100%)	—	—
162	52	37 (71.2%)	18 (34.6%)	4 (7.7%)	—	15 (28.9%)	15 (28.9%)	29 (55.8%)	1 (1.9%)	—
163	57	47 (82.5%)	38 (66.7%)	14 (24.6%)	5 (8.8%)	34 (59.6%)	35 (61.4%)	18 (31.6%)	—	—
164	574	404 (70.4%)	196 (34.1%)	88 (15.3%)	2 (0.3%)	127 (22.1%)	127 (22.1%)	302 (52.6%)	7 (1.2%)	7 (1.2%)
165	33	24 (72.7%)	9 (27.3%)	—	—	9 (27.3%)	9 (27.3%)	14 (42.4%)	—	—
166	957	792 (82.8%)	499 (52.1%)	159 (16.6%)	412 (43.0%)	33 (3.5%)	436 (45.6%)	365 (38.1%)	7 (0.7%)	1 (0.1%)
167	301	234 (77.7%)	177 (58.8%)	—	26 (8.6%)	174 (57.8%)	177 (58.8%)	131 (43.5%)	—	1 (0.3%)
169	1	—	—	—	—	—	—	1 (100%)	—	—
173	113	40 (35.4%)	1 (0.9%)	1 (0.9%)	—	—	—	111 (98.2%)	—	—
174	50	33 (66.0%)	1 (2.0%)	1 (2.0%)	—	—	—	37 (74.0%)	—	—
175	2	2 (100%)	—	—	—	—	—	—	—	—
176	189	110 (58.2%)	33 (17.5%)	1 (0.5%)	11 (5.8%)	32 (16.9%)	32 (16.9%)	128 (67.7%)	3 (1.6%)	—
177	1	—	—	—	—	—	—	1 (100%)	—	—

180	28	18 (64.3%)	—	—	—	—	—	19 (67.9%)	5 (17.9%)	—
181	8	5 (62.5%)	—	—	—	—	—	8 (100%)	—	—
182	33	26 (78.8%)	2 (6.1%)	2 (6.1%)	—	—	—	23 (69.7%)	—	—
183	1	—	—	—	—	—	—	1 (100%)	—	—
185	49	31 (63.3%)	2 (4.1%)	2 (4.1%)	—	—	—	36 (73.5%)	3 (6.1%)	—
186	370	203 (54.9%)	—	—	—	—	—	314 (84.9%)	—	—
187	154	123 (79.9%)	1 (0.7%)	1 (0.7%)	—	—	—	77 (50.0%)	3 (1.9%)	—
188	20	4 (20.0%)	—	—	—	—	—	19 (95.0%)	—	—
189	537	483 (89.9%)	2 (0.4%)	2 (0.4%)	—	—	—	121 (22.5%)	3 (0.6%)	—
190	41	25 (61.0%)	2 (4.9%)	2 (4.9%)	—	—	—	29 (70.7%)	—	—
191	452	449 (99.3%)	4 (0.9%)	4 (0.9%)	—	—	—	8 (1.8%)	69 (15.3%)	—
192	2	—	—	—	—	—	—	2 (100%)	—	—
193	270	258 (95.6%)	2 (0.7%)	2 (0.7%)	—	—	—	43 (15.9%)	10 (3.7%)	—
194	1530	1285 (84.0%)	31 (2.0%)	31 (2.0%)	—	—	—	532 (34.8%)	142 (9.3%)	—
195	1	—	—	—	—	—	—	1 (100%)	—	—
196	1	1 (100%)	—	—	—	—	—	1 (100%)	—	—
197	20	10 (50.0%)	—	—	—	—	—	20 (100%)	—	—
198	170	77 (45.3%)	—	—	—	—	—	168 (98.8%)	—	—
199	32	9 (28.1%)	—	—	—	—	—	32 (100%)	—	—
200	22	17 (77.3%)	1 (4.5%)	1 (4.5%)	—	—	—	12 (54.5%)	—	—
201	6	6 (100%)	5 (83.3%)	—	5 (83.3%)	—	5 (83.3%)	1 (16.7%)	—	—
202	18	13 (72.2%)	7 (38.9%)	7 (38.9%)	—	—	—	13 (72.2%)	—	—
203	6	5 (83.3%)	5 (83.3%)	2 (33.3%)	5 (83.3%)	—	5 (83.3%)	1 (16.7%)	—	—
204	145	123 (84.8%)	—	—	—	—	—	120 (82.8%)	5 (3.5%)	—
205	130	62 (47.7%)	24 (18.5%)	24 (18.5%)	—	—	—	111 (85.4%)	—	—
206	60	30 (50.0%)	—	—	—	—	—	58 (96.7%)	2 (3.3%)	—
208	2	2 (100%)	—	—	—	—	—	2 (100%)	—	—
210	1	1 (100%)	1 (100%)	1 (100%)	—	—	—	—	—	—
211	1	1 (100%)	—	—	—	—	—	—	—	—
212	14	8 (57.1%)	—	—	—	—	—	14 (100%)	—	—
213	22	17 (77.3%)	—	—	—	—	—	22 (100%)	—	—
214	13	7 (53.9%)	—	—	—	—	—	13 (100%)	—	—
215	53	25 (47.2%)	3 (5.7%)	3 (5.7%)	—	—	—	39 (73.6%)	—	—
216	751	600 (79.9%)	301 (40.1%)	301 (40.1%)	—	—	—	440 (58.6%)	—	—
217	108	66 (61.1%)	1 (0.9%)	1 (0.9%)	—	—	—	82 (75.9%)	3 (2.8%)	—
218	42	13 (30.9%)	1 (2.4%)	1 (2.4%)	—	—	—	41 (97.6%)	—	—
219	8	5 (62.5%)	—	—	—	—	—	8 (100%)	—	—
220	142	115 (81.0%)	5 (3.5%)	5 (3.5%)	—	—	—	119 (83.8%)	—	—
221	1334	1171 (87.8%)	8 (0.6%)	8 (0.6%)	—	—	—	278 (20.8%)	237 (17.8%)	—
223	217	214 (98.6%)	—	—	—	—	—	34 (15.7%)	24 (11.1%)	—
224	16	9 (56.2%)	—	—	—	—	—	11 (68.8%)	—	—
225	1651	1293 (78.3%)	168 (10.2%)	168 (10.2%)	—	—	—	959 (58.1%)	78 (4.7%)	—
226	43	42 (97.7%)	—	—	—	—	—	4 (9.3%)	1 (2.3%)	—
227	816	684 (83.8%)	71 (8.7%)	71 (8.7%)	—	—	—	539 (66.0%)	21 (2.6%)	—
229	205	185 (90.2%)	2 (1.0%)	2 (1.0%)	—	—	—	61 (29.8%)	30 (14.6%)	—
230	6	5 (83.3%)	—	—	—	—	—	3 (50.0%)	2 (33.3%)	—
Total	36163	26660 (73.7%)	9789 (27.1%)	1293 (3.6%)	8387 (23.2%)	982 (2.7%)	8856 (24.5%)	16725 (46.2%)	1138 (3.1%)	28 (0.1%)

Table S21: Nonmagnetic unique materials without  $f$  electrons in which one or more associated ICSD entries exhibit a connected grouping of bands with dimension  $\geq 130$  in the presence of SOC. In order, for each unique material containing a grouping of bands with connectivity  $\geq 130$  with SOC, the columns in this table list the chemical formula, the SG number, the SG symbol, the ICSD number, the stable topological classification at  $E_F$ , the number of valence electrons (num  $e^-$ ), and the largest number of connected bands across the electronic band structures of all of the ICSDs associated to the unique material (noting that the VASP calculations performed in this work have been truncated at fillings of  $\sim 2N_e$ , see S4 for further calculation details). In the right-most column of this table, we also list in parentheses a percentage corresponding to the ratio of the maximum band connectivity with SOC in the unique material relative to  $2N_e$ , which is the approximate total number of bands in each VASP calculation performed with SOC. A chemical formula with a \* indicates that only some (but not all) of the ICSDs associated to the same unique material (defined using its topological class with SOC) contain a connected grouping of bands with dimension  $\geq 130$  in the presence of SOC.

Chem. formula	SG #	SG symbol	ICSD	Top. subclass.	num $e^-$	nbr connected bands
Cu <sub>3</sub> P*	165	<i>P</i> 3 <i>c</i> 1	<b>628626</b>	ES	228	144 (31.58%)
AgCd <sub>3</sub> Hf <sub>3</sub> F <sub>20</sub>	176	<i>P</i> 6 <sub>3</sub> / <i>m</i>	<b>78893</b>	ESFD	398	136 (17.09%)
Cu <sub>3</sub> P	185	<i>P</i> 6 <sub>3</sub> <i>c</i> <i>m</i>	<b>15056</b>	ES	228	164 (35.96%)
Hf <sub>5</sub> ZnSb <sub>3</sub>	193	<i>P</i> 6 <sub>3</sub> / <i>mcm</i>	<b>42913</b>	ESFD	94	145 (77.13%)
Nb <sub>5</sub> Ge <sub>3</sub>	193	<i>P</i> 6 <sub>3</sub> / <i>mcm</i>	<b>637215</b>	ESFD	154	157 (50.97%)
K <sub>6</sub> (BiCl <sub>6</sub> )Cl <sub>2</sub> (H <sub>3</sub> F <sub>4</sub> )	194	<i>P</i> 6 <sub>3</sub> / <i>mmc</i>	<b>68226</b>	LCEBR	292	156 (26.71%)
Ga <sub>5</sub> V <sub>6</sub>	194	<i>P</i> 6 <sub>3</sub> / <i>mmc</i>	<b>108499</b>	ESFD	90	164 (91.11%)
Mg <sub>17</sub> Sr <sub>2</sub>	194	<i>P</i> 6 <sub>3</sub> / <i>mmc</i>	<b>150736</b>	ES	108	145 (67.13%)
Hf <sub>9</sub> (HfMo <sub>3</sub> )Si	194	<i>P</i> 6 <sub>3</sub> / <i>mmc</i>	<b>603654</b>	ES	124	136 (54.84%)
W <sub>10</sub> Co <sub>3</sub> C <sub>4</sub>	194	<i>P</i> 6 <sub>3</sub> / <i>mmc</i>	<b>617464</b>	ESFD	206	136 (33.01%)
Hf <sub>9</sub> Mo <sub>4</sub> Si*	194	<i>P</i> 6 <sub>3</sub> / <i>mmc</i>	<b>638632</b>	ES	128	132 (51.56%)
Cu <sub>5</sub> Zn <sub>8</sub>	217	<i>I</i> 43 <i>m</i>	<b>2092</b>	ESFD	302	156 (25.83%)
CaHg <sub>11</sub>	221	<i>P</i> m <sub>3</sub> <i>m</i>	<b>58902</b>	ES	402	150 (18.66%)
BaHg <sub>11</sub> *	221	<i>P</i> m <sub>3</sub> <i>m</i>	<b>107486</b>	SEBR	426	172 (20.19%)
KHg <sub>11</sub>	221	<i>P</i> m <sub>3</sub> <i>m</i>	<b>410566</b>	ESFD	423	130 (15.37%)
Ba <sub>8</sub> Au <sub>6</sub> Si <sub>40</sub>	223	<i>P</i> m <sub>3</sub> <i>n</i>	<b>40567</b>	ESFD	306	132 (21.57%)
Ru <sub>4</sub> Y <sub>3</sub> Ge <sub>13</sub>	223	<i>P</i> m <sub>3</sub> <i>n</i>	<b>53900</b>	ESFD	234	216 (46.15%)
Ni <sub>3</sub> Ba <sub>4</sub> Ge <sub>20</sub>	223	<i>P</i> m <sub>3</sub> <i>n</i>	<b>57034</b>	ESFD	300	136 (22.67%)
Pd <sub>3</sub> Ba <sub>4</sub> Ge <sub>20</sub>	223	<i>P</i> m <sub>3</sub> <i>n</i>	<b>57035</b>	ESFD	300	136 (22.67%)
Au <sub>3</sub> Ba <sub>4</sub> Ge <sub>20</sub>	223	<i>P</i> m <sub>3</sub> <i>n</i>	<b>57037</b>	ESFD	306	136 (22.22%)
AuZn <sub>3</sub>	223	<i>P</i> m <sub>3</sub> <i>n</i>	<b>58626</b>	ES	376	132 (17.55%)
Ca <sub>3</sub> Rh <sub>4</sub> Sn <sub>13</sub>	223	<i>P</i> m <sub>3</sub> <i>n</i>	<b>58930</b>	ESFD	188	168 (44.68%)
Cs <sub>8</sub> Sn <sub>46</sub>	223	<i>P</i> m <sub>3</sub> <i>n</i>	<b>62352</b>	ES	256	177 (34.57%)
Ba <sub>6</sub> Si <sub>46</sub>	223	<i>P</i> m <sub>3</sub> <i>n</i>	<b>94263</b>	ESFD	244	212 (43.44%)
Si <sub>46</sub>	223	<i>P</i> m <sub>3</sub> <i>n</i>	<b>186544</b>	LCEBR	184	173 (47.01%)
Si	223	<i>P</i> m <sub>3</sub> <i>n</i>	<b>189393</b>	LCEBR	184	157 (42.66%)
Na <sub>2</sub> Ba <sub>6</sub> Si <sub>46</sub>	223	<i>P</i> m <sub>3</sub> <i>n</i>	<b>409912</b>	ESFD	246	152 (30.89%)
Ca <sub>3</sub> Ir <sub>4</sub> Ge <sub>13</sub>	223	<i>P</i> m <sub>3</sub> <i>n</i>	<b>619308</b>	ES	188	216 (57.45%)
Y <sub>3</sub> Co <sub>4</sub> Ge <sub>13</sub>	223	<i>P</i> m <sub>3</sub> <i>n</i>	<b>623663</b>	ESFD	242	132 (27.27%)
Cs <sub>4</sub> Sn <sub>23</sub>	223	<i>P</i> m <sub>3</sub> <i>n</i>	<b>627107</b>	ESFD	256	177 (34.57%)
Cs <sub>4</sub> Sn <sub>23</sub>	223	<i>P</i> m <sub>3</sub> <i>n</i>	<b>627108</b>	ES	256	177 (34.57%)
Y <sub>3</sub> Ir <sub>4</sub> Ge <sub>13</sub>	223	<i>P</i> m <sub>3</sub> <i>n</i>	<b>636763</b>	ESFD	242	160 (33.06%)
Y <sub>3</sub> Os <sub>4</sub> Ge <sub>13</sub>	223	<i>P</i> m <sub>3</sub> <i>n</i>	<b>637488</b>	ESFD	234	216 (46.15%)
Y <sub>3</sub> Rh <sub>4</sub> Ge <sub>13</sub>	223	<i>P</i> m <sub>3</sub> <i>n</i>	<b>637724</b>	ESFD	242	192 (39.67%)
Cd <sub>13</sub> K*	226	<i>F</i> m <sub>3</sub> <i>c</i>	<b>102002</b>	ESFD	330	184 (27.88%)
BaCu <sub>13</sub>	226	<i>F</i> m <sub>3</sub> <i>c</i>	<b>108093</b>	ESFD	306	176 (28.76%)
Ag <sub>13</sub> OsO <sub>6</sub>	226	<i>F</i> m <sub>3</sub> <i>c</i>	<b>413193</b>	ESFD	374	172 (22.99%)
YRu <sub>2</sub> Zn <sub>20</sub>	227	<i>F</i> d <sub>3</sub> <i>m</i>	<b>152110</b>	ESFD	534	156 (14.61%)

$\text{Ag}_{16}\text{Ca}_6\text{N}$	229	$I\bar{m}3\bar{m}$	78395	ESFD	193	188 (48.7%)
$\text{Ag}_8\text{Ca}_3$	229	$I\bar{m}3\bar{m}$	107145	ESFD	188	184 (48.94%)
$\text{Al}_4\text{Ni}_3$	230	$I\bar{a}3\bar{d}$	58042	SEBR	336	192 (28.57%)
$\text{Bi}_4\text{Rh}$	230	$I\bar{a}3\bar{d}$	58854	ESFD	348	249 (35.78%)
$\text{Ga}_4\text{Ni}_3$	230	$I\bar{a}3\bar{d}$	103864	ES	336	256 (38.1%)
$\text{Ga}_3\text{Ni}_3\text{Zn}$	230	$I\bar{a}3\bar{d}$	103898	ESFD	408	184 (22.55%)

## S9. REPEAT-TOPOLOGY AND SUPERTOPOLOGY

In this work, we introduce the concept of a *repeat-topological* (RTopo) material – a material in which the gap at the Fermi level, as well as the next gap below the Fermi level as measured by band connectivity, exhibit cumulative symmetry-indicated stable topology [see Fig. S4A]. We additionally introduce the concept of a *supertopological* (STopo) material – a material in which *every* energetically isolated set of bands in the spectrum obtained from our first-principles calculations (see S4) exhibits symmetry-indicated stable topology [see Fig. S4B]. In this section, we will first rigorously define repeat-topology in S9 A. Then, in S9 B, we will further define supertopology. Lastly, in S9 C, we will provide a detailed statistical breakdown of the STopo unique materials with SOC in the ICSD.

### A. Definition of Repeat-Topology

In this section, we introduce and rigorously define *repeat-topological* (RTopo) materials. In this work, to define RTopo materials, we first restrict to ICSD entries in which the entire valence manifold exhibits cumulative stable (NLC or SEBR) topology (*i.e.* the summed stable topological indices of all of the occupied bands are nontrivial). Next, using the compatibility relations (see S2 and Refs. [28, 43, 58, 92, 93]), we determine the next-highest electronic filling at which an insulating gap is permitted. If the valence manifold in an ICSD entry when filled up to the next-highest gap below  $E_F$  is also stable topological [see Fig. S4A], then we define the ICSD entry to be RTopo. We emphasize that by this definition, it is possible for the isolated bands between  $E_F$  and the next-highest gap below  $E_F$  to be topologically trivial [see Fig. S4C]. Crucially however, the definition of repeat-topology employed in this work is motivated from an experimental perspective. Specifically, we have in this work defined RTopo materials as exhibiting consecutive stable topological gaps at  $E_F$  and just below  $E_F$  because topological boundary states below  $E_F$  can straightforwardly be observed through ARPES, whereas states above  $E_F$  can only be observed by doping or by performing more complicated pump-probe experiments [153–156], and because topological response effects and boundary states in solid-state materials occur as a consequence of *gaps* with nontrivial cumulative band topology, as opposed to isolated topological *bands*. From a physical perspective, idealized RTopo materials will exhibit two sets of surface or hinge states within consecutive bulk gaps that both lie at energies accessible to ARPES probes without doping ( $\sim 1.5$  eV below  $E_F$ ). Hence, the repeated topological surface and hinge states of RTopo ICSD entries in consecutive bulk band gaps are analogous to the Fermi-arc “quantum ladder” recently observed in the unconventional chiral semimetal alloy  $\text{Rh}_x\text{Ni}_y\text{Si}$  [71]. Specifically, while  $\text{Rh}_x\text{Ni}_y\text{Si}$  is gapless at  $E_F$  and below  $E_F$ ,  $\text{Rh}_x\text{Ni}_y\text{Si}$  nevertheless exhibits topological Fermi-arc surface states at  $E_F$  and at a filling of two electrons below  $E_F$ , representing a closely-related semimetallic analog of the topological (crystalline) insulating RTopo materials discovered in this work.

Next, we extend the definition of RTopo beyond individual ICSD entries to groups of ICSD entries associated to unique materials. In this work, we define a unique material as a material that exhibits the same topological features (*i.e.* topological class or nodal crossing points) with SOC at the Fermi level (see S4). Therefore, away from  $E_F$ , it is possible for two ICSD entries grouped into the same unique material to have isolated sets of bands with different topology. Because we wish to define RTopo materials in a manner that is robust to numerical uncertainty, we define a unique material to be RTopo if *any* of the ICSD entries associated to the unique material are themselves RTopo. In S11 B, we list the RTopo TIs and TCIs on <https://www.topologicalquantumchemistry.com/> with the fewest number of bulk Fermi pockets when the Fermi level is set to 0, or set to the next highest filling at which an insulating gap is permitted by band connectivity.

Lastly, in the main text, we have highlighted  $\text{Bi}_2\text{Mg}_3$  [ICSD 659569, SG 164 ( $P\bar{3}m1$ )] as a prototypical RTopo (and STopo, see S9B) material. In Table S1 of S3, we previously computed the symmetry-indicated stable and fragile topology of all of the isolated sets of bands in  $\text{Bi}_2\text{Mg}_3$  using the updated version of the **Check Topological Mat** program on the **BCS** implemented for this work. Next, in Fig. 5D of the main text, we have plotted the (0001)-surface states of  $\text{Bi}_2\text{Mg}_3$  obtained from surface Green's functions. To compute the (0001)-surface spectrum shown in Fig. 5D of the main text, we first used WANNIER90 [85] to construct a Wannier-based tight-binding model from the *s* and *p* orbitals of Mg and the *p* orbitals of Bi, which we found to accurately reproduce the bulk electronic band structure of  $\text{Bi}_2\text{Mg}_3$  obtained from *ab initio* calculations (see ICSD 659569 on <https://www.topologicalquantumchemistry.com/>). We next placed the Wannier-based tight-binding model in a *z*-(*c*-axis) directed slab geometry with 100 layers (slab unit cells) in the stacking (*c*-axis) direction, and then computed the *z*-normal [(0001)-] surface states using the iterative Green's function method as implemented in WANNIERTOOLS [157]. In the (0001)-surface spectrum of  $\text{Bi}_2\text{Mg}_3$  shown in Fig. 5D of the main text, we observe topological twofold Dirac-cone surface states in both the projected gap at  $E_F$  [labeled the “0003  $E_F$  gap” in Fig. 5D of the main text], and just below  $E_F$  [labeled the “0013 RTopo gap” in Fig. 5D of the main text]. Most interesting, previous ARPES experiments on  $\text{Bi}_2\text{Mg}_3$  samples have also detected surface states below the Fermi level, which were labeled as “surface resonance bands” in the earlier works [72, 158, 159]. Hence in this work, we recognize the surface resonance bands detected in Refs. [72, 158, 159] to in fact be the RTopo surface states of  $\text{Bi}_2\text{Mg}_3$  in the first gap below  $E_F$  as determined by band connectivity (see S2).

## B. Definition of Supertopology

In this section, we introduce and define *supertopological* (STopo) materials. Similar to the definition of RTopo materials introduced in S9A, in this work, we first define an ICSD entry to be STopo if all of the energetically isolated, connected sets of bands with SOC included in our calculations (see S4) exhibit symmetry-indicated stable (NLC or SEBR) topology [see Fig. S4B]. We note that by this definition, semimetals (ES or ESFD) and trivial insulators (LCEBR) are also capable of being STopo materials, because the definition of supertopology is independent of the Fermi level (*i.e.* supertopology is independent of the electronic filling). We additionally emphasize that the electronic band structures calculated for this work only contain bands originating from valence atomic orbitals and at least the same number of bands originating from conduction atomic orbitals; we do not consider the topology of bands originating from core-shell atomic orbitals, which are free to be topologically trivial in an STopo material (which is physically motivated, because core-shell atomic orbitals typically lie at energies that are inaccessible in experimental probes). We additionally emphasize that STopo materials are not necessarily also RTopo. For example in an STopo material, it is possible for the isolated bands just below  $E_F$  to exhibit stable topological indices that combine with the stable topological indices of the other sets of bands below  $E_F$  to sum to trivial values [see Fig. S4D].

As previously with RTopo materials in S9A, we next extend the definition of STopo beyond individual ICSD entries to groups of ICSD entries associated to unique materials. Specifically, in this work, we define a unique material to be STopo if *any* of the ICSD entries associated to the unique material are themselves STopo, thus providing a definition that is less sensitive to numerical uncertainty in materials with small band gaps away from  $E_F$ . We find that bismuth (Bi) crystals in SG 166 ( $R\bar{3}m$ ) – recently discovered to be higher-order TIs (HOTIs) [22] – represent a prototypical example of both repeat-topology and supertopology. In Table S22, we show the output of the **Check Topological Mat** program (see S3) applied to two different ICSD entries for Bi [ICSD 64703 and (ICSD 53797)] that are associated to the same unique material. Notably, we find that, while both Bi (ICSD 64703) and Bi (ICSD 53797) exhibit the cumulative stable indices of a HOTI at the Fermi level [ $(Z_{2,1}, Z_{2,2}, Z_{2,3}, Z_4) = (0, 0, 0, 2)$  at valence filling  $\nu = 10$ , see S11 A 3], Bi (ICSD 64703) is STopo and RTopo, whereas Bi (ICSD 53797) is RTopo, but not STopo. Crucially, from a physical perspective, Bi (ICSD 64703) and Bi (ICSD 53797) only differ by weak band inversion away from the Fermi level, and both Bi (ICSD 64703) and Bi (ICSD 53797) exhibit topologically nontrivial (SEBR) gaps with the indices  $(Z_{2,1}, Z_{2,2}, Z_{2,3}, Z_4) = (0, 0, 0, 3)$  just below the Fermi level (see Fig. S5). This indicates that, whether a particular bismuth crystal sample is more closely characterized by the ICSD entry Bi (ICSD 64703) or by Bi (ICSD 53797), ARPES investigations of band gaps below the Fermi level may still reveal fully filled topological surface states (specifically, twofold Dirac cones). In general, when

using [Check Topological Mat](#), topological surface and hinge states away from  $E_F$  can be predicted by searching the “top. type/all” column (labeled in violet in Table S22) for NLC and SEBR entries at experimentally accessible gaps away from  $E_F$ .

A Bi SG 166 ( $R\bar{3}m$ ) <a href="#">ICSD 64703</a>										
$\Gamma$	T	F	L	dim	top. type	ind/band	filling $\nu$	top. type/all	ind/all	
-GM8(2)	-T9(2)	-F5-F6(2)	-L3-L4(2)	2	SEBR	1 1 1 0	2	SEBR	1 1 1 0	
-GM9(2)	-T8(2)	-F3-F4(2)	-L5-L6(2)	2	SEBR	1 1 1 0	4	LCEBR	0 0 0 0	
-GM8(2)	-T9(2)	-F3-F4(2)	-L3-L4(2)	2	SEBR	1 1 1 1	6	SEBR	1 1 1 1	
-GM8(2)	-T8(2)	-F5-F6(2)	-L5-L6(2)	2	SEBR	1 1 1 2	8	SEBR	0 0 0 3	
-GM4-GM5(2)	-T6-T7(2)	-F5-F6(2)	-L5-L6(2)	2	SEBR	0 0 0 3	10	SEBR	0 0 0 2	
-GM9(2)	-T8(2)	-F3-F4(2)	-L3-L4(2)	2	SEBR	0 0 0 1	12	SEBR	0 0 0 3	
-GM9(2)	-T9(2)	-F3-F4(2)	-L3-L4(2)	2	SEBR	1 1 1 2	14	SEBR	1 1 1 1	
-GM6-GM7(2)	-T4-T5(2)	-F3-F4(2)	-L5-L6(2)	2	SEBR	1 1 1 0	16	SEBR	0 0 0 1	
-GM9(2)	-T9(2)	-F5-F6(2)	-L3-L4(2)	2	SEBR	1 1 1 1	18	SEBR	1 1 1 2	

B Bi SG 166 ( $R\bar{3}m$ ) <a href="#">ICSD 53797</a>										
$\Gamma$	T	F	L	dim	top. type	ind/band	filling $\nu$	top. type/all	ind/all	
-GM8(2)	-T9(2)	-F5-F6(2)	-L3-L4(2)	2	SEBR	1 1 1 0	2	SEBR	1 1 1 0	
-GM9(2)	-T8(2)	-F3-F4(2)	-L5-L6(2)	2	SEBR	1 1 1 0	4	LCEBR	0 0 0 0	
-GM8(2)	-T9(2)	-F3-F4(2)	-L5-L6(2)	2	LCEBR	0 0 0 0	6	LCEBR	0 0 0 0	
-GM8(2)	-T8(2)	-F5-F6(2)	-L3-L4(2)	2	SEBR	0 0 0 3	8	SEBR	0 0 0 3	
-GM4-GM5(2)	-T6-T7(2)	-F5-F6(2)	-L5-L6(2)	2	SEBR	0 0 0 3	10	SEBR	0 0 0 2	
-GM9(2)	-T8(2)	-F3-F4(2)	-L3-L4(2)	2	SEBR	0 0 0 1	12	SEBR	0 0 0 3	
-GM9(2)	-T9(2)	-F3-F4(2)	-L3-L4(2)	2	SEBR	1 1 1 2	14	SEBR	1 1 1 1	
-GM6-GM7(2)	-T4-T5(2)	-F3-F4(2)	-L5-L6(2)	2	SEBR	1 1 1 0	16	SEBR	0 0 0 1	
-GM9(2)	-T9(2)	-F5-F6(2)	-L3-L4(2)	2	SEBR	1 1 1 1	18	SEBR	1 1 1 2	

Table S22. A typical table generated by [Check Topological Mat](#). Here, we have used as examples two different ICSD entries A: Bi ([ICSD 64703](#)) and B: Bi ([ICSD 53797](#)) for the repeat-topological (RTopo) and supertopological (STopo) unique material Bi. In this table, the horizontal lines indicate the electronic fillings  $\nu$  at which the occupied bands satisfy the compatibility relations. Columns  $\Gamma$ , T, F, and L contain the coreps at each maximal k point for each energetically isolated set of bands that satisfy the compatibility relations. Column “dim” shows the dimension of each set of bands, Column “top. type” indicates the topology of the isolated bands [which can either be LCEBR, FRAGILE, NLC, or SEBR], and Column “ind/band” contains the stable SIs ( $Z_{2,1}$   $Z_{2,2}$   $Z_{2,3}$   $Z_4$ ) that result from subducing onto SG 2 ( $P\bar{1}$ ). The remaining three columns contain the cumulative information of several combined sets of energetically isolated bands that are filled up to a total number of valence electrons specified by the column “filling  $\nu$ .” Column “top. type/all” provides the cumulative topology (LCEBR, FRAGILE, NLC, or SEBR) at the gap specified by the electronic filling in the “filling  $\nu$ ” column, and Column “ind/all” provides the cumulative stable SIs of all of the filled bands up to the same gap. Hence, the values of “ind/all” at each filling  $\nu$  listed in this table can be obtained by summing the values in the “ind/band” column up to the same filling  $\nu$ . In both A: Bi ([ICSD 64703](#)) and B: Bi ([ICSD 53797](#)), the Fermi level lies at the valence filling  $\nu = 10$ , indicating that the gap at the Fermi level exhibits the subduced stable SIs (0002). However away from  $E_F$ , the bands at valence filling  $\nu = 6$  exhibit trivial symmetry-indicated (LCEBR) topology in B, whereas all of the energetically isolated bands in A are classified as stable topological (SEBR). Therefore, A: Bi ([ICSD 64703](#)) is an STopo ICSD entry, whereas B: Bi ([ICSD 53797](#)) is not; however, because A and B are associated to the same unique material, then as a whole, we consider Bi in SG 166 ( $R\bar{3}m$ ) with (0002) SEBR topology at the Fermi level to be an STopo unique material.

### C. Statistics for Supertopological Materials in the ICSD

In this section, we provide detailed statistics and lists for all of the STopo unique materials in the ICSD with SOC. As previously discussed in [S9 B](#), because the STopo classification is insensitive to the Fermi level, then materials in all of the topological classes (NLC, SEBR, ES, ESFD, and LCEBR) may be STopo. First, in Table S23, we list statistics for all of the STopo unique materials in the ICSD with SOC subdivided by the topology at  $E_F$  and by SG. Then, in Tables S24, S25, S26 and S27, we respectively list all of the stoichiometric, nonmagnetic unique STopo materials in the ICSD without  $f$  electrons that are classified as NLC, SEBR, ES, ESFD, and LCEBR at  $E_F$ .

Table S23: Statistics for supertopological (STopo) materials. The first and second columns respectively list the SG and the number of unique materials in the SG. In order, the next columns list the number of unique materials in the SG that are STopo (defined in S9 B), the number that are STopo in which all of the bands are NLC (STopo-NLC), and the number that are STopo in which all of the bands are SEBR (STopo-SEBR). In the final five columns, we respectively list the number of unique STopo materials in the SG that are classified as NLC, SEBR, ES, ESFD, and LCEBR at  $E_F$ . For all of the STopo material sub-classifications listed in this table, each number of materials is accompanied by the percentage of unique materials in the SG with the STopo sub-classification. When there are no unique materials with the STopo sub-classification, the table entry is marked with a dashed horizontal line.

SG	# Mat.	STopo	STopo-NLC	STopo-SEBR	STopo and NLC	STopo and SEBR	STopo and ES	STopo and ESFD	STopo and LCEBR
2	1574	7 (0.4%)	7 (0.4%)	—	—	—	—	—	7 (0.4%)
10	38	1 (2.6%)	1 (2.6%)	—	—	—	—	—	1 (2.6%)
11	587	1 (0.2%)	1 (0.2%)	—	1 (0.2%)	—	—	—	—
12	1345	9 (0.7%)	—	—	5 (0.4%)	3 (0.2%)	—	—	1 (0.1%)
13	195	1 (0.5%)	1 (0.5%)	—	—	—	—	—	1 (0.5%)
14	2665	24 (0.9%)	24 (0.9%)	—	5 (0.2%)	—	1 (0.0%)	—	18 (0.7%)
51	107	2 (1.9%)	2 (1.9%)	—	—	—	—	2 (1.9%)	—
55	394	5 (1.3%)	5 (1.3%)	—	—	—	—	—	5 (1.3%)
58	208	1 (0.5%)	1 (0.5%)	—	—	—	—	—	1 (0.5%)
61	122	9 (7.4%)	9 (7.4%)	—	—	—	—	—	9 (7.4%)
62	3006	3 (0.1%)	3 (0.1%)	—	1 (0.0%)	—	—	—	2 (0.1%)
63	1396	6 (0.4%)	2 (0.1%)	—	3 (0.2%)	1 (0.1%)	—	1 (0.1%)	1 (0.1%)
64	257	5 (1.9%)	—	5 (1.9%)	—	4 (1.6%)	—	—	1 (0.4%)
65	241	2 (0.8%)	—	—	2 (0.8%)	—	—	—	—
74	218	2 (0.9%)	2 (0.9%)	—	2 (0.9%)	—	—	—	—
83	10	1 (10.0%)	—	—	1 (10.0%)	—	—	—	—
87	181	1 (0.6%)	—	—	—	1 (0.6%)	—	—	—
88	139	1 (0.7%)	—	1 (0.7%)	—	—	—	—	1 (0.7%)
122	124	4 (3.2%)	—	4 (3.2%)	—	—	—	—	4 (3.2%)
123	473	41 (8.7%)	14 (3.0%)	—	5 (1.1%)	1 (0.2%)	14 (3.0%)	20 (4.2%)	1 (0.2%)
127	403	6 (1.5%)	6 (1.5%)	—	1 (0.2%)	—	—	4 (1.0%)	1 (0.2%)
129	884	1 (0.1%)	—	—	1 (0.1%)	—	—	—	—
139	1622	43 (2.6%)	—	15 (0.9%)	—	14 (0.9%)	11 (0.7%)	12 (0.7%)	6 (0.4%)
140	457	45 (9.8%)	2 (0.4%)	—	9 (2.0%)	2 (0.4%)	10 (2.2%)	21 (4.6%)	3 (0.7%)
141	267	2 (0.8%)	—	1 (0.4%)	—	1 (0.4%)	—	—	1 (0.4%)
164	598	13 (2.2%)	—	12 (2.0%)	—	3 (0.5%)	—	1 (0.2%)	9 (1.5%)
166	1029	6 (0.6%)	—	6 (0.6%)	—	6 (0.6%)	—	—	—
176	206	5 (2.4%)	—	2 (1.0%)	—	—	2 (1.0%)	2 (1.0%)	1 (0.5%)
187	158	1 (0.6%)	1 (0.6%)	—	—	—	—	1 (0.6%)	—
189	592	10 (1.7%)	—	—	—	—	5 (0.8%)	5 (0.8%)	—
191	506	63 (12.4%)	—	63 (12.4%)	—	11 (2.2%)	20 (4.0%)	32 (6.3%)	—
193	302	3 (1.0%)	—	3 (1.0%)	—	—	2 (0.7%)	1 (0.3%)	—
194	1619	130 (8.0%)	2 (0.1%)	38 (2.4%)	—	15 (0.9%)	71 (4.4%)	33 (2.0%)	11 (0.7%)
204	151	1 (0.7%)	—	1 (0.7%)	—	—	—	1 (0.7%)	—
205	130	2 (1.5%)	2 (1.5%)	—	—	—	—	1 (0.8%)	1 (0.8%)
206	61	4 (6.6%)	—	4 (6.6%)	—	—	—	2 (3.3%)	2 (3.3%)
216	777	1 (0.1%)	1 (0.1%)	—	—	—	—	1 (0.1%)	—
221	1352	196 (14.5%)	—	55 (4.1%)	1 (0.1%)	36 (2.7%)	24 (1.8%)	129 (9.5%)	6 (0.4%)
223	222	9 (4.0%)	—	9 (4.0%)	—	—	1 (0.5%)	7 (3.1%)	1 (0.5%)
224	17	1 (5.9%)	—	1 (5.9%)	—	—	—	1 (5.9%)	—
225	1693	37 (2.2%)	—	37 (2.2%)	—	5 (0.3%)	5 (0.3%)	25 (1.5%)	2 (0.1%)
227	841	33 (3.9%)	—	25 (3.0%)	—	4 (0.5%)	10 (1.2%)	12 (1.4%)	7 (0.8%)

229	210	31 (14.8%)	—	29 (13.8%)	—	2 (0.9%)	2 (0.9%)	25 (11.9%)	2 (0.9%)
Total	38298	769 (2.0%)	86 (0.2%)	311 (0.8%)	37 (0.1%)	109 (0.3%)	178 (0.5%)	339 (0.9%)	106 (0.3%)

Table S24: Supertopological (STopo) nonmagnetic unique materials without  $f$  electrons that are also NLC-classified at  $E_F$  with SOC. In order, the columns list the chemical formula, the SG number, the SG symbol, the ICSD number, whether all of the bands in the STopo material are NLC, whether all of the bands in the STopo material are SEBR, the number of valence electrons, and the cumulative stable SIs at  $E_F$  (see S11). A chemical formula with a \* indicates that only some (but not all) of the ICSDs associated to the same unique material (defined using its topological class with SOC) are STopo.

Chem. formula	SG #	SG symbol	ICSD	All NLC	All SEBR	num $e^-$	Topological Indices
GeH <sub>4</sub>	11	<i>P</i> 2 <sub>1</sub> / <i>m</i>	183082	Yes	No	16	$Z_{2,1} = 0 \ Z_{2,2} = 0 \ Z_{2,3} = 1 \ Z_4 = 3$
WH <sub>6</sub> <sup>*</sup>	12	<i>C</i> 2/ <i>m</i>	247613	No	No	24	$Z_{2,1} = 0 \ Z_{2,2} = 0 \ Z_{2,3} = 0 \ Z_4 = 1$
SN <sup>*</sup>	14	<i>P</i> 2 <sub>1</sub> / <i>c</i>	41966	Yes	No	44	$Z_{2,1} = 1 \ Z_{2,2} = 0 \ Z_{2,3} = 0 \ Z_4 = 2$
ZrGe <sub>2</sub> <sup>*</sup>	63	<i>C</i> mcm	56054	No	No	24	$Z_{2,1} = 1 \ Z_{2,2} = 1 \ Z_{2,3} = 0 \ Z_4 = 1$
ZrSi <sub>2</sub> <sup>*</sup>	63	<i>C</i> mcm	95179	Yes	No	24	$Z_{2,1} = 1 \ Z_{2,2} = 1 \ Z_{2,3} = 0 \ Z_4 = 1$
Ga <sub>2</sub> Sc	65	<i>C</i> mmm	103956	No	No	18	$Z_{2,1} = 0 \ Z_{2,2} = 0 \ Z_{2,3} = 1 \ Z_4 = 1$
Ga <sub>3</sub> Ti <sub>2</sub>	83	<i>P</i> 4/ <i>m</i>	103995	No	No	34	$Z_{2,1} = 1 \ Z_{2,2} = 1 \ Z_{2,3} = 1 \ Z_4 = 1 \ Z_{4m,\pi} = 1 \ Z_2 = 1 \ Z_8 = 1$
MoPt <sub>3</sub>	123	<i>P</i> 4/ <i>mmm</i>	161108	No	No	36	$Z_{2,1} = 1 \ Z_{2,2} = 1 \ Z_{2,3} = 1 \ Z_4 = 3 \ Z_{4m,\pi} = 1 \ Z_2 = 1 \ Z_8 = 7$
Cu <sub>2</sub> NiZn	123	<i>P</i> 4/ <i>mmm</i>	103079	No	No	44	$Z_{2,1} = 0 \ Z_{2,2} = 0 \ Z_{2,3} = 0 \ Z_4 = 1 \ Z_{4m,\pi} = 2 \ Z_2 = 1 \ Z_8 = 1$
Pd <sub>5</sub> Ti <sub>3</sub>	123	<i>P</i> 4/ <i>mmm</i>	105726	No	No	62	$Z_{2,1} = 0 \ Z_{2,2} = 0 \ Z_{2,3} = 1 \ Z_4 = 3 \ Z_{4m,\pi} = 1 \ Z_2 = 1 \ Z_8 = 3$
Sc	129	<i>P</i> 4/ <i>nmm</i>	52412	No	No	12	$Z_{2,1} = 0 \ Z_{2,2} = 0 \ Z_{2,3} = 0 \ Z_4 = 3 \ Z_2 = 1$
Sc	140	<i>I</i> 4/ <i>mcm</i>	246445	No	No	12	$Z_{2,1} = 1 \ Z_{2,2} = 1 \ Z_{2,3} = 1 \ Z_4 = 3 \ Z_2 = 1 \ Z_8 = 7$
PtTl <sub>2</sub>	140	<i>I</i> 4/ <i>mcm</i>	102797	Yes	No	32	$Z_{2,1} = 0 \ Z_{2,2} = 0 \ Z_{2,3} = 0 \ Z_4 = 3 \ Z_2 = 1 \ Z_8 = 7$
FeZr <sub>2</sub>	140	<i>I</i> 4/ <i>mcm</i>	103712	No	No	32	$Z_{2,1} = 0 \ Z_{2,2} = 0 \ Z_{2,3} = 0 \ Z_4 = 1 \ Z_2 = 1 \ Z_8 = 5$
Pb <sub>2</sub> Pt	140	<i>I</i> 4/ <i>mcm</i>	54316	No	No	36	$Z_{2,1} = 1 \ Z_{2,2} = 1 \ Z_{2,3} = 1 \ Z_4 = 1 \ Z_2 = 1 \ Z_8 = 1$
NiHf <sub>2</sub>	140	<i>I</i> 4/ <i>mcm</i>	102808	No	No	36	$Z_{2,1} = 1 \ Z_{2,2} = 1 \ Z_{2,3} = 1 \ Z_4 = 1 \ Z_2 = 1 \ Z_8 = 1$
HfRu	221	<i>P</i> m̄3 <i>m</i>	104268	No	No	12	$Z_{2,1} = 0 \ Z_{2,2} = 0 \ Z_{2,3} = 0 \ Z_4 = 2 \ Z_{4m,\pi} = 0 \ Z_2 = 0 \ Z_8 = 6$

Table S25: Supertopological (STopo) nonmagnetic unique materials without  $f$  electrons that are also SEBR-classified at  $E_F$  with SOC. In order, the columns list the chemical formula, the SG number, the SG symbol, the ICSD number, whether all of the bands in the STopo material are NLC, whether all of the bands in the STopo material are SEBR, the number of valence electrons, and the cumulative stable SIs at  $E_F$  (see S11). A chemical formula with a \* indicates that only some (but not all) of the ICSDs associated to the same unique material (defined using its topological class with SOC) are STopo.

Chem. formula	SG #	SG symbol	ICSD	All NLC	All SEBR	num $e^-$	Topological Indices
Bi	12	<i>C</i> 2/ <i>m</i>	409752	No	No	10	$Z_{2,1} = 0 \ Z_{2,2} = 0 \ Z_{2,3} = 1 \ Z_4 = 2$
TaSb <sub>2</sub> <sup>*</sup>	12	<i>C</i> 2/ <i>m</i>	651600	No	No	30	$Z_{2,1} = 1 \ Z_{2,2} = 1 \ Z_{2,3} = 1 \ Z_4 = 2$
Si <sub>2</sub> Ti <sup>*</sup>	63	<i>C</i> mcm	168418	No	No	24	$Z_{2,1} = 1 \ Z_{2,2} = 1 \ Z_{2,3} = 0 \ Z_4 = 0$
Ca	64	<i>C</i> mce	107510	No	Yes	8	$Z_{2,1} = 0 \ Z_{2,2} = 0 \ Z_{2,3} = 0 \ Z_4 = 3$
Ga	64	<i>C</i> mce	43388	No	Yes	12	$Z_{2,1} = 1 \ Z_{2,2} = 1 \ Z_{2,3} = 0 \ Z_4 = 1$
MoNi <sub>4</sub>	87	<i>I</i> 4/ <i>m</i>	105047	No	No	46	$Z_{2,1} = 0 \ Z_{2,2} = 0 \ Z_{2,3} = 0 \ Z_4 = 3 \ Z_2 = 1 \ Z_8 = 7$
TiH <sub>2</sub>	139	<i>I</i> 4/ <i>mmm</i>	56184	No	No	6	$Z_{2,1} = 0 \ Z_{2,2} = 0 \ Z_{2,3} = 0 \ Z_4 = 3 \ Z_2 = 1 \ Z_8 = 7$
Hf <sub>3</sub> Te <sub>2</sub>	139	<i>I</i> 4/ <i>mmm</i>	75936	No	No	24	$Z_{2,1} = 0 \ Z_{2,2} = 0 \ Z_{2,3} = 0 \ Z_4 = 0 \ Z_2 = 0 \ Z_8 = 4$
Al <sub>3</sub> Zr <sup>*</sup>	139	<i>I</i> 4/ <i>mmm</i>	107903	No	No	26	$Z_{2,1} = 0 \ Z_{2,2} = 0 \ Z_{2,3} = 0 \ Z_4 = 3 \ Z_2 = 1 \ Z_8 = 7$
HfAl <sub>3</sub>	139	<i>I</i> 4/ <i>mmm</i>	608102	No	No	26	$Z_{2,1} = 1 \ Z_{2,2} = 1 \ Z_{2,3} = 1 \ Z_4 = 2 \ Z_2 = 0 \ Z_8 = 6$
CaCo <sub>2</sub> Ge <sub>2</sub>	139	<i>I</i> 4/ <i>mmm</i>	406	No	Yes	28	$Z_{2,1} = 1 \ Z_{2,2} = 1 \ Z_{2,3} = 1 \ Z_4 = 3 \ Z_2 = 1 \ Z_8 = 3$
CaCo <sub>2</sub> Si <sub>2</sub>	139	<i>I</i> 4/ <i>mmm</i>	420974	No	Yes	28	$Z_{2,1} = 1 \ Z_{2,2} = 1 \ Z_{2,3} = 1 \ Z_4 = 0 \ Z_2 = 1 \ Z_8 = 3$
CaNi <sub>2</sub> Ge <sub>2</sub>	139	<i>I</i> 4/ <i>mmm</i>	408	No	No	30	$Z_{2,1} = 1 \ Z_{2,2} = 1 \ Z_{2,3} = 1 \ Z_4 = 0 \ Z_2 = 0 \ Z_8 = 4$
MoBe <sub>12</sub>	139	<i>I</i> 4/ <i>mmm</i>	616334	No	No	30	$Z_{2,1} = 0 \ Z_{2,2} = 0 \ Z_{2,3} = 0 \ Z_4 = 3 \ Z_2 = 1 \ Z_8 = 7$
Ba <sub>2</sub> Bi	139	<i>I</i> 4/ <i>mmm</i>	2141	No	No	50	$Z_{2,1} = 0 \ Z_{2,2} = 0 \ Z_{2,3} = 0 \ Z_4 = 1 \ Z_2 = 1 \ Z_8 = 5$

Bi*	140	<i>I4/mcm</i>	<a href="#">51674</a>	No	No	20	$Z_{2,1} = 1 \ Z_{2,2} = 1 \ Z_{2,3} = 1 \ Z_4 = 0 \ Z_2 = 0 \ Z_8 = 0$ $Z_{2,1} = 0 \ Z_{2,2} = 0 \ Z_{2,3} = 0 \ Z_4 = 2 \ Z_2 = 0 \ Z_8 = 6$ $Z_{2,1} = 0 \ Z_{2,2} = 0 \ Z_{2,3} = 0 \ Z_4 = 1 \ Z_2 = 1$ $Z_{2,1} = 0 \ Z_{2,2} = 0 \ Z_{2,3} = 0 \ Z_4 = 3$ $Z_{2,1} = 0 \ Z_{2,2} = 0 \ Z_{2,3} = 0 \ Z_4 = 3$ $Z_{2,1} = 0 \ Z_{2,2} = 0 \ Z_{2,3} = 0 \ Z_4 = 3$ $Z_{2,1} = 1 \ Z_{2,2} = 1 \ Z_{2,3} = 1 \ Z_4 = 3$ $Z_{2,1} = 1 \ Z_{2,2} = 0 \ Z_{2,3} = 0 \ Z_4 = 2$ $Z_{2,1} = 1 \ Z_{2,2} = 1 \ Z_{2,3} = 1 \ Z_4 = 1$ $Z_{2,1} = 1 \ Z_{2,2} = 1 \ Z_{2,3} = 1 \ Z_4 = 3$ $Z_{2,1} = 0 \ Z_{2,2} = 0 \ Z_{2,3} = 0 \ Z_4 = 2$ $Z_{2,1} = 0 \ Z_{2,2} = 0 \ Z_{2,3} = 0 \ Z_4 = 1$
Ga <sub>2</sub> Sc <sub>3</sub>	140	<i>I4/mcm</i>	<a href="#">103957</a>	No	No	120	
Si	141	<i>I4<sub>1</sub>/amd</i>	<a href="#">52460</a>	No	No	8	
Bi <sub>2</sub> Mg <sub>3</sub> *	164	<i>P̄3m1</i>	<a href="#">659569</a>	No	Yes	16	
PtTe <sub>2</sub>	164	<i>P̄3m1</i>	<a href="#">41385</a>	No	Yes	22	
PdTe <sub>2</sub> *	164	<i>P̄3m1</i>	<a href="#">83642</a>	No	Yes	22	
As*	166	<i>R̄3m</i>	<a href="#">16516</a>	No	Yes	10	
P	166	<i>R̄3m</i>	<a href="#">53301</a>	No	Yes	10	
Sb	166	<i>R̄3m</i>	<a href="#">55402</a>	No	Yes	10	
Sb*	166	<i>R̄3m</i>	<a href="#">64695</a>	No	Yes	10	
Bi*	166	<i>R̄3m</i>	<a href="#">64703</a>	No	Yes	10	
CaGe <sub>2</sub> *	166	<i>R̄3m</i>	<a href="#">110107</a>	No	Yes	20	
Si	191	<i>P6/mmm</i>	<a href="#">52456</a>	No	Yes	4	
ZrB <sub>2</sub>	191	<i>P6/mmm</i>	<a href="#">30327</a>	No	Yes	10	
TiB <sub>2</sub>	191	<i>P6/mmm</i>	<a href="#">30330</a>	No	Yes	10	
HfB <sub>2</sub>	191	<i>P6/mmm</i>	<a href="#">30422</a>	No	Yes	10	
CaSi <sub>2</sub>	191	<i>P6/mmm</i>	<a href="#">154433</a>	No	Yes	10	
Ti	191	<i>P6/mmm</i>	<a href="#">52521</a>	No	Yes	12	
Ti <sub>2</sub> Zr	191	<i>P6/mmm</i>	<a href="#">247962</a>	No	Yes	12	
CaNi <sub>4</sub> B	191	<i>P6/mmm</i>	<a href="#">36504</a>	No	Yes	90	
Mg	194	<i>P6<sub>3</sub>/mmc</i>	<a href="#">52260</a>	No	Yes	4	
Mg	194	<i>P6<sub>3</sub>/mmc</i>	<a href="#">170902</a>	No	Yes	4	
Zn	194	<i>P6<sub>3</sub>/mmc</i>	<a href="#">52259</a>	No	Yes	24	
Ti <sub>2</sub> PbC	194	<i>P6<sub>3</sub>/mmc</i>	<a href="#">42926</a>	No	No	32	
Ti <sub>2</sub> SnC*	194	<i>P6<sub>3</sub>/mmc</i>	<a href="#">161064</a>	No	No	32	
HfAl <sub>2</sub>	194	<i>P6<sub>3</sub>/mmc</i>	<a href="#">109245</a>	No	Yes	40	
WBe <sub>2</sub>	194	<i>P6<sub>3</sub>/mmc</i>	<a href="#">616501</a>	No	No	40	
WB <sub>2.0</sub>	194	<i>P6<sub>3</sub>/mmc</i>	<a href="#">23716</a>	No	No	48	
HfCr <sub>2</sub>	194	<i>P6<sub>3</sub>/mmc</i>	<a href="#">109213</a>	No	No	64	
AlSc	221	<i>Pm̄3m</i>	<a href="#">58098</a>	No	No	6	
BeTi	221	<i>Pm̄3m</i>	<a href="#">58743</a>	No	No	6	
AlCo	221	<i>Pm̄3m</i>	<a href="#">57596</a>	No	Yes	12	
Allr	221	<i>Pm̄3m</i>	<a href="#">57928</a>	No	No	12	
AgLi	221	<i>Pm̄3m</i>	<a href="#">58310</a>	No	Yes	12	
CaPd	221	<i>Pm̄3m</i>	<a href="#">58926</a>	No	Yes	12	
HfOs	221	<i>Pm̄3m</i>	<a href="#">104252</a>	No	Yes	12	
MgPd	221	<i>Pm̄3m</i>	<a href="#">104847</a>	No	No	12	
MnV	221	<i>Pm̄3m</i>	<a href="#">104998</a>	No	No	12	
OsZr	221	<i>Pm̄3m</i>	<a href="#">105580</a>	No	No	12	
RuTi	221	<i>Pm̄3m</i>	<a href="#">106004</a>	No	No	12	
RuZr	221	<i>Pm̄3m</i>	<a href="#">106022</a>	No	No	12	
TiRu	221	<i>Pm̄3m</i>	<a href="#">150936</a>	No	No	12	
ZrRu	221	<i>Pm̄3m</i>	<a href="#">181289</a>	No	No	12	
MgNi	221	<i>Pm̄3m</i>	<a href="#">187256</a>	No	No	12	
TiFe*	221	<i>Pm̄3m</i>	<a href="#">189112</a>	No	No	12	
FeTi*	221	<i>Pm̄3m</i>	<a href="#">190972</a>	No	No	12	
OsHf	221	<i>Pm̄3m</i>	<a href="#">290935</a>	No	No	12	
AlAu	221	<i>Pm̄3m</i>	<a href="#">57495</a>	No	No	14	
AgGa	221	<i>Pm̄3m</i>	<a href="#">104466</a>	No	No	14	
AgIn	221	<i>Pm̄3m</i>	<a href="#">605384</a>	No	No	14	
CoMn	221	<i>Pm̄3m</i>	<a href="#">187981</a>	No	No	16	
Co <sub>3</sub> V	221	<i>Pm̄3m</i>	<a href="#">187965</a>	No	No	32	
TIPd <sub>3</sub> H	221	<i>Pm̄3m</i>	<a href="#">247273</a>	No	No	34	
HfRh <sub>3</sub> B	221	<i>Pm̄3m</i>	<a href="#">614447</a>	No	Yes	34	
ZrRh <sub>3</sub> B	221	<i>Pm̄3m</i>	<a href="#">615353</a>	No	Yes	34	
Ni <sub>3</sub> Cr	221	<i>Pm̄3m</i>	<a href="#">188231</a>	No	No	36	

Pt <sub>3</sub> Zn	221	<i>Pm</i> 3̄ <i>m</i>	105853	No	No	42	$Z_{2,1} = 0 \ Z_{2,2} = 0 \ Z_{2,3} = 0 \ Z_4 = 2 \ Z_{4m,\pi} = 2 \ Z_2 = 0 \ Z_8 = 6$
AuCu <sub>3</sub>	221	<i>Pm</i> 3̄ <i>m</i>	40351	No	No	44	$Z_{2,1} = 1 \ Z_{2,2} = 1 \ Z_{2,3} = 1 \ Z_4 = 0 \ Z_{4m,\pi} = 1 \ Z_2 = 0 \ Z_8 = 4$
Ca	225	<i>Fm</i> 3̄ <i>m</i>	44348	No	Yes	2	$Z_{2,1} = 0 \ Z_{2,2} = 0 \ Z_{2,3} = 0 \ Z_4 = 0 \ Z_2 = 0 \ Z_8 = 4$
Mg	225	<i>Fm</i> 3̄ <i>m</i>	180453	No	Yes	2	$Z_{2,1} = 0 \ Z_{2,2} = 0 \ Z_{2,3} = 0 \ Z_4 = 0 \ Z_2 = 0 \ Z_8 = 4$
TiH <sub>2</sub>	225	<i>Fm</i> 3̄ <i>m</i>	56182	No	Yes	6	$Z_{2,1} = 0 \ Z_{2,2} = 0 \ Z_{2,3} = 0 \ Z_4 = 3 \ Z_2 = 1 \ Z_8 = 7$
In <sub>2</sub> LiRh	225	<i>Fm</i> 3̄ <i>m</i>	106806	No	Yes	16	$Z_{2,1} = 0 \ Z_{2,2} = 0 \ Z_{2,3} = 0 \ Z_4 = 3 \ Z_2 = 1 \ Z_8 = 7$
MgIn <sub>2</sub>	227	<i>Fd</i> 3̄ <i>m</i>	423608	No	Yes	16	$Z_{2,1} = 0 \ Z_{2,2} = 0 \ Z_{2,3} = 0 \ Z_4 = 3 \ Z_2 = 1$
Ti <sub>2</sub> C	227	<i>Fd</i> 3̄ <i>m</i>	77473	No	Yes	48	$Z_{2,1} = 0 \ Z_{2,2} = 0 \ Z_{2,3} = 0 \ Z_4 = 1 \ Z_2 = 1$
Hf <sub>2</sub> Pd	227	<i>Fd</i> 3̄ <i>m</i>	638772	No	No	144	$Z_{2,1} = 0 \ Z_{2,2} = 0 \ Z_{2,3} = 0 \ Z_4 = 1 \ Z_2 = 1$

Table S26: Supertopological (STopo) nonmagnetic unique materials without *f* electrons that are also ES-classified at  $E_F$  with SOC. In order, the columns list the chemical formula, the SG number, the SG symbol, the ICSD number, whether all of the bands in the STopo material are NLC, whether all of the bands in the STopo material are SEBR, and the number of valence electrons. A chemical formula with a \* indicates that only some (but not all) of the ICSDs associated to the same unique material (defined using its topological class with SOC) are STopo.

Chem. formula	SG #	SG symbol	ICSD	All NLC	All SEBR	num e <sup>-</sup>
IrV	123	<i>P4/mmm</i>	104589	Yes	No	14
RhV*	123	<i>P4/mmm</i>	169385	Yes	No	14
MgNiH <sub>2</sub>	123	<i>P4/mmm</i>	187258	No	No	14
RuSi <sub>2</sub>	123	<i>P4/mmm</i>	154013	No	No	16
AuCu	123	<i>P4/mmm</i>	42574	Yes	No	22
NiZn	123	<i>P4/mmm</i>	105469	No	No	22
PdZn	123	<i>P4/mmm</i>	105752	Yes	No	22
Sn	139	<i>I4/mmm</i>	108748	No	No	4
Ge <sub>2</sub> W	139	<i>I4/mmm</i>	9978	No	Yes	14
WSi <sub>2</sub>	139	<i>I4/mmm</i>	26869	No	No	14
CaGa <sub>4</sub>	139	<i>I4/mmm</i>	58892	No	Yes	14
CrSi <sub>2</sub>	139	<i>I4/mmm</i>	71499	No	No	14
Al <sub>4</sub> Ca	139	<i>I4/mmm</i>	151189	No	Yes	14
TiS <sub>2</sub>	139	<i>I4/mmm</i>	181504	No	No	16
Au <sub>2</sub> Hf	139	<i>I4/mmm</i>	611956	No	Yes	26
Be <sub>12</sub> Pd	139	<i>I4/mmm</i>	109314	No	Yes	34
Ga <sub>5</sub> Mg <sub>2</sub>	139	<i>I4/mmm</i>	23227	No	No	38
Zr <sub>2</sub> Si	140	<i>I4/mcm</i>	652615	No	No	24
RuSn <sub>2</sub>	140	<i>I4/mcm</i>	105993	No	No	32
FeZr <sub>2</sub>	140	<i>I4/mcm</i>	634145	No	No	32
Hf <sub>2</sub> Ni	140	<i>I4/mcm</i>	151466	No	No	36
V <sub>4</sub> SiSb <sub>2</sub>	140	<i>I4/mcm</i>	82564	No	No	68
TlTe*	140	<i>I4/mcm</i>	69027	No	No	72
Ti <sub>5</sub> FeSb <sub>2</sub>	140	<i>I4/mcm</i>	96143	No	No	76
Mo <sub>5</sub> Si <sub>3</sub> *	140	<i>I4/mcm</i>	35756	No	No	84
W <sub>5</sub> Zr <sub>3</sub>	140	<i>I4/mcm</i>	653434	No	No	84
ScIr <sub>3</sub> B <sub>4</sub>	176	<i>P6<sub>3</sub>/m</i>	44424	No	Yes	84
Sn <sub>4</sub> Ir <sub>7</sub> B <sub>3</sub>	176	<i>P6<sub>3</sub>/m</i>	78985	No	Yes	176
MoB <sub>2</sub> *	191	<i>P6/mmm</i>	614799	No	Yes	12
Ti <sub>2</sub> TaN <sub>3</sub>	191	<i>P6/mmm</i>	186418	No	Yes	28
ScCo <sub>3</sub> B <sub>2</sub>	191	<i>P6/mmm</i>	44179	No	Yes	36
CaPt <sub>5</sub>	191	<i>P6/mmm</i>	58929	No	Yes	52
NaPt <sub>3</sub> B	191	<i>P6/mmm</i>	68092	No	Yes	68
MgFe <sub>6</sub> Ge <sub>6</sub>	191	<i>P6/mmm</i>	188716	No	Yes	74
TiFe <sub>6</sub> Ge <sub>6</sub> *	191	<i>P6/mmm</i>	92173	No	Yes	76
CaNi <sub>4</sub> B	191	<i>P6/mmm</i>	612693	No	Yes	90

Zr <sub>5</sub> AgIn <sub>3</sub>	193	<i>P</i> 6 <sub>3</sub> / <i>mcm</i>	190116	No	Yes	80	
Ti*	194	<i>P</i> 6 <sub>3</sub> / <i>mmc</i>	168830	No	Yes	8	
Ge*	194	<i>P</i> 6 <sub>3</sub> / <i>mmc</i>	189805	No	Yes	8	
Cr*	194	<i>P</i> 6 <sub>3</sub> / <i>mmc</i>	151375	No	Yes	12	
Ru	194	<i>P</i> 6 <sub>3</sub> / <i>mmc</i>	40354	No	No	16	
Fe	194	<i>P</i> 6 <sub>3</sub> / <i>mmc</i>	53450	No	No	16	
CaIn <sub>2</sub>	194	<i>P</i> 6 <sub>3</sub> / <i>mmc</i>	58686	No	Yes	16	
CaGa <sub>2</sub>	194	<i>P</i> 6 <sub>3</sub> / <i>mmc</i>	58891	No	Yes	16	
Ga <sub>2</sub> Mg	194	<i>P</i> 6 <sub>3</sub> / <i>mmc</i>	103792	No	Yes	16	
CaLi <sub>2</sub>	194	<i>P</i> 6 <sub>3</sub> / <i>mmc</i>	106349	No	Yes	16	
TcB	194	<i>P</i> 6 <sub>3</sub> / <i>mmc</i>	168897	No	No	20	
CaMg <sub>2</sub>	194	<i>P</i> 6 <sub>3</sub> / <i>mmc</i>	58912	No	Yes	24	
RhB	194	<i>P</i> 6 <sub>3</sub> / <i>mmc</i>	193833	No	Yes	24	
ReB <sub>3</sub>	194	<i>P</i> 6 <sub>3</sub> / <i>mmc</i>	24361	No	Yes	32	
AlAuTi	194	<i>P</i> 6 <sub>3</sub> / <i>mmc</i>	57506	No	No	36	
Be <sub>2</sub> Re	194	<i>P</i> 6 <sub>3</sub> / <i>mmc</i>	58732	No	No	44	
Ag	194	<i>P</i> 6 <sub>3</sub> / <i>mmc</i>	64707	No	No	44	
FeWN <sub>2</sub>	194	<i>P</i> 6 <sub>3</sub> / <i>mmc</i>	81488	No	No	48	
BaNa <sub>2</sub>	194	<i>P</i> 6 <sub>3</sub> / <i>mmc</i>	106313	No	No	48	
MoC*	194	<i>P</i> 6 <sub>3</sub> / <i>mmc</i>	44987	No	No	60	
Mg <sub>2</sub> Y*	194	<i>P</i> 6 <sub>3</sub> / <i>mmc</i>	642901	No	Yes	60	
Cr <sub>2</sub> Ti*	194	<i>P</i> 6 <sub>3</sub> / <i>mmc</i>	102854	No	No	64	
Re <sub>2</sub> Sc	194	<i>P</i> 6 <sub>3</sub> / <i>mmc</i>	105890	No	No	68	
Mn <sub>2</sub> Sc	194	<i>P</i> 6 <sub>3</sub> / <i>mmc</i>	108596	No	No	68	
ScMn <sub>2</sub> *	194	<i>P</i> 6 <sub>3</sub> / <i>mmc</i>	109246	No	No	68	
TaB <sub>4</sub>	194	<i>P</i> 6 <sub>3</sub> / <i>mmc</i>	182094	No	No	68	
Cr <sub>2</sub> Ta*	194	<i>P</i> 6 <sub>3</sub> / <i>mmc</i>	626859	No	No	68	
WB <sub>4</sub>	194	<i>P</i> 6 <sub>3</sub> / <i>mmc</i>	43193	No	No	72	
HfRe <sub>2</sub>	194	<i>P</i> 6 <sub>3</sub> / <i>mmc</i>	150512	No	No	72	
MoB <sub>4</sub>	194	<i>P</i> 6 <sub>3</sub> / <i>mmc</i>	182095	No	No	72	
Re <sub>2</sub> Zr*	194	<i>P</i> 6 <sub>3</sub> / <i>mmc</i>	650208	No	No	72	
ScRu <sub>2</sub>	194	<i>P</i> 6 <sub>3</sub> / <i>mmc</i>	150514	No	No	76	
CaHg <sub>3</sub>	194	<i>P</i> 6 <sub>3</sub> / <i>mmc</i>	619356	No	Yes	76	
Os <sub>2</sub> Sc	194	<i>P</i> 6 <sub>3</sub> / <i>mmc</i>	647766	No	No	76	
TiOs <sub>2</sub>	194	<i>P</i> 6 <sub>3</sub> / <i>mmc</i>	290936	No	No	80	
ZrOs <sub>2</sub>	194	<i>P</i> 6 <sub>3</sub> / <i>mmc</i>	290937	No	No	80	
Re <sub>2</sub> W	194	<i>P</i> 6 <sub>3</sub> / <i>mmc</i>	650203	No	No	80	
Ru <sub>2</sub> Zr*	194	<i>P</i> 6 <sub>3</sub> / <i>mmc</i>	650790	No	No	80	
MoN*	194	<i>P</i> 6 <sub>3</sub> / <i>mmc</i>	106926	No	Yes	88	
WFe <sub>2</sub> *	194	<i>P</i> 6 <sub>3</sub> / <i>mmc</i>	600061	No	Yes	88	
MoFe <sub>2</sub> *	194	<i>P</i> 6 <sub>3</sub> / <i>mmc</i>	601488	No	No	88	
Mg <sub>5</sub> Rh <sub>2</sub>	194	<i>P</i> 6 <sub>3</sub> / <i>mmc</i>	104860	No	No	112	
Mg <sub>5</sub> Pd <sub>2</sub> *	194	<i>P</i> 6 <sub>3</sub> / <i>mmc</i>	246978	No	No	120	
KAg <sub>2</sub>	194	<i>P</i> 6 <sub>3</sub> / <i>mmc</i>	150142	No	No	124	
HfMo <sub>2</sub> *	194	<i>P</i> 6 <sub>3</sub> / <i>mmc</i>	638615	No	No	128	
Al <sub>5</sub> Rh <sub>2</sub> *	194	<i>P</i> 6 <sub>3</sub> / <i>mmc</i>	58153	No	No	132	
SrZn <sub>2</sub>	194	<i>P</i> 6 <sub>3</sub> / <i>mmc</i>	246194	No	No	136	
Pd <sub>3</sub> Ti*	194	<i>P</i> 6 <sub>3</sub> / <i>mmc</i>	649037	No	No	136	
YZn <sub>2</sub>	194	<i>P</i> 6 <sub>3</sub> / <i>mmc</i>	290900	No	No	140	
AlRe	221	<i>Pm</i> 3 <i>m</i>	58146	No	No	10	
RuSi	221	<i>Pm</i> 3 <i>m</i>	44616	No	Yes	12	
AlRh	221	<i>Pm</i> 3 <i>m</i>	58151	No	No	12	
BePd	221	<i>Pm</i> 3 <i>m</i>	58728	No	Yes	12	
InRh	221	<i>Pm</i> 3 <i>m</i>	59515	No	No	12	
GaIr	221	<i>Pm</i> 3 <i>m</i>	103760	No	No	12	
GaRh	221	<i>Pm</i> 3 <i>m</i>	103948	No	Yes	12	

OsTi	221	<i>Pm</i> $\bar{3}m$	105572	No	No	12
TcV	221	<i>Pm</i> $\bar{3}m$	106143	No	No	12
OsC	221	<i>Pm</i> $\bar{3}m$	185989	No	Yes	12
ZnZr	221	<i>Pm</i> $\bar{3}m$	106235	No	No	16
NiZn	221	<i>Pm</i> $\bar{3}m$	105470	No	No	22
ZrRu <sub>3</sub>	221	<i>Pm</i> $\bar{3}m$	185641	No	No	28
Cd(TiO <sub>3</sub> )	221	<i>Pm</i> $\bar{3}m$	33667	No	No	34
Fe <sub>3</sub> Pd	221	<i>Pm</i> $\bar{3}m$	103586	No	No	34
ScPd <sub>3</sub> B	221	<i>Pm</i> $\bar{3}m$	190796	No	Yes	36
Cr	223	<i>Pm</i> $\bar{3}m$	108326	No	Yes	48
Mo	225	<i>Fm</i> $\bar{3}m$	41513	No	Yes	6
PtIn <sub>2</sub>	225	<i>Fm</i> $\bar{3}m$	56259	No	Yes	16
Al <sub>2</sub> Pd	225	<i>Fm</i> $\bar{3}m$	58116	No	Yes	16
RuSi <sub>2</sub>	225	<i>Fm</i> $\bar{3}m$	154014	No	Yes	16
CdGeP <sub>2</sub>	225	<i>Fm</i> $\bar{3}m$	52804	No	Yes	26
CaPt <sub>2</sub>	227	<i>Fd</i> $\bar{3}m$	108147	No	Yes	44
Cr <sub>2</sub> Ni	227	<i>Fd</i> $\bar{3}m$	188278	No	No	44
Ni <sub>2</sub> Zr	227	<i>Fd</i> $\bar{3}m$	105480	No	Yes	48
PbAu <sub>2</sub>	227	<i>Fd</i> $\bar{3}m$	56261	No	No	52
Be <sub>22</sub> Mo*	227	<i>Fd</i> $\bar{3}m$	58718	No	Yes	100
Pb <sub>2</sub> Sn <sub>2</sub> O <sub>6</sub>	227	<i>Fd</i> $\bar{3}m$	15308	No	No	104
Sc <sub>4</sub> Ru <sub>7</sub> Ge <sub>6</sub>	229	<i>I</i> $m\bar{3}m$	637747	No	Yes	92

Table S27: Supertopological (STopo) nonmagnetic unique materials without  $f$  electrons that are also ESFD-classified at  $E_F$  with SOC. In order, the columns list the chemical formula, the SG number, the SG symbol, the ICSD number, whether all of the bands in the STopo material are NLC, whether all of the bands in the STopo material are SEBR, and the number of valence electrons. A chemical formula with a \* indicates that only some (but not all) of the ICSDs associated to the same unique material (defined using its topological class with SOC) are STopo.

Chem. formula	SG #	SG symbol	ICSD	All NLC	All SEBR	num $e^-$
MoRh	51	<i>Pmma</i>	108608	Yes	No	30
CaRhIn <sub>4</sub>	51	<i>Pmma</i>	410891	Yes	No	46
Ga	63	<i>Cmcm</i>	43539	Yes	No	6
AlTi*	123	<i>P4/mmm</i>	58187	Yes	No	7
GaTi	123	<i>P4/mmm</i>	103989	No	No	7
RhTi	123	<i>P4/mmm</i>	105951	No	No	13
RuTa	123	<i>P4/mmm</i>	105995	No	No	13
PtV	123	<i>P4/mmm</i>	105835	Yes	No	15
ReC <sub>2</sub>	123	<i>P4/mmm</i>	184664	No	No	15
CuGa <sub>2</sub>	123	<i>P4/mmm</i>	102906	No	No	17
HfNiGa <sub>5</sub>	123	<i>P4/mmm</i>	634319	No	No	29
Pt <sub>3</sub> Al	123	<i>P4/mmm</i>	109235	No	No	33
Cu <sub>3</sub> Pd*	123	<i>P4/mmm</i>	103083	No	No	43
ReO <sub>3</sub>	127	<i>P4/mbm</i>	77680	Yes	No	50
Sc <sub>2</sub> SiIr <sub>5</sub> B <sub>2</sub>	127	<i>P4/mbm</i>	85629	Yes	No	122
Sc <sub>5</sub> Rh <sub>4</sub> Si <sub>10</sub> *	127	<i>P4/mbm</i>	602226	Yes	No	182
Sc <sub>5</sub> Co <sub>4</sub> Si <sub>10</sub> *	127	<i>P4/mbm</i>	624958	Yes	No	182
Sc*	139	<i>I</i> $4/mmm$	52410	No	No	3
In*	139	<i>I</i> $4/mmm$	639813	No	Yes	3
TiGa <sub>3</sub>	139	<i>I</i> $4/mmm$	98937	No	No	13
Ga <sub>4</sub> Na	139	<i>I</i> $4/mmm$	103822	No	No	13
CuTi <sub>2</sub> *	139	<i>I</i> $4/mmm$	629388	No	No	19
ScNi <sub>2</sub> Si <sub>2</sub>	139	<i>I</i> $4/mmm$	106839	No	No	31

Be <sub>12</sub> Ag	139	<i>I</i> 4/ <i>mmm</i>	109313	No	No	35
GaHf <sub>2</sub>	140	<i>I</i> 4/ <i>mcm</i>	102809	No	No	22
Hf <sub>2</sub> Al	140	<i>I</i> 4/ <i>mcm</i>	150773	No	No	22
Zr <sub>2</sub> Al	140	<i>I</i> 4/ <i>mcm</i>	150774	No	No	22
Ti <sub>2</sub> B	140	<i>I</i> 4/ <i>mcm</i>	189385	No	No	22
Ta <sub>2</sub> B	140	<i>I</i> 4/ <i>mcm</i>	42525	No	No	26
Mo <sub>2</sub> B	140	<i>I</i> 4/ <i>mcm</i>	24278	No	No	30
W <sub>2</sub> B	140	<i>I</i> 4/ <i>mcm</i>	24279	No	No	30
Cr <sub>2</sub> B	140	<i>I</i> 4/ <i>mcm</i>	76127	No	No	30
Al <sub>2</sub> Cu*	140	<i>I</i> 4/ <i>mcm</i>	42517	No	No	34
Mn <sub>2</sub> B	140	<i>I</i> 4/ <i>mcm</i>	42529	No	No	34
CoZr <sub>2</sub>	140	<i>I</i> 4/ <i>mcm</i>	102740	No	No	34
RhPb <sub>2</sub> *	140	<i>I</i> 4/ <i>mcm</i>	102802	No	No	34
RhZr <sub>2</sub>	140	<i>I</i> 4/ <i>mcm</i>	102807	No	No	34
IrZr <sub>2</sub>	140	<i>I</i> 4/ <i>mcm</i>	641204	No	No	34
CoTa <sub>2</sub> *	140	<i>I</i> 4/ <i>mcm</i>	102815	Yes	No	38
Tc <sub>2</sub> Al <sub>3</sub>	164	<i>P</i> 3 <i>m</i> 1	609482	No	Yes	23
HfIr <sub>3</sub> B <sub>4</sub>	176	<i>P</i> 6 <sub>3</sub> / <i>m</i>	1518	No	No	86
ZrIr <sub>3</sub> B <sub>4</sub>	176	<i>P</i> 6 <sub>3</sub> / <i>m</i>	614583	No	No	86
AlB <sub>2</sub>	191	<i>P</i> 6/ <i>mmm</i>	43851	No	Yes	9
ScB <sub>2</sub>	191	<i>P</i> 6/ <i>mmm</i>	44491	No	Yes	9
TaB <sub>2</sub> *	191	<i>P</i> 6/ <i>mmm</i>	30420	No	Yes	11
VB <sub>2</sub> *	191	<i>P</i> 6/ <i>mmm</i>	165125	No	Yes	11
AgB <sub>2</sub>	191	<i>P</i> 6/ <i>mmm</i>	43821	No	Yes	17
AuB <sub>2</sub>	191	<i>P</i> 6/ <i>mmm</i>	52699	No	Yes	17
Hg <sub>2</sub> Na	191	<i>P</i> 6/ <i>mmm</i>	104327	No	Yes	25
Zr <sub>4</sub> Al <sub>3</sub> *	191	<i>P</i> 6/ <i>mmm</i>	603486	No	Yes	25
Hf <sub>4</sub> Al <sub>3</sub>	191	<i>P</i> 6/ <i>mmm</i>	608072	No	Yes	25
CaRh <sub>3</sub> B <sub>2</sub>	191	<i>P</i> 6/ <i>mmm</i>	66767	No	Yes	35
Co <sub>3</sub> HfB <sub>2</sub>	191	<i>P</i> 6/ <i>mmm</i>	23550	No	Yes	37
CoSn*	191	<i>P</i> 6/ <i>mmm</i>	55564	No	Yes	39
PbRh	191	<i>P</i> 6/ <i>mmm</i>	105607	No	Yes	39
NiIn*	191	<i>P</i> 6/ <i>mmm</i>	161111	No	Yes	39
Al <sub>9</sub> CaCo <sub>2</sub>	191	<i>P</i> 6/ <i>mmm</i>	57535	No	Yes	47
CaCu <sub>5</sub>	191	<i>P</i> 6/ <i>mmm</i>	58882	No	Yes	57
LiNi <sub>6</sub> Ge <sub>6</sub>	191	<i>P</i> 6/ <i>mmm</i>	41463	No	Yes	255
Ta <sub>5</sub> N <sub>6</sub> *	193	<i>P</i> 6 <sub>3</sub> / <i>mcm</i>	29329	No	Yes	110
Na	194	<i>P</i> 6 <sub>3</sub> / <i>mmc</i>	44758	No	Yes	2
Li	194	<i>P</i> 6 <sub>3</sub> / <i>mmc</i>	44760	No	Yes	2
Tc	194	<i>P</i> 6 <sub>3</sub> / <i>mmc</i>	52498	No	No	14
WH	194	<i>P</i> 6 <sub>3</sub> / <i>mmc</i>	247586	Yes	No	14
Re*	194	<i>P</i> 6 <sub>3</sub> / <i>mmc</i>	650069	No	No	14
Ag	194	<i>P</i> 6 <sub>3</sub> / <i>mmc</i>	56269	No	No	22
ReB <sub>2</sub> *	194	<i>P</i> 6 <sub>3</sub> / <i>mmc</i>	23871	No	No	26
AuSn	194	<i>P</i> 6 <sub>3</sub> / <i>mmc</i>	56262	No	No	30
ReC <sub>2</sub> *	194	<i>P</i> 6 <sub>3</sub> / <i>mmc</i>	184660	No	No	30
AuMg <sub>3</sub> *	194	<i>P</i> 6 <sub>3</sub> / <i>mmc</i>	58541	No	No	34
V <sub>2</sub> CP*	194	<i>P</i> 6 <sub>3</sub> / <i>mmc</i>	29284	No	No	38
V <sub>2</sub> AsC	194	<i>P</i> 6 <sub>3</sub> / <i>mmc</i>	43874	No	No	38
MnMoN <sub>2</sub>	194	<i>P</i> 6 <sub>3</sub> / <i>mmc</i>	81489	No	No	46
MoCoP <sub>2</sub>	194	<i>P</i> 6 <sub>3</sub> / <i>mmc</i>	624219	No	Yes	50
AlPt <sub>2</sub> Zr	194	<i>P</i> 6 <sub>3</sub> / <i>mmc</i>	58139	No	No	54
HfAlPt <sub>2</sub>	194	<i>P</i> 6 <sub>3</sub> / <i>mmc</i>	608138	No	Yes	54
W <sub>2</sub> B <sub>5</sub>	194	<i>P</i> 6 <sub>3</sub> / <i>mmc</i>	615696	No	No	54
Ir <sub>3</sub> Mo	194	<i>P</i> 6 <sub>3</sub> / <i>mmc</i>	104506	No	No	66
Ir <sub>3</sub> W	194	<i>P</i> 6 <sub>3</sub> / <i>mmc</i>	104598	No	No	66

MoRh <sub>3</sub>	194	<i>P</i> 6 <sub>3</sub> /mmc	105085	No	No	66	
Nb <sub>2</sub> AsC*	194	<i>P</i> 6 <sub>3</sub> /mmc	43011	No	No	70	
CaNiAl <sub>9</sub>	194	<i>P</i> 6 <sub>3</sub> /mmc	63626	No	Yes	78	
Hg <sub>3</sub> Sc	194	<i>P</i> 6 <sub>3</sub> /mmc	104343	No	Yes	78	
V <sub>6</sub> Ga <sub>5</sub> *	194	<i>P</i> 6 <sub>3</sub> /mmc	635613	No	No	90	
Al <sub>10</sub> Mn <sub>3</sub>	194	<i>P</i> 6 <sub>3</sub> /mmc	57974	No	No	102	
Hf <sub>9</sub> W <sub>4</sub> Co	194	<i>P</i> 6 <sub>3</sub> /mmc	623810	No	No	138	
Zr <sub>9</sub> Mo <sub>4</sub> Co	194	<i>P</i> 6 <sub>3</sub> /mmc	624247	No	No	138	
Al <sub>23</sub> V <sub>4</sub>	194	<i>P</i> 6 <sub>3</sub> /mmc	58203	No	No	178	
ReO <sub>3</sub> *	204	<i>I</i> m $\bar{3}$	77721	No	Yes	100	
AlSb	205	<i>P</i> a $\bar{3}$	41994	Yes	No	64	
C	206	<i>I</i> a $\bar{3}$	5390	No	Yes	32	
C <sub>8</sub>	206	<i>I</i> a $\bar{3}$	74655	No	Yes	32	
MgSc	221	<i>P</i> m $\bar{3}$ <i>m</i>	108583	No	No	5	
As*	221	<i>P</i> m $\bar{3}$ <i>m</i>	162842	No	Yes	5	
TcB	221	<i>P</i> m $\bar{3}$ <i>m</i>	168900	No	Yes	10	
AlOs	221	<i>P</i> m $\bar{3}$ <i>m</i>	58107	No	No	11	
BeRh	221	<i>P</i> m $\bar{3}$ <i>m</i>	58734	No	Yes	11	
CaTl <sub>3</sub>	221	<i>P</i> m $\bar{3}$ <i>m</i>	58942	No	No	11	
HfTc	221	<i>P</i> m $\bar{3}$ <i>m</i>	104277	No	No	11	
MgRh	221	<i>P</i> m $\bar{3}$ <i>m</i>	104859	No	Yes	11	
ReTi	221	<i>P</i> m $\bar{3}$ <i>m</i>	105896	No	No	11	
TcTi	221	<i>P</i> m $\bar{3}$ <i>m</i>	106142	No	No	11	
OsSi	221	<i>P</i> m $\bar{3}$ <i>m</i>	43417	No	No	12	
RhSi	221	<i>P</i> m $\bar{3}$ <i>m</i>	44385	No	Yes	13	
AlNi	221	<i>P</i> m $\bar{3}$ <i>m</i>	58037	No	No	13	
AlPd	221	<i>P</i> m $\bar{3}$ <i>m</i>	58113	No	No	13	
AlPt	221	<i>P</i> m $\bar{3}$ <i>m</i>	58128	No	No	13	
AgMg	221	<i>P</i> m $\bar{3}$ <i>m</i>	58322	No	Yes	13	
BeCu	221	<i>P</i> m $\bar{3}$ <i>m</i>	58700	No	No	13	
InNi*	221	<i>P</i> m $\bar{3}$ <i>m</i>	59432	No	No	13	
InPd	221	<i>P</i> m $\bar{3}$ <i>m</i>	59473	No	No	13	
GaNi	221	<i>P</i> m $\bar{3}$ <i>m</i>	103853	No	No	13	
HfRh	221	<i>P</i> m $\bar{3}$ <i>m</i>	104265	No	No	13	
IrZr	221	<i>P</i> m $\bar{3}$ <i>m</i>	104606	No	No	13	
PtSc	221	<i>P</i> m $\bar{3}$ <i>m</i>	105784	No	Yes	13	
RhTi	221	<i>P</i> m $\bar{3}$ <i>m</i>	105953	No	No	13	
HfIr	221	<i>P</i> m $\bar{3}$ <i>m</i>	185632	No	No	13	
IrC	221	<i>P</i> m $\bar{3}$ <i>m</i>	185990	No	Yes	13	
ZrAl <sub>3</sub> *	221	<i>P</i> m $\bar{3}$ <i>m</i>	192029	No	Yes	13	
HfAl <sub>3</sub>	221	<i>P</i> m $\bar{3}$ <i>m</i>	248537	No	Yes	13	
AuSc	221	<i>P</i> m $\bar{3}$ <i>m</i>	58582	No	Yes	14	
CuSc	221	<i>P</i> m $\bar{3}$ <i>m</i>	103095	No	No	14	
HfPt	221	<i>P</i> m $\bar{3}$ <i>m</i>	104257	No	No	14	
PtZr	221	<i>P</i> m $\bar{3}$ <i>m</i>	105857	No	No	14	
HfPd	221	<i>P</i> m $\bar{3}$ <i>m</i>	185630	No	No	14	
CoTa	221	<i>P</i> m $\bar{3}$ <i>m</i>	187978	No	No	14	
ScZn	221	<i>P</i> m $\bar{3}$ <i>m</i>	106041	No	No	15	
RhZn	221	<i>P</i> m $\bar{3}$ <i>m</i>	107574	No	Yes	21	
CuZn	221	<i>P</i> m $\bar{3}$ <i>m</i>	56276	No	No	23	
AgZn	221	<i>P</i> m $\bar{3}$ <i>m</i>	58384	No	No	23	
AuCd*	221	<i>P</i> m $\bar{3}$ <i>m</i>	58410	No	No	23	
AuTi <sub>3</sub>	221	<i>P</i> m $\bar{3}$ <i>m</i>	58604	No	Yes	23	
AuZn*	221	<i>P</i> m $\bar{3}$ <i>m</i>	58625	No	No	23	
TiRu <sub>3</sub>	221	<i>P</i> m $\bar{3}$ <i>m</i>	185635	No	No	28	
ZrOs <sub>3</sub>	221	<i>P</i> m $\bar{3}$ <i>m</i>	185644	No	Yes	28	

Mn <sub>3</sub> Rh	221	<i>Pm</i> $\bar{3}m$	104961	No	Yes	30
Rh <sub>3</sub> Sc	221	<i>Pm</i> $\bar{3}m$	105920	No	No	30
Ir <sub>3</sub> Sc	221	<i>Pm</i> $\bar{3}m$	108568	No	No	30
HfIr <sub>3</sub> <sup>*</sup>	221	<i>Pm</i> $\bar{3}m$	104212	No	Yes	31
Ir <sub>3</sub> Zr	221	<i>Pm</i> $\bar{3}m$	104610	No	No	31
Rh <sub>3</sub> Ti	221	<i>Pm</i> $\bar{3}m$	105955	No	No	31
ScIr <sub>3</sub> B	221	<i>Pm</i> $\bar{3}m$	44423	No	No	33
Rh <sub>3</sub> ScB	221	<i>Pm</i> $\bar{3}m$	44561	No	Yes	33
AlPt <sub>3</sub>	221	<i>Pm</i> $\bar{3}m$	58131	No	No	33
Pd <sub>3</sub> Sc <sup>*</sup>	221	<i>Pm</i> $\bar{3}m$	105674	No	No	33
Au <sub>3</sub> Li	221	<i>Pm</i> $\bar{3}m$	58525	No	Yes	34
Fe <sub>3</sub> Pt	221	<i>Pm</i> $\bar{3}m$	103598	No	Yes	34
Pt <sub>3</sub> Zr	221	<i>Pm</i> $\bar{3}m$	105858	No	Yes	34
TiPt <sub>3</sub>	221	<i>Pm</i> $\bar{3}m$	185640	No	No	34
ZrPd <sub>3</sub>	221	<i>Pm</i> $\bar{3}m$	185643	No	No	34
Ag <sub>3</sub> Mg	221	<i>Pm</i> $\bar{3}m$	58323	No	Yes	35
ScPt <sub>3</sub> B	221	<i>Pm</i> $\bar{3}m$	190790	No	Yes	36
TiZn <sub>3</sub>	221	<i>Pm</i> $\bar{3}m$	106185	No	No	40
AgPt <sub>3</sub>	221	<i>Pm</i> $\bar{3}m$	58347	No	No	41
VZn <sub>3</sub>	221	<i>Pm</i> $\bar{3}m$	106240	No	No	41
AuPd <sub>3</sub>	221	<i>Pm</i> $\bar{3}m$	180876	No	No	41
HgPt <sub>3</sub>	221	<i>Pm</i> $\bar{3}m$	639147	No	No	42
Cu <sub>3</sub> Pd	221	<i>Pm</i> $\bar{3}m$	103084	No	Yes	43
Au <sub>3</sub> Pd	221	<i>Pm</i> $\bar{3}m$	180872	No	Yes	43
Cu <sub>3</sub> Pt	221	<i>Pm</i> $\bar{3}m$	628749	No	No	43
Au <sub>3</sub> Cu <sup>*</sup>	221	<i>Pm</i> $\bar{3}m$	56266	No	No	44
Tl <sub>3</sub> Au	223	<i>Pm</i> $\bar{3}n$	186643	No	Yes	40
Mo <sub>3</sub> Zr	223	<i>Pm</i> $\bar{3}n$	105118	No	Yes	44
V <sub>3</sub> Fe	223	<i>Pm</i> $\bar{3}n$	634028	No	Yes	46
Mo <sub>3</sub> Os	223	<i>Pm</i> $\bar{3}n$	105054	No	Yes	52
IrMo <sub>3</sub>	223	<i>Pm</i> $\bar{3}n$	640816	No	Yes	54
Na <sub>4</sub> Si <sub>2</sub> <sub>3</sub>	223	<i>Pm</i> $\bar{3}n$	194245	No	Yes	192
PtO <sub>2</sub>	224	<i>Pn</i> $\bar{3}m$	77654	No	Yes	44
Sc	225	<i>Fm</i> $\bar{3}m$	41502	No	Yes	3
Tl <sup>*</sup>	225	<i>Fm</i> $\bar{3}m$	104199	No	Yes	3
Al <sup>*</sup>	225	<i>Fm</i> $\bar{3}m$	191766	No	Yes	3
Ti	225	<i>Fm</i> $\bar{3}m$	41503	No	Yes	4
Hf	225	<i>Fm</i> $\bar{3}m$	41519	No	Yes	4
ZrB <sup>*</sup>	225	<i>Fm</i> $\bar{3}m$	44605	No	Yes	7
VH <sub>2</sub>	225	<i>Fm</i> $\bar{3}m$	56191	No	Yes	7
HfB <sup>*</sup>	225	<i>Fm</i> $\bar{3}m$	76128	No	Yes	7
Rh <sup>*</sup>	225	<i>Fm</i> $\bar{3}m$	41516	No	Yes	9
Pd	225	<i>Fm</i> $\bar{3}m$	41517	No	Yes	10
Pt <sup>*</sup>	225	<i>Fm</i> $\bar{3}m$	64921	No	Yes	10
TcB	225	<i>Fm</i> $\bar{3}m$	168899	No	Yes	10
Cu	225	<i>Fm</i> $\bar{3}m$	43493	No	Yes	11
Au	225	<i>Fm</i> $\bar{3}m$	44362	No	Yes	11
Ag	225	<i>Fm</i> $\bar{3}m$	44387	No	Yes	11
ReC <sup>*</sup>	225	<i>Fm</i> $\bar{3}m$	77350	No	Yes	11
In <sub>2</sub> LiRu	225	<i>Fm</i> $\bar{3}m$	639896	No	Yes	15
Al <sub>2</sub> Au	225	<i>Fm</i> $\bar{3}m$	57501	No	Yes	17
AuIn <sub>2</sub>	225	<i>Fm</i> $\bar{3}m$	58489	No	Yes	17
Be <sub>2</sub> Ta	227	<i>Fd</i> $\bar{3}m$	58739	No	Yes	18
NaAs <sub>2</sub>	227	<i>Fd</i> $\bar{3}m$	182161	No	Yes	22
CdLi	227	<i>Fd</i> $\bar{3}m$	102008	No	Yes	26
Cr <sub>2</sub> Ti	227	<i>Fd</i> $\bar{3}m$	102851	No	No	32

$\text{Cr}_2\text{Zr}$	227	$Fd\bar{3}m$	102860	No	Yes	32
$\text{Mo}_2\text{Zr}$	227	$Fd\bar{3}m$	105115	No	No	32
$\text{Ir}_2\text{Sc}$	227	$Fd\bar{3}m$	104558	No	Yes	42
$\text{LiPt}_2$	227	$Fd\bar{3}m$	104778	No	No	42
$\text{CaPd}_2$	227	$Fd\bar{3}m$	58927	No	Yes	44
$\text{Ag}_2\text{Na}$	227	$Fd\bar{3}m$	58337	No	Yes	46
Li	229	$Im\bar{3}m$	44367	No	Yes	1
$\text{Ca}^*$	229	$Im\bar{3}m$	44349	No	Yes	2
Zr	229	$Im\bar{3}m$	52544	No	Yes	4
Hf	229	$Im\bar{3}m$	53023	No	Yes	4
V	229	$Im\bar{3}m$	43420	No	Yes	5
Ta	229	$Im\bar{3}m$	53793	No	Yes	5
W	229	$Im\bar{3}m$	43421	No	Yes	6
Mo	229	$Im\bar{3}m$	52267	No	Yes	6
Cu	229	$Im\bar{3}m$	183263	No	Yes	11
$\text{CrGa}_4$	229	$Im\bar{3}m$	626026	No	Yes	18
$\text{Mg}_4\text{Rh}_7\text{As}_6$	229	$Im\bar{3}m$	94391	No	Yes	101
$\text{Pt}_3\text{Ga}_7^*$	229	$Im\bar{3}m$	635137	No	Yes	102
$\text{Ag}_8\text{Ca}_3$	229	$Im\bar{3}m$	107145	No	No	188

Table S28: Supertopological (STopo) nonmagnetic unique materials without  $f$  electrons that are LCEBR-classified at  $E_F$  with SOC. In order, the columns list the chemical formula, the SG number, the SG symbol, the ICSD number, whether all of the bands in the STopo material are NLC, whether all of the bands in the STopo material are SEBR, and the number of valence electrons. A chemical formula with a \* indicates that only some (but not all) of the ICSDs associated to the same unique material (defined using its topological class with SOC) are STopo.

Chem. formula	SG #	SG symbol	ICSD	All NLC	All SEBR	num $e^-$
$\text{NaCaH}_3$	2	$P\bar{1}$	168714	Yes	No	12
$\text{LiBeH}_3$	2	$P\bar{1}$	162771	Yes	No	36
$\text{NaSbS}_2$	2	$P\bar{1}$	200597	Yes	No	36
$\text{MnP}_4^*$	2	$P\bar{1}$	100786	Yes	No	54
$\text{Mg}(\text{SiO}_4\text{H}_2)^*$	10	$P2/m$	190936	Yes	No	32
$\text{BaPbO}_3^*$	12	$C2/m$	67811	No	No	64
$\text{Al}_2\text{O}_3$	13	$P2/c$	169723	Yes	No	96
$\text{Li}(\text{AlH}_4)$	14	$P2_1/c$	22247	Yes	No	32
$\text{SiH}_4$	14	$P2_1/c$	159307	Yes	No	32
$\text{GeH}_4$	14	$P2_1/c$	183080	Yes	No	32
$\text{LiNH}_2$	14	$P2_1/c$	237209	Yes	No	32
$\text{RhSi}^*$	14	$P2_1/c$	79235	Yes	No	52
$\text{SiH}_3\text{I}$	14	$P2_1/c$	65044	Yes	No	56
$\text{ZrO}_2^*$	14	$P2_1/c$	57158	Yes	No	64
$\text{HfO}_2^*$	14	$P2_1/c$	173158	Yes	No	64
$(\text{NH}_3(\text{OH}))\text{Cl}^*$	14	$P2_1/c$	14204	Yes	No	88
$\text{Tl}(\text{BS}_3)$	14	$P2_1/c$	73085	Yes	No	96
$\text{As}_2\text{Se}_3^*$	14	$P2_1/c$	43226	Yes	No	112
$(\text{NH}_4)(\text{H}_2\text{PO}_3)$	14	$P2_1/c$	49544	Yes	No	136
$\text{Ca}(\text{TiSiO}_5)^*$	14	$P2_1/c$	158653	Yes	No	160
$\text{LiSc}(\text{Si}_2\text{O}_6)^*$	14	$P2_1/c$	152076	Yes	No	192
$\text{Pb}_3\text{O}_4^*$	55	$Pbam$	9754	Yes	No	144
$\text{SnPb}_2\text{O}_4^*$	55	$Pbam$	31484	Yes	No	144
$\text{Pb}_2\text{PtO}_4$	55	$Pbam$	202214	Yes	No	168
$\text{SiO}_2$	55	$Pbam$	170516	Yes	No	256
$\text{MgH}_2$	61	$Pbca$	155811	Yes	No	32

TiO <sub>2</sub> <sup>*</sup>	61	Pbca	15409	Yes	No	128
(NH <sub>2</sub> )(CN)	61	Pbca	40446	Yes	No	128
SnO <sub>2</sub> <sup>*</sup>	61	Pbca	181280	Yes	No	128
CoAsSe	61	Pbca	41731	Yes	No	160
CoPSe*	61	Pbca	53060	Yes	No	160
CoSbS*	61	Pbca	624859	Yes	No	160
CaH <sub>2</sub> <sup>*</sup>	62	Pnma	23870	Yes	No	16
NaMgH <sub>3</sub> <sup>*</sup>	62	Pnma	91795	Yes	No	24
Na(NbO <sub>3</sub> ) <sup>*</sup>	63	Cmcm	280098	No	No	128
Ca	64	Cmce	162255	No	Yes	8
Na(AlH <sub>4</sub> ) <sup>*</sup>	88	I4 <sub>1</sub> /a	8022	No	Yes	16
LiPN <sub>2</sub> <sup>*</sup>	122	I4̄2d	32713	No	Yes	32
MgCN <sub>2</sub>	122	I4̄2d	44110	No	Yes	32
BeSiN <sub>2</sub>	122	I4̄2d	44112	No	Yes	32
Bi <sub>2</sub> ZnTiO <sub>6</sub>	123	P4/mmm	186800	No	No	62
Na(TaO <sub>3</sub> )	127	P4/mbm	23322	Yes	No	48
Sn <sup>*</sup>	139	I4/mmm	236686	No	No	4
CaAl <sub>2</sub> Ga <sub>2</sub>	139	I4/mmm	300209	No	Yes	14
Si	139	I4/mmm	181908	No	Yes	16
C <sup>*</sup>	139	I4/mmm	190716	No	Yes	16
K <sub>2</sub> MgF <sub>4</sub>	139	I4/mmm	33519	No	No	48
TlGaTe <sub>2</sub> <sup>*</sup>	140	I4/mcm	635524	No	No	36
InSn <sub>2</sub> I <sub>5</sub> <sup>*</sup>	140	I4/mcm	151995	No	No	92
InPb <sub>2</sub> I <sub>5</sub> <sup>*</sup>	140	I4/mcm	151998	No	No	92
LiAl	141	I4 <sub>1</sub> /amd	240114	No	Yes	8
CaB <sub>2</sub> H <sub>2</sub>	164	P̄3m1	183134	No	Yes	10
Mg <sub>3</sub> Sb <sub>2</sub> <sup>*</sup>	164	P̄3m1	2142	No	Yes	16
CaMg <sub>2</sub> Sb <sub>2</sub>	164	P̄3m1	100045	No	Yes	16
CaAl <sub>2</sub> Ge <sub>2</sub>	164	P̄3m1	409570	No	Yes	16
CaBe <sub>2</sub> As <sub>2</sub>	164	P̄3m1	609867	No	Yes	16
MgBe <sub>2</sub> As <sub>2</sub>	164	P̄3m1	609872	No	Yes	16
Ba <sub>2</sub> H <sub>3</sub> I	164	P̄3m1	423520	No	Yes	30
C <sup>*</sup>	194	P6 <sub>3</sub> /mmc	27422	No	Yes	16
TlInS <sub>2</sub>	194	P6 <sub>3</sub> /mmc	25355	No	No	36
KTl	194	P6 <sub>3</sub> /mmc	262071	No	No	48
CuScO <sub>2</sub> <sup>*</sup>	194	P6 <sub>3</sub> /mmc	60847	No	No	52
Ni <sub>3</sub> Zr	194	P6 <sub>3</sub> /mmc	105482	No	No	68
HfMn <sub>2</sub> <sup>*</sup>	194	P6 <sub>3</sub> /mmc	104214	No	No	72
ZrMn <sub>2</sub>	194	P6 <sub>3</sub> /mmc	109269	No	No	72
ZrTc <sub>2</sub>	194	P6 <sub>3</sub> /mmc	423221	No	No	72
HfTc <sub>2</sub> <sup>*</sup>	194	P6 <sub>3</sub> /mmc	638955	No	Yes	72
MgH <sub>2</sub>	205	Pa $\bar{3}$	168832	Yes	No	16
Ca <sub>3</sub> N <sub>2</sub> <sup>*</sup>	206	Ia $\bar{3}$	34678	No	Yes	128
Li <sub>3</sub> (ScN <sub>2</sub> )	206	Ia $\bar{3}$	98140	No	Yes	128
Ca(SiO <sub>3</sub> ) <sup>*</sup>	221	Pm $\bar{3}m$	40658	No	No	24
Ca(SnO <sub>3</sub> )	221	Pm $\bar{3}m$	56095	No	Yes	24
Pb(GeO <sub>3</sub> )	221	Pm $\bar{3}m$	185693	No	No	26
Sn(TiO <sub>3</sub> )	221	Pm $\bar{3}m$	186724	No	No	26
C <sub>3</sub> N <sub>2</sub>	221	Pm $\bar{3}m$	185974	No	No	88
Si <sub>46</sub>	223	Pm $\bar{3}n$	186544	No	Yes	184
MgH <sub>2</sub>	225	Fm $\bar{3}m$	166234	No	Yes	4
LiAl <sup>*</sup>	227	Fd $\bar{3}m$	1924	No	Yes	8
Si <sup>*</sup>	227	Fd $\bar{3}m$	29287	No	Yes	8
Ge	227	Fd $\bar{3}m$	41980	No	Yes	8
GaLi	227	Fd $\bar{3}m$	103775	No	Yes	8
AlH <sub>3</sub>	227	Fd $\bar{3}m$	182535	No	Yes	24

$\text{SiO}_2^*$	227	$Fd\bar{3}m$	<a href="#">35536</a>	No	Yes	32
$\text{Zn}_2\text{Zr}^*$	227	$Fd\bar{3}m$	<a href="#">653507</a>	No	No	56
Si	229	$Im\bar{3}m$	<a href="#">189392</a>	No	Yes	24

## S10. SOC-DRIVEN TOPOLOGICAL PHASE TRANSITIONS

In this section, we provide statistics for the SOC-driven topological phase transitions in the materials studied in this work. To begin, there are two broad mechanisms by which a material can be driven into a topological (crystalline) insulating phase. The first mechanism occurs when a semimetal w/o SOC gaps directly into a TI or TCI under the introduction of SOC; in this case, the TI or TCI phase originates from *splitting* bands that were previously connected in the absence of SOC (and possibly in the presence of additional crystal symmetries that are subsequently broken by Rashba- or Dresselhaus-like SOC). The prototypical example of SOC-driven topological splitting occurs in the Kane-Mele model of graphene, which is an ESFD semimetal in the absence of SOC [28, 31, 160], and an SEBR 2D TI when the (weak) effects of SOC are taken into consideration [3, 127]. The second mechanism for realizing a TI or TCI is SOC-driven *band inversion*. In the case of band inversion, a narrow-gap, topologically trivial semiconductor w/o SOC becomes a TI or TCI when introducing SOC changes the band ordering at a small number of  $k$  points in the BZ. In real materials, band inversion arises due to the interplay of SOC and other interactions, which are typically controlled by doping and chemical substitution. A prototypical of example of SOC- and dopant-driven band inversion occurs in the family of (higher-order) topological crystalline and trivial insulators  $\text{Pb}_{1-x}\text{Sn}_x\text{Te}$  (see Refs. [12, 16, 30, 105, 121, 161–164] and S11 A 5).

In S6, we reviewed the previously established result that all 3D, symmetry-indicated topological phases w/o SOC are topological semimetals (either NLC-SM, SEBR-SM, ES, or ESFD). In the case of ES and ESFD semimetals w/o SOC, introducing SOC may split bands and open a topological gap, as occurs in the hourglass insulator KHgSb (ICSD 56201, see Refs. [13, 14, 110, 128, 129] and S11 A 6), or the bulk may remain gapless, as occurs in B20 compounds in the CoSi family of chiral crystals (ICSD 189221, see Refs. [9, 23–25, 131, 135, 136] and S11 C 1). However, in the case of NLC-SM- and SEBR-SM-classified semimetals w/o SOC, infinitesimal SOC will always open a direct gap if the bulk is a centrosymmetric nodal-line semimetal [31, 34, 36], but will conversely not open a gap if the bulk is a noncentrosymmetric spinless (spin-degenerate) Weyl semimetal in the absence of SOC [165]. Specifically, if the bulk is a spinless Weyl semimetal when the effects of SOC are neglected, then introducing infinitesimal SOC will *not* generically open a bulk gap – whether or not the spinless SIs in the absence of SOC are nontrivial – as the two Weyl points within each spin-degenerate pair carry the same chiral charges (Chern numbers), and hence cannot pairwise annihilate [36, 112, 165].

In the tables below, we provide detailed statistics comparing the topology of all of the stoichiometric unique materials in the ISCD at the Fermi level with and w/o SOC (we emphasize that in this work, a unique material is defined by the topological classification or crossing points at  $E_F$  with SOC, see S4 for further details). Specifically, in Tables S29, S30, S31, S32, and S33, we respectively list the number of unique materials in each SG that are classified w/o SOC as ES, ESFD, LCEBR, NLC-SM, and SEBR-SM, which we then further divide by the topological classification of the same material in the presence of SOC. Notably, there are relatively few materials in the ICSD that are classified as NLC-SM (Table S32) or SEBR-SM (Table S33 [see S6 A for a more detailed discussion of NLC-SM and SEBR-SM materials in the ICSD].

Table S29: SOC-driven topological phase transition statistics for ES-classified semimetals w/o SOC. In order, the first two columns in this table list the SG and the number of ES-classified unique materials in the SG w/o SOC. If an SG is not listed in the first column, then there are no ES-classified unique materials in the SG w/o SOC. In the remaining five columns, restricting to the same unique materials listed in the second column, we respectively list the number of unique materials that become classified as NLC, SEBR, ES, ESFD, and LCEBR when the effects of SOC are incorporated. For all of the topological classification categories in the table, each number of materials is accompanied by the percentage of materials in the SG in the topological class. When there are no materials in the topological class, the table entry is marked with a dashed horizontal line.

SG	# Mat.	NLC	SEBR	ES	ESFD	LCEBR
3	7	—	—	—	—	7 (100.00%)
4	14	—	—	—	—	14 (100.00%)
5	19	—	—	—	—	19 (100.00%)
6	4	—	—	—	—	4 (100.00%)
7	6	—	—	—	—	6 (100.00%)
8	14	—	—	—	—	14 (100.00%)
9	4	—	—	—	—	4 (100.00%)
10	16	15 (93.75%)	—	—	—	1 (6.25%)
11	97	74 (76.29%)	—	—	—	23 (23.71%)
12	406	177 (43.60%)	160 (39.41%)	—	—	69 (17.00%)
13	21	12 (57.14%)	—	—	—	9 (42.86%)
14	330	227 (68.79%)	—	41 (12.42%)	—	62 (18.79%)
15	137	78 (56.93%)	—	—	—	59 (43.07%)
16	1	—	—	—	—	1 (100.00%)
17	3	—	—	—	—	3 (100.00%)
18	4	—	—	—	—	4 (100.00%)
19	9	—	—	—	—	9 (100.00%)
20	3	—	—	—	—	3 (100.00%)
21	3	—	—	—	—	3 (100.00%)
22	11	—	—	—	—	11 (100.00%)
23	3	—	—	—	—	3 (100.00%)
25	12	—	—	—	—	12 (100.00%)
26	8	—	—	—	—	8 (100.00%)
28	5	—	—	—	—	5 (100.00%)
29	1	—	—	—	—	1 (100.00%)
30	1	—	—	—	—	1 (100.00%)
31	19	—	—	—	—	19 (100.00%)
33	20	—	—	—	—	20 (100.00%)
34	2	—	—	—	—	2 (100.00%)
35	2	—	—	—	—	2 (100.00%)
36	21	—	—	—	—	21 (100.00%)
38	38	—	—	—	—	38 (100.00%)
39	3	—	—	—	—	3 (100.00%)
40	3	—	—	—	—	3 (100.00%)
41	9	—	—	—	—	9 (100.00%)
43	8	—	—	—	—	8 (100.00%)
44	24	—	—	—	—	24 (100.00%)
45	2	—	—	—	—	2 (100.00%)
46	23	—	—	—	—	23 (100.00%)
47	29	25 (86.21%)	—	—	—	4 (13.79%)
48	1	—	—	—	—	1 (100.00%)
50	5	3 (60.00%)	1 (20.00%)	—	—	1 (20.00%)
51	42	40 (95.24%)	—	—	—	2 (4.76%)
53	3	—	2 (66.67%)	—	—	1 (33.33%)

54	4	3 (75.00%)	—	—	—	1 (25.00%)
55	211	173 (81.99%)	—	—	—	38 (18.01%)
56	1	—	—	—	—	1 (100.00%)
57	31	25 (80.65%)	—	—	—	6 (19.35%)
58	62	37 (59.68%)	—	8 (12.90%)	—	17 (27.42%)
59	78	27 (34.62%)	33 (42.31%)	—	—	18 (23.08%)
60	20	13 (65.00%)	—	—	—	7 (35.00%)
61	16	8 (50.00%)	—	4 (25.00%)	—	4 (25.00%)
62	777	572 (73.62%)	—	—	—	205 (26.38%)
63	454	236 (51.98%)	153 (33.70%)	—	—	65 (14.32%)
64	72	—	50 (69.44%)	6 (8.33%)	—	16 (22.22%)
65	123	68 (55.28%)	44 (35.77%)	—	—	11 (8.94%)
66	7	4 (57.14%)	—	—	—	3 (42.86%)
67	11	9 (81.82%)	—	—	—	2 (18.18%)
68	2	—	—	—	—	2 (100.00%)
69	25	—	22 (88.00%)	—	—	3 (12.00%)
70	36	—	28 (77.78%)	—	—	8 (22.22%)
71	162	—	134 (82.72%)	—	—	28 (17.28%)
72	51	25 (49.02%)	13 (25.49%)	—	—	13 (25.49%)
74	75	51 (68.00%)	—	—	—	24 (32.00%)
76	1	—	—	1 (100.00%)	—	—
82	10	8 (80.00%)	—	—	—	2 (20.00%)
83	2	—	1 (50.00%)	1 (50.00%)	—	—
84	4	2 (50.00%)	—	2 (50.00%)	—	—
85	3	—	3 (100.00%)	—	—	—
86	9	—	1 (11.11%)	6 (66.67%)	—	2 (22.22%)
87	15	—	6 (40.00%)	9 (60.00%)	—	—
88	12	—	2 (16.67%)	4 (33.33%)	—	6 (50.00%)
90	2	—	—	—	—	2 (100.00%)
91	1	—	—	—	—	1 (100.00%)
92	6	—	—	4 (66.67%)	—	2 (33.33%)
94	1	—	—	—	—	1 (100.00%)
95	1	—	—	1 (100.00%)	—	—
99	1	—	—	—	—	1 (100.00%)
100	1	—	—	—	—	1 (100.00%)
102	3	—	—	1 (33.33%)	—	2 (66.67%)
105	1	—	—	—	—	1 (100.00%)
107	13	—	—	10 (76.92%)	—	3 (23.08%)
108	2	—	—	1 (50.00%)	—	1 (50.00%)
109	7	—	—	—	—	7 (100.00%)
110	2	—	—	1 (50.00%)	—	1 (50.00%)
111	1	—	—	—	—	1 (100.00%)
113	5	2 (40.00%)	—	—	—	3 (60.00%)
114	3	—	2 (66.67%)	1 (33.33%)	—	—
115	1	—	—	—	—	1 (100.00%)
116	3	—	1 (33.33%)	—	—	2 (66.67%)
117	3	—	—	—	—	3 (100.00%)
118	2	1 (50.00%)	—	—	—	1 (50.00%)
119	8	—	—	—	—	8 (100.00%)
120	3	2 (66.67%)	—	—	—	1 (33.33%)
121	17	—	14 (82.35%)	—	—	3 (17.65%)
122	11	—	10 (90.91%)	—	—	1 (9.09%)
123	66	22 (33.33%)	17 (25.76%)	25 (37.88%)	—	2 (3.03%)
124	4	—	—	4 (100.00%)	—	—
125	7	1 (14.29%)	3 (42.86%)	3 (42.86%)	—	—
126	2	—	—	2 (100.00%)	—	—

127	78	30 (38.46%)	—	42 (53.85%)	—	6 (7.69%)	
128	12	—	5 (41.67%)	7 (58.33%)	—	—	
129	213	50 (23.47%)	83 (38.97%)	43 (20.19%)	—	37 (17.37%)	
130	10	2 (20.00%)	1 (10.00%)	1 (10.00%)	—	6 (60.00%)	
131	11	4 (36.36%)	—	4 (36.36%)	—	3 (27.27%)	
132	1	—	—	1 (100.00%)	—	—	
135	9	2 (22.22%)	—	6 (66.67%)	—	1 (11.11%)	
136	95	—	24 (25.26%)	49 (51.58%)	—	22 (23.16%)	
137	10	—	6 (60.00%)	3 (30.00%)	—	1 (10.00%)	
138	4	—	—	1 (25.00%)	—	3 (75.00%)	
139	332	—	203 (61.14%)	100 (30.12%)	—	29 (8.73%)	
140	100	32 (32.00%)	16 (16.00%)	39 (39.00%)	—	13 (13.00%)	
141	77	—	43 (55.84%)	19 (24.68%)	—	15 (19.48%)	
142	11	—	5 (45.45%)	2 (18.18%)	—	4 (36.36%)	
147	1	—	—	—	—	1 (100.00%)	
148	5	—	—	5 (100.00%)	—	—	
150	4	—	—	1 (25.00%)	—	3 (75.00%)	
152	2	—	—	1 (50.00%)	—	1 (50.00%)	
153	1	—	—	—	—	1 (100.00%)	
154	1	—	—	—	—	1 (100.00%)	
155	2	—	—	1 (50.00%)	—	1 (50.00%)	
156	7	—	—	4 (57.14%)	—	3 (42.86%)	
157	2	—	—	—	—	2 (100.00%)	
158	1	—	—	—	—	1 (100.00%)	
160	6	—	—	—	—	6 (100.00%)	
161	3	—	—	2 (66.67%)	—	1 (33.33%)	
162	5	—	3 (60.00%)	2 (40.00%)	—	—	
163	3	—	3 (100.00%)	—	—	—	
164	47	—	33 (70.21%)	7 (14.89%)	—	7 (14.89%)	
165	6	—	3 (50.00%)	1 (16.67%)	—	2 (33.33%)	
166	153	—	96 (62.75%)	30 (19.61%)	—	27 (17.65%)	
167	21	—	6 (28.57%)	11 (52.38%)	—	4 (19.05%)	
173	11	—	—	10 (90.91%)	—	1 (9.09%)	
176	5	—	3 (60.00%)	2 (40.00%)	—	—	
180	2	—	—	—	1 (50.00%)	1 (50.00%)	
181	1	—	—	—	—	1 (100.00%)	
182	5	—	—	4 (80.00%)	—	1 (20.00%)	
185	10	—	—	6 (60.00%)	—	4 (40.00%)	
186	40	—	—	30 (75.00%)	2 (5.00%)	8 (20.00%)	
187	31	9 (29.03%)	—	19 (61.29%)	—	3 (9.68%)	
189	94	—	53 (56.38%)	40 (42.55%)	—	1 (1.06%)	
190	3	2 (66.67%)	—	1 (33.33%)	—	—	
191	63	—	22 (34.92%)	41 (65.08%)	—	—	
193	24	—	10 (41.67%)	14 (58.33%)	—	—	
194	235	—	98 (41.70%)	124 (52.77%)	—	13 (5.53%)	
198	1	—	—	—	—	1 (100.00%)	
199	1	—	—	—	—	1 (100.00%)	
200	2	—	2 (100.00%)	—	—	—	
204	4	—	4 (100.00%)	—	—	—	
205	9	6 (66.67%)	—	1 (11.11%)	—	2 (22.22%)	
206	1	—	1 (100.00%)	—	—	—	
208	2	—	—	—	—	2 (100.00%)	
212	2	—	—	2 (100.00%)	—	—	
213	1	—	—	1 (100.00%)	—	—	
214	1	—	—	—	1 (100.00%)	—	
216	21	13 (61.90%)	—	2 (9.52%)	1 (4.76%)	5 (23.81%)	

217	6	—	1 (16.67%)	—	2 (33.33%)	3 (50.00%)	
219	2	—	—	—	—	2 (100.00%)	
220	15	10 (66.67%)	—	—	4 (26.67%)	1 (6.67%)	
221	107	4 (3.74%)	50 (46.73%)	46 (42.99%)	6 (5.61%)	1 (0.93%)	
223	13	—	3 (23.08%)	9 (69.23%)	1 (7.69%)	—	
225	74	—	34 (45.95%)	33 (44.59%)	3 (4.05%)	4 (5.41%)	
226	3	—	1 (33.33%)	1 (33.33%)	1 (33.33%)	—	
227	131	—	71 (54.20%)	37 (28.24%)	13 (9.92%)	10 (7.63%)	
229	8	—	2 (25.00%)	3 (37.50%)	3 (37.50%)	—	
230	1	—	—	1 (100.00%)	—	—	
Total	6006	2,104 (35.03%)	1,585 (26.39%)	944 (15.72%)	38 (0.63%)	1,335 (22.23%)	

Table S30: SOC-driven topological phase transition statistics for ESFD-classified semimetals w/o SOC. In order, the first two columns in this table list the SG and the number of ESFD-classified unique materials in the SG w/o SOC. If an SG is not listed in the first column, then there are no ESFD-classified unique materials in the SG w/o SOC. In the remaining five columns, restricting to the same unique materials listed in the second column, we respectively list the number of unique materials that become classified as NLC, SEBR, ES, ESFD, and LCEBR when the effects of SOC are incorporated. For all of the topological classification categories in the table, each number of materials is accompanied by the percentage of materials in the SG in the topological class. When there are no materials in the topological class, the table entry is marked with a dashed horizontal line.

SG	# Mat.	NLC	SEBR	ES	ESFD	LCEBR
1	9	—	—	—	9 (100.00%)	—
2	112	1 (0.89%)	—	—	111 (99.11%)	—
4	6	—	—	6 (100.00%)	—	—
5	12	—	—	—	12 (100.00%)	—
6	1	—	—	—	1 (100.00%)	—
7	3	—	—	3 (100.00%)	—	—
8	12	—	—	—	12 (100.00%)	—
9	11	—	—	11 (100.00%)	—	—
10	5	—	—	—	5 (100.00%)	—
11	96	—	—	—	95 (98.96%)	1 (1.04%)
12	191	—	—	—	191 (100.00%)	—
13	20	—	—	—	20 (100.00%)	—
14	137	—	—	—	137 (100.00%)	—
15	173	—	—	—	173 (100.00%)	—
18	2	—	—	—	2 (100.00%)	—
19	19	—	—	19 (100.00%)	—	—
20	2	—	—	2 (100.00%)	—	—
21	6	—	—	—	6 (100.00%)	—
23	2	—	—	—	2 (100.00%)	—
25	2	—	—	—	2 (100.00%)	—
26	4	—	—	—	4 (100.00%)	—
28	2	—	—	2 (100.00%)	—	—
29	1	—	—	1 (100.00%)	—	—
30	1	—	—	—	1 (100.00%)	—
31	14	—	—	—	14 (100.00%)	—
33	23	—	—	23 (100.00%)	—	—
34	3	—	—	—	3 (100.00%)	—
35	2	—	—	—	2 (100.00%)	—
36	32	—	—	—	32 (100.00%)	—
38	31	—	—	—	31 (100.00%)	—
40	4	—	—	4 (100.00%)	—	—

41	1	—	—	1 (100.00%)	—	—
43	13	—	—	—	13 (100.00%)	—
44	11	—	—	—	11 (100.00%)	—
46	7	—	—	7 (100.00%)	—	—
47	13	—	—	—	13 (100.00%)	—
51	35	—	—	—	35 (100.00%)	—
52	4	—	—	4 (100.00%)	—	—
53	3	—	—	—	3 (100.00%)	—
54	2	—	—	2 (100.00%)	—	—
55	41	—	—	—	41 (100.00%)	—
56	4	—	—	4 (100.00%)	—	—
57	17	—	—	17 (100.00%)	—	—
58	35	—	—	—	35 (100.00%)	—
59	65	—	—	—	65 (100.00%)	—
60	9	—	—	9 (100.00%)	—	—
61	2	—	—	2 (100.00%)	—	—
62	674	—	—	674 (100.00%)	—	—
63	470	—	—	—	470 (100.00%)	—
64	39	—	—	—	39 (100.00%)	—
65	70	—	—	—	70 (100.00%)	—
66	9	—	—	—	9 (100.00%)	—
67	6	—	—	—	6 (100.00%)	—
68	4	—	—	—	4 (100.00%)	—
69	18	—	—	—	18 (100.00%)	—
70	11	—	—	—	11 (100.00%)	—
71	153	—	—	—	153 (100.00%)	—
72	58	—	—	—	58 (100.00%)	—
73	1	—	—	1 (100.00%)	—	—
74	77	—	—	—	77 (100.00%)	—
75	2	—	—	—	2 (100.00%)	—
76	1	—	—	1 (100.00%)	—	—
79	1	—	—	1 (100.00%)	—	—
81	3	—	—	—	—	3 (100.00%)
82	25	7 (28.00%)	—	—	10 (40.00%)	8 (32.00%)
83	6	2 (33.33%)	2 (33.33%)	2 (33.33%)	—	—
84	3	—	—	1 (33.33%)	2 (66.67%)	—
85	9	—	—	1 (11.11%)	8 (88.89%)	—
86	29	—	8 (27.59%)	10 (34.48%)	11 (37.93%)	—
87	89	—	14 (15.73%)	13 (14.61%)	59 (66.29%)	3 (3.37%)
88	15	—	2 (13.33%)	—	12 (80.00%)	1 (6.67%)
90	2	—	—	—	2 (100.00%)	—
91	2	—	—	1 (50.00%)	—	1 (50.00%)
92	12	—	—	7 (58.33%)	5 (41.67%)	—
96	1	—	—	1 (100.00%)	—	—
97	1	—	—	1 (100.00%)	—	—
98	1	—	—	—	—	1 (100.00%)
99	26	—	—	7 (26.92%)	15 (57.69%)	4 (15.38%)
100	13	—	—	1 (7.69%)	11 (84.62%)	1 (7.69%)
102	3	—	—	1 (33.33%)	1 (33.33%)	1 (33.33%)
103	3	—	—	—	3 (100.00%)	—
104	1	—	—	—	1 (100.00%)	—
106	1	—	—	1 (100.00%)	—	—
107	88	—	—	6 (6.82%)	51 (57.95%)	31 (35.23%)
108	5	—	—	1 (20.00%)	3 (60.00%)	1 (20.00%)
109	16	—	—	—	13 (81.25%)	3 (18.75%)
110	1	—	—	1 (100.00%)	—	—

111	6	—	1 (16.67%)	—	4 (66.67%)	1 (16.67%)
113	21	—	—	—	19 (90.48%)	2 (9.52%)
114	3	—	—	—	—	3 (100.00%)
115	14	—	4 (28.57%)	—	6 (42.86%)	4 (28.57%)
117	3	1 (33.33%)	—	—	1 (33.33%)	1 (33.33%)
118	1	—	—	—	1 (100.00%)	—
119	9	2 (22.22%)	—	—	6 (66.67%)	1 (11.11%)
120	3	—	—	2 (66.67%)	—	1 (33.33%)
121	39	—	4 (10.26%)	—	20 (51.28%)	15 (38.46%)
122	12	—	3 (25.00%)	1 (8.33%)	8 (66.67%)	—
123	325	28 (8.62%)	18 (5.54%)	64 (19.69%)	210 (64.62%)	5 (1.54%)
124	15	1 (6.67%)	—	3 (20.00%)	11 (73.33%)	—
125	25	3 (12.00%)	3 (12.00%)	5 (20.00%)	14 (56.00%)	—
126	2	—	—	—	2 (100.00%)	—
127	248	32 (12.90%)	—	46 (18.55%)	167 (67.34%)	3 (1.21%)
128	33	—	8 (24.24%)	14 (42.42%)	10 (30.30%)	1 (3.03%)
129	478	51 (10.67%)	34 (7.11%)	48 (10.04%)	330 (69.04%)	15 (3.14%)
130	13	1 (7.69%)	—	2 (15.38%)	9 (69.23%)	1 (7.69%)
131	25	3 (12.00%)	—	5 (20.00%)	17 (68.00%)	—
133	2	1 (50.00%)	—	1 (50.00%)	—	—
134	3	—	—	—	3 (100.00%)	—
135	6	2 (33.33%)	—	1 (16.67%)	3 (50.00%)	—
136	93	—	9 (9.68%)	21 (22.58%)	58 (62.37%)	5 (5.38%)
137	27	—	2 (7.41%)	7 (25.93%)	17 (62.96%)	1 (3.70%)
138	3	1 (33.33%)	—	1 (33.33%)	—	1 (33.33%)
139	1052	—	251 (23.86%)	180 (17.11%)	582 (55.32%)	39 (3.71%)
140	219	18 (8.22%)	8 (3.65%)	22 (10.05%)	167 (76.26%)	4 (1.83%)
141	92	—	8 (8.70%)	4 (4.35%)	73 (79.35%)	7 (7.61%)
142	24	—	4 (16.67%)	10 (41.67%)	10 (41.67%)	—
143	5	—	—	1 (20.00%)	3 (60.00%)	1 (20.00%)
144	2	—	—	—	1 (50.00%)	1 (50.00%)
146	20	—	—	5 (25.00%)	9 (45.00%)	6 (30.00%)
147	15	—	5 (33.33%)	5 (33.33%)	3 (20.00%)	2 (13.33%)
148	184	—	37 (20.11%)	22 (11.96%)	102 (55.43%)	23 (12.50%)
149	5	—	—	1 (20.00%)	2 (40.00%)	2 (40.00%)
150	11	—	—	2 (18.18%)	8 (72.73%)	1 (9.09%)
152	7	—	—	1 (14.29%)	6 (85.71%)	—
154	1	—	—	1 (100.00%)	—	—
155	17	—	—	2 (11.76%)	7 (41.18%)	8 (47.06%)
156	9	—	—	2 (22.22%)	6 (66.67%)	1 (11.11%)
157	3	—	—	1 (33.33%)	2 (66.67%)	—
158	2	—	—	1 (50.00%)	1 (50.00%)	—
159	6	—	—	3 (50.00%)	2 (33.33%)	1 (16.67%)
160	52	—	—	7 (13.46%)	33 (63.46%)	12 (23.08%)
161	15	—	—	6 (40.00%)	7 (46.67%)	2 (13.33%)
162	21	—	2 (9.52%)	6 (28.57%)	11 (52.38%)	2 (9.52%)
163	22	—	1 (4.55%)	8 (36.36%)	10 (45.45%)	3 (13.64%)
164	271	—	58 (21.40%)	37 (13.65%)	150 (55.35%)	26 (9.59%)
165	18	—	1 (5.56%)	6 (33.33%)	8 (44.44%)	3 (16.67%)
166	463	—	84 (18.14%)	68 (14.69%)	281 (60.69%)	30 (6.48%)
167	100	—	5 (5.00%)	16 (16.00%)	66 (66.00%)	13 (13.00%)
173	28	—	—	24 (85.71%)	2 (7.14%)	2 (7.14%)
174	33	—	—	2 (6.06%)	31 (93.94%)	—
175	2	—	—	—	2 (100.00%)	—
176	77	—	3 (3.90%)	16 (20.78%)	52 (67.53%)	6 (7.79%)
180	16	—	—	6 (37.50%)	9 (56.25%)	1 (6.25%)

181	4	—	—	1 (25.00%)	3 (75.00%)	—
182	19	—	—	16 (84.21%)	2 (10.53%)	1 (5.26%)
185	19	—	—	4 (21.05%)	15 (78.95%)	—
186	163	—	—	38 (23.31%)	116 (71.17%)	9 (5.52%)
187	92	3 (3.26%)	—	31 (33.70%)	58 (63.04%)	—
188	4	—	—	2 (50.00%)	2 (50.00%)	—
189	389	—	47 (12.08%)	81 (20.82%)	260 (66.84%)	1 (0.26%)
190	22	2 (9.09%)	—	4 (18.18%)	16 (72.73%)	—
191	384	—	51 (13.28%)	130 (33.85%)	203 (52.86%)	—
193	233	—	5 (2.15%)	84 (36.05%)	140 (60.09%)	4 (1.72%)
194	1043	—	107 (10.26%)	414 (39.69%)	505 (48.42%)	17 (1.63%)
196	1	—	—	—	1 (100.00%)	—
197	10	—	—	—	9 (90.00%)	1 (10.00%)
198	76	—	—	2 (2.63%)	74 (97.37%)	—
199	8	—	—	1 (12.50%)	7 (87.50%)	—
200	15	—	1 (6.67%)	—	13 (86.67%)	1 (6.67%)
201	4	—	1 (25.00%)	—	3 (75.00%)	—
202	10	—	—	—	10 (100.00%)	—
203	1	—	—	1 (100.00%)	—	—
204	119	—	7 (5.88%)	—	104 (87.39%)	8 (6.72%)
205	40	2 (5.00%)	—	2 (5.00%)	34 (85.00%)	2 (5.00%)
206	29	—	9 (31.03%)	2 (6.90%)	13 (44.83%)	5 (17.24%)
210	1	—	—	—	1 (100.00%)	—
211	1	—	—	—	1 (100.00%)	—
212	6	—	—	1 (16.67%)	5 (83.33%)	—
213	16	—	—	2 (12.50%)	14 (87.50%)	—
214	6	—	—	1 (16.67%)	5 (83.33%)	—
215	23	—	3 (13.04%)	—	13 (56.52%)	7 (30.43%)
216	496	45 (9.07%)	—	15 (3.02%)	412 (83.06%)	24 (4.84%)
217	60	—	5 (8.33%)	1 (1.67%)	50 (83.33%)	4 (6.67%)
218	12	—	1 (8.33%)	6 (50.00%)	5 (41.67%)	—
219	3	—	—	2 (66.67%)	1 (33.33%)	—
220	100	1 (1.00%)	—	2 (2.00%)	95 (95.00%)	2 (2.00%)
221	1063	—	63 (5.93%)	114 (10.72%)	878 (82.60%)	8 (0.75%)
223	201	—	6 (2.99%)	37 (18.41%)	158 (78.61%)	—
224	9	—	—	1 (11.11%)	8 (88.89%)	—
225	1203	—	128 (10.64%)	135 (11.22%)	904 (75.15%)	36 (2.99%)
226	39	—	1 (2.56%)	4 (10.26%)	34 (87.18%)	—
227	542	—	69 (12.73%)	108 (19.93%)	325 (59.96%)	40 (7.38%)
229	177	—	5 (2.82%)	15 (8.47%)	156 (88.14%)	1 (0.56%)
230	4	—	1 (25.00%)	—	3 (75.00%)	—
Total	13997	207 (1.48%)	1,089 (7.78%)	2,792 (19.95%)	9,423 (67.32%)	486 (3.47%)

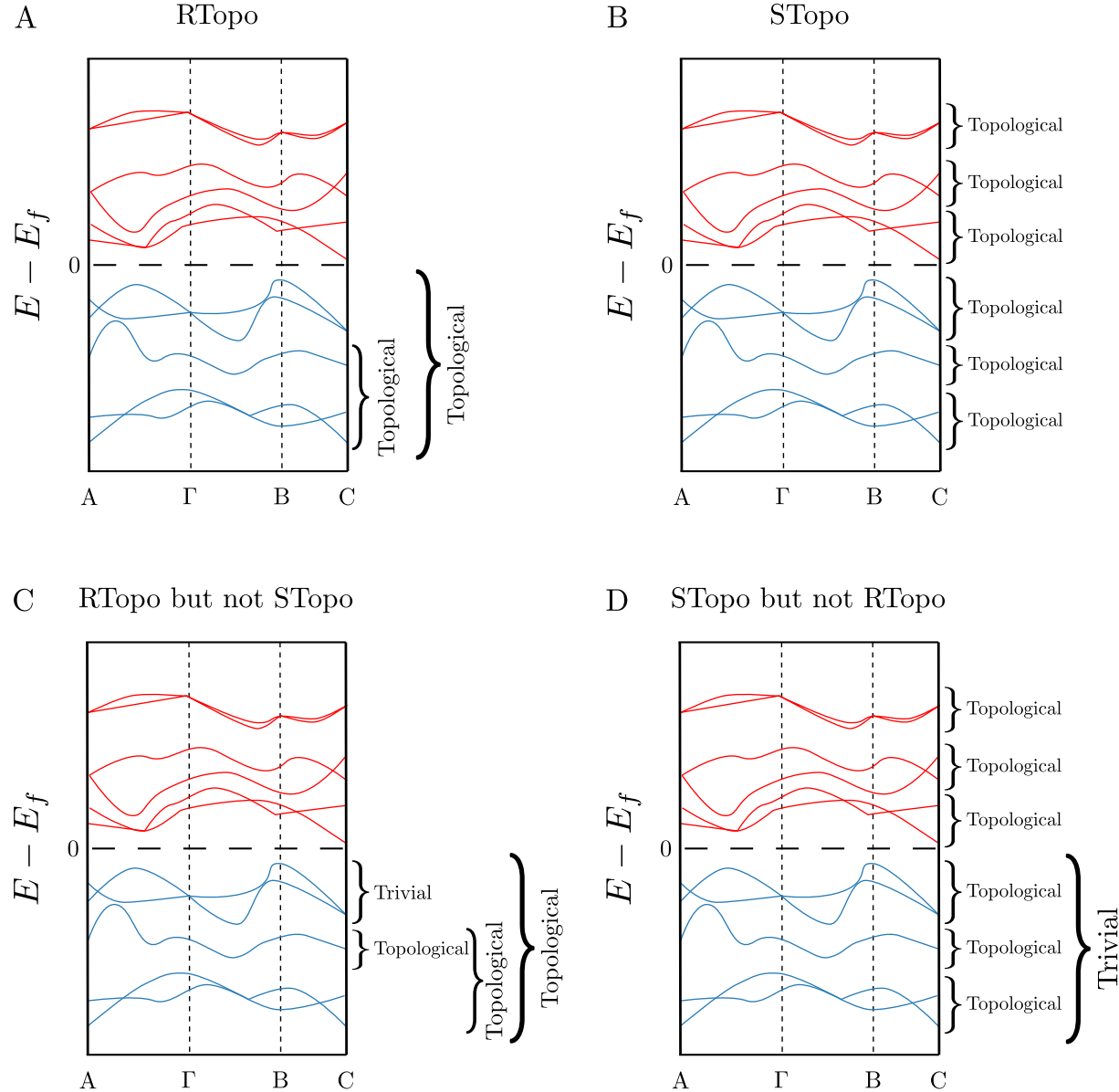


Figure S4. Repeat-topological and supertopological materials. A: A schematic depiction of a repeat-topological (RTopo) band structure. In RTopo materials, the gap at  $E_F$ , as well as the next gap below  $E_F$  as measured by band connectivity (see S2), exhibit cumulative symmetry-indicated stable topology (*i.e.* the *summed* stable topological indices of all of the bands up to  $E_F$  and up to the next gap below  $E_F$  are nontrivial, see S9 A). B: A schematic depiction of a supertopological (STopo) band structure. In STopo materials, *every* energetically isolated set of bands in the spectrum exhibits symmetry-indicated stable topology (see S9 B). It is important to emphasize that because repeat-topology is focused on cumulative topology (*i.e.* topological gaps), whereas supertopology is defined by the appearance of topological *bands* that may together exhibit cumulative *trivial* topology, then not all RTopo materials are STopo, and not all STopo materials are RTopo. In panel C, we show a schematic example of a band structure that is RTopo, but not STopo. Similarly, in panel D, we show a schematic example of a band structure that is STopo, but not RTopo.

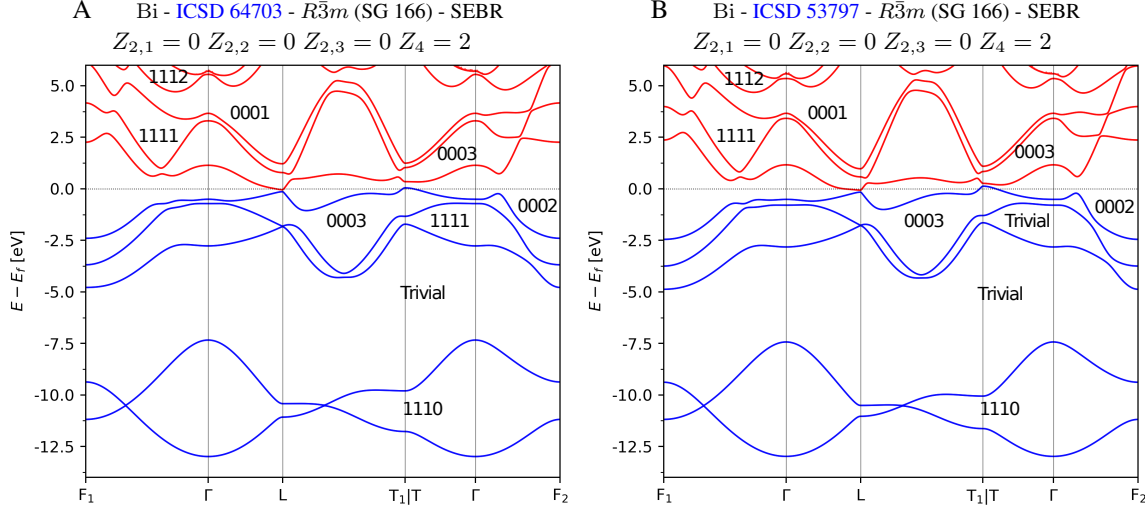


Figure S5. Bulk bands and topology for two ICSD entries associated to the same unique material Bi. Blue (red) colors are used to indicate valence (conduction) bands, and the four numbers listed in each gap indicate the cumulative stable SIs that result from subducing onto SG 2 ( $P\bar{1}$ ):  $Z_{2,1}, Z_{2,2}, Z_{2,3}, Z_4$ , reproduced from the “ind/all” column in Table S22. In both panels A and B, the word “Trivial” indicates a gap in which the cumulative values  $(Z_{2,1}, Z_{2,2}, Z_{2,3}, Z_4) = (0, 0, 0, 0)$ . In A [B], we show the bulk bands and cumulative stable SIs of A: Bi (ICSD 64703) [B: Bi (ICSD 53797)], which is [not] STopo. Conversely, because the gap at  $E_F$  [(0002)] and the next gap below  $E_F$  [(0003)] exhibit cumulative symmetry-indicated stable topology, then Bi (ICSD 64703) in A and Bi (ICSD 53797) in B are both RTopo ICSD entries (see S9 A). Crucially, though the topological classifications of A and B differ away from  $E_F$ , both A and B exhibit the characteristic stable SIs of a HOTI [22] at  $E_F$   $[(Z_{2,1}, Z_{2,2}, Z_{2,3}, Z_4) = (0, 0, 0, 2)]$ , see S11 A 3.

Table S31: SOC-driven topological phase transition statistics for LCEBR-classified materials w/o SOC. In order, the first two columns in this table list the SG and the number of LCEBR-classified unique materials in the SG w/o SOC. If an SG is not listed in the first column, then there are no LCEBR-classified unique materials in the SG w/o SOC. In the remaining five columns, restricting to the same unique materials listed in the second column, we respectively list the number of unique materials that become classified as NLC, SEBR, ES, ESFD, and LCEBR when the effects of SOC are incorporated. For all of the topological classification categories in the table, each number of materials is accompanied by the percentage of materials in the SG in the topological class. When there are no materials in the topological class, the table entry is marked with a dashed horizontal line.

SG	# Mat.	NLC	SEBR	ES	ESFD	LCEBR
1	142	—	—	—	—	142 (100.00%)
2	1189	—	—	—	—	1,189 (100.00%)
3	3	—	—	—	—	3 (100.00%)
4	199	—	—	—	—	199 (100.00%)
5	117	—	—	—	—	117 (100.00%)
6	23	—	—	—	—	23 (100.00%)
7	76	—	—	—	—	76 (100.00%)
8	115	—	—	—	—	115 (100.00%)
9	182	—	—	—	—	182 (100.00%)
10	12	—	—	—	—	12 (100.00%)
11	350	2 (0.57%)	—	—	—	348 (99.43%)
12	629	7 (1.11%)	3 (0.48%)	—	—	619 (98.41%)
13	122	—	—	—	—	122 (100.00%)
14	2029	6 (0.30%)	—	1 (0.05%)	—	2,022 (99.66%)
15	1070	2 (0.19%)	—	—	—	1,068 (99.81%)
16	1	—	—	—	—	1 (100.00%)
17	5	—	—	—	—	5 (100.00%)
18	24	—	—	—	—	24 (100.00%)
19	233	—	—	—	—	233 (100.00%)
20	53	—	—	—	—	53 (100.00%)
21	6	—	—	—	—	6 (100.00%)
22	3	—	—	—	—	3 (100.00%)
23	10	—	—	—	—	10 (100.00%)
24	2	—	—	—	—	2 (100.00%)
25	31	—	—	—	—	31 (100.00%)
26	47	—	—	—	—	47 (100.00%)
27	1	—	—	—	—	1 (100.00%)
28	4	—	—	—	—	4 (100.00%)
29	57	—	—	—	—	57 (100.00%)
30	3	—	—	—	—	3 (100.00%)
31	125	—	—	—	—	125 (100.00%)
32	10	—	—	—	—	10 (100.00%)
33	208	—	—	—	—	208 (100.00%)
34	16	—	—	—	—	16 (100.00%)
35	4	—	—	—	—	4 (100.00%)
36	188	—	—	—	—	188 (100.00%)
37	5	—	—	—	—	5 (100.00%)
38	26	—	—	—	—	26 (100.00%)
39	9	—	—	—	—	9 (100.00%)
40	47	—	—	—	—	47 (100.00%)
41	21	—	—	—	—	21 (100.00%)
42	4	—	—	—	—	4 (100.00%)
43	62	—	—	—	—	62 (100.00%)

44	27	—	—	—	—	—	27 (100.00%)
45	6	—	—	—	—	—	6 (100.00%)
46	25	—	—	—	—	—	25 (100.00%)
47	3	—	—	—	—	—	3 (100.00%)
48	2	—	—	—	—	—	2 (100.00%)
50	2	—	—	—	—	—	2 (100.00%)
51	23	1 (4.35%)	—	—	—	—	22 (95.65%)
52	32	—	—	—	—	—	32 (100.00%)
53	12	—	—	—	—	—	12 (100.00%)
54	12	—	—	—	—	—	12 (100.00%)
55	84	—	—	—	—	—	84 (100.00%)
56	14	—	—	—	—	—	14 (100.00%)
57	80	—	—	—	—	—	80 (100.00%)
58	104	1 (0.96%)	—	—	—	—	103 (99.04%)
59	65	—	—	—	—	—	65 (100.00%)
60	109	—	—	—	—	—	109 (100.00%)
61	101	—	—	—	—	—	101 (100.00%)
62	1349	17 (1.26%)	—	—	—	—	1,332 (98.74%)
63	353	2 (0.57%)	3 (0.85%)	—	—	—	348 (98.58%)
64	133	—	—	—	—	—	133 (100.00%)
65	20	—	—	—	—	—	20 (100.00%)
66	18	1 (5.56%)	—	—	—	—	17 (94.44%)
67	12	—	—	—	—	—	12 (100.00%)
68	13	—	—	—	—	—	13 (100.00%)
69	22	—	—	—	—	—	22 (100.00%)
70	83	—	—	—	—	—	83 (100.00%)
71	70	—	—	—	—	—	70 (100.00%)
72	73	—	—	—	—	—	73 (100.00%)
73	15	—	—	—	—	—	15 (100.00%)
74	50	1 (2.00%)	—	—	—	—	49 (98.00%)
75	3	—	—	—	—	—	3 (100.00%)
76	10	—	—	—	—	—	10 (100.00%)
77	2	—	—	—	—	—	2 (100.00%)
78	2	—	—	—	—	—	2 (100.00%)
79	10	—	—	—	—	—	10 (100.00%)
80	3	—	—	—	—	—	3 (100.00%)
81	9	—	—	—	—	—	9 (100.00%)
82	93	2 (2.15%)	—	—	—	—	91 (97.85%)
83	1	—	—	—	—	—	1 (100.00%)
84	21	—	—	—	—	—	21 (100.00%)
85	22	—	—	—	—	—	22 (100.00%)
86	11	—	1 (9.09%)	—	—	—	10 (90.91%)
87	69	—	—	—	—	—	69 (100.00%)
88	102	—	—	—	—	—	102 (100.00%)
90	1	—	—	—	—	—	1 (100.00%)
91	4	—	—	—	—	—	4 (100.00%)
92	29	—	—	—	—	—	29 (100.00%)
95	2	—	—	—	—	—	2 (100.00%)
96	15	—	—	—	—	—	15 (100.00%)
97	1	—	—	—	—	—	1 (100.00%)
98	3	—	—	—	—	—	3 (100.00%)
99	71	—	—	—	—	—	71 (100.00%)
100	6	—	—	—	—	—	6 (100.00%)
102	6	—	—	—	—	—	6 (100.00%)
104	2	—	—	—	—	—	2 (100.00%)
105	3	—	—	—	—	—	3 (100.00%)

107	11	—	—	—	—	—	11 (100.00%)
108	7	—	—	—	—	—	7 (100.00%)
109	14	—	—	—	1 (7.14%)	—	13 (92.86%)
110	5	—	—	—	—	—	5 (100.00%)
111	13	—	—	—	—	—	13 (100.00%)
112	4	—	—	—	—	—	4 (100.00%)
113	45	—	—	—	—	—	45 (100.00%)
114	25	—	—	—	—	—	25 (100.00%)
115	6	—	—	—	—	—	6 (100.00%)
116	14	—	—	—	—	—	14 (100.00%)
117	5	—	—	—	—	—	5 (100.00%)
118	8	—	—	—	—	—	8 (100.00%)
119	18	—	—	—	—	—	18 (100.00%)
120	9	—	—	—	—	—	9 (100.00%)
121	67	—	—	—	—	—	67 (100.00%)
122	101	—	3 (2.97%)	1 (0.99%)	—	—	97 (96.04%)
123	59	—	—	—	—	—	59 (100.00%)
124	3	—	—	—	—	—	3 (100.00%)
125	17	—	—	—	—	—	17 (100.00%)
126	7	—	—	1 (14.29%)	—	—	6 (85.71%)
127	42	1 (2.38%)	—	—	—	—	41 (97.62%)
128	26	—	—	—	—	—	26 (100.00%)
129	170	1 (0.59%)	—	5 (2.94%)	—	—	164 (96.47%)
130	14	—	—	—	—	—	14 (100.00%)
131	7	—	—	—	—	—	7 (100.00%)
132	9	—	—	—	—	—	9 (100.00%)
133	1	—	—	—	—	—	1 (100.00%)
134	1	—	—	—	—	—	1 (100.00%)
135	11	—	—	—	—	—	11 (100.00%)
136	63	—	1 (1.59%)	—	—	—	62 (98.41%)
137	31	—	—	—	—	—	31 (100.00%)
138	9	—	—	—	—	—	9 (100.00%)
139	159	—	2 (1.26%)	3 (1.89%)	—	—	154 (96.86%)
140	112	1 (0.89%)	—	—	—	—	111 (99.11%)
141	77	—	1 (1.30%)	1 (1.30%)	—	—	75 (97.40%)
142	38	—	—	—	—	—	38 (100.00%)
143	12	—	—	1 (8.33%)	—	—	11 (91.67%)
144	11	—	—	—	—	—	11 (100.00%)
145	5	—	—	—	—	—	5 (100.00%)
146	63	—	—	—	1 (1.59%)	—	62 (98.41%)
147	52	—	—	1 (1.92%)	—	—	51 (98.08%)
148	255	—	1 (0.39%)	—	—	—	254 (99.61%)
149	5	—	—	—	—	—	5 (100.00%)
150	49	—	—	—	—	—	49 (100.00%)
151	4	—	—	—	—	—	4 (100.00%)
152	31	—	—	1 (3.23%)	2 (6.45%)	28 (90.32%)	28 (90.32%)
154	15	—	—	—	1 (6.67%)	14 (93.33%)	14 (93.33%)
155	31	—	—	—	—	—	31 (100.00%)
156	41	—	—	1 (2.44%)	—	40 (97.56%)	40 (97.56%)
157	9	—	—	—	—	—	9 (100.00%)
159	18	—	—	—	—	—	18 (100.00%)
160	100	—	—	—	—	—	100 (100.00%)
161	69	—	—	—	—	—	69 (100.00%)
162	25	—	—	—	—	—	25 (100.00%)
163	32	—	1 (3.12%)	—	—	—	31 (96.88%)
164	254	—	13 (5.12%)	2 (0.79%)	—	—	239 (94.09%)

165	9	—	—	15 (4.45%)	3 (0.89%)	—	9 (100.00%)
166	337	—	—	15 (4.45%)	3 (0.89%)	—	319 (94.66%)
167	179	—	—	—	—	—	179 (100.00%)
169	1	—	—	—	—	—	1 (100.00%)
173	74	—	—	—	—	—	74 (100.00%)
174	17	—	—	—	—	—	17 (100.00%)
176	107	—	—	—	—	—	107 (100.00%)
177	1	—	—	—	—	—	1 (100.00%)
180	10	—	—	—	—	—	10 (100.00%)
181	3	—	—	—	—	—	3 (100.00%)
182	9	—	—	—	—	—	9 (100.00%)
183	1	—	—	—	—	—	1 (100.00%)
185	20	—	—	2 (10.00%)	—	—	18 (90.00%)
186	167	—	—	3 (1.80%)	—	—	164 (98.20%)
187	31	—	—	—	—	—	31 (100.00%)
188	16	—	—	—	—	—	16 (100.00%)
189	54	—	2 (3.70%)	—	—	—	52 (96.30%)
190	16	—	—	—	—	—	16 (100.00%)
191	5	—	—	—	—	—	5 (100.00%)
192	2	—	—	—	—	—	2 (100.00%)
193	13	—	—	—	—	—	13 (100.00%)
194	252	—	4 (1.59%)	6 (2.38%)	—	—	242 (96.03%)
195	1	—	—	—	—	—	1 (100.00%)
197	10	—	—	—	—	—	10 (100.00%)
198	93	—	—	—	1 (1.08%)	—	92 (98.92%)
199	23	—	—	—	—	—	23 (100.00%)
200	5	—	—	—	1 (20.00%)	—	4 (80.00%)
201	2	—	—	—	—	—	2 (100.00%)
202	8	—	—	—	—	—	8 (100.00%)
203	5	—	—	—	—	—	5 (100.00%)
204	22	—	—	—	1 (4.55%)	—	21 (95.45%)
205	81	1 (1.23%)	—	1 (1.23%)	—	—	79 (97.53%)
206	30	—	1 (3.33%)	—	1 (3.33%)	—	28 (93.33%)
212	6	—	—	—	—	—	6 (100.00%)
213	5	—	—	—	—	—	5 (100.00%)
214	6	—	—	—	—	—	6 (100.00%)
215	30	—	—	—	—	—	30 (100.00%)
216	234	3 (1.28%)	—	6 (2.56%)	8 (3.42%)	—	217 (92.74%)
217	42	—	—	—	—	—	42 (100.00%)
218	30	—	—	—	—	—	30 (100.00%)
219	3	—	—	—	—	—	3 (100.00%)
220	27	—	—	—	—	—	27 (100.00%)
221	164	—	12 (7.32%)	1 (0.61%)	—	—	151 (92.07%)
223	3	—	—	—	—	—	3 (100.00%)
224	7	—	—	1 (14.29%)	—	—	6 (85.71%)
225	374	—	14 (3.74%)	—	6 (1.60%)	—	354 (94.65%)
226	1	—	—	—	—	—	1 (100.00%)
227	143	—	1 (0.70%)	—	2 (1.40%)	—	140 (97.90%)
229	20	—	—	—	—	—	20 (100.00%)
230	1	—	—	—	—	—	1 (100.00%)
Total	15865	49 (0.31%)	78 (0.49%)	42 (0.26%)	24 (0.15%)	—	15,672 (98.78%)

Table S32: SOC-driven topological phase transition statistics for NLC-SM-classified semimetals w/o SOC. In order, the first two columns in this table list the SG and the number of NLC-SM-classified unique materials in the SG w/o SOC. If an SG is not listed in the first column, then there are no NLC-SM-classified unique materials in the SG w/o SOC. In the remaining five columns, restricting to the same unique materials listed in the second column, we respectively list the number of unique materials that become classified as NLC, SEBR, ES, ESFD, and LCEBR when the effects of SOC are incorporated. For all of the topological classification categories in the table, each number of materials is accompanied by the percentage of materials in the SG in the topological class. When there are no materials in the topological class, the table entry is marked with a dashed horizontal line.

SG	# Mat.	NLC	SEBR	ES	ESFD	LCEBR
2	165	158 (95.76%)	—	—	—	7 (4.24%)
11	4	4 (100.00%)	—	—	—	—
12	24	2 (8.33%)	20 (83.33%)	—	—	2 (8.33%)
13	1	1 (100.00%)	—	—	—	—
14	24	23 (95.83%)	—	—	—	1 (4.17%)
15	22	18 (81.82%)	—	—	—	4 (18.18%)
58	1	—	—	1 (100.00%)	—	—
60	1	1 (100.00%)	—	—	—	—
81	1	—	—	—	—	1 (100.00%)
82	2	1 (50.00%)	—	1 (50.00%)	—	—
85	2	—	—	—	—	2 (100.00%)
87	2	—	2 (100.00%)	—	—	—
166	2	—	2 (100.00%)	—	—	—
Total	251	208 (82.87%)	24 (9.56%)	2 (0.8%)	—	17 (6.77%)

Table S33: SOC-driven topological phase transition statistics for SEBR-SM-classified semimetals w/o SOC. In order, the first two columns in this table list the SG and the number of SEBR-SM-classified unique materials in the SG w/o SOC. If an SG is not listed in the first column, then there are no SEBR-SM-classified unique materials in the SG w/o SOC. In the remaining five columns, restricting to the same unique materials listed in the second column, we respectively list the number of unique materials that become classified as NLC, SEBR, ES, ESFD, and LCEBR when the effects of SOC are incorporated. For all of the topological classification categories in the table, each number of materials is accompanied by the percentage of materials in the SG in the topological class. When there are no materials in the topological class, the table entry is marked with a dashed horizontal line.

SG	# Mat.	NLC	SEBR	ES	ESFD	LCEBR
147	3	—	3 (100.00%)	—	—	—
148	35	—	29 (82.86%)	5 (14.29%)	—	1 (2.86%)
162	1	—	1 (100.00%)	—	—	—
164	2	—	2 (100.00%)	—	—	—
166	2	—	2 (100.00%)	—	—	—
167	1	—	1 (100.00%)	—	—	—
Total	44	—	38 (86.36%)	5 (11.36%)	—	1 (2.27%)

## S11. LISTS OF REPRESENTATIVE TOPOLOGICAL MATERIALS

In this section, we will provide representative examples of materials on <https://www.topologicalquantumchemistry.com/> with nontrivial bulk topology that can be

identified from symmetry eigenvalues and band connectivity (TQC) [28, 43, 58, 92, 93]. Though many of the materials listed in this section have been identified in previous theoretical and experimental works, most of the materials listed in this section were not previously recognized as hosting nontrivial electronic band topology. In each part of this section, we will highlight the most well-studied examples of known topological materials. First, in S11A, we will enumerate the 3D topological insulators (TIs) [5, 30, 142], topological crystalline insulators (TCIs) [11–14, 110, 161, 166], and higher-order TIs (HOTIs) [15–17, 22, 33, 34, 87, 102, 105, 111, 163, 167] with the fewest electron and hole pockets at the Fermi energy ( $E_F$ ). Next, in S11C, we will list the topological semimetals with the simplest bulk Fermi surfaces, including examples of both conventional Dirac [6, 19, 59, 115, 116, 168–173] as well as unconventional fermion [7–9, 23–25, 131, 132, 135, 136] semimetals. Then, in S11D, we will provide representative examples of spin-orbit-coupling- (SOC-) driven semimetal-to-insulator transitions that result in topological (crystalline) insulators with large gaps at  $E_F$ . Finally, in S11E, we will show the materials with the cleanest insulating or semimetallic Fermi surfaces that host fragile topological bands [43–48, 96–101, 174] at or near  $E_F$ . We note that in this section, we only display electronic structures and topological data calculated in the presence of SOC; for each material, the electronic structure and topological data calculated in the absence of SOC can be accessed by clicking on the ICSD number listed above each plot. In Fig. S6, we provide an example detailing the labeling scheme and information contained within each of the band-structure plots shown in this section.

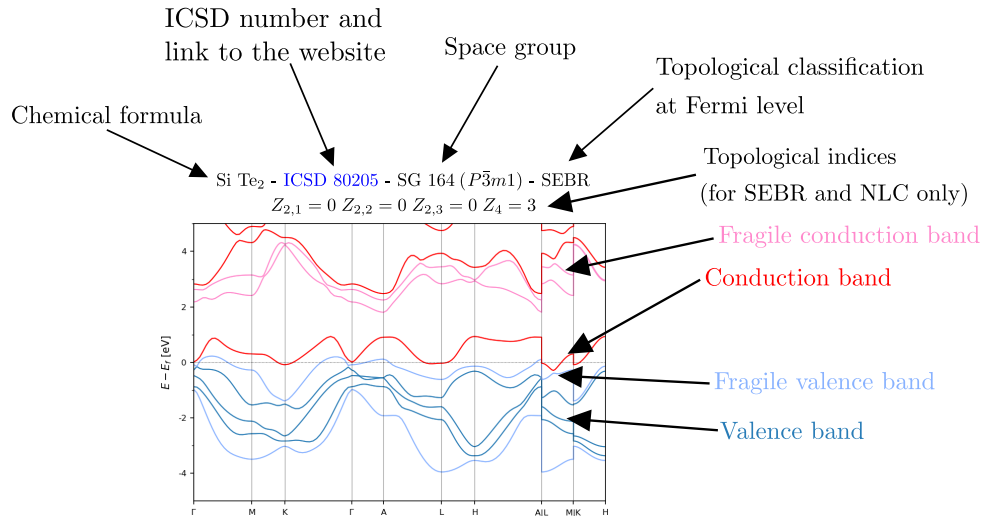


Figure S6. Example band-structure plot. In this figure, we show the band structure and topological indices of SiTe<sub>2</sub> [ICSD 80205, SG 164 ( $P\bar{3}m1$ )] as an example of the labeling scheme and information contained within each of the band-structure plots shown in this section. First, at the top of each band-structure plot, we provide the chemical formula, the ICSD number with a hyperlink to <https://www.topologicalquantumchemistry.com/>, the space group symbol and number, and the topological classification at the Fermi level (e.g. NLC, SEBR, ES, or ESFD). If the ICSD entry is classified as SEBR or NLC at  $E_F$ , then we further list the cumulative symmetry-based topological indices (stable SIs) at  $E_F$  in the notation established in Ref. [16]. In the band-structure plot, trivial and stable topological conduction (valence) bands are labeled in red (blue), and fragile conduction (valence) bands are labeled in pink (light blue).

We additionally emphasize that for the materials highlighted in this section, we cannot preclude the existence of non-symmetry-indicated topological (crystalline) insulating (e.g. hourglass insulating [13, 14, 110, 166] or high-fold mirror-Chern TCI [161, 175]) or Weyl semimetal [20, 21, 143] phases. These non-symmetry-indicated phases cannot be identified through TQC alone, and must instead be diagnosed by performing additional (nested) Wilson-loop calculations [13, 14, 34, 102, 108–112, 176].

### A. Symmetry-Indicated TIs, TCIs, and HOTIs

In this section, we will list the 3D TIs, TCIs, and HOTIs that can be diagnosed from their symmetry eigenvalues through the topological-index formulas established in Refs. [5, 16, 17, 30, 87]. First, in S11 A1, we will list the 3D strong TIs indicated through the Fu-Kane parity criterion [5, 30]. Next, in S11 A2, we will list the  $S_{4z}$  rotoinversion-indicated 3D TIs and Weyl semimetals [16, 17, 112]. Then, in S11 A3, S11 A4, S11 A5, S11 A6, and S11 A7, we will list the TCIs and HOTIs diagnosed through the symmetry-based indicators (stable SIs) more recently introduced in Refs. [16, 17, 22, 33, 34, 87, 163]. Lastly, in S11 B, we will list the repeat-topological (RTop) TIs and TCIs (rigorously defined in S9 A), which exhibit symmetry-indicated stable topology at the Fermi level and at the next gap below  $E_F$  as determined by band connectivity (see S2).

#### I. 3D Strong TIs

In this section, we list the symmetry-indicated 3D strong TIs with the largest band gaps or the fewest and smallest bulk Fermi pockets. First, in Figs. S7, S8, S9, S10, and S11, we list the 3D TIs classified as NLC, and then, in Figs. S12, S13, S14, S15, and S16, we list the 3D TIs classified as SEBR. 3D TIs characteristically exhibit odd numbers of twofold Dirac-cone surface states [5, 18, 30, 177] that are protected by time-reversal ( $\mathcal{T}$ ) symmetry. Though it was originally recognized that 3D TIs could be identified through a  $\mathbb{Z}_2$ -valued (Fu-Kane) index based on parity [inversion ( $\mathcal{I}$ )] eigenvalues [5, 30], a more exhaustive consideration of eigenvalue indicators (stable SIs, see Refs. [16, 17, 22, 33, 34, 87, 163] and S2) has revealed that the Fu-Kane parity index is in fact subsumed by a  $\mathbb{Z}_4$ -valued index  $Z_4$  that includes both HOTIs and strong TIs. In the notation of Ref. [16], which we use throughout this work, 3D TIs are indicated either by  $Z_4 = 1, 3$  (which coincide with the Fu-Kane parity criterion). The most well known example of a 3D TI [18] –  $\text{Bi}_2\text{Se}_3$  [ICSD 617079, SG 166 ( $R\bar{3}m$ )] – is classified as SEBR, and accordingly appears in Fig. S14.

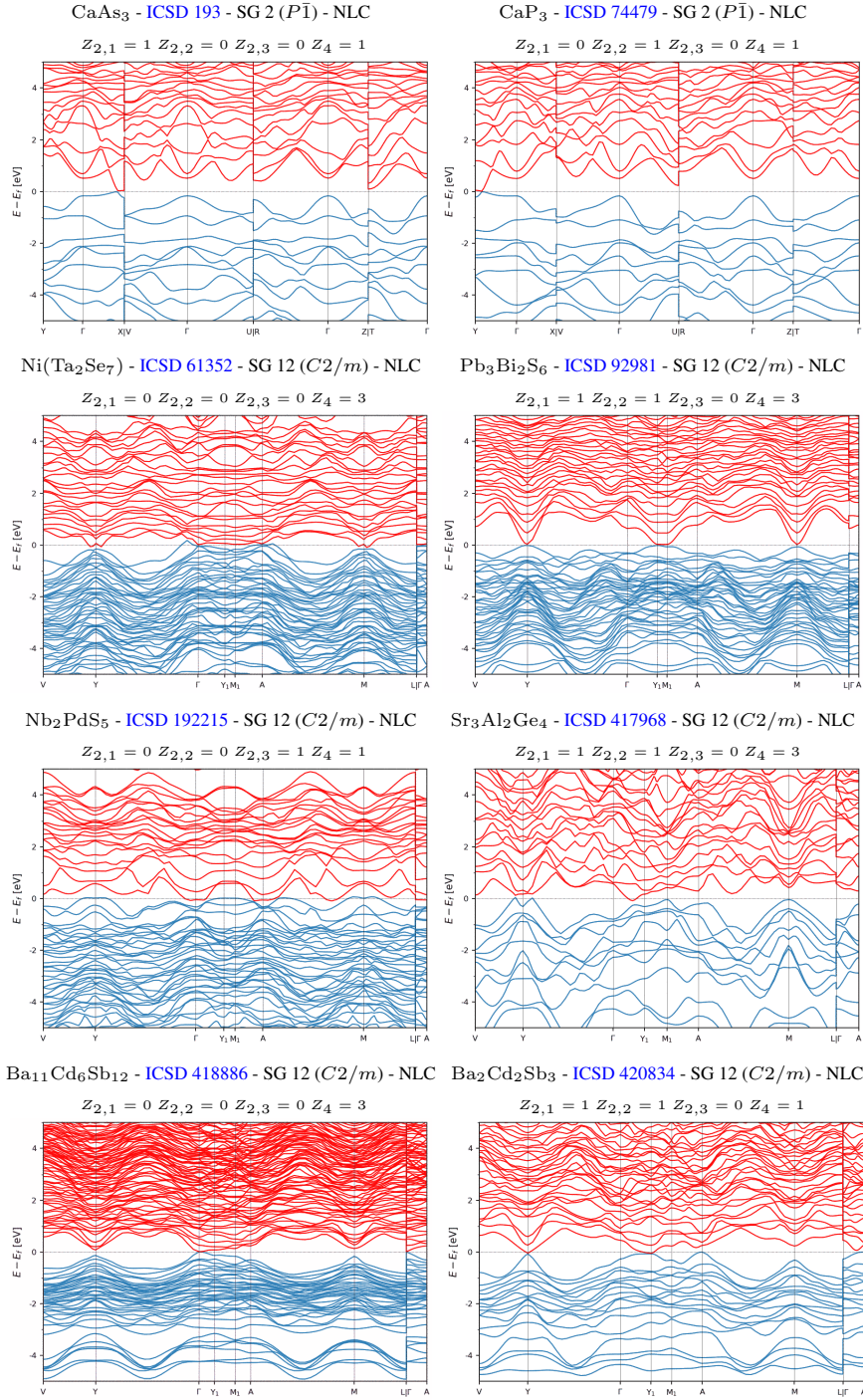


Figure S7. The NLC-classified 3D strong TIs with the largest band gaps or the fewest and smallest bulk Fermi pockets. (part 1/5)

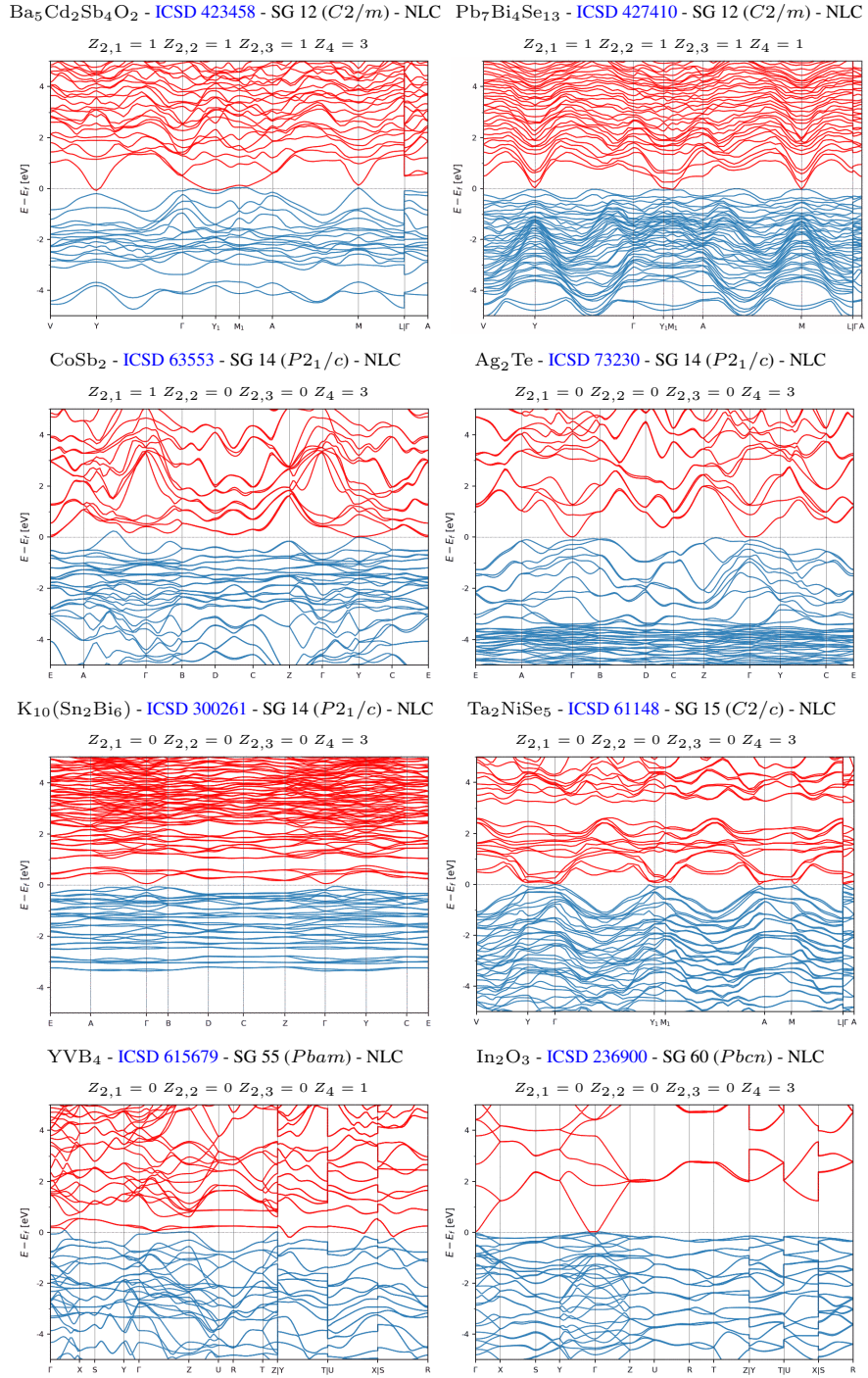


Figure S8. The NLC-classified 3D strong TIs with the largest band gaps or the fewest and smallest bulk Fermi pockets. (part 2/5)

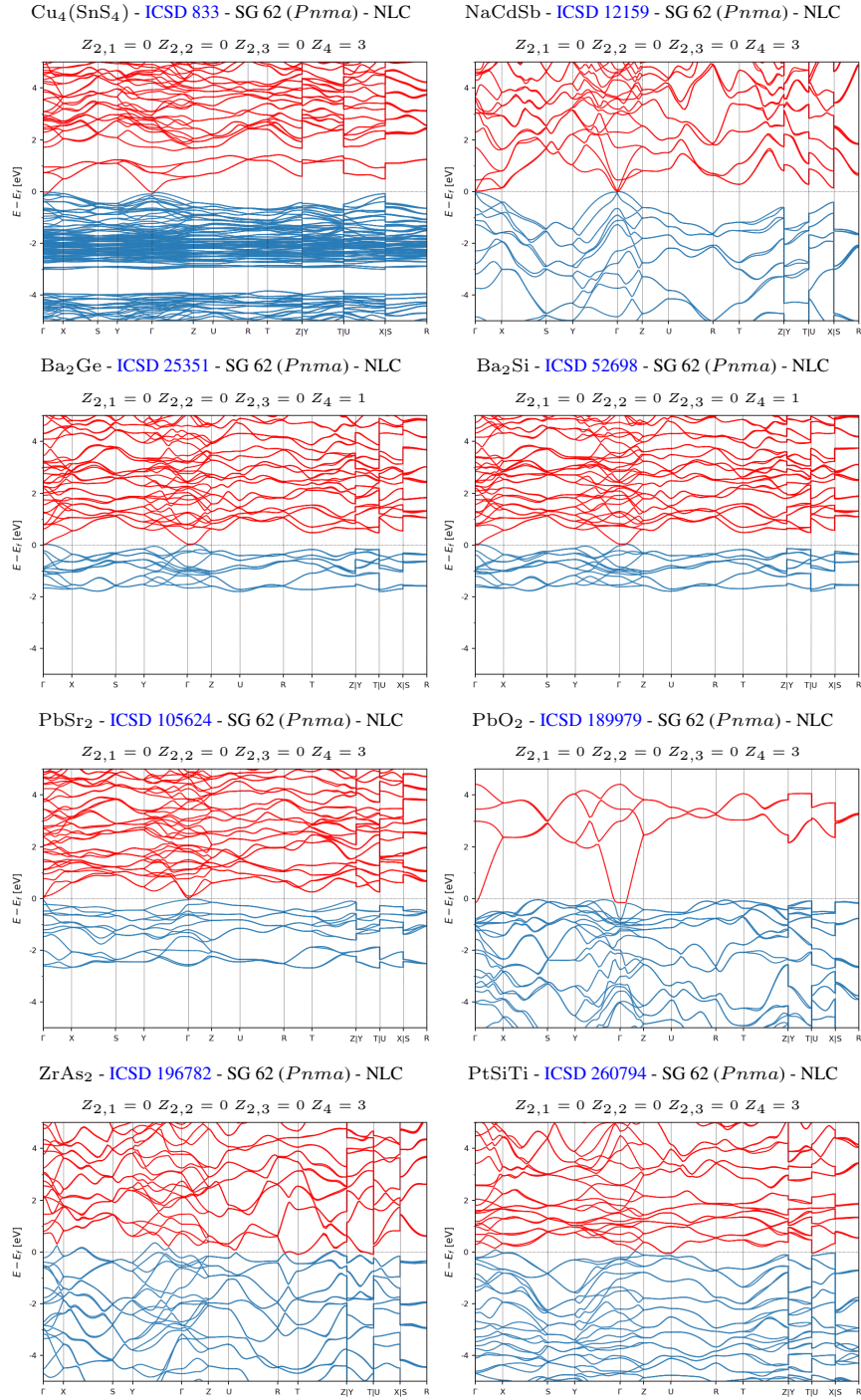


Figure S9. The NLC-classified 3D strong TIs with the largest band gaps or the fewest and smallest bulk Fermi pockets. (part 3/5)

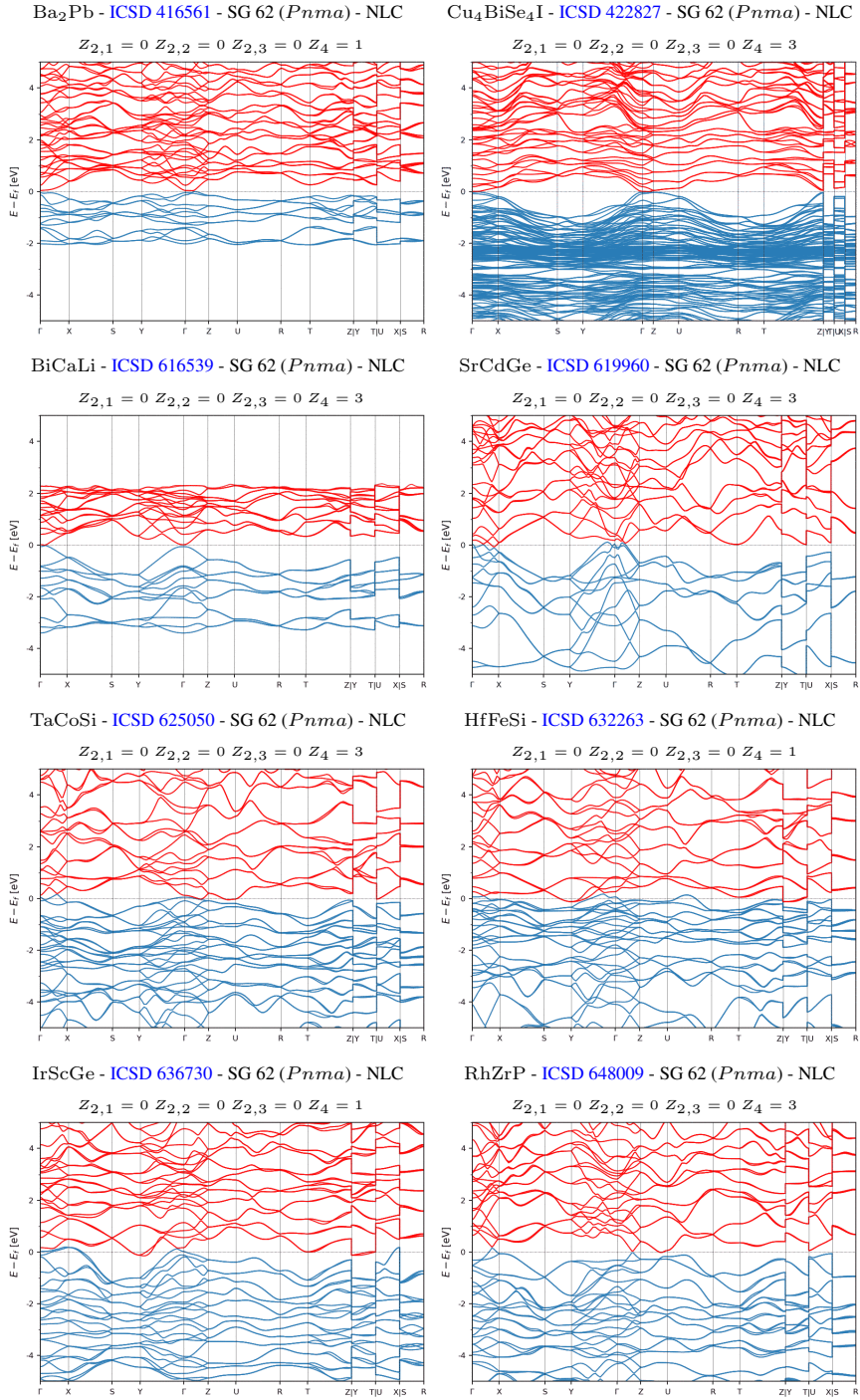


Figure S10. The NLC-classified 3D strong TIs with the largest band gaps or the fewest and smallest bulk Fermi pockets. (part 4/5)

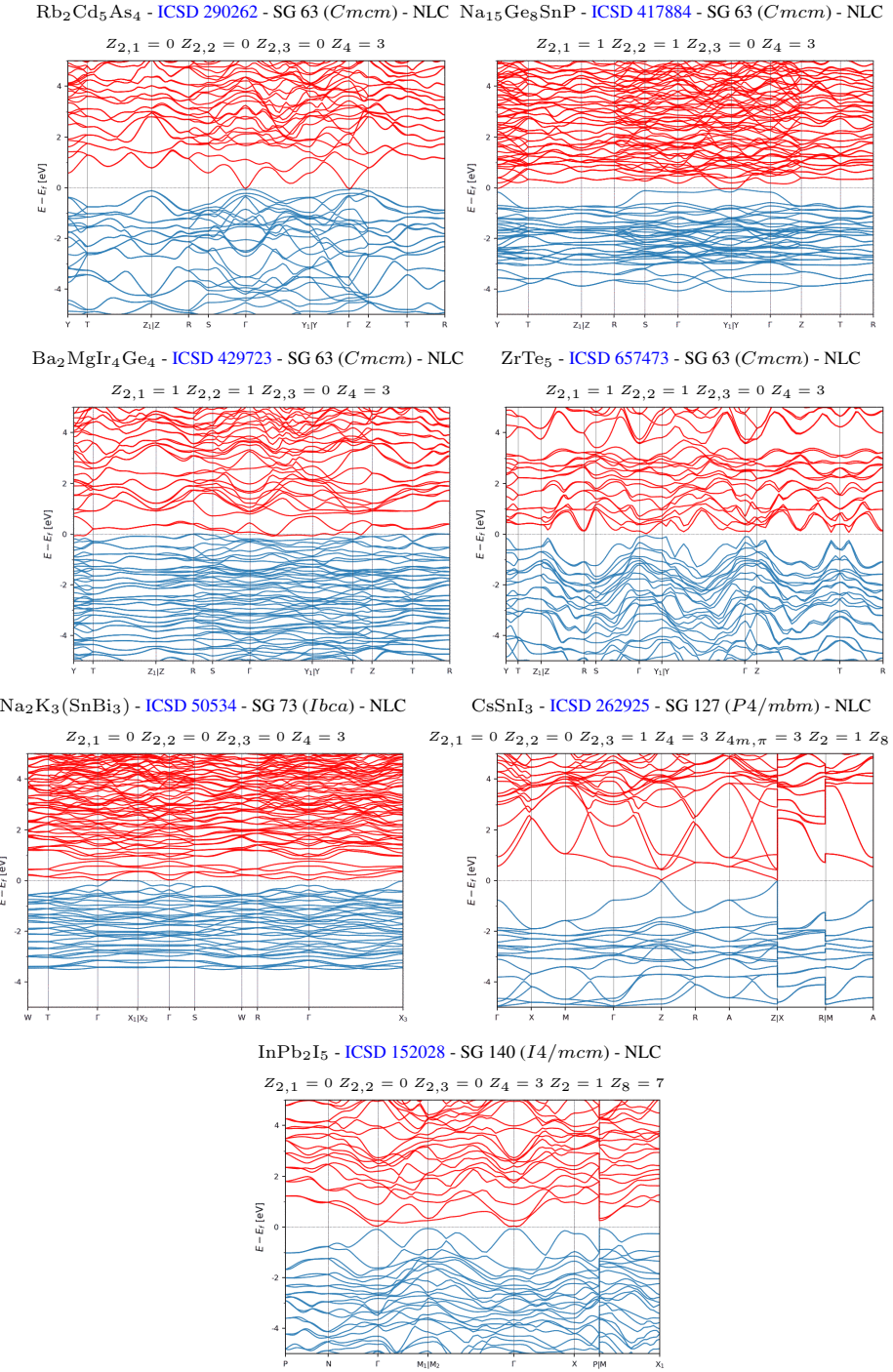


Figure S11. The NLC-classified 3D strong TIs with the largest band gaps or the fewest and smallest bulk Fermi pockets. (part 5/5)

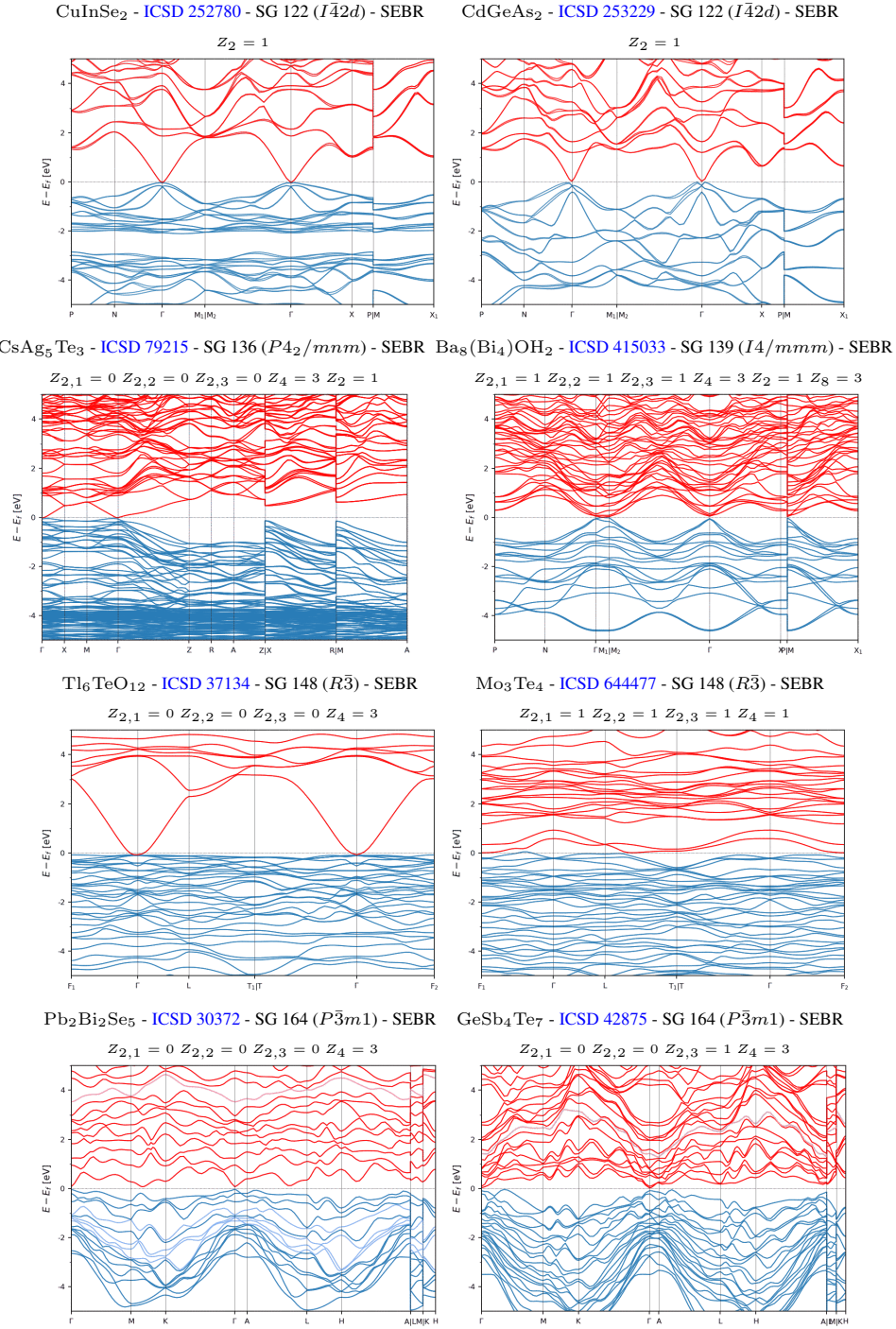


Figure S12. The SEBR-classified 3D strong TIs with the largest band gaps or the fewest and smallest bulk Fermi pockets. (part 1/5)

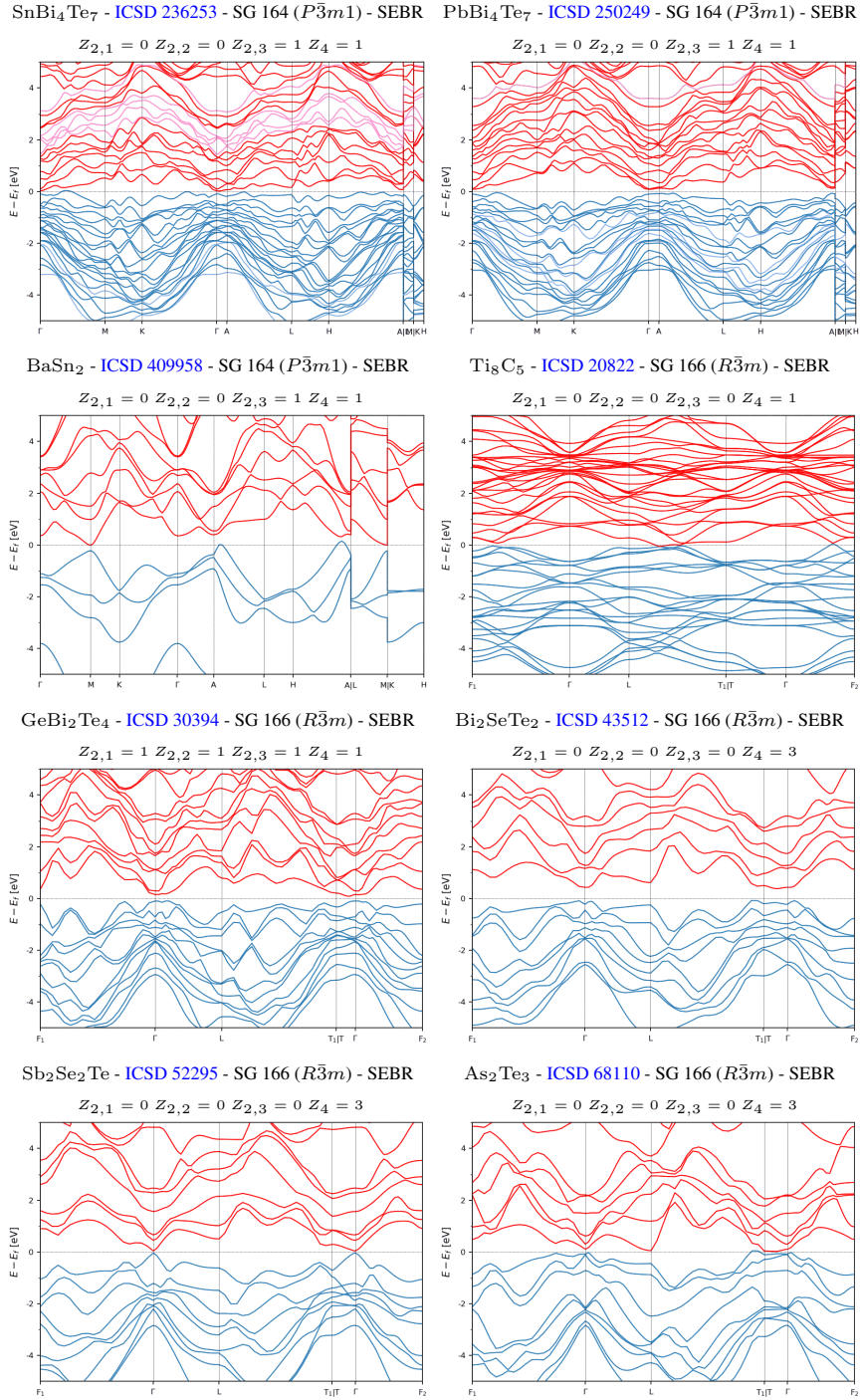


Figure S13. The SEBR-classified 3D strong TIs with the largest band gaps or the fewest and smallest bulk Fermi pockets. (part 2/5)

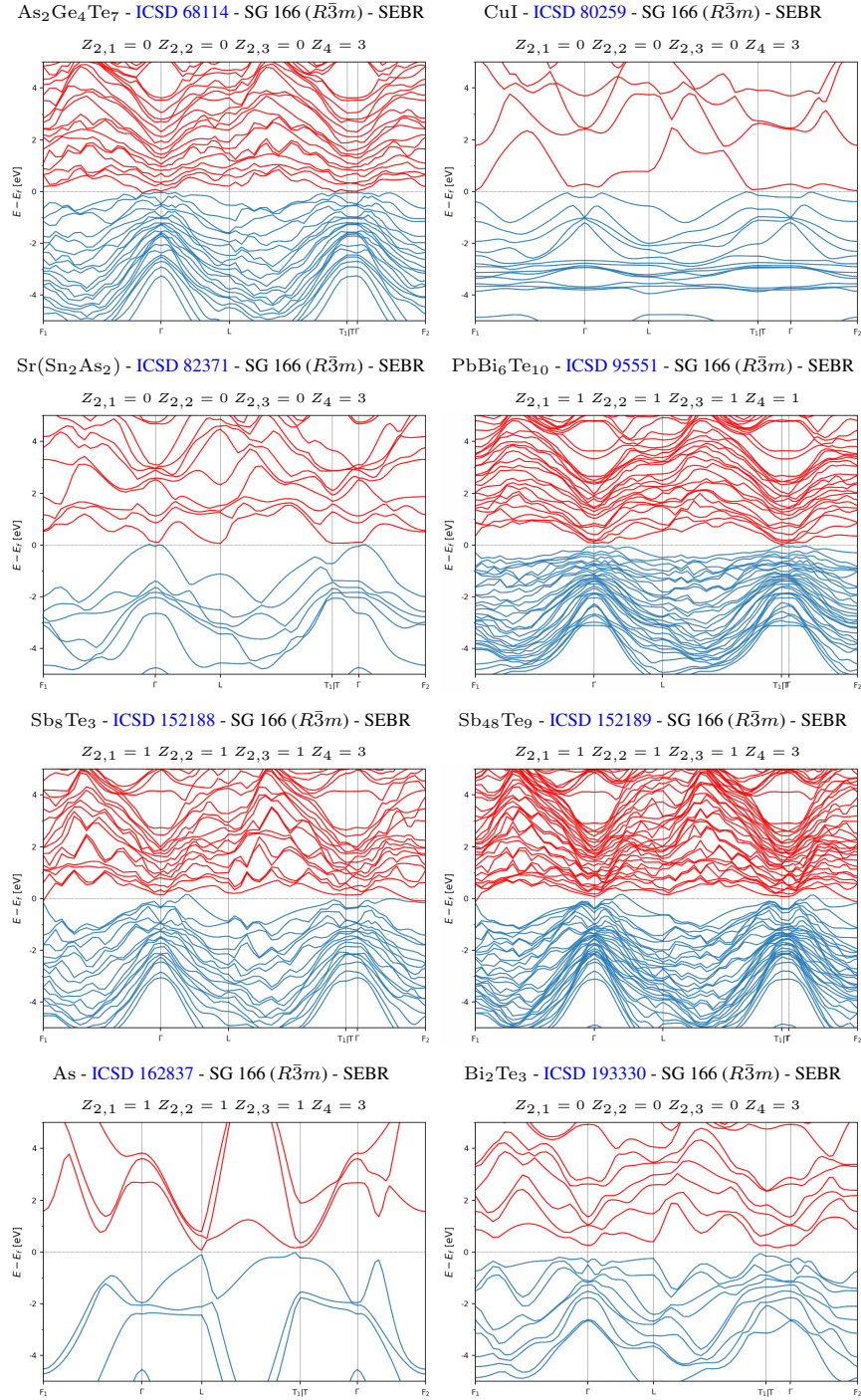


Figure S14. The SEBR-classified 3D strong TIs with the largest band gaps or the fewest and smallest bulk Fermi pockets. (part 3/5)

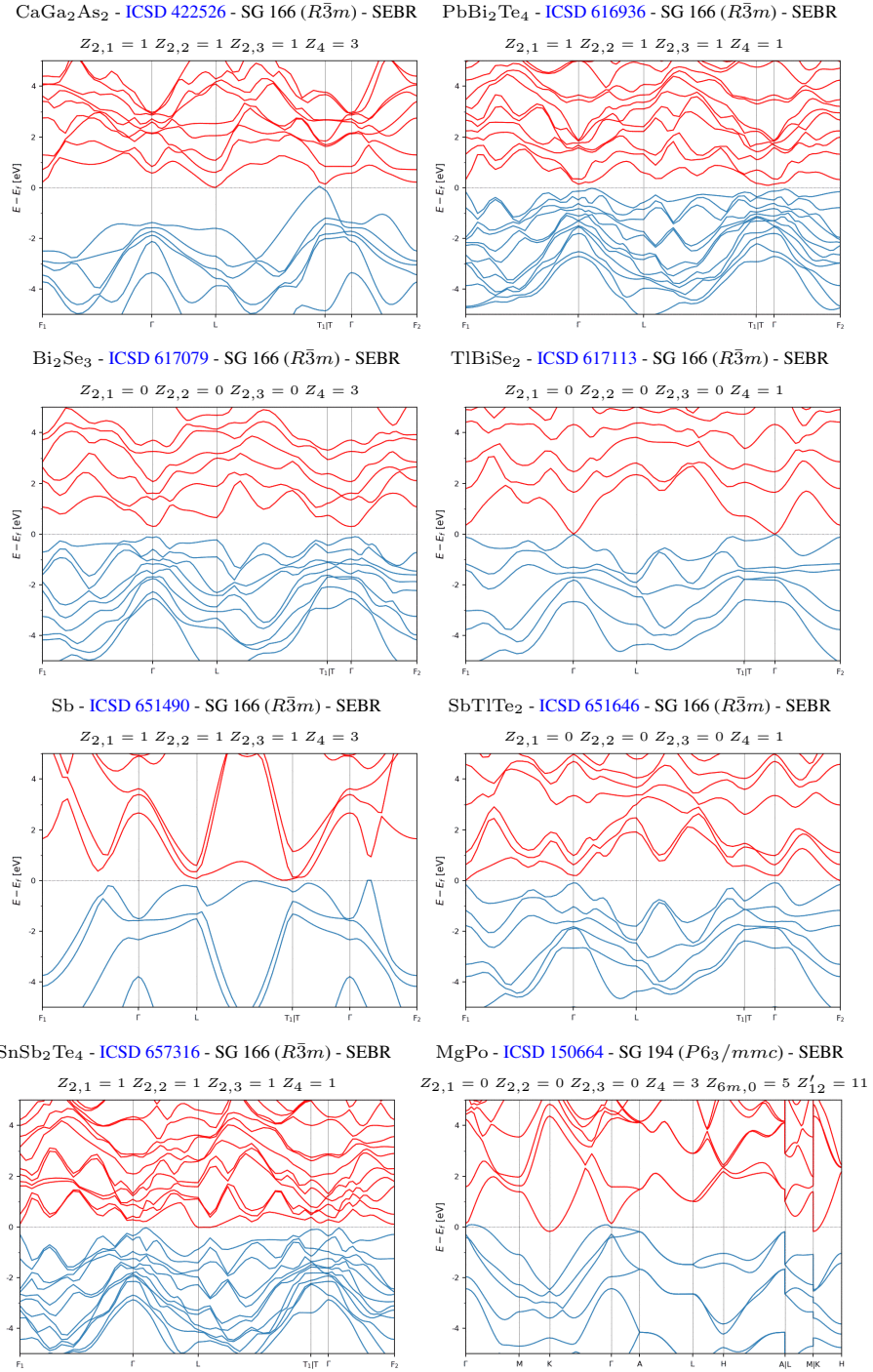


Figure S15. The SEBR-classified 3D strong TIs with the largest band gaps or the fewest and smallest bulk Fermi pockets. (part 4/5)

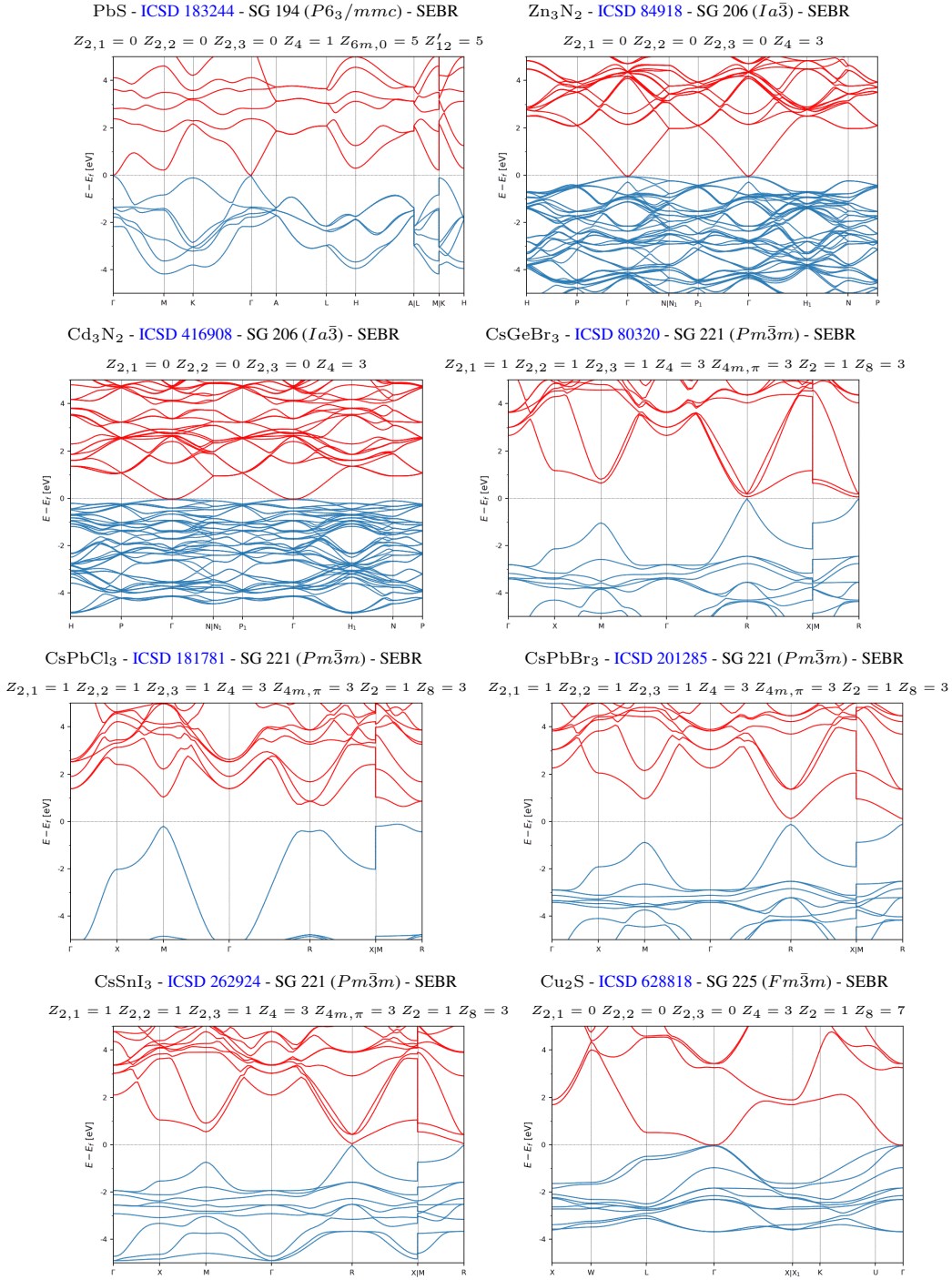


Figure S16. The SEBR-classified 3D strong TIs with the largest band gaps or the fewest and smallest bulk Fermi pockets. (part 5/5)

## 2. $S_4$ -Rotoinversion-Indicated Strong TIs and Weyl Semimetals

In this section, we list the noncentrosymmetric stable topological materials with fourfold rotoinversion  $S_4 = C_4 \times \mathcal{I}$  symmetry and with the largest gaps or the fewest Fermi pockets along all high-symmetry BZ lines. As shown in Ref. [16], these materials can either be strong 3D TIs or Weyl semimetals, and can only be further distinguished by performing an additional calculation beyond symmetry-based indicators [112]. In terms of the indices introduced in Ref. [16], the materials listed in this section exhibit  $Z_2 = 1$  (which is not to be confused with the Fu-Kane parity criterion [5, 30], see S11A 1 for further details), and do not have a well-defined  $Z_4$  index, because they are noncentrosymmetric. First, in Fig. S17, we list the  $S_4$  TIs and Weyl semimetals classified as NLC, and then, in Fig. S18, we list the  $S_4$  TIs and Weyl semimetals classified as SEBR. Among the stoichiometric materials in the ICSD, we find that there are relatively few examples of noncentrosymmetric  $S_4$ -symmetry-indicated TIs and Weyl semimetals that either have SGs in which the only stable SI is  $Z_2$ , or which have trivial values for all stable SIs aside from  $Z_2$ .

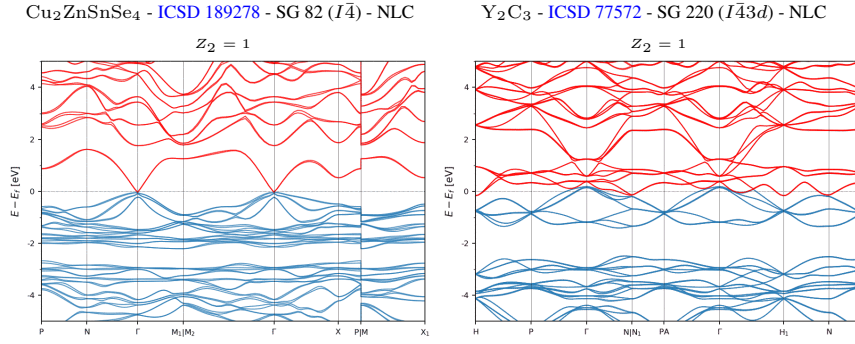
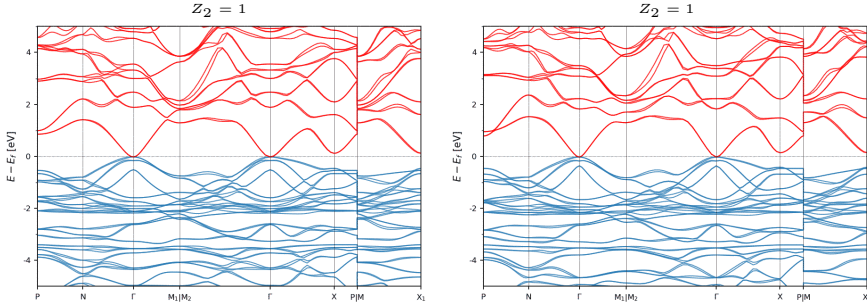
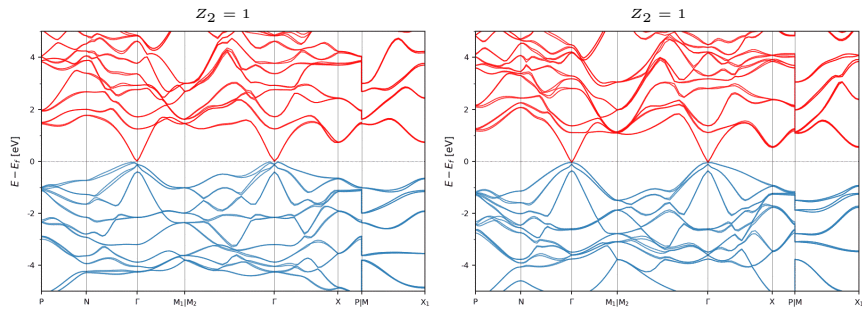


Figure S17. The NLC-classified,  $S_4$ -rotoinversion-indicated, noncentrosymmetric 3D strong TIs and Weyl semimetals with the largest band gaps along high-symmetry lines or the fewest and smallest bulk Fermi pockets.

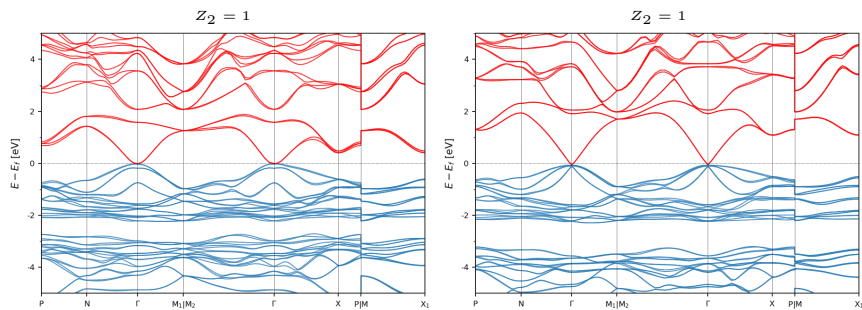
$\text{Cu}_2\text{HgSnSe}_4$  - ICSD 95119 - SG 121 ( $I\bar{4}2m$ ) - SEBR     $\text{Cu}_2\text{HgGeSe}_4$  - ICSD 152761 - SG 121 ( $I\bar{4}2m$ ) - SEBR



$\text{CdGeAs}_2$  - ICSD 16736 - SG 122 ( $I\bar{4}2d$ ) - SEBR



$\text{CuTlSe}_2$  - ICSD 28743 - SG 122 ( $I\bar{4}2d$ ) - SEBR



$\text{CdSnAs}_2$  - ICSD 609982 - SG 122 ( $I\bar{4}2d$ ) - SEBR

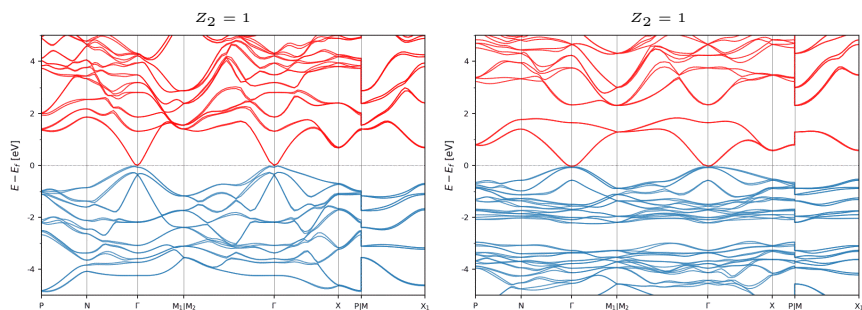


Figure S18. The SEBR-classified,  $S_4$ -rotoinversion-indicated, noncentrosymmetric 3D strong TIs and Weyl semimetals with the largest band gaps along high-symmetry lines or the fewest and smallest bulk Fermi pockets.

### 3. Inversion-Symmetry-Protected HOTIs

In this section, we list the inversion-symmetry-indicated HOTIs with the largest bulk gaps or the fewest and smallest bulk Fermi pockets. In ideal models of inversion-symmetry-indicated HOTIs, when symmetries other than  $\mathcal{I}$  and  $\mathcal{T}$  are relaxed, finite samples exhibit gapped 2D surfaces and gapless 1D hinges with anomalous helical modes [16, 17, 22, 33, 34, 105]. In the presence of additional symmetries, such as mirror reflection and twofold rotation ( $C_2$ ), inversion-symmetry-indicated HOTIs may also exhibit  $2 + 4n$  twofold Dirac cones on specific, high-symmetry surfaces [14, 16, 17, 105]. In terms of the indices introduced in Ref. [16], the materials listed in this section are characterized by  $Z_4 = 2$ , and exhibit trivial values for all other independent stable SIs. First, in Figs. S19, S20, S21, S22, S23, and S24, we list the HOTIs classified as NLC, and then, in Figs. S25 and S26, we list the HOTIs classified as SEBR. The materials listed in this section include the recently identified HOTIs bismuth [ICSD 64705, SG 166 ( $R\bar{3}m$ )] [22, 178] and BiBr [ICSD 1560, SG 12 ( $C2/m$ )] [179–183], which are classified as SEBR, and MoTe<sub>2</sub> [ICSD 14349, SG 11 ( $P2_1/m$ )] [34, 180], which is classified as NLC. Bismuth, BiBr, and MoTe<sub>2</sub>, as well as members of closely-related material families have been the subject of recent intense theoretical and experimental investigations seeking to distinguish  $\mathcal{I}$ - and  $\mathcal{T}$ -symmetric HOTIs from weak TIs and other TI and TCI phases [29, 184–189]. Notably,  $\mathcal{I}$ - and  $\mathcal{T}$ -symmetric HOTIs exhibit trivial axion angles  $\theta \bmod 2\pi = 0$ , and it remains an open and urgent question whether there exist quantized electromagnetic response effects beyond the axionic magnetoelectric effect that can distinguish  $\mathcal{I}$ - and  $\mathcal{T}$ -symmetric HOTI phases from other TCIs and from trivial insulators [29, 102, 149].

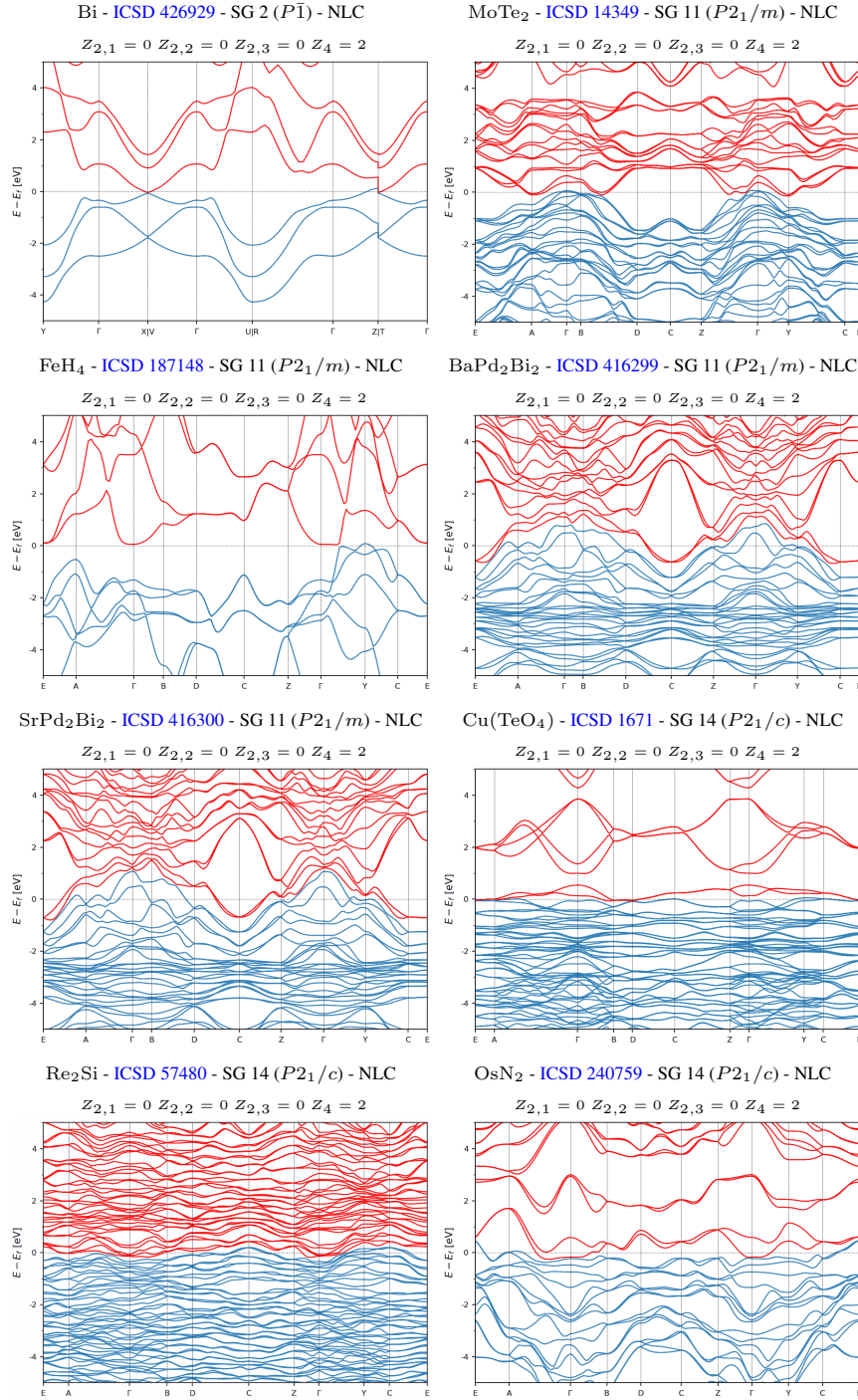


Figure S19. The NLC-classified, inversion-symmetry-indicated HOTIs with the largest band gaps or the fewest and smallest bulk Fermi pockets. (part 1/6)

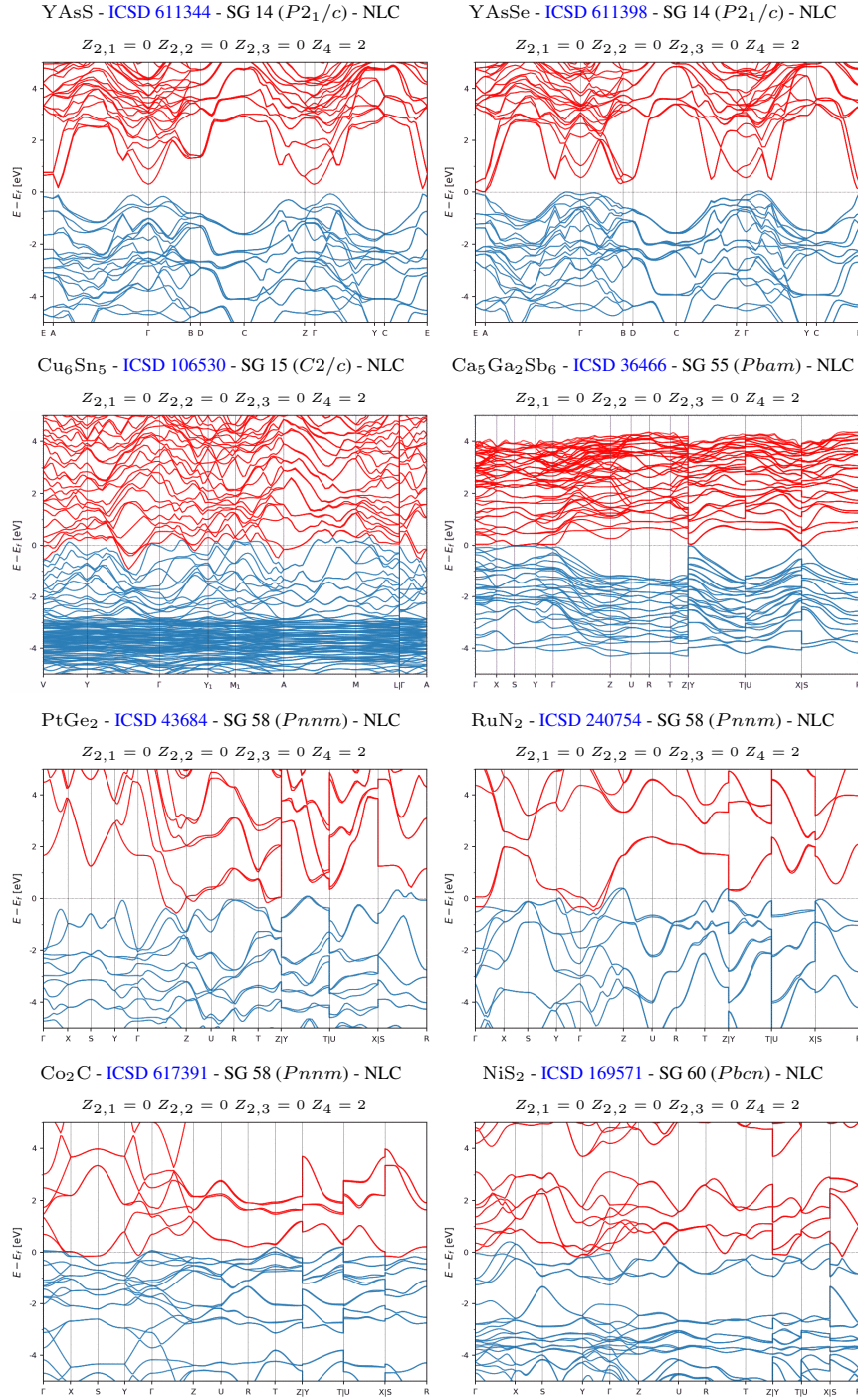


Figure S20. The NLC-classified, inversion-symmetry-indicated HOTIs with the largest band gaps or the fewest and smallest bulk Fermi pockets. (part 2/6)

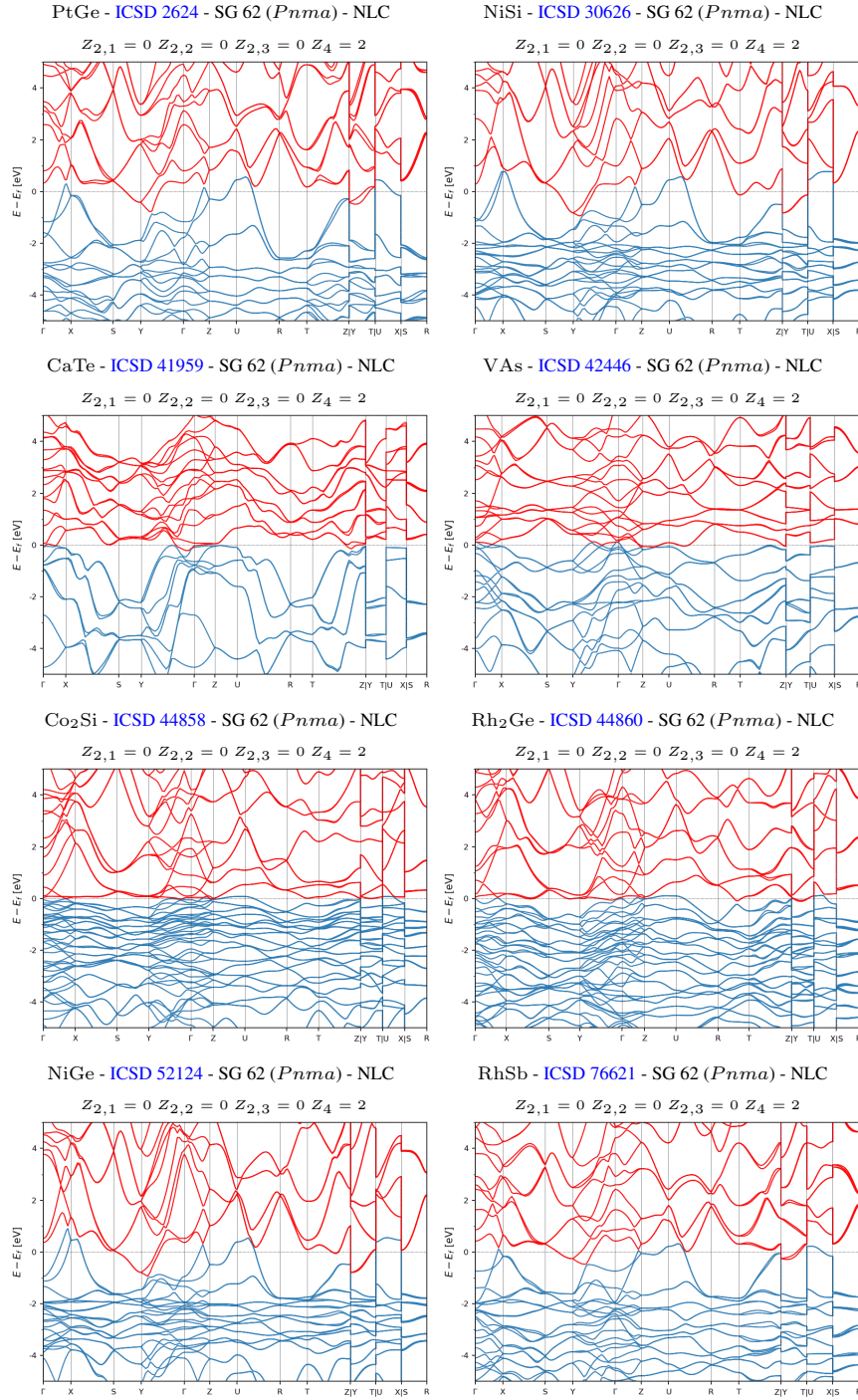


Figure S21. The NLC-classified, inversion-symmetry-indicated HOTIs with the largest band gaps or the fewest and smallest bulk Fermi pockets. (part 3/6)

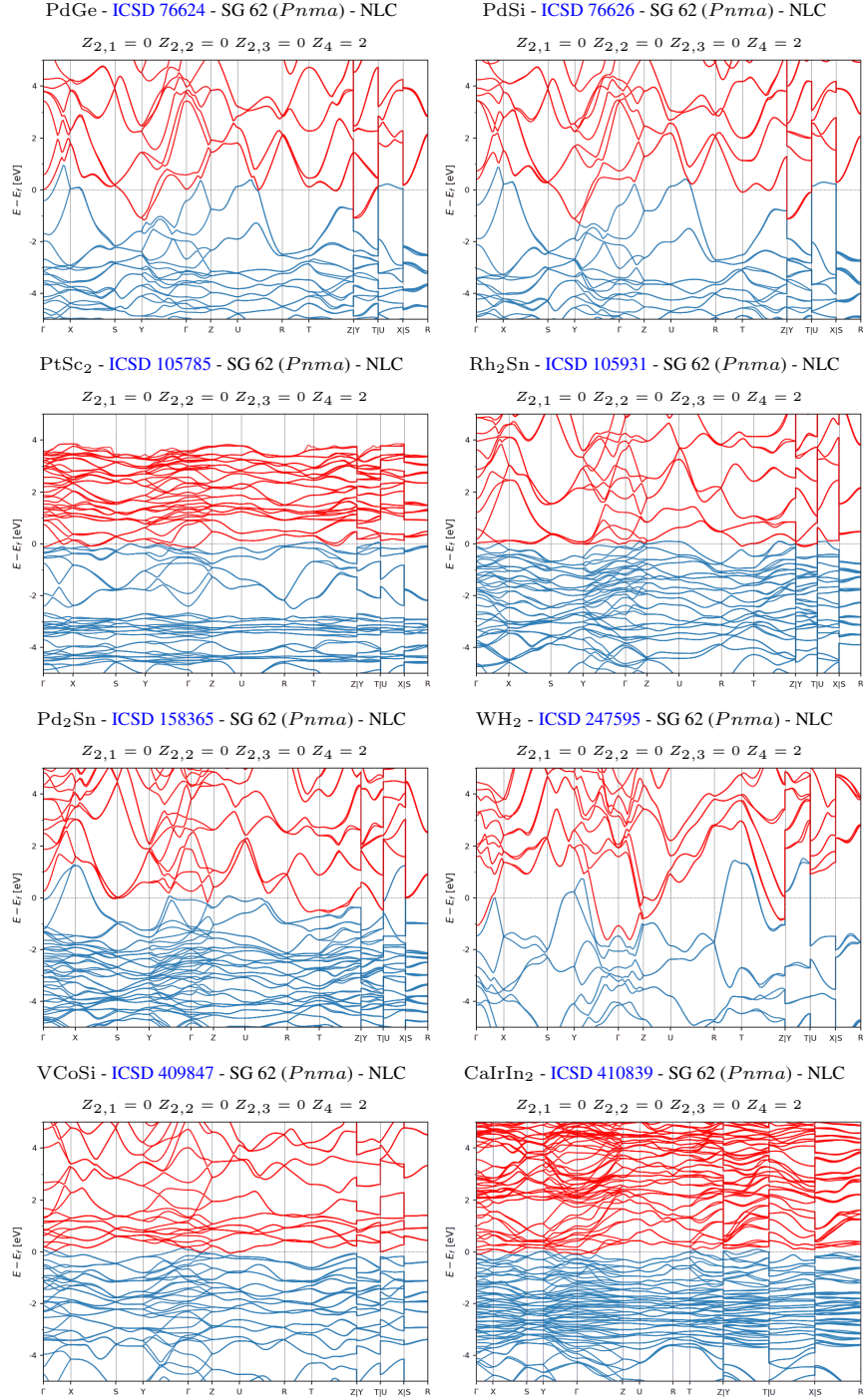


Figure S22. The NLC-classified, inversion-symmetry-indicated HOTIs with the largest band gaps or the fewest and smallest bulk Fermi pockets. (part 4/6)

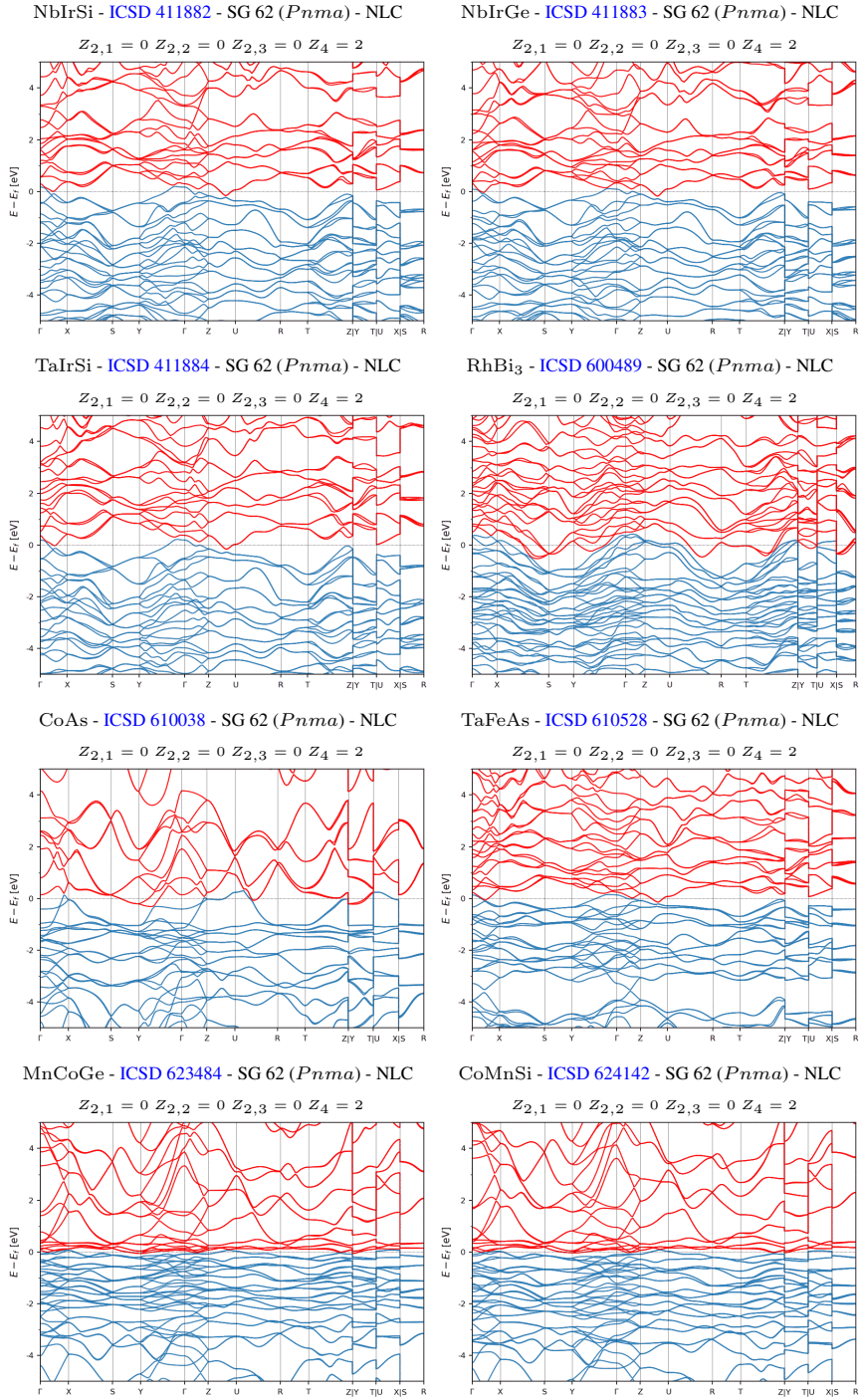


Figure S23. The NLC-classified, inversion-symmetry-indicated HOTIs with the largest band gaps or the fewest and smallest bulk Fermi pockets. (part 5/6)

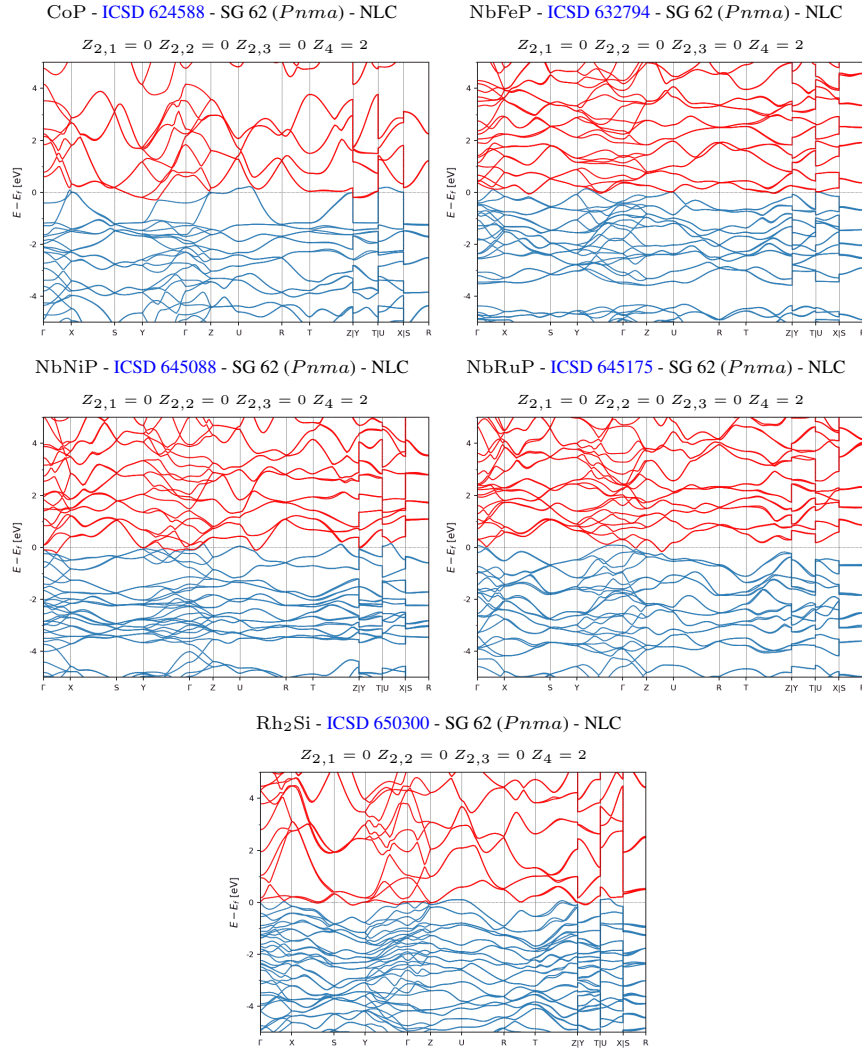


Figure S24. The NLC-classified, inversion-symmetry-indicated HOTIs with the largest band gaps or the fewest and smallest bulk Fermi pockets. (part 6/6)

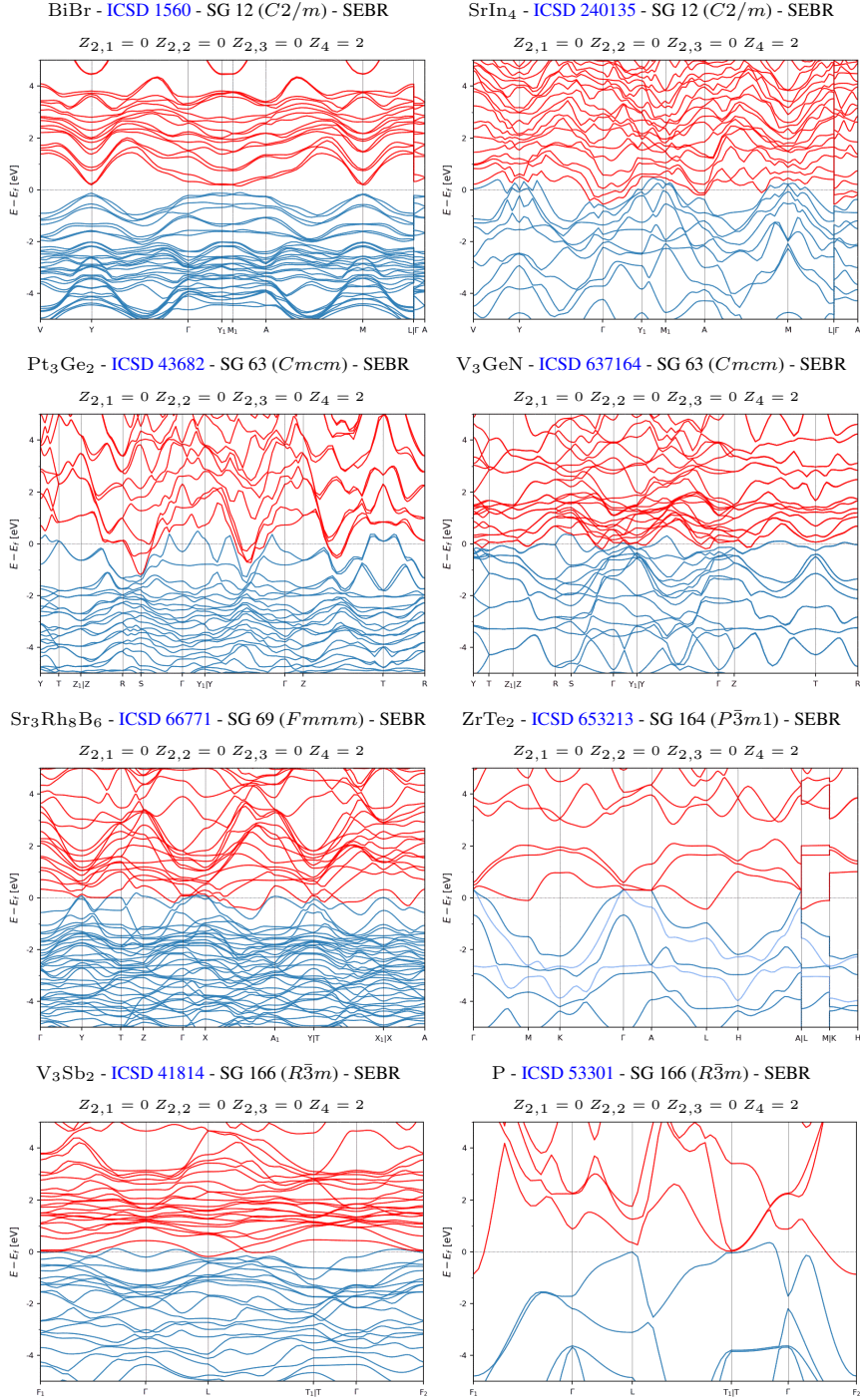


Figure S25. The SEBR-classified, inversion-symmetry-indicated HOTIs with the largest band gaps or the fewest and smallest bulk Fermi pockets. (part 1/2)

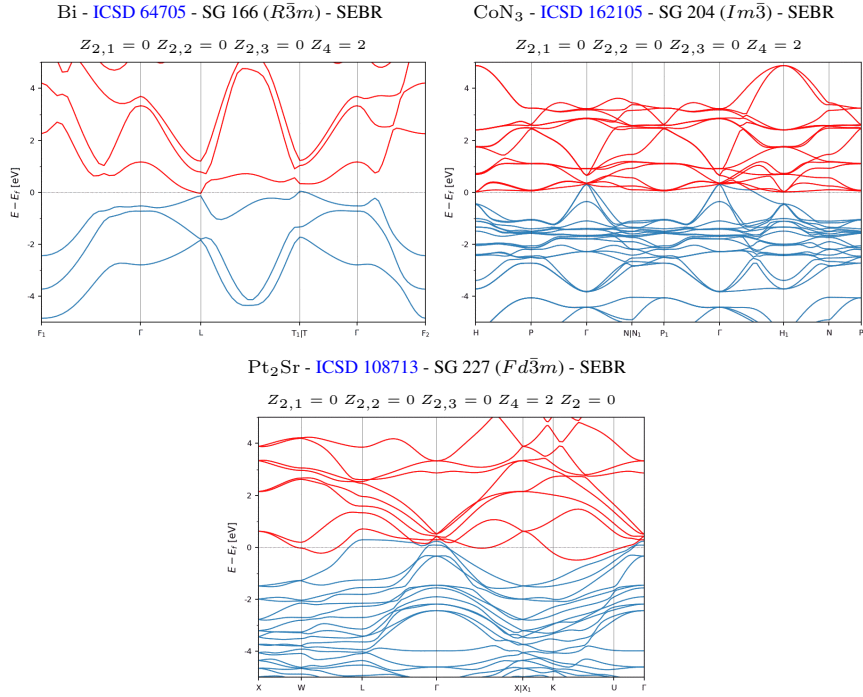


Figure S26. The SEBR-classified, inversion-symmetry-indicated HOTIs with the largest band gaps or the fewest and smallest bulk Fermi pockets. (part 2/2)

#### 4. Inversion-Symmetry-Indicated Weak TIs and TCIs

In this section, we list the inversion-symmetry-indicated weak TIs and TCIs with the largest bulk gaps or the fewest and smallest bulk Fermi pockets. Like the HOTIs previously listed in S11 A 3, the weak TIs and TCIs listed in this section have 2D surfaces with even numbers of massless or massive twofold Dirac cones, depending on the Miller indices of the surfaces [5, 30, 147, 148]. In terms of the indices introduced in Ref. [16], the materials in this section are characterized by  $Z_4 = 2$ , and exhibit nontrivial values for some or all other independent stable SIs. First, in Figs. S27 and S28, we list the weak TIs and TCIs classified as NLC, and then, in Figs. S29, S30, S31, S32, S33, S34, S35, S36, S37, S38, S39, S40, S41, and S42, we list the weak TIs and TCIs classified as SEBR. The materials listed in this section include the experimentally confirmed weak TI BiI [ICSD 1559, SG 12 ( $C2/m$ )] [179, 182, 183, 190], which is classified as SEBR.

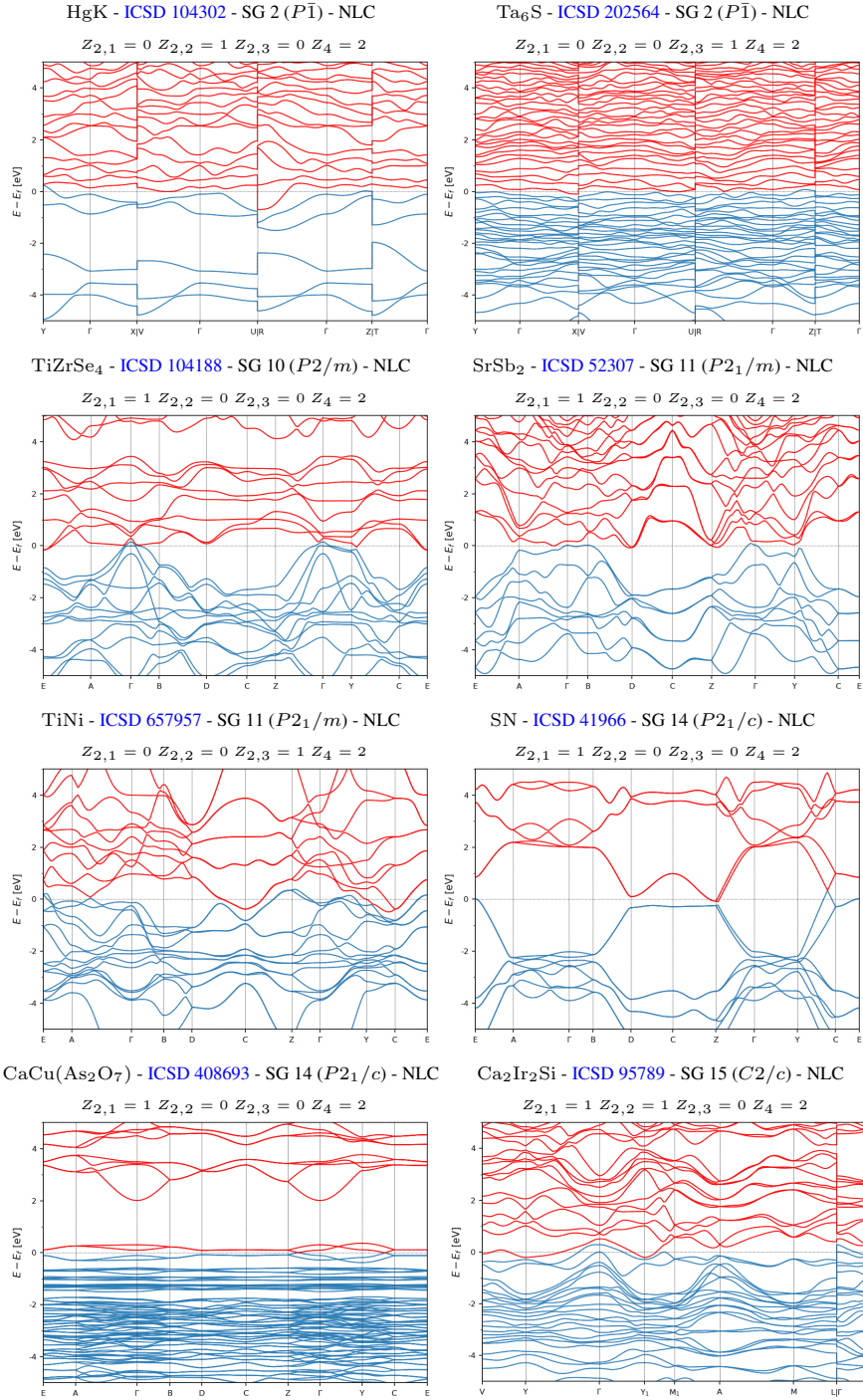


Figure S27. The NLC-classified, inversion-symmetry-indicated weak TIs and TCIs with the largest band gaps or the fewest and smallest bulk Fermi pockets. (part 1/2)

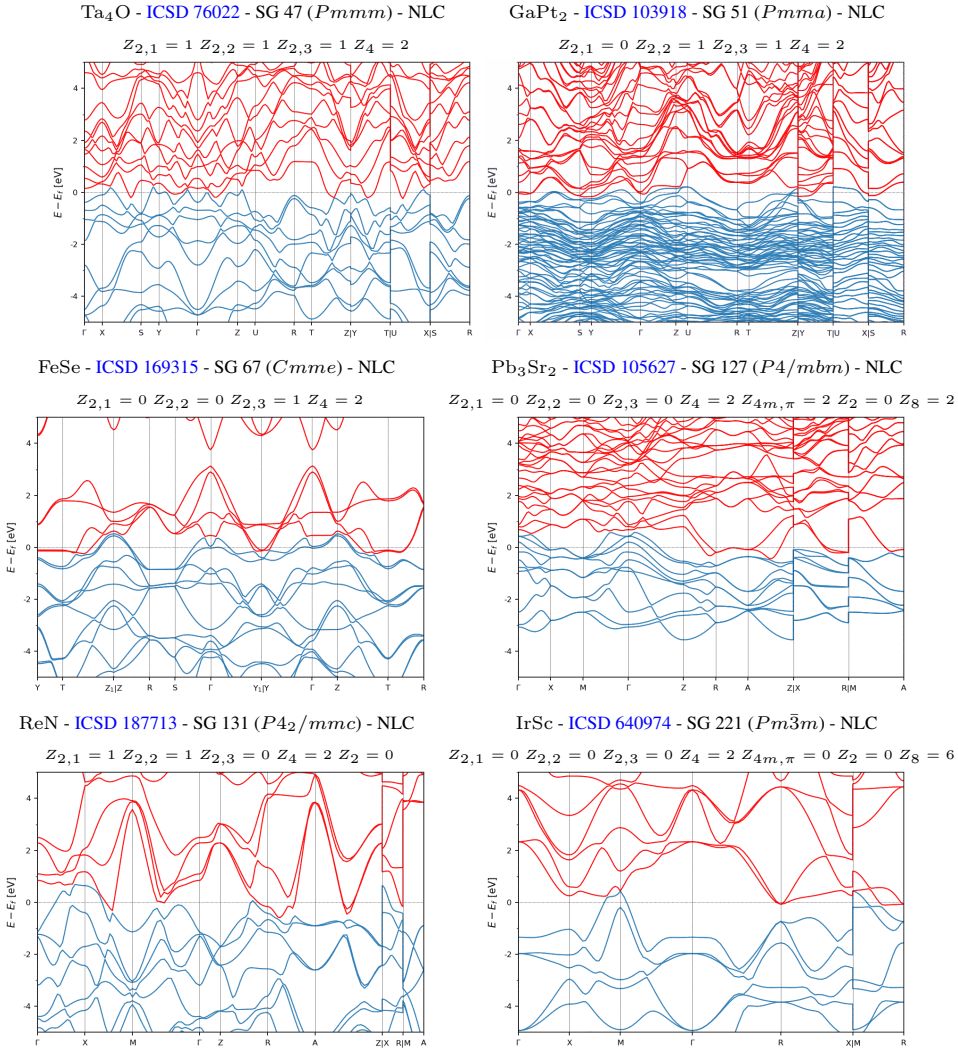


Figure S28. The NLC-classified, inversion-symmetry-indicated weak TIs and TCIs with the largest band gaps or the fewest and smallest bulk Fermi pockets. (part 2/2)

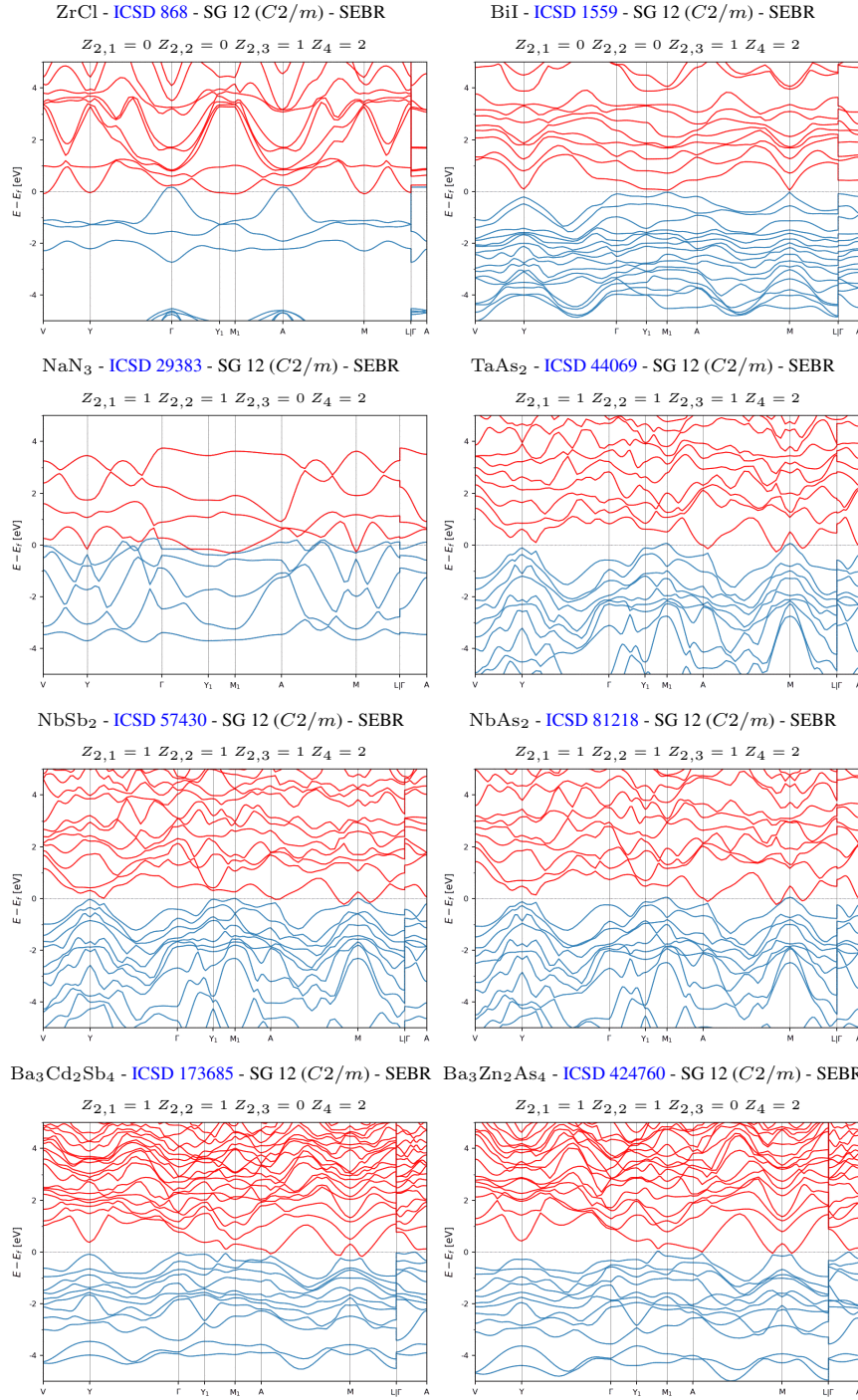


Figure S29. The SEBR-classified, inversion-symmetry-indicated weak TIs and TCIs with the largest band gaps or the fewest and smallest bulk Fermi pockets. (part 1/14)

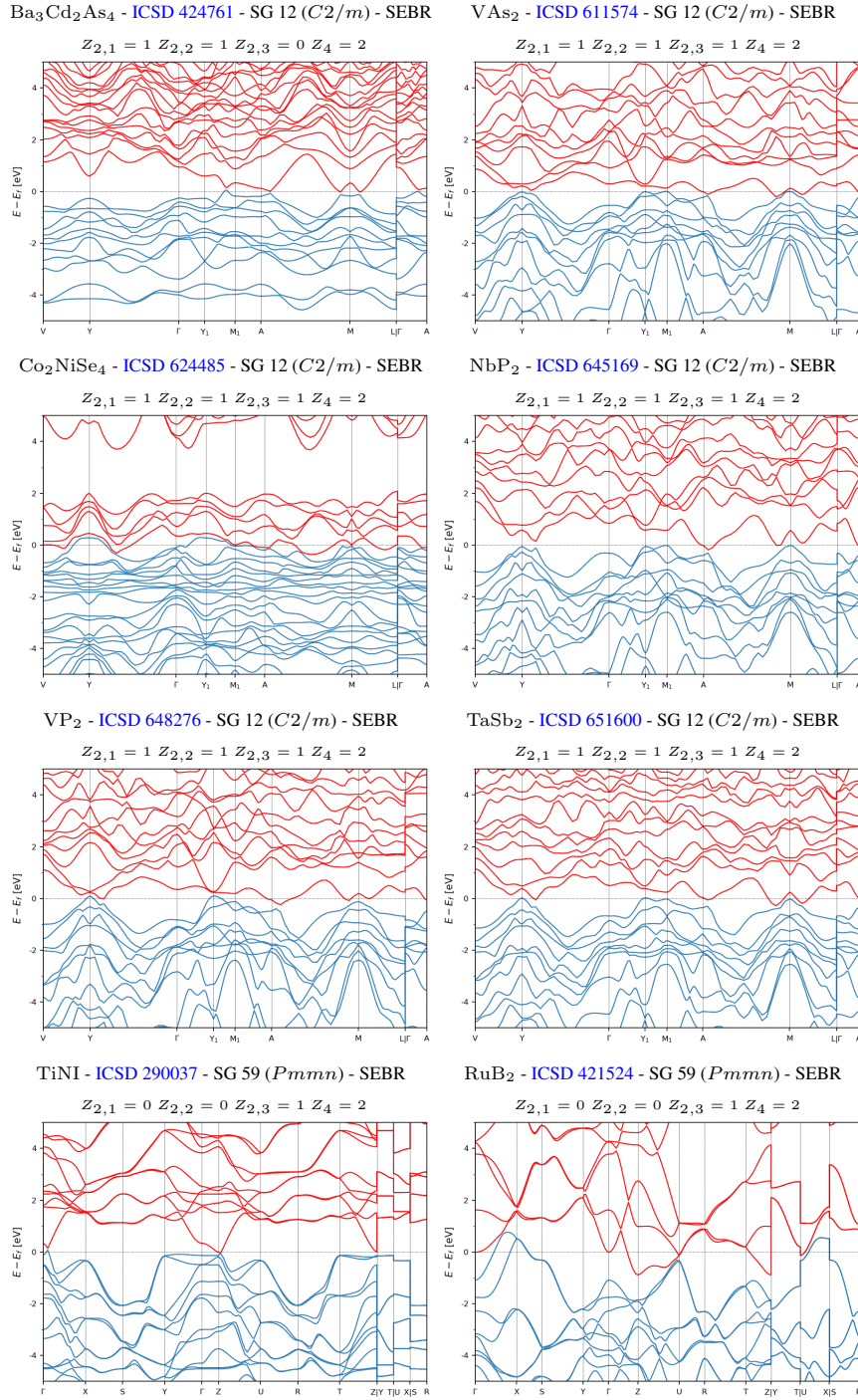


Figure S30. The SEBR-classified, inversion-symmetry-indicated weak TIs and TCIs with the largest band gaps or the fewest and smallest bulk Fermi pockets. (part 2/14)

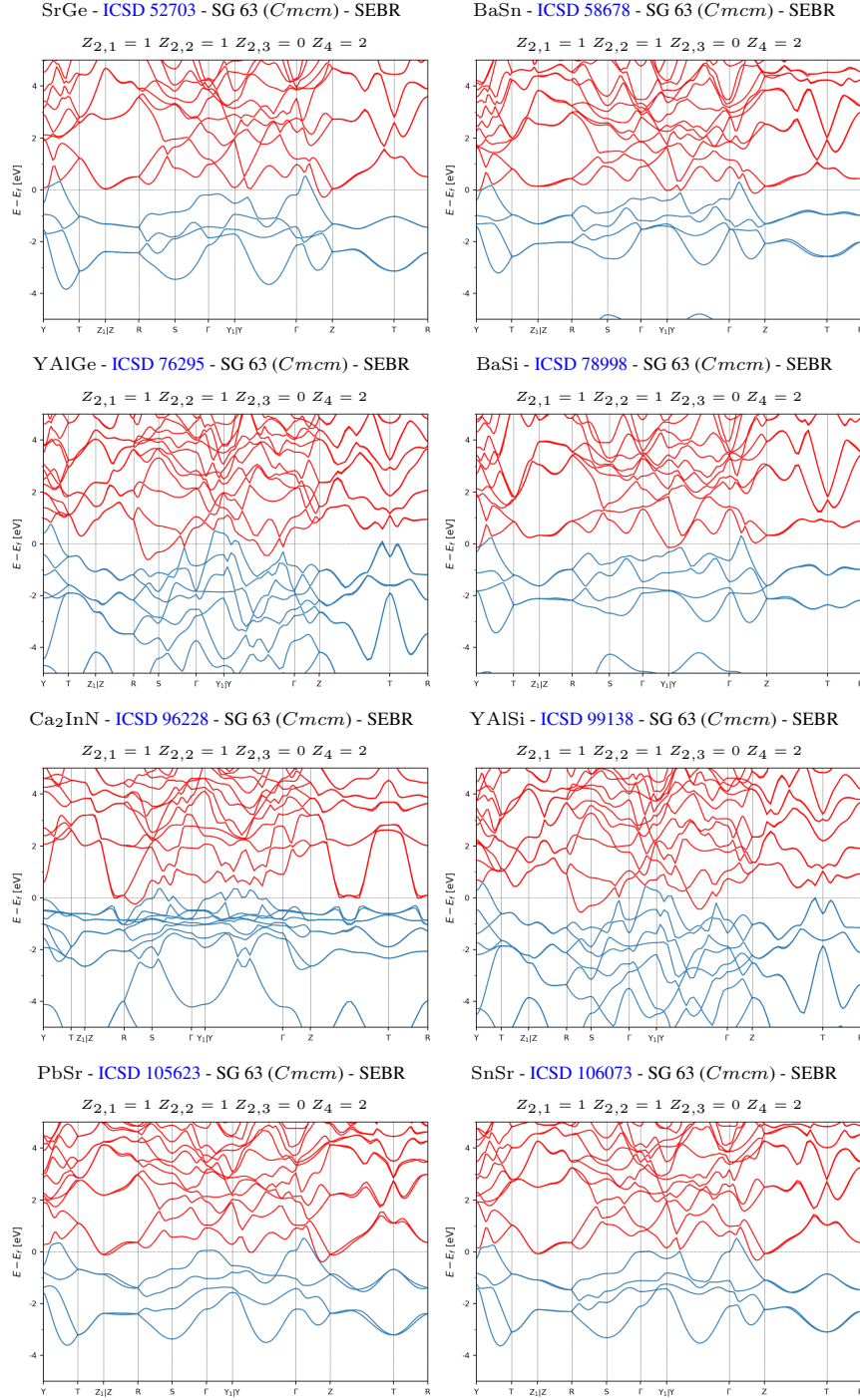


Figure S31. The SEBR-classified, inversion-symmetry-indicated weak TIs and TCIs with the largest band gaps or the fewest and smallest bulk Fermi pockets. (part 3/14)

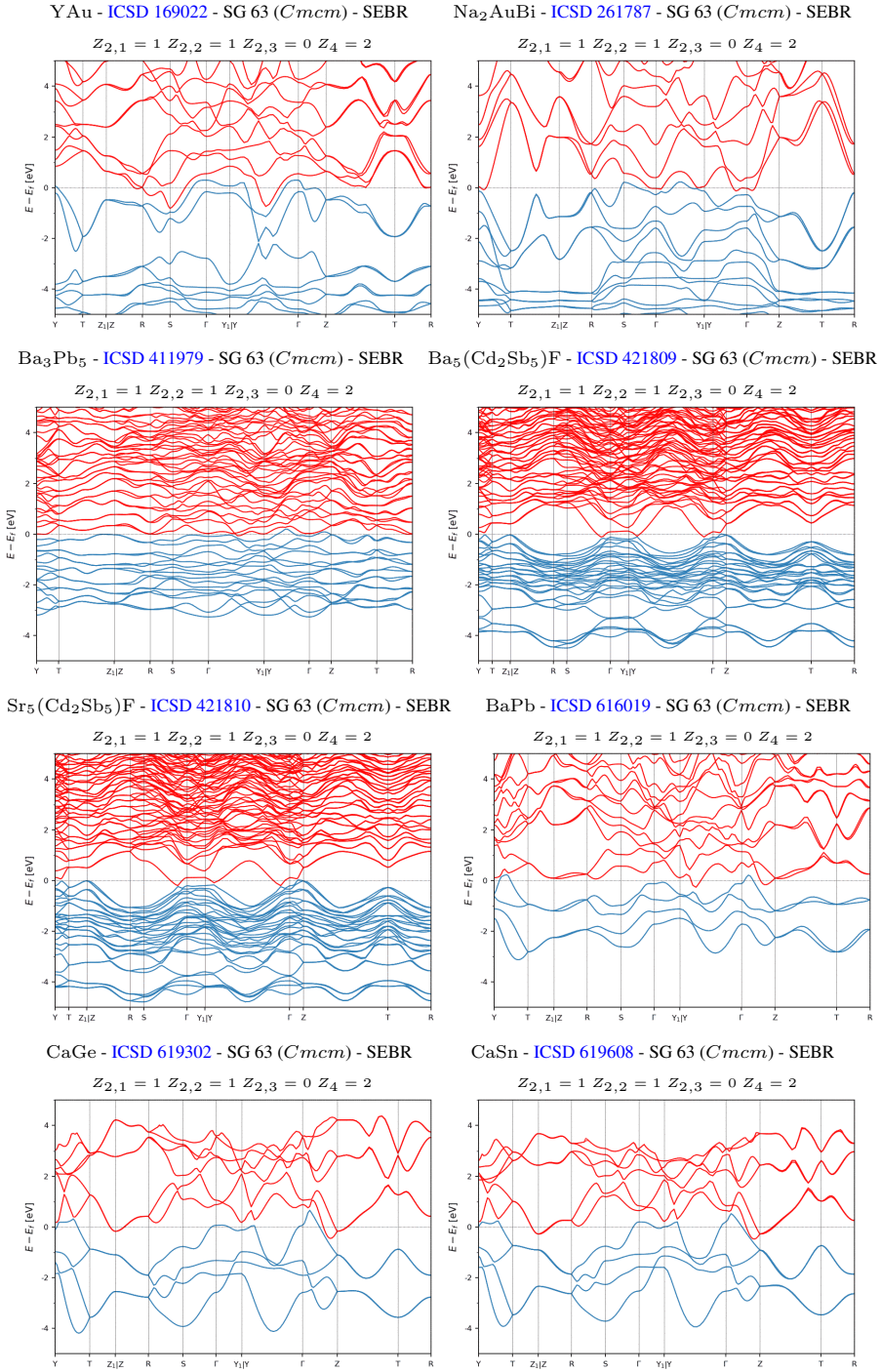


Figure S32. The SEBR-classified, inversion-symmetry-indicated weak TIs and TCIs with the largest band gaps or the fewest and smallest bulk Fermi pockets. (part 4/14)

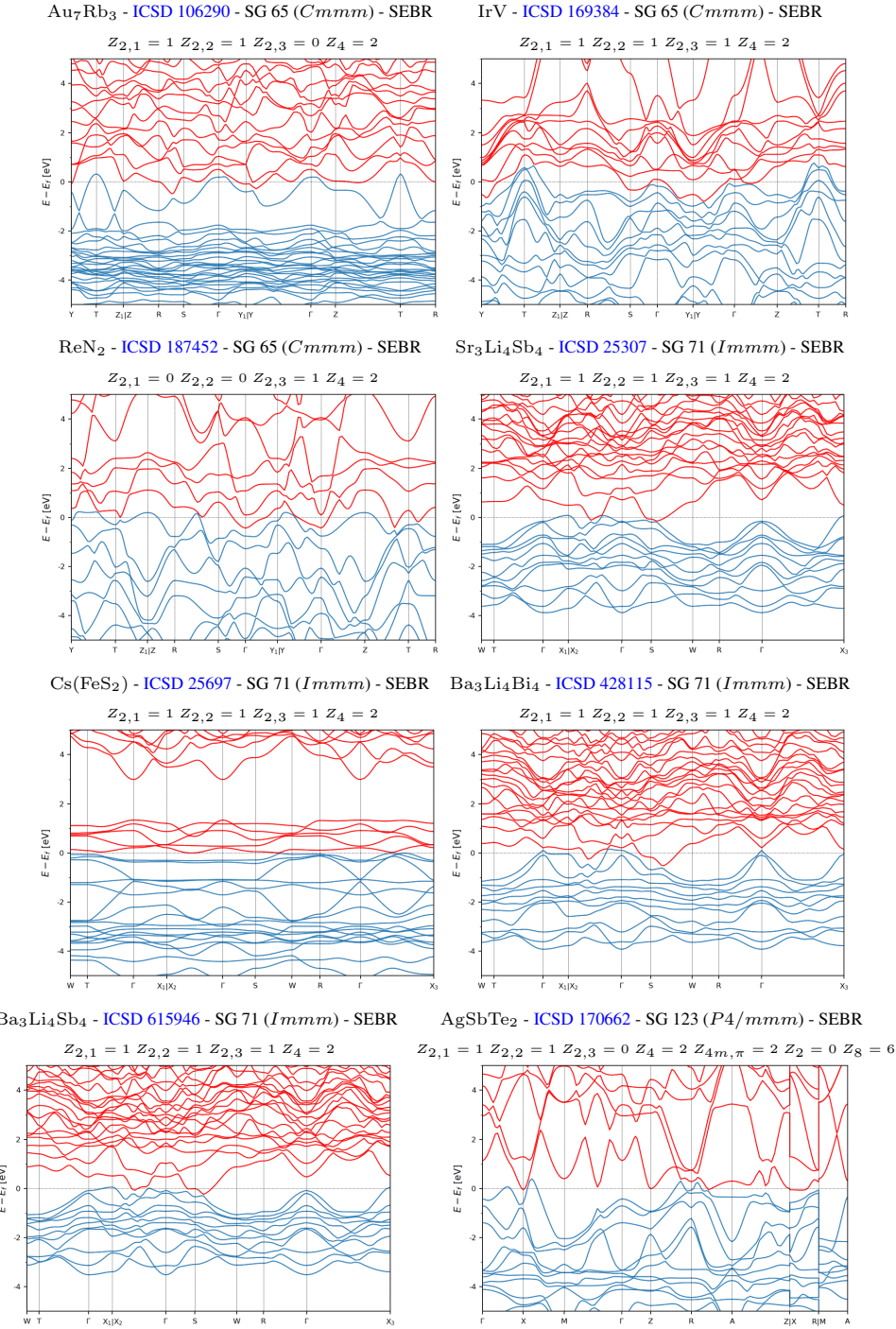


Figure S33. The SEBR-classified, inversion-symmetry-indicated weak TIs and TCIs with the largest band gaps or the fewest and smallest bulk Fermi pockets. (part 5/14)

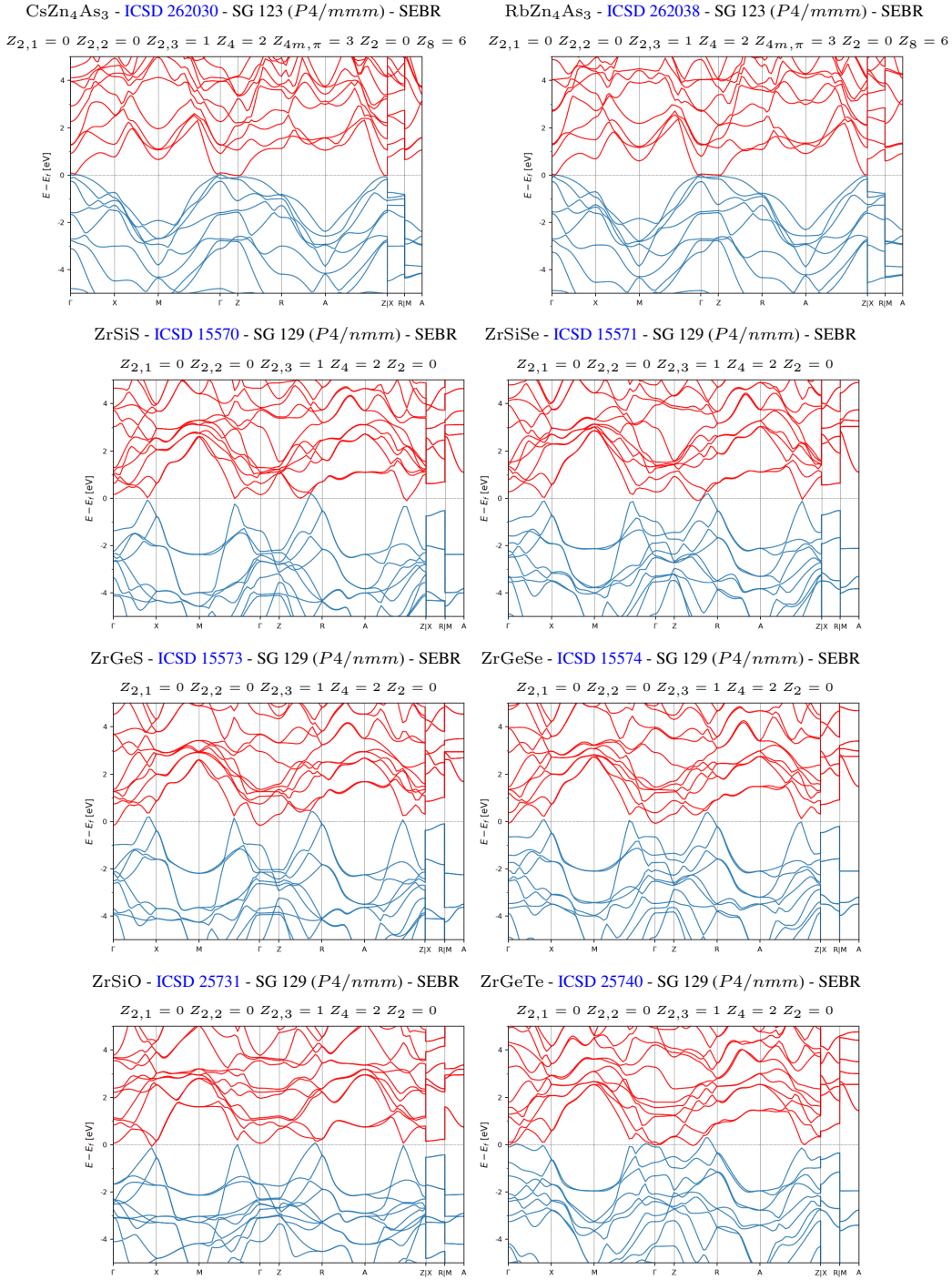
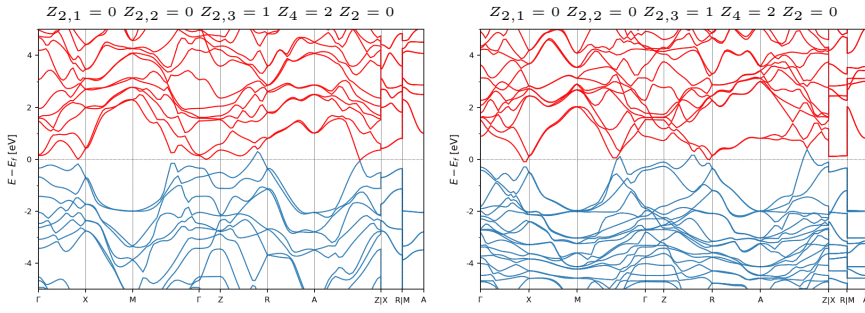
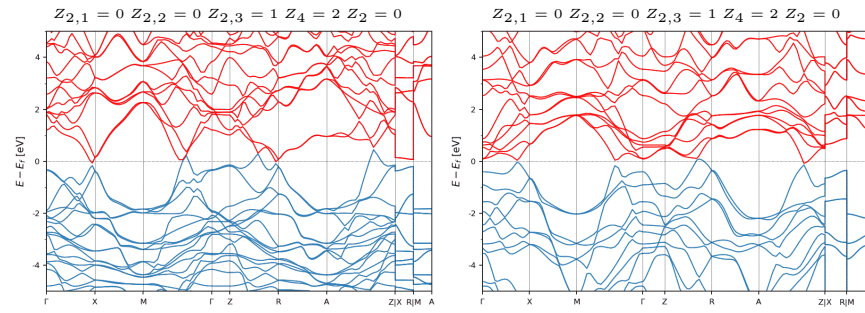


Figure S34. The SEBR-classified, inversion-symmetry-indicated weak TIs and TCIs with the largest band gaps or the fewest and smallest bulk Fermi pockets. (part 6/14)

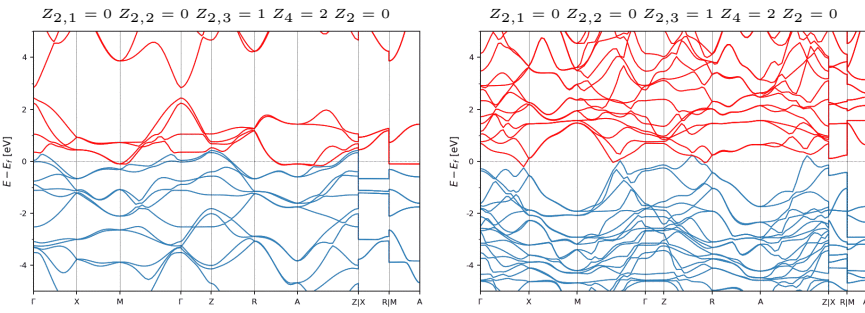
HfGeTe - ICSD 25743 - SG 129 ( $P4/nmm$ ) - SEBR ZrCuSiAs - ICSD 42165 - SG 129 ( $P4/nmm$ ) - SEBR



ZrCuSiP - ICSD 59594 - SG 129 ( $P4/nmm$ ) - SEBR ZrSnTe - ICSD 80190 - SG 129 ( $P4/nmm$ ) - SEBR



FeSe - ICSD 169269 - SG 129 ( $P4/nmm$ ) - SEBR TiCuSiAs - ICSD 185854 - SG 129 ( $P4/nmm$ ) - SEBR



TiCuGeAs - ICSD 185857 - SG 129 ( $P4/nmm$ ) - SEBR ZrCuGeAs - ICSD 185858 - SG 129 ( $P4/nmm$ ) - SEBR

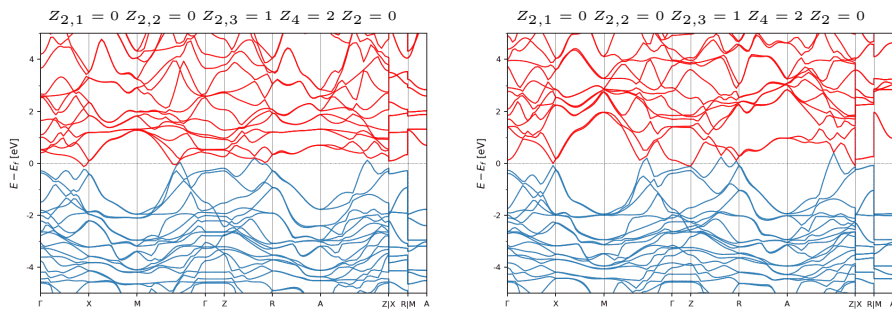


Figure S35. The SEBR-classified, inversion-symmetry-indicated weak TIs and TCIs with the largest band gaps or the fewest and smallest bulk Fermi pockets. (part 7/14)

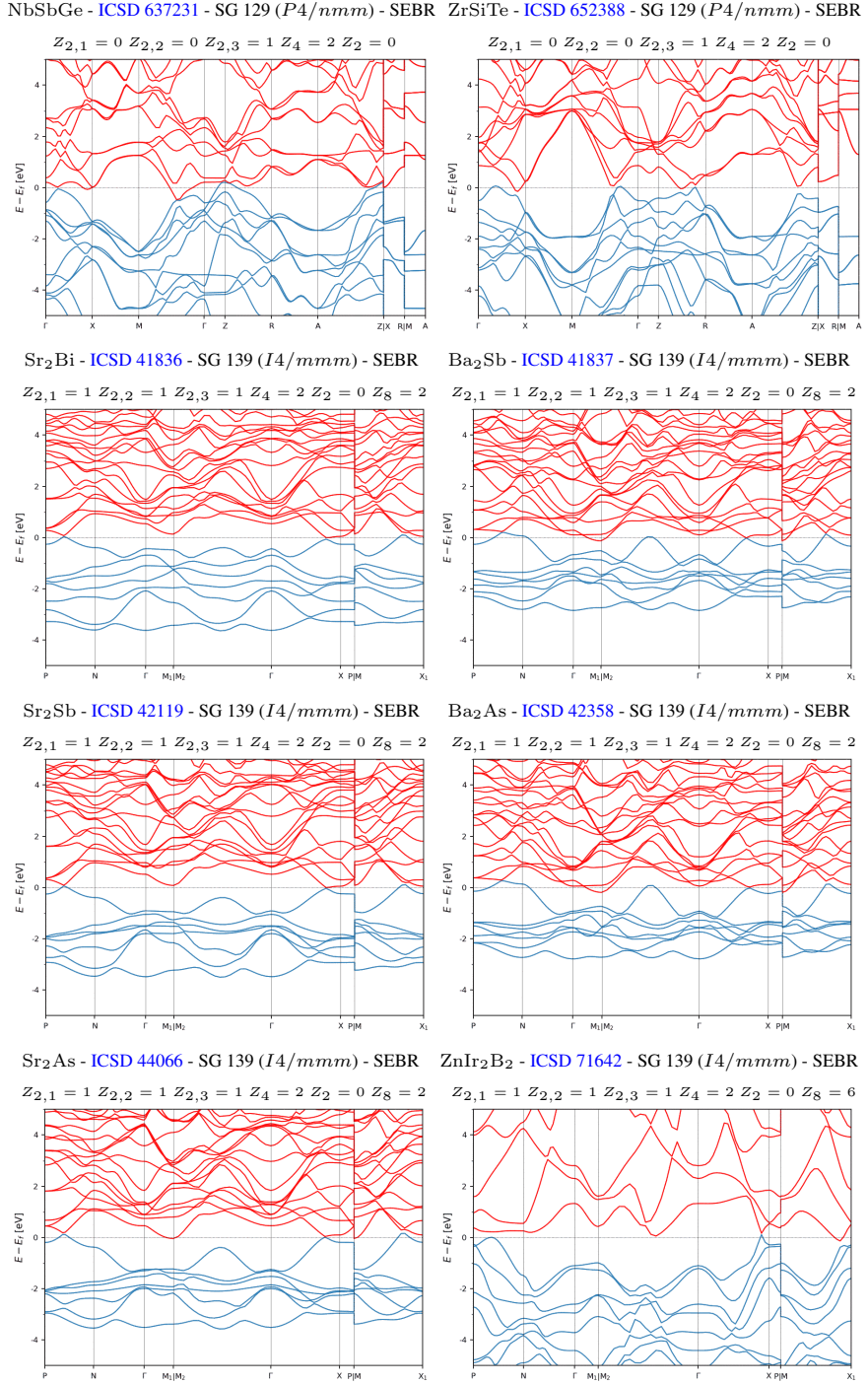


Figure S36. The SEBR-classified, inversion-symmetry-indicated weak TIs and TCIs with the largest band gaps or the fewest and smallest bulk Fermi pockets. (part 8/14)

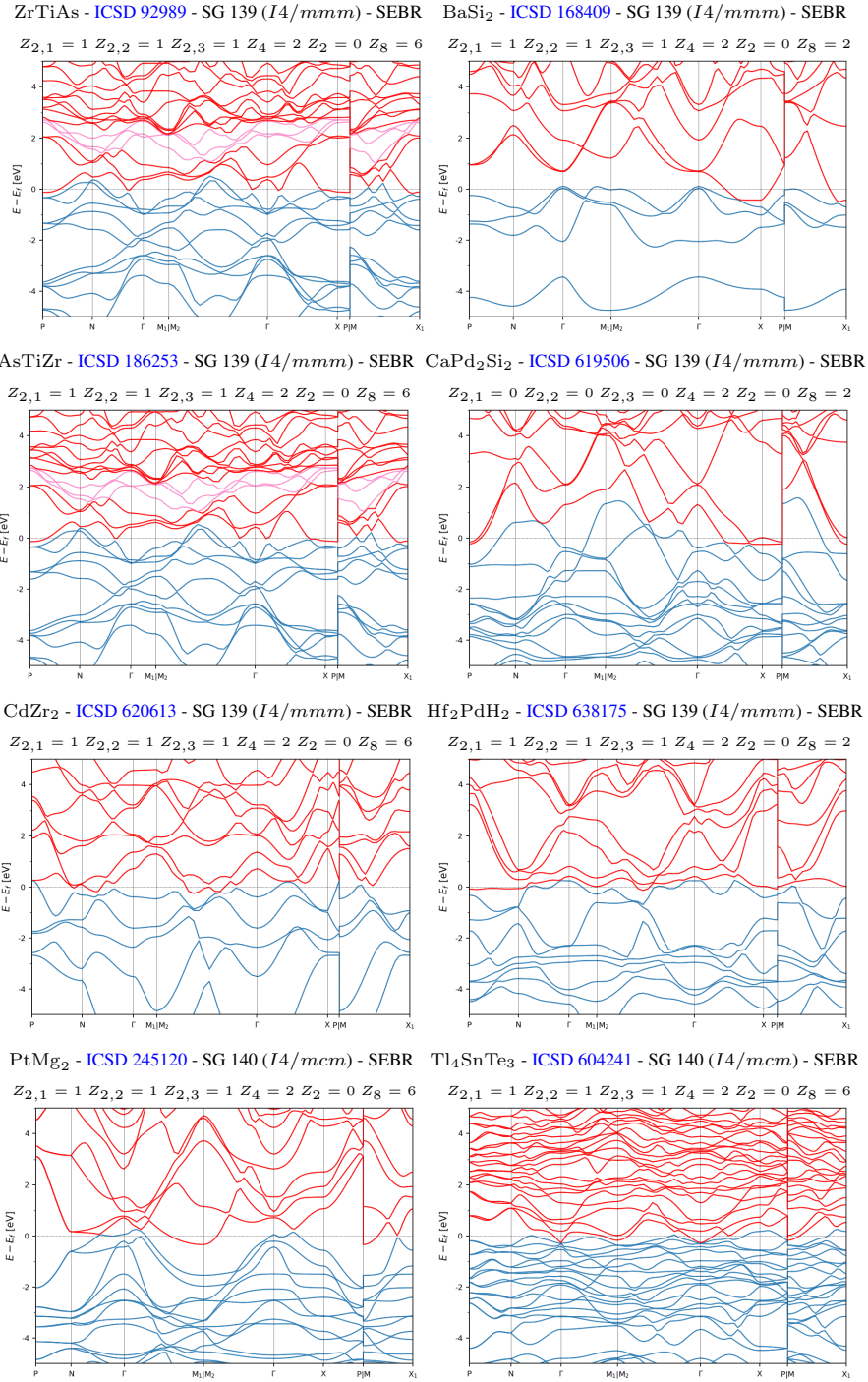


Figure S37. The SEBR-classified, inversion-symmetry-indicated weak TIs and TCIs with the largest band gaps or the fewest and smallest bulk Fermi pockets. (part 9/14)

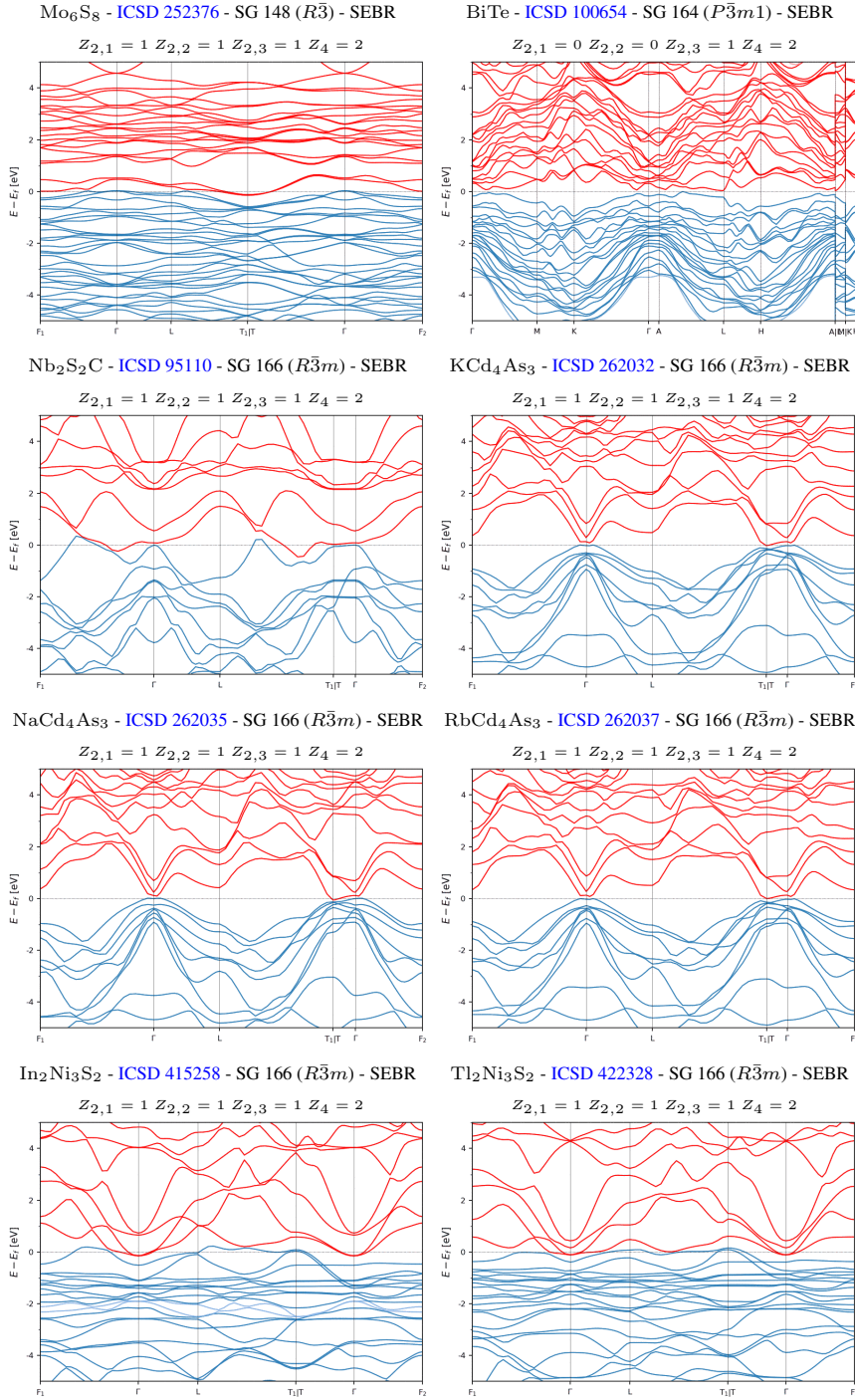


Figure S38. The SEBR-classified, inversion-symmetry-indicated weak TIs and TCIs with the largest band gaps or the fewest and smallest bulk Fermi pockets. (part 10/14)

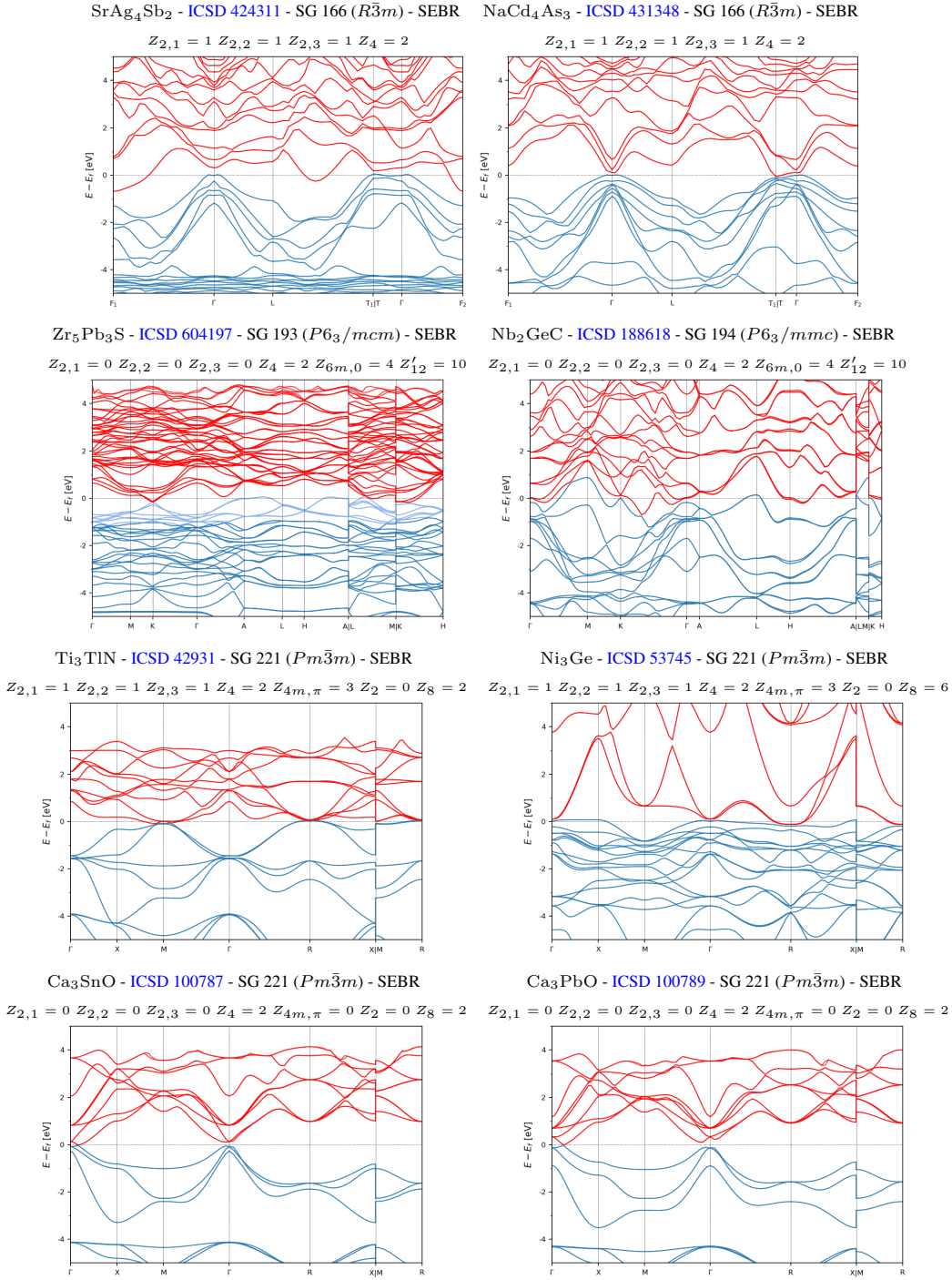


Figure S39. The SEBR-classified, inversion-symmetry-indicated weak TIs and TCIs with the largest band gaps or the fewest and smallest bulk Fermi pockets. (part 11/14)

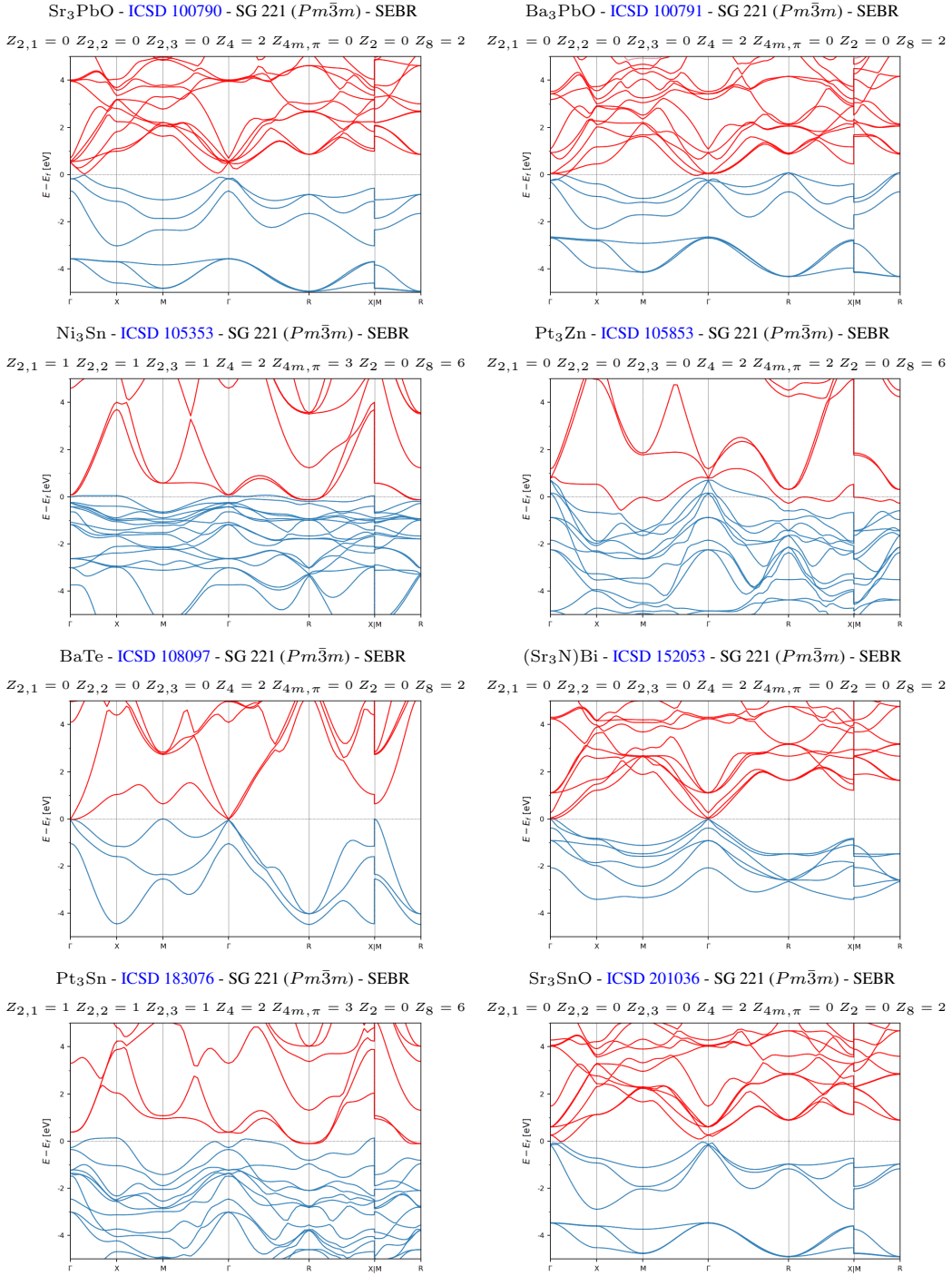


Figure S40. The SEBR-classified, inversion-symmetry-indicated weak TIs and TCIs with the largest band gaps or the fewest and smallest bulk Fermi pockets. (part 12/14)

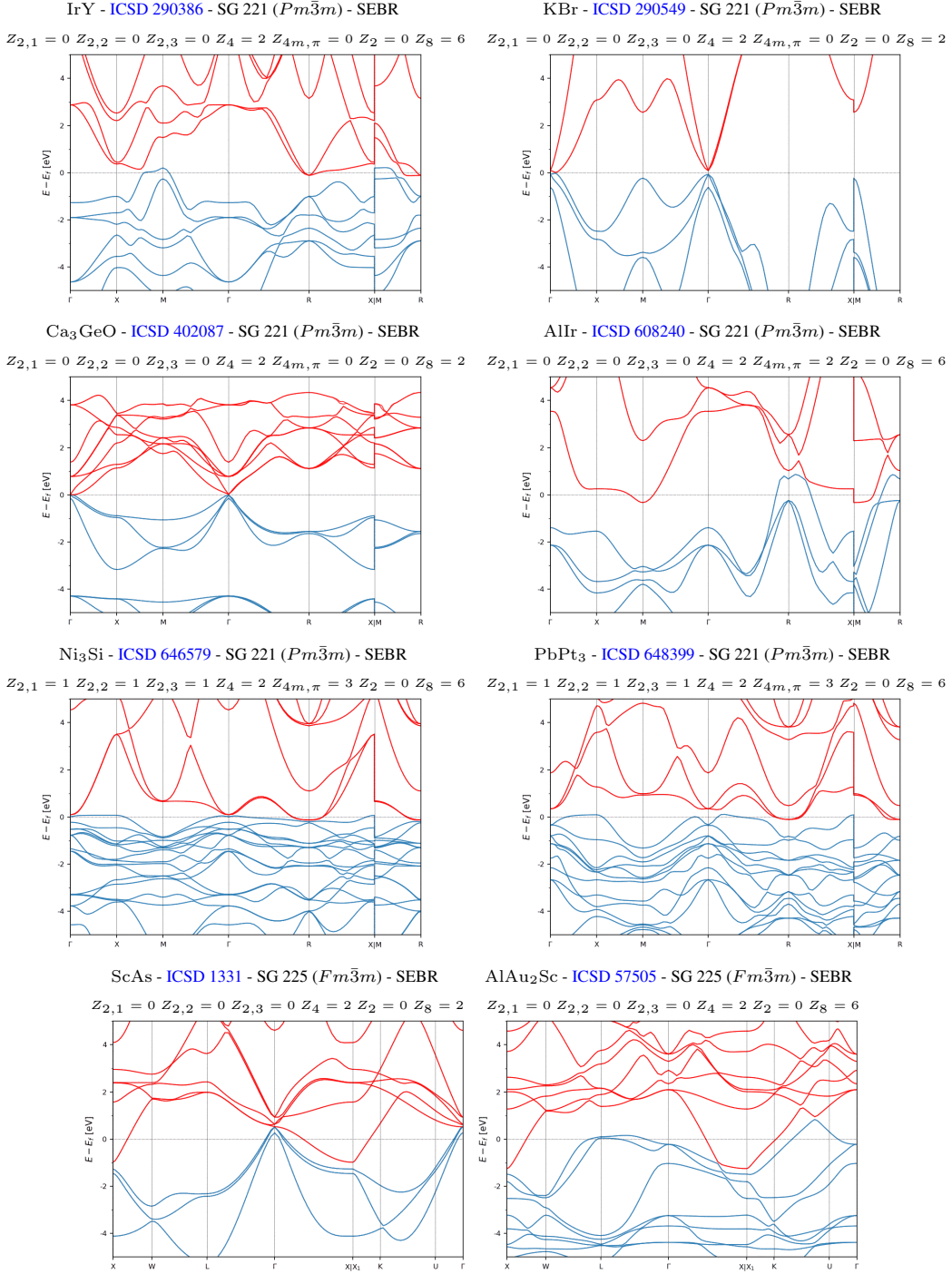


Figure S41. The SEBR-classified, inversion-symmetry-indicated weak TIs and TCIs with the largest band gaps or the fewest and smallest bulk Fermi pockets. (part 13/14)

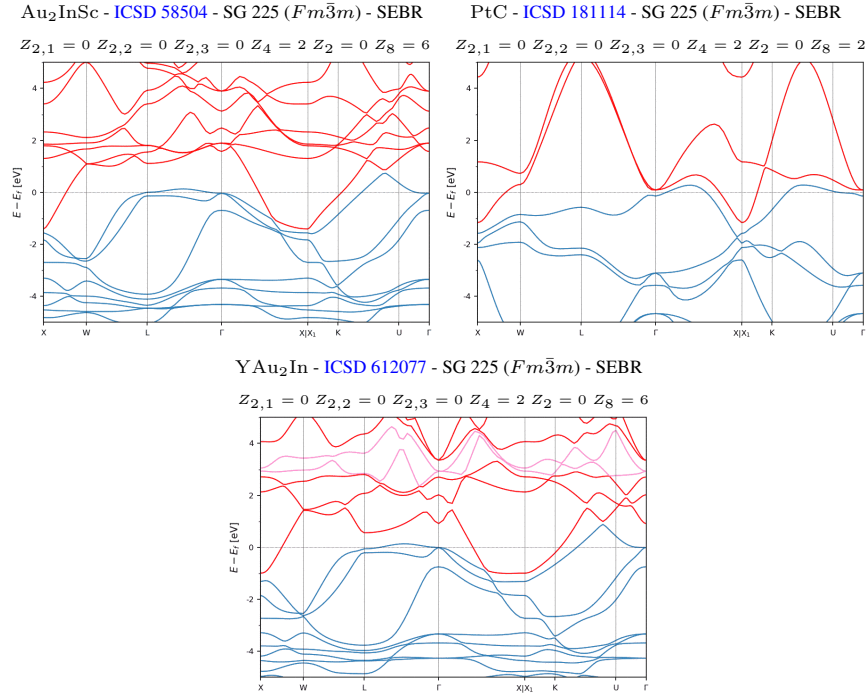


Figure S42. The SEBR-classified, inversion-symmetry-indicated weak TIs and TCIs with the largest band gaps or the fewest and smallest bulk Fermi pockets. (part 14/14)

### 5. Rotation-Anomaly TCIs and High-Fold-Rotation Mirror TCIs

In this section, we list the symmetry-indicated rotation-anomaly and high-fold-rotation mirror TCIs [16, 17, 87, 102, 105, 175] with the largest bulk gaps or the fewest and smallest bulk Fermi pockets. The TCIs listed in this section exhibit varying, even numbers of massless or massive twofold surface Dirac cones, depending on the Miller indices of the surfaces [16, 17, 87, 102, 105]. On the edges between gapped surfaces, helical hinge modes may also be present, depending on the crystallographic (Miller) indices of the hinges. In terms of the stable SIs introduced in Ref. [16], the materials in this section either exhibit  $Z_8 = 4$  or  $Z'_{12} = 6$ ; we do not find any examples of band insulators with  $Z_{12} = 6$  and few bulk Fermi pockets. First, in Fig. S43, we list the few sixfold-rotation-anomaly TCIs with  $Z'_{12} = 6$ , all of which are classified as SEBR. In Fig. S44, we then show the only TCI with  $Z_8 = 4$  and a relatively clean Fermi surface that is classified as NLC. Finally, in Figs. S45, S46, S47, and S48, we list the TCIs with  $Z_8 = 4$  that are classified as SEBR. The materials identified in this section include members of the well-studied SnTe family, including SnTe [ICSD 652759, SG 225 ( $Fm\bar{3}m$ )] [12, 16, 105, 161–163] – a prototypical fourfold rotation-anomaly TCI – and PbTe [ICSD 648615, SG 225 ( $Fm\bar{3}m$ )] [121, 164], which also appears as a fourfold-rotation anomaly TCI, depending on the choice of lattice parameters and DFT functionals. SnTe and PbTe are both classified as SEBR and thus appear in Figs. S47 and S48, respectively.

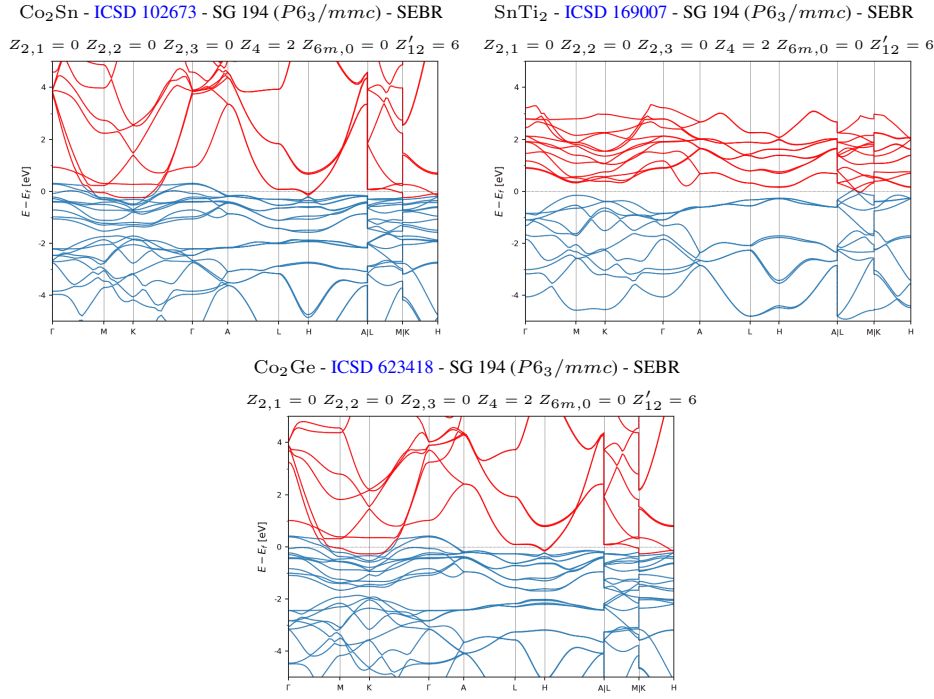


Figure S43. The sixfold-rotation-anomaly TCIs with the largest band gaps or the fewest and smallest bulk Fermi pockets. All of these materials exhibit  $Z'_{12} = 6$ , and are classified as SEBR.

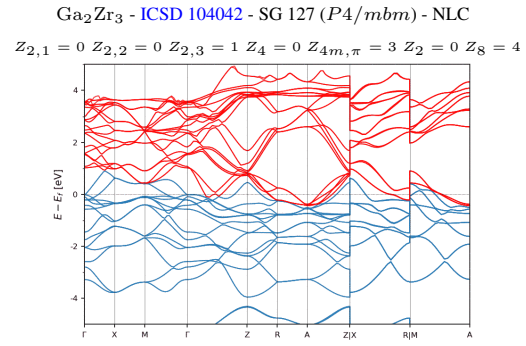


Figure S44. The NLC-classified, fourfold-rotation-anomaly weak TI characterized by  $Z_8 = 4$  with the fewest and smallest bulk Fermi pockets.

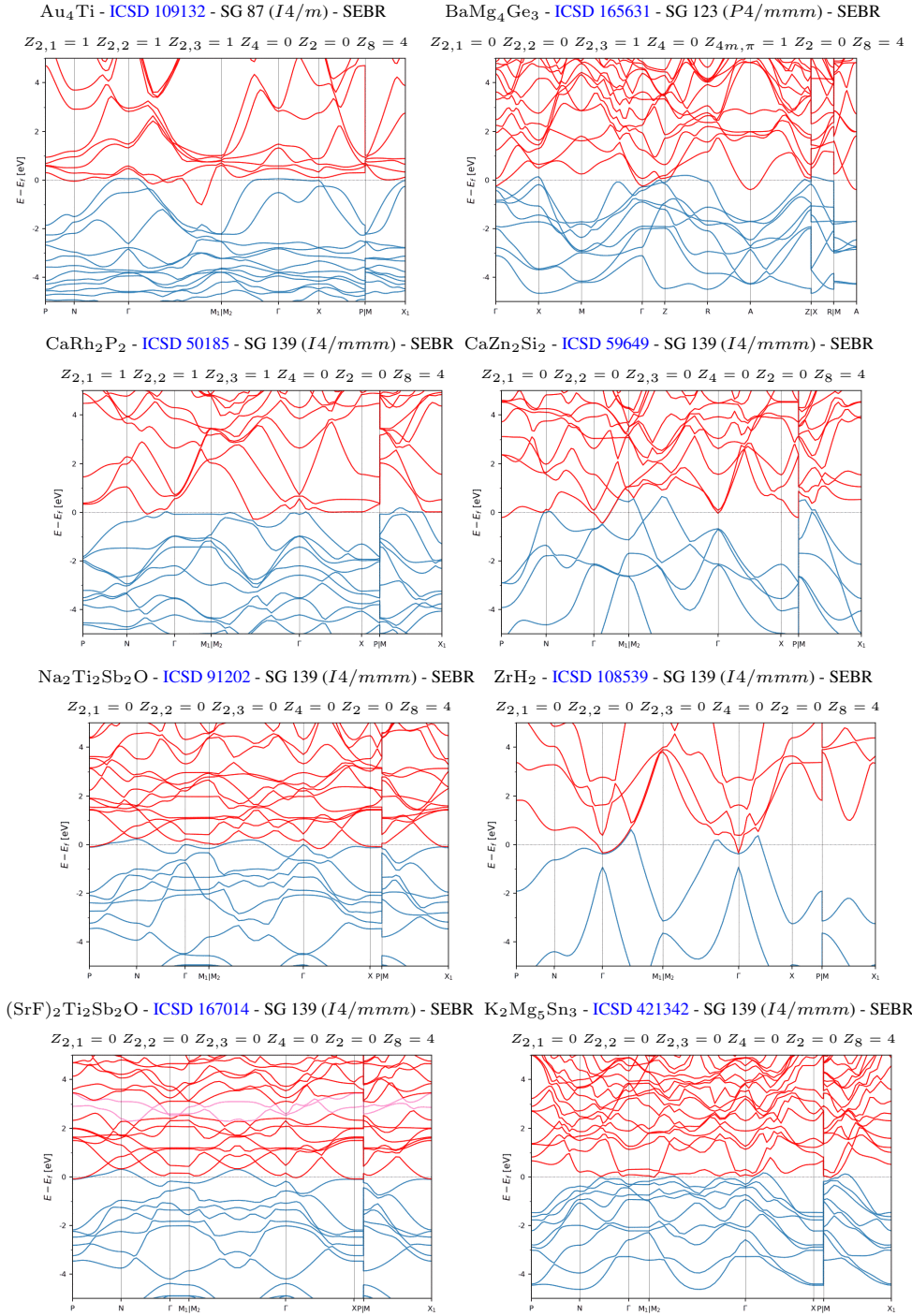


Figure S45. The SEBR-classified, fourfold-rotation-anomaly and mirror TCIs characterized by  $Z_8 = 4$  with the largest band gaps or the fewest and smallest bulk Fermi pockets. (part 1/4)

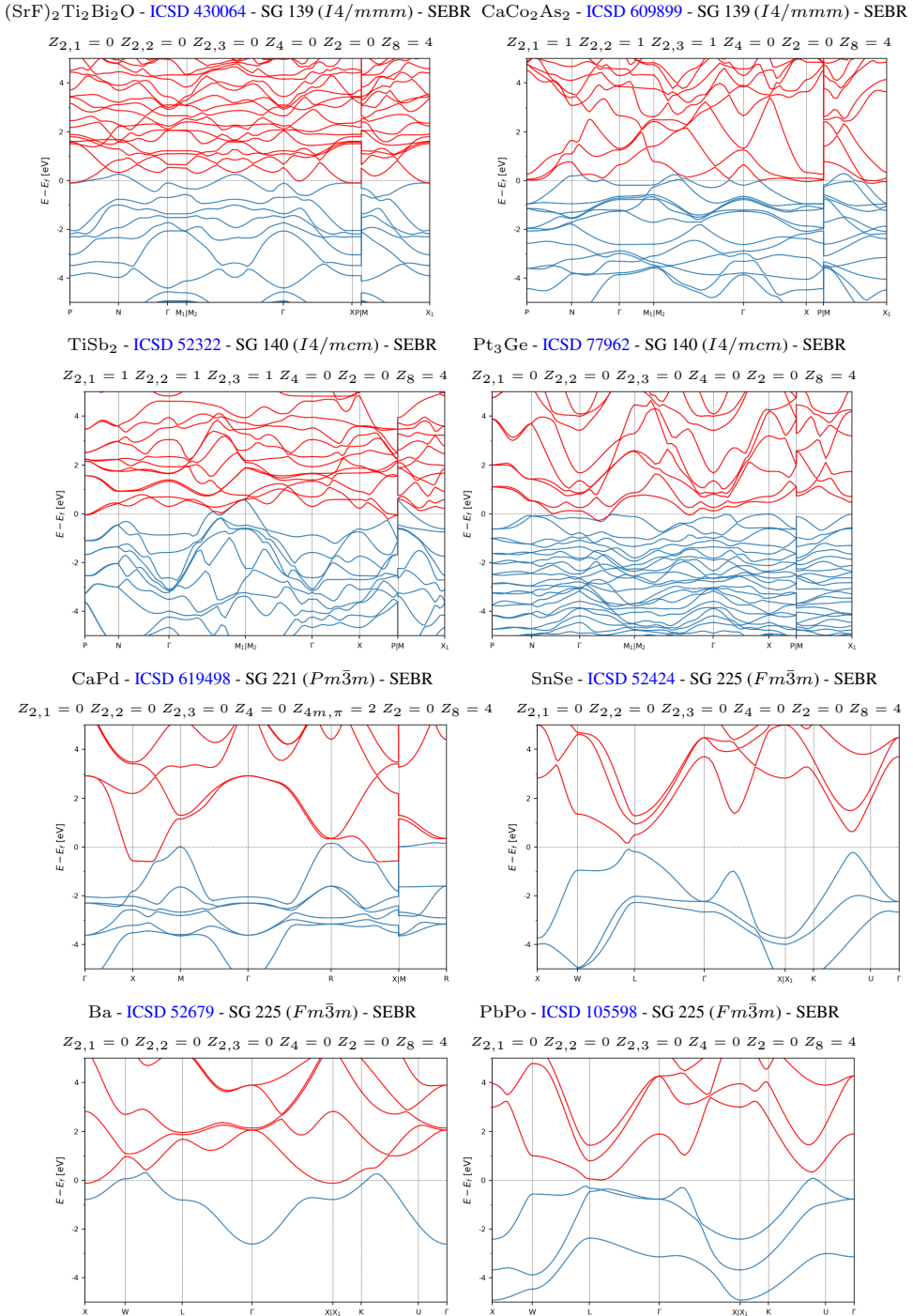


Figure S46. The SEBR-classified, fourfold-rotation-anomaly and mirror TCIs characterized by  $Z_8 = 4$  with the largest band gaps or the fewest and smallest bulk Fermi pockets. (part 2/4)

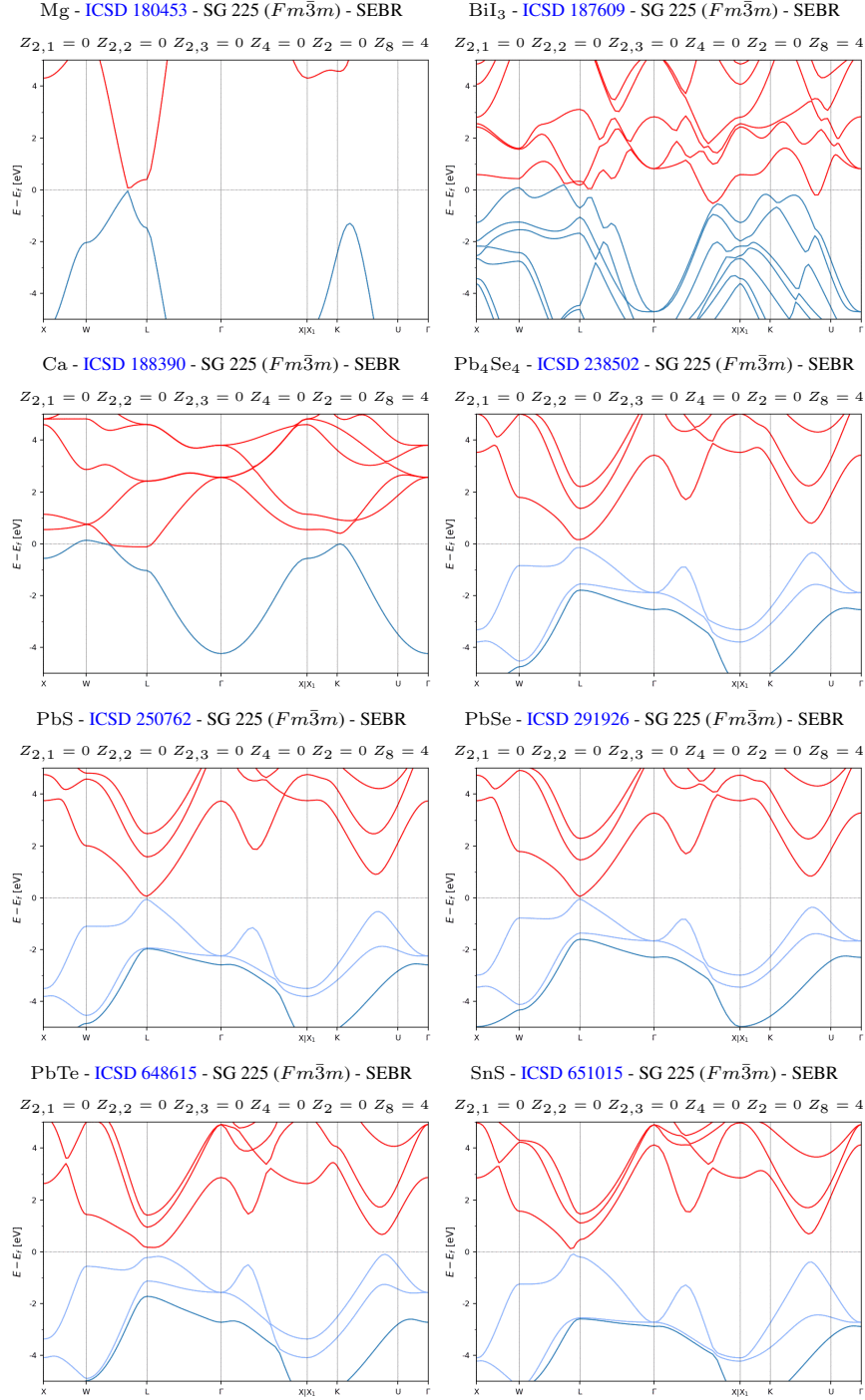


Figure S47. The SEBR-classified, fourfold-rotation-anomaly and mirror TCIs characterized by  $Z_8 = 4$  with the largest band gaps or the fewest and smallest bulk Fermi pockets. (part 3/4)

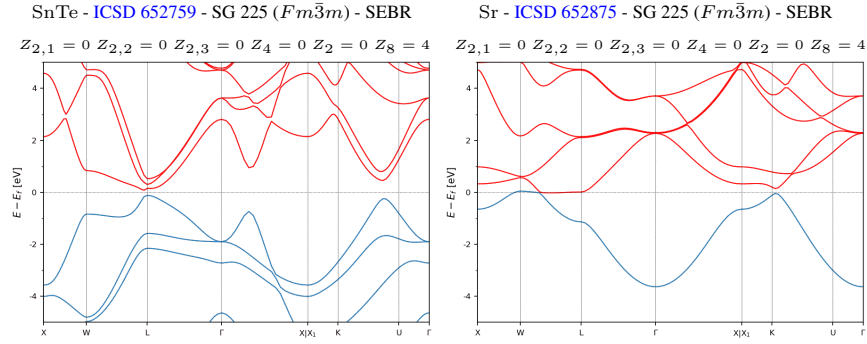


Figure S48. The SEBR-classified, fourfold-rotation-anomaly and mirror TCIs characterized by  $Z_8 = 4$  with the largest band gaps or the fewest and smallest bulk Fermi pockets. (part 4/4)

### 6. Other TCIs with Trivial $Z_4$ Indices

In this section, we list the remaining TCIs with trivial strong  $Z_4$  indices and nontrivial values for at least one other stable SI, and which have simple bulk Fermi surfaces or insulating gaps. In terms of the stable SIs introduced in Ref. [16], the materials listed in this section specifically exhibit  $Z_4 = 0$  and nontrivial values for at least one other stable SI, excluding the cases of  $Z_8 = 4$  or  $Z'_{12} = 6$ , which were previously addressed in S11A5. The TCIs listed in this section exhibit differing numbers of twofold surface Dirac cones, whose presence is indicated through a combination of weak indices and mirror and rotation-anomaly TCI indices.

Notably, a subset of the TCIs listed in this section exhibit completely trivial strong indices (*i.e.*  $Z_4 = 0$  without any other nontrivial strong indices). As shown in Refs. [16, 26, 149, 150], materials with  $Z_4 = 0$  and nontrivial weak indices realize “obstructed” weak-TI phases that differ from weak-TI phases by fractional lattice translation. Specifically, when the weak indices  $Z_{2,i}$  are nontrivial, the value of the strong index  $Z_4$  can be advanced by 2 (mod 4) by shifting the origin of the unit cell by half of a lattice translation along the direction of the weak-index vector. In an obstructed weak-TI phase, the bulk is topologically equivalent to a stack of 2D TIs oriented along the weak-index vector, but crucially a stack in which the 2D TI layers in each stack unit cell are displaced from the origin by half of a lattice translation along the stacking direction, analogous to the obstructed-atomic-limit phase of the Su-Schrieffer-Heeger model of polyacetylene [90, 149, 150, 191–193]. Like weak TIs, obstructed weak TIs exhibit twofold Dirac-cone surface states and topological defect bound states [149, 150, 185, 194].

Below, in Fig. S49, we first list the  $Z_4 = 0$  TCIs that are classified as NLC, and then, in Figs. S50, S51, S52, and S53, we list the  $Z_4 = 0$  TCIs that are classified as SEBR. In addition to obstructed weak-TI phases, the materials listed in this section include members of the KHgSb family [ICSD 56201, SG 194 ( $P6_3/mmc$ )], which have been shown theoretically and experimentally [13, 14, 110, 128, 129] to exhibit a combination of symmetry-indicated mirror-TCI surface states and non-symmetry-indicated glide-protected surface states. In particular, KHgSb itself is classified as SEBR, and thus appears in Fig. S52 under the alternative chemical formula HgKSB.

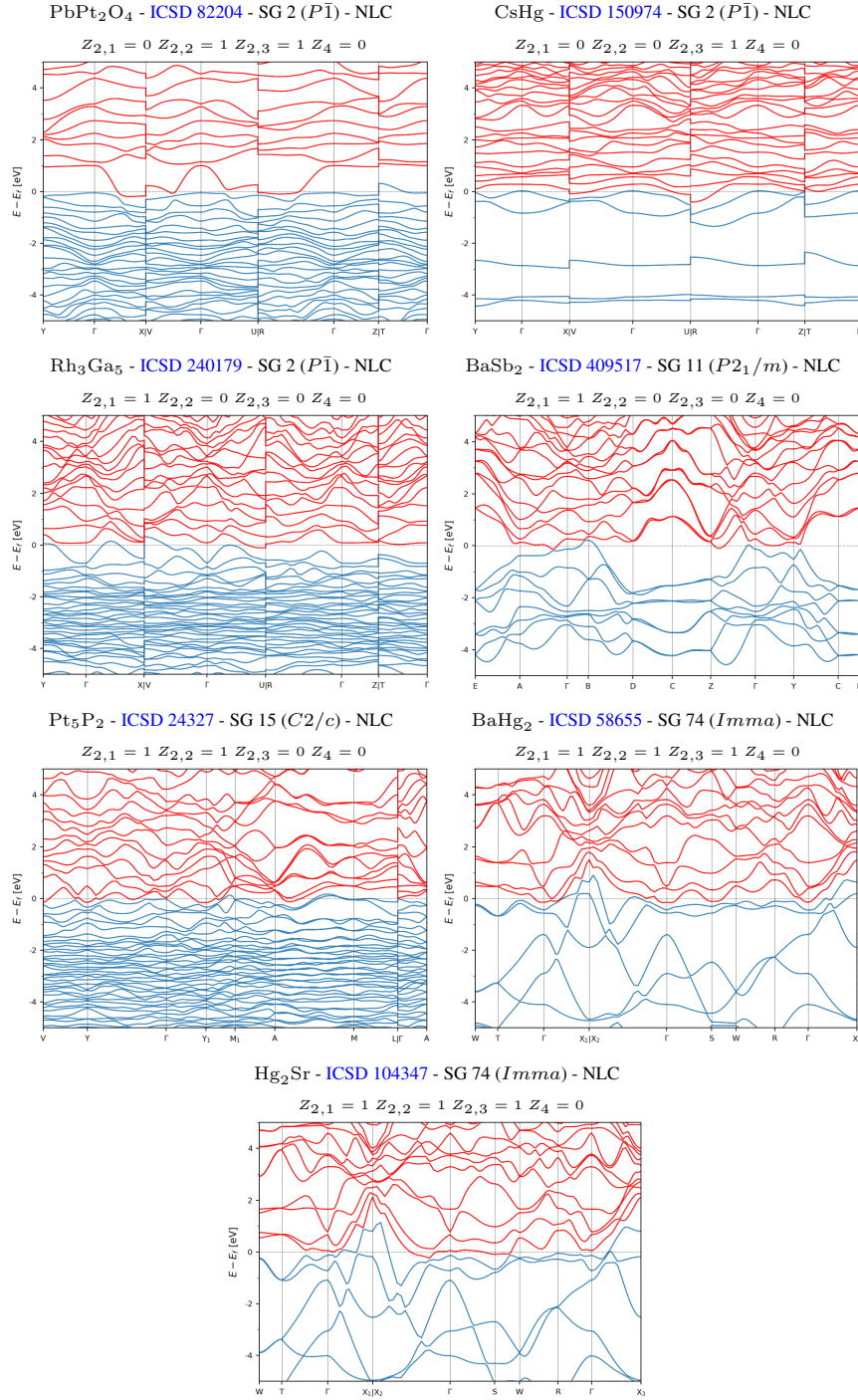


Figure S49. The NLC-classified TCIs with the largest band gaps or the fewest and smallest bulk Fermi pockets whose topology is characterized by  $Z_4 = 0$  and undefined or trivial values of  $Z_8$ .

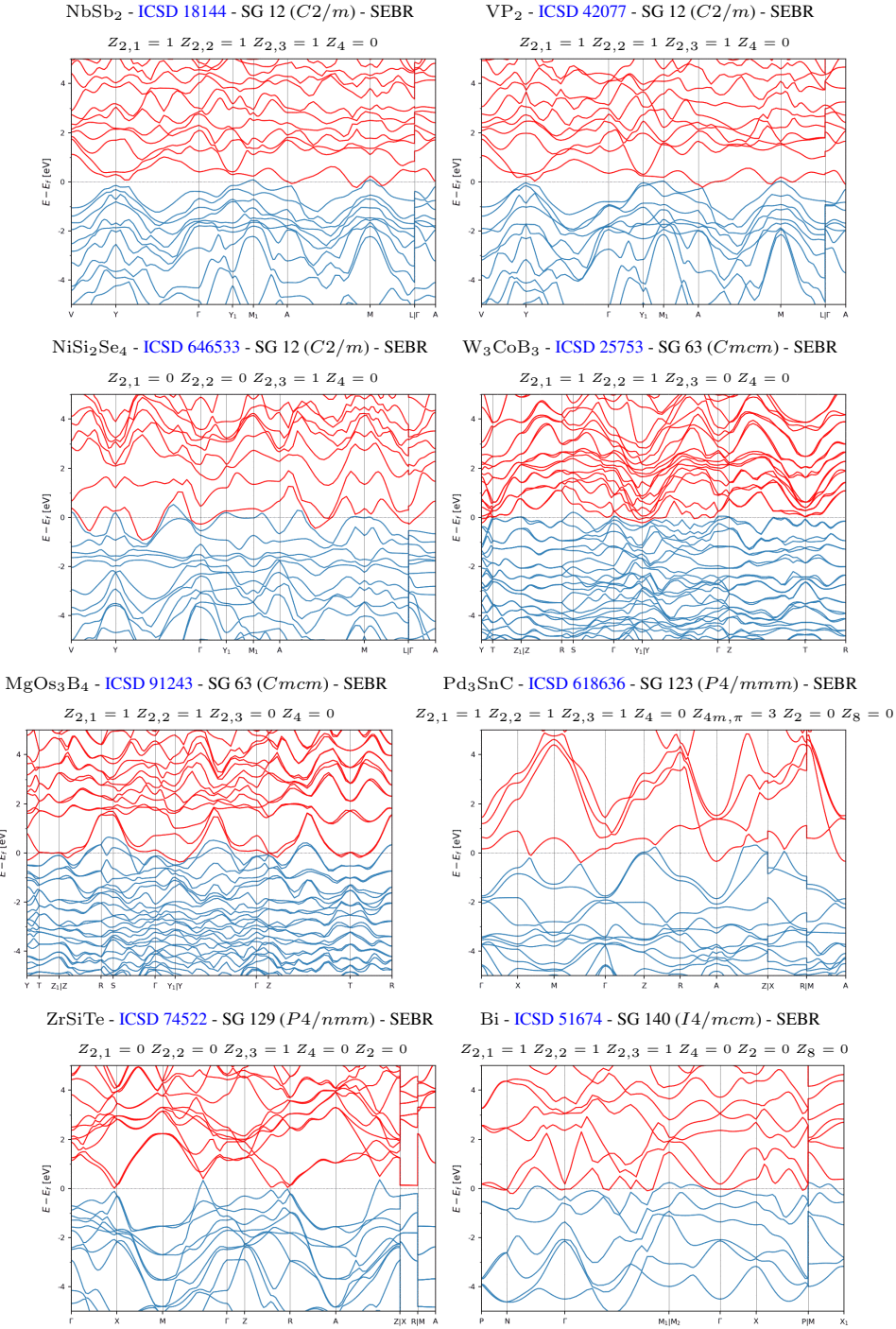


Figure S50. The SEBR-classified TCIs with the largest band gaps or the fewest and smallest bulk Fermi pockets whose topology is characterized by  $Z_4 = 0$  and undefined or trivial values of  $Z_8$ . (part 1/4)

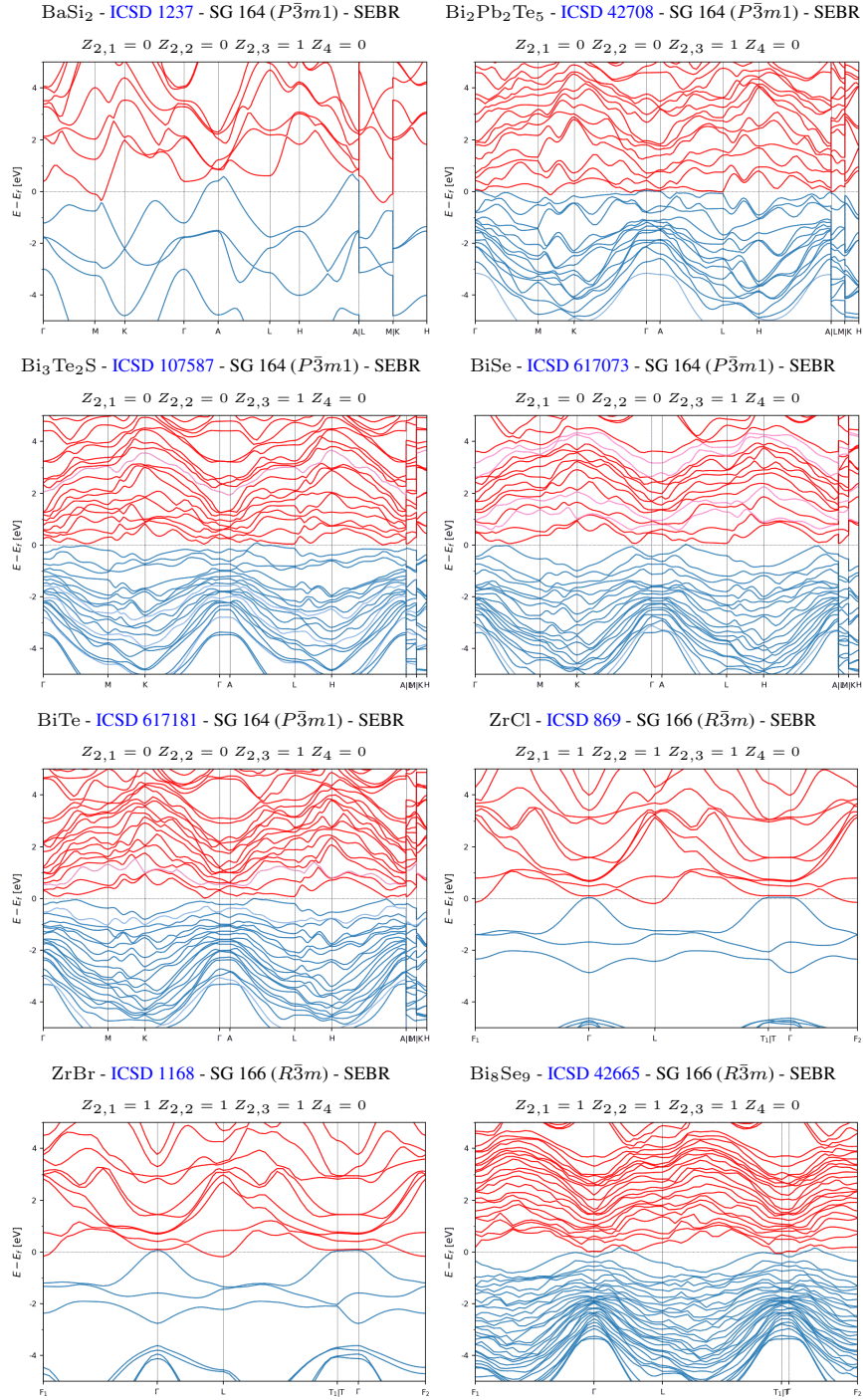


Figure S51. The SEBR-classified TCIs with the largest band gaps or the fewest and smallest bulk Fermi pockets whose topology is characterized by  $Z_4 = 0$  and undefined or trivial values of  $Z_8$ . (part 2/4)

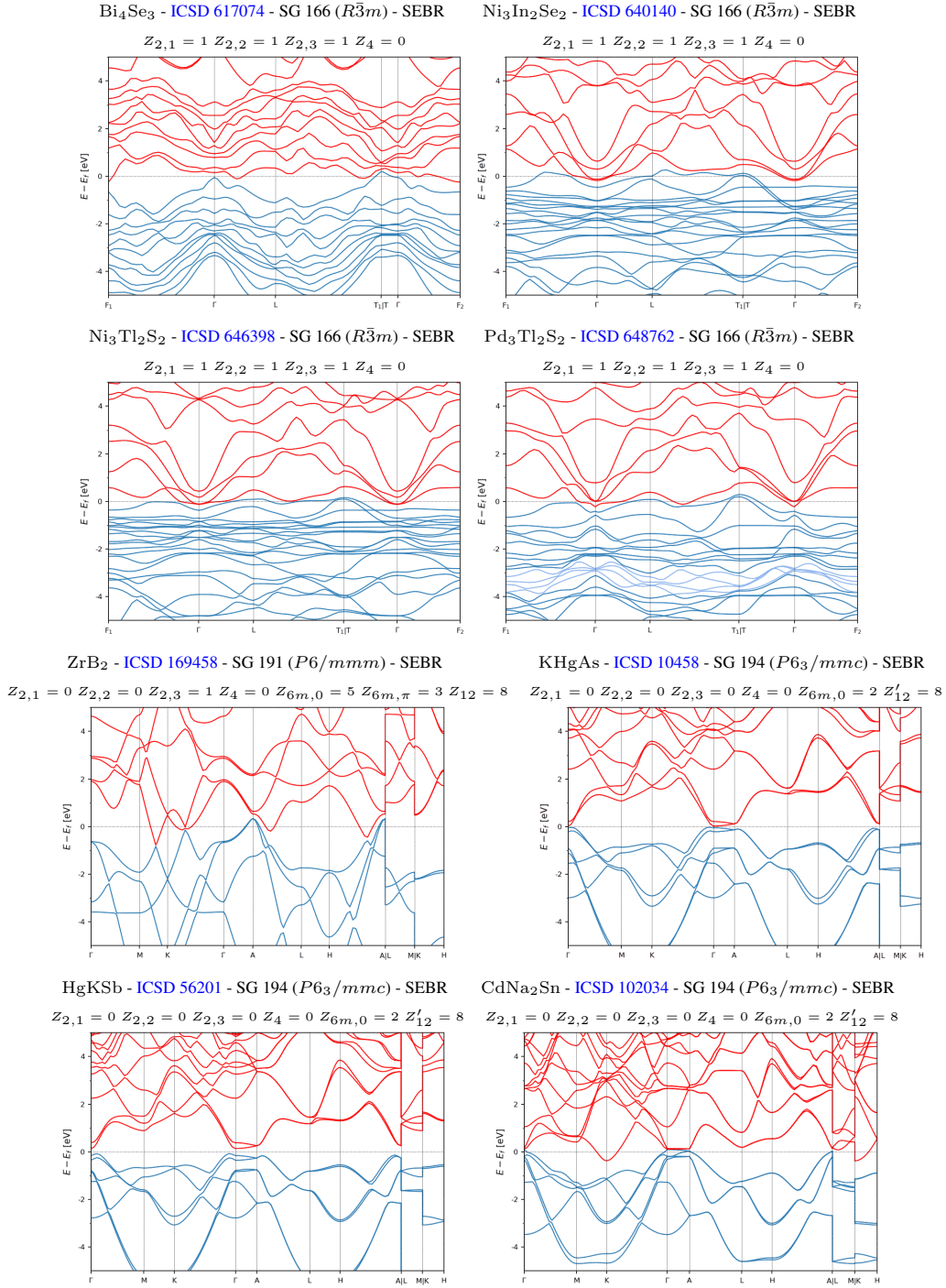


Figure S52. The SEBR-classified TCIs with the largest band gaps or the fewest and smallest bulk Fermi pockets whose topology is characterized by  $Z_4 = 0$  and undefined or trivial values of  $Z_8$ . (part 3/4)

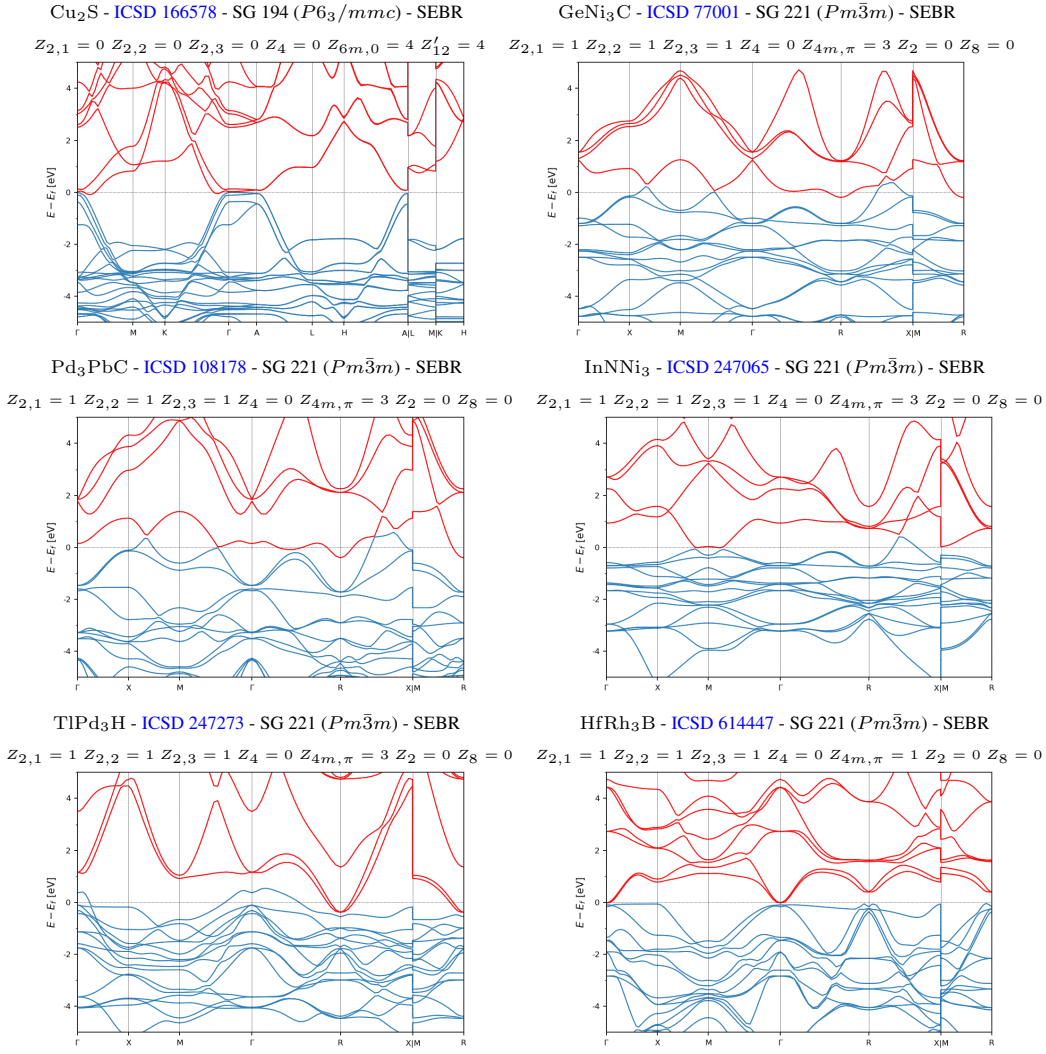


Figure S53. The SEBR-classified TCIs with the largest band gaps or the fewest and smallest bulk Fermi pockets whose topology is characterized by  $Z_4 = 0$  and undefined or trivial values of  $Z_8$ . (part 4/4)

### 7. TCIs with Threefold Rotation Symmetry

In this section, we list the TCIs with threefold rotation symmetry and nontrivial  $Z_{3m0,\pi}$  indices. As discussed in Refs. [16, 17, 29], TCIs with nontrivial  $Z_{3m0,\pi}$  indices may also be 3D TIs. Specifically,  $Z_{3m0,\pi}$  respectively indicate the mirror Chern numbers in the  $k_z = 0, \pi$  planes modulo 3. Insulators with net-odd momentum-space mirror Chern numbers  $C_{M_z}$  are 3D TIs – however, because insulators with  $C_{M_z} = 2$  and  $C_{M_z} = -1$  exhibit the same mirror Chern numbers modulo 3, then further Wilson-loop [13, 14, 108–110, 176] or surface-state calculations must be performed to determine whether insulators with nontrivial  $Z_{3m0,\pi}$  are additionally 3D TIs.

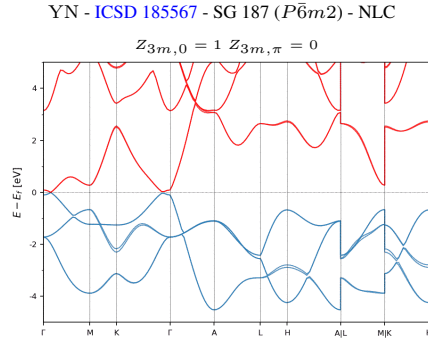


Figure S54. The NLC-classified, threefold-rotation-indicated TCI with the fewest and smallest bulk Fermi pockets.

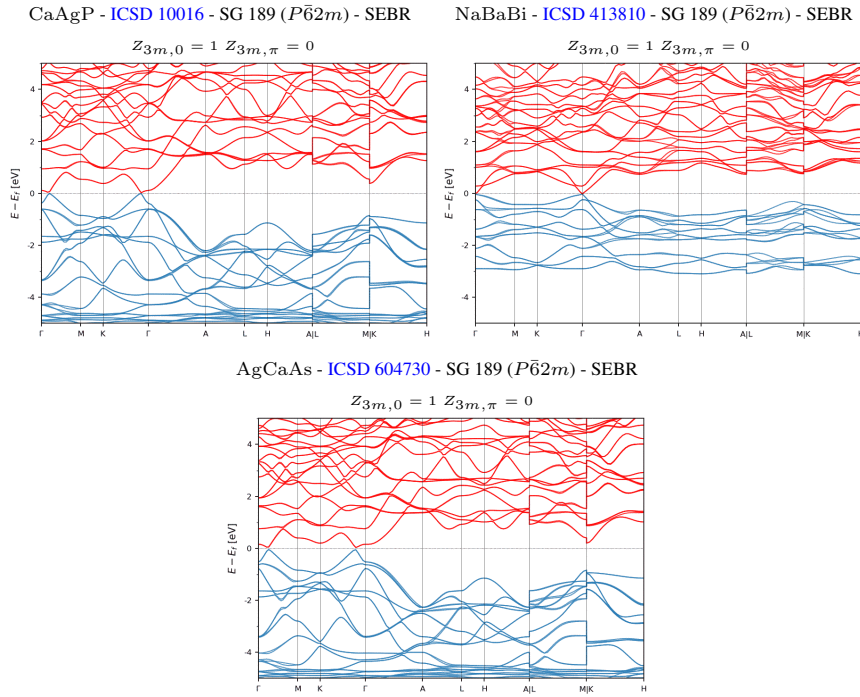


Figure S55. The SEBR-classified, threefold-rotation-indicated TIs and TCIs with the largest band gaps or the fewest and smallest bulk Fermi pockets.

### B. Repeat-Topological Materials

In this section, we list the RTopo TIs and TCIs with the largest band gaps or the fewest and smallest bulk Fermi pockets when the Fermi level is set to 0, and when the Fermi level is set to the next highest filling below  $E_F$  at which an insulating gap is permitted by band connectivity (see S9 A for further details and a rigorous definition of RTopo materials). As introduced in this work, RTopo materials specifically exhibit stable topological gaps at  $E_F$ , and at the next-highest gap below  $E_F$  as determined by band connectivity through TQC (see S2 and S9 A). First in Figs. S56 and S57, we list the RTopo materials that are classified as NLC at  $E_F$ , and then, in Figs. S58, S59, S60, S61, S62, and S63, we list the RTopo materials that are classified as SEBR at  $E_F$ .

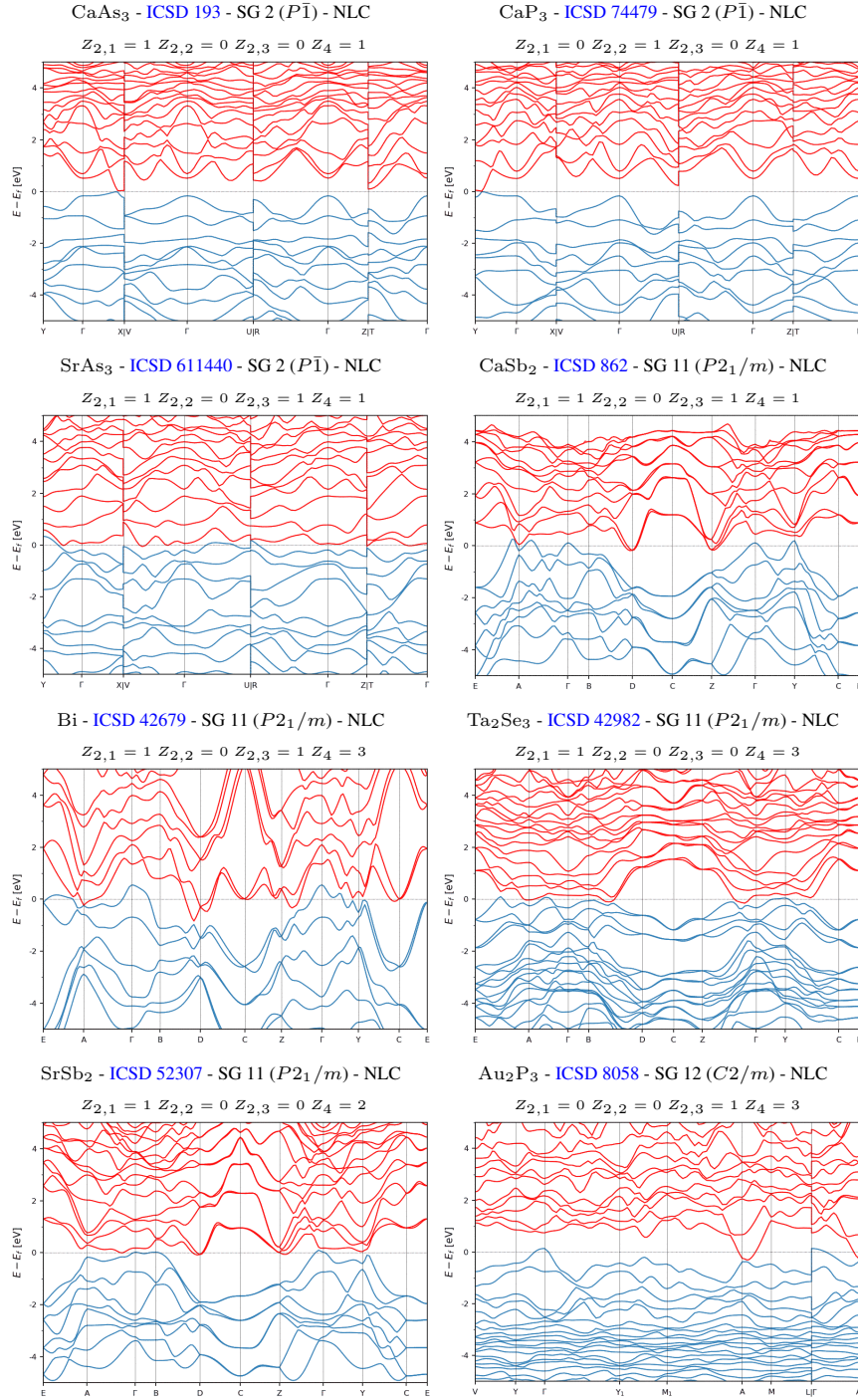


Figure S56. The RTopo TIs and TCIs that are NLC-classified at the Fermi level and have the fewest and smallest bulk Fermi pockets when the Fermi level is set to 0, or set to the next highest filling at which an insulating gap is permitted by band connectivity. (part 1/2)

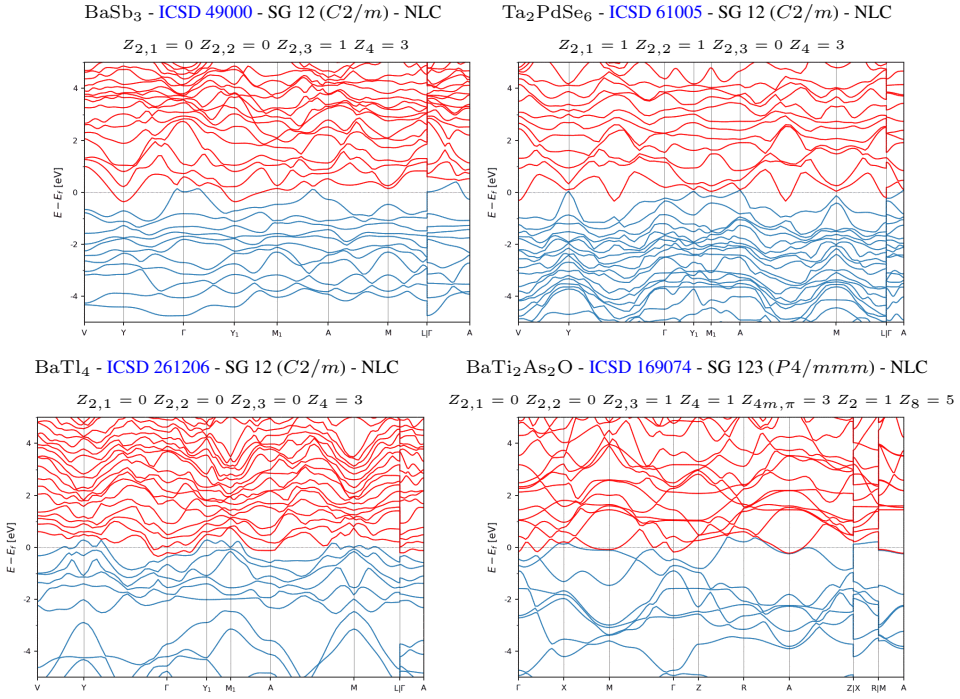


Figure S57. The RTopo TIs and TCIs that are NLC-classified at the Fermi level and have the fewest and smallest bulk Fermi pockets when the Fermi level is set to 0, or set to the next highest filling at which an insulating gap is permitted by band connectivity. (part 2/2)

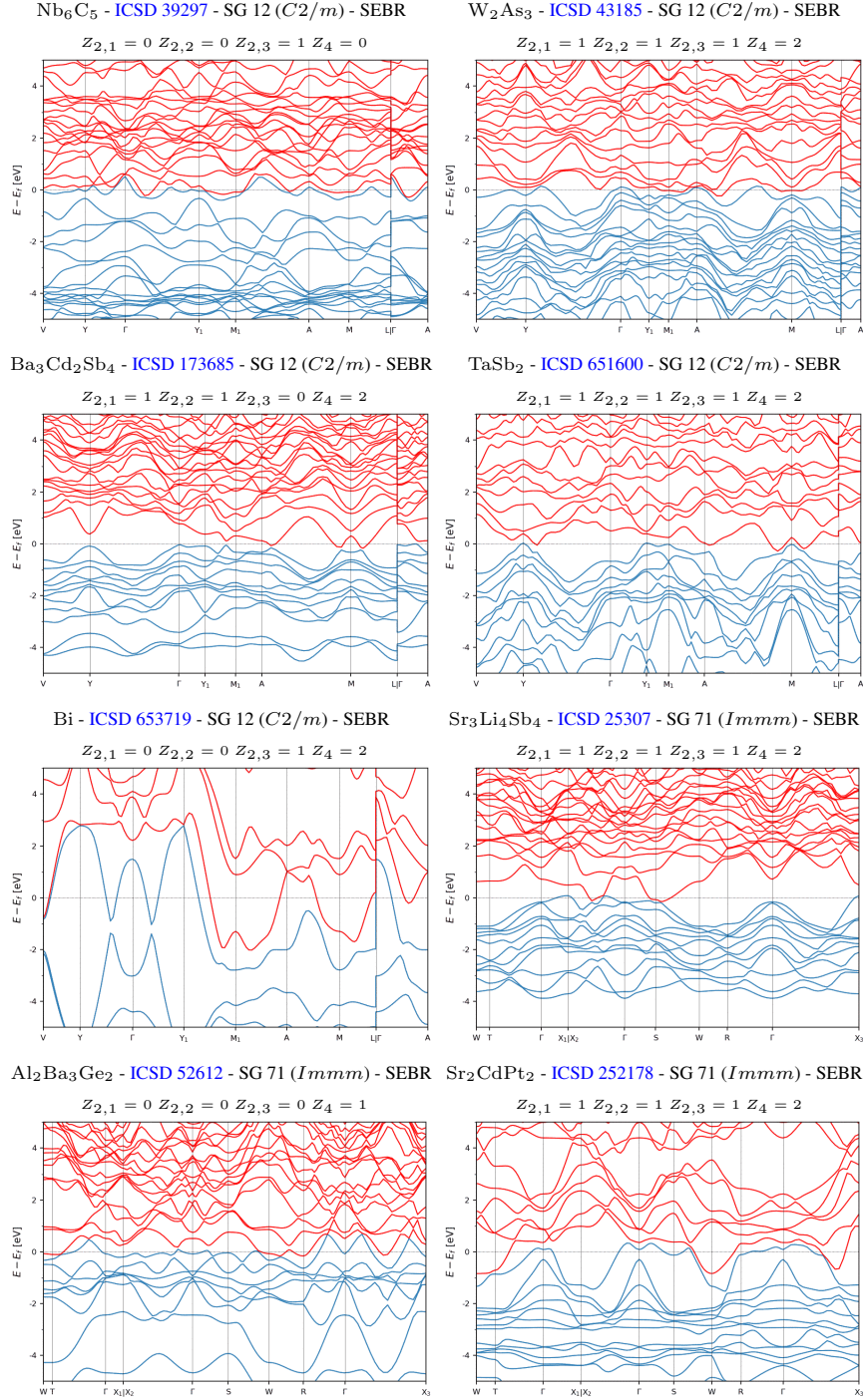


Figure S58. The RTopo TIs and TCIs that are SEBR-classified at the Fermi level and have the fewest and smallest bulk Fermi pockets when the Fermi level is set to 0, or set to the next highest filling at which an insulating gap is permitted by band connectivity. (part 1/6)

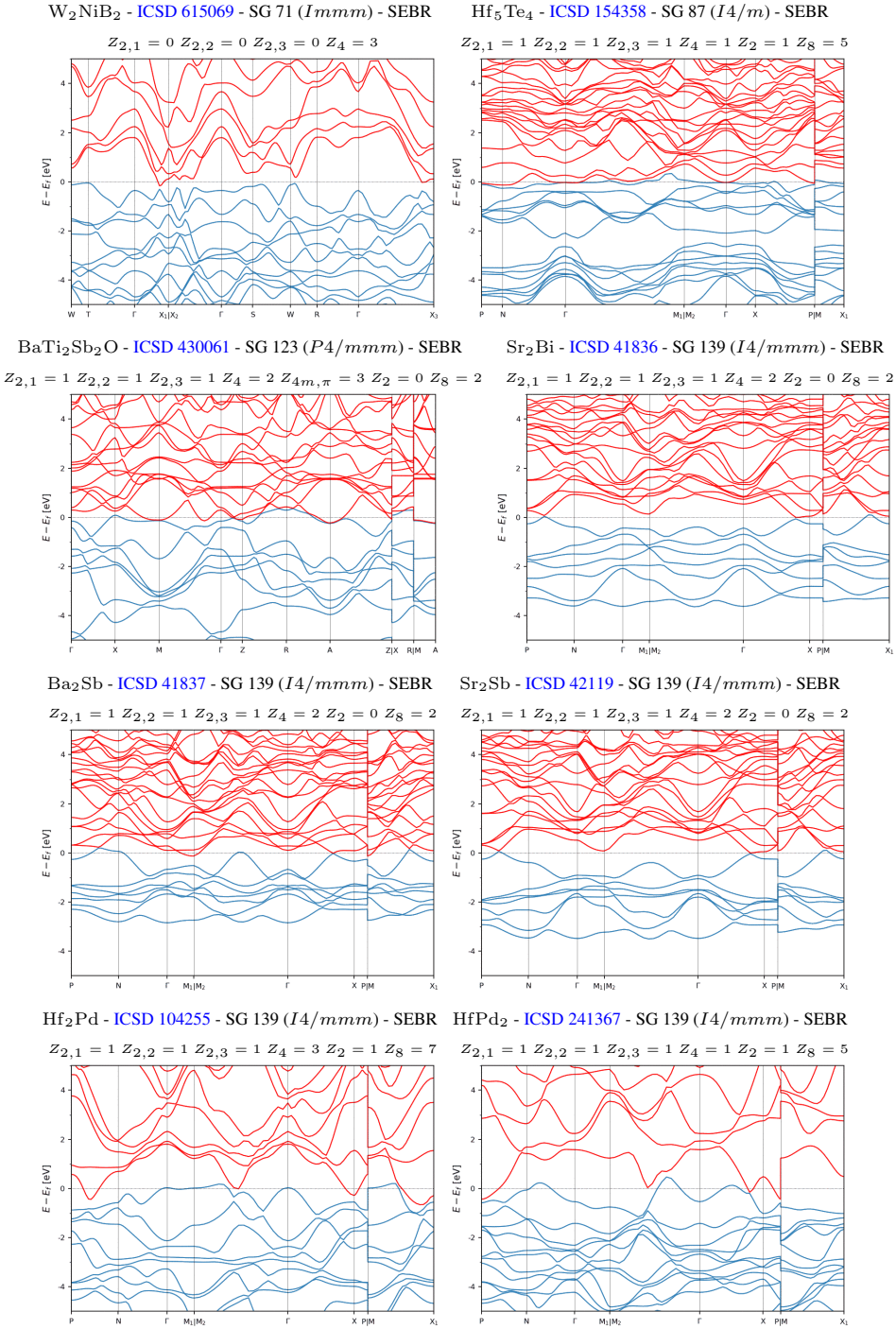


Figure S59. The RTopo TIs and TCIs that are SEBR-classified at the Fermi level and have the fewest and smallest bulk Fermi pockets when the Fermi level is set to 0, or set to the next highest filling at which an insulating gap is permitted by band connectivity. (part 2/6)

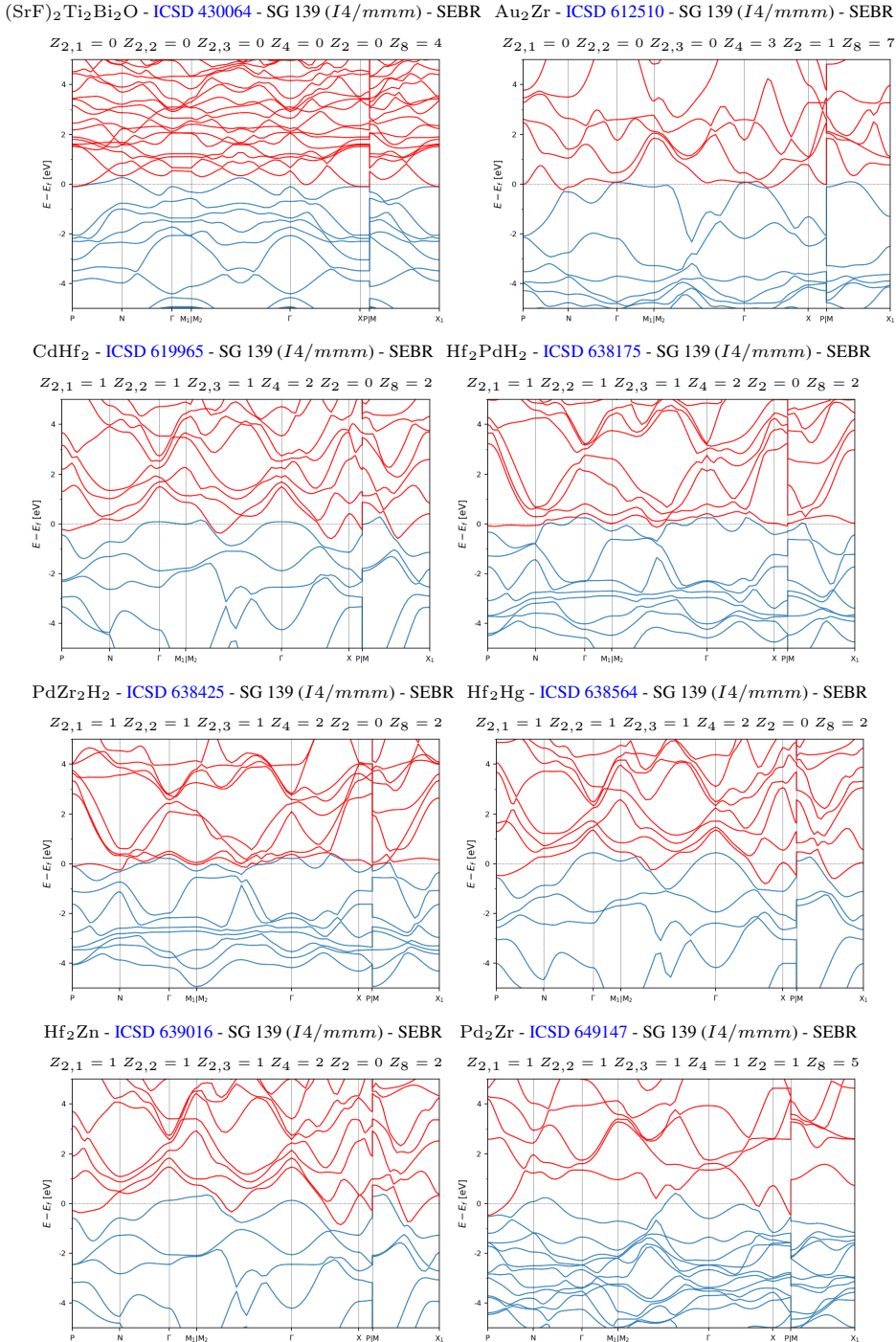


Figure S60. The RTopo TIs and TCIs that are SEBR-classified at the Fermi level and have the fewest and smallest bulk Fermi pockets when the Fermi level is set to 0, or set to the next highest filling at which an insulating gap is permitted by band connectivity. (part 3/6)

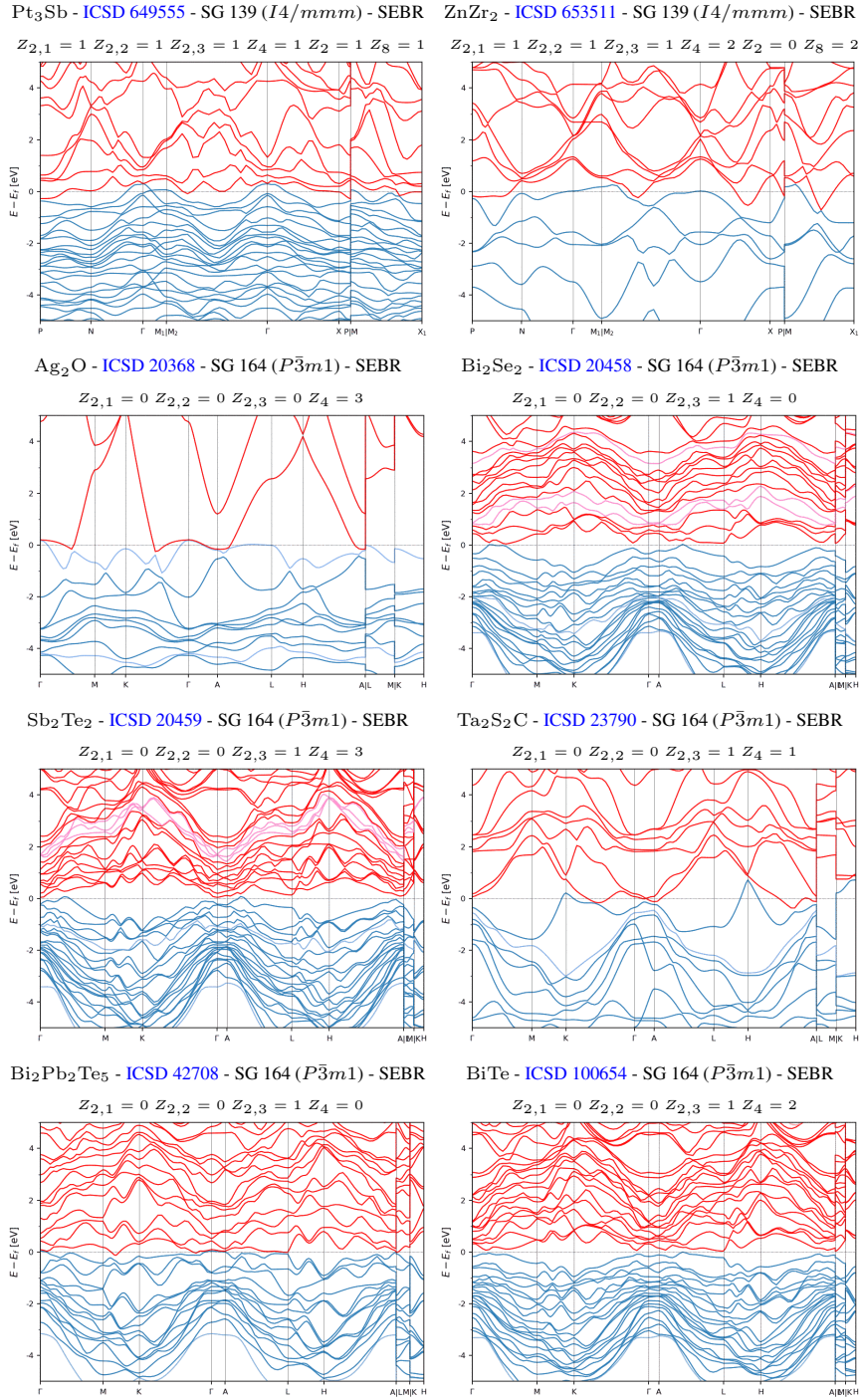


Figure S61. The RTopo TIs and TCIs that are SEBR-classified at the Fermi level and have the fewest and smallest bulk Fermi pockets when the Fermi level is set to 0, or set to the next highest filling at which an insulating gap is permitted by band connectivity. (part 4/6)

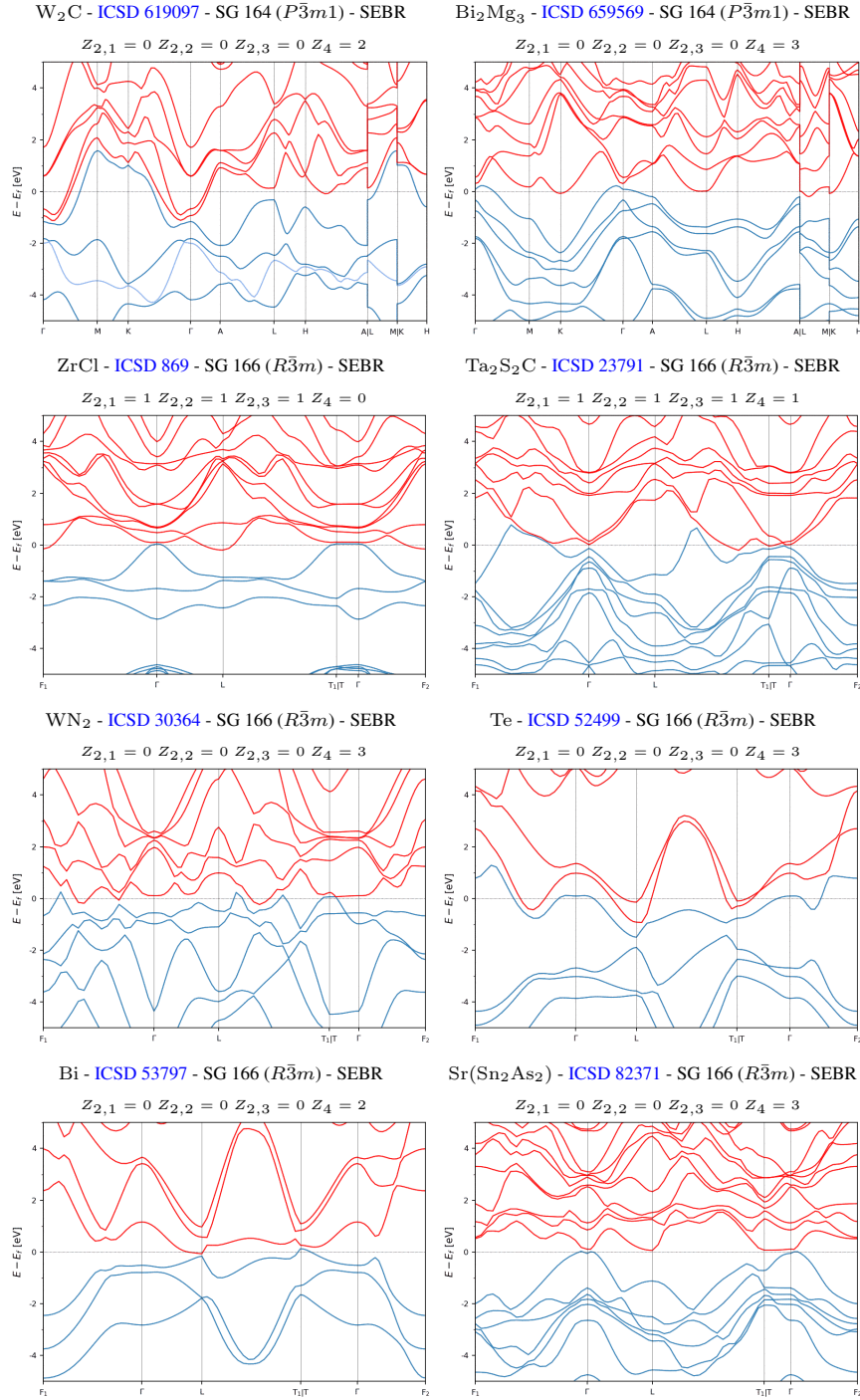


Figure S62. The RTopo TIs and TCIs that are SEBR-classified at the Fermi level and have the fewest and smallest bulk Fermi pockets when the Fermi level is set to 0, or set to the next highest filling at which an insulating gap is permitted by band connectivity. (part 5/6)

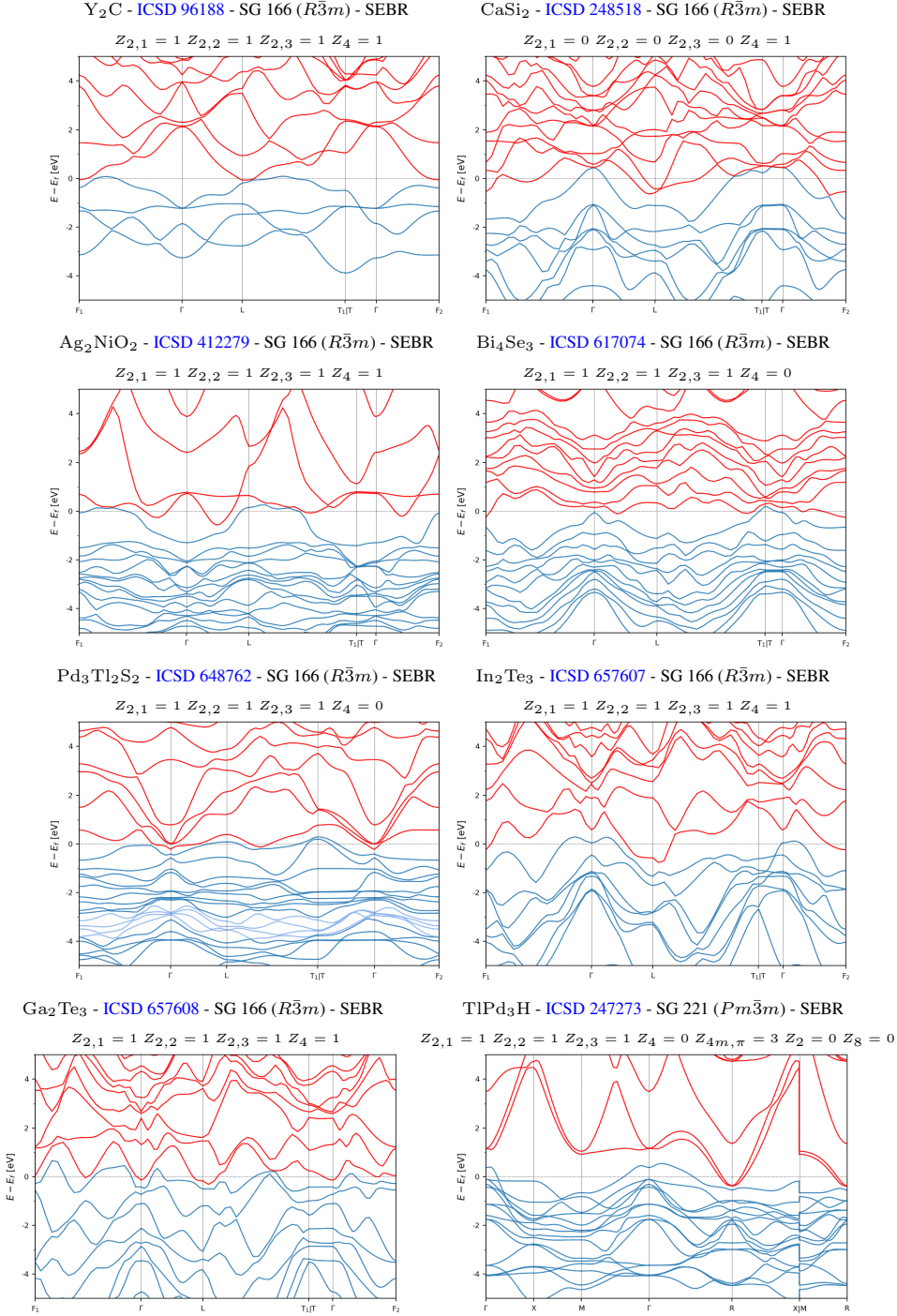


Figure S63. The RTopo TIs and TCIs that are SEBR-classified at the Fermi level and have the fewest and smallest bulk Fermi pockets when the Fermi level is set to 0, or set to the next highest filling at which an insulating gap is permitted by band connectivity. (part 6/6)

### C. Enforced Topological Semimetals

In this section, we will list the enforced semimetals with the smallest bulk Fermi pockets. First, in [S11 C 1](#), we will list the enforced semimetals whose nodal degeneracies are pinned to high-symmetry BZ points (ESFD), and then, in [S11 C 2](#), we will list the enforced semimetals whose nodal degeneracies lie along high-symmetry BZ lines (ES).

#### 1. ESFD-Classified Semimetals

In this section, we list the enforced semimetals whose nodal degeneracies are pinned to high-symmetry BZ points (ESFD in the nomenclature established in Ref. [38]). Most generally, ESFD phases can include both conventional (filling-) [130, 151, 195] enforced Dirac [152, 169, 170, 196] and Weyl [132] semimetals, as well as unconventional (multifold) fermion [7–9, 131, 132, 197] semimetals. Depending on whether or not the little groups of the  $\mathbf{k}$  points of the enforced nodal degeneracies (as well as the full space group) contain rotoinversion symmetries, the ESFD semimetals identified in this section may further be classified as topologically chiral or achiral [131, 132]. ESFD phases in structurally chiral crystals have in particular been highlighted for hosting monopole-like spin textures [132, 198], exhibiting photoresponse signatures of topological chirality [133, 199–202], and as possible venues for realizing topological superconductivity [203–205].

First, in Fig. [S64](#), we list the ESFD materials with the simplest bulk Fermi surfaces and threefold-degenerate spin-1 fermions [8] close to  $E_F$ . Because the spin-1 fermions in the materials in Fig. [S64](#) all lie at high-symmetry  $\mathbf{k}$  points with rotoinversion (specifically  $S_4$ ) symmetry, then the threefold degeneracies carry net-zero chiral charges, and do not exhibit associated topological surface Fermi arcs [131, 132]. Next, in Figs. [S65](#), [S66](#), [S67](#), [S68](#), [S69](#), [S70](#), [S71](#), [S72](#), [S73](#), and [S74](#), we list the materials with well-isolated achiral fourfold-degenerate spin-3/2 fermions [8] close to  $E_F$ . Then, in Figs. [S75](#), [S76](#), [S77](#), [S78](#), [S79](#), and [S80](#), we list the cubic ESFD materials with chiral crystal structures and enforced chiral fermions [8, 9, 131, 132] close to  $E_F$ , which in most cases include chiral fourfold-degenerate spin-3/2 fermions and chiral sixfold-degenerate double-spin-1 fermions. The materials in Figs. [S75](#), [S76](#), [S77](#), [S78](#), [S79](#), and [S80](#) notably include members of the B20 chiral crystal family, such as CoSi [ICSD 189221, SG 198 ( $P2_13$ )], which have been shown in recent theoretical and experimental investigations to exhibit large topological surface Fermi arcs [9, 23–25, 131, 135, 136]. In the following figures – Figs. [S81](#), [S82](#), and [S83](#) – we then show the ESFD materials with eightfold-degenerate double Dirac fermions [7, 8] close to  $E_F$  that do not exhibit clear magnetic instabilities in DFT. Specifically, in a number of ESFD compounds – most notably candidate double Dirac semimetals such as CuBi<sub>2</sub>O<sub>4</sub> [ICSD 15865, SG 130 ( $P4/ncc$ )] [8, 206, 207] – experimental investigations have revealed that the nodal degeneracies become gapped by electron-electron interactions, leading to correlated Mott – or possibly more exotic – insulating phases, even above the transition temperature for magnetic ordering. The candidate double Dirac semimetals shown in Figs. [S81](#), [S82](#), and [S83](#) exhibit less sharply peaked densities of states at  $E_F$  than CuBi<sub>2</sub>O<sub>4</sub>, and may therefore be less susceptible to interaction-driven (semi)metal-insulator transitions. Finally, in Figs. [S84](#) and [S85](#), we list the ESFD materials with other forms of nodal fermions at  $E_F$ , such as fourfold degeneracies with quadratic dispersion.

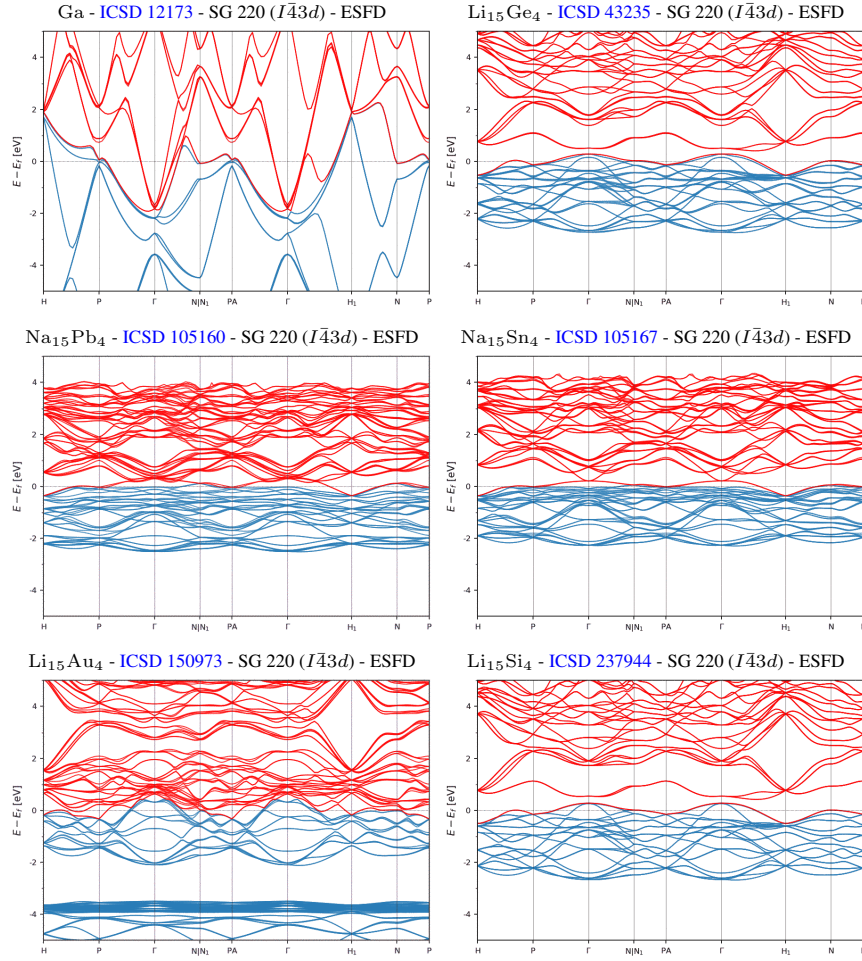


Figure S64. The ESFD-classified topological semimetals with the simplest bulk Fermi surfaces and threefold-degenerate spin-1 fermions close to  $E_F$ .

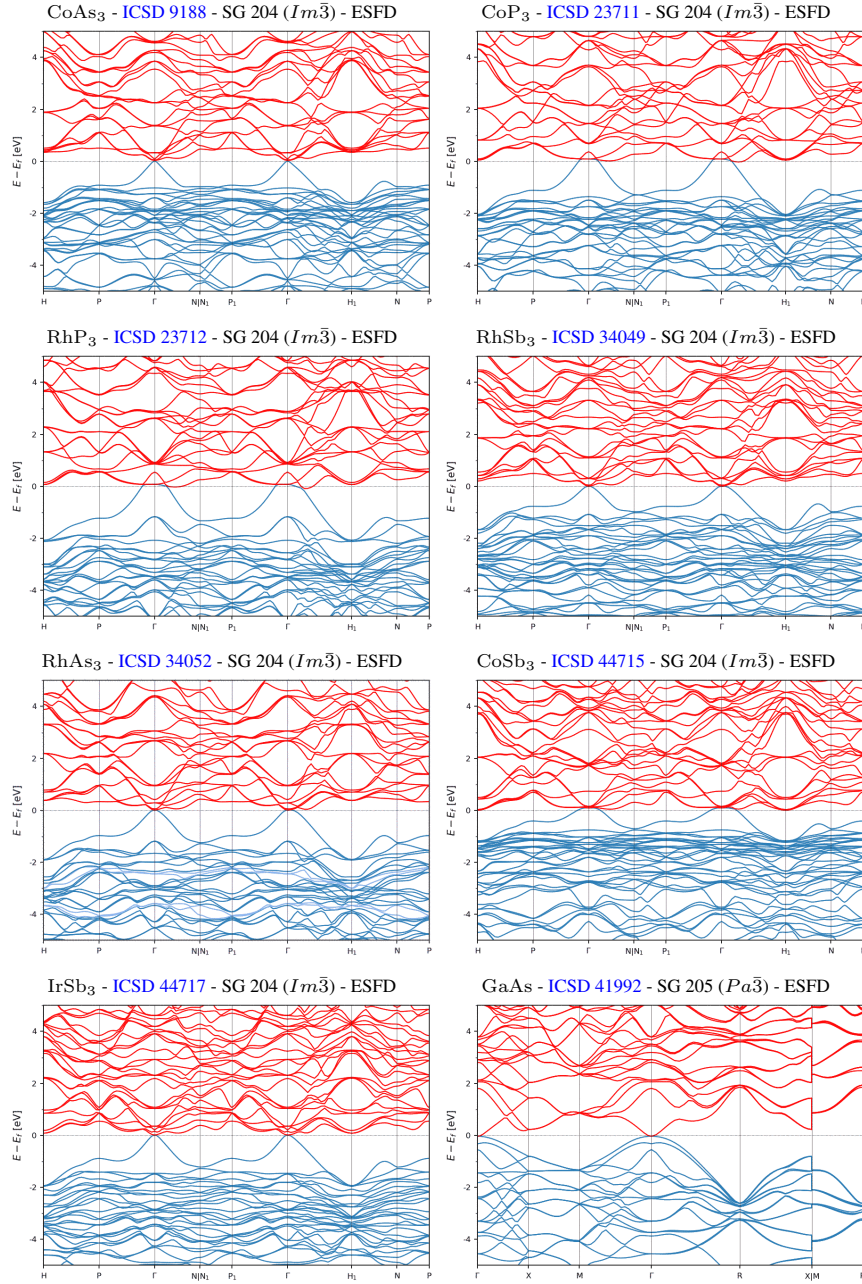


Figure S65. The ESFD-classified topological semimetals with the simplest bulk Fermi surfaces and fourfold-degenerate, achiral spin-3/2 fermions close to  $E_F$ . (part 1/10)

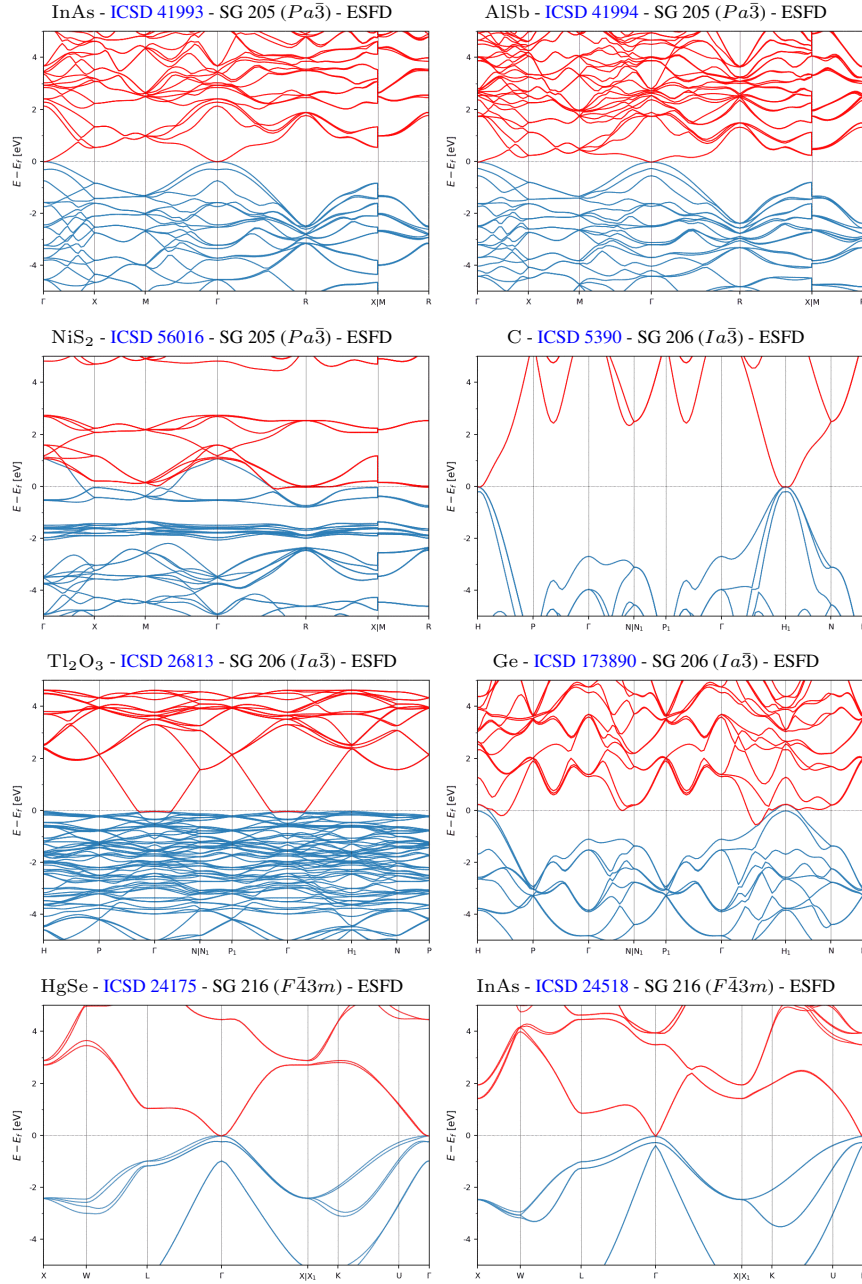


Figure S66. The ESFD-classified topological semimetals with the simplest bulk Fermi surfaces and fourfold-degenerate, achiral spin-3/2 fermions close to  $E_F$ . (part 2/10)

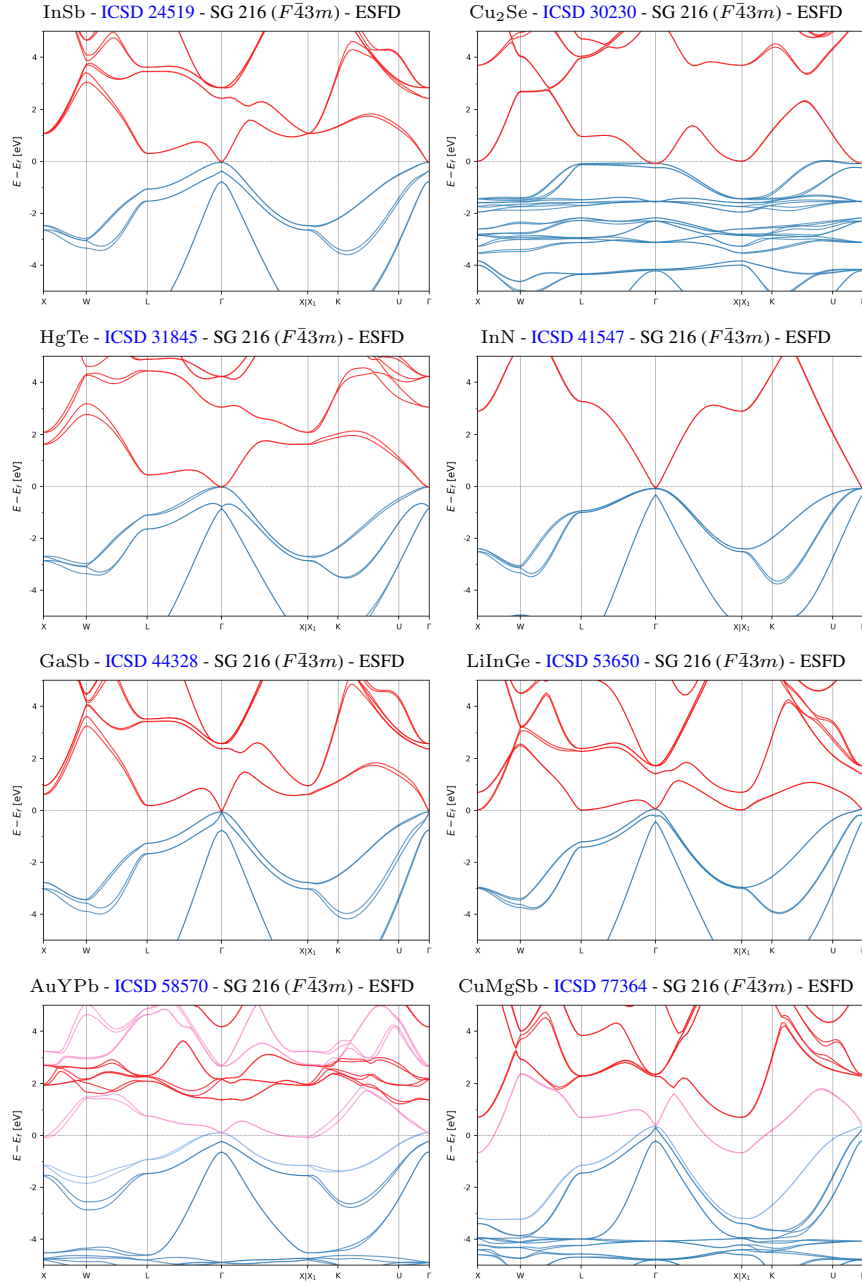


Figure S67. The ESFD-classified topological semimetals with the simplest bulk Fermi surfaces and fourfold-degenerate, achiral spin-3/2 fermions close to  $E_F$ . (part 3/10)

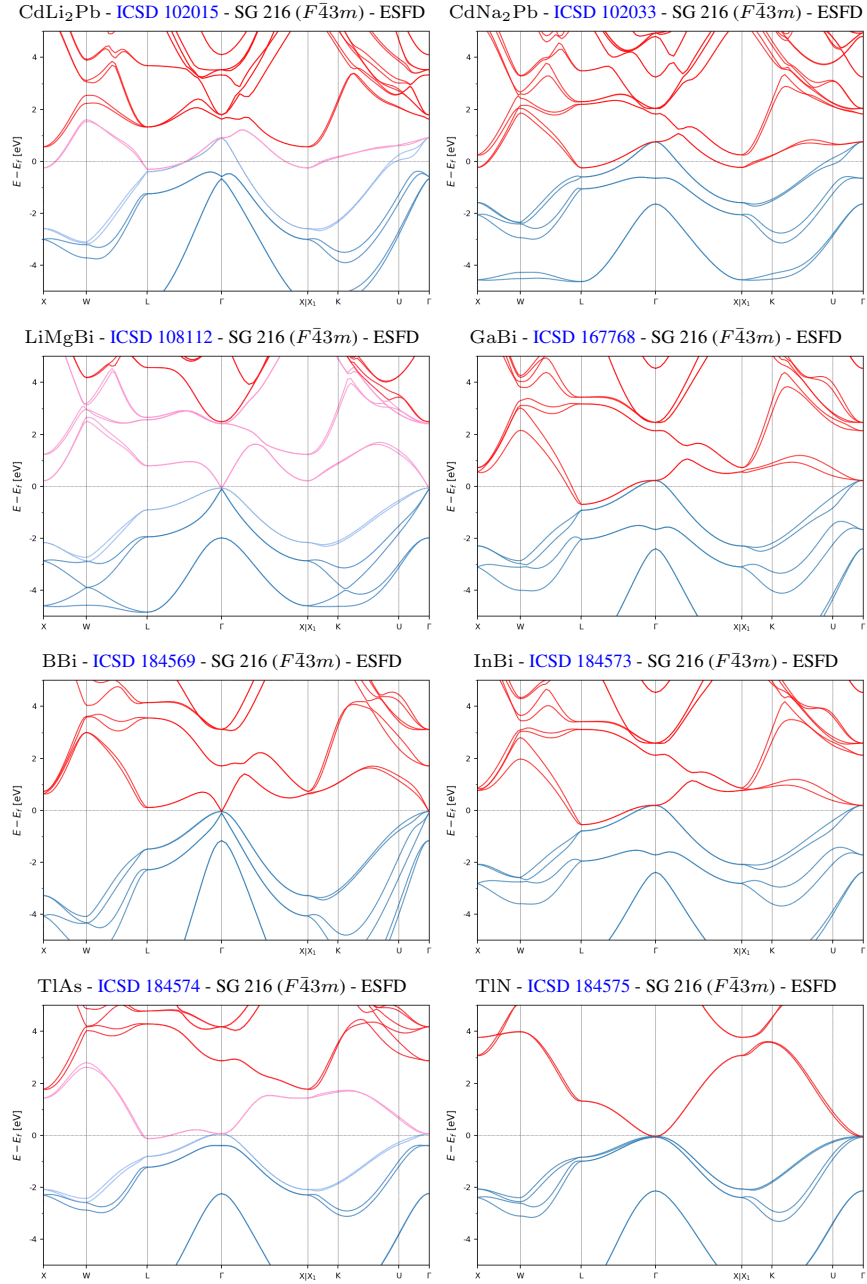


Figure S68. The ESFD-classified topological semimetals with the simplest bulk Fermi surfaces and fourfold-degenerate, achiral spin-3/2 fermions close to  $E_F$ . (part 4/10)

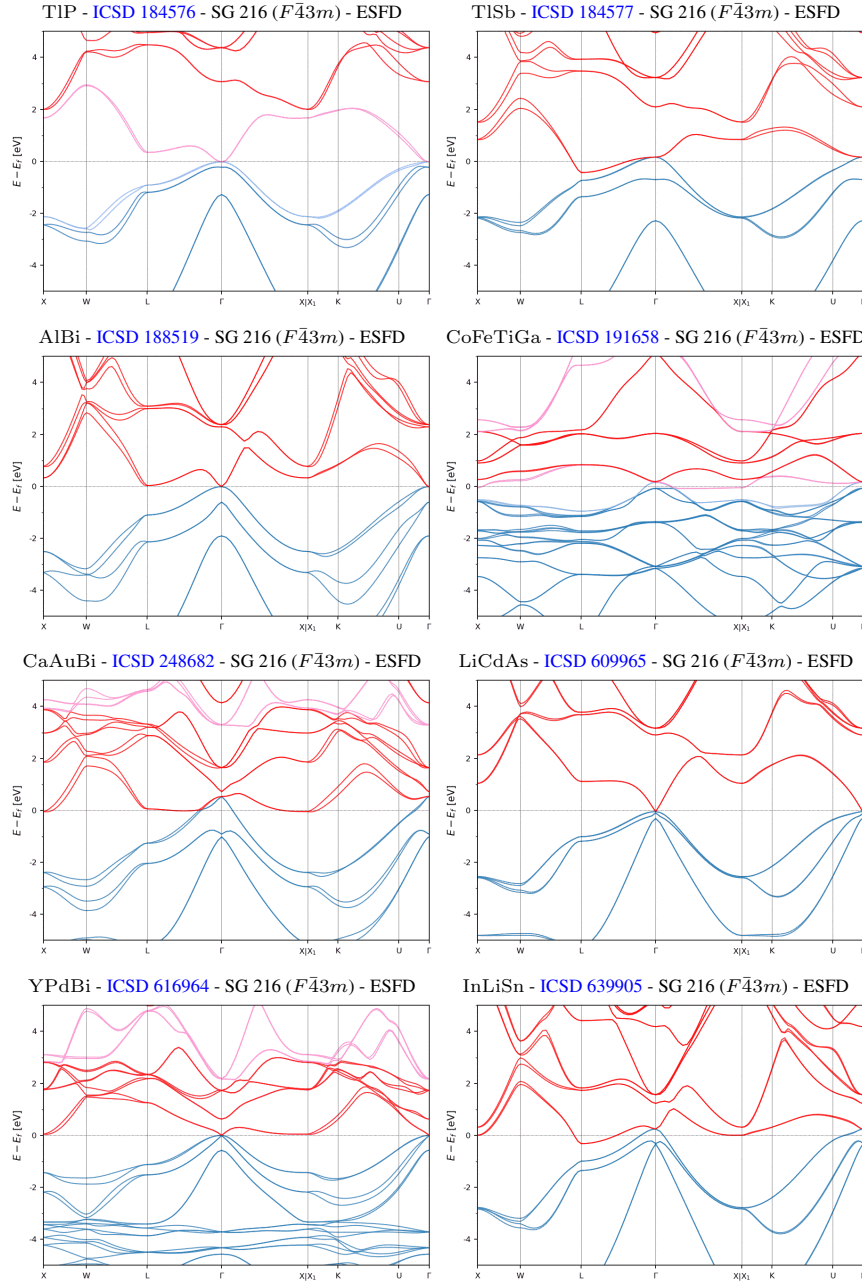


Figure S69. The ESFD-classified topological semimetals with the simplest bulk Fermi surfaces and fourfold-degenerate, achiral spin-3/2 fermions close to  $E_F$ . (part 5/10)

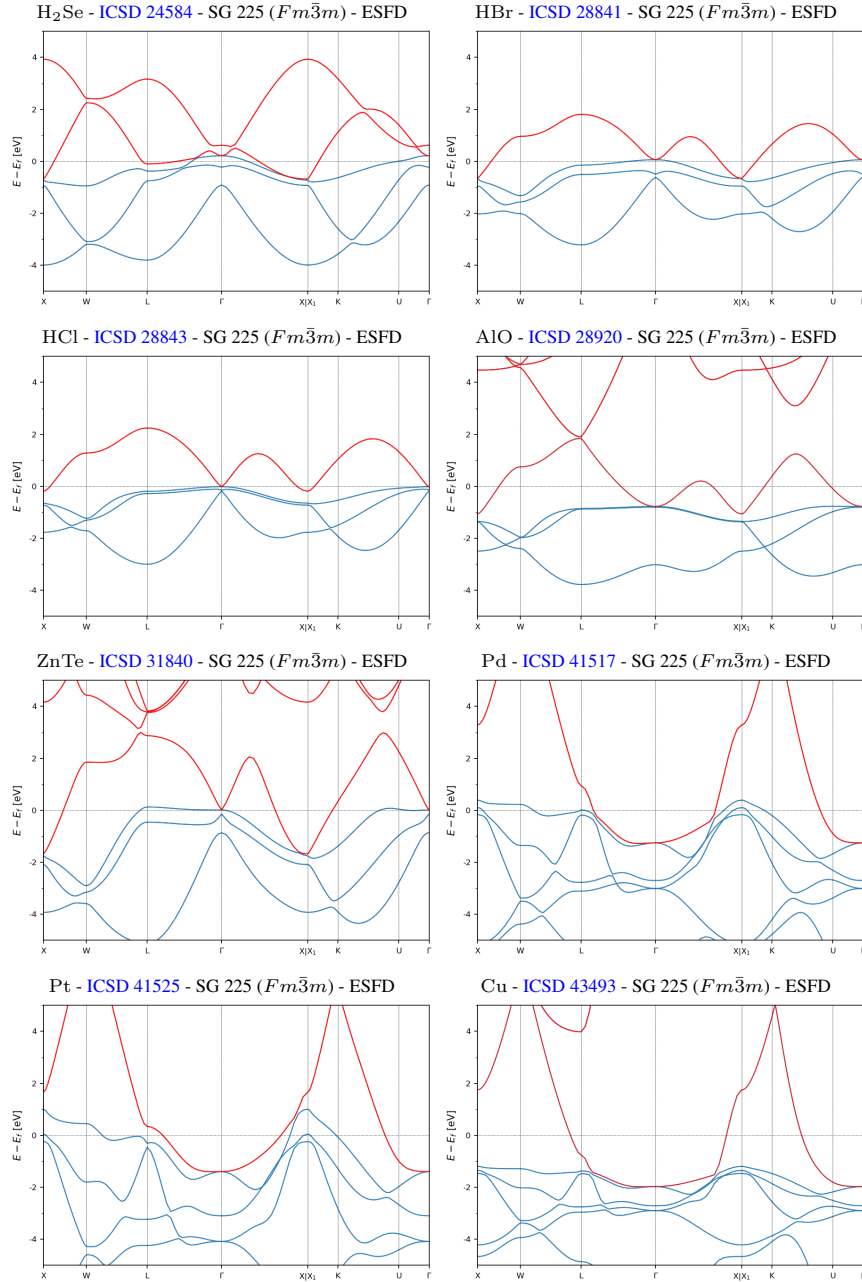


Figure S70. The ESFD-classified topological semimetals with the simplest bulk Fermi surfaces and fourfold-degenerate, achiral spin-3/2 fermions close to  $E_F$ . (part 6/10)

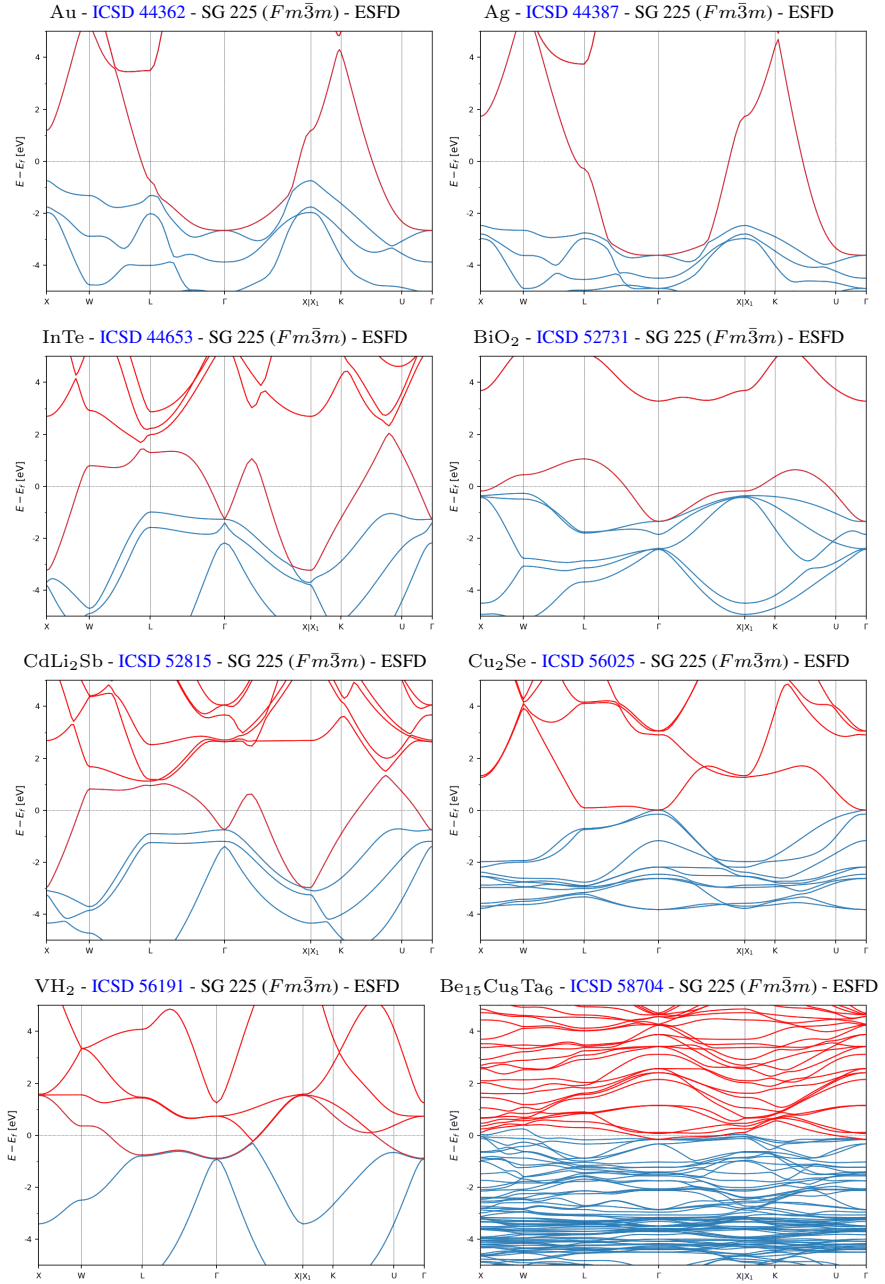


Figure S71. The ESFD-classified topological semimetals with the simplest bulk Fermi surfaces and fourfold-degenerate, achiral spin-3/2 fermions close to  $E_F$ . (part 7/10)

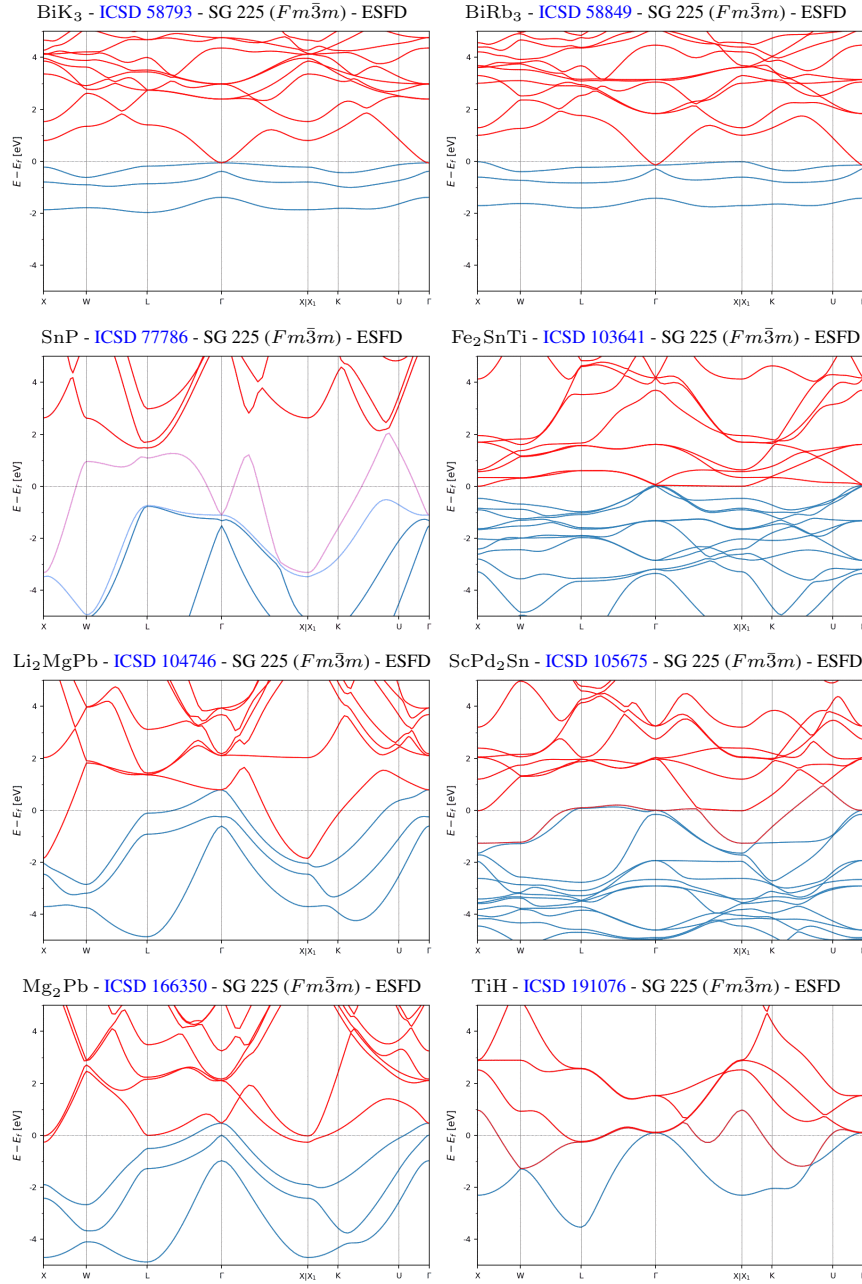


Figure S72. The ESFD-classified topological semimetals with the simplest bulk Fermi surfaces and fourfold-degenerate, achiral spin-3/2 fermions close to  $E_F$ . (part 8/10)

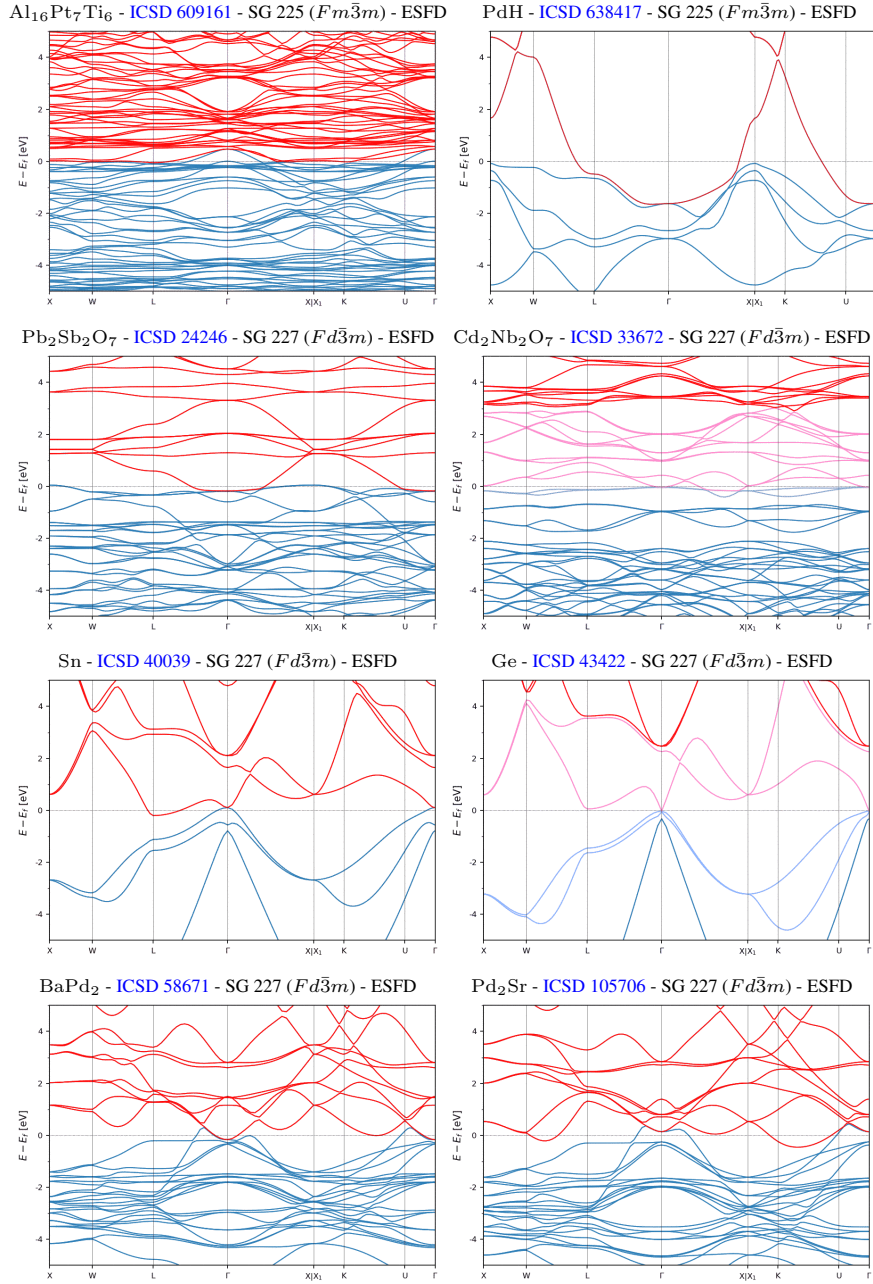


Figure S73. The ESFD-classified topological semimetals with the simplest bulk Fermi surfaces and fourfold-degenerate, achiral spin-3/2 fermions close to  $E_F$ . (part 9/10)

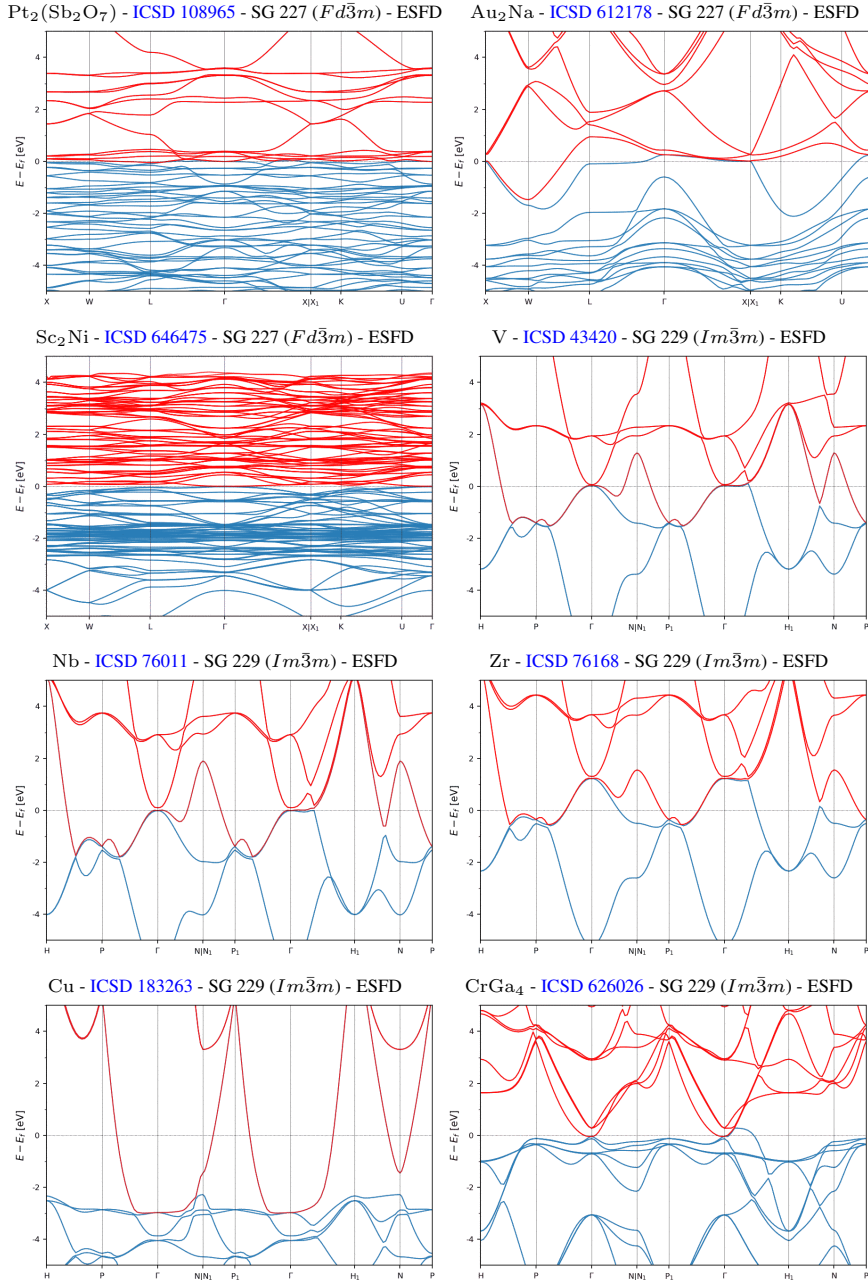


Figure S74. The ESFD-classified topological semimetals with the simplest bulk Fermi surfaces and fourfold-degenerate, achiral spin-3/2 fermions close to  $E_F$ . (part 10/10)

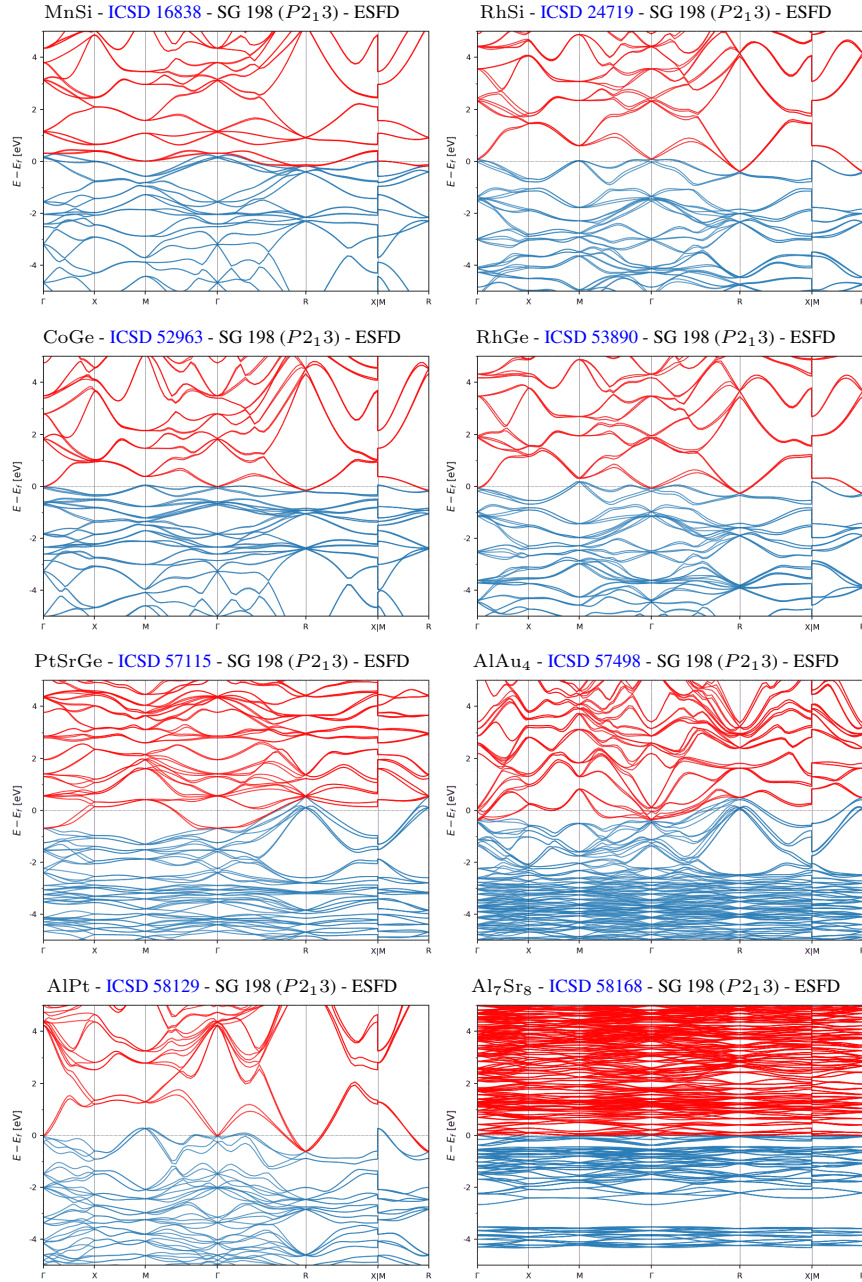


Figure S75. The ESFD-classified topological semimetals in chiral space groups with the simplest bulk Fermi surfaces and enforced chiral fermions close to  $E_F$ . (part 1/6)

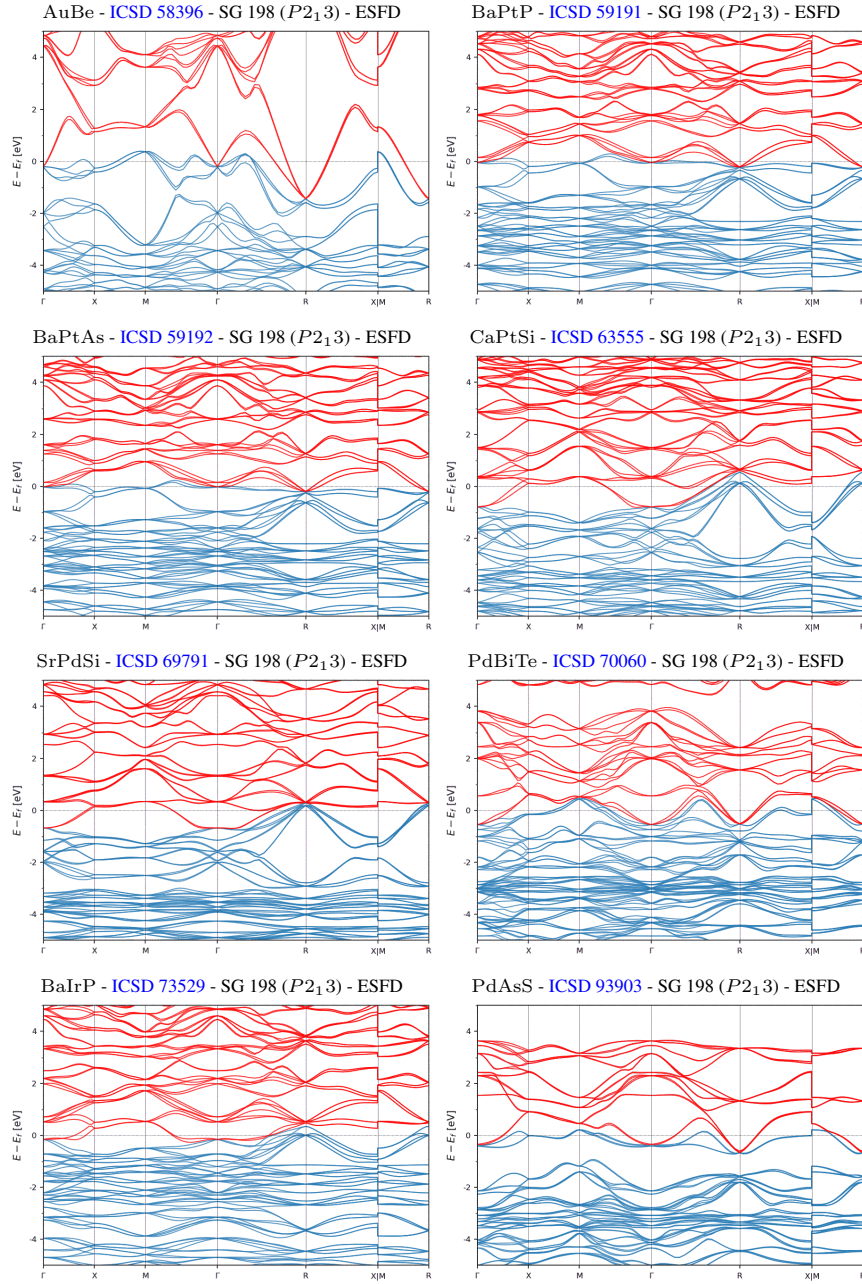


Figure S76. The ESFD-classified topological semimetals in chiral space groups with the simplest bulk Fermi surfaces and enforced chiral fermions close to  $E_F$ . (part 2/6)

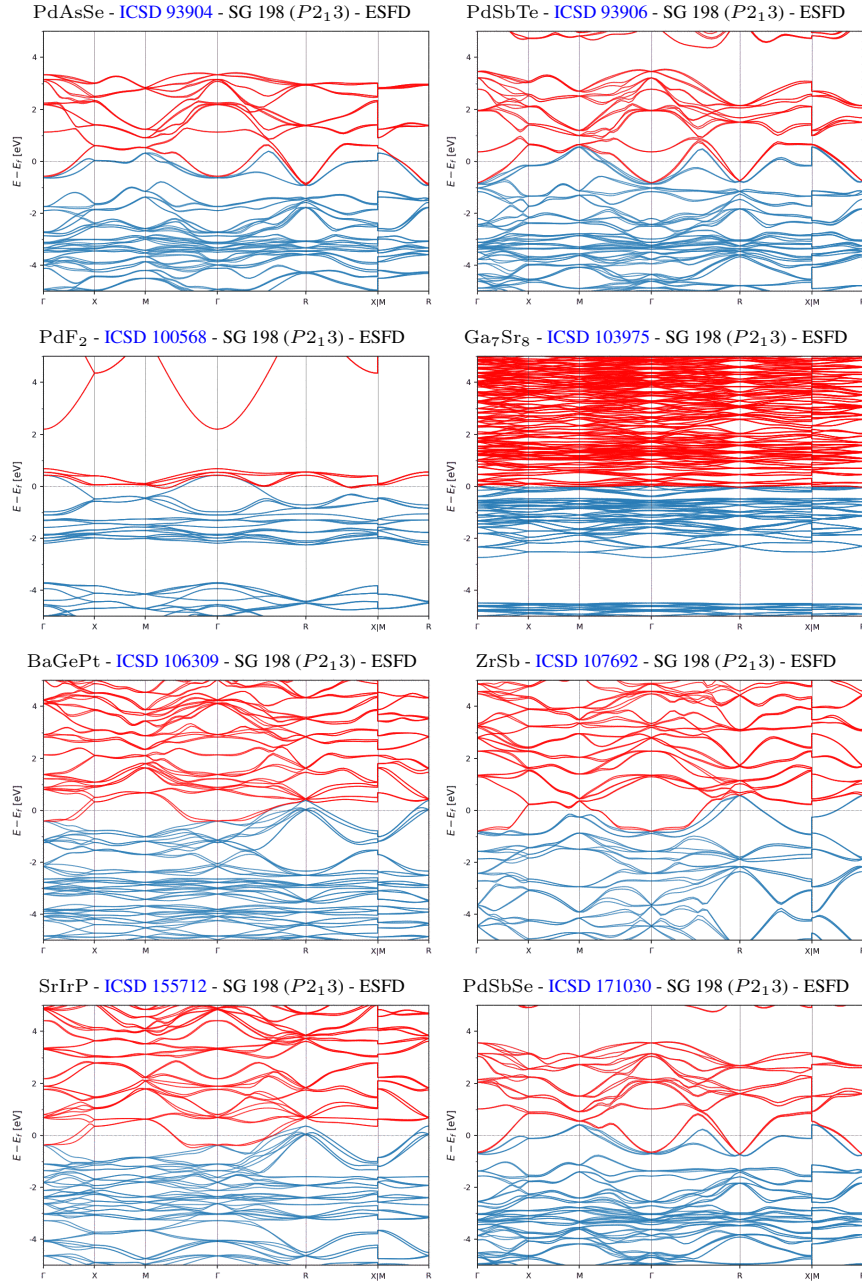


Figure S77. The ESFD-classified topological semimetals in chiral space groups with the simplest bulk Fermi surfaces and enforced chiral fermions close to  $E_F$ . (part 3/6)

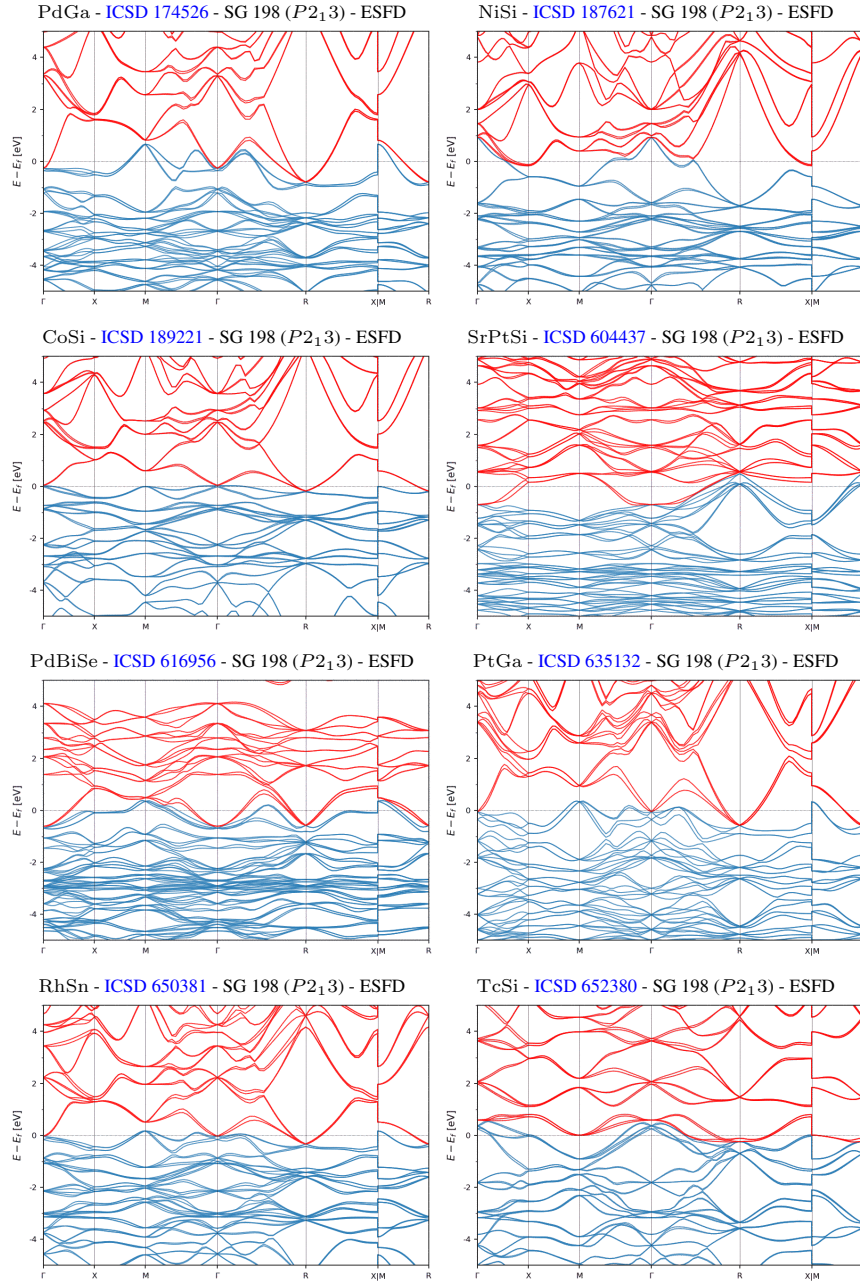


Figure S78. The ESFD-classified topological semimetals in chiral space groups with the simplest bulk Fermi surfaces and enforced chiral fermions close to  $E_F$ . (part 4/6)

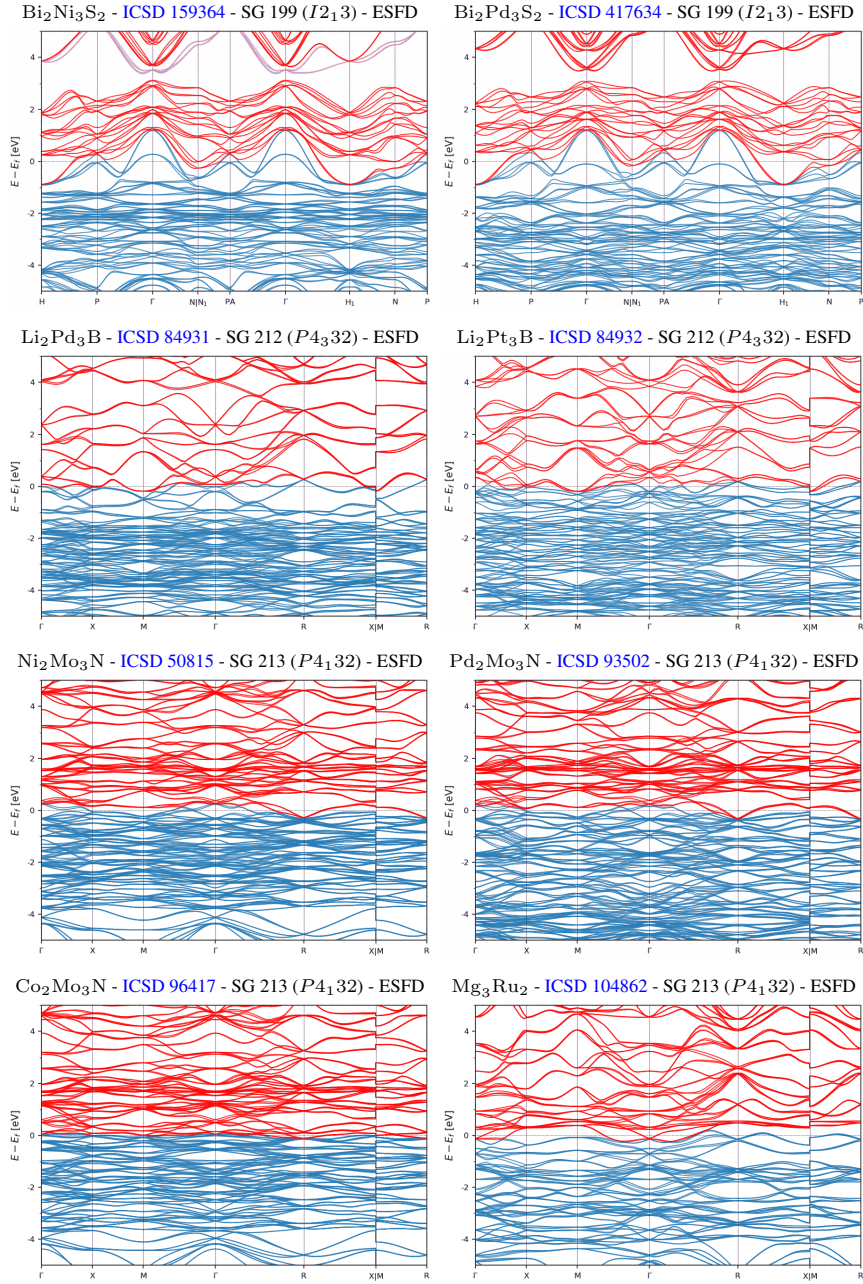


Figure S79. The ESFD-classified topological semimetals in chiral space groups with the simplest bulk Fermi surfaces and enforced chiral fermions close to  $E_F$ . (part 5/6)

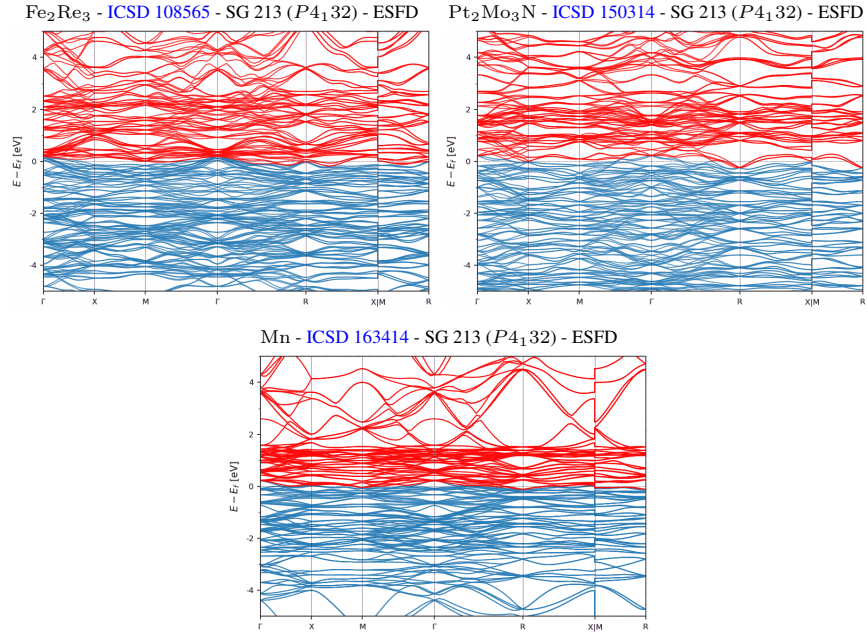


Figure S80. The ESFD-classified topological semimetals in chiral space groups with the simplest bulk Fermi surfaces and enforced chiral fermions close to  $E_F$ . (part 6/6)

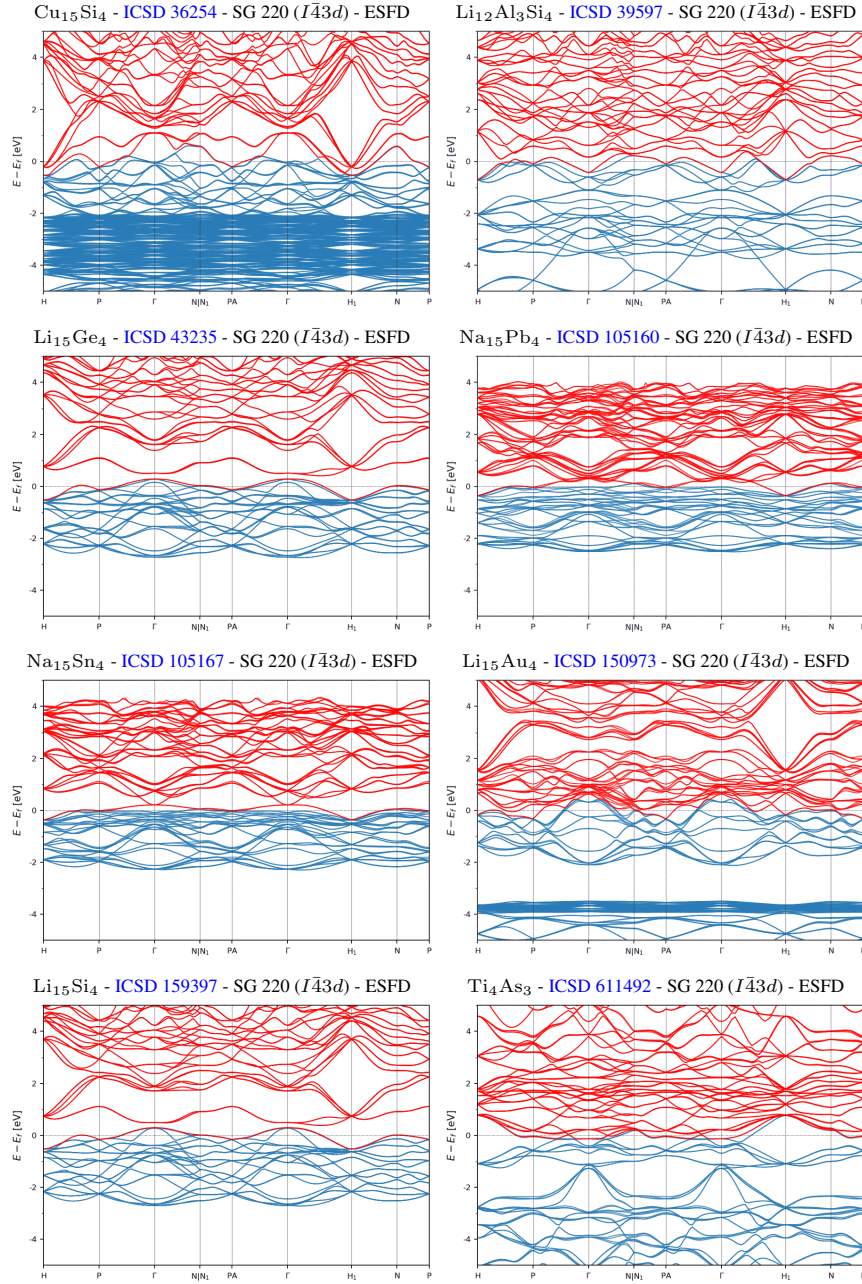


Figure S81. The ESFD-classified topological semimetals with the simplest bulk Fermi surfaces and eightfold-degenerate double Dirac fermions close to  $E_F$ . (part 1/3)

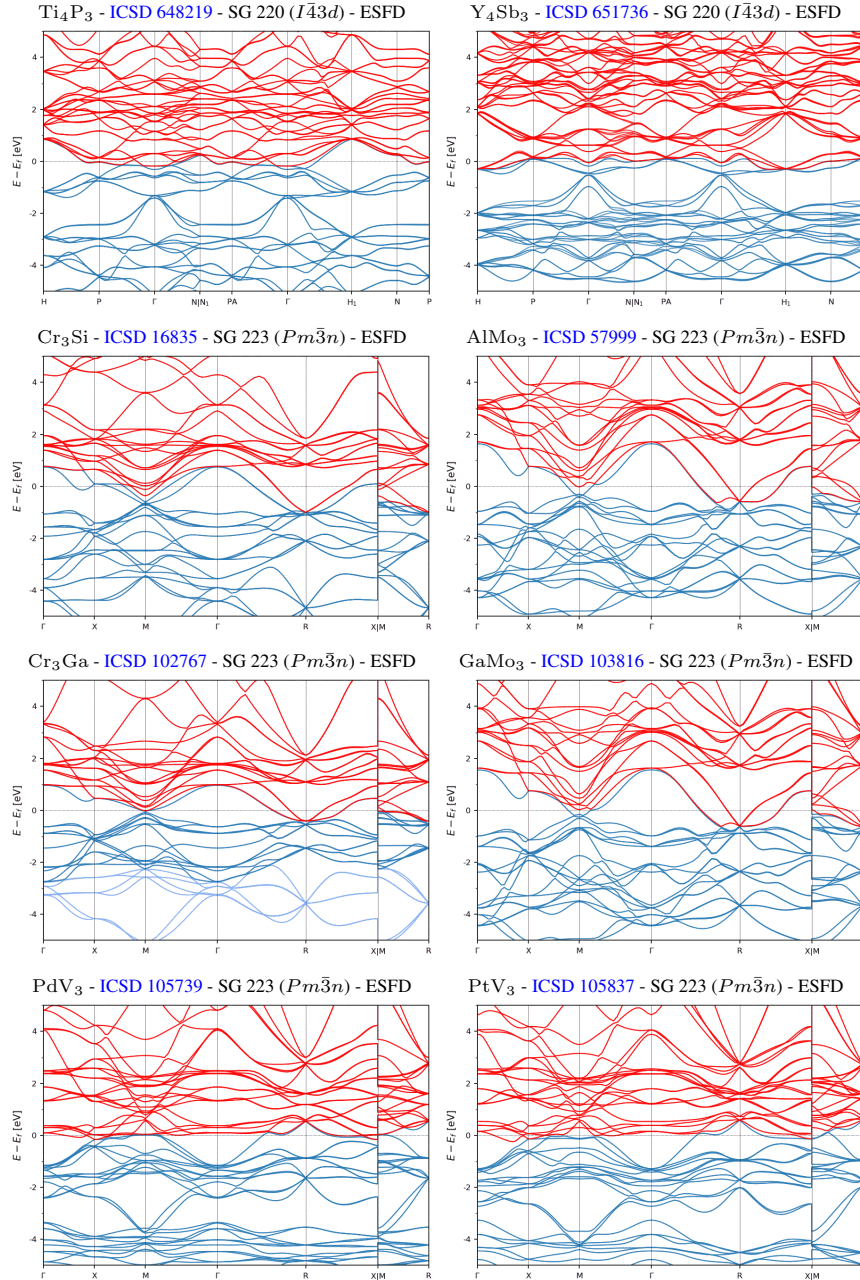


Figure S82. The ESFD-classified topological semimetals with the simplest bulk Fermi surfaces and eightfold-degenerate double Dirac fermions close to  $E_F$ . (part 2/3)

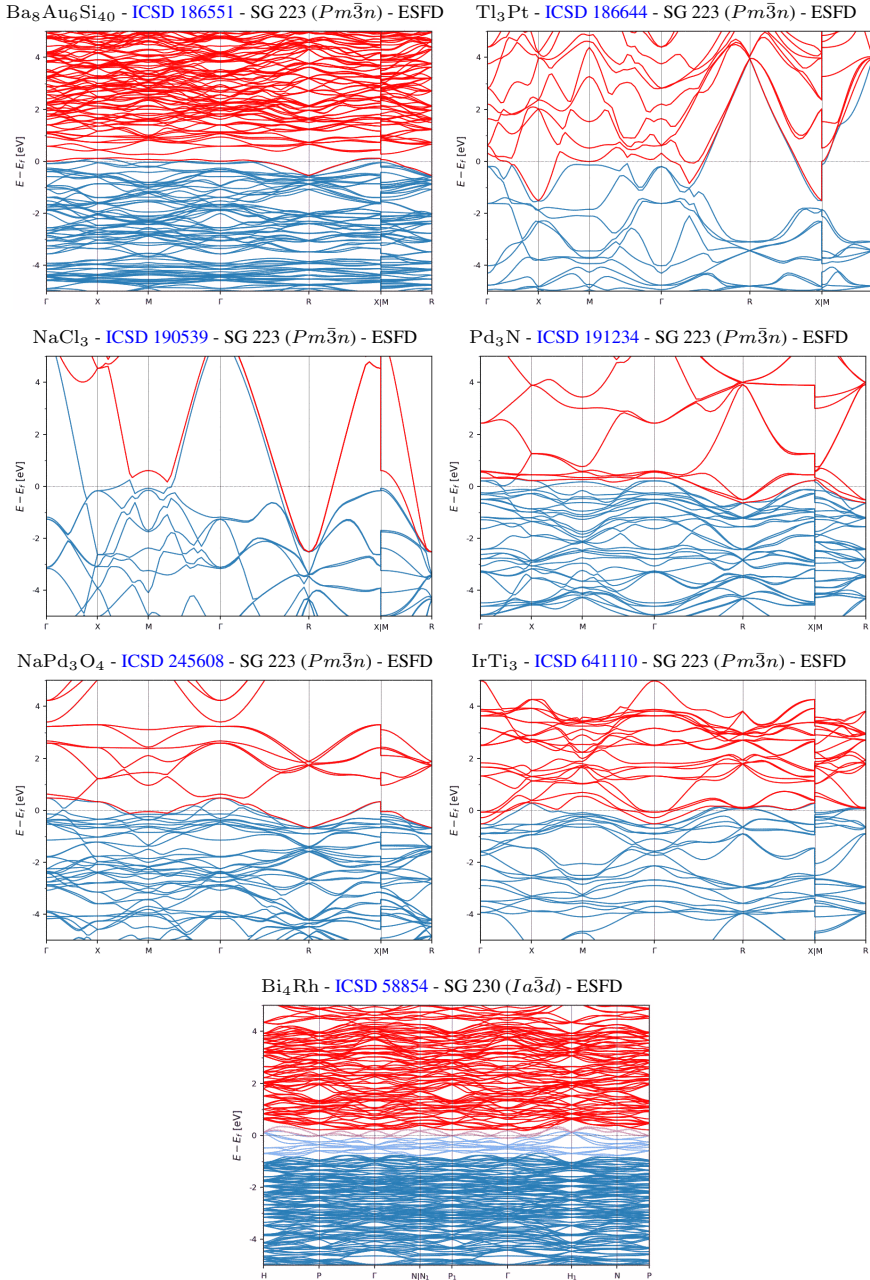


Figure S83. The ESFD-classified topological semimetals with the simplest bulk Fermi surfaces and eightfold-degenerate double Dirac fermions close to  $E_F$ . (part 3/3)

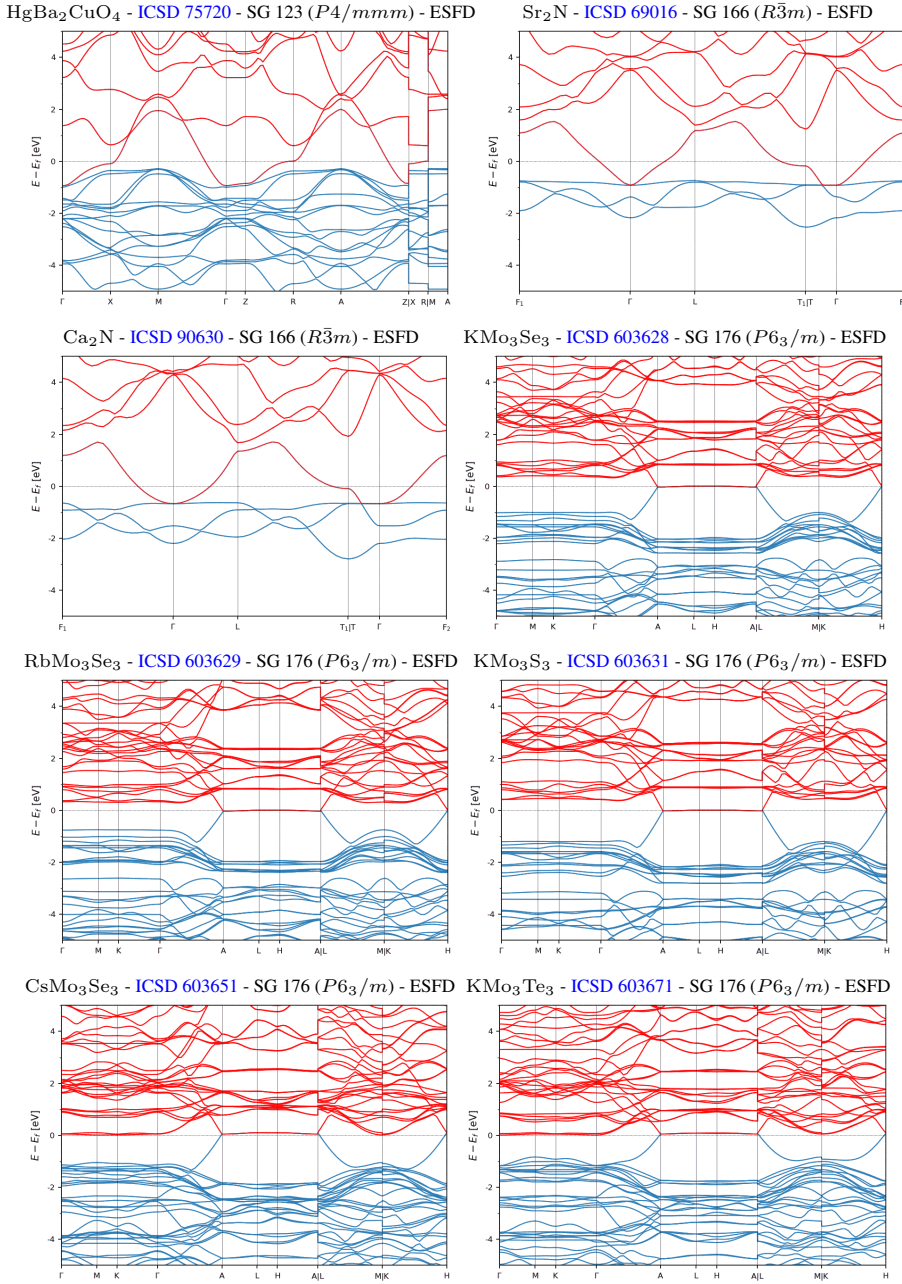


Figure S84. The ESFD-classified topological semimetals with the simplest bulk Fermi surfaces beyond those shown in Figs. S64 through S83. (part 1/2)

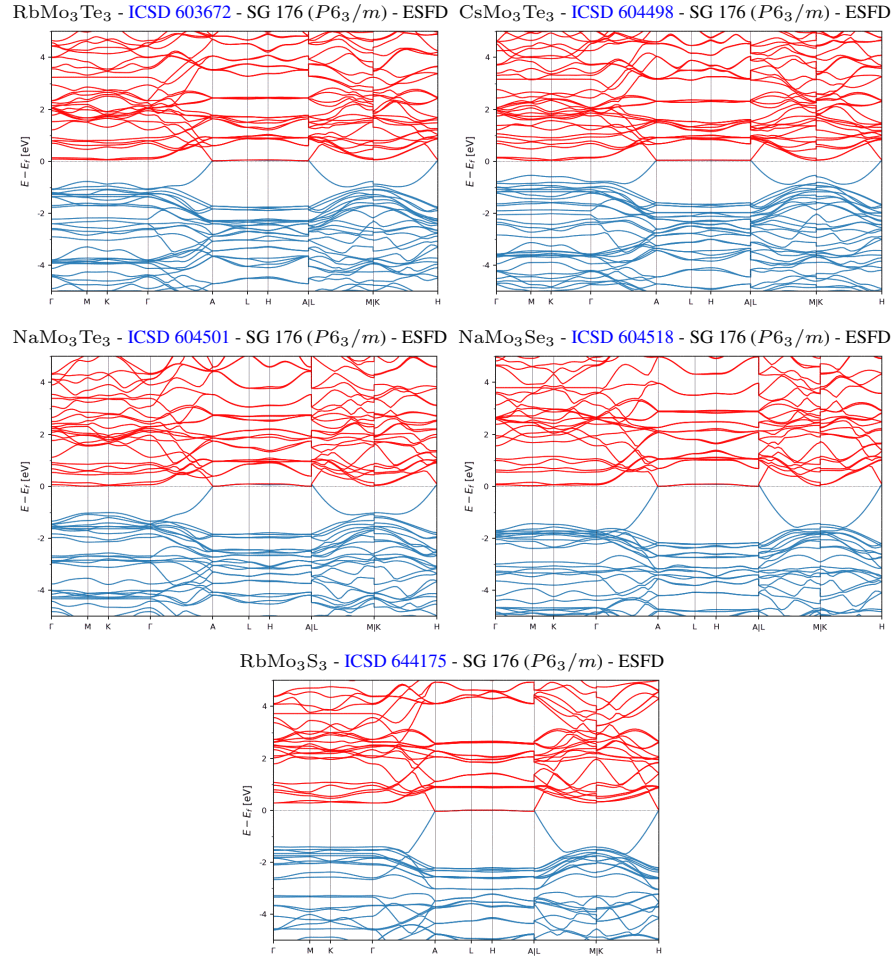


Figure S85. The ESFD-classified topological semimetals with the simplest bulk Fermi surfaces beyond those shown in Figs. S64 through S83. (part 2/2)

## 2. ES-Classified Semimetals

In this section, we list in Figs. S86, S87, S88, S89, S90, and S91 the enforced semimetals with the simplest bulk Fermi surfaces whose nodal degeneracies lie along high-symmetry BZ lines (ES in the nomenclature established in Ref. [38]). Typically, the bulk Fermi pockets of ES materials are characterized by fourfold-degenerate, linearly dispersing Dirac fermions [6, 168, 208, 209]. However, it is also possible for ES materials to host chiral fermions with larger Chern numbers [210–214], threefold-degenerate “nexus” fermions [215–220], or more exotic mixtures of chiral and achiral fermions [221]. Almost all of the materials shown in Figs. S86, S87, S88, S89, S90, and S91 are conventional Dirac semimetals, with two exceptions. First, In<sub>2</sub>ZnS<sub>4</sub> [ICSD 15636 and ICSD 65725, SG 160 (*R*3*m*)] in Fig. S87 is a nexus fermion semimetal with narrowly separated threefold degeneracies. Second, Ta<sub>2</sub>ISe<sub>8</sub> [ICSD 35190, SG 97 (*I*422)] in Fig. S86 is a structurally chiral, quasi-1D Weyl semimetal that, as demonstrated in recent theoretical and experimental investigations, becomes gapped by a topological (axionic) charge-density wave when cooled just below room temperature [26, 27, 70, 222–224]. Most notably, Figs. S86 and S90 respectively include the archetypal, experimentally confirmed Dirac semimetals Cd<sub>3</sub>As<sub>2</sub> [ICSD 107918, SG 137 (*P*4<sub>2</sub>/*nmc*)] [6, 19, 115, 116] and Na<sub>3</sub>Bi [ICSD 26881, SG 194 *P*6<sub>3</sub>/*mmc*] [168, 172, 173]. As recently shown in Ref. [59], Dirac points with 4*mm* or higher symmetry also exhibit topological hinge states; because a significant number of the Dirac semimetals in Figs. S86, S87, S88, S89, S90, and S91 have SGs whose point groups contain 4*mm*, then the listed Dirac semimetals may also be classified as higher-order topological semimetals. Finally, the results of Refs. [34, 59, 96, 225–231] also imply the presence of hinge states in additional ES materials without fourfold symmetry, including the materials shown in Figs. S86, S87, S88, S89, S90, and S91 with threefold or sixfold rotational symmetries.

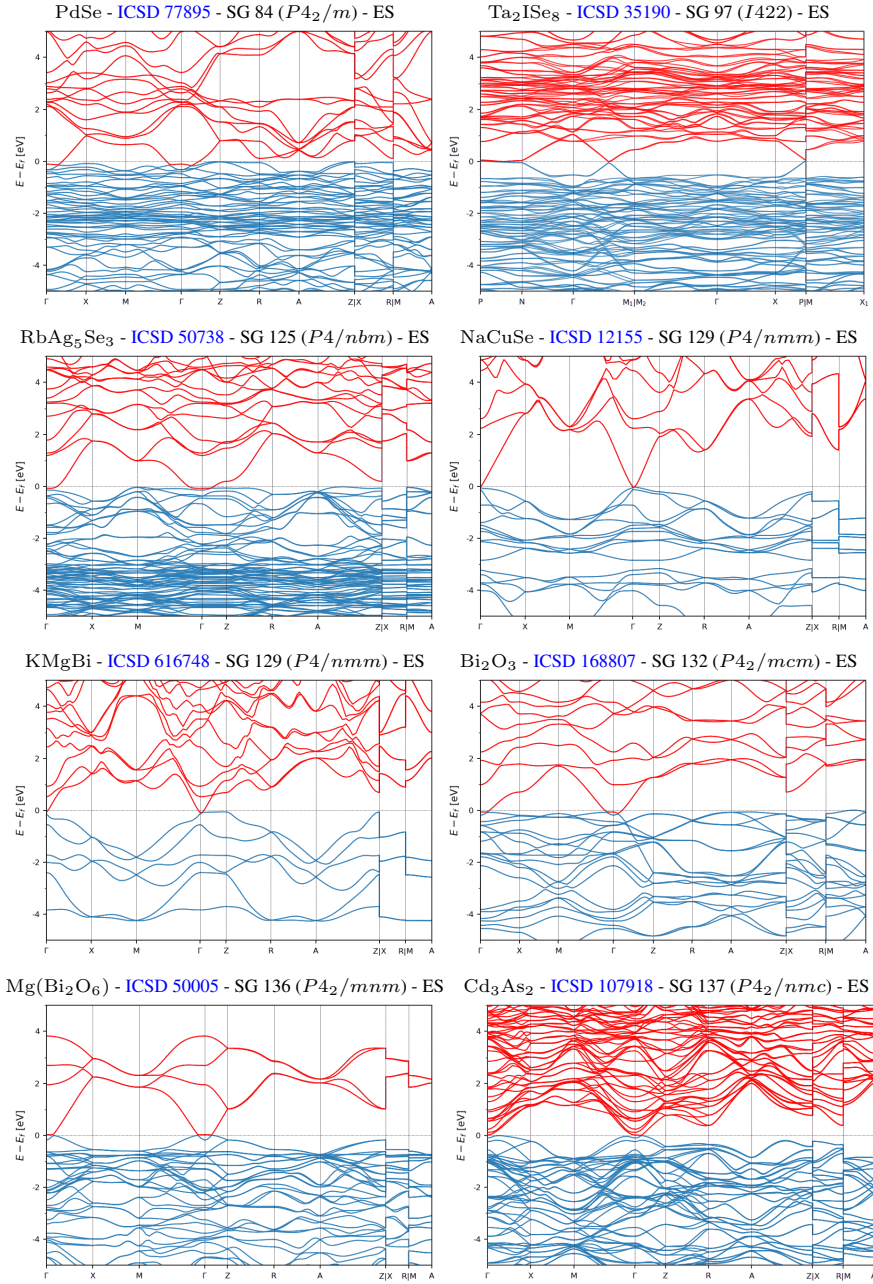


Figure S86. The ES-classified topological semimetals with the simplest bulk Fermi surfaces. (part 1/6)

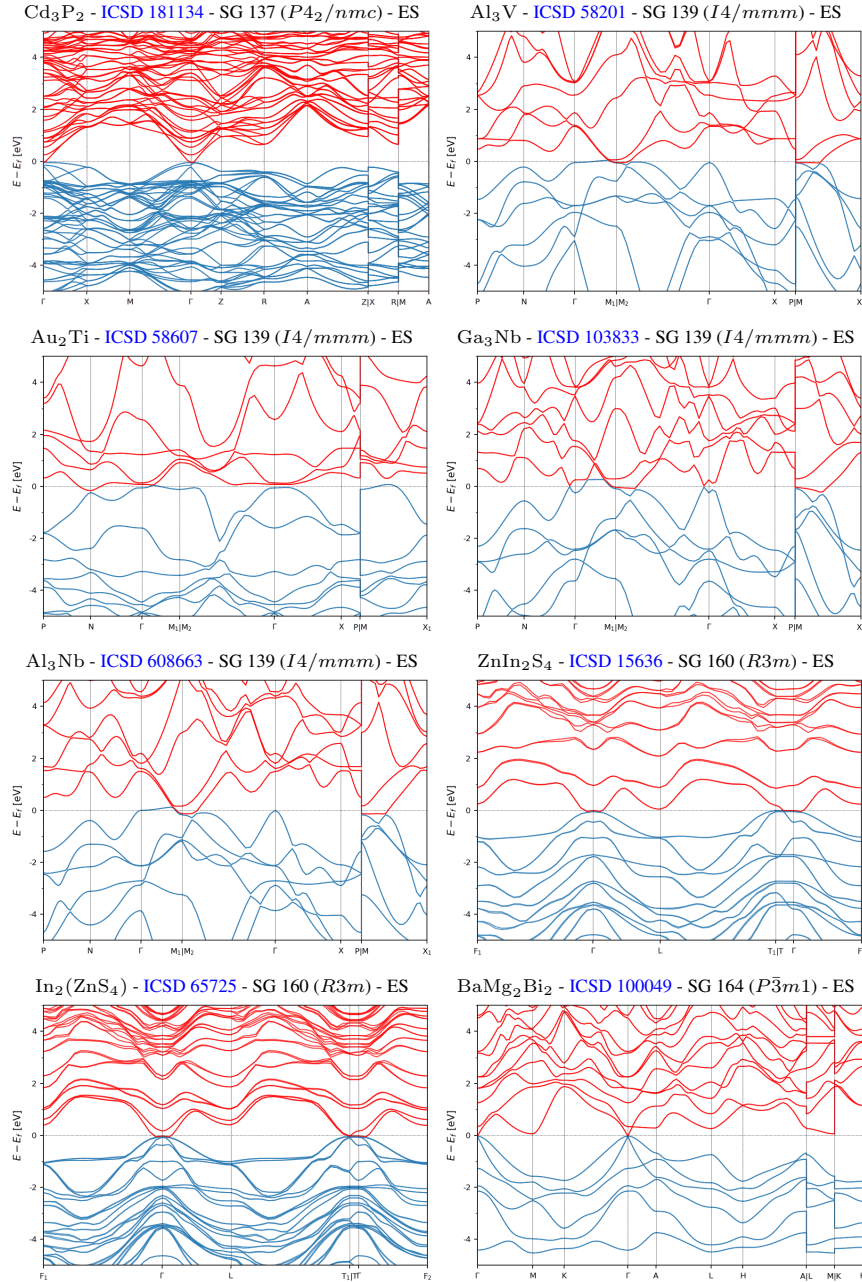


Figure S87. The ES-classified topological semimetals with the simplest bulk Fermi surfaces. (part 2/6)

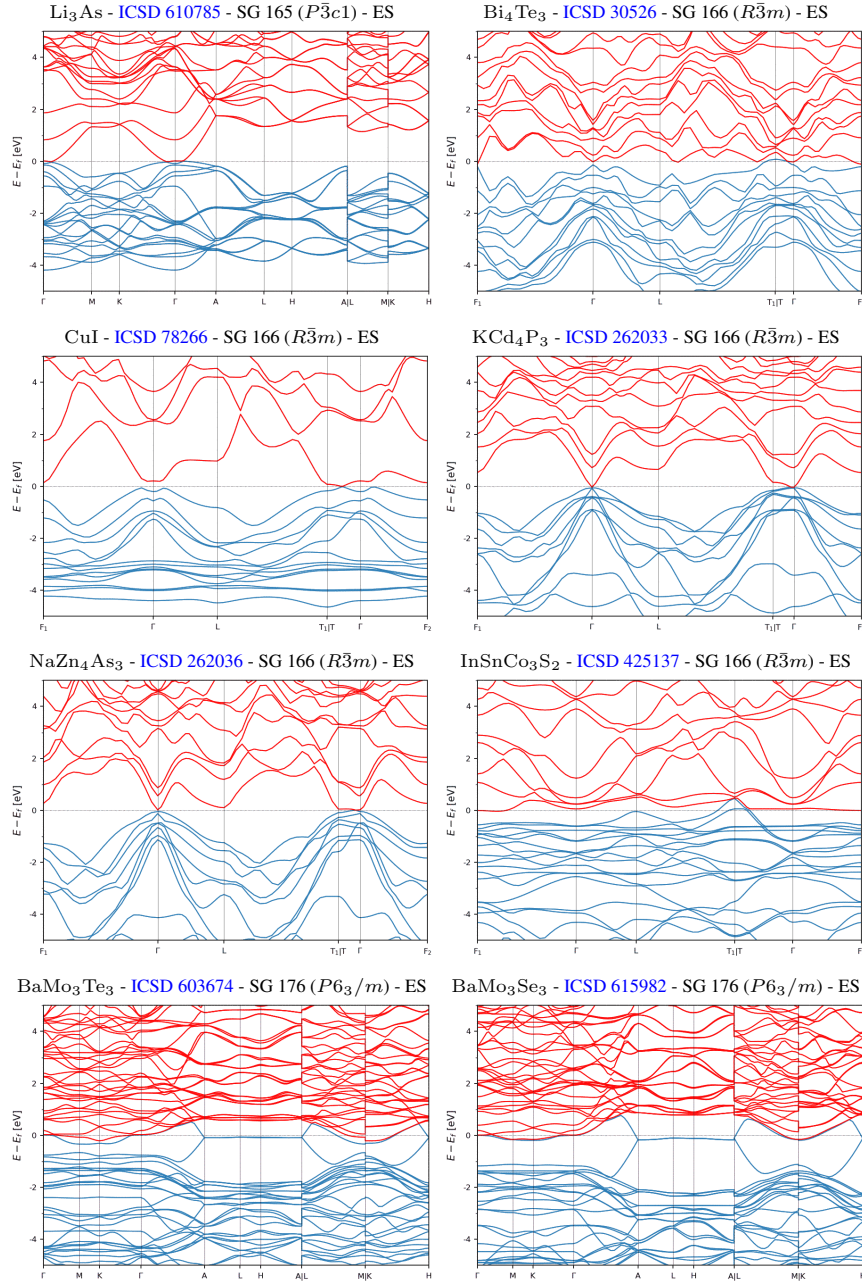


Figure S88. The ES-classified topological semimetals with the simplest bulk Fermi surfaces. (part 3/6)

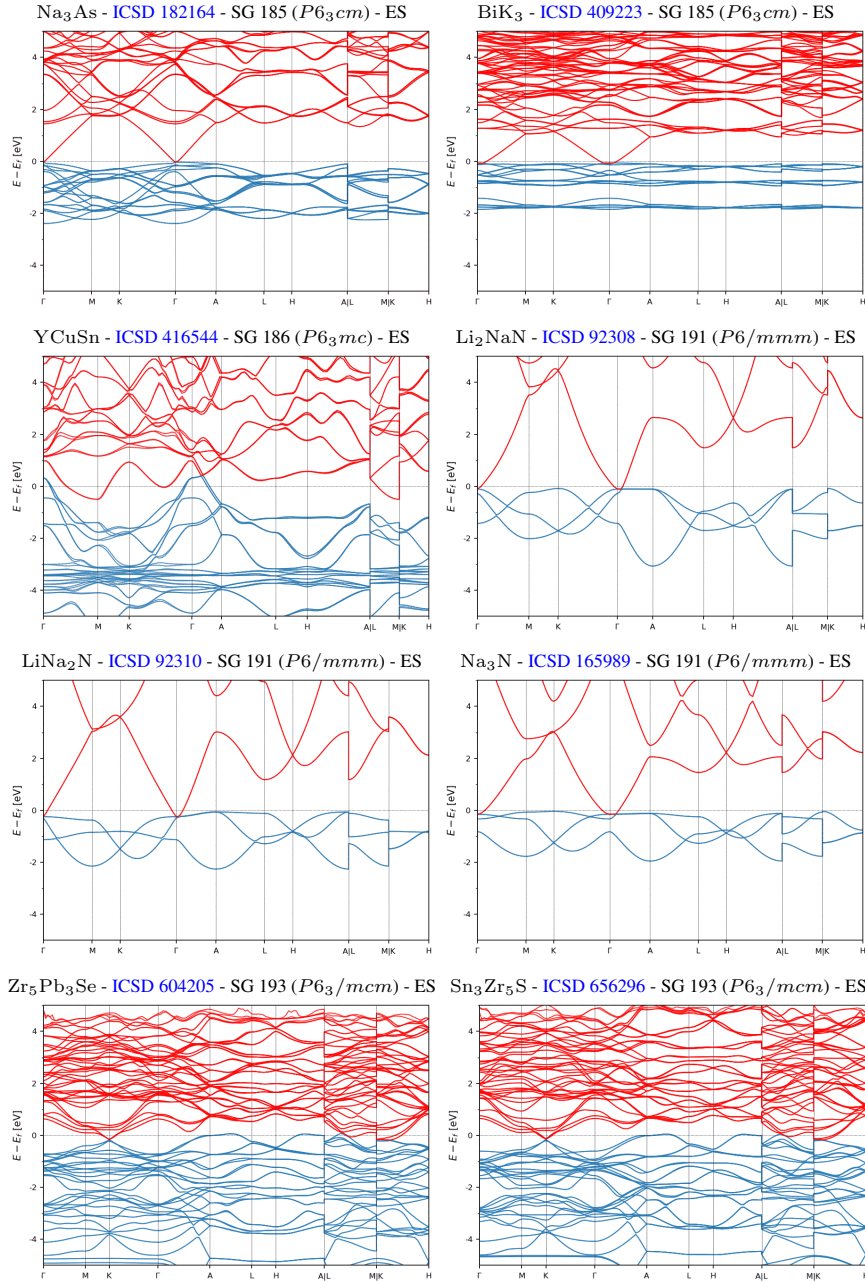


Figure S89. The ES-classified topological semimetals with the simplest bulk Fermi surfaces. (part 4/6)

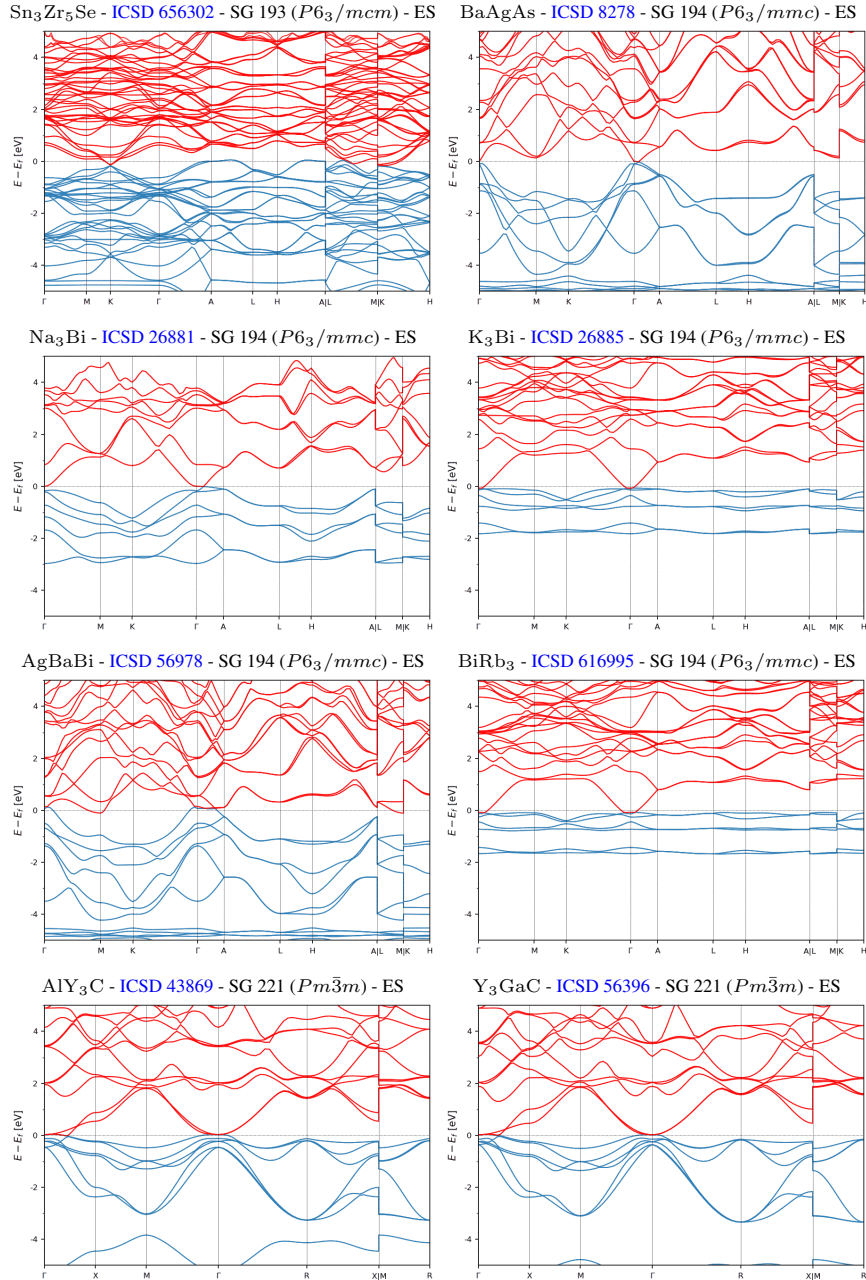


Figure S90. The ES-classified topological semimetals with the simplest bulk Fermi surfaces. (part 5/6)

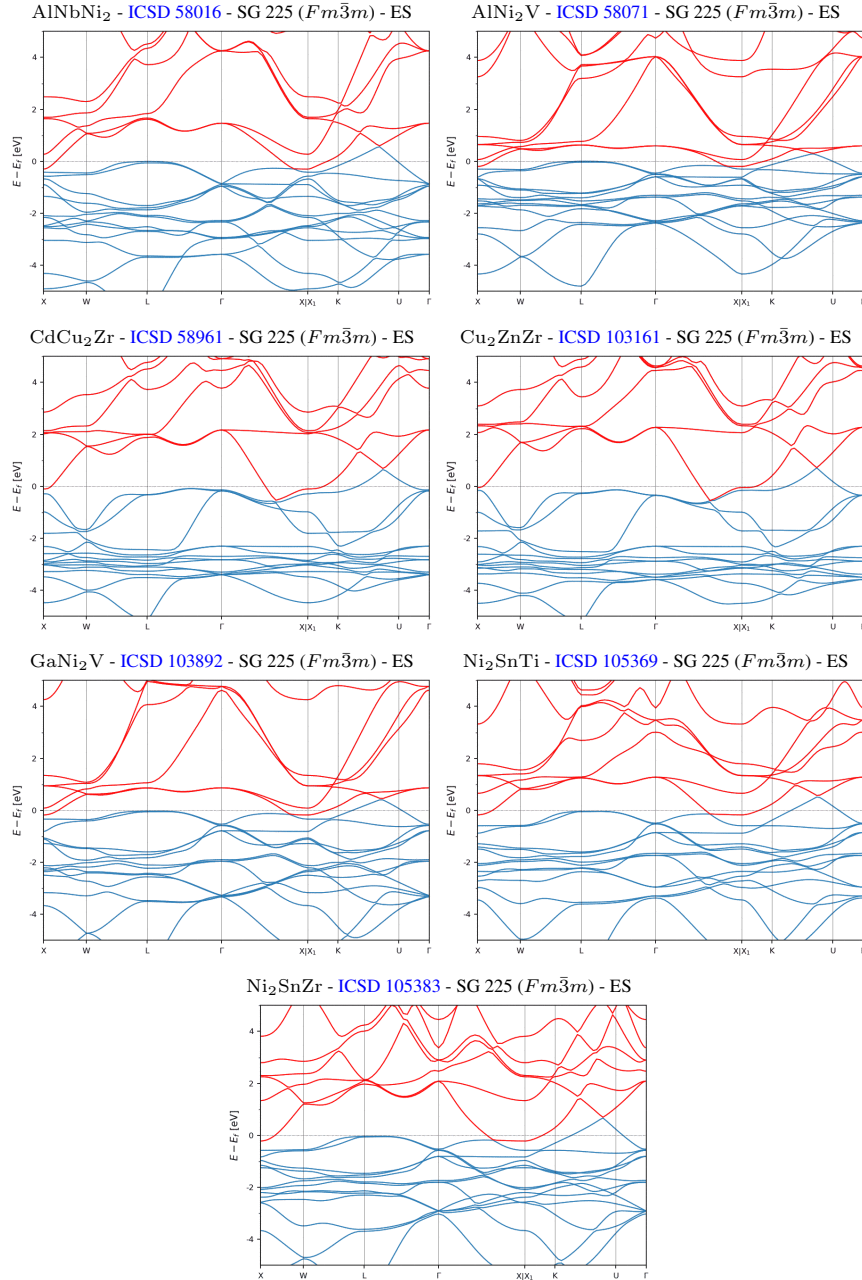


Figure S91. The ES-classified topological semimetals with the simplest bulk Fermi surfaces. (part 6/6)

#### D. Semimetal-Insulator Transitions Driven by Spin-Orbit Coupling

In this section, we show the materials with the largest gaps at  $E_F$  or the fewest and smallest bulk Fermi pockets that are topological insulating in the presence of SOC and enforced or symmetry-indicated semimetals when the effects of SOC are neglected. Specifically, when the strength of SOC is artificially tuned to zero without (un)inverting bands (*i.e.* without changing the bulk band ordering), the bulk gaps of spinful TI, TCI, and HOTI phases necessarily close and the bulk transitions into a spinless (spin-degenerate) topological semimetal phase [31, 34, 36]. The prototypical example of an SOC-driven transition between a spinless topological semimetal phase without SOC and a TI phase with SOC occurs in graphene, which is an ESFD semimetal in the absence of SOC [28, 31, 160], and a 2D TI when the (weak) effects of SOC are taken into consideration [3, 127] (see S10). In Figs. S92, S93, S94, S95, S96, and S97, we respectively show the spinful topological (crystalline) insulators that originate from weak-SOC ESFD, ES, NLC-symmetry-indicated (NLC-SM), and SEBR-symmetry-indicated (SEBR-SM) topological semimetals. For concision, in Figs. S92, S93, S94, S95, S96, and S97, we only show material band structures calculated incorporating the effects of SOC; the corresponding band structures and topological information calculated without SOC can be accessed for each material by clicking on the ICSD number listed above each plot.

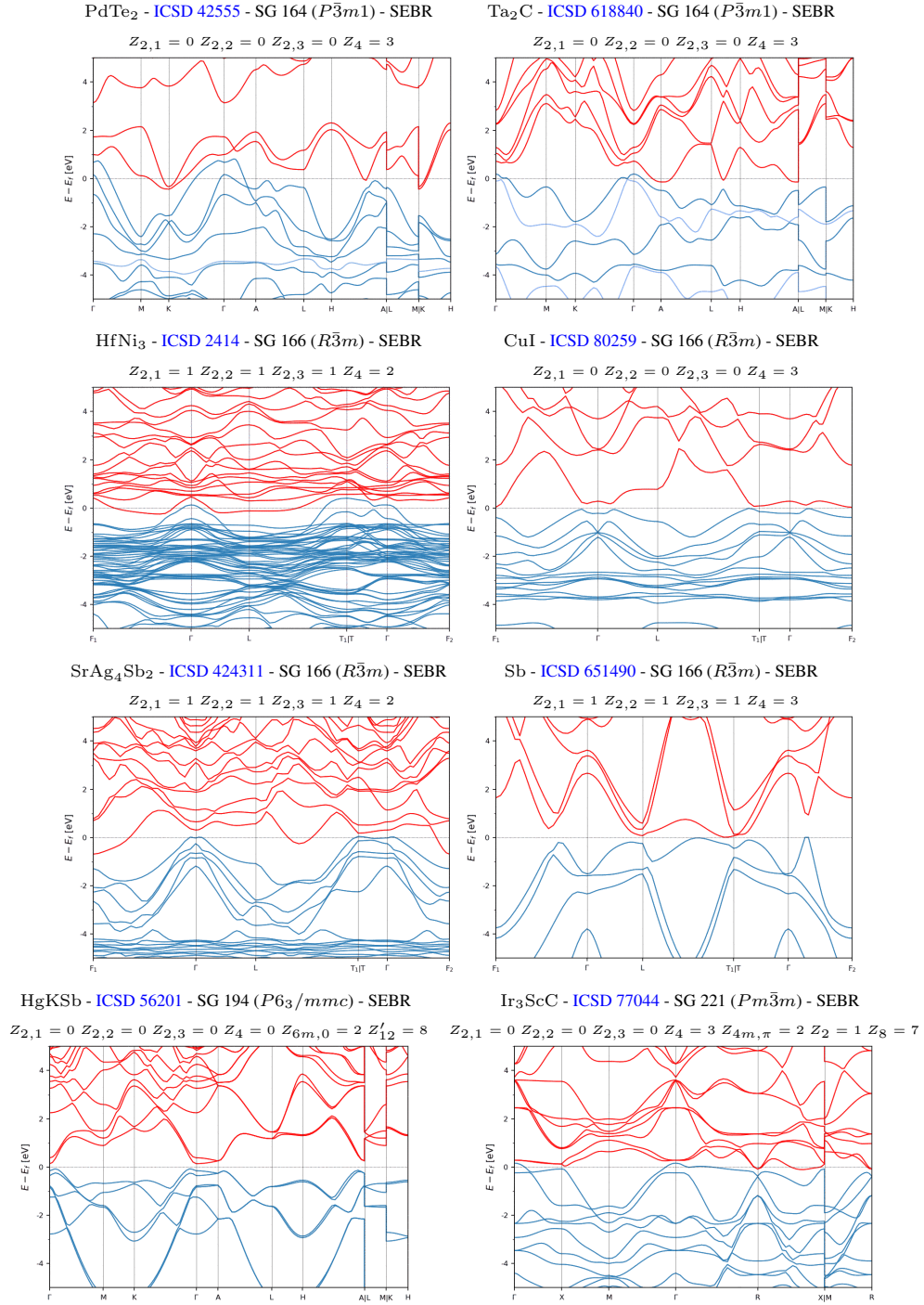


Figure S92. The spinful topological (crystalline) insulators with the largest bulk gaps or the fewest Fermi pockets that are classified as ESFD topological semimetals when the effects of SOC are neglected. (part 1/2)

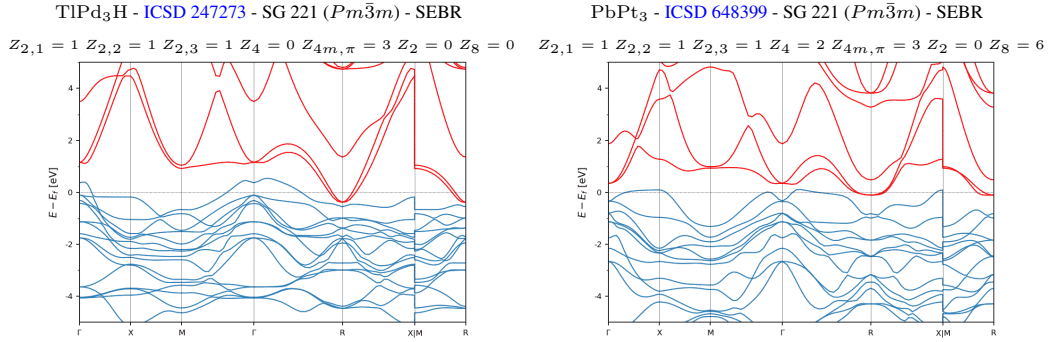


Figure S93. The spinful topological (crystalline) insulators with the largest bulk gaps or the fewest Fermi pockets that are classified as ESFD topological semimetals when the effects of SOC are neglected. (part 2/2)

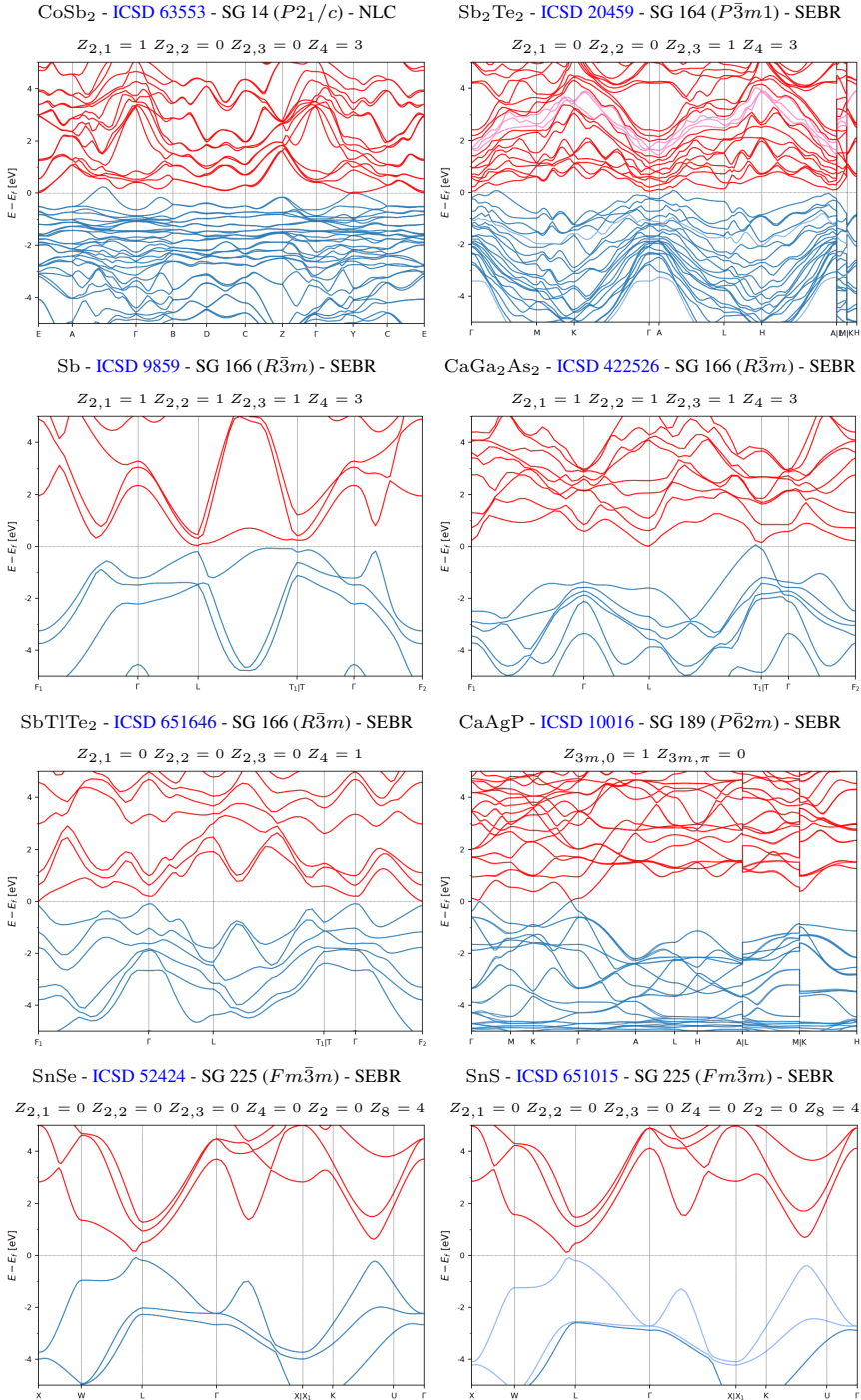


Figure S94. The spinful topological (crystalline) insulators with the largest bulk gaps or the fewest Fermi pockets that are classified as ES topological semimetals when the effects of SOC are neglected. (part 1/2)

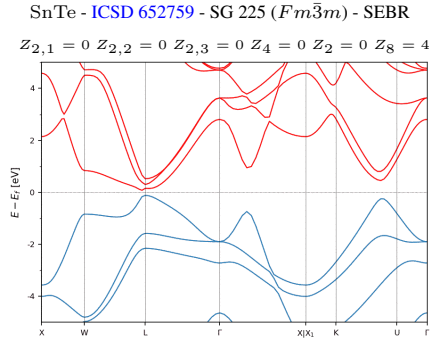


Figure S95. The spinful topological (crystalline) insulators with the largest bulk gaps or the fewest Fermi pockets that are classified as ES topological semimetals when the effects of SOC are neglected. (part 2/2)

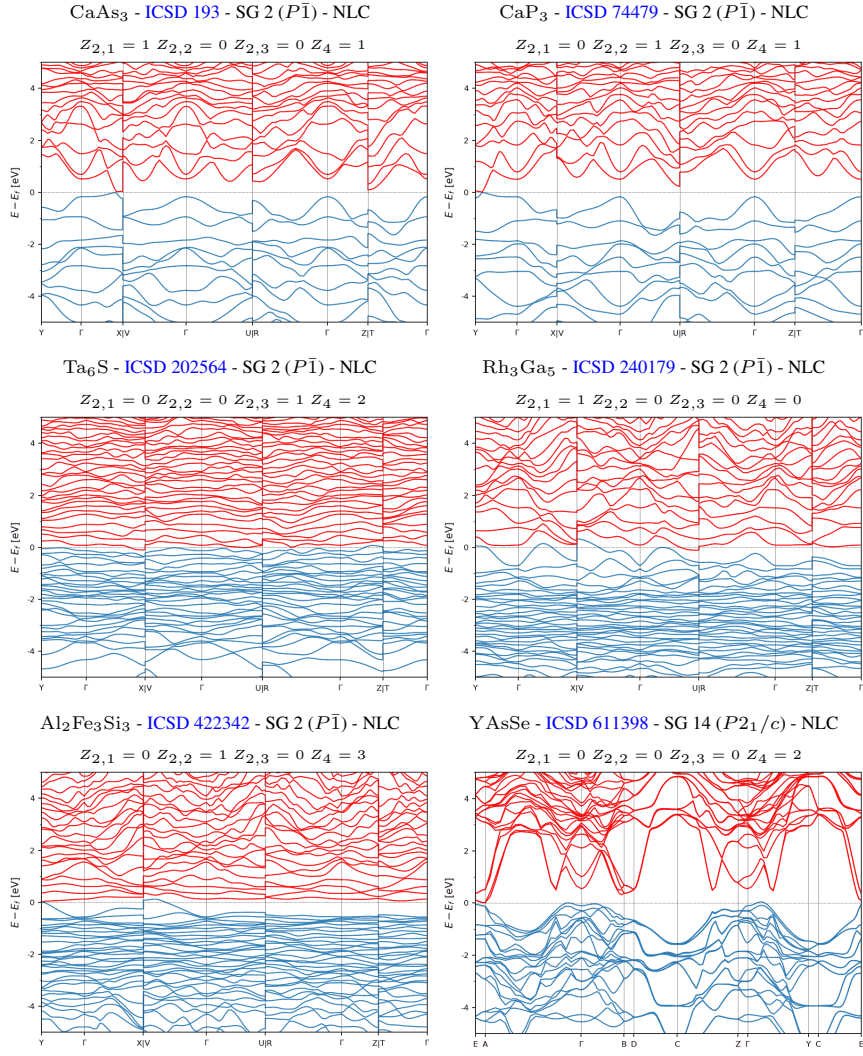


Figure S96. The spinful topological (crystalline) insulators with the largest bulk gaps or the fewest Fermi pockets that are classified as NLC-SM topological semimetals when the effects of SOC are neglected.

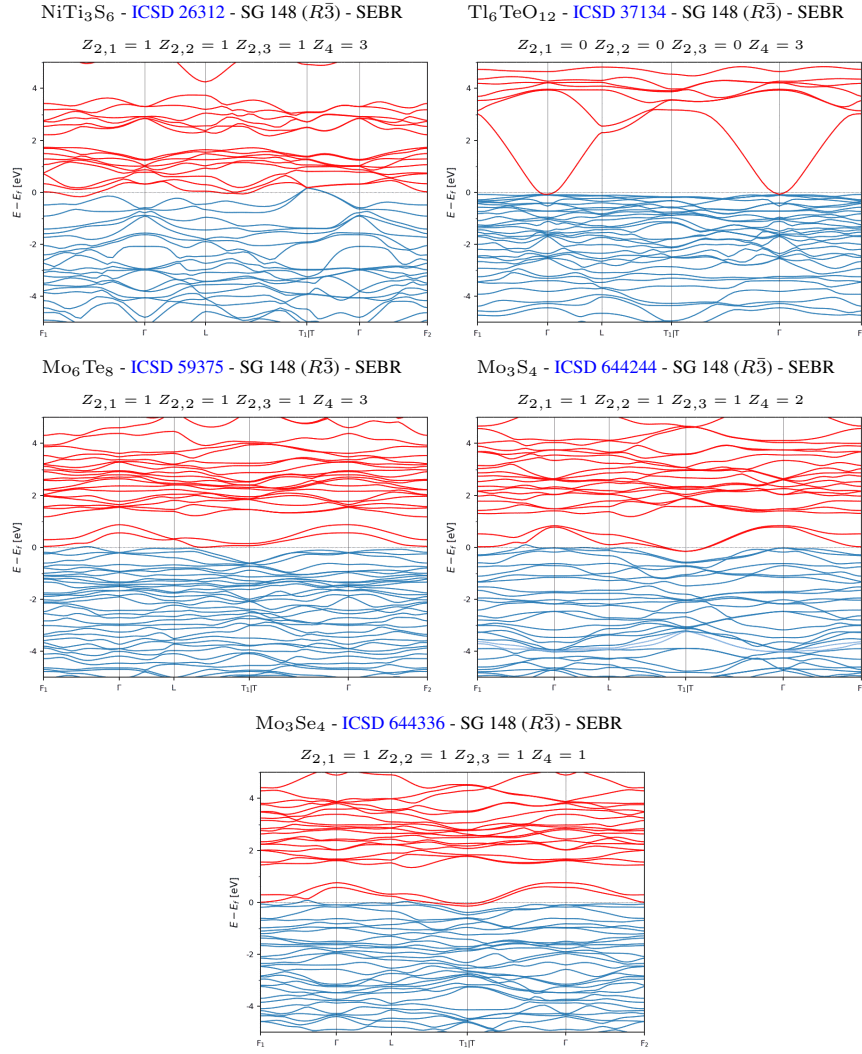


Figure S97. The spinful topological (crystalline) insulators with the largest bulk gaps or the fewest Fermi pockets that are classified as SEBR-SM topological semimetals when the effects of SOC are neglected.

### E. Materials with Fragile Topological Bands at or Close to $E_F$

In this section, we show the materials with the largest gaps at  $E_F$  or the fewest and smallest bulk Fermi pockets that host groups of well-isolated bands at or near  $E_F$  with symmetry-indicated fragile topology [43–48, 96–101, 174]. Specifically, as derived in Refs. [43, 45, 46], in some cases, isolated groups of bands within the spectrum can be diagnosed as fragile topological, even if the entire valence (or conduction) manifold does not exhibit fragile topology. In Figs. S98, S99, S100, S101, S102, and S103, we respectively show representative examples of SEBR-, ESFD-, ES-, and LCEBR-classified materials with well-isolated fragile bands close to  $E_F$  [we do not find any examples of NLC-classified topological (crystalline) insulators with few bulk Fermi pockets and well-isolated fragile bands close to  $E_F$ ]. Though just over half of the materials listed in Figs. S98, S99, S100, S101, S102, and S103 were previously identified in Ref. [45] as hosting fragile bands, the remaining materials in this section have not been previously highlighted for hosting fragile topology. The materials with well-isolated fragile bands not previously listed in Ref. [45] are Sb<sub>2</sub>Te<sub>2</sub> [ICSD 20459, SG 164 ( $P\bar{3}m1$ )], Ta<sub>2</sub>S<sub>2</sub>C [ICSD 23790, SG 164 ( $P\bar{3}m1$ )], Pb<sub>2</sub>Bi<sub>2</sub>Se<sub>5</sub> [ICSD 30372, SG 164 ( $P\bar{3}m1$ )], BiTe [ICSD 30525, SG 164 ( $P\bar{3}m1$ )], As<sub>2</sub>Ge<sub>5</sub>Te<sub>8</sub> [ICSD 63174, SG 164 ( $P\bar{3}m1$ )], Ta<sub>2</sub>C [ICSD 409555, SG 164 ( $P\bar{3}m1$ )], BiSe [ICSD 617073, SG 164 ( $P\bar{3}m1$ )], and TiS<sub>2</sub> [ICSD 72042, SG 227 ( $Fd\bar{3}m$ )] in Figs. S98 and S99; TaSe<sub>2</sub> [ICSD 24313, SG 164 ( $P\bar{3}m1$ )], BiTe [ICSD 44984, SG 225 ( $Fm\bar{3}m$ )], and Bi<sub>4</sub>Rh [ICSD 58854, SG 230 ( $Ia\bar{3}d$ )] in Figs. S100 and S101; SrZn<sub>2</sub>Sb<sub>2</sub> [ICSD 12152, SG 164 ( $P\bar{3}m1$ )], Sc<sub>2</sub>C [ICSD 280743, SG 164 ( $P\bar{3}m1$ )], and TaN [ICSD 105123, SG 194 ( $P6_3/mmc$ )] in Fig. S102; and TiS<sub>2</sub> [ICSD 91579, SG 164 ( $P\bar{3}m1$ )] and Al<sub>5</sub>C<sub>3</sub>N [ICSD 36303, SG 186 ( $P6_3mc$ )] in Fig. S103.

Finally, because recent works have demonstrated that insulators with fragile topological bands can exhibit anomalous corner modes [34, 46, 59, 96, 99, 102] and nontrivial twisted-boundary [47, 100] and topological defect responses [107], then the materials highlighted in this section represent new avenues for experimentally investigating novel topological response effects in solid-state systems.

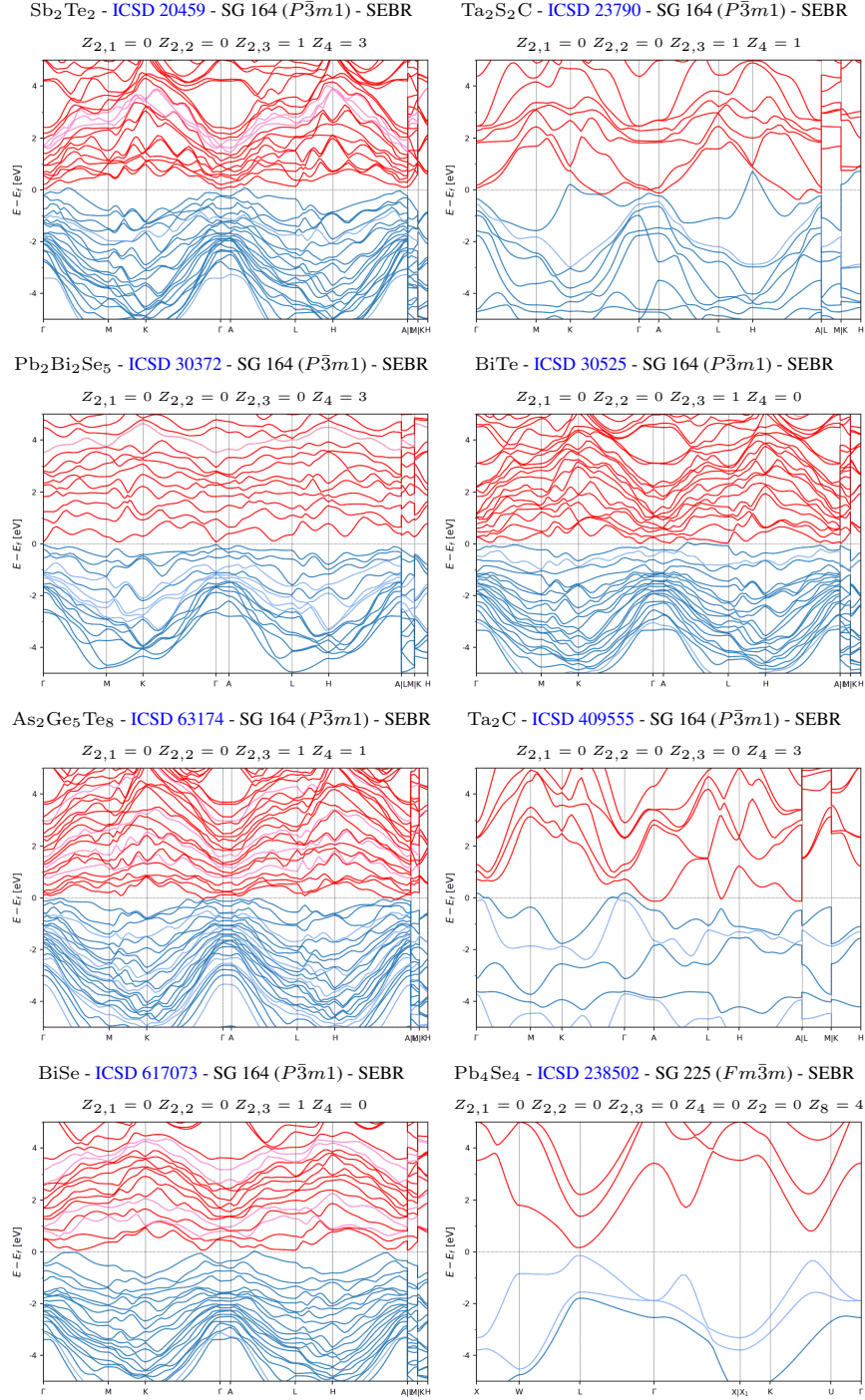


Figure S98. The SEBR-classified topological (crystalline) insulators with the largest bulk gaps or the fewest and smallest bulk Fermi pockets that host well-isolated fragile bands at or close to  $E_F$ . (part 1/2)

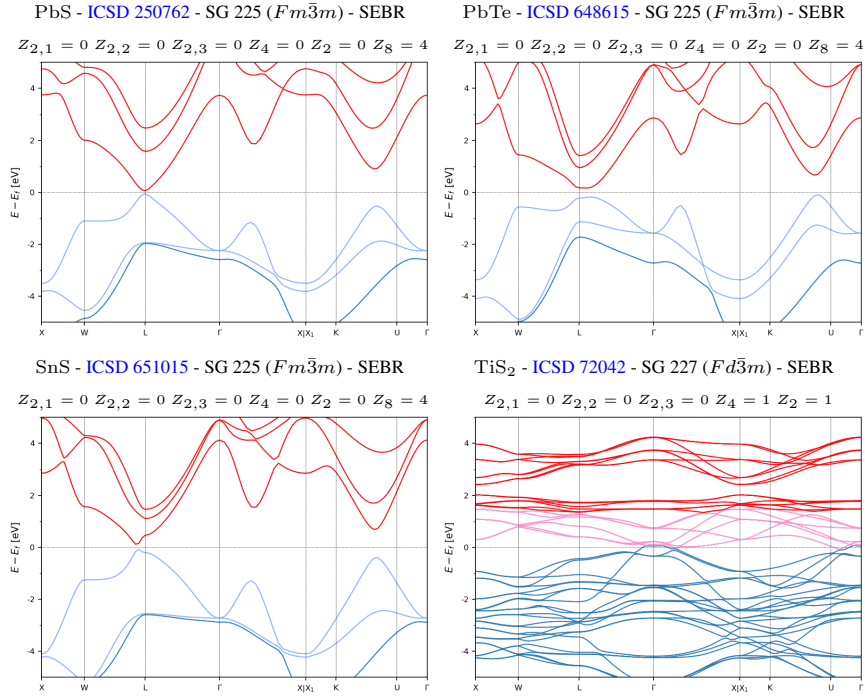


Figure S99. The SEBR-classified topological (crystalline) insulators with the largest bulk gaps or the fewest and smallest bulk Fermi pockets that host well-isolated fragile bands at or close to  $E_F$ . (part 2/2)

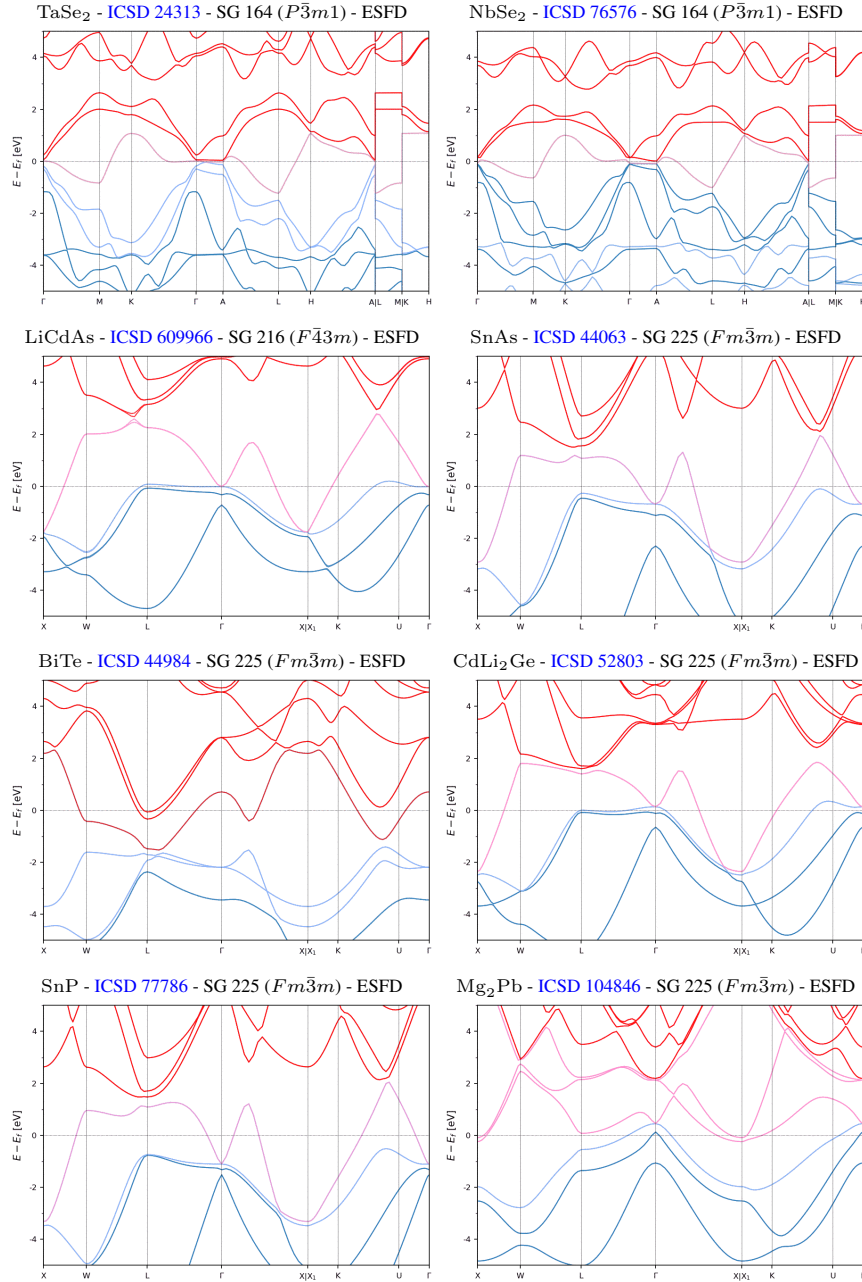


Figure S100. The ESFD-classified topological semimetals with the simplest bulk Fermi surfaces and well-isolated fragile bands at or close to  $E_F$ . (part 1/2)

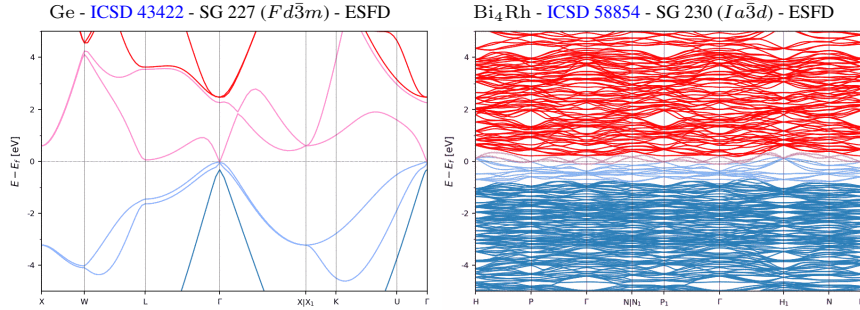


Figure S101. The ESFD-classified topological semimetals with the simplest bulk Fermi surfaces and well-isolated fragile bands at or close to  $E_F$ . (part 2/2)

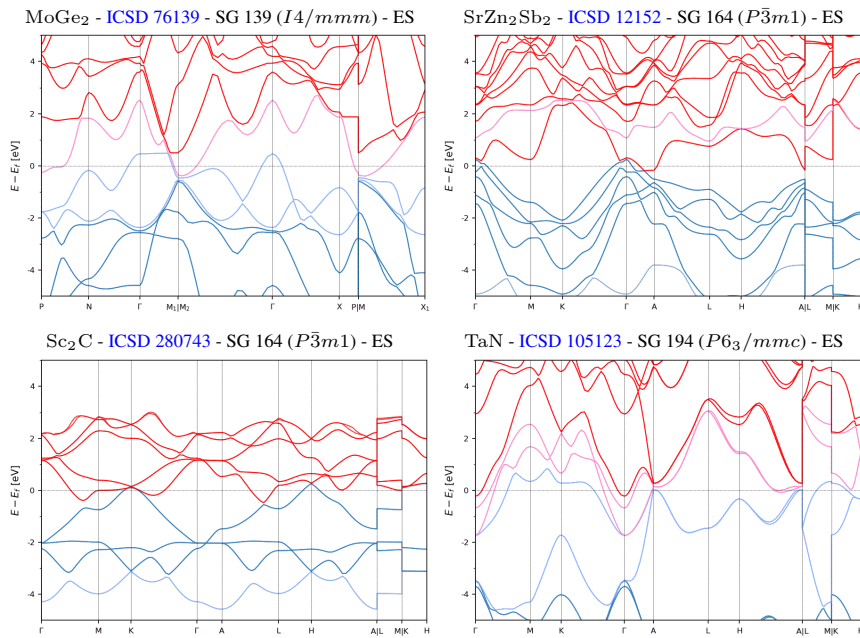


Figure S102. The ES-classified topological semimetals with the simplest bulk Fermi surfaces and well-isolated fragile bands at or close to  $E_F$ .

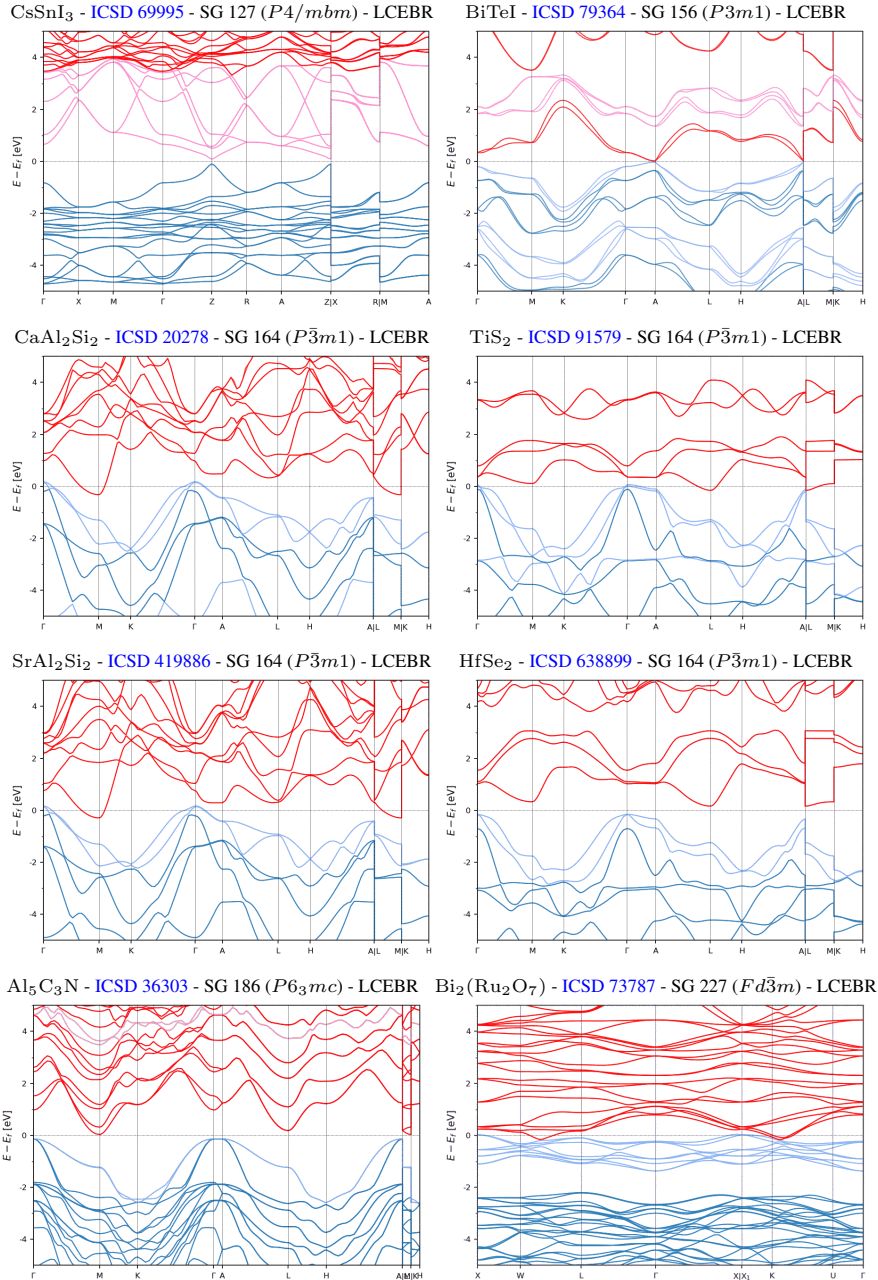


Figure S103. Representative examples of LCEBR-classified insulators with trivial symmetry-indicated strong topology and well-isolated fragile bands at or close to  $E_F$ .

## References and Notes

1. B. J. Wieder, B. Bradlyn, J. Cano, Z. Wang, M. G. Vergniory, L. Elcoro, A. A. Soluyanov, C. Felser, T. Neupert, N. Regnault, B. A. Bernevig, Topological materials discovery from crystal symmetry. *Nat. Rev. Mater.* **7**, 196–216 (2022).  
[doi:10.1038/s41578-021-00380-2](https://doi.org/10.1038/s41578-021-00380-2)
2. M. Z. Hasan, C. L. Kane, Topological insulators. *Rev. Mod. Phys.* **82**, 3045–3067 (2010).  
[doi:10.1103/RevModPhys.82.3045](https://doi.org/10.1103/RevModPhys.82.3045)
3. C. L. Kane, E. J. Mele,  $Z_2$  topological order and the quantum spin Hall effect. *Phys. Rev. Lett.* **95**, 146802 (2005). [doi:10.1103/PhysRevLett.95.146802](https://doi.org/10.1103/PhysRevLett.95.146802) [Medline](#)
4. B. A. Bernevig, T. L. Hughes, S.-C. Zhang, Quantum spin Hall effect and topological phase transition in HgTe quantum wells. *Science* **314**, 1757–1761 (2006).  
[doi:10.1126/science.1133734](https://doi.org/10.1126/science.1133734) [Medline](#)
5. L. Fu, C. L. Kane, E. J. Mele, Topological insulators in three dimensions. *Phys. Rev. Lett.* **98**, 106803 (2007). [doi:10.1103/PhysRevLett.98.106803](https://doi.org/10.1103/PhysRevLett.98.106803) [Medline](#)
6. Z. Wang, H. Weng, Q. Wu, X. Dai, Z. Fang, Three-dimensional Dirac semimetal and quantum transport in Cd<sub>3</sub>As<sub>2</sub>. *Phys. Rev. B* **88**, 125427 (2013). [doi:10.1103/PhysRevB.88.125427](https://doi.org/10.1103/PhysRevB.88.125427)
7. B. J. Wieder, Y. Kim, A. M. Rappe, C. L. Kane, Double Dirac Semimetals in Three Dimensions. *Phys. Rev. Lett.* **116**, 186402 (2016). [doi:10.1103/PhysRevLett.116.186402](https://doi.org/10.1103/PhysRevLett.116.186402) [Medline](#)
8. B. Bradlyn, J. Cano, Z. Wang, M. G. Vergniory, C. Felser, R. J. Cava, B. A. Bernevig, Beyond Dirac and Weyl fermions: Unconventional quasiparticles in conventional crystals. *Science* **353**, aaf5037 (2016). [doi:10.1126/science.aaf5037](https://doi.org/10.1126/science.aaf5037) [Medline](#)
9. P. Tang, Q. Zhou, S.-C. Zhang, Multiple Types of Topological Fermions in Transition Metal Silicides. *Phys. Rev. Lett.* **119**, 206402 (2017). [doi:10.1103/PhysRevLett.119.206402](https://doi.org/10.1103/PhysRevLett.119.206402) [Medline](#)
10. N. P. Armitage, E. J. Mele, A. Vishwanath, Weyl and Dirac semimetals in three-dimensional solids. *Rev. Mod. Phys.* **90**, 015001 (2018). [doi:10.1103/RevModPhys.90.015001](https://doi.org/10.1103/RevModPhys.90.015001)

11. L. Fu, Topological crystalline insulators. *Phys. Rev. Lett.* **106**, 106802 (2011).  
[doi:10.1103/PhysRevLett.106.106802](https://doi.org/10.1103/PhysRevLett.106.106802) [Medline](#)
12. T. H. Hsieh, H. Lin, J. Liu, W. Duan, A. Bansil, L. Fu, Topological crystalline insulators in the SnTe material class. *Nat. Commun.* **3**, 982 (2012). [doi:10.1038/ncomms1969](https://doi.org/10.1038/ncomms1969) [Medline](#)
13. Z. Wang, A. Alexandradinata, R. J. Cava, B. A. Bernevig, Hourglass fermions. *Nature* **532**, 189–194 (2016). [doi:10.1038/nature17410](https://doi.org/10.1038/nature17410) [Medline](#)
14. B. J. Wieder, B. Bradlyn, Z. Wang, J. Cano, Y. Kim, H. D. Kim, A. M. Rappe, C. L. Kane, B. A. Bernevig, Wallpaper fermions and the nonsymmorphic Dirac insulator. *Science* **361**, 246–251 (2018). [doi:10.1126/science.aan2802](https://doi.org/10.1126/science.aan2802) [Medline](#)
15. W. A. Benalcazar, B. A. Bernevig, T. L. Hughes, Electric multipole moments, topological multipole moment pumping, and chiral hinge states in crystalline insulators. *Phys. Rev. B* **96**, 245115 (2017). [doi:10.1103/PhysRevB.96.245115](https://doi.org/10.1103/PhysRevB.96.245115)
16. Z. Song, T. Zhang, Z. Fang, C. Fang, Quantitative mappings between symmetry and topology in solids. *Nat. Commun.* **9**, 3530 (2018). [doi:10.1038/s41467-018-06010-w](https://doi.org/10.1038/s41467-018-06010-w) [Medline](#)
17. E. Khalaf, H. C. Po, A. Vishwanath, H. Watanabe, Symmetry Indicators and Anomalous Surface States of Topological Crystalline Insulators. *Phys. Rev. X* **8**, 031070 (2018).  
[doi:10.1103/PhysRevX.8.031070](https://doi.org/10.1103/PhysRevX.8.031070)
18. D. Hsieh, Y. Xia, D. Qian, L. Wray, J. H. Dil, F. Meier, J. Osterwalder, L. Patthey, J. G. Checkelsky, N. P. Ong, A. V. Fedorov, H. Lin, A. Bansil, D. Grauer, Y. S. Hor, R. J. Cava, M. Z. Hasan, A tunable topological insulator in the spin helical Dirac transport regime. *Nature* **460**, 1101–1105 (2009). [doi:10.1038/nature08234](https://doi.org/10.1038/nature08234) [Medline](#)
19. S. Borisenko, Q. Gibson, D. Evtushinsky, V. Zabolotnyy, B. Büchner, R. J. Cava, Experimental realization of a three-dimensional Dirac semimetal. *Phys. Rev. Lett.* **113**, 027603 (2014). [doi:10.1103/PhysRevLett.113.027603](https://doi.org/10.1103/PhysRevLett.113.027603) [Medline](#)
20. S.-Y. Xu, I. Belopolski, N. Alidoust, M. Neupane, G. Bian, C. Zhang, R. Sankar, G. Chang, Z. Yuan, C.-C. Lee, S.-M. Huang, H. Zheng, J. Ma, D. S. Sanchez, B. Wang, A. Bansil, F. Chou, P. P. Shibayev, H. Lin, S. Jia, M. Z. Hasan, Discovery of a Weyl fermion

semimetal and topological Fermi arcs. *Science* **349**, 613–617 (2015).

[doi:10.1126/science.aaa9297](https://doi.org/10.1126/science.aaa9297) [Medline](#)

21. H. Weng, C. Fang, Z. Fang, B. A. Bernevig, X. Dai, Weyl Semimetal Phase in Noncentrosymmetric Transition-Metal Monophosphides. *Phys. Rev. X* **5**, 011029 (2015).  
[doi:10.1103/PhysRevX.5.011029](https://doi.org/10.1103/PhysRevX.5.011029)
22. F. Schindler, Z. Wang, M. G. Vergniory, A. M. Cook, A. Murani, S. Sengupta, A. Y. Kasumov, R. Deblock, S. Jeon, I. Drozdov, H. Bouchiat, S. Guéron, A. Yazdani, B. A. Bernevig, T. Neupert, Higher-order topology in bismuth. *Nat. Phys.* **14**, 918–924 (2018).  
[doi:10.1038/s41567-018-0224-7](https://doi.org/10.1038/s41567-018-0224-7) [Medline](#)
23. D. S. Sanchez, I. Belopolski, T. A. Cochran, X. Xu, J.-X. Yin, G. Chang, W. Xie, K. Manna, V. Süß, C.-Y. Huang, N. Alidoust, D. Multer, S. S. Zhang, N. Shumiya, X. Wang, G.-Q. Wang, T.-R. Chang, C. Felser, S.-Y. Xu, S. Jia, H. Lin, M. Z. Hasan, Topological chiral crystals with helicoid-arc quantum states. *Nature* **567**, 500–505 (2019).  
[doi:10.1038/s41586-019-1037-2](https://doi.org/10.1038/s41586-019-1037-2) [Medline](#)
24. Z. Rao, H. Li, T. Zhang, S. Tian, C. Li, B. Fu, C. Tang, L. Wang, Z. Li, W. Fan, J. Li, Y. Huang, Z. Liu, Y. Long, C. Fang, H. Weng, Y. Shi, H. Lei, Y. Sun, T. Qian, H. Ding, Observation of unconventional chiral fermions with long Fermi arcs in CoSi. *Nature* **567**, 496–499 (2019). [doi:10.1038/s41586-019-1031-8](https://doi.org/10.1038/s41586-019-1031-8) [Medline](#)
25. N. B. M. Schröter, S. Stoltz, K. Manna, F. de Juan, M. G. Vergniory, J. A. Krieger, D. Pei, T. Schmitt, P. Dudin, T. K. Kim, C. Cacho, B. Bradlyn, H. Borrmann, M. Schmidt, R. Widmer, V. N. Strocov, C. Felser, Observation and control of maximal Chern numbers in a chiral topological semimetal. *Science* **369**, 179–183 (2020).  
[doi:10.1126/science.aaz3480](https://doi.org/10.1126/science.aaz3480) [Medline](#)
26. W. Shi, B. J. Wieder, H. L. Meyerheim, Y. Sun, Y. Zhang, Y. Li, L. Shen, Y. Qi, L. Yang, J. Jena, P. Werner, K. Koepernik, S. Parkin, Y. Chen, C. Felser, B. A. Bernevig, Z. Wang, A charge-density-wave topological semimetal. *Nat. Phys.* **17**, 381–387 (2021).  
[doi:10.1038/s41567-020-01104-z](https://doi.org/10.1038/s41567-020-01104-z)
27. J. Goeth, B. Bradlyn, S. Honnali, C. Schindler, N. Kumar, J. Noky, Y. Qi, C. Shekhar, Y. Sun, Z. Wang, B. A. Bernevig, C. Felser, Axionic charge-density wave in the Weyl

semimetal  $(\text{TaSe}_4)_2\text{I}$ . *Nature* **575**, 315–319 (2019). [doi:10.1038/s41586-019-1630-4](https://doi.org/10.1038/s41586-019-1630-4)  
[Medline](#)

28. B. Bradlyn, L. Elcoro, J. Cano, M. G. Vergniory, Z. Wang, C. Felser, M. I. Aroyo, B. A. Bernevig, Topological quantum chemistry. *Nature* **547**, 298–305 (2017).  
[doi:10.1038/nature23268](https://doi.org/10.1038/nature23268) [Medline](#)
29. L. Elcoro, B. J. Wieder, Z. Song, Y. Xu, B. Bradlyn, B. A. Bernevig, Magnetic topological quantum chemistry. *Nat. Commun.* **12**, 5965 (2021). [doi:10.1038/s41467-021-26241-8](https://doi.org/10.1038/s41467-021-26241-8)  
[Medline](#)
30. L. Fu, C. L. Kane, Topological insulators with inversion symmetry. *Phys. Rev. B* **76**, 045302 (2007). [doi:10.1103/PhysRevB.76.045302](https://doi.org/10.1103/PhysRevB.76.045302)
31. Y. Kim, B. J. Wieder, C. L. Kane, A. M. Rappe, Dirac Line Nodes in Inversion-Symmetric Crystals. *Phys. Rev. Lett.* **115**, 036806 (2015). [doi:10.1103/PhysRevLett.115.036806](https://doi.org/10.1103/PhysRevLett.115.036806)  
[Medline](#)
32. J. Kruthoff, J. de Boer, J. van Wezel, C. L. Kane, R.-J. Slager, Topological Classification of Crystalline Insulators through Band Structure Combinatorics. *Phys. Rev. X* **7**, 041069 (2017). [doi:10.1103/PhysRevX.7.041069](https://doi.org/10.1103/PhysRevX.7.041069)
33. H. C. Po, A. Vishwanath, H. Watanabe, Symmetry-based indicators of band topology in the 230 space groups. *Nat. Commun.* **8**, 50 (2017). [doi:10.1038/s41467-017-00133-2](https://doi.org/10.1038/s41467-017-00133-2) [Medline](#)
34. Z. Wang, B. J. Wieder, J. Li, B. Yan, B. A. Bernevig, Higher-Order Topology, Monopole Nodal Lines, and the Origin of Large Fermi Arcs in Transition Metal Dichalcogenides  $\text{XTe}_2$  ( $\text{X}=\text{Mo}, \text{W}$ ). *Phys. Rev. Lett.* **123**, 186401 (2019).  
[doi:10.1103/PhysRevLett.123.186401](https://doi.org/10.1103/PhysRevLett.123.186401) [Medline](#)
35. H. Watanabe, H. C. Po, A. Vishwanath, Structure and topology of band structures in the 1651 magnetic space groups. *Sci. Adv.* **4**, eaat8685 (2018). [doi:10.1126/sciadv.aat8685](https://doi.org/10.1126/sciadv.aat8685)  
[Medline](#)
36. Z. Song, T. Zhang, C. Fang, Diagnosis for Nonmagnetic Topological Semimetals in the Absence of Spin-Orbital Coupling. *Phys. Rev. X* **8**, 031069 (2018).  
[doi:10.1103/PhysRevX.8.031069](https://doi.org/10.1103/PhysRevX.8.031069)

37. Y. Xu, L. Elcoro, Z.-D. Song, B. J. Wieder, M. G. Vergniory, N. Regnault, Y. Chen, C. Felser, B. A. Bernevig, High-throughput calculations of magnetic topological materials. *Nature* **586**, 702–707 (2020). [doi:10.1038/s41586-020-2837-0](https://doi.org/10.1038/s41586-020-2837-0) [Medline](#)
38. M. G. Vergniory, L. Elcoro, C. Felser, N. Regnault, B. A. Bernevig, Z. Wang, A complete catalogue of high-quality topological materials. *Nature* **566**, 480–485 (2019). [doi:10.1038/s41586-019-0954-4](https://doi.org/10.1038/s41586-019-0954-4) [Medline](#)
39. T. Zhang, Y. Jiang, Z. Song, H. Huang, Y. He, Z. Fang, H. Weng, C. Fang, Catalogue of topological electronic materials. *Nature* **566**, 475–479 (2019). [doi:10.1038/s41586-019-0944-6](https://doi.org/10.1038/s41586-019-0944-6) [Medline](#)
40. F. Tang, H. C. Po, A. Vishwanath, X. Wan, Comprehensive search for topological materials using symmetry indicators. *Nature* **566**, 486–489 (2019). [doi:10.1038/s41586-019-0937-5](https://doi.org/10.1038/s41586-019-0937-5) [Medline](#)
41. G. Bergerhoff, R. Hundt, R. Sievers, I. D. Brown, The inorganic crystal structure data base. *J. Chem. Inf. Comput. Sci.* **23**, 66–69 (1983). [doi:10.1021/ci00038a003](https://doi.org/10.1021/ci00038a003)
42. See supplementary materials.
43. J. Cano, B. Bradlyn, Z. Wang, L. Elcoro, M. G. Vergniory, C. Felser, M. I. Aroyo, B. A. Bernevig, Topology of Disconnected Elementary Band Representations. *Phys. Rev. Lett.* **120**, 266401 (2018). [doi:10.1103/PhysRevLett.120.266401](https://doi.org/10.1103/PhysRevLett.120.266401) [Medline](#)
44. H. C. Po, H. Watanabe, A. Vishwanath, Fragile Topology and Wannier Obstructions. *Phys. Rev. Lett.* **121**, 126402 (2018). [doi:10.1103/PhysRevLett.121.126402](https://doi.org/10.1103/PhysRevLett.121.126402) [Medline](#)
45. Z.-D. Song, L. Elcoro, Y.-F. Xu, N. Regnault, B. A. Bernevig, Fragile Phases as Affine Monoids: Classification and Material Examples. *Phys. Rev. X* **10**, 031001 (2020). [doi:10.1103/PhysRevX.10.031001](https://doi.org/10.1103/PhysRevX.10.031001)
46. Y. Hwang, J. Ahn, B.-J. Yang, Fragile topology protected by inversion symmetry: Diagnosis, bulk-boundary correspondence, and Wilson loop. *Phys. Rev. B* **100**, 205126 (2019). [doi:10.1103/PhysRevB.100.205126](https://doi.org/10.1103/PhysRevB.100.205126)
47. Z.-D. Song, L. Elcoro, B. A. Bernevig, Twisted bulk-boundary correspondence of fragile topology. *Science* **367**, 794–797 (2020). [doi:10.1126/science.aaz7650](https://doi.org/10.1126/science.aaz7650)

48. Z. Song, Z. Wang, W. Shi, G. Li, C. Fang, B. A. Bernevig, All Magic Angles in Twisted Bilayer Graphene are Topological. *Phys. Rev. Lett.* **123**, 036401 (2019).  
[doi:10.1103/PhysRevLett.123.036401](https://doi.org/10.1103/PhysRevLett.123.036401) [Medline](#)
49. H. C. Po, L. Zou, T. Senthil, A. Vishwanath, Faithful tight-binding models and fragile topology of magic-angle bilayer graphene. *Phys. Rev. B* **99**, 195455 (2019).  
[doi:10.1103/PhysRevB.99.195455](https://doi.org/10.1103/PhysRevB.99.195455)
50. Topological Materials Database, [www.topologicalquantumchemistry.com/](http://www.topologicalquantumchemistry.com/).
51. D. N. Basov, R. D. Averitt, D. Hsieh, Towards properties on demand in quantum materials. *Nat. Mater.* **16**, 1077–1088 (2017). [doi:10.1038/nmat5017](https://doi.org/10.1038/nmat5017) [Medline](#)
52. S. Peotta, P. Törmä, Superfluidity in topologically nontrivial flat bands. *Nat. Commun.* **6**, 8944 (2015). [doi:10.1038/ncomms9944](https://doi.org/10.1038/ncomms9944) [Medline](#)
53. F. Xie, Z. Song, B. Lian, B. A. Bernevig, Topology-Bounded Superfluid Weight in Twisted Bilayer Graphene. *Phys. Rev. Lett.* **124**, 167002 (2020).  
[doi:10.1103/PhysRevLett.124.167002](https://doi.org/10.1103/PhysRevLett.124.167002) [Medline](#)
54. VASP2Trace, <https://github.com/zjwang11/irvsp>.
55. Check Topological Mat, [www.cryst.ehu.es/cryst/checktopologicalmat](http://www.cryst.ehu.es/cryst/checktopologicalmat).
56. C. Bradley, A. Cracknell, *The Mathematical Theory of Symmetry in Solids: Representation Theory for Point Groups and Space Groups* (Clarendon, 1972).
57. A. A. Soluyanov, D. Vanderbilt, Wannier representation of  $Z_2$  topological insulators. *Phys. Rev. B* **83**, 035108 (2011). [doi:10.1103/PhysRevB.83.035108](https://doi.org/10.1103/PhysRevB.83.035108)
58. L. Elcoro, B. Bradlyn, Z. Wang, M. G. Vergniory, J. Cano, C. Felser, B. A. Bernevig, D. Orobengoa, G. de la Flor, M. I. Aroyo, Double crystallographic groups and their representations on the Bilbao Crystallographic Server. *J. Appl. Crystallogr.* **50**, 1457–1477 (2017). [doi:10.1107/S1600576717011712](https://doi.org/10.1107/S1600576717011712)
59. B. J. Wieder, Z. Wang, J. Cano, X. Dai, L. M. Schoop, B. Bradlyn, B. A. Bernevig, Strong and fragile topological Dirac semimetals with higher-order Fermi arcs. *Nat. Commun.* **11**, 627 (2020). [doi:10.1038/s41467-020-14443-5](https://doi.org/10.1038/s41467-020-14443-5) [Medline](#)

60. C.-Z. Li, A.-Q. Wang, C. Li, W.-Z. Zheng, A. Brinkman, D.-P. Yu, Z.-M. Liao, Reducing Electronic Transport Dimension to Topological Hinge States by Increasing Geometry Size of Dirac Semimetal Josephson Junctions. *Phys. Rev. Lett.* **124**, 156601 (2020). [doi:10.1103/PhysRevLett.124.156601](https://doi.org/10.1103/PhysRevLett.124.156601) [Medline](#)
61. A. Marrazzo, M. Gibertini, D. Campi, N. Mounet, N. Marzari, Relative Abundance of  $Z_2$  Topological Order in Exfoliable Two-Dimensional Insulators. *Nano Lett.* **19**, 8431–8440 (2019). [doi:10.1021/acs.nanolett.9b02689](https://doi.org/10.1021/acs.nanolett.9b02689) [Medline](#)
62. D. Wang, F. Tang, J. Ji, W. Zhang, A. Vishwanath, H. C. Po, X. Wan, Two-dimensional topological materials discovery by symmetry-indicator method. *Phys. Rev. B* **100**, 195108 (2019). [doi:10.1103/PhysRevB.100.195108](https://doi.org/10.1103/PhysRevB.100.195108)
63. Y. Li, V. Balédent, N. Barisić, Y. Cho, B. Fauqué, Y. Sidis, G. Yu, X. Zhao, P. Bourges, M. Greven, Unusual magnetic order in the pseudogap region of the superconductor  $HgBa_2CuO_{4+\delta}$ . *Nature* **455**, 372–375 (2008). [doi:10.1038/nature07251](https://doi.org/10.1038/nature07251) [Medline](#)
64. J. Zhou, J. Lin, X. Huang, Y. Zhou, Y. Chen, J. Xia, H. Wang, Y. Xie, H. Yu, J. Lei, D. Wu, F. Liu, Q. Fu, Q. Zeng, C.-H. Hsu, C. Yang, L. Lu, T. Yu, Z. Shen, H. Lin, B. I. Yakobson, Q. Liu, K. Suenaga, G. Liu, Z. Liu, A library of atomically thin metal chalcogenides. *Nature* **556**, 355–359 (2018). [doi:10.1038/s41586-018-0008-3](https://doi.org/10.1038/s41586-018-0008-3) [Medline](#)
65. Y. Chen, W. Ruan, M. Wu, S. Tang, H. Ryu, H.-Z. Tsai, R. L. Lee, S. Kahn, F. Liou, C. Jia, O. R. Albertini, H. Xiong, T. Jia, Z. Liu, J. A. Sobota, A. Y. Liu, J. E. Moore, Z.-X. Shen, S. G. Louie, S.-K. Mo, M. F. Crommie, Strong correlations and orbital texture in single-layer 1T-TaSe<sub>2</sub>. *Nat. Phys.* **16**, 218–224 (2020). [doi:10.1038/s41567-019-0744-9](https://doi.org/10.1038/s41567-019-0744-9)
66. K. Dolui, S. Sanvito, Dimensionality-driven phonon softening and incipient charge density wave instability in TiS<sub>2</sub>. *Europhys. Lett.* **115**, 47001 (2016). [doi:10.1209/0295-5075/115/47001](https://doi.org/10.1209/0295-5075/115/47001)
67. Y. F. Lu, H. Kono, T. I. Larkin, A. W. Rost, T. Takayama, A. V. Boris, B. Keimer, H. Takagi, Zero-gap semiconductor to excitonic insulator transition in Ta<sub>2</sub>NiSe<sub>5</sub>. *Nat. Commun.* **8**, 14408 (2017). [doi:10.1038/ncomms14408](https://doi.org/10.1038/ncomms14408) [Medline](#)

68. G. Mazza, M. Rösner, L. Windgätter, S. Latini, H. Hübener, A. J. Millis, A. Rubio, A. Georges, Nature of Symmetry Breaking at the Excitonic Insulator Transition: Ta<sub>2</sub>NiSe<sub>5</sub>. *Phys. Rev. Lett.* **124**, 197601 (2020). [doi:10.1103/PhysRevLett.124.197601](https://doi.org/10.1103/PhysRevLett.124.197601) [Medline](#)
69. R. M. Fleming, S. A. Sunshine, C. H. Chen, L. F. Schneemeyer, J. V. Waszczak, Defect-inhibited incommensurate distortion in Ta<sub>2</sub>NiSe<sub>7</sub>. *Phys. Rev. B* **42**, 4954–4959 (1990). [doi:10.1103/PhysRevB.42.4954](https://doi.org/10.1103/PhysRevB.42.4954) [Medline](#)
70. Q.-G. Mu, D. Nenno, Y.-P. Qi, F.-R. Fan, C. Pei, M. ElGhazali, J. Gooth, C. Felser, P. Narang, S. Medvedev, Suppression of axionic charge density wave and onset of superconductivity in the chiral Weyl semimetal Ta<sub>2</sub>Se<sub>8</sub>I. *Phys. Rev. Mater.* **5**, 084201 (2021). [doi:10.1103/PhysRevMaterials.5.084201](https://doi.org/10.1103/PhysRevMaterials.5.084201)
71. T. A. Cochran *et al.*, A Fermi Arc Quantum Ladder. arXiv 2004.11365 (2020).
72. T.-R. Chang, I. Pletikosic, T. Kong, G. Bian, A. Huang, J. Denlinger, S. K. Kushwaha, B. Sinkovic, H.-T. Jeng, T. Valla, W. Xie, R. J. Cava, Realization of a Type-II Nodal-Line Semimetal in Mg<sub>3</sub>Bi<sub>2</sub>. *Adv. Sci.* **6**, 1800897 (2018). [doi:10.1002/advs.201800897](https://doi.org/10.1002/advs.201800897) [Medline](#)
73. A. A. Soluyanov, D. Gresch, Z. Wang, Q. Wu, M. Troyer, X. Dai, B. A. Bernevig, Type-II Weyl semimetals. *Nature* **527**, 495–498 (2015). [doi:10.1038/nature15768](https://doi.org/10.1038/nature15768) [Medline](#)
74. J. Gao, Y. Qian, S. Nie, Z. Fang, H. Weng, Z. Wang, High-throughput screening for Weyl semimetals with S<sub>4</sub> symmetry. *Sci. Bull.* **66**, 667–675 (2021). [doi:10.1016/j.scib.2020.12.028](https://doi.org/10.1016/j.scib.2020.12.028)
75. K. Choudhary, K. F. Garrity, N. J. Ghimire, N. Anand, F. Tavazza, High-throughput search for magnetic topological materials using spin-orbit spillage, machine learning, and experiments. *Phys. Rev. B* **103**, 155131 (2021). [doi:10.1103/PhysRevB.103.155131](https://doi.org/10.1103/PhysRevB.103.155131)
76. Z. Guo, D. Yan, H. Sheng, S. Nie, Y. Shi, Z. Wang, Quantum spin Hall effect in Ta<sub>2</sub>M<sub>3</sub>Te<sub>5</sub> (M = Pd, Ni). *Phys. Rev. B* **103**, 115145 (2021). [doi:10.1103/PhysRevB.103.115145](https://doi.org/10.1103/PhysRevB.103.115145)
77. X. Wang *et al.*, Observation of quantum spin Hall states in Ta<sub>2</sub>Pd<sub>3</sub>Te<sub>5</sub>. arXiv 2012.07293 (2020).

78. G. Kresse, J. Furthmüller, Efficiency of ab-initio total energy calculations for metals and semiconductors using a plane-wave basis set. *Comput. Mater. Sci.* **6**, 15–50 (1996).  
[doi:10.1016/0927-0256\(96\)00008-0](https://doi.org/10.1016/0927-0256(96)00008-0)
79. G. Kresse, J. Furthmüller, Efficient iterative schemes for *ab initio* total-energy calculations using a plane-wave basis set. *Phys. Rev. B* **54**, 11169–11186 (1996).  
[doi:10.1103/PhysRevB.54.11169](https://doi.org/10.1103/PhysRevB.54.11169) [Medline](#)
80. G. Kresse, J. Hafner, *Ab initio* molecular dynamics for open-shell transition metals. *Phys. Rev. B* **48**, 13115–13118 (1993). [doi:10.1103/PhysRevB.48.13115](https://doi.org/10.1103/PhysRevB.48.13115) [Medline](#)
81. G. Kresse, D. Joubert, From ultrasoft pseudopotentials to the projector augmented-wave method. *Phys. Rev. B* **59**, 1758–1775 (1999). [doi:10.1103/PhysRevB.59.1758](https://doi.org/10.1103/PhysRevB.59.1758)
82. J. P. Perdew, K. Burke, M. Ernzerhof, Generalized Gradient Approximation Made Simple. *Phys. Rev. Lett.* **77**, 3865–3868 (1996). [doi:10.1103/PhysRevLett.77.3865](https://doi.org/10.1103/PhysRevLett.77.3865) [Medline](#)
83. D. Hobbs, G. Kresse, J. Hafner, Fully unconstrained noncollinear magnetism within the projector augmented-wave method. *Phys. Rev. B* **62**, 11556–11570 (2000).  
[doi:10.1103/PhysRevB.62.11556](https://doi.org/10.1103/PhysRevB.62.11556)
84. J. Gao, Q. Wu, C. Persson, Z. Wang, Irvsp: To obtain irreducible representations of electronic states in the VASP. *Comput. Phys. Commun.* **261**, 107760 (2021).  
[doi:10.1016/j.cpc.2020.107760](https://doi.org/10.1016/j.cpc.2020.107760)
85. G. Pizzi, V. Vitale, R. Arita, S. Blügel, F. Freimuth, G. Géranton, M. Gibertini, D. Gresch, C. Johnson, T. Koretsune, J. Ibañez-Azpiroz, H. Lee, J.-M. Lihm, D. Marchand, A. Marrazzo, Y. Mokrousov, J. I. Mustafa, Y. Nohara, Y. Nomura, L. Paulatto, S. Poncé, T. Ponweiser, J. Qiao, F. Thöle, S. S. Tsirkin, M. Wierzbowska, N. Marzari, D. Vanderbilt, I. Souza, A. A. Mostofi, J. R. Yates, Wannier90 as a community code: New features and applications. *J. Phys. Condens. Matter* **32**, 165902 (2020). [doi:10.1088/1361-648X/ab51ff](https://doi.org/10.1088/1361-648X/ab51ff) [Medline](#)
86. Data for “All Topological Bands of All Nonmagnetic Stoichiometric Materials”; <https://doi.org/10.5281/zenodo.6123281>.

87. Z. Song, Z. Fang, C. Fang, ( $d - 2$ )-Dimensional Edge States of Rotation Symmetry Protected Topological States. *Phys. Rev. Lett.* **119**, 246402 (2017).  
[doi:10.1103/PhysRevLett.119.246402](https://doi.org/10.1103/PhysRevLett.119.246402) [Medline](#)
88. L. Michel, J. Zak, Connectivity of energy bands in crystals. *Phys. Rev. B* **59**, 5998–6001 (1999). [doi:10.1103/PhysRevB.59.5998](https://doi.org/10.1103/PhysRevB.59.5998)
89. L. Michel, J. Zak, Elementary energy bands in crystals are connected. *Phys. Rep.* **341**, 377–395 (2001). [doi:10.1016/S0370-1573\(00\)00093-4](https://doi.org/10.1016/S0370-1573(00)00093-4)
90. J. Cano, L. Elcoro, M. I. Aroyo, B. A. Bernevig, B. Bradlyn, Topology invisible to eigenvalues in obstructed atomic insulators. arXiv 2107.00647 (2021).
91. J. Zak, Symmetry Specification of Bands in Solids. *Phys. Rev. Lett.* **45**, 1025–1028 (1980).  
[doi:10.1103/PhysRevLett.45.1025](https://doi.org/10.1103/PhysRevLett.45.1025)
92. M. G. Vergniory, L. Elcoro, Z. Wang, J. Cano, C. Felser, M. I. Aroyo, B. A. Bernevig, B. Bradlyn, Graph theory data for topological quantum chemistry. *Phys. Rev. E* **96**, 023310 (2017). [doi:10.1103/PhysRevE.96.023310](https://doi.org/10.1103/PhysRevE.96.023310) [Medline](#)
93. J. Cano, B. Bradlyn, Z. Wang, L. Elcoro, M. G. Vergniory, C. Felser, M. I. Aroyo, B. A. Bernevig, Building blocks of topological quantum chemistry: Elementary band representations. *Phys. Rev. B* **97**, 035139 (2018). [doi:10.1103/PhysRevB.97.035139](https://doi.org/10.1103/PhysRevB.97.035139)
94. M. I. Aroyo, J. M. Perez-Mato, C. Capillas, E. Kroumova, S. Ivantchev, G. Madariaga, A. Kirov, H. Wondratschek, Bilbao Crystallographic Server: I. Databases and crystallographic computing programs. *Z. Kristallogr. Cryst. Mater.* **221**, 15–27 (2006).  
[doi:10.1524/zkri.2006.221.1.15](https://doi.org/10.1524/zkri.2006.221.1.15)
95. M. I. Aroyo, A. Kirov, C. Capillas, J. M. Perez-Mato, H. Wondratschek, Bilbao Crystallographic Server. II. Representations of crystallographic point groups and space groups. *Acta Crystallogr. A* **62**, 115–128 (2006). [doi:10.1107/S0108767305040286](https://doi.org/10.1107/S0108767305040286) [Medline](#)
96. S. Liu, A. Vishwanath, E. Khalaf, Shift Insulators: Rotation-Protected Two-Dimensional Topological Crystalline Insulators. *Phys. Rev. X* **9**, 031003 (2019).  
[doi:10.1103/PhysRevX.9.031003](https://doi.org/10.1103/PhysRevX.9.031003)

97. B. Bradlyn, Z. Wang, J. Cano, B. A. Bernevig, Disconnected elementary band representations, fragile topology, and Wilson loops as topological indices: An example on the triangular lattice. *Phys. Rev. B* **99**, 045140 (2019).  
[doi:10.1103/PhysRevB.99.045140](https://doi.org/10.1103/PhysRevB.99.045140)
98. A. Bouhon, A. M. Black-Schaffer, R.-J. Slager, Wilson loop approach to fragile topology of split elementary band representations and topological crystalline insulators with time-reversal symmetry. *Phys. Rev. B* **100**, 195135 (2019). [doi:10.1103/PhysRevB.100.195135](https://doi.org/10.1103/PhysRevB.100.195135)
99. J. Ahn, S. Park, B.-J. Yang, Failure of Nielsen-Ninomiya Theorem and Fragile Topology in Two-Dimensional Systems with Space-Time Inversion Symmetry: Application to Twisted Bilayer Graphene at Magic Angle. *Phys. Rev. X* **9**, 021013 (2019).  
[doi:10.1103/PhysRevX.9.021013](https://doi.org/10.1103/PhysRevX.9.021013)
100. V. Peri, Z.-D. Song, M. Serra-Garcia, P. Engeler, R. Queiroz, X. Huang, W. Deng, Z. Liu, B. A. Bernevig, S. D. Huber, Experimental characterization of fragile topology in an acoustic metamaterial. *Science* **367**, 797–800 (2020). [doi:10.1126/science.aaz7654](https://doi.org/10.1126/science.aaz7654)  
[Medline](#)
101. A. Nelson, T. Neupert, T. Bzdušek, A. Alexandradinata, Multicellularity of Delicate Topological Insulators. *Phys. Rev. Lett.* **126**, 216404 (2021).  
[doi:10.1103/PhysRevLett.126.216404](https://doi.org/10.1103/PhysRevLett.126.216404) [Medline](#)
102. B. J. Wieder, B. A. Bernevig, The Axion Insulator as a Pump of Fragile Topology. arXiv 1810.02373 (2018).
103. A. Kitaev, V. Lebedev, M. Feigel'man, Periodic table for topological insulators and superconductors. *AIP Conf. Proc.* **1134**, 22–30 (2009). [doi:10.1063/1.3149495](https://doi.org/10.1063/1.3149495)
104. X.-L. Qi, T. L. Hughes, S.-C. Zhang, Topological field theory of time-reversal invariant insulators. *Phys. Rev. B* **78**, 195424 (2008). [doi:10.1103/PhysRevB.78.195424](https://doi.org/10.1103/PhysRevB.78.195424)
105. C. Fang, L. Fu, New classes of topological crystalline insulators having surface rotation anomaly. *Sci. Adv.* **5**, eaat2374 (2019). [doi:10.1126/sciadv.aat2374](https://doi.org/10.1126/sciadv.aat2374)
106. S.-J. Huang, H. Song, Y.-P. Huang, M. Hermele, Building crystalline topological phases from lower-dimensional states. *Phys. Rev. B* **96**, 205106 (2017).  
[doi:10.1103/PhysRevB.96.205106](https://doi.org/10.1103/PhysRevB.96.205106)

107. W. A. Benalcazar, T. Li, T. L. Hughes, Quantization of fractional corner charge in  $C_n$ -symmetric higher-order topological crystalline insulators. *Phys. Rev. B* **99**, 245151 (2019). [doi:10.1103/PhysRevB.99.245151](https://doi.org/10.1103/PhysRevB.99.245151)
108. L. Fidkowski, T. S. Jackson, I. Klich, Model characterization of gapless edge modes of topological insulators using intermediate Brillouin-zone functions. *Phys. Rev. Lett.* **107**, 036601 (2011). [doi:10.1103/PhysRevLett.107.036601](https://doi.org/10.1103/PhysRevLett.107.036601) [Medline](#)
109. R. Yu, X. L. Qi, A. Bernevig, Z. Fang, X. Dai, Equivalent expression of  $Z_2$  topological invariant for band insulators using the non-Abelian Berry connection. *Phys. Rev. B* **84**, 075119 (2011). [doi:10.1103/PhysRevB.84.075119](https://doi.org/10.1103/PhysRevB.84.075119)
110. A. Alexandradinata, Z. Wang, B. A. Bernevig, Topological Insulators from Group Cohomology. *Phys. Rev. X* **6**, 021008 (2016). [doi:10.1103/PhysRevX.6.021008](https://doi.org/10.1103/PhysRevX.6.021008)
111. W. A. Benalcazar, B. A. Bernevig, T. L. Hughes, Quantized electric multipole insulators. *Science* **357**, 61–66 (2017). [doi:10.1126/science.aah6442](https://doi.org/10.1126/science.aah6442) [Medline](#)
112. Y. Qian, J. Gao, Z. Song, S. Nie, Z. Wang, H. Weng, Z. Fang, Weyl semimetals with  $S_4$  symmetry. *Phys. Rev. B* **101**, 155143 (2020). [doi:10.1103/PhysRevB.101.155143](https://doi.org/10.1103/PhysRevB.101.155143)
113. VASP2Trace may be accessed to compute the topological classification of a material by selecting the function CHECKTOPOLOGICAL at <https://cryst.ehu.es/cgi-bin/cryst/programs/topological.pl>.
114. L. Elcoro, Z. Song, B. A. Bernevig, Application of induction procedure and Smith decomposition in calculation and topological classification of electronic band structures in the 230 space groups. *Phys. Rev. B* **102**, 035110 (2020).  
[doi:10.1103/PhysRevB.102.035110](https://doi.org/10.1103/PhysRevB.102.035110)
115. M. N. Ali, Q. Gibson, S. Jeon, B. B. Zhou, A. Yazdani, R. J. Cava, The crystal and electronic structures of  $Cd_3As_2$ , the three-dimensional electronic analogue of graphene. *Inorg. Chem.* **53**, 4062–4067 (2014). [doi:10.1021/ic403163d](https://doi.org/10.1021/ic403163d) [Medline](#)
116. Z. K. Liu, J. Jiang, B. Zhou, Z. J. Wang, Y. Zhang, H. M. Weng, D. Prabhakaran, S.-K. Mo, H. Peng, P. Dudin, T. Kim, M. Hoesch, Z. Fang, X. Dai, Z. X. Shen, D. L. Feng, Z. Hussain, Y. L. Chen, A stable three-dimensional topological Dirac semimetal  $Cd_3As_2$ . *Nat. Mater.* **13**, 677–681 (2014). [doi:10.1038/nmat3990](https://doi.org/10.1038/nmat3990) [Medline](#)

117. M. I. Aroyo, Ed., *International Tables for Crystallography, Volume A: Space-Group Symmetry* (International Union of Crystallography, 2016).
118. J. Perez-Mato, S. V. Gallego, E. S. Tasci, L. Elcoro, G. de la Flor, M. I. Aroyo, Symmetry-Based Computational Tools for Magnetic Crystallography. *Annu. Rev. Mater. Res.* **45**, 217–248 (2015). [doi:10.1146/annurev-matsci-070214-021008](https://doi.org/10.1146/annurev-matsci-070214-021008)
119. P. Hohenberg, W. Kohn, Inhomogeneous Electron Gas. *Phys. Rev.* **136**, B864–B871 (1964). [doi:10.1103/PhysRev.136.B864](https://doi.org/10.1103/PhysRev.136.B864)
120. W. Kohn, L. J. Sham, Self-Consistent Equations Including Exchange and Correlation Effects. *Phys. Rev.* **140**, A1133–A1138 (1965). [doi:10.1103/PhysRev.140.A1133](https://doi.org/10.1103/PhysRev.140.A1133)
121. I. Robredo, M. G. Vergniory, B. Bradlyn, Higher-order and crystalline topology in a phenomenological tight-binding model of lead telluride. *Phys. Rev. Mater.* **3**, 041202 (2019). [doi:10.1103/PhysRevMaterials.3.041202](https://doi.org/10.1103/PhysRevMaterials.3.041202)
122. A. Hjorth Larsen, J. Jørgen Mortensen, J. Blomqvist, I. E. Castelli, R. Christensen, M. Dulak, J. Friis, M. N. Groves, B. Hammer, C. Hargus, E. D. Hermes, P. C. Jennings, P. Bjerre Jensen, J. Kermode, J. R. Kitchin, E. Leonhard Kolsbjerg, J. Kubal, K. Kaasbjerg, S. Lysgaard, J. Bergmann Maronsson, T. Maxson, T. Olsen, L. Pastewka, A. Peterson, C. Rostgaard, J. Schiøtz, O. Schütt, M. Strange, K. S. Thygesen, T. Vegge, L. Vilhelmsen, M. Walter, Z. Zeng, K. W. Jacobsen, The atomic simulation environment—a Python library for working with atoms. *J. Phys. Condens. Matter* **29**, 273002 (2017). [doi:10.1088/1361-648X/aa680e](https://doi.org/10.1088/1361-648X/aa680e) [Medline](#)
123. A. Togo, I. Tanaka, First principles phonon calculations in materials science. *Scr. Mater.* **108**, 1–5 (2015). [doi:10.1016/j.scriptamat.2015.07.021](https://doi.org/10.1016/j.scriptamat.2015.07.021)
124. W. Setyawan, S. Curtarolo, High-throughput electronic band structure calculations: Challenges and tools. *Comput. Mater. Sci.* **49**, 299–312 (2010). [doi:10.1016/j.commatsci.2010.05.010](https://doi.org/10.1016/j.commatsci.2010.05.010)
125. Y. Hinuma, G. Pizzi, Y. Kumagai, F. Oba, I. Tanaka, Band structure diagram paths based on crystallography. *Comput. Mater. Sci.* **128**, 140–184 (2017). [doi:10.1016/j.commatsci.2016.10.015](https://doi.org/10.1016/j.commatsci.2016.10.015)

126. A. Jain, S. P. Ong, G. Hautier, W. Chen, W. D. Richards, S. Dacek, S. Cholia, D. Gunter, D. Skinner, G. Ceder, K. A. Persson, The Materials Project: A materials genome approach to accelerating materials innovation. *APL Mater.* **1**, 011002 (2013). [doi:10.1063/1.4812323](https://doi.org/10.1063/1.4812323)
127. C. L. Kane, E. J. Mele, Quantum spin Hall effect in graphene. *Phys. Rev. Lett.* **95**, 226801 (2005). [doi:10.1103/PhysRevLett.95.226801](https://doi.org/10.1103/PhysRevLett.95.226801) [Medline](#)
128. J. Ma, C. Yi, B. Lv, Z. Wang, S. Nie, L. Wang, L. Kong, Y. Huang, P. Richard, P. Zhang, K. Yaji, K. Kuroda, S. Shin, H. Weng, B. A. Bernevig, Y. Shi, T. Qian, H. Ding, Experimental evidence of hourglass fermion in the candidate nonsymmorphic topological insulator KHgSb. *Sci. Adv.* **3**, e1602415 (2017). [doi:10.1126/sciadv.1602415](https://doi.org/10.1126/sciadv.1602415)
129. S. Liang, S. Kushwaha, T. Gao, M. Hirschberger, J. Li, Z. Wang, K. Stolze, B. Skinner, B. A. Bernevig, R. J. Cava, N. P. Ong, A gap-protected zero-Hall effect state in the quantum limit of the non-symmorphic metal KHgSb. *Nat. Mater.* **18**, 443–447 (2019). [doi:10.1038/s41563-019-0303-x](https://doi.org/10.1038/s41563-019-0303-x) [Medline](#)
130. B. J. Wieder, C. L. Kane, Spin-orbit semimetals in the layer groups. *Phys. Rev. B* **94**, 155108 (2016). [doi:10.1103/PhysRevB.94.155108](https://doi.org/10.1103/PhysRevB.94.155108)
131. G. Chang, S.-Y. Xu, B. J. Wieder, D. S. Sanchez, S.-M. Huang, I. Belopolski, T.-R. Chang, S. Zhang, A. Bansil, H. Lin, M. Z. Hasan, Unconventional Chiral Fermions and Large Topological Fermi Arcs in RhSi. *Phys. Rev. Lett.* **119**, 206401 (2017). [doi:10.1103/PhysRevLett.119.206401](https://doi.org/10.1103/PhysRevLett.119.206401) [Medline](#)
132. G. Chang, B. J. Wieder, F. Schindler, D. S. Sanchez, I. Belopolski, S.-M. Huang, B. Singh, D. Wu, T.-R. Chang, T. Neupert, S.-Y. Xu, H. Lin, M. Z. Hasan, Topological quantum properties of chiral crystals. *Nat. Mater.* **17**, 978–985 (2018). [doi:10.1038/s41563-018-0169-3](https://doi.org/10.1038/s41563-018-0169-3) [Medline](#)
133. F. Flicker, F. de Juan, B. Bradlyn, T. Morimoto, M. G. Vergniory, A. G. Grushin, Chiral optical response of multifold fermions. *Phys. Rev. B* **98**, 155145 (2018). [doi:10.1103/PhysRevB.98.155145](https://doi.org/10.1103/PhysRevB.98.155145)
134. M. Nespolo, M. I. Aroyo, B. Souvignier, Crystallographic shelves: Space-group hierarchy explained. *J. Appl. Crystallogr.* **51**, 1481–1491 (2018). [doi:10.1107/S1600576718012724](https://doi.org/10.1107/S1600576718012724)

135. D. Takane, Z. Wang, S. Souma, K. Nakayama, T. Nakamura, H. Oinuma, Y. Nakata, H. Iwasawa, C. Cacho, T. Kim, K. Horiba, H. Kumigashira, T. Takahashi, Y. Ando, T. Sato, Observation of Chiral Fermions with a Large Topological Charge and Associated Fermi-Arc Surface States in CoSi. *Phys. Rev. Lett.* **122**, 076402 (2019).  
[doi:10.1103/PhysRevLett.122.076402](https://doi.org/10.1103/PhysRevLett.122.076402) [Medline](#)
136. N. B. M. Schröter, D. Pei, M. G. Vergniory, Y. Sun, K. Manna, F. de Juan, J. A. Krieger, V. Süss, M. Schmidt, P. Dudin, B. Bradlyn, T. K. Kim, T. Schmitt, C. Cacho, C. Felser, V. N. Strocov, Y. Chen, Chiral topological semimetal with multifold band crossings and long Fermi arcs. *Nat. Phys.* **15**, 759–765 (2019). [doi:10.1038/s41567-019-0511-y](https://doi.org/10.1038/s41567-019-0511-y)
137. R. Yu, H. Weng, Z. Fang, X. Dai, X. Hu, Topological Node-Line Semimetal and Dirac Semimetal State in Antiperovskite Cu<sub>3</sub>PdN. *Phys. Rev. Lett.* **115**, 036807 (2015).  
[doi:10.1103/PhysRevLett.115.036807](https://doi.org/10.1103/PhysRevLett.115.036807) [Medline](#)
138. C. Fang, Y. Chen, H.-Y. Kee, L. Fu, Topological nodal line semimetals with and without spin-orbital coupling. *Phys. Rev. B* **92**, 081201 (2015). [doi:10.1103/PhysRevB.92.081201](https://doi.org/10.1103/PhysRevB.92.081201)
139. J. Ahn, D. Kim, Y. Kim, B.-J. Yang, Band Topology and Linking Structure of Nodal Line Semimetals with Z<sub>2</sub> Monopole Charges. *Phys. Rev. Lett.* **121**, 106403 (2018).  
[doi:10.1103/PhysRevLett.121.106403](https://doi.org/10.1103/PhysRevLett.121.106403) [Medline](#)
140. A. Bouhon, A. M. Black-Schaffer, Bulk topology of line-nodal structures protected by space group symmetries in class AI. arXiv 1710.04871 (2017).
141. T. Bzdušek, M. Sigrist, Robust doubly charged nodal lines and nodal surfaces in centrosymmetric systems. *Phys. Rev. B* **96**, 155105 (2017).  
[doi:10.1103/PhysRevB.96.155105](https://doi.org/10.1103/PhysRevB.96.155105)
142. T. L. Hughes, E. Prodan, B. A. Bernevig, Inversion-symmetric topological insulators. *Phys. Rev. B* **83**, 245132 (2011). [doi:10.1103/PhysRevB.83.245132](https://doi.org/10.1103/PhysRevB.83.245132)
143. X. Wan, A. M. Turner, A. Vishwanath, S. Y. Savrasov, Topological semimetal and Fermi-arc surface states in the electronic structure of pyrochlore iridates. *Phys. Rev. B* **83**, 205101 (2011). [doi:10.1103/PhysRevB.83.205101](https://doi.org/10.1103/PhysRevB.83.205101)

144. T. Zhang, L. Lu, S. Murakami, Z. Fang, H. Weng, C. Fang, Diagnosis scheme for topological degeneracies crossing high-symmetry lines. *Phys. Rev. Res.* **2**, 022066 (2020). [doi:10.1103/PhysRevResearch.2.022066](https://doi.org/10.1103/PhysRevResearch.2.022066)
145. I. Tateishi, Mapping rules from nodal line semimetal to topological crystalline insulator in face centered cubic lattice. *Phys. Rev. Res.* **2**, 043112 (2020).  
[doi:10.1103/PhysRevResearch.2.043112](https://doi.org/10.1103/PhysRevResearch.2.043112)
146. I. Tateishi, Nodal lines and mapping to mirror Chern numbers in Ca<sub>2</sub>As family. *Phys. Rev. B* **102**, 155111 (2020). [doi:10.1103/PhysRevB.102.155111](https://doi.org/10.1103/PhysRevB.102.155111)
147. Z. Ringel, Y. E. Kraus, A. Stern, Strong side of weak topological insulators. *Phys. Rev. B* **86**, 045102 (2012). [doi:10.1103/PhysRevB.86.045102](https://doi.org/10.1103/PhysRevB.86.045102)
148. J. E. Moore, L. Balents, Topological invariants of time-reversal-invariant band structures. *Phys. Rev. B* **75**, 121306 (2007). [doi:10.1103/PhysRevB.75.121306](https://doi.org/10.1103/PhysRevB.75.121306)
149. B. J. Wieder, K.-S. Lin, B. Bradlyn, Axionic band topology in inversion-symmetric Weyl-charge-density waves. *Phys. Rev. Res.* **2**, 042010 (2020).  
[doi:10.1103/PhysRevResearch.2.042010](https://doi.org/10.1103/PhysRevResearch.2.042010)
150. J. Yu, B. J. Wieder, C.-X. Liu, Dynamical piezomagnetic effect in time-reversal-invariant Weyl semimetals with axionic charge density waves. *Phys. Rev. B* **104**, 174406 (2021).  
[doi:10.1103/PhysRevB.104.174406](https://doi.org/10.1103/PhysRevB.104.174406)
151. H. Watanabe, H. C. Po, A. Vishwanath, M. Zaletel, Filling constraints for spin-orbit coupled insulators in symmorphic and nonsymmorphic crystals. *Proc. Natl. Acad. Sci. U.S.A.* **112**, 14551–14556 (2015). [doi:10.1073/pnas.1514665112](https://doi.org/10.1073/pnas.1514665112) [Medline](#)
152. S. M. Young, B. J. Wieder, Filling-Enforced Magnetic Dirac Semimetals in Two Dimensions. *Phys. Rev. Lett.* **118**, 186401 (2017). [doi:10.1103/PhysRevLett.118.186401](https://doi.org/10.1103/PhysRevLett.118.186401) [Medline](#)
153. H. Yang, A. Liang, C. Chen, C. Zhang, N. B. M. Schroeter, Y. Chen, Visualizing electronic structures of quantum materials by angle-resolved photoemission spectroscopy. *Nat. Rev. Mater.* **3**, 341–353 (2018). [doi:10.1038/s41578-018-0047-2](https://doi.org/10.1038/s41578-018-0047-2)

154. B. Lv, T. Qian, H. Ding, Angle-resolved photoemission spectroscopy and its application to topological materials. *Nat. Rev. Phys.* **1**, 609–626 (2019). [doi:10.1038/s42254-019-0088-5](https://doi.org/10.1038/s42254-019-0088-5)
155. I. Belopolski, P. Yu, D. S. Sanchez, Y. Ishida, T.-R. Chang, S. S. Zhang, S.-Y. Xu, H. Zheng, G. Chang, G. Bian, H.-T. Jeng, T. Kondo, H. Lin, Z. Liu, S. Shin, M. Z. Hasan, Signatures of a time-reversal symmetric Weyl semimetal with only four Weyl points. *Nat. Commun.* **8**, 942 (2017). [doi:10.1038/s41467-017-00938-1](https://doi.org/10.1038/s41467-017-00938-1) Medline
156. I. Belopolski, D. S. Sanchez, Y. Ishida, X. Pan, P. Yu, S.-Y. Xu, G. Chang, T.-R. Chang, H. Zheng, N. Alidoust, G. Bian, M. Neupane, S.-M. Huang, C.-C. Lee, Y. Song, H. Bu, G. Wang, S. Li, G. Eda, H.-T. Jeng, T. Kondo, H. Lin, Z. Liu, F. Song, S. Shin, M. Z. Hasan, Discovery of a new type of topological Weyl fermion semimetal state in  $\text{Mo}_x\text{W}_{1-x}\text{Te}_2$ . *Nat. Commun.* **7**, 13643 (2016). [doi:10.1038/ncomms13643](https://doi.org/10.1038/ncomms13643) Medline
157. Q. Wu, S. Zhang, H.-F. Song, M. Troyer, A. A. Soluyanov, WannierTools: An open-source software package for novel topological materials. *Comput. Phys. Commun.* **224**, 405–416 (2018). [doi:10.1016/j.cpc.2017.09.033](https://doi.org/10.1016/j.cpc.2017.09.033)
158. X. Zhang, L. Jin, X. Dai, G. Liu, Topological Type-II Nodal Line Semimetal and Dirac Semimetal State in Stable Kagome Compound  $\text{Mg}_3\text{Bi}_2$ . *J. Phys. Chem. Lett.* **8**, 4814–4819 (2017). [doi:10.1021/acs.jpclett.7b02129](https://doi.org/10.1021/acs.jpclett.7b02129) Medline
159. T. Zhou, X.-G. Zhu, M. Tong, Y. Zhang, X.-B. Luo, X. Xie, W. Feng, Q. Chen, S. Tan, Z.-Y. Wang, T. Jiang, Y. Tang, X.-C. Lai, X. Yang, Experimental Evidence of Topological Surface States in  $\text{Mg}_3\text{Bi}_2$  Films Grown by Molecular Beam Epitaxy. *Chin. Phys. Lett.* **36**, 117303 (2019). [doi:10.1088/0256-307X/36/11/117303](https://doi.org/10.1088/0256-307X/36/11/117303)
160. A. H. Castro Neto, F. Guinea, N. M. R. Peres, K. S. Novoselov, A. K. Geim, The electronic properties of graphene. *Rev. Mod. Phys.* **81**, 109–162 (2009). [doi:10.1103/RevModPhys.81.109](https://doi.org/10.1103/RevModPhys.81.109)
161. J. C. Y. Teo, L. Fu, C. L. Kane, Surface states and topological invariants in three-dimensional topological insulators: Application to  $\text{Bi}_{1-x}\text{Sb}_x$ . *Phys. Rev. B* **78**, 045426 (2008). [doi:10.1103/PhysRevB.78.045426](https://doi.org/10.1103/PhysRevB.78.045426)

162. Y. Tanaka, Z. Ren, T. Sato, K. Nakayama, S. Souma, T. Takahashi, K. Segawa, Y. Ando, Experimental realization of a topological crystalline insulator in SnTe. *Nat. Phys.* **8**, 800–803 (2012). [doi:10.1038/nphys2442](https://doi.org/10.1038/nphys2442)
163. F. Schindler, A. M. Cook, M. G. Vergniory, Z. Wang, S. S. P. Parkin, B. A. Bernevig, T. Neupert, Higher-order topological insulators. *Sci. Adv.* **4**, eaat0346 (2018).  
[doi:10.1126/sciadv.aat0346](https://doi.org/10.1126/sciadv.aat0346) [Medline](#)
164. E. Fradkin, E. Dagotto, D. Boyanovsky, Physical realization of the parity anomaly in condensed matter physics. *Phys. Rev. Lett.* **57**, 2967–2970 (1986).  
[doi:10.1103/PhysRevLett.57.2967](https://doi.org/10.1103/PhysRevLett.57.2967) [Medline](#)
165. G. Chang, S.-Y. Xu, D. S. Sanchez, S.-M. Huang, C.-C. Lee, T.-R. Chang, G. Bian, H. Zheng, I. Belopolski, N. Alidoust, H.-T. Jeng, A. Bansil, H. Lin, M. Z. Hasan, A strongly robust type II Weyl fermion semimetal state in Ta<sub>3</sub>S<sub>2</sub>. *Sci. Adv.* **2**, e1600295 (2016).  
[doi:10.1126/sciadv.1600295](https://doi.org/10.1126/sciadv.1600295)
166. K. Shiozaki, M. Sato, K. Gomi, Z<sub>2</sub> topology in nonsymmorphic crystalline insulators: Möbius twist in surface states. *Phys. Rev. B* **91**, 155120 (2015).  
[doi:10.1103/PhysRevB.91.155120](https://doi.org/10.1103/PhysRevB.91.155120)
167. J. Langbehn, Y. Peng, L. Trifunovic, F. von Oppen, P. W. Brouwer, Reflection-Symmetric Second-Order Topological Insulators and Superconductors. *Phys. Rev. Lett.* **119**, 246401 (2017). [doi:10.1103/PhysRevLett.119.246401](https://doi.org/10.1103/PhysRevLett.119.246401) [Medline](#)
168. Z. Wang, Y. Sun, X.-Q. Chen, C. Franchini, G. Xu, H. Weng, X. Dai, Z. Fang, Dirac semimetal and topological phase transitions in A<sub>3</sub>Bi (A = Na, K, Rb). *Phys. Rev. B* **85**, 195320 (2012). [doi:10.1103/PhysRevB.85.195320](https://doi.org/10.1103/PhysRevB.85.195320)
169. S. M. Young, S. Zaheer, J. C. Y. Teo, C. L. Kane, E. J. Mele, A. M. Rappe, Dirac semimetal in three dimensions. *Phys. Rev. Lett.* **108**, 140405 (2012).  
[doi:10.1103/PhysRevLett.108.140405](https://doi.org/10.1103/PhysRevLett.108.140405) [Medline](#)
170. J. A. Steinberg, S. M. Young, S. Zaheer, C. L. Kane, E. J. Mele, A. M. Rappe, Bulk Dirac points in distorted spinels. *Phys. Rev. Lett.* **112**, 036403 (2014).  
[doi:10.1103/PhysRevLett.112.036403](https://doi.org/10.1103/PhysRevLett.112.036403) [Medline](#)

171. B.-J. Yang, N. Nagaosa, Classification of stable three-dimensional Dirac semimetals with nontrivial topology. *Nat. Commun.* **5**, 4898 (2014). [doi:10.1038/ncomms5898](https://doi.org/10.1038/ncomms5898) [Medline](#)
172. Z. K. Liu, B. Zhou, Y. Zhang, Z. J. Wang, H. M. Weng, D. Prabhakaran, S.-K. Mo, Z. X. Shen, Z. Fang, X. Dai, Z. Hussain, Y. L. Chen, Discovery of a three-dimensional topological Dirac semimetal, Na<sub>3</sub>Bi. *Science* **343**, 864–867 (2014). [doi:10.1126/science.1245085](https://doi.org/10.1126/science.1245085) [Medline](#)
173. S.-Y. Xu, C. Liu, S. K. Kushwaha, R. Sankar, J. W. Krizan, I. Belopolski, M. Neupane, G. Bian, N. Alidoust, T. R. Chang, H. T. Jeng, C. Y. Huang, W. F. Tsai, H. Lin, P. P. Shibayev, F. C. Chou, R. J. Cava, M. Z. Hasan, Observation of Fermi arc surface states in a topological metal. *Science* **347**, 294–298 (2015). [doi:10.1126/science.1256742](https://doi.org/10.1126/science.1256742) [Medline](#)
174. M. B. de Paz, M. G. Vergniory, D. Bercioux, A. García-Etxarri, B. Bradlyn, Engineering fragile topology in photonic crystals: Topological quantum chemistry of light. *Phys. Rev. Res.* **1**, 032005 (2019). [doi:10.1103/PhysRevResearch.1.032005](https://doi.org/10.1103/PhysRevResearch.1.032005)
175. C. Fang, M. J. Gilbert, B. A. Bernevig, Bulk topological invariants in noninteracting point group symmetric insulators. *Phys. Rev. B* **86**, 115112 (2012). [doi:10.1103/PhysRevB.86.115112](https://doi.org/10.1103/PhysRevB.86.115112)
176. A. Alexandradinata, X. Dai, B. A. Bernevig, Wilson-loop characterization of inversion-symmetric topological insulators. *Phys. Rev. B* **89**, 155114 (2014). [doi:10.1103/PhysRevB.89.155114](https://doi.org/10.1103/PhysRevB.89.155114)
177. D. Hsieh, D. Qian, L. Wray, Y. Xia, Y. S. Hor, R. J. Cava, M. Z. Hasan, A topological Dirac insulator in a quantum spin Hall phase. *Nature* **452**, 970–974 (2008). [doi:10.1038/nature06843](https://doi.org/10.1038/nature06843) [Medline](#)
178. C.-H. Hsu, X. Zhou, T.-R. Chang, Q. Ma, N. Gedik, A. Bansil, S.-Y. Xu, H. Lin, L. Fu, Topology on a new facet of bismuth. *Proc. Natl. Acad. Sci. U.S.A.* **116**, 13255–13259 (2019). [doi:10.1073/pnas.1900527116](https://doi.org/10.1073/pnas.1900527116) [Medline](#)
179. C.-C. Liu, J.-J. Zhou, Y. Yao, F. Zhang, Weak Topological Insulators and Composite Weyl Semimetals: β-Bi<sub>4</sub>X<sub>4</sub> (X=Br, I). *Phys. Rev. Lett.* **116**, 066801 (2016). [doi:10.1103/PhysRevLett.116.066801](https://doi.org/10.1103/PhysRevLett.116.066801) [Medline](#)

180. F. Tang, H. C. Po, A. Vishwanath, X. Wan, Efficient topological materials discovery using symmetry indicators. *Nat. Phys.* **15**, 470–476 (2019). [doi:10.1038/s41567-019-0418-7](https://doi.org/10.1038/s41567-019-0418-7)
181. C.-H. Hsu, X. Zhou, Q. Ma, N. Gedik, A. Bansil, V. M. Pereira, H. Lin, L. Fu, S.-Y. Xu, T.-R. Chang, Purely rotational symmetry-protected topological crystalline insulator  $\alpha$ -Bi<sub>4</sub>Br<sub>4</sub>. *2D Mater.* **6**, 031004 (2019).
182. C. Yoon, C.-C. Liu, H. Min, F. Zhang, Quasi-One-Dimensional Higher-Order Topological Insulators. arXiv 2005.14710 (2020).
183. R. Noguchi, M. Kobayashi, Z. Jiang, K. Kuroda, T. Takahashi, Z. Xu, D. Lee, M. Hirayama, M. Ochi, T. Shirasawa, P. Zhang, C. Lin, C. Bareille, S. Sakuragi, H. Tanaka, S. Kunisada, K. Kurokawa, K. Yaji, A. Harasawa, V. Kandyba, A. Giampietri, A. Barinov, T. K. Kim, C. Cacho, M. Hashimoto, D. Lu, S. Shin, R. Arita, K. Lai, T. Sasagawa, T. Kondo, Evidence for a higher-order topological insulator in a three-dimensional material built from van der Waals stacking of bismuth-halide chains. *Nat. Mater.* **20**, 473–479 (2021). [doi:10.1038/s41563-020-00871-7](https://doi.org/10.1038/s41563-020-00871-7) [Medline](#)
184. A. K. Nayak, J. Reiner, R. Queiroz, H. Fu, C. Shekhar, B. Yan, C. Felser, N. Avraham, H. Beidenkopf, Resolving the topological classification of bismuth with topological defects. *Sci. Adv.* **5**, eaax6996 (2019). [doi:10.1126/sciadv.aax6996](https://doi.org/10.1126/sciadv.aax6996) [Medline](#)
185. R. Queiroz, I. C. Fulga, N. Avraham, H. Beidenkopf, J. Cano, Partial Lattice Defects in Higher-Order Topological Insulators. *Phys. Rev. Lett.* **123**, 266802 (2019). [doi:10.1103/PhysRevLett.123.266802](https://doi.org/10.1103/PhysRevLett.123.266802) [Medline](#)
186. F.-T. Huang, S. Joon Lim, S. Singh, J. Kim, L. Zhang, J.-W. Kim, M.-W. Chu, K. M. Rabe, D. Vanderbilt, S.-W. Cheong, Polar and phase domain walls with conducting interfacial states in a Weyl semimetal MoTe<sub>2</sub>. *Nat. Commun.* **10**, 4211 (2019). [doi:10.1038/s41467-019-11949-5](https://doi.org/10.1038/s41467-019-11949-5) [Medline](#)
187. Y.-B. Choi, Y. Xie, C.-Z. Chen, J. Park, S.-B. Song, J. Yoon, B. J. Kim, T. Taniguchi, K. Watanabe, J. Kim, K. C. Fong, M. N. Ali, K. T. Law, G.-H. Lee, Evidence of higher-order topology in multilayer WTe<sub>2</sub> from Josephson coupling through anisotropic hinge states. *Nat. Mater.* **19**, 974–979 (2020). [doi:10.1038/s41563-020-0721-9](https://doi.org/10.1038/s41563-020-0721-9) [Medline](#)

188. A. Kononov, G. Abulizi, K. Qu, J. Yan, D. Mandrus, K. Watanabe, T. Taniguchi, C. Schönenberger, One-Dimensional Edge Transport in Few-Layer WTe<sub>2</sub>. *Nano Lett.* **20**, 4228–4233 (2020). [doi:10.1021/acs.nanolett.0c00658](https://doi.org/10.1021/acs.nanolett.0c00658) [Medline](#)
189. W. Wang, S. Kim, M. Liu, F. A. Cevallos, R. J. Cava, N. P. Ong, Evidence for an edge supercurrent in the Weyl superconductor MoTe<sub>2</sub>. *Science* **368**, 534–537 (2020). [doi:10.1126/science.aaw9270](https://doi.org/10.1126/science.aaw9270) [Medline](#)
190. R. Noguchi, T. Takahashi, K. Kuroda, M. Ochi, T. Shirasawa, M. Sakano, C. Bareille, M. Nakayama, M. D. Watson, K. Yaji, A. Harasawa, H. Iwasawa, P. Dudin, T. K. Kim, M. Hoesch, V. Kandyba, A. Giampietri, A. Barinov, S. Shin, R. Arita, T. Sasagawa, T. Kondo, A weak topological insulator state in quasi-one-dimensional bismuth iodide. *Nature* **566**, 518–522 (2019). [doi:10.1038/s41586-019-0927-7](https://doi.org/10.1038/s41586-019-0927-7) [Medline](#)
191. W. P. Su, J. R. Schrieffer, A. J. Heeger, Solitons in Polyacetylene. *Phys. Rev. Lett.* **42**, 1698–1701 (1979). [doi:10.1103/PhysRevLett.42.1698](https://doi.org/10.1103/PhysRevLett.42.1698)
192. C. K. Chiang, C. R. Fincher, Y. W. Park, A. J. Heeger, H. Shirakawa, E. J. Louis, S. C. Gau, A. G. MacDiarmid, Electrical Conductivity in Doped Polyacetylene. *Phys. Rev. Lett.* **39**, 1098–1101 (1977). [doi:10.1103/PhysRevLett.39.1098](https://doi.org/10.1103/PhysRevLett.39.1098)
193. J.-N. Fuchs, F. Piéchon, Orbital embedding and topology of one-dimensional two-band insulators. *Phys. Rev. B* **104**, 235428 (2021). [doi:10.1103/PhysRevB.104.235428](https://doi.org/10.1103/PhysRevB.104.235428)
194. Y. Ran, Y. Zhang, A. Vishwanath, One-dimensional topologically protected modes in topological insulators with lattice dislocations. *Nat. Phys.* **5**, 298–303 (2009). [doi:10.1038/nphys1220](https://doi.org/10.1038/nphys1220)
195. Y.-M. Xie, X.-J. Gao, X. Y. Xu, C.-P. Zhang, J.-X. Hu, J. Z. Gao, K. T. Law, Kramers nodal line metals. *Nat. Commun.* **12**, 3064 (2021). [doi:10.1038/s41467-021-22903-9](https://doi.org/10.1038/s41467-021-22903-9) [Medline](#)
196. S. M. Young, C. L. Kane, Dirac Semimetals in Two Dimensions. *Phys. Rev. Lett.* **115**, 126803 (2015). [doi:10.1103/PhysRevLett.115.126803](https://doi.org/10.1103/PhysRevLett.115.126803) [Medline](#)
197. N. Kumar, M. Yao, J. Nayak, M. G. Vergniory, J. Bannies, Z. Wang, N. B. M. Schröter, V. N. Strocov, L. Müchler, W. Shi, E. D. L. Rienks, J. L. Mañes, C. Shekhar, S. S. P. Parkin, J. Fink, G. H. Fecher, Y. Sun, B. A. Bernevig, C. Felser, Signatures of Sixfold

Degenerate Exotic Fermions in a Superconducting Metal PdSb<sub>2</sub>. *Adv. Mater.* **32**, e1906046 (2020). [doi:10.1002/adma.201906046](https://doi.org/10.1002/adma.201906046) [Medline](#)

198. G. Gatti, D. Gosálbez-Martínez, S. S. Tsirkin, M. Fanciulli, M. Puppin, S. Polishchuk, S. Moser, L. Testa, E. Martino, S. Roth, P. Bugnon, L. Moreschini, A. Bostwick, C. Jozwiak, E. Rotenberg, G. Di Santo, L. Petaccia, I. Vobornik, J. Fujii, J. Wong, D. Jariwala, H. A. Atwater, H. M. Rønnow, M. Chergui, O. V. Yazyev, M. Grioni, A. Crepaldi, Radial Spin Texture of the Weyl Fermions in Chiral Tellurium. *Phys. Rev. Lett.* **125**, 216402 (2020). [doi:10.1103/PhysRevLett.125.216402](https://doi.org/10.1103/PhysRevLett.125.216402) [Medline](#)
199. F. de Juan, A. G. Grushin, T. Morimoto, J. E. Moore, Quantized circular photogalvanic effect in Weyl semimetals. *Nat. Commun.* **8**, 15995 (2017). [doi:10.1038/ncomms15995](https://doi.org/10.1038/ncomms15995) [Medline](#)
200. D. Rees, K. Manna, B. Lu, T. Morimoto, H. Borrmann, C. Felser, J. E. Moore, D. H. Torchinsky, J. Orenstein, Helicity-dependent photocurrents in the chiral Weyl semimetal RhSi. *Sci. Adv.* **6**, eaba0509 (2020). [doi:10.1126/sciadv.aba0509](https://doi.org/10.1126/sciadv.aba0509) [Medline](#)
201. B. Xu, Z. Fang, M.-Á. Sánchez-Martínez, J. W. F. Venderbos, Z. Ni, T. Qiu, K. Manna, K. Wang, J. Paglione, C. Bernhard, C. Felser, E. J. Mele, A. G. Grushin, A. M. Rappe, L. Wu, Optical signatures of multifold fermions in the chiral topological semimetal CoSi. *Proc. Natl. Acad. Sci. U.S.A.* **117**, 27104–27110 (2020). [doi:10.1073/pnas.2010752117](https://doi.org/10.1073/pnas.2010752117) [Medline](#)
202. Z. Ni, K. Wang, Y. Zhang, O. Pozo, B. Xu, X. Han, K. Manna, J. Paglione, C. Felser, A. G. Grushin, F. de Juan, E. J. Mele, L. Wu, Giant topological longitudinal circular photogalvanic effect in the chiral multifold semimetal CoSi. *Nat. Commun.* **12**, 154 (2021). [doi:10.1038/s41467-020-20408-5](https://doi.org/10.1038/s41467-020-20408-5) [Medline](#)
203. D. J. Rebar, S. M. Birnbaum, J. Singleton, M. Khan, J. C. Ball, P. W. Adams, J. Y. Chan, D. P. Young, D. A. Browne, J. F. DiTusa, Fermi surface, possible unconventional fermions, and unusually robust resistive critical fields in the chiral-structured superconductor AuBe. *Phys. Rev. B* **99**, 094517 (2019). [doi:10.1103/PhysRevB.99.094517](https://doi.org/10.1103/PhysRevB.99.094517)
204. J. Z. S. Gao *et al.*, Topological Superconductivity in Multifold Fermion Metals. arXiv 2012.11287 (2020).

205. E. Emmanouilidou, S. Mardanya, J. Xing, P. V. S. Reddy, A. Agarwal, T.-R. Chang, N. Ni, Fermiology and type-I superconductivity in the chiral superconductor NbGe<sub>2</sub> with Kramers-Weyl fermions. *Phys. Rev. B* **102**, 235144 (2020).  
[doi:10.1103/PhysRevB.102.235144](https://doi.org/10.1103/PhysRevB.102.235144)
206. G. Sharma, Z. Zhao, P. Sarker, B. A. Nail, J. Wang, M. N. Huda, F. E. Osterloh, Electronic structure, photovoltage, and photocatalytic hydrogen evolution with p-CuBi<sub>2</sub>O<sub>4</sub> nanocrystals. *J. Mater. Chem. A* **4**, 2936–2942 (2016). [doi:10.1039/C5TA07040F](https://doi.org/10.1039/C5TA07040F)
207. D. Di Sante, A. Hausoel, P. Barone, J. M. Tomczak, G. Sangiovanni, R. Thomale, Realizing double Dirac particles in the presence of electronic interactions. *Phys. Rev. B* **96**, 121106 (2017). [doi:10.1103/PhysRevB.96.121106](https://doi.org/10.1103/PhysRevB.96.121106)
208. J. F. Khouri, A. J. E. Rettie, M. A. Khan, N. J. Ghimire, I. Robredo, J. E. Pfluger, K. Pal, C. Wolverton, A. Bergara, J. S. Jiang, L. M. Schoop, M. G. Vergniory, J. F. Mitchell, D. Y. Chung, M. G. Kanatzidis, A New Three-Dimensional Subsulfide Ir<sub>2</sub>In<sub>8</sub>S with Dirac Semimetal Behavior. *J. Am. Chem. Soc.* **141**, 19130–19137 (2019).  
[doi:10.1021/jacs.9b10147](https://doi.org/10.1021/jacs.9b10147) [Medline](#)
209. L. M. Schoop, A. Topp, J. Lippmann, F. Orlandi, L. Müchler, M. G. Vergniory, Y. Sun, A. W. Rost, V. Duppel, M. Krivenkov, S. Sheoran, P. Manuel, A. Varykhalov, B. Yan, R. K. Kremer, C. R. Ast, B. V. Lotsch, Tunable Weyl and Dirac states in the nonsymmorphic compound CeSbTe. *Sci. Adv.* **4**, eaar2317 (2018). [doi:10.1126/sciadv.aar2317](https://doi.org/10.1126/sciadv.aar2317) [Medline](#)
210. C. Fang, M. J. Gilbert, X. Dai, B. A. Bernevig, Multi-Weyl topological semimetals stabilized by point group symmetry. *Phys. Rev. Lett.* **108**, 266802 (2012).  
[doi:10.1103/PhysRevLett.108.266802](https://doi.org/10.1103/PhysRevLett.108.266802) [Medline](#)
211. G. Xu, H. Weng, Z. Wang, X. Dai, Z. Fang, Chern semimetal and the quantized anomalous Hall effect in HgCr<sub>2</sub>Se<sub>4</sub>. *Phys. Rev. Lett.* **107**, 186806 (2011).  
[doi:10.1103/PhysRevLett.107.186806](https://doi.org/10.1103/PhysRevLett.107.186806) [Medline](#)
212. S.-M. Huang, S.-Y. Xu, I. Belopolski, C.-C. Lee, G. Chang, T.-R. Chang, B. Wang, N. Alidoust, G. Bian, M. Neupane, D. Sanchez, H. Zheng, H.-T. Jeng, A. Bansil, T. Neupert, H. Lin, M. Z. Hasan, New type of Weyl semimetal with quadratic double Weyl fermions.

*Proc. Natl. Acad. Sci. U.S.A.* **113**, 1180–1185 (2016). [doi:10.1073/pnas.1514581113](https://doi.org/10.1073/pnas.1514581113)  
[Medline](#)

213. S. S. Tsirkin, I. Souza, D. Vanderbilt, Composite Weyl nodes stabilized by screw symmetry with and without time-reversal invariance. *Phys. Rev. B* **96**, 045102 (2017).  
[doi:10.1103/PhysRevB.96.045102](https://doi.org/10.1103/PhysRevB.96.045102)
214. W. Wu, Z.-M. Yu, X. Zhou, Y. X. Zhao, S. A. Yang, Higher-order Dirac fermions in three dimensions. *Phys. Rev. B* **101**, 205134 (2020). [doi:10.1103/PhysRevB.101.205134](https://doi.org/10.1103/PhysRevB.101.205134)
215. H. Weng, C. Fang, Z. Fang, X. Dai, Topological semimetals with triply degenerate nodal points in  $\theta$ -phase tantalum nitride. *Phys. Rev. B* **93**, 241202 (2016).  
[doi:10.1103/PhysRevB.93.241202](https://doi.org/10.1103/PhysRevB.93.241202)
216. Z. Zhu, G. W. Winkler, Q. Wu, J. Li, A. A. Soluyanov, Triple Point Topological Metals. *Phys. Rev. X* **6**, 031003 (2016). [doi:10.1103/PhysRevX.6.031003](https://doi.org/10.1103/PhysRevX.6.031003)
217. G. Chang, S.-Y. Xu, S.-M. Huang, D. S. Sanchez, C.-H. Hsu, G. Bian, Z.-M. Yu, I. Belopolski, N. Alidoust, H. Zheng, T.-R. Chang, H.-T. Jeng, S. A. Yang, T. Neupert, H. Lin, M. Z. Hasan, Nexus fermions in topological symmorphic crystalline metals. *Sci. Rep.* **7**, 1688 (2017). [doi:10.1038/s41598-017-01523-8](https://doi.org/10.1038/s41598-017-01523-8) [Medline](#)
218. B. J. Wieder, Threes company. *Nat. Phys.* **14**, 329–330 (2018). [doi:10.1038/s41567-017-0032-5](https://doi.org/10.1038/s41567-017-0032-5)
219. B. Q. Lv, Z.-L. Feng, Q.-N. Xu, X. Gao, J.-Z. Ma, L.-Y. Kong, P. Richard, Y.-B. Huang, V. N. Strocov, C. Fang, H.-M. Weng, Y.-G. Shi, T. Qian, H. Ding, Observation of three-component fermions in the topological semimetal molybdenum phosphide. *Nature* **546**, 627–631 (2017). [doi:10.1038/nature22390](https://doi.org/10.1038/nature22390) [Medline](#)
220. J.-Z. Ma, J.-B. He, Y.-F. Xu, B. Q. Lv, D. Chen, W.-L. Zhu, S. Zhang, L.-Y. Kong, X. Gao, L.-Y. Rong, Y.-B. Huang, P. Richard, C.-Y. Xi, E. S. Choi, Y. Shao, Y.-L. Wang, H.-J. Gao, X. Dai, C. Fang, H.-M. Weng, G.-F. Chen, T. Qian, H. Ding, Three-component fermions with surface Fermi arcs in tungsten carbide. *Nat. Phys.* **14**, 349–354 (2018).  
[doi:10.1038/s41567-017-0021-8](https://doi.org/10.1038/s41567-017-0021-8)
221. H. Gao, Y. Kim, J. W. F. Venderbos, C. L. Kane, E. J. Mele, A. M. Rappe, W. Ren, Dirac-Weyl Semimetal: Coexistence of Dirac and Weyl Fermions in Polar Hexagonal ABC

Crystals. *Phys. Rev. Lett.* **121**, 106404 (2018). [doi:10.1103/PhysRevLett.121.106404](#)  
[Medline](#)

222. C. Tournier-Colletta, L. Moreschini, G. Autès, S. Moser, A. Crepaldi, H. Berger, A. L. Walter, K. S. Kim, A. Bostwick, P. Monceau, E. Rotenberg, O. V. Yazyev, M. Grioni, Electronic instability in a zero-gap semiconductor: The charge-density wave in  $(\text{TaSe}_4)_2\text{I}$ . *Phys. Rev. Lett.* **110**, 236401 (2013). [doi:10.1103/PhysRevLett.110.236401](#) [Medline](#)
223. Y. Zhang, L.-F. Lin, A. Moreo, S. Dong, E. Dagotto, First-principles study of the low-temperature charge density wave phase in the quasi-one-dimensional Weyl chiral compound  $(\text{TaSe}_4)_2\text{I}$ . *Phys. Rev. B* **101**, 174106 (2020).  
[doi:10.1103/PhysRevB.101.174106](#)
224. H. Yi, Z. Huang, W. Shi, L. Min, R. Wu, C. M. Polley, R. Zhang, Y.-F. Zhao, L.-J. Zhou, J. Adell, X. Gui, W. Xie, M. H. W. Chan, Z. Mao, Z. Wang, W. Wu, C.-Z. Chang, Surface charge induced Dirac band splitting in a charge density wave material  $(\text{TaSe}_4)_2\text{I}$ . *Phys. Rev. Res.* **3**, 013271 (2021). [doi:10.1103/PhysRevResearch.3.013271](#)
225. M. Lin, T. L. Hughes, Topological quadrupolar semimetals. *Phys. Rev. B* **98**, 241103 (2018). [doi:10.1103/PhysRevB.98.241103](#)
226. D. Călugăru, V. Juričić, B. Roy, Higher-order topological phases: A general principle of construction. *Phys. Rev. B* **99**, 041301 (2019). [doi:10.1103/PhysRevB.99.041301](#)
227. A. L. Szabó, R. Moessner, B. Roy, Strain-engineered higher-order topological phases for spin-3/2 Luttinger fermions. *Phys. Rev. B* **101**, 121301 (2020).  
[doi:10.1103/PhysRevB.101.121301](#)
228. A. L. Szabó, B. Roy, Dirty higher-order Dirac semimetal: Quantum criticality and bulk-boundary correspondence. *Phys. Rev. Res.* **2**, 043197 (2020).  
[doi:10.1103/PhysRevResearch.2.043197](#)
229. S. A. A. Ghorashi, T. Li, T. L. Hughes, Higher-Order Weyl Semimetals. *Phys. Rev. Lett.* **125**, 266804 (2020). [doi:10.1103/PhysRevLett.125.266804](#) [Medline](#)
230. H.-X. Wang, Z.-K. Lin, B. Jiang, G.-Y. Guo, J.-H. Jiang, Higher-Order Weyl Semimetals. *Phys. Rev. Lett.* **125**, 146401 (2020). [doi:10.1103/PhysRevLett.125.146401](#) [Medline](#)

231. S. Nie, B. A. Bernevig, Z. Wang, Sixfold excitations in electrides. *Phys. Rev. Res.* **3**, L012028 (2021). [doi:10.1103/PhysRevResearch.3.L012028](https://doi.org/10.1103/PhysRevResearch.3.L012028)